September 2015

Understanding and Managing Environmental Roadblocks to Shale Gas Development: An Analysis of Shallow Gas, NORM, and Trace Metals

Final Report
June 14, 2013 to September 30, 2015

RPSEA Award No 11122-56

by
J.-P. Nicot, P. Mickler, T. Larson, M.C. Castro
R. Darvari, R. Smyth, K. Uhlman, C. Omelon
with participation of
L. Bouvier, Tao Wen, Z.L. Hildenbrand, M. Slotten, J.M. Aldrige, C.M. Hall, R. Costley, J. Anderson, R. Reedy, J. Lu, Yuan Liu, K. Romanak, S.L. Porse, and Texas Water Development Board

Bureau of Economic Geology
Jackson School of Geosciences
The University of Texas at Austin
Austin, Texas 78713-8924

Understanding and Managing Environmental Roadblocks to Shale Gas Development: An Analysis of Shallow Gas, NORM, and Trace Metals

Jean-Philippe Nicot[1], Patrick Mickler[1], Toti Larson[2], M. Clara Castro[3]
Roxana Darvari[1], Rebecca Smyth[1], Kristine Uhlman[+1], Christopher Omelon[2]
with participation of
L. Bouvier[+3], Tao Wen[3], Z.L. Hildenbrand[4], M. Slotten[+5], J.M. Aldrige[+5],
C.M. Hall[3], R. Costley[1], J. Anderson[1], R. Reedy[1], J. Lu[1], Yuan Liu[+1],
K. Romanak[1], S.L. Porse[+1], and TWDB[6]

[1]: Bureau of Economic Geology, The University of Texas at Austin
[2]: Department of Geological Sciences, The University of Texas at Austin
[3]: Department of Earth and Environmental Sciences, University of Michigan at Ann Arbor
[4]: Inform Environmental LLC, Dallas, TX
[5]: Environmental Management and Sustainability Program, St. Edwards University, Austin, TX
[6]: Texas Water Development Board, Austin, TX
[+]: previously at

Bureau of Economic Geology
Jackson School of Geosciences
The University of Texas at Austin
Austin, Texas 78713-8924

Disclaimer

From DOE/NETL:

"This report was prepared as an account of work sponsored by an agency of the United States Government. Neither the United States Government nor any agency thereof, nor any of their employees, makes any warranty, express or implied, or assumes any legal liability or responsibility for the accuracy, completeness, or usefulness of any information, apparatus, product, or process disclosed, or represents that its use would not infringe privately owned rights. Reference herein to any specific commercial product, process, or service by trade name, trademark, manufacturer, or otherwise does not necessarily constitute or imply its endorsement, recommendation, or favoring by the United States Government or any agency thereof. The views and opinions of authors expressed herein do not necessarily state or reflect those of the United States Government or any agency thereof."

From RPSEA:

"Funding for this project is provided by RPSEA through the "Ultra-Deepwater and Unconventional Natural Gas and Other Petroleum Resources" program authorized by the U.S. Energy Policy Act of 2005. RPSEA (www.rpsea.org) is a nonprofit corporation whose mission is to provide a stewardship role in ensuring the focused research, development and deployment of safe and environmentally responsible technology that can effectively deliver hydrocarbons from domestic resources to the citizens of the United States. RPSEA, operating as a consortium of premier U.S. energy research universities, industry, and independent research organizations, manages the program under a contract with the U.S. Department of Energy's National Energy Technology Laboratory."

Abstract

The main objective of the project was to document occurrences of shallow gas in fresh-water aquifers in Texas either dissolved or free phase and identify controlling processes. A secondary somewhat independent objective was to contribute to the understanding of the nature and variability of flowback and produced water associated with hydraulic fracturing in the context of rock-water interactions.

We undertook a large sampling campaign of aquifers in the footprint of major Texas plays (900+ water samples): Barnett in north-central Texas (555 unique locations), Eagle Ford in South Texas (118 unique locations), Haynesville in East Texas (70 unique locations), and in the Delaware Basin of West Texas (40 unique locations). Most of the wells (2/3) are relatively shallow residential wells sampled at or as close as possible to the wellhead but many wells are irrigation, municipal, or rig-supply wells. All samples were analyzed for major ions, dissolved gases, and, when CH_4>0.1 mg/L, for methane and light alkanes carbon isotopes and trace elements. The vast majority of wells show some measurable methane and ~100 wells show methane >0.1 mg/L. A total of ~20 wells have methane concentrations >10 mg/L, these high concentrations were observed in all plays and present at least a thermogenic component. Some wells, generally with a <10 mg/L concentration, show a clear microbial origin for methane. A number of samples show mixing between the two origins but also more complex behavior such as methane degradation. Samples with thermogenic methane are generally spatially organized in clusters. Overall the source of the dissolved methane is likely natural sourced from shallow natural gas accumulations in the Barnett Shale, lignite beds associated with a fault in the Haynesville shale, and lignite and degradation of oil and deep organic matter associated with a fractured zone in the Eagle Ford Shale. The Delaware Basin samples show no dissolved methane other than associated to a recent blowout.

We also performed autoclave experiments in controlled conditions exposing shale core fragments to various fluids, examining reacted and unreacted rocks and documenting chemical composition of the evolving fluid through time. The experiments demonstrated that shales undergo typical geochemical processes during hydraulic fracturing such as carbonate and feldspar dissolution as well as ion exchange resulting in an increase in dissolved solids. Observations suggest that rock permeability is increased two to –three-fold and that porosity is increased by 50%.

Baseline sampling as it is currently practiced is not sufficient to resolve ambiguity of the source of the dissolved methane even if of thermogenic origin because it still could be natural. Additional analyses such as noble gases and isotopes are needed to better constrain origin of the methane.

Executive Summary

The main objective of the project was to enhance our understanding of shallow natural gas which is sometimes found unexpectedly in groundwater wells. The visibility of this topic has considerably increased in the past few years because of a possible connection with hydraulic fracturing (HF). A second objective, only loosely connected to the first one, was to understand the nature of the flowback and produced water flowing from wells stimulated by HF. We addressed the first objective by sampling hundreds of water wells across the state of Texas and performing detailed chemical analysis of the water. The second objective was accomplished by performing rock-water interaction experiments at high temperature and pressure in a laboratory autoclave.

Methane is a nontoxic but explosive gas that has been documented to exist in many groundwater aquifers. Methane in the subsurface is formed through two major types of processes: biodegradation of organic material (for example, organic matter from soil, oil, lignite debris), termed microbial, or abiotic maturation of organic matter when it is buried to form coal of various rank, oil and gas; this methane is termed thermogenic. The two endmembers can be identified through their isotopic signature and other geochemical characteristics. At the onset on the project it was expected that several methane studies already existed in the state and that the project would focus on understanding mechanisms of its migration. It turned out that a large sampling campaign was needed. We focused the sampling on the footprint of some major unconventional plays: the Barnett Shale in northcentral Texas (only its section with condensate- and gas-producing wells), the Haynesville Shale in East Texas, the Eagle Ford in South Texas, and the plays of the Delaware Basin in West Texas.

Autoclave experiments were done using Barnett Shale core fragments that were exposed to water of various salinities (0, 2000, and 20,000 ppm) and composition (either sodium, potassium, or calcium chloride) for three weeks. Unreacted and reacted samples were examined using classic (SEM, EDS, XRD) and more recent (ion-milling) technologies. A few flowback water and produced gas samples were also taken in the Barnett Shale footprint. Chemical analyses of the groundwater samples and rock-water interactions samples were performed at UT (IC for major ions and ICP for trace metals). Dissolved gas (CH_4 and other light alkanes, N_2, O_2, Ar) and isotopic (^{13}C –if CH_4>0.1 mg/L, D, ^{15}N) analyses were also performed at UT. All the dissolved gas samples were carefully taken at the wellhead and shipped promptly to Austin. Dissolved noble gases were sampled following the copper tube approach and analyses were performed at the University of Michigan. A few microbial mass samples were also taken to better document methane production or attenuation in the areas with high methane concentrations.

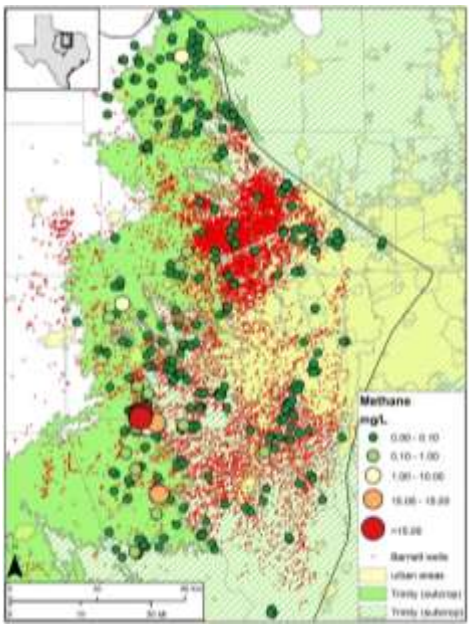

We sampled 555 unique water wells in the Barnett Shale footprint (shale at ~6000 ft below ground surface), sometimes sampling several times the same well. See opposite map showing gas wells (small red dots) and sampled water wells. Most water wells sampled on the

western edge of the project area were domestic wells tapping the Trinity aquifer but towards the east in the direction of more populated area and increasing depth of the producing aquifers, many sampled water wells were deeper municipal or irrigation wells (but still completed in the Trinity and allied formations of Cretaceous age). The vast majority of wells show no to very little methane that is, when present, mostly thermogenic. There is one well-documented cluster on the Parker-Hood county line with 20+ water wells with methane, the Parker-Hood cluster, but other smaller clusters exist. Some have been sampled (North Parker and Somervell clusters), others not (Palo Pinto County). Although some samples with low methane concentrations are clearly microbial, all high dissolved methane samples are thermogenic, genetically related to shallow reservoirs in the Strawn Formation of Paleozoic age and seem to be mostly natural. We spent some efforts on the Parker-Hood cluster sampling for noble gas and nitrogen isotope analyses in order to refine our understanding of this highly publicized contamination case ("Range Resources" case, involving in several lawsuits this company and its experts as well as the state RRC and federal EPA and several well owners).

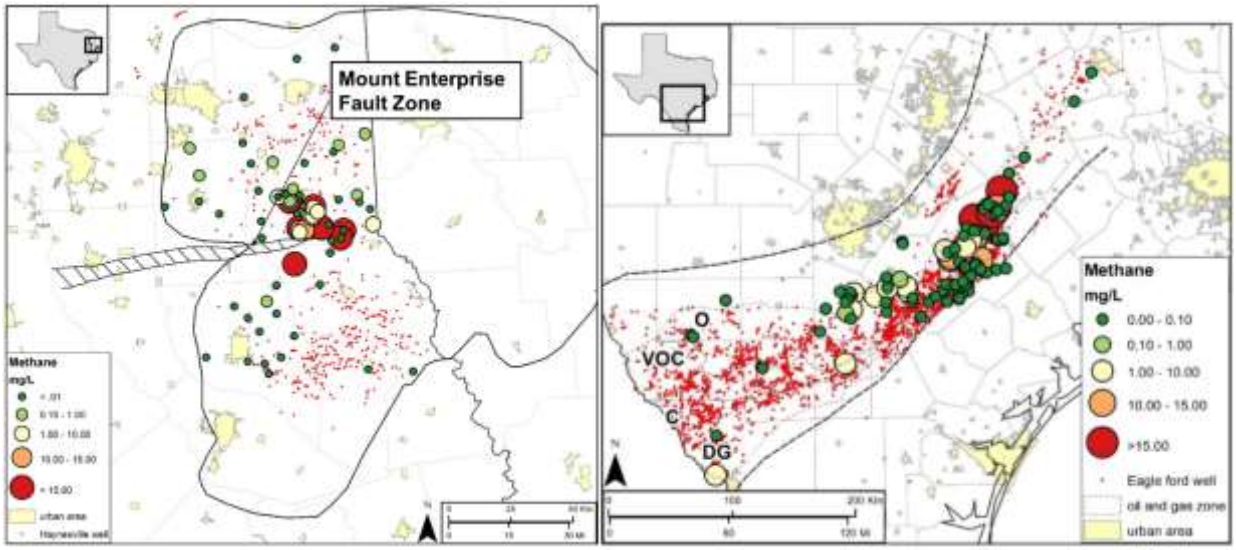

The Haynesville Shale of Jurassic age (see map above) straddles the Texas-Louisiana state line and is found at depths of ~11,000 ft and more. We took a total of 70 samples (in Texas only) mostly of domestic wells in the Wilcox aquifer. Again many wells show little methane except a cluster next to the Panola-Shelby county line. Several samples with methane are clearly of either microbial or thermogenic origin whereas other samples are of mixed character. Spatially the methane-rich samples are associated with the end of a major fault zone, the Mount Enterprise fault zone. Unlike the Barnett Shale area where the only major source of methane is the shale itself and related overlying conventional accumulations, the Haynesville Shale footprint contains several lignite deposits, including in the Panola-Shelby cluster, in particular at the base of the Wilcox. We hypothesize that methane in the groundwater originated in the lignite and migrated along the fault to the shallow subsurface. Some of the methane may also undergo anaerobic sulfate reduction.

We took a total of 118 samples in the eastern section of the footprint of the Cretaceous Eagle Ford Shale (shale at depths of ~8,000 ft and more) from domestic, irrigation and rig-supply water wells. See map above. We sampled the several aquifers that overlap on the narrow strip formed by the productive Eagle Ford in south central Texas. The dissolved methane, mostly of mixed

thermogenic and biogenic origin depending on the sample, is present at all depths (to 3000 ft) in several aquifers and also shows signs of biodegradation (low sulfate, shift to heavier $\delta^{13}C$). In this case, we hypothesize that methane originated from lignite beds and from action of well-known vertical structural features (increased fracture density in Karnes Trough, Wilcox fault zone) leaking oil from the Eagle Ford or other reservoirs which is then consumed by microbes.

The Delaware basin in West Texas include plays such as the Bone Spring and Wolfcamp at depths >5000 ft. We sampled several aquifers (Pecos alluvium, Dockum, and Rustler) mostly from rig-supply and industrial wells because the area has a very low population density. The samples show no methane except in water wells next to a known blowout.

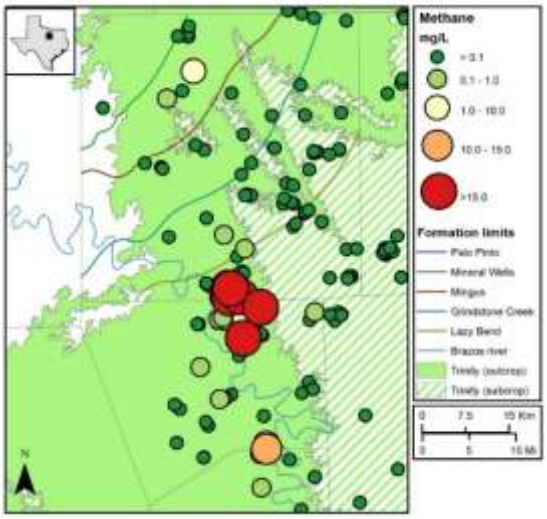

After the reconnaissance sampling of the four areas described above, we focused on the Parker-Hood cluster (see opposite map) by doing supplemental sampling that including duplicating all analyses and adding noble gas (35 unique wells) and nitrogen isotope (25 unique wells) analyses. The geology consists of the feathering edge of a Cretaceous cover (including the Trinity aquifer at the base) unconformably overlying thick Paleozoic Strawn sediments. All samples, except those specifically chosen as background, contain dissolved methane. The noble gas results, not fully finalized yet, show abundant crustal production, likely from the thick mostly shaly Strawn. The nitrogen isotopes provide a qualitative measurement of interactions between aquifer water and migrating gas. The Parker-Hood cluster subcrop contains several shallow natural accumulations, at least one of which has been commercially produced at a depth of ~400 ft, but several similar accumulations have been penetrated by water wells at similar depths. Such observations are consistent with the geological model of the upper Lower Strawn described as sand bodies of fluvial origin embedded within a more silty or shaly matrix. These water wells are characterized by two-phase flow in the formation (as visualized by video camera), water pump gas lock, hydrocarbon smell, and effervescing methane. They also show a nitrogen isotope shift suggesting strong imprint of the natural gas on the water. On the other hand, many water wells, although sometimes high in methane, do not show strong interactions with the water, suggesting they tap the halo of dissolved gas surrounding gas accumulations. Generally water wells penetrating the Strawn beyond the unconformity display higher methane when present. There is some evidence of mixing between thermogenic and microbial gas but limited evidence of biodegradation. All elements of the study point to natural methane contamination in the Parker-Hood cluster. Methane concentrations do not show an obvious relationship with distance to Barnett gas wells (see opposite figure).

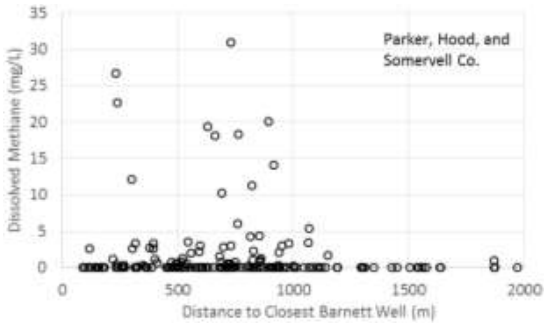

The autoclave experiments suggest that rock-water interactions increase porosity and permeability of the rock in significant amounts (50% and ×2-3) by dissolving carbonates (5-10%

of the rock is calcite) and some minor feldspar. The quartz (40-45% of the rock) and illite (30% of the rock) do not react in the time scale of the experiments. Exposure of the Barnett core fragments to the proxy HF fluids mobilized all elements either through mineral dissolution or desorption. Some scale-forming elements such as Ba (and then Ra) and Sr were also mobilized and could then be in the flowback but other troublesome elements such as As precipitated back after an initial peak.

The overall conclusion of the study is that methane is indeed naturally present in many aquifers across the state but only in the aggregate sense. It cannot be ruled out a priori that a particular water well has been contaminated by oil and gas activities without further detailed studies. Well integrity issues have been documented in many historical instances. In addition to well integrity, other methane mobilization mechanisms have been put forward such as water level drop or air drilling. In terms of improving current practices, continued technological progress of surface casing of oil/gas wells, in particular connection between rock and cement, and requiring venting systems be installed on water wells in areas with known dissolved methane are two reasonable lines of action. In terms of acquiring knowledge about dissolved methane, baseline / predrill sampling is a great reconnaissance tool but, as evidenced by the current controversies on the source of the dissolved methane, discriminating between well leakage and natural leakage requires more sophisticated analyses, including noble gas and isotopes beyond ^{13}C.

Table of Contents

List of Figures

List of Tables

Acknowledgments

The authors would like to thank the RPSEA program for funding this research and the state-sponsored STARR program and the Jackson School of Geosciences at The University of Texas at Austin for providing the cost share. We are also grateful to the project managers Charlotte Schroeder at RPSEA and then Sandra McSurdy at NETL for helping in the course of the research and to Peter Pope at the RRC in Austin for his help and knowledge of the field. The project would not have been possible without the hundreds of well owners who let us sample, sometimes several times, their wells and the various groundwater districts for their help in contacting well owners. Watts Drilling provided well logs and some well owner contact information. TWDB sampled many water wells for dissolved methane under the direction of Janie Hopkins, in particular Doug Coker, but also Chris Muller, Andrew Finnell, Chuck Crawford and Josh Oyer. Thanks to Tongwei Zhang (BEG) for occasional use of his equipment and hydrocarbon gas analyses. Nathan Miller at the UT Department of Geological Sciences completed the ICP-MS analyses. The authors are also grateful to the Jackson School of Geosciences for the financial help in setting up the high-pressure and -temperature laboratory and to IHS for free access to their Enerdeq oil and gas database.

Acronyms

BEG	Bureau of Economic Geology
BMP	Best management practices
BTEX	Benzene, toluene, ethylbenzene, and xylenes
CBM	Coal-bed methane
CZWX	Carrizo-Wilcox (aquifer)
DFW	Dallas Fort Worth
DI water	Deionized water
DIC	Dissolved inorganic carbon
DOE	Department of Energy
DRO	Diesel range organics
EDS	Energy dispersive X-ray spectroscopy
EF	Eagle Ford
FeOx	Iron oxyhydroxides
FID	Flame ionization detector
Fm.	Formation
Fms.	Formations
FP	Flowback and produced water
FR	Friction reducer
GAM	Groundwater availability model
GAT	Geological atlas of Texas
GC	Gas chromatograph
GRO	Gasoline range organics
HEM	N-Hexane Extractable Material
HF	Hydraulic fracturing
HF'ed	Hydraulically fractured
ICP-MS	Inductively-coupled-plasma-mass-spectrometer
IC	Ion chromatography
LHS	Left-hand side
LUST	Leaking underground storage tank
MCL	Maximum contaminant level
MTBE	Methyl tert-butyl ether (gasoline additive)
MW	Molecular weight
NETL	National Energy Technology Laboratory
NGO	Non-governmental organization
NORM	Naturally occurring radioactive materials

OM	Organic matter
PAH	Polycyclic aromatic hydrocarbon
PAM	Polyacrylamide
PMP	Project management plan
PWS	Public Water Supply
QCSP	Queen City-Sparta (aquifer)
RHS	Right-hand side
RPSEA	Research Partnership to Secure Energy for America
RRC	Railroad Commission of Texas
UST	Underground storage tank
SEM	Scanning electron microscope
STARR	State of Texas Advanced Resource Recovery
TCEQ	Texas Commission on Environmental Quality
TDLR	Texas Department of Licensing and Regulation
TDS	Total dissolved solids
TPH	Total petroleum hydrocarbons
TSS	Total suspended solids
TWDB	Texas Water Development Board
VSMOW	Vienna Standard Mean Ocean Water
UT	University of Texas at Austin
UTA	University of Texas at Arlington
XRD	X-ray diffraction
ZPC	Zero point charge

Chemical Elements:

Symbol	Name	Symbol	Name	Symbol	Name	Symbol	Name
Ag	Silver	Cs	Cesium	Na	Sodium	Sr	Strontium
Al	Aluminum	Cu	Copper	Ne	Neon	Th	Thorium
Ar	Argon	D	Deuterium	Ni	Nickel	Ti	Titanium
As	Arsenic	F	Fluorine	O	Oxygen	Tl	Thallium
B	Boron	Fe	Iron	P	Phosphorus	U	Uranium
Ba	Barium	H	Hydrogen	Pb	Lead	V	Vanadium
Bi	Bismuth	He	Helium	Rb	Rubidium	Xe	Xenon
Br	Bromine	K	Potassium	Ra	Radium	Zn	Zinc
C	Carbon	Kr	Krypton	Rn	Radon	Zr	Zirconium
Ca	Calcium	Li	Lithium	S	Sulfur		
Cd	Cadmium	Mg	Magnesium	Sb	Antimony	SO_4	Sulfate
Cl	Chlorine	Mn	Manganese	Se	Selenium	NO_3	Nitrate
Co	Cobalt	Mo	Molybdenum	Si	Silicon	NH_4	Ammonium
Cr	Chromium	N	Nitrogen	Sn	Tin		

I. Introduction

This research untitled "*Understanding and Managing Environmental Roadblocks to Shale Gas Development: An Analysis of Shallow Gas, NORM, and Trace Metals*" consists in two loosely connected parts: (1) assessing, documenting, and understanding the presence of methane in Texas aquifers, and (2) understanding the nature of flowback through laboratory experiments. The objectives are listed in the proposal as:

> *The objectives of this study are to enhance (1) understanding of naturally-occurring shallow gas either dissolved or free phase (to facilitate rational analysis of accusations of groundwater contamination with gas, trace metals, and naturally occurring radioactive materials) and (2) understanding of nature and variability of flowback (to adjust and optimize flowback treatment and possibly frac fluid composition). This understanding will be used to develop a best management practice manual for baseline monitoring and fingerprinting sources and processes affecting shallow gas.*

I-1. Motivation

The use of hydraulic fracturing (HF) stimulation for oil and gas production has considerably increased in the past 20 years and many reports and peer-reviewed papers have documented interactions between the newly perfected technology and water resources. The impact of HF on water resources have been well-documented early on, especially in Texas (Bené et al., 2007; Nicot et al., 2011; Nicot et al., 2012), responding to a concern of the general public and other local water stakeholders. On the other hand, a different type of issue emerged in response to early production from the Marcellus Shale in the Northeastern U.S.. There, stakeholders were concerned about methane in groundwater and potential degradation of water quality. Several research papers have documented the initial state of knowledge (Osborn et al., 2011; Jackson, Vengosh et al., 2013; Molofsky et al., 2013). A quick search of Texas databases determined that there was very little information on this topic in the state and given the large footprint of the oil and gas industry, such a study was warranted. The major part of this project consisted in documenting and understanding methane distribution in Texas aquifers. In particular, the study endeavored to obtain a better understanding of the Barnett Shale in North-Central Texas, the oldest play in which hydraulic fracturing became a major stimulation technique (Nicot et al., 2014) by sampling hundreds of relatively shallow domestic wells as well as deeper wells in the footprint of the play with a focus on the natural systems.

As a clarification, our goal was not to determine whether a particular water well was contaminated by operations related to HF but rather to consider all the sampling results in aggregate and propose, if appropriate, a natural explanation that would satisfy all observations. Undoubtedly accidents happen and some of the high-methane in water wells we sampled could actually be the result of recent contamination. In the light of the results of the study, we believe these wells are in small number if they exist. Similarly, we did not try to prove that no methane contamination took place, proving a negative is arduous if not impossible and future evidence would likely prove us wrong. Our starting hypothesis was that, in general the presence of methane in groundwater is mostly natural in origin or can be explained by legacy events (blowouts) or legacy contamination when rules were not as stringent as currently. A corollary goal of this work in addition to confirm methane concentrations observed in Parker County (Barnett Shale) was to try to determine fluxes and average residence times.

The choice of Texas to perform this large scale reconnaissance study is justified by the number of unconventional plays in the state (Figure 1 and Figure 2) and the significant contribution of Texas to the U.S. overall oil and gas production.

The other part of the study, which consisted in autoclave experiments and their interpretation, was concerned about explaining the chemical nature of the flowback and produced (FP) water and the contribution of rock-water interactions to it. FP water, although typically less in volume but of poorer quality than the water used for HF, are either (1) disposed of in deep injection wells or (2) recycled or reused. The latter option is growing because of the concern about induced seismicity caused by the former.

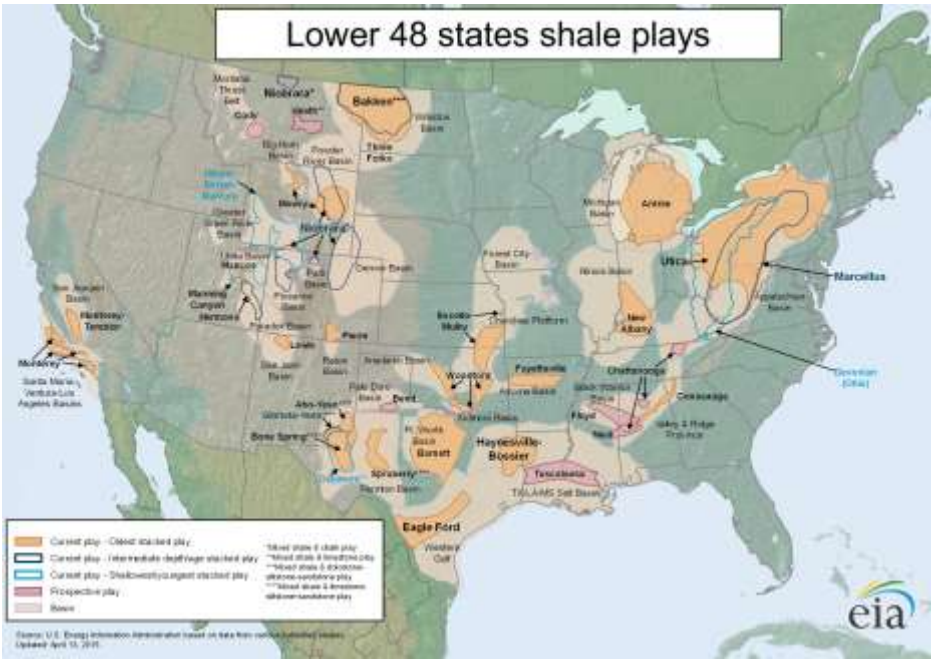

Source: EIA (April 13, 2015); http://www.eia.gov/oil_gas/rpd/shale_gas.pdf (accessed 8/19/2015)

Figure 1. Map of shale plays in the U.S.

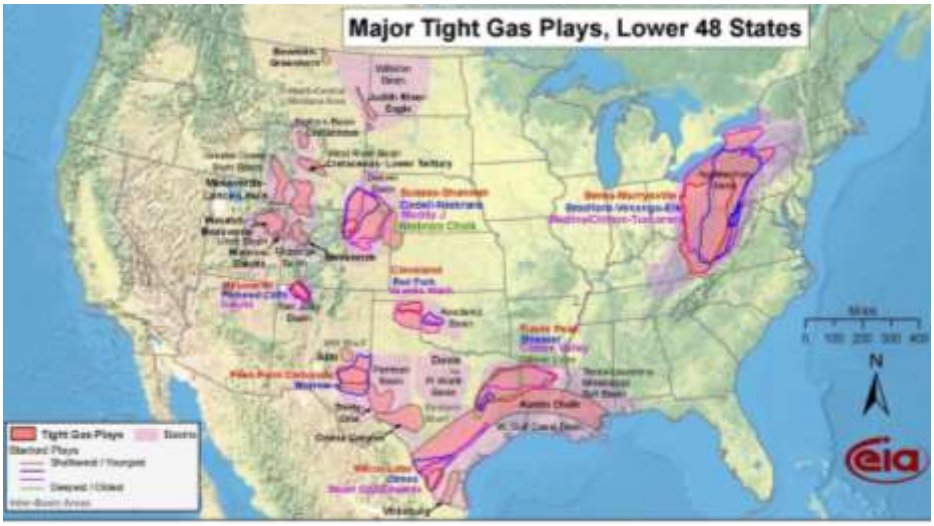

Source: EIA (June 6, 2010)

Figure 2. Map of tight gas plays in the U.S.

I-2. Administrative Matters

This research was done in response to a Request for Proposal put out by Research Partnership to Secure Energy for America (RPSEA) in December 2011 (RFP2011UN001 Unconventional Onshore Program). The University of Texas Bureau of Economic Geology (UT-BEG) in collaboration with Dr. Clara Castro at the University of Michigan (UMI) Earth and Environmental Sciences Department submitted its proposal on March 2012 and was selected for award in November 2012 (award No 11122-56). After a period to adjust the scope of work and resolve other administrative matters, the contract between UT and RPSEA became effective on June 14, 2013 for a period of 2 years (Ms. Charlotte Schroeder, RPSEA, Project Manager). RPSEA's participation amounted to $1,291,318 whereas the 20% cost-share were provided by the state-funded State of Texas Advanced Resource Recovery (STARR) program and some of the researcher salary support granted by the Jackson School of Geosciences of which BEG is one of the three components (a total of $325,269). In June 2014, the project oversight was transferred to the National Energy Technology Laboratory (NETL) for the rest of the project (Ms. Sandra McSurdy, Project Manager). In February 2015, we requested a no-cost extension to September 30, 2015, which was granted in April 2015.

Note that another RPSEA project untitled "*Reducing the Environmental Impact of Gas Shale Development: Advanced Analytical Methods for Air and Stray Gas Emissions and Produced Brine Characterization*" (award No 11122-45) awarded to GSI Environmental during the same round in response to the same RFP shows interesting overlap with our own project and we met with the GSI team regularly as the company has an office in Austin, TX.

I-3. Flow and Timing of the Research

Effective work started in June 2013 with benchtop experiments on the Barnett Shale core samples while preparing for field work for methane sampling. We performed six autoclave experiments in June-November 2013 during which time we met with officials at the Railroad Commission (RRC), agency in charge of regulating the oil and gas industry in Texas, and at the Texas Commission on Environmental Quality (TCEQ), state agency in charge of water quality. In parallel we also prepared the reconnaissance sampling campaigns focusing on four areas: Barnett Shale footprint in North-Central Texas, Haynesville shale footprint in East Texas, Eagle Ford Shale footprint in South Texas, and the Delaware Basin (Loving County) in Far-West Texas. Training of the various teams to sample water wells in following the BEG approach to do the reconnaissance sampling also occurred during this period. The Barnett Shale water samples were taken by Dr. Zacariah Hildenbrand from Inform Environmental, LLC (573 samples from November 2013 to June 2014, including duplicates and triplicates). Note that Dr. Hildenbrand, in a cost-cutting effort, also sampled the same wells at the same time on behalf of the University of Texas at Arlington (UTA) for a study unrelated to the one described in this document. The Haynesville samples were taken by Mr. Michael Slotten and Ms. Jordan Aldridge, volunteer MS students in the Environmental Management and Sustainability program at St. Edwards University in Austin, TX (31 samples from February 2014 to May 2014). The Eagle Ford Shale area was sampled by Dr. Hildenbrand (77 samples and duplicates from July 2014 to December 2014) and the water sampling group at TWDB (33 samples from May 2014 to August 2014). It is moderately difficult to find wells to sample in South Texas because the area is generally sparsely populated. The TWDB team also took a few samples in the Haynesville area (33 samples in May and June 2014). TWDB generally sampled deeper Public Water Supply (PWS) wells whereas the

other groups sampled mostly domestic wells. West Texas was sampled by Ms. Rebecca Smyth and Dr. Pat Mickler (both BEG) in 3 trips from February 2014 to January 2015 (45 samples and duplicates). Sampling in West Texas is more difficult than in the eastern half of the state because of the paucity of water wells and of the large distances.

As the laboratory work and reconnaissance field sampling continued, we also tentatively made progress on the understanding of the basic processes involved in the migration of dissolved gas in the subsurface (diffusion, solubility, phase transfer, etc). We hired Dr. Yuan Liu as a postdoctoral fellow on November 2013 to develop this topic both theoretically and in laboratory experiments (see Liu et al., 2014) but unfortunately she had to leave soon afterward (April 2014).

A second sampling campaign focusing on the Parker County area with high dissolved methane concentrations took place in November 2014 including the sampling of two "water" wells for which we hired a contractor (Watts Drilling) to enter the well with a video camera and observe the origin of the effervescing gas (August 2014). The UMI noble gas team traveled to Texas to perform the noble gas sampling using the copper tube technique in November 2014. We also performed microbial sampling at the same time. In January 2015 (Parker County) and April 2015 (Wise County) we were also able to sample Barnett and Strawn gas-producing wells in the same vicinity (a total of 9 gas wells). During the April 2015 in Wise County, we were also able to sample flowback water from a recently hydraulically fractured (HF'ed) well.

We also sought constant interaction with the industry. They own a vast amount of data not in the public domain. BEG has led / is leading several studies related to HF involving industry participation and many opportunities to discuss dissolved methane sampling and flowback composition arose. These interactions resulted mostly in soft but invaluable information, that is, limited amount of hard data –such as gas and flowback samples, but confirmation that our findings, especially in terms of methane concentration, were consistent with the much larger data set colleted by the industry as a whole.

I-4. Organization of the Report

The project consisted of two somewhat independent components: a field component and a laboratory component, each with their own independent tasks (Tasks 5 and 6 of contract, respectively). The field component focused on documenting natural accumulations of methane in the subsurface and the processes acting on and leading to them. The purpose of the laboratory component is to understand the nature of FP water and of downhole rock-water interactions after injection of HF fluid. Task 7 translated the findings into outcomes useful to operators and other stakeholders. The agreed-upon scope of work calls for the following tasks. **Task 5**: "Source of Shallow/Stray Gas in Groundwater Wells" was oriented toward field work and comprised three subtasks: (1) inventory of shallow methane occurrences and reconnaissance sampling; (2) detailed field sampling of selected areas; and (3) results and data interpretation. The objective of **Task 6**: "NORMs and trace elements" was to assess quantity and mobilization mechanisms of trace metals and NORMs using laboratory batch experiments with synthetic HF water. **Task 7**: "Best Management Practices" summarized the findings.

The report first presents a few generalities on HF, methane, noble gases, and flowback. The next section describes field and laboratory methodology approaches. The following section details the results of the reconnaissance sampling in the four areas of interest (Barnett, Haynesville, and Eagle Ford footprints and Delaware basin) with an additional section of the dense sampling in

the Parker County area. Discussion and best management practices (BMP) sections follow the results section.

Some of the material was transferred to the Appendix section to avoid burdening the flow of the report and some of the Appendices contain supplementary information. Appendix A lists abstracts and papers resulting from this work. Appendix B reports discussion with RRC districts about methane contamination whereas Appendix C discusses underground blowouts in Texas. Appendix D documents the results of a water quality analysis in the footprint of the various plays studied. A short comparison of our methane with that of Isotech for QA purposes is presented in Appendix E. Appendix F compares dissolved methane concentrations to that of other aqueous species. A summary of the noble gas analysis is presented in Appendix G whereas Appendix H contains results of the West Texas study. Appendix I describes the Wise County investigations in the footprint of the Barnett Shale where several early lawsuits related to dissolved methane in fresh aquifers took place. Appendix J presents the results and conclusions of the autoclave and benchtop experiments.

Field work was accomplished by many individuals as listed above. Among other tasks, Ms. Kristine Ulhman coordinated the Parker County sampling campaigns. Drs. Jiemin Lu and Pat Mickler with the help of Ms. Roxana Darvari did the autoclave and benchtop experiments. Dr. Clara Castro and her team at UMI (Ms. Laura Bouvier, Mr. Tao Wen, and Mr. Chris Hall) did the noble gas sampling, measurements and analyses. Dr. Toti Larson did dissolved methane and isotopic laboratory measurements. Dr. Chris Omelon did the microbial study. Ms. Rebecca Smyth did the West Texas study. In addition to researchers interpreting their own results, Dr. J.-P. Nicot with the help of Drs. Larson and Mickler and Mss. Roxana Darvari and Ruth Costley put the report together and integrated the interpretation of the measurements.

II. Background Information

II-1. Hydraulic Fracturing

HF combined with horizontal drilling has become the technology of choice to extract oil and gas directly from source rocks ("shales") and from other tight formations (somewhat conventional reservoirs but with a very low permeability). Although both technologies were initiated several decades ago, 1950's for HF and 1980's for horizontal drilling, their application at a large scale started in the early 2000's in the Barnett Shale (Nicot et al., 2011; Nicot et al., 2014). Each horizontal well uses millions of gallons of which only a variable fraction return to the surface as flowback followed by produced water that must be either recycled/reused or disposed of. Like all industrial activities, extracting oil and gas from the subsurface involves risks (Vengosh et al., 2014; Small et al., 2014) and the well itself is generally seen as a weak element (Jackson, Gorody et al., 2013; Jackson et al., 2014). Exploiting a play through HF requires many more wells than a conventional play and the increase in well count mechanically increases the overall risks. Risks to groundwater resulting from a direct connection between the HF'ed interval and the fresh water aquifers (Myers, 2012; Hazen and Sawyer, 2009) have been dismissed as remote. Surface hazards related to HF operations are recognized as the most likely to impact groundwater: spills of various fluids on well pads or during transportation, defective pipe lines. Surface accidents and incidents have the advantage of being visible and potentially immediately subject to corrective action. On the other hand, subsurface contamination is more insidious as it may take some time (maybe decades) before it is recognized as such. A problem that has plagued the industry for many decades is the integrity of the oil and gas well wellbores as they must be drilled through fresh water and slightly saline aquifers. Technology and regulations have continuously improved in stages during the past decades (Nicot, 2009) but problems persist.

Interest in methane dissolved in groundwater aquifers has considerably increased in the past few years due to a possible relationship with HF activities. Substantial sampling campaigns have been undertaken in the Marcellus Shale in the northwest US by several entities: federal (Kappel and Nystrom, 2012; Revesz et al., 2012; Heisig and Scott, 2013; Senior, 2014; Sloto, 2014), academic (Osborn et al., 2011; Jackson, Vengosh et al., 2013; McPhillips et al., 2014; Siegel et al., 2015), industry (Wilson, 2012) or consultancy (Molofsky et al., 2013). Other areas have not been covered as thoroughly but studies exist (non comprehensive list): Bakken in North Dakota (McMahon et al., 2015), Fayetteville in Arkansas (Kresse at al., 2011; Warner et al., 2013), in Colorado (Li and Carlson, 2014), and outside of the US, in particular in Alberta (Cheung et al., 2010; Dr. Bernhard Mayer, U. of Calgary), Ontario (McIntosh et al., 2014), New Brunswick (Al et al., 2013), c; Moritz et al., 2015) and the United Kingdom (BGS, 2015). The goals of these

studies were (1) to document the current methane status of aquifers in areas with potential HF activities and (2) to determine the source of the methane.

Several mechanisms have been put forward to explain occurrences of methane in groundwater, in particular, some related to human activities such as the transition from a dissolved state to a gas phase because of aquifer depressurization in a process similar to producing water from a coal seam to mobilize methane (coal-bed methane, CBM) or a defective or not deep enough surface casing which does not protect fresh water as designed to. The presence of methane and other light hydrocarbons in groundwater is sometimes called "*stray gas*". Stray gas can be defined as "*gaseous material of undetermined origin found in an area where the gas has impacted the shallow subsurface, potable water supplies or has the potential to present a threat to public health and safety*" (Baldassare et al., 2014). Stray gas in the oil and gas industry has also been defined as any unexpected gas kick while drilling. Methane can be microbial (likely not anthropogenic) or thermogenic (natural or anthropogenic) and previous studies have shown both types in shallow groundwater. In the Marcellus footprint where methane is clearly mostly thermogenic, it is assumed linked to HF (Osborn et al., 2011; Jackson, Vengosh et al., 2013 both in PA) or natural related to topography (Molofsky et al., 2013; Siegel et al., 2015 both in PA; Heisig and Scott, 2013 in central NY) or not (McPhillips et al., 2014 in central NY)]. A USGS study in West Virginia assumed that the methane was sourced from coal and stated that "methane concentrations exceeding 10 mg/L were found in wells located in valleys and on hillsides but not in wells located on hilltops." (White and Mathes, 2006). Elsewhere it has been described mostly as microbial: Ontario studies (Aravena et al., 1995; McIntosh et al., 2014), Colorado study (Li and Carlson, 2014), and Bakken study (McMahon et al., 2015) or mixed: Quebec study (Pinti et al., 2013).

II-2. Methane and Other Light Alkanes

Methane is a nontoxic but explosive gas. Dissolved methane is not included within the National Primary Drinking Water Maximum Contaminant Level (MCL) listing. The list was developed following the passage of the Clean Water Act (the 1972 amendment to the 1948 Federal Water Pollution Control Act) enforced by the U.S. EPA and individual state agencies assure compliance with concentration limits. Consuming methane dissolved in water is not considered a health risk. Methane has been documented to be very common in the subsurface in particular in oil and gas provinces and coal-mining areas (Keech and Gaber, 1982; NGWA, 2013). Solubility in water at 1 atm varies between 25 and 30 mg/L depending on temperature. As for all gases, solubility increases with pressure and decrease with temperature. For example, saturation is ~400 mg/L at a depth of ~500 ft. It may be accompanied by other gases including H_2S, Rn, CO_2, He, N_2, and may include other saturated gaseous hydrocarbons (alkanes) such as ethane, propane, and butanes (Saunders et. al., 1999; Klusman, et. al., 2000; Gorody, 2012; Rowan and Kraemer, 2012). Methane is so common in the deep subsurface that several researchers and companies have looked into the feasibility of producing brine to extract the dissolved gas (Taggart, 2010; Chacko et al., 1998; Gregory et al., 1980; Buckley et al., 1958). It is also common in the shallow subsurface where it accompanies dissolved atmospheric gases (N_2, O_2, Ar, CO_2), atmospheric methane concentration is ~1ppm that translates into an equilibrium dissolved value of <1ppb at atmospheric pressure. CO_2 and H_2S are also the result of mostly biochemical reactions in the aquifer.

Methane, the major component of natural gas that could also include ethane, propane, and butanes, has two main common origins: (1) biogenic or microbial from the degradation of fresh organic matter in reducing conditions at shallow depth where microbes are active and numerous (bottom of lakes and ponds, landfills, hydrocarbon spills or leaking underground storage tanks – UST, of which there are many examples) and (2) thermogenic resulting from the impact of pressure and temperature on recalcitrant organic matter buried with sediments. In the latter case, methane can result from the direct degradation of organic matter / kerogen or from the degradation of already generated HC (oil or C2+ gas and condensate components). Microbial methane can be generated by fermentation (two copies of the organic substrate, one being reduced, the other oxidized, yielding energy, methane and CO_2) or by CO_2 reduction (organic substrate using CO_2 as an electron acceptor which is then reduced to CH_4 while releasing energy). The two mechanisms to produce microbial methane can be revealed by the H isotopes of methane (Whiticar, 1999). CO_2 reduction produces methane with lighter C but heavier H than fermentation.

There are many documented natural seeps of thermogenic methane across the world (Etiope, 2009; Link, 1952), the U.S. (Etiope et al., 2013), and Texas (Link, 1952 and older USGS and BEG reports). Link (1952) documented three gas seeps in the Barnett Shale footprint one each in Erath, Palo Pinto and Young counties, counties mostly west of currently active Barnett and production. He also described another gas seep in Harrison County in the Haynesville footprint just north of Panola County (county with the highest water well sampling density of this study in East Texas. A few additional gas and oil seeps exist in Webb, Atascosa, and Gonzales counties in the footprint of the Eagle Ford. Most of the seeps listed in Link (1952) are in the northern Gulf Coast of Texas, very likely related to the numerous salt diapirs in the area ("Houston Salt Basin"). No seeps are described in the Permian Basin, fact to relate to the mostly unfolded nature of the sediments and to the presence of evaporitic seals. Early oil and gas exploration often relied on seeps to guess the location of subsurface reservoirs (Fuex, 1977; Jones and Drozd, 1983). When hydrocarbon reservoirs are ruptured gases are the first to escape. The presence of sulfurous gas seeping from the soil near Beaumont, Texas, led to the discovery of the Spindeltop oil field 1901 (Knowles, 1978) and of other fields associated with salt domes (Carlton, 1929). The Spindeltop discovery initiated the Texas Oil Boom and exploration across the state. The Conroe Oil Field (Michaux and Buck, 1936) was discovered 1931 based on gas seeps that then instigated a structural analysis of the subsurface to provide an explanation for the seeps (and development of the field). Historic blowouts of production wells in the Conroe Field in 1936 and 1968 were later blamed for the development of new oil and gas seeps in 1972 and stray gas in domestic wells in the same time period (RRC, 1973). Although oil and gas seeps have been the predominant means of oil field discovery, in Texas, as described above, there are comparatively few when compared to other oil regions of the world. Methane gas seeps have been identified in the field by "paraffin-dirt" indications, an obsolete colloquialism found in Texas records dating to 1913 (Gardner, 1951; Glass, 1953). "Paraffin-dirt" consists of organic matter that represents degraded bacterial lipid and fungal residues which thrived on a seep of natural gas (Simoneit and Didyk, 1978). Chemical and isotopic analysis can differentiate between active and extinct methane seeps (Simoneit, et al., 1980). Use of the term 'paraffin-dirt' has fallen from modern usage. In addition to providing evidence to support oil/gas exploration, methane seeps are indicative of the potential for transport of gases though the subsurface

Often conventional plays are located above the unconventional plays being HF'ed. This fact is not surprising as the conventional accumulations were sourced from the source rocks that are

now a target. For example, gas from Bend Conglomerate reservoirs originated from the Barnett Shale, Austin Chalk collected oil escaping the immediately underlying Eagle Ford Shale, and Haynesville Shale gas filled reservoirs of the Cotton Valley tight gas reservoirs. One of the common characteristics of Texas unconventional plays is that the area in which they are located have a history of oil and gas production as well as legacy brine and/or hydrocarbon contamination.

There are a number of potential sources of shallow gas, including landfills, gas storage reservoirs, pipelines, abandoned coal mines, coal bed methane, improperly abandoned gas wells, deep shale gas, well blowouts, and hydraulic fracturing operations. Although most of the current coal production is from open-pit lignite mines, Texas has several bituminous coal deposits in the footprint of shale plays that were historically produced through underground mining.

Across the nation, there has been well-documented cases of house explosion due to methane leakage (often but not always related to integrity of old or new wells): Bainbridge, Ohio (ODNR, 2008), several instances in Pennsylvania (Baldassare and Laughrey, 1997), and more generally simple well leakage in Lloydminster, Alberta (CAPP, 1995, 1996), in Bammel, Texas. This well-known latter case occurred in 1942 at the Bammel Field in Harris County (Houston area) and severely impacted fresh-water aquifers. USGS (Rose and Alexander, 1945) documented the incident with consequences still discernable and impacting municipal wells more than four decades (Cartwright, 1987; Gutierez, 1990; Gutierrez and Bremer, 1990) and six decades (LeBlanc and Jones, 2004) later.

Action Levels:

Action levels are generally established at 10 and 28 mg/L of dissolved methane. One often-cited source is the Department of Interior Surface of Mining (Eltschlager et al., 2001, Table 9) (Table 1). Some states have more stringent regulations, for example, Pennsylvania action level is 7 mg/L.

Table 1. Methane action levels

Table 9. Recommended Action Levels for Methane

Action Level	Atmospheric (Percent Volume)		Dissolved in Water (mg/liter)	Soil Gas (Percent Volume)
	Occupiable Spaces (homes)	Un-Occupiable Spaces		
Immediate Action	>1.0%	>3.0%	>28 mg/L	>5.0%
Warning, Investigate	>0.5% but <1.0%	>1.0% but <3.0%	>10 mg/L but <28 mg/L	>3.0% but <5.0%
Monitor to Determine Concentration Trends	>0.25% but <0.5%			<3.0% but >1.0%
No Immediate Action	<0.25%	<1.0%	<10 mg/L	

The so-called Bernard plot (Bernard et al., 1976) (Figure 3) displays $\delta^{13}C$ of methane on the x-axis against the log10 of ratio of methane concentration over that of heavier hydrocarbon gas (C2-C3 or C2-C5). Most authors use the molar ratio whereas others use the weight ratio. Because if $(CH_4/C_2H_6)_{molar}$ equals 1, $(CH_4/C_2H_6)_{weight}$ equals 0.53, that is, a small difference in a log space

that spans 5 orders of magnitude and because of the uncertainties inherent to (1) sampling and analysis and (2) boundaries of the plot areas of interest, use either ratio would lead to similar conclusions. Typically microbial and thermogenic methane reside in opposite corners of the plot (i.e., Withicar, 1999, reproduced in Figure 3). Thermogenic gas is classically recognized to be in the -50 – -20 ‰ PDB range whereas microbial methane ranges from -100 to -50 ‰ PDB. Thermogenic methane is heavier because methanogenic microbes would selectively use molecules with lighter carbon atoms. Microbes also rarely produce ethane and C3+ (Davis and Squires, 1954; Bernard et al., 1977, p.4061; Taylor et al., 2000). It is habitually accepted than a C1/C2+C3 ratio <100 is indicative of thermogenic gas whereas a ratio >1000 would indicate a microbial origin. Note that ethane concentrations are typically one order of magnitude less that methane and that of propane are even lower, it follows that the ratio is somewhat uncertain in samples with low methane concentration. Data points falling in the other two quarters of the Bernard plot require adding complexity to the system.

Mixing between the two origins (such as thermogenic gas migrating to an aquifer with active methane production) would fall in the lower LHS corner. Endmembers of mixing lines can vary. Thermogenic gas offers all the gradations between (1) wet gas, such as in the Barnett with high C2+, in which case it would tend to be plotted towards the bottom of the plot and (2) dry gas, such as in the Haynesville, with little C2+. The nature of the kerogen and the geologic evolution of the source rock will also impact the position of the data points on the x-axis (i.e., Zumberge et al., 2012).

Migration and chromatographic-like separation can explain data points falling in the upper LHS quarter. Methane diffuses faster the C2+ molecules and is less soluble in water, that is, would be relatively favored in an advancing gas phase in equilibrium with the water, gas phase that is buoyant and typically travels faster than water. Diffusion and phase exchange do not impact much the isotopic signature compared to the other processes involving chemical reactions so a migration process would appear mostly as points on a vertical band. Biodegradation by methanotrophs and other microbes will move the isotopic signature towards the heavy side because microbes would favor lighter methane molecules to consume. That is, methane of microbial origin may appear thermogenic if partly consumed by other microbes. Note that the microbial oxidation arrow on the plot assumes that methane will be preferentially degraded relative to C2+, which might be the case on the ocean floor (Whiticar, 1999, p.308) but the reverse has also been observed frequently in aquifers, that is, the methane oxidation arrow would point to the top of the plot. The discrepancy may have something to do with the redox state of the system. In the anaerobic sulfate reduction zone (anaerobic oxidation of methane –AOM-, $CH_4 + SO_4^{2-} \rightarrow HCO_3^- + HS^- + H_2O$) common in shallow oceanic sediment, methane is preferred whereas in aquifers under aerobic conditions, C2+ hydrocarbons are more easily processed than methane. Methane is produced only when sulfate has reached low concentration values (Bernard et al., 1977; Zhang et al., 1998) because sulfate reducers are favored compare to methanogens. Zang et al. (1998, p.62) working on Central Texas aquifers put this threshold at 1 mM sulfate (~100 mg/L).

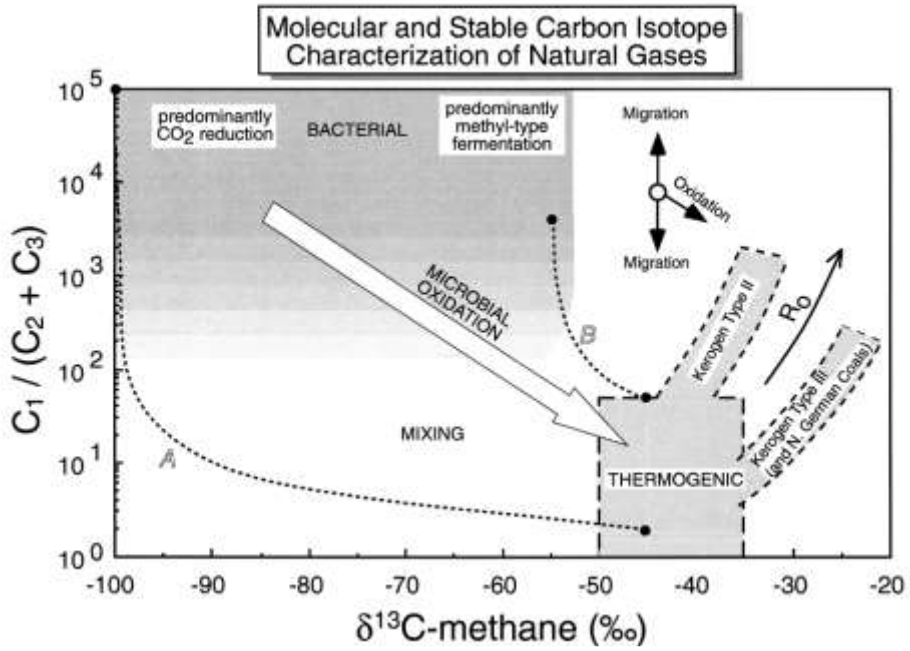

Fig. 12. Natural gas interpretative (''Bernard'') diagram (after Bernard et al., 1978) combining the molecular and isotope compositional information. Lines A and $\tilde{j}$ are calculated mixing lines for possible gas bacterial and thermogenic mixtures with end-member isotope ($\delta^{13}C_{CH_4}$) and molecular $[C_1/(C_2+C_3)]$ compositions of −100‰, 10^5; −45‰, 2 (A) and −55‰, 5000; −45‰, 50 ($\tilde{j}$), respectively. The relative compositional effects of migration or oxidation are also indicated.

Source: Whiticar (1999, Fig.12); original caption

Figure 3. Interpretative Bernard plot

Two other plots of lesser importance to this study are the CD (Carbon-Deuterium; D is a heavy isotope of hydrogen) methane plot in which $\delta^{13}C$ and. dD, both of methane, are plotted, (Figure 4) and the $\delta^{13}C$ methane and CO_2 plot in which the $\delta^{13}C$ of methane and of CO_2 are plotted against each other (Figure 5). The CD methane plot offers a confirmation to the Bernard plot relative to the thermogenic vs. microbial origin of the methane but it also allows a better determination of the methanogenesis mechanism: CO_2 reduction [$CO_2 + 4H_2 \rightarrow CH_4 + 2H_2O$] or fermentation [$*CH_3COOH \rightarrow *CH_4 + CO_2$]. The same way biodegraded methane on a Bernard plot is shifted towards less light C13 signature and shows a decrease in the relative amount of ethane, biodegraded methane on a CD plot would move towards heavier C13 and D. Note that Grossman et al. (1989, p.495), following Klass (1984), stated that even if it appears that CO_2 reduction should consume CO_2 (and thus decrease DIC) and fermentation should produce it, these reactions represent only the final step of a series of reactions. In the complete breakdown of a compound like glucose, similar amounts of CO_2 are produced whether the reaction follows the CO_2 reduction pathway or the fermentation pathway. The δC CH_4-CO_2 plot combined with a CH_4 vs. DIC concentration plot helps elucidate mechanisms as well.

Another plot of interest but not used in this study because of a lack of ethane isotopic data is methane/ethane ratio vs. $\delta^{13}C$ of ethane. Similarly to methane, biodegraded ethane will become heavier as microbes will use lighter ethane first. Microbes will also use ethane first, translating generally into an increasing methane/ethane ratio.

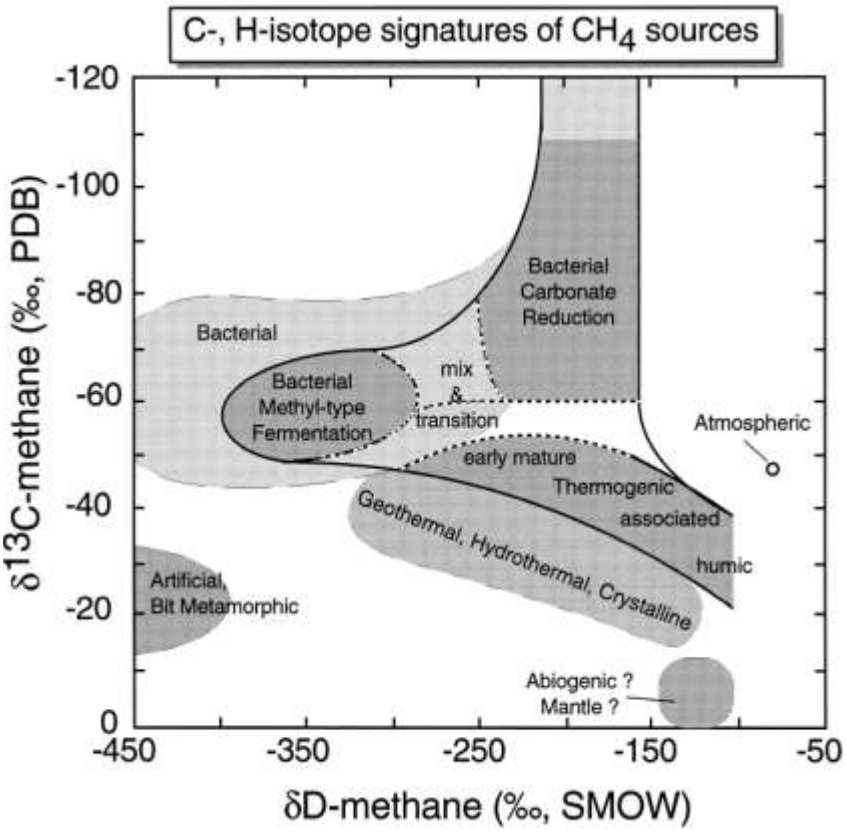

Source: Whiticar (1999, Fig.4)

Figure 4. Interpretative CD methane plot

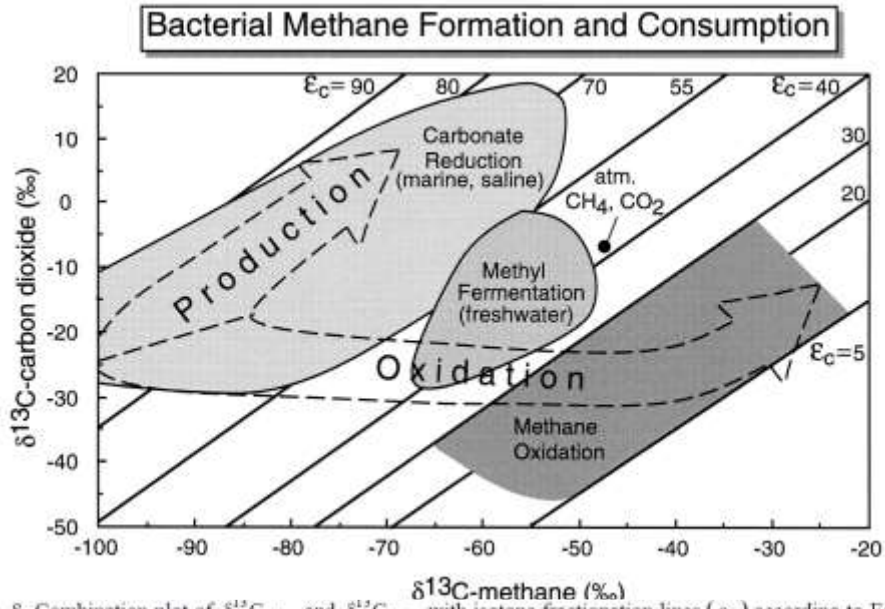

Fig. 8. Combination plot of $\delta^{13}C_{CH_4}$ and $\delta^{13}C_{CO_2}$ with isotope fractionation lines (ε_C) according to Eq. (7). Methanogenesis by carbonate reduction (saline, marine region) has a larger CO_2–CH_4 isotope separation than by methyl-type fermentation (freshwater region) or methane consumption. The figure also shows the observed CO_2–CH_4 carbon isotope partitioning trajectories resulting from both bacterial methane formation and oxidation processes.

Source: Whiticar (1999, Fig.8); original caption; $\varepsilon c = \delta^{13}C(CO_2) - \delta^{13}C(CH_4)$

Figure 5. Interpretative CD methane plot

II-3. Noble Gas

See Appendix G: Noble Gases and Stable Isotopes

II-4. Baseline Sampling

We make the distinction between baseline sampling and monitoring. Baseline sampling consists in taking samples in water wells in the vicinity of a future gas or oil wells in order to compare its chemical characteristics to samples taken after activities have started. Many entities, state (GWPC, 2013), NGO's, trade associations (WRF-AWWA, 2011), have published about their concept of baseline sampling. See Section VI-3 Baseline Sampling and Monitoring for more details.

II-5. Flowback and Produced Water

The amount of water flowing back to the surface is very variable and tends to follow oil and gas production pattern, that is, initial high rates followed by a sharp decrease. Some plays such as the Marcellus or Eagle Ford (Scanlon et al., 2014a,b) display a low flowback rate (less than 30-40% on average) whereas plays such as the Bakken and the Barnett (Nicot and Scanlon, 2012) produce back almost as much as or more than the HF fluid volume injected (but of lesser quality).

II-6. NORMs

Naturally-occurring radioactive materials (NORMs) are common in oil field produced water and not uncommon in aquifers (Szabo et al., 2012). For example, the Hickory Sandstone of Cambrian age is used for municipal and domestic water supply in counties north of the Precambrian Llano uplift, just a couple of counties south of Parker/ Hood counties and contains high levels of Ra (20-40 pCi/L gross alpha) (Kim et al., 1995; George et al., 2011). The Hickory Formation (Fm.) thins out just South of Hood County in which area the water is saline and higher in Ra. The Barnett Shale is separated from the Hickory Sandstone by the thick karstic dolomitic Ellenburger Fm. (Ordovician age) and a few other thin older formations. The EPA drinking water MCLs for Ra and gross alpha are respectively 5 and 15 pCi/L.

Oil-field NORM is typically an issue because of the formation of scales in water lines and other equipment where Ra can build up (Ra-226 and Ra-228 daughter products of U-238 and Th-232, respectively) to level of thousands of pCi/g. It is not so much of a concern when Ra is in the water itself because of its low concentration unless in case of repeated ingestion of, for example, drinking water slightly contaminated by Ra-rich produced water. Ra has a chemistry similar to that of Ba (alkaline earth element with Ca and Sr), has only one redox state and is relatively soluble except when exposed to sulfate. Ra is released into solution from sorbed U and Th or U and Th minerals. Conventional produced water ranges from 100 to 1000 pCi/L Ra, typically increasing with salinity (Fisher, 1998). Some water samples show concentrations of several thousand pCi/L. Sludges resulting from the treatment of produced water can show much higher activity as high as several hundreds of pCi/g (Fisher, 1995; Zielinski and Otton, 1999). Shales are good metal scavengers and they show U concentrations (8-20 ppm, Fisher, 1995, Table 2) higher than that of sandstones or carbonates (<10 ppm, Fisher, 1995, Table 2), common conventional reservoir rocks.

Alley et al. (2011) and Hamlat et al. (2001) both collated literature produced water values from a variety of fields around the world. Hamlat et al. (2001) found ranges of Ra-226 in Algeria to be 5.1-14.8 Bq/L (138-400 pCi/L) , in Norway at 0.3-10.4 Bq/L (8-280 pCi/L), and USA ranges from 0.1 to 9.7 Bq/L (2.7-262 pCi/L) [with 1 Bq/L = 27 pCi/L]. For Texas, Stephenson (1992) found Ra-226 values from Panhandle and Gulf Coast produced waters can range from 0.1 to 1620 pCi/L. Ra-228 values for the same areas were found to range between 8.3 and 1507 pCi/L (Stephenson, 1992). Laul et al. (1985) found that samples of brine from the Wolfcamp Fm. in the Palo Duro Basin (Texas Panhandle) had Ra-226 and Ra-228 concentrations of 227 and 21.4 pCi/L respectively. Additionally, Snavely (1989) found Ra-226 values in produced waters from the Texas Panhandle ranged from 3-1560 pCi/L, while Texas Gulf Coast oil and gas wells had concentration ranges of 1.3-437 and 0.1-1580 pCi/L respectively. As far as Ra-226 concentrations, Snavely (1989) did not collect values from the Panhandle, but found Gulf Coast concentration ranges for oil and gas wells at 204-575 and 19-1507 pCi/L respectively.

For comparison purposes, we discuss the Marcellus produced water which is known for its high Ra content. Haluszczak et al. (2013) reported that Marcellus flow back waters have average measured total Ra-226 amounts of 812 pCi/L with the highest at 6540 pCi/L. Silva et al. (2014) gave a range of 2730-17,800 pCi/L for Ra-226. Warner et al. (2013b, their Table 2) reported that average Ra-226 concentration in Marcellus produced water is 3231 pCi/L with little Ra-228. Nelson et al. (2014) measured ~670 Bq/L (18,110 pCi/L) in the Marcellus produced water. Rowan et al. (2011, Figure 8) measured a range from ~0 to ~17,000 pCi/L in the Marcellus produced water. Analyses we recently performed on Marcellus produced water in a different study (Nicot et al., 2015) returned a range of 16-25 pCi/g, that is, roughly equivalent to 16,000-25,000 pCi/L. All values considerably higher than in conventional reservoirs.

Specific data for the Barnett Shale are given in Almond et al. (2014) which mentioned a low mean Ra-226 value of 6.5 Bq/L (175 pCi/L) and a single Ra-228 reading of 0.04 Bq/L (1 pCi/L).

The USGS produced water database (Blondes et al., 2014) does not contain NORM information in Texas.

III. Field and Laboratory Methodology

III-1. Field Sampling

Organization. We obtained well owners contact information by placing ads in local papers and occasionally by contacting GCD's and Underground Water Conservation Districts (UWCD's): Prairielands, Upper Trinity, and North Texas GCD's in the Barnett footprint, Evergreen, Live Oak, and Gonzales County UWCD's and Bee GDC in the Eagle Ford area and Panola County GCD in the Haynesville area. The TWDB arranged sampling to the wells they regularly sample. And the sampling in West Texas started thanks to personal contacts. It follows that the sampling is not random but biased towards those well owners willing to let us sample their water well. However, given the density of the sampling we do not think the bias is significant in terms of result interpretation.

Most of the water samples were taken at the wellhead or close to the wellhead before any treatment (Figure 6, Figure 7, and Figure 8). The presence of submersible pumps whose removal for a simple single sampling event would be hard to justify and cost-prohibitive, makes downhole sampling impossible. We were able to enter a single water well with no pump but with flowing methane (in Hood County). Several authors have documented seasonal variations but the variations rarely show large swings from high methane to none. We sampled several wells two or three times, particularly in the Parker County area, with good agreement between sampling events. No big changes were observed in this study in the few instances multiple samples were taken, that is, individual wells may display some variations but the variations will not impact the interpretation of the results as it relies on the aggregate of the results not on that of a specific well.

We also used portable flame ionization detector (FID) to test the air around the wellheads for methane and hydrocarbons at ~150+ sample locations but, in addition to the device being capricious in windy and cold weather conditions, we did not find any correlation with dissolved methane values so the FID measurements were discontinued. Note that we did not measure well headspace concentrations.

Sampling methodology. Direct fill and inverted bottle approaches compare well to isoflask®, assumed to be more accurate, up to 15-10 mg/L of methane (Richardson, S., 2014) but then they plateau (gas escaping?) whereas higher methane concentrations can still be measured using the isoflask® approach. We used a slightly different method (Figure 9). Samples analyzed for dissolved methane were collected by diverting a small portion of the well outflow through tubing ending in a syringe needle. A BD 1 inch, 23 gauge hypodermic needle was pushed through a thick Bellco Glass Inc. 20 mm rubber septa (cat # 2048-11800A) of a sealed 60 ml serum vial. A second needle was also inserted through the serum vial that acted as a vent so the vial could be completely filled with groundwater. Water was allowed to flow through the serum vial for approximately 15 minutes, allowing for multiple volumes of water to cycle through the serum vial. The outflow needle was then removed followed immediately by the inflow needle leaving the vial filled with groundwater that had no contact with the atmosphere during sampling. Samples were then stored upside down such that the gas bubble that sometimes form is not in contact with the rubber septum at ~4°C. They are then shipped or otherwise transported to the BEG in Austin, TX within a week. These methods are good to sample dissolved methane below saturation at atmospheric pressure but give only semi-quantitative if the concentration at depth is

above saturation at the surface because the formation of bubbles limit the likelihood of having a representative sample. In addition, we also used IsoFlasks® sent to the well-known Isotech lab as quality control for dissolved methane concentrations.

Credit: JP Nicot, BEG (a) (b

Figure 6. Water sampling for noble gas analysis (a) at the wellhead and (b) removed from the wellhead but before the tank (Barnett Shale area)

Credit: P. Mickler, BEG

Figure 7. Sampling of a Lake County Acres PWS well (Parker County). Note the sign about the presence of methane.

Credit: R. Smyth, BEG

Credit: R. Smyth, BEG

Figure 8. Water sampling of rig supply water wells in West Texas

The dissolved oxygen (DO) and oxidation-reduction potential (ORP, also referred to as electrode potential) measurements were taken on separate probes on the YSI instrument. We also measured water temperature, pH, Eh, TDS, and field conditions (wind, air temperature, cloudiness, atmospheric pressure). We did not do any ^{14}C activity or Sr isotope analyses of water

that could have helped constrain the water flow model. We did not analyze for ^{14}C activity of the methane, which would have clearly showed at least some gas of microbial origin.

Credit: JP Nicot, BEG (a) (b

Figure 9. Dissolved gas sampling (a) and methane exsolving (Barnett Shale area)

Credit: JP Nicot, BEG

Figure 10. Video camera being inserted in water well (Barnett Shale area)

Credit: JP Nicot, BEG (a) (b

Figure 11. Video camera screenshots showing the bubbling well of Figure 10 at the atmosphere-water interface (a) and close to the bottom of the wellbore (b).

Wells

There are millions of water wells in Texas and location and depth is known only for a subset of them. Most of the water well samples come from domestic wells along with a few irrigation and municipal wells (~2/3 residential and the rest split between irrigation and municipal with a few (~25) water supply wells to the industry). There are two major databases with useful information: (1) the TWDB groundwater database that contains a relatively small subset of selected wells (each well has a state well number) regularly sampled by the agency (https://www.twdb.texas.gov/groundwater/data/gwdbrpt.asp; Microsoft Access format; a GIS Viewer is available at http://www.beg.utexas.edu/asun/gwdb.html) and (2) the larger TDLR database (with no well numbering system) that collects mandatory information about all newly drilled water well (since 2001) (http://www.twdb.texas.gov/groundwater/data/drillersdb.asp; text format or ArcGIS format; http://wiid.twdb.texas.gov/). Information about water wells older than 2001 do exist but in a paper format sometime scanned as pdfs. There is a small overlap between the TWDB and TDLR databases. The TCEQ public water supply (PWS) database contains a much smaller dataset of water wells (each well has an ID) in the state and overlaps slightly the TWDB database. The TWDB database is the best in terms of quality of information. The TDLR is typically filed by drillers and the information provided is of uneven quality. We collected information from the well owners as much as possible and crosschecked it with the TDLR (mostly) and TWDB databases.

Exact water well location is determined by (1) using a GPS manual device while sampling the well, and (2) ensuring its appropriate location using Google earth. Elevation of the well, use to determine which formation the screen interval(s) in in when not given in any of the databases, is determined by its location on the USGS national elevation dataset 1/3-arc second (10 meter resolution), appropriate because of the relatively flat nature of the terrane.

Most water wells do not state which formation they draw water from (although most “TWDB wells” do). We estimated the water producing formation by matching the screen interval(s) depth (well owners’ information confirmed by a look at the driller log stored in the TDLR database or

by drilling logs of neighboring water wells) and with regional groundwater model structural information. Starting almost 20 years ago, the state of Texas has embarked on a state-wide program to model all fresh-water aquifers in the state with periodic updates. Incidentally, a new program is about to start to model brackish water aquifer. In this work, we used the following groundwater availability models (GAM's): Carrizo-Wilcox (CZWX) and Queen City-Sparta (QCSP) aquifer model (Kelley et al., 2004) for the Eagle Ford and Haynesville shales, Trinity aquifer for the Barnett shale (Harden et al., 2004), and the Dockum (Ewing et al., 2008), Rustler (Ewing et al., 2012), and Pecos Valley Alluvium (Anaya and Jones, 2009) aquifers for the Delaware Basin. The entire model of any aquifer can be ordered at a small processing fee from the TWDB (http://www.twdb.texas.gov/groundwater/models/gam/index.asp).

Gas Well Gas sampling

We used IsoTubes® (Isotech) and copper tubes

Credit: J. Lu and P. Mickler, BEG (a) (b)

Figure 12. Produced gas sampling in the Barnett Shale area showing (a) IsoTube® for hydrocarbon and atmospheric gas collection and (b) copper tube for noble gas analysis.

Produced Water Sampling

We sampled produced water.

Credit: R. Darvari, BEG (a) (b)

Figure 13. Sampling in the Barnett Shale area: (a) farmer's pond at the end of HF operations and (b) flowback into an open tank.

Microbial sampling

Microbial biomass was collected in the Parker County area by filtering groundwater through both 0.45 µm glass fiber filters and 0.22 µm cellulose acetate filters for a minimum of 20 minutes at the same time samples were taken for dissolved methane and noble gas analysis (Figure 14). Filters were subsequently stored 4°C for a few days until return to Austin and then stored long-term at -20°C until laboratory processing.

Credit: JP Nicot, BEG

Figure 14. Field setting showing microbial biomass sampling (Barnett Shale area)

Water Well Gas Sampling

We used an inflatable bladder as packer to isolate a short section of the wellbore above the water level and use a Bennett compressed air-operated submersible piston pump (http://www.bennettsamplepump.com/index.htm). We used isobags from Isotech and copper tubes to sample the gas.

III-2. Autoclave and Benchtop Experiments

Details on the autoclave and benchtop experiments are given in Appendix J: A Study of Rock-Water Interactions during Hydraulic Fracturing (Barnett Shale).

III-3. Laboratory Analyses

We used a staged approach for chemical and isotopic analyses. All well water samples were analyzed for major ions and dissolved methane. If the latter is >0.5 mg/L (later 0.2 mg/L), we performed an isotopic analysis ($\delta^{13}C$ of methane) and also analyzed for minor and trace elements.

III-3-1 Major, Minor and Trace Elements Analyses

Major and other cations (Li, Na, NH_4, K, Mg, Ca) and anions (F, Cl, Br, NO_3, PO_4, SO_4) of water samples were analyzed on two Dionex ICS-1100 Ion Chromatography systems equipped with an AS-AP auto sampler at the BEG. Samples were diluted after collection as needed using de-ionized water for ion chromatography (IC) such that Ca and SO_4 concentrations did not exceed 500 ppm. Trace and other elements (B, Mg, Al, Si, P, K, Ca, Ti, V, Cr, Mn, Fe, Co, Ni, Cu, Zn, As, Se, Rb, Sr, Zr, Mo, Ag, Cd, Sn, Sb, Cs, Ba, Tl, Pb, Bi, Th, U) were analyzed on an Agilent 7500ce quadrupole inductively coupled plasma-mass-spectrometer (ICP-MS) at the UT Department of Geological sciences http://www.geo.utexas.edu/isochem/default.htm). Samples for trace metals were acidified with 2% HNO_3 immediately after collection and diluted so that the total dissolved solid content was close to 500 mg/L.

III-3-2 Dissolved Hydrocarbons Analyses

We screened for dissolved methane to a low level (<0.001 mg/L). A new more accurate dissolved methane analysis along with isotopic analyses was then performed if methane concentration is >0.5 mg/L (at the beginning of the project) or >0.2 mg/L (work on the Parker County area).

The analysis method makes use of the sampling in a vial with a thick rubber septum (tested in an earlier project as able not to let any gas diffuse out). Prior to analysis, by using two separate syringes, 5 ml of Helium gas was injected into the serum vial as 5 ml of fluid was simultaneously withdrawn resulting in a serum vial with 5 ml of head space and an internal pressure of 1 atmosphere. This sample was shaken for 25 to 30 minutes at 23.5°C to allow the headspace gas to equilibrate with the aqueous solution. Approximately 0.2 ml of the headspace gas was removed from the vial for analysis.

A 0.2 ml aliquot of head space gas from the serum vial was injected into an Agilent 7890A gas chromatograph equipped with a 30 meter 5Å mol sieve GC column and a thermal conductivity detector (TCD). Ar, O_2, N_2, and CH_4 concentrations in the headspace gas were measured using

the TCD. This gas chromatograph is coupled to a combustion interface Isotope Ratio mass Spectrometer (IRMS) for carbon isotope ratio ($\delta^{13}C$) measurement in methane (see below).

Dissolved gas concentrations in the sample were calculated using the Henry's Law EPA method (EPA, 2004) where the important model input values are the concentration of the gas component in the headspace, Henry's law constant for the gas, the temperature of the sample, the volume of the sample bottle, the headspace volume, and the molecular weight of the gaseous analyte.

Detection limits are estimated at ~1, ~2, ~3 ppb for methane, ethane, and propane, respectively.

III-3-3 Isotopic Analyses

The analysis approach shares its few first steps with the dissolved gas analysis. Upon analysis, reconnaissance sample vials received 5 ml of helium gas as 5 ml of fluid was simultaneously withdrawn (by using two separate syringes), resulting in a serum vial with 5 ml of head space and an internal pressure of 1 atmosphere. This sample was shaken for 25 to 30 minutes at 23.5°C to allow the headspace gas to equilibrate with the aqueous solution. Approximately 0.2 ml of the headspace gas was then removed from the vial for analysis. A 0.2 ml aliquot of head space gas from the serum vial was injected into an Agilent 7890A gas chromatograph equipped with a 30 meter 5Å mol sieve GC column and a thermal conductivity detector (TCD). Ar, O_2, N_2, and CH_4 concentrations in the headspace gas were measured using the TCD. Dissolved gas concentrations in the sample were calculated using the Henry's Law EPA method where the important model input values are the concentration of the gas component in the headspace, Henry's law constant for the gas, the temperature of the sample, the volume of the sample bottle, the headspace volume, and the molecular weight of the gaseous analyte.

This gas chromatograph is coupled to a combustion interface Isotope Ratio mass Spectrometer (IRMS) for carbon isotope ratio ($\delta^{13}C$) measurement in methane. Briefly, the eluent gas from the TCD is passed through a copper oxide-packed reactor heated to 700°C. This reactor quantitatively combusts the methane to CO¬2 for $\delta^{13}C$ measurement. The stream of gas with the CO_2 is then passed through a methanol cold trap (-20°C) to remove H_2O vapor from the gas. The dry CO_2 gas is then analyzed for $\delta^{13}C$ using a ThermoElectron Delta V plus continuous flow mass spectrometer. $\delta^{13}C$ values are reported in standard per mill (‰) notation relative to VPDB with NBS-19 = +1.95‰.

When done, hydrogen isotope ratios were measured using a Thermal Conversion Elemental Analyzer (TCEA) coupled to a ThermoElectron MAT 253 Isotope Ratio Mass Spectrometer. This method is similar to the previously described method, with the critical difference being the reduction of methane to H_2 gas through a ceramic reactor packed with glassy carbon at 1450°C. The evolved hydrogen gas is separated from N_2, O_2, and Ar using a 5Å mol sieve GC column. Hydrogen isotope ratios (δD values) are measured on the purified hydrogen gas and are reported in standard per mill (‰) notation relative to VSMOW (Vienna Standard Mean Ocean Water) water =0‰ normalized such that the δΔ of SLAP water = -428‰.

III-3-4 Noble Gas Analyses

See Appendix G: Noble Gases and Stable Isotopes

III-3-5 Microbial Analyses

Filters taken in the field and stored were processed in the laboratory to extract genomic DNA by placing them in 15 ml centrifuge tubes containing 10 ml Tris-EDTA buffer and 270 µl lysozyme and incubating at 37°C for five minutes. 540 µl 10% sodium dodecyl sulfate and 54 µl 20 mg/ml Proteinase K were subsequently added and filters incubated for 1 hour at 55˚C, followed by incubation at 65°C for 1 hour with the addition of 1.35 ml 5M NaCl and 1.35 ml cetyltrimethylammonium bromide/NaCl solution. After the addition of 650 µl of 24:1 chloroform:isoamyl the tubes were gently shaken for 2 minutes and solutions transferred to new 15 ml tubes and centrifuged at 14,000 rpm at room temperature for 15 minutes. The top aqueous layer was transferred to new 2.0 ml microcentrifuge tubes and 650 µl 25:24:1 phenol:chloroform:isoamyl alcohol added, after which the solutions were gently mixed for 2 minutes and centrifuged at 14,000 g for 10 minutes at room temperature. The top aqueous later was then transferred to 1.5 ml microcentrifuge tubes in 900 µl aliquots and DNA precipitated by adding 0.6 volumes isopropanol and stored at -20°C overnight.

DNA was pelleted by centrifugation at 14,000 rpm at room temperature, washed with 70% ethanol, air dried, and resuspended in Tris-EDTA buffer. DNA concentration was quantified by fluorometric quantitation and samples submitted for whole genome shotgun metagenomic sequencing to the Genomic Sequencing and Analysis Facility at the University of Texas at Austin.

IV. Results

IV-1. Previous Dissolved Methane Knowledge in Texas

We turned to two main sources of information to collect dissolved methane data: (1) state agencies and (2) scientific literature. The TWDB is responsible for overseeing the water resources of the state. An early examination of the TWDB groundwater database that collects most of the public domain taken from water wells showed that very few methane analyses were listed (http://www.twdb.texas.gov/groundwater/data/gwdbrpt.asp) and discussion with TWDB staff confirmed that they do not routinely sample for dissolved methane. Propane and C4+ results were more common in the database because they are typically analyzed by TCEQ in contamination cases. The TCEQ is the regulatory agency in charge of enforcing the Safe Drinking Water Act of 1974 to assure compliance with concentration limits, or Maximum Contaminant Levels (MCLs) in drinking water. Groundwater-based public water providers must report to TCEQ analytical results from annual testing - dissolved methane is not included within the National Primary Drinking Water MCL listing, however constituents that may be associated with the presence of methane may be detected under standardized analysis of Total Petroleum Hydrocarbons (TPH) or Volatile Organic Compounds (VOC). Contaminated drinking water sources that appear to be impacted by petroleum constituents naturally occurring or not are forwarded to the RRC for follow-up. Domestic drinking water wells are exempt from regulation in Texas, and water quality complaints that may be associated with petroleum hydrocarbons are also forwarded to the RRC. The Site Remediation Section of the RRC was contacted in September of 2013, in addition, the nine District Office of the RRC were individually contacted and queried about drinking water well complaints. Interviews with the district offices unearthed wells with dissolved methane (Appendix B) although it is difficult to assign the true source of the methane in many cases. On receipt of a drinking water complaint, a RRC representative will investigate and may collect a water sample. Sample analysis consists of TPH and VOC, but may include additional testing if gas is found or the gas is flaring. Most complaints that reach the District offices are for H_2S gas and many contaminant issues are found to be related to nearby oil/gas pipeline, well casing failures or blowouts. Files are retained in the district offices and archived in the main Austin facility of the RRC. We also contacted other organizations such as the Rural Water Association of Texas, the Texas Water Well Association, and some GCD's. We also tried to acquire more information through the court system for these cases that went through litigation but it turned out to be a dead-end as it would be a very time-intensive endeavor.

Early research work in Texas includes the following papers, essentially representing the body of work on this topic by Dr. Grossman from Texas A&M (Grossman et al., 1995; Zhang, 1994): Sampling used the direct fill method with large (>300 mL) glass bottles. He and his students sampled central Texas water wells, essentially around the footprint of what is now called the Eaglebine, northern extensions of the Eagle Ford where it meets with the Woodbine Fm. sandstones. The HF activity in this area is currently moderate.
Grossman et al. (1986): 6 wells out of 25 Sparta wells with methane, a mixture of thermogenic and microbial origins, all concentrations <0.1 mg/L except one at 3.9 mg/L,
Grossman et al. (1989): 16 wells out of 45 Sparta and Yegua wells showing microbial methane in the 0.5-2 mg/L range,
and Zhang et al. (1998): 40 wells in east-central and central Texas. They concluded that the methane (concentrations <2ppm) was microbial with active methane consumption and sulfate

reduction moving the $\delta^{13}C$ into the thermogenic range. The area of study covers areas termed the Eaglebine extension of the Eagle Ford Shale into the East Texas Basin (more than half of their samples are in Burleson, Brazos, and Robertson counties). The other samples are outside of currently producing shales. Samples seemed to have been collected using the direct-fill approach. Most (19) samples show methane concentration <1 mg/L, 4 are between 1 and 10 mg/L and the maximum is 26 mg/L [unit in paper is μM]. Ethane was detected in 4 of the 5 samples with methane concentration >1 mg/L but with a very high C1/C2 ratio suggesting a microbial origin supported by the microbial isotopic signal. Methane origin is attributed to consumption of woody remnants in sandy Eocene aquifers. Another set of 16 samples was collected in Cretaceous aquifers in Bexar and Travis counties, they show barely any methane (<0.07 mg/L) but 4 samples show traces of ethane with a much smaller C1/C2 ratio and an isotopic signature underlining a possible thermogenic influence. The authors attributed the thermogenic gas to deep brines migrating from overpressured GOM formations.

More recent work (Carlson and Horn, 2013; Carlson and Horn, 2014) was done in Louisiana just across the state line in the footprint of the Haynesville. Recent work by Dr. Murgulet (Texas A&M Corpus Christi) in the Eagle Ford (Hampton et al., 2013; Murgulet et al., 2015) suggest mixed thermogenic and microbial sources there. Recent work also includes a peer-reviewed paper published in the course of this study by Darrah et al. (2014) mostly discussing the Marcellus Shale but including a few Barnett samples from the Parker-Hood cluster revisiting the well-known "Range Resources" case. Previous methane sampling in the Parker-Hood cluster is limited to a small area with high ethane concentrations strongly suggesting thermogenic origin. Our sampling confirmed the high concentration values. Section IV-4 give additional details.

The Gulf Coast region has also many documented shallow groundwater with methane. A TWDB-sponsored geochemical study of Gulf Coast system aquifers included systematic dissolved methane sampling (Kreitler et al., 2013a; Kreitler et al., 2013b; Young et al., 2014). We did not perform a thorough analysis of their dissolved methane results but a preliminary look suggest that the methane is mostly microbial and degraded microbial as illustrated on the Bernard plot (Figure 15) displaying those samples with methane >0.1 mg/L. The biodegradation of methane pushes the remaining methane into the thermogenic field for $\delta^{13}C$ but the quasi absence of ethane and propane lessens the likelihood of a thermogenic origin (it is unlikely that gas with high methane concentrations would not show some ethane even if ethane is preferentially consumed).

EPA (2015c; 2012a, p.153; 2012b) selected Wise County as one of the five cases for a retrospective study of potential HF-related contamination. EPA investigated three sites in the county, including one located within the area of the Wise County lawsuit (Appendix I); water sampling was conducted between September 2011 and May 2013 on several occasions. Low methane concentrations (<0.025 mg/L) were detected and no isotopic analysis was performed.

Lawsuits can sometimes bring to light many technical details or, on the other hand, sequester them from the public domain. In the past few decades, three major lawsuits have been related to methane and groundwater contamination, all in the Barnett Shale footprint, labelled after the county the events occurred: Wise, Parker, and Palo Pinto, only the latter is still active. The oldest, in Wise County, is summarized in Gold (2014) and described in Appendix I: Wise County Litigation. This Wise County lawsuit against Mitchell Energy took place because their surface casings were allegedly too short and that resulted in methane contamination of the

Trinity aquifer (gas came from the Bend Conglomerate, Boonsville field). Our limited sampling did not catch any dissolved methane in Wise County.

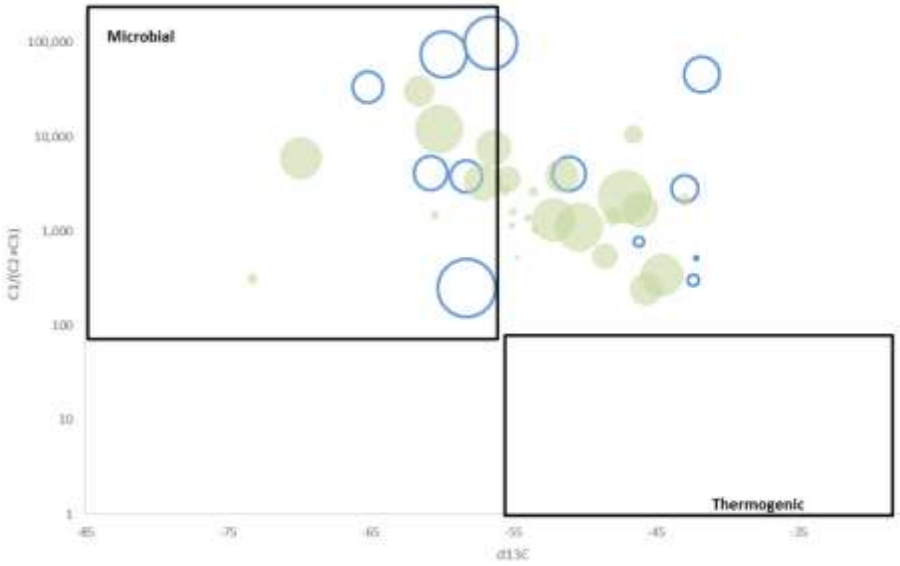

Source: Kreitler et al. (2013a), Kreitler et al. (2013b), Young et al. (2014) and TWDB database
Note: circle areas are proportional to methane concentrations; maximum and minimum concentrations are ~23 and 0.1 mg/L; empty blue circles = Gulf Coast and filled light green circles = CZWX.

Figure 15. Bernard plot of TWDB measurements in the Gulf Coast system and CZWX aquifers

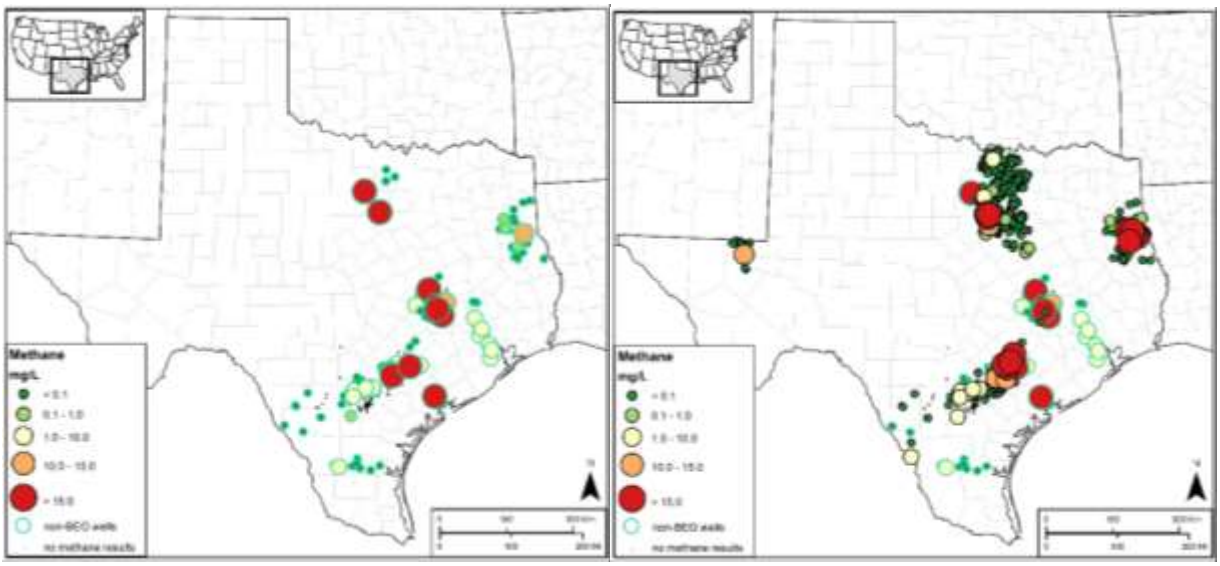

Before After

Figure 16. Public domain data on dissolved methane before and after this study

The second major lawsuit(s) were against Range Resources and the matter is discussed in the next sections. In the course of this project, a water well blowout occurred in Palo Pinto County near the town of Oran at the eastern edge of the economically viable Barnett Shale but still clearly within its overall footprint and produced the third lawsuit. The RRC is still currently investigating after releasing preliminary information (RRC, 2015). Five ~220 ft-dep water wells were sampled and four of them show methane concentrations at 55, 38, 14, 2.4 mg/L with

significant ethane (thermogenic origin corroborated by C isotope signature). The water well dissolved gas shows some sign of biodegradation, which suggests, as it did in the Parker-Hood cluster, that microbes are acclimated to the presence of natural gas and therefore that it is not a recent incursion.

There has been a few studies dedicated to assess potential contamination related to HF but not necessarily focusing on methane. For example, UT Arlington proceeded to take water samples in the Barnett Shale area but focused on arsenic and other trace metals as well as organics. (Fontenot et al., 2013; Hildenbrand et al., 2015 [note many of the samples described in this 2015 paper were taken at the same time and in the same wells described in this report]).

IV-2. Overview of Methane Sources

Potential sources of methane in Texas include the following:

Oil and Gas reservoirs: The many oil and gas accumulations in Texas originated from the shales and other source rocks currently subject to HF. In general these accumulations occur between the ground surface and the source rock following secondary migration of the hydrocarbons.

Coal: The lignite belt forms an arc from the Mexican border to the Louisiana state line (Figure 17). Several large open-pit mines provide fuel for mouth-of-mine coal-fired power plants. The continuation of this belt within the Wilcox Fm. of Eocene into Louisiana has been studied for deep coal-bed methane (Warwick et al., 2008). Warwick et al. (2008) concluded that most of the gas is of biogenic origin (CO_2 reduction). Cretaceous-age and Paleozoic-age subbituminous coal deposits occur west of the lignite belt and were produced mostly in the first half of the 20th century. Both the Eagle Ford and Haynesville shales are stratigraphically located underneath the Wilcox deposits. The Barnett Shale is located east of the previously produced coal accumulations but non-commercial accumulations of Paleozoic-age (including in the Strawn Fm.) but younger than the Barnett have been described in its footprint.

Legacy contamination and gas blow outs: The long history of oil and gas production in Texas with practices that were not up to current standards have generated legacy contaminated sites, some known and documented but likely many forgotten. Common contamination cases involve brine pits that could give the appearance of a leaky well, particularly if combined with detectable methane. However, the most likely origin of the methane would be the biodegradation of spilled oil, which would have then a biogenic signature. On the other hand, gas blowouts can contaminate groundwater for decades with thermogenic gas so it is important to rule them out in a state with a long history of oil and gas production when high concentration methane are discovered. For example, it is documented that twelve blowouts occurred in Montgomery County between 1932 and 1933, resulting in methane seeps bubbling from creek beds (Michaux, 1936) and of the 105 wells drilled in the Conroe Oil field in Montgomery County by 1999, fifteen wells were blowouts, impacting water wells nearby (Adams, 1999) but many more across the state are likely forgotten. Oil blowouts would also generate mostly microbial gas. The RRC has a web list of known blowouts (http://www.rrc.state.tx.us/oil-gas/compliance-enforcement/blowouts-and-well-control-problems/blowouts-and-well-control-problems-11-15/). We expand on the RRC database in Appendix C and RRC-documented blowouts are displayed on Figure 77. Drinking water well contamination following a blowout is common, with both domestic and public water supply wells reported to be impacted by methane and occasionally free-phase petroleum hydrocarbons years after the initial incident (RRC, 1973; Kelly et al., 1985; Gutierrez and

Bremer, 1990; Stagg, 2002). The only high methane water well sampled in the Delaware Basin (Loving County) is related to a recent blowout whereas Parker and Hood counties have no documented blowout close to the high-methane area (Figure 78 and Figure 79).

Historical contamination cases: We collected contamination cases from the RRC to (1) evaluate spatial density of contamination and potential clustering in areas with high methane; and (2) assess typical contaminant and check if markers can be identified.

Landfills and pipelines: Landfills are a well-documented source of microbial methane, sometimes with persistent plumes (e.g., Cozarelli et al., 2011). Figure 18 shows their distribution across the state. Pipelines are also numerous crisscrossing the state of Texas. Figure 20 focuses on the four plays/basin of interest in this study. Catastrophic leaks are rare and pipelines are constantly monitored by operators for minor leaks. If the fluids transported is crude oil or gasoline, the methane resulting from a leak will be microbial from the degradation of the HC. The signature of methane will be thermogenic only when natural gas is carried in the pipeline.

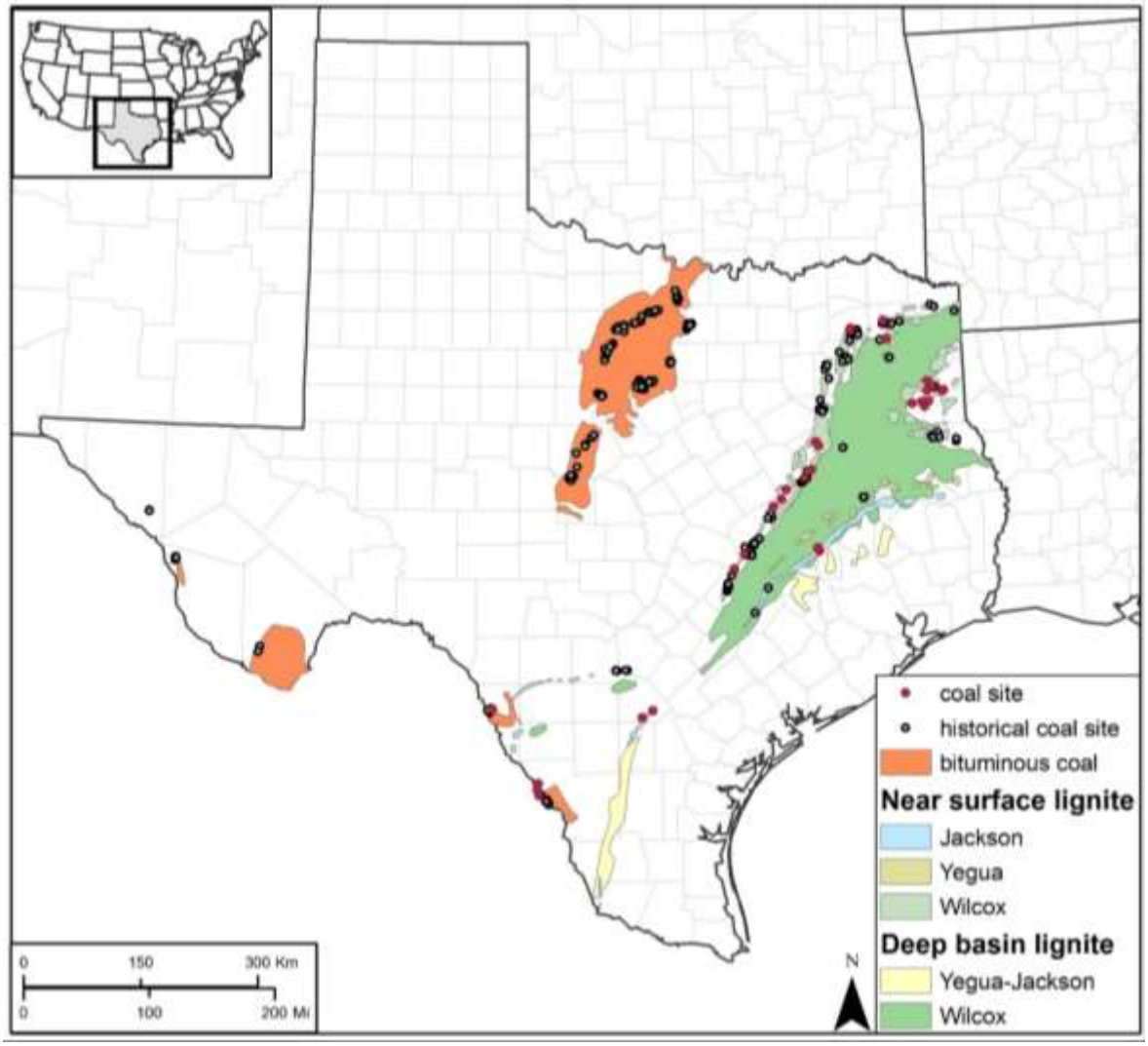

Source: Evans (1974) and Mapel (1967) for bituminous coal;

Figure 17. Coal-containing formations and coal mines in Texas

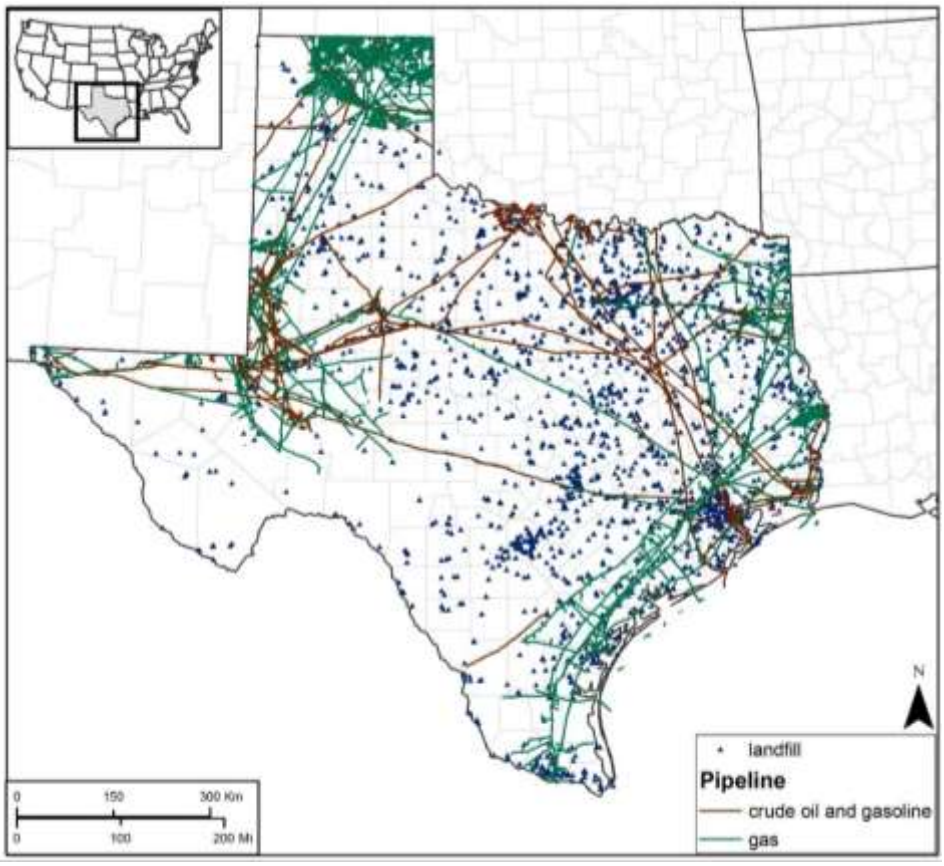

Source: landfills: TCEQ GIS data: http://www.tceq.state.tx.us/gis/download-tceq-gis-data (last accessed, 8/26/2015)
Pipelines: RRC data for purchase: http://www.rrc.state.tx.us/about-us/resource-center/research/data-sets-available-for-purchase/pipeline-data/ (purchased on or before 2013)

Figure 18. Landfills and major gas pipelines in Texas.

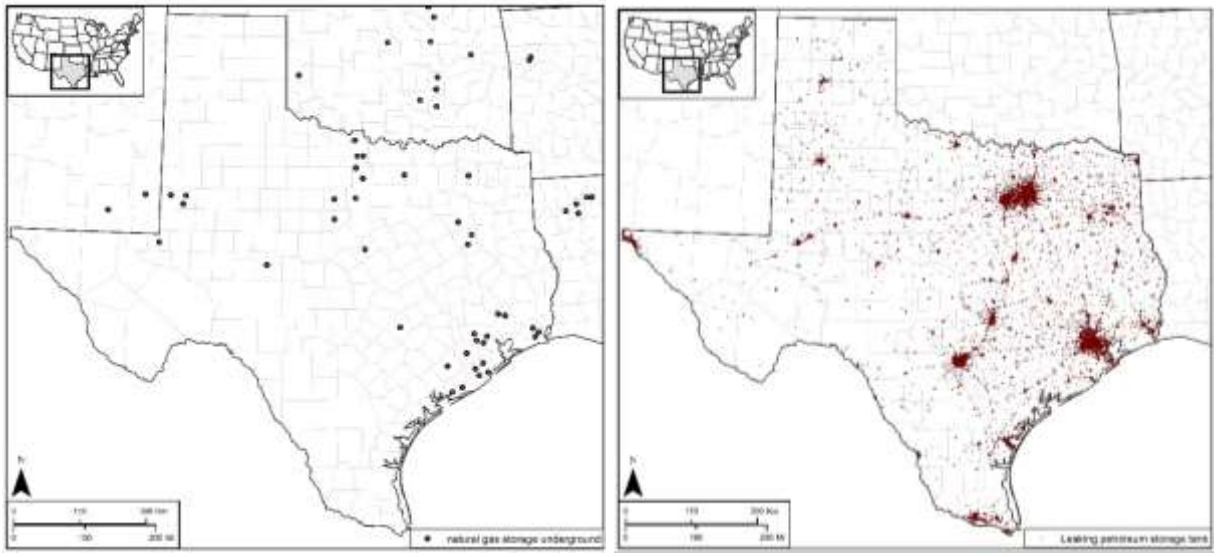

Source: EIA (July 2014) and TCEC (August 2015): https://www.tceq.texas.gov/agency/data/lookup-data/pst-datasets-records.html

Figure 19. Underground gas storage facilities (a) and leaking petroleum underground storage tanks(b)

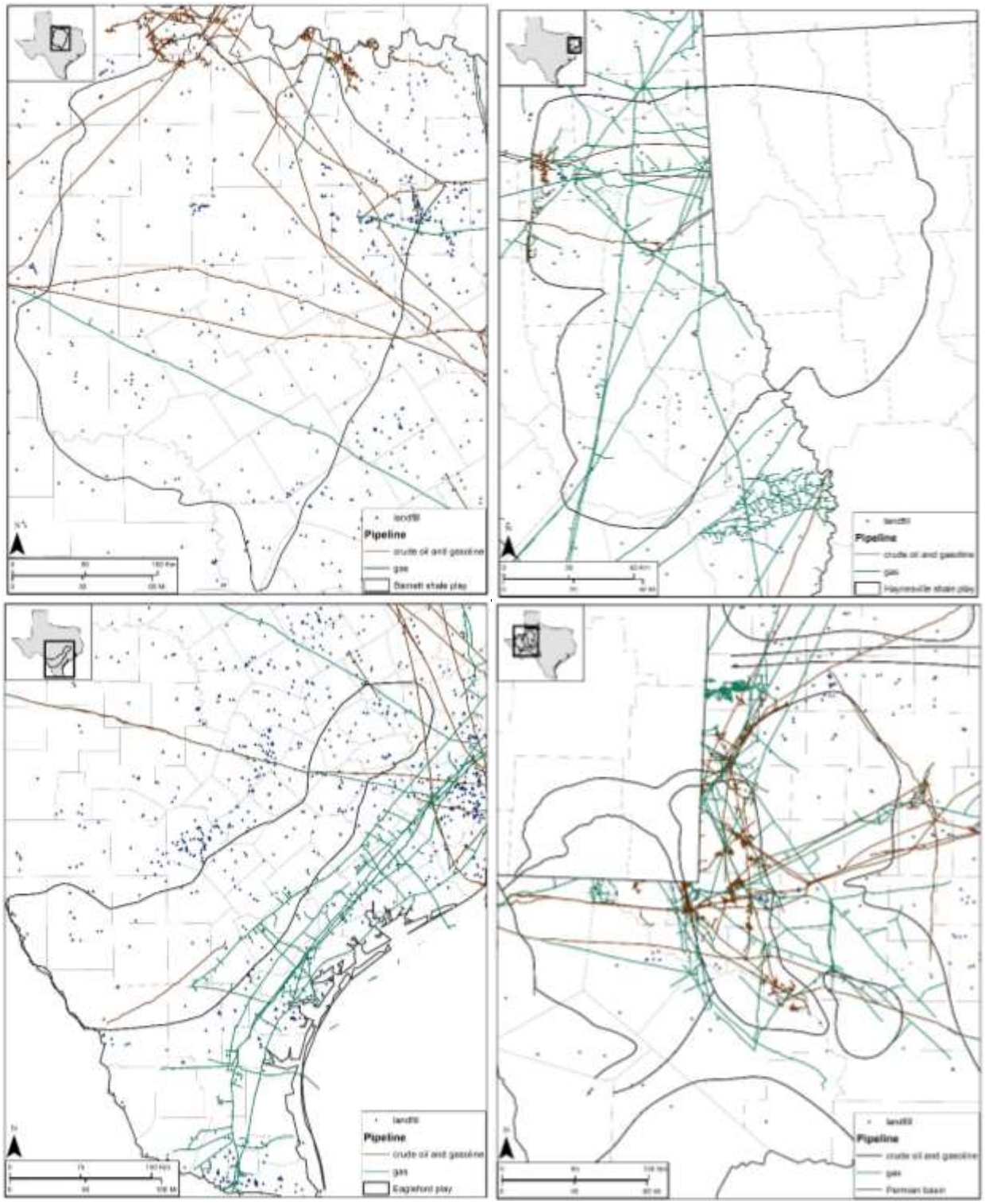

Figure 20. Landfills and major gas pipelines in Texas in (a) Barnett Shale play; (b) Haynesville Shale play; (c) Eagle Ford play: and (d) Permian Basin.

IV-3. Reconnaissance Sampling

In this section we examine the four plays / areas: Barnett, Haynesville, and Eagle Ford shales and Delaware basin.

IV-3-1 Barnett Shale Footprint

This study endeavored to obtain a better understanding of the impact of gas production from the Barnett Shale in north central Texas on groundwater quality. The Barnett is the oldest play in which hydraulic fracturing became a major stimulation technique (Nicot et al., 2014). We sampled hundreds of relatively shallow domestic wells as well as deeper wells in the footprint of the play (Figure 22). Production started in what is called the core area that has been drilled intensively and consists of Wise, Denton, and Tarrant counties in the Fort Worth area.

IV-3-1.1 Play Characteristics

Barnett Shale and Paleozoic Formations Geology: The Barnett Shale is a siliceous mudrock composed mostly of quartz and clay minerals with some minor calcite (Loucks and Ruppel, 2007; Appendix J) and deposited in what is now the Fort Worth Basin. The Barnett Shale Fm. exists under wide areas in Texas and crops out on the flanks of the Llano Uplift 150 miles to the south of the core area. Most current boundaries of the formation are erosional but it is bounded by tectonic features to the east by the Ouachita thrust foldbelt (old, eroded, and buried mountain range) and to the north by uplifted material (Muenster and Red River Arches). A depositional equivalent is present farther west in the Delaware Basin, a large sub-basin of the Permian Basin. The Barnett Shale gets thicker and deeper toward the NE close to the core area and dips gently toward the core area and the Muenster Arch from the south and west where it thins considerably. Its base reaches a maximum depth of ~8,500 ft (subsea) in the NE confines of its extent. The depth to the top of the Barnett ranges from about ~4,500 ft in northwestern Jack County to about ~2,500 ft in southwest Palo Pinto County to about ~3,500 ft in northern Hamilton County to about ~6,000 ft in western McLennan County to about 7,000 to 8,000 ft in the Dallas-Fort Worth area. Further west in Throckmorton, Shackelford, and Callahan Counties where it is not an exploration target, the depth to the Barnett varies between ~4,000 and 2,000 ft.

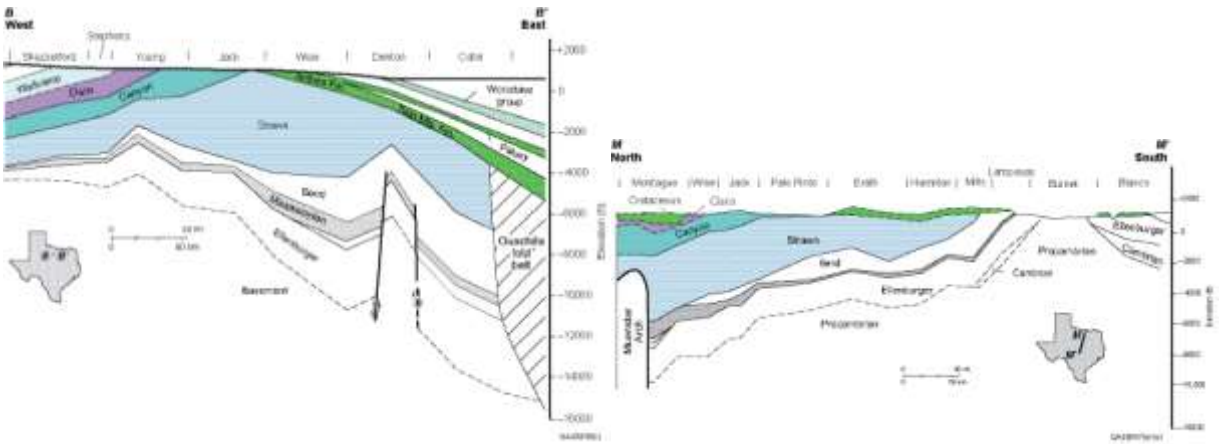

Source: Nicot et al. (2013b) (modified from CLI, 1972)

Figure 21. EW and NS Generalized ross-sections through the Fort Worth Basin

The Mississippian Barnett Shale was deposited in a calm anoxic environment at the edge a large continental mass and where it collected and preserved significant amounts of organic matter. It overlies the Ellenburger dolomite of Ordovician age, itself resting on a Precambrian basement with an intervening Cambrian sandstone. Uneventful mostly carbonate sedimentation continues with breaks until early in the Pennsylvanian period when sedimentation nature and amount changed due to an approaching continent. Sedimentation increased substantially, progressively lost its marine origin, and became more siliciclastic with sediments coming from the north and east. The continental collision created the now buried (in Texas) Ouichita Mountains and drove some of the Barnett rocks into the pressure and temperature zone favorable for oil and gas production. The Barnett Shale became thermogenetically mature during the Permian and Mesozoic periods during which time most of the migration and trapping occurred (Montgomery et al., 2005; Pollastro et al., 2007). This study is concerned with these counties where the Barnett Shale has acted as a source rock and produced hydrocarbons (Figure 22).

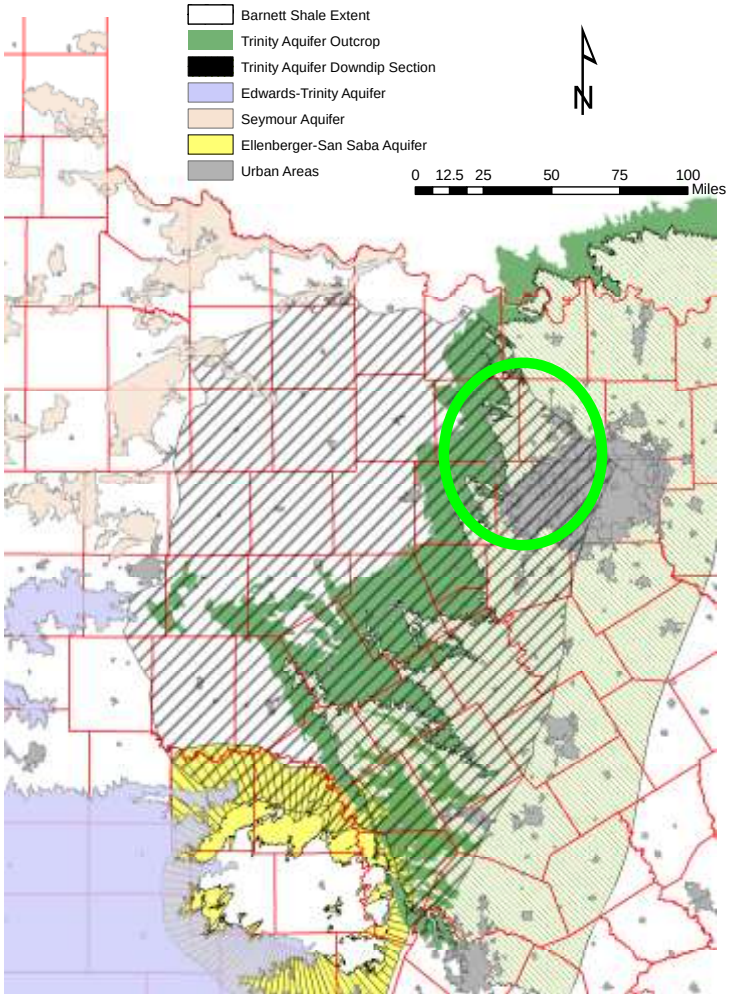

Note: Barnett extent is approximate and will change with new studies. Llano uplift is outlined by the Ellenburger Aquifer. The lower downdip limit of the aquifers is set when salinity reaches 3,000 ppm. Green circle represents the core area.

Figure 22. Barnett Shale extent and TWDB major aquifers.

The Pennsylvanian sediments include the Bend conglomerate that contains important gas reservoirs produced mostly in the 1950's through the 1970's and other formations from the Bend

Group of Atokan age. They underlie the Strawn Fm. (Brown et al., 1973; Cleaves, 1975) of direct interest to this study. Younger Pennsylvanian formations such as those in the Canyon and Cisco Groups crop out further to the west (Nicot et al., 2014) and are not of concern to this study. The Canyon sediments stand out compared to the Strawn (older) and Cisco (younger) sediments because of the relative abundance of bank and shelf carbonates. The Atoka-Strawn sediments can reach 5000+ ft close to the Ouachita thrust belt but decrease considerably on the Bend Arch, 100 miles to the west.

The Barnett Shale is mostly a gas play, that is, most of the formation has entered the gas window. However to the North (Montague County) and to the West, substantial amounts of condensate are produced as the formation is still in the oil window (Pollastro et al., 2007). The Barnett Shale crops out to the south next to the Llano uplift exposing Precambrian rocks. The Barnett gets thicker and deeper toward the NE close to the so-called core area that has been drilled intensively. The core area is located under the city of Fort Worth and neighboring communities, for example, Denton in Wise County.

Shallow Geology: The main aquifer in the area is the Trinity aquifer system of Cretaceous age (Harden et al, 2004; Bené et al., 2007; Intera, 2014 US EPA. 2015c; and references therein) and on the western edge of our study area small aquifers of Paleozoic age (Nicot et al., 2013b). The Trinity aquifer dips towards the west whereas Strawn formations dip towards the northwest with a major unconformity in between.

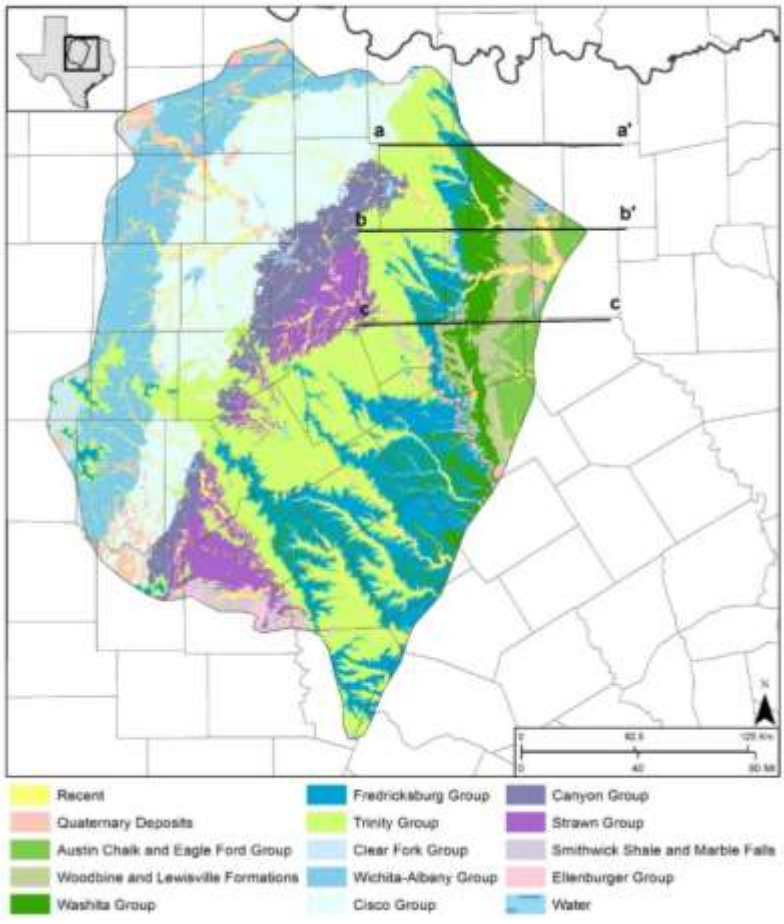

Figure 23. Geologic map of the Barnett Shale footprint.

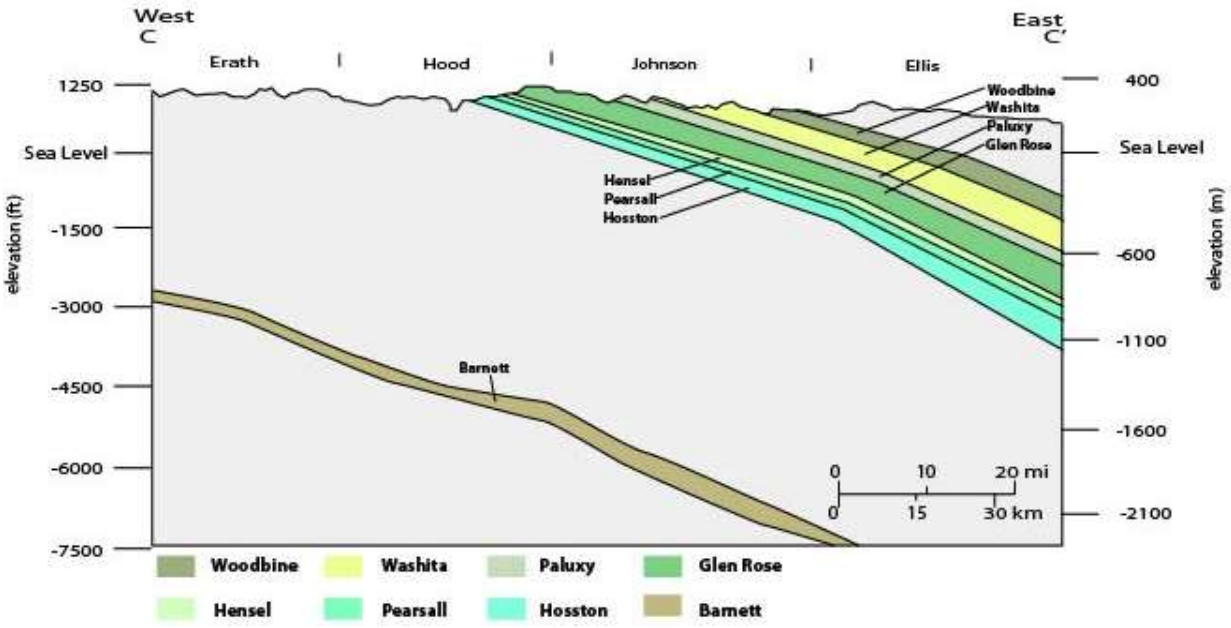

Figure 24. EW cross-section of the Barnett Shale footprint along the Parker-Hood county line.

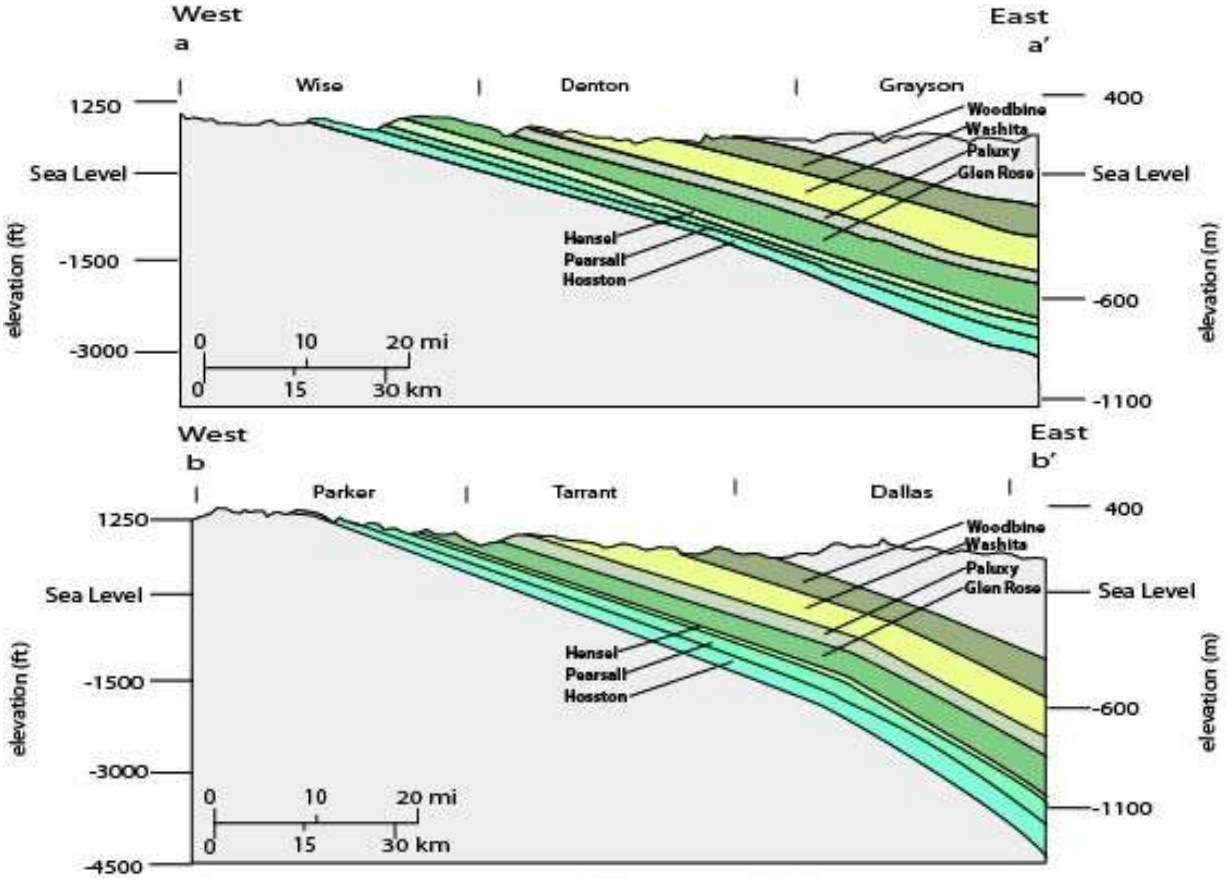

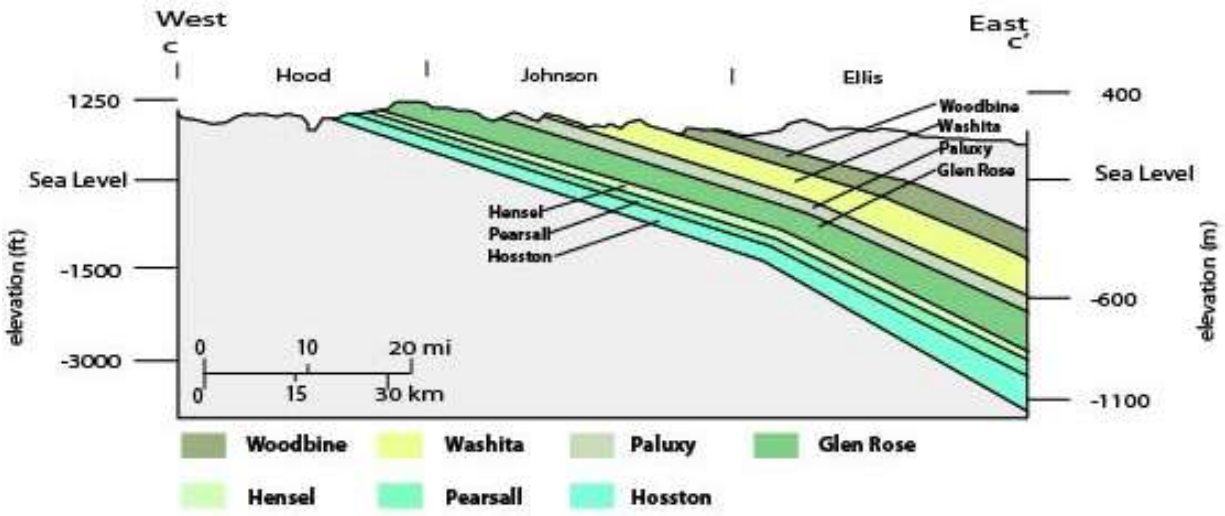

Figure 25. EW cross-sections of the shallow vertical section of the Barnett Shale footprint.

Presence of Faults: In addition to the Ouichita thrust belt on the eastern edge of the Barnett, a major fault, "the Mineral Wells fault", trending SW-NE has been described in southern Denton and northern Parker counties. It seems to be a fault rooted in the basement and that has been active to the end of the Paleozoic (Pollastro et al., 2007, p.412). Several minor normal faults parallel to it are present in the basin including in southern Parker County (see below and map by Ewing, 1991). There is not fault at the surface in the Parker County area of interest but several exist at depth impacting at least some of the Paleozoic section. Flippin (1982, p.142) commenting on Erath County suggests that the fault could impact the Strawn Fm..

Natural sources of thermogenic methane: The Barnett Shale is recognized as the major source of hydrocarbons in the Fort Worth Basin. However, there are potential source rocks in the Pennsylvanian section, for example, many thin (10-20 ft) organic-bearing shale beds exist in the Bend Conglomerate section (Hackley et al., 2009). Pollastro et al. (2007, Figs.3 and 4) also recognized that the Barnett Shale is the major source rock in the basin but add as minor sources the Marble Falls limestone, the Bend conglomerate, and the Smithwick shale, all pre-Strawn and of early Pennsylvanian age. The same formations contain many mostly gas reservoirs. The overlying Strawn also contains many reservoirs, several very shallow. The Strawn and the overlying Cretaceous also include minor coal seams (see Section IV-4 on Parker County).

IV-3-1.2 Results

We sampled mostly domestic wells in the eastern half of the producing Barnett footprint (Figure 26a) then we turned to municipal and irrigation wells to the East as (1) the Trinity aquifer deepens following its dip and (2) the area becomes more urbanized with many less domestic wells to sample from. During the sampling many well owners complained about H_2S that we were also able to experience, it is more widespread than dissolved methane and may be more related to well maintenance rather than a regional contaminant (Figure 26b). We sampled 555 wells, most within the Barnett footprint but ~100 outside of the footprint to the east (Ellis and Hill counties) and north (Cooke and Denton counties) as a reference point and collected 612 samples (with du- and tri-plicates).

The vast majority of the water samples shows no or very little methane (Figure 27) except in the Parker-Hood cluster which is the most publicized area with high methane levels in Texas. An initial study by the RRC (RRC, 2014) determined that the gas is thermogenic. Although the number of samples is large, the area of interest is also large and the overall sampling density is <0.1 sample/mi^2. There are other areas such as the Oran area in northeastern Palo Pinto County (RRC, 2015) in an area not sampled for this study where dissolved methane is clearly present. Some domestic wells in RRC District 9 (Bowie area in Montague County to the NW of DFW) have been described by RRC staff as potentially containing dissolved methane but they have attributed it to shallow coal seams. The City of Bowie PWS is currently provided by surface water, not groundwater. The single sample with dissolved methane in Montague County turned out to be microbial. It is possible that other areas with dissolved methane we did not sample exist but they are unlikely to be as large as the Parker-Hood cluster; complaints from residents would have reached the RRC.

The three areas with dissolved methane in Parker, Hood, and Somervell counties (Figure 27) are discussed below in a further section.

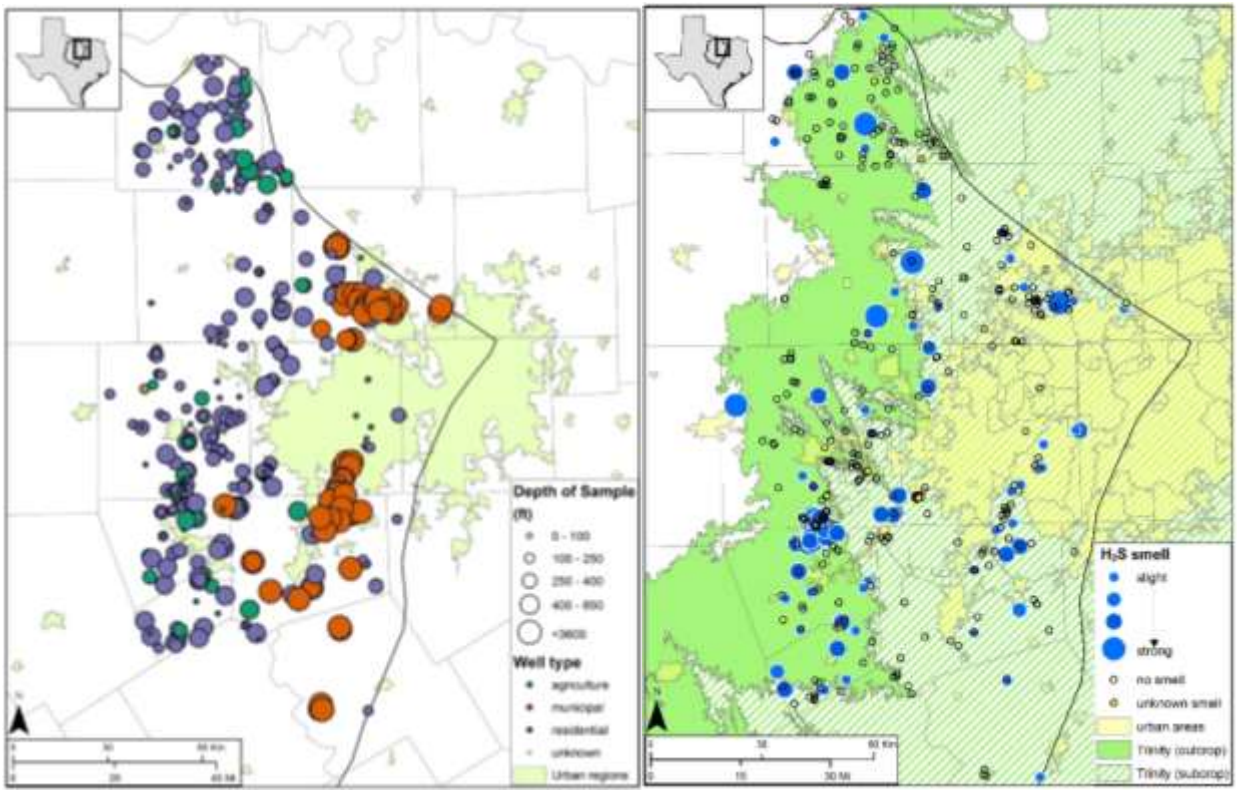

(a) (b)

Figure 26. Depth and type of sampled water well and qualitative estimate of H_2S amount

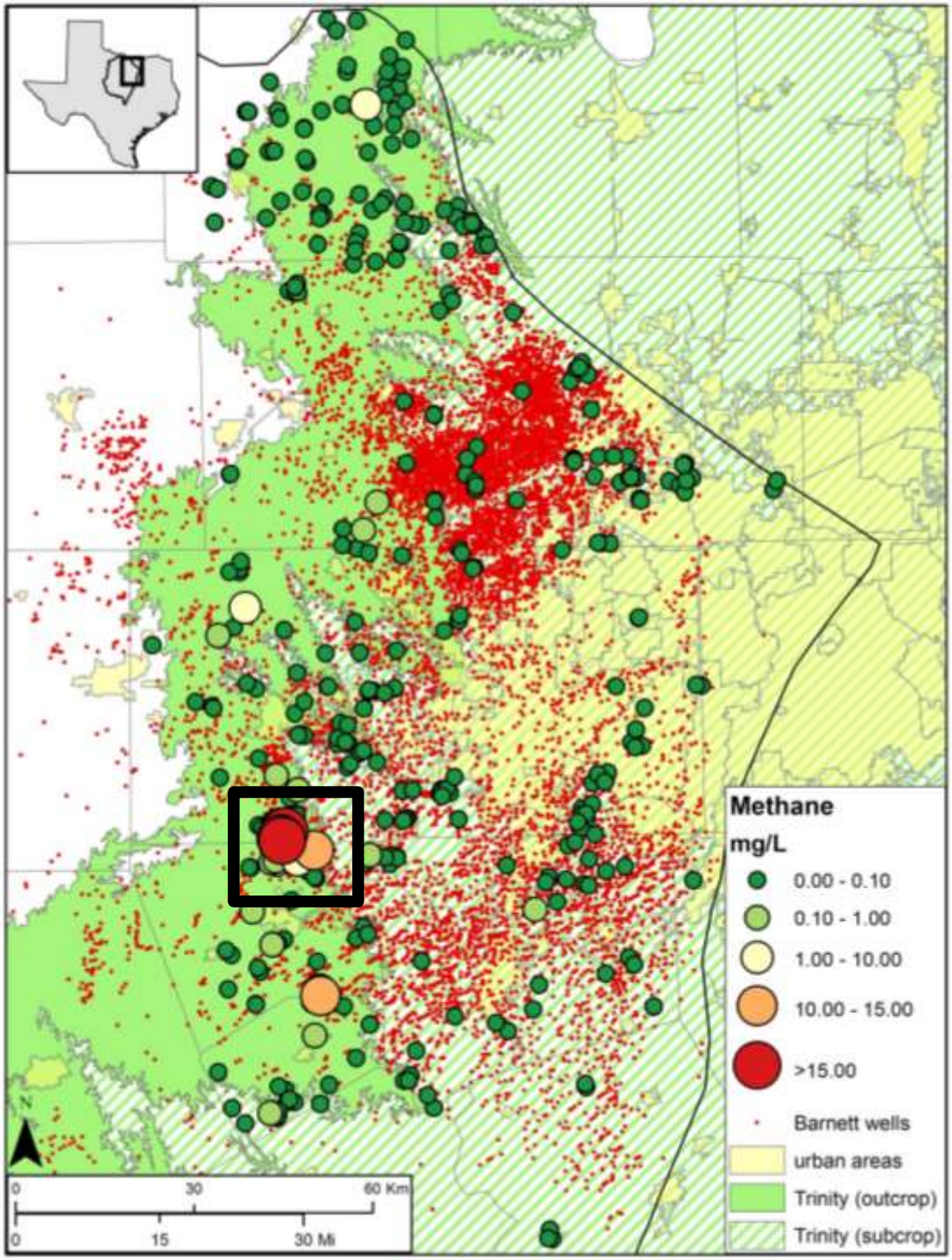

Note: square with black line delimits the boundaries of Figure 65; 18,022 Barnett wells on the map including

Figure 27. Distribution of dissolved methane concentration in aquifers (Barnett)

IV-3-2 Haynesville Footprint

HF and gas production from the Haynesville Shale started in the mid-2000's (Nicot et al, 2011) but drilling have seriously declined in the past few years. Overlying the Haynesville, the clastic Cotton Valley Fm. has been producing gas for several decades and operators have started using HF and horizontal wells there as well (Nicot et al, 2011; Nicot and Scanlon, 2012). The Bossier Shale is another shale overlying the Haynesville with prospective interest. The Haynesville Shale is deep (>10,000 ft) and overpressured.

IV-3-2.1 Play Characteristics

The Haynesville Shale of Jurassic age straddles the Texas-Louisiana state line and is found at depths of ~11,000 ft and more (Figure 29b). Its thickness can reach several hundred feet. The Shale and its regional framework have been described in several publications (Mancini et al., 2008; Hammes et al., 2011; Hammes and Frebourg, 2012; Nunn, 2012). The surface geology displays the Sabine Uplift, a prominent East Texas feature around which early Eocene formations starting with the Wilcox groups crops out, progressively younger formations ring the uplift: Carrizo, Queen City, Sparta, Yegua and Jackson Fms (Figure 28). All five formations in addition to the Wilcox contain local aquifers (Figure 30): Carrizo-Wilcox, Queen City, Sparta, and Yegua-Jackson aquifers.

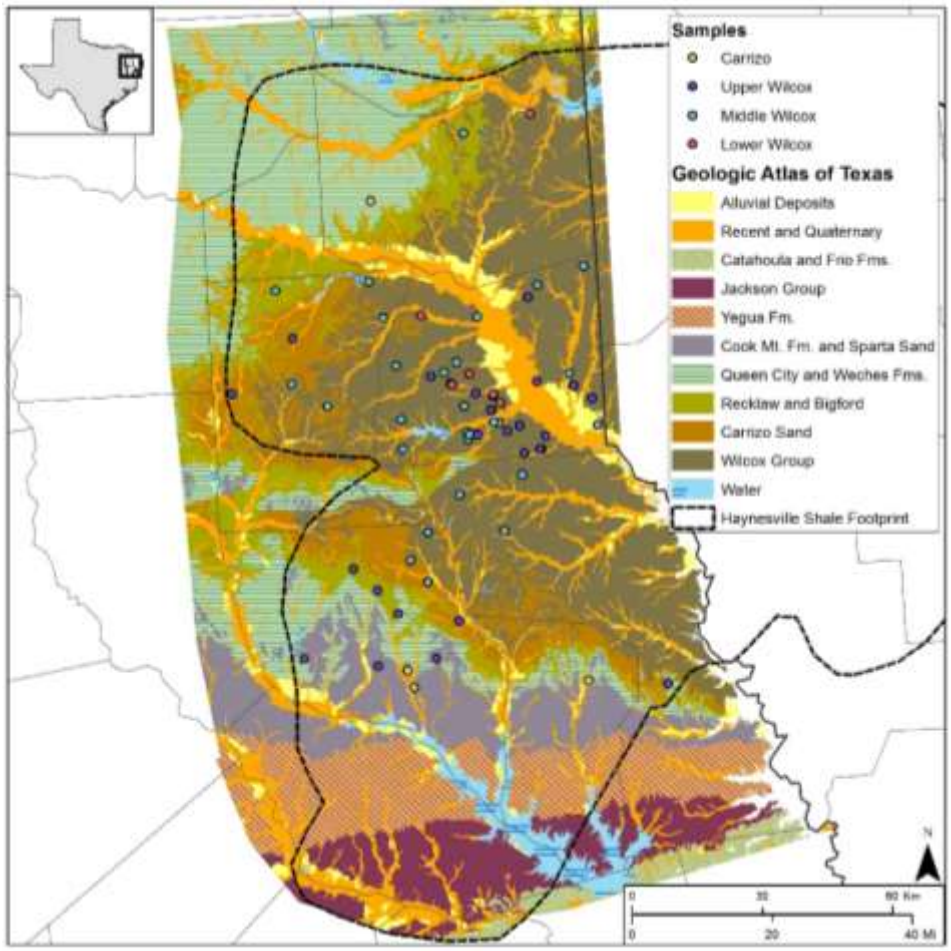

Figure 28. Geologic map of the Haynesville Shale footprint (Texas)

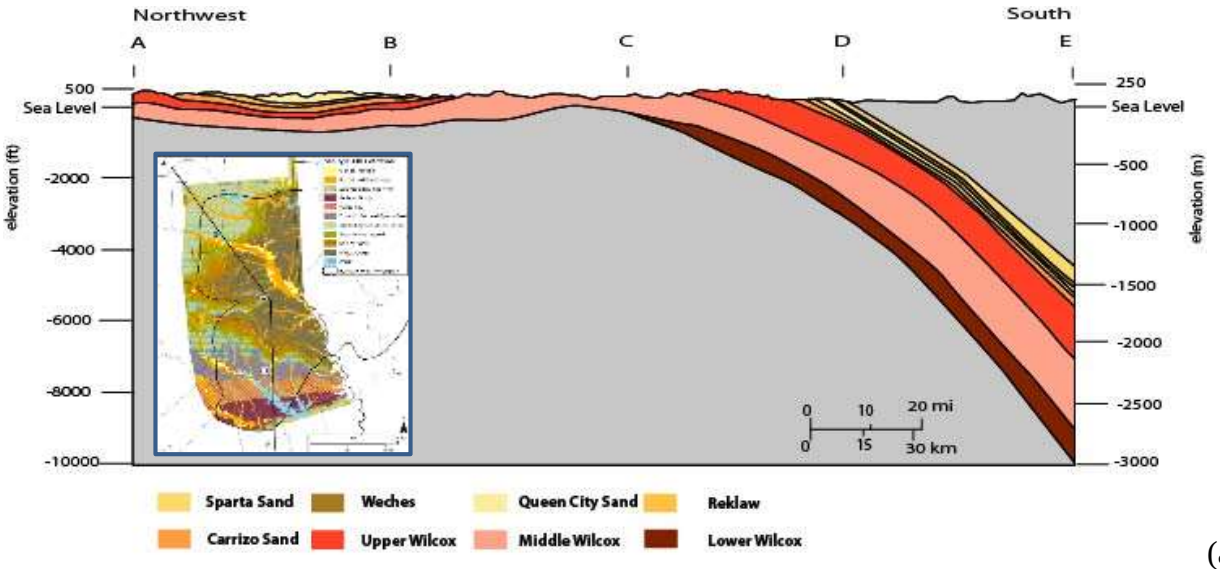

(a)

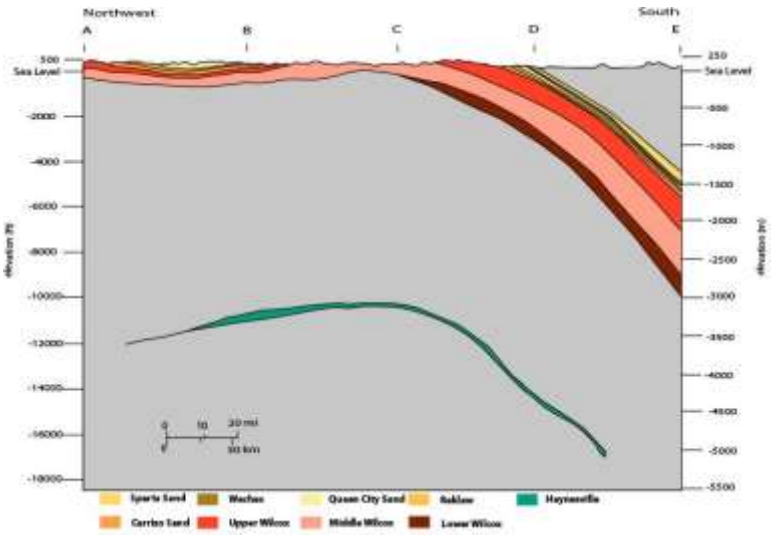

(b)

Figure 29. Cross-section of the Haynesville Shale footprint not including (a) and including (b) the Haynesville Fm.

Shallow subsurface. Aquifer hydrogeology is described in Kelly et al. (2004) and more specifically about Panola County in Oliver and Lupton (2013) and Lupton et al. (2015).

Presence of Faults. A well-known if not well understood fault zone exists on the Panola-Shelby county line in the footprint of the Haynesville Shale. It consists of the eastern expression of the Mount Enterprise Fault System which manifests itself in a series of parallel and en-echelon normal faults trending E-W with general downthrow to the north (unlike many faults in the Gulf Coast area that present an overall downthrow to the coast).

Natural sources of thermogenic methane. In addition to the Haynesville and Bossier shales, the area contains lignite and CBM. Kaiser (1990) and more recently Warwick et al. (2005) describe prospective CBM wells in Panola County targeting the Lower Wilcox. The Lower Wilcox contains lignite intervals, most extensive in Panola and Shelby counties, including beneath the Panola-Shelby cluster (Kaiser, 1990, pl.15), when and where the Wilcox Fm. transitions from the

mostly marine underlying Midway Fm. to the deltaic Wilcox Fm.. Lignite mines operate further to the north and also in Rusk County where the lignite is of Upper Wilcox age (Kaiser, 1990). A small patch of lignite of Upper Wilcox age is mapped on the Panola-Shelby county line beneath the Panola-Shelby cluster (Kaiser, 1990, pl.15). Warwick et al. (2005) described the exploratory well USGS-PA-2 drilled to a depth of 400 ft to the coal seams, located close to the Panola-Shelby county line and close to the Panola-Shelby dissolved methane cluster. Hydrocarbon analyses indicate that the CBM gas is very dry with a C1/C2+C3 ratio of 103. Isotopic analyses of the methane indicate a $\delta^{13}C$ of -55.82‰ and a δD of -194.6‰ (San Filipo et al., 2000; Warwick et al., 2005, p.147). Warwick et al. (2004, p.18) suggested the methane may have originated from mixing of thermogenic and microbial gases. CBM gas from the Wilcox in Louisiana is clearly biogenic (CO_2 reduction) with of a $\delta^{13}C$ of -62.05‰ and a δD of -187.9‰ as given in Warwick and Breland (2005) and confirmed in Warwick et al. (2008).

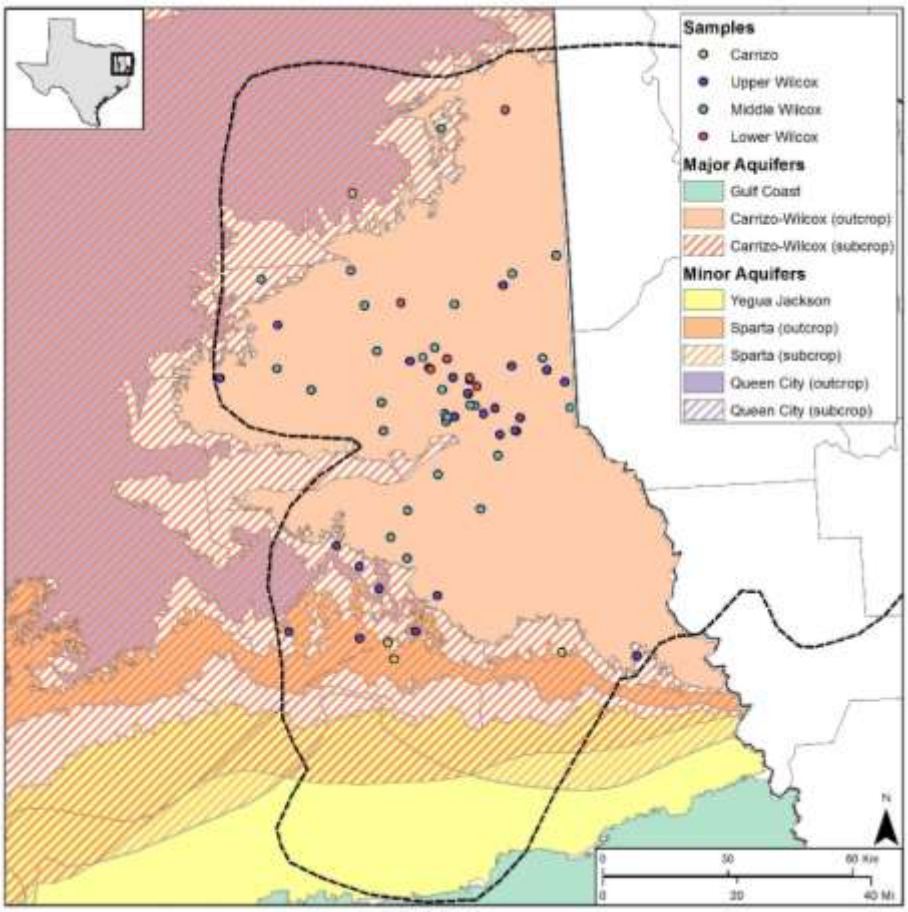

Figure 30. Aquifers in the Haynesville Shale footprint showing sampled well locations and position of screened interval

IV-3-2.2 Results

A total of 70 samples were taken in the Haynesville shale footprint (only in Texas). Because of field and budget constraints the coverage is not even across the play (Figure 31) but still points out to an area with significantly higher dissolved methane than elsewhere on the Panola-Shelby county line. Sampling in Louisiana also shows a relatively low dissolved methane concentration

across the play (Carlson and Horn, 2014). Carlson and Horn (2014) sampled 1000+ water wells in three parishes in the Haynesville footprint across from the state line. Most dissolved water concentrations were <1 mg/L with a few in the 1-3 mg/L range (their Appendix D). They used a modified direct fill method in which the headspace (250 ml) was created in the field by partially filling a 1-L bottle with the water to be tested. Then there is a direct relation between GC-measured headspace and dissolved concentration (2 ppm headspace methane, ethane, and propane corresponds to ~0.7, ~1.4, and ~2 ppm dissolved methane, ethane, and propane, respectively). The authors examined correlation of methane concentration with presence of Wilcox lignite, number of Haynesville wells, and density of historical conventional wells but did not find any strong correlation with any either way. However, relatively high methane concentrations were associated with oil and gas fields which can be attributed to natural seeps corroborated by the fact that in general the deeper the sand layer screened the higher the methane concentration. Unfortunately C2+ gases and C isotopes were not analyzed in Carlson and Horn (2014) which leaves many questions unanswered. Darling (2014) also observed biogenic methane in LA. An older study (Harder et al., 1965) catalogued water wells with high methane concentrations in southwestern Louisiana. Although the authors stated that concentrations were higher next to oil and gas fields, they also reported that there is typically no dissolved C2+ suggesting biogenic origin.

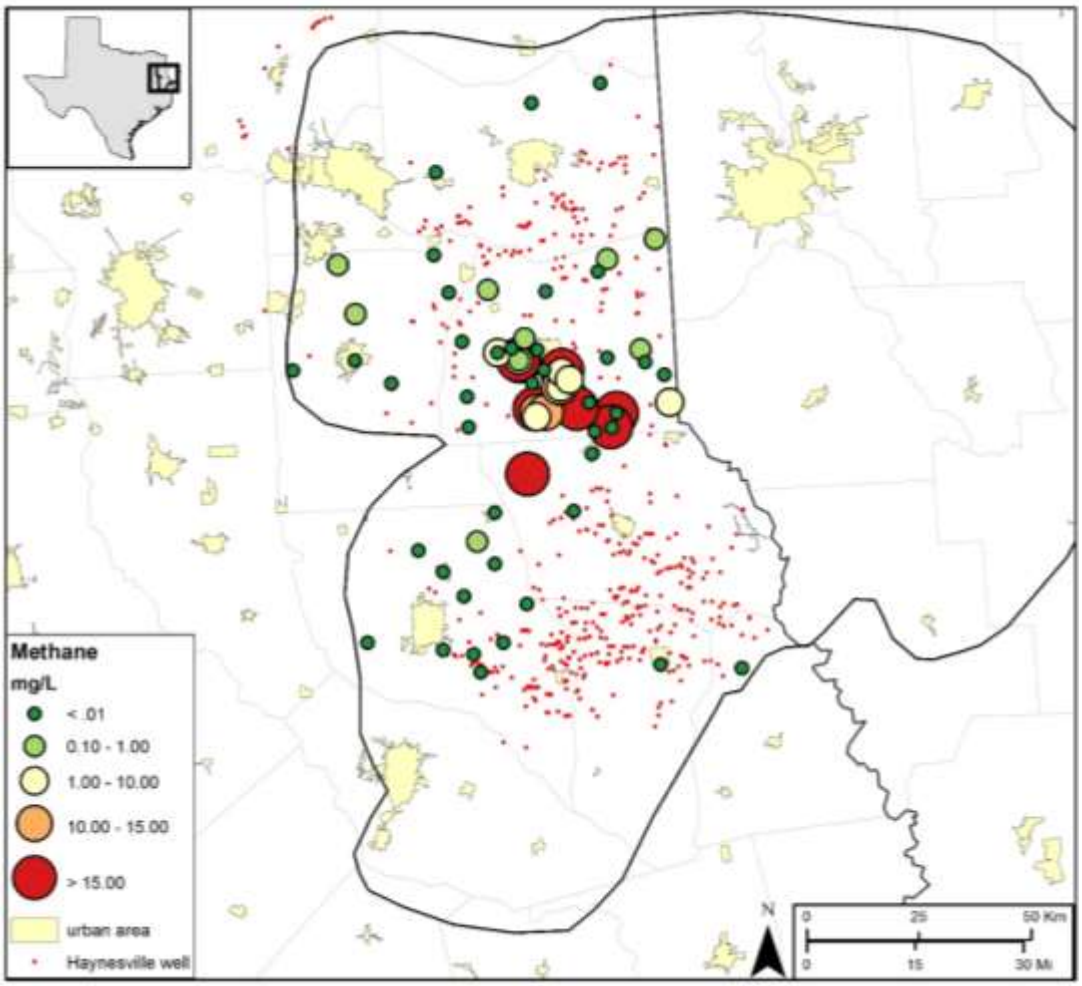

Figure 31. Distribution of dissolved methane concentration in aquifers (Haynesville)

Analyses for dissolved methane are mostly negative except in the Panola-Shelby cluster where all the high values are clustered (Figure 31). Adams (2013, p.31), Panola County GCD, also reported bubbling methane in a water well in the same vicinity (between Gary City in southern Panola County and Tenaha in northern Shelby County).

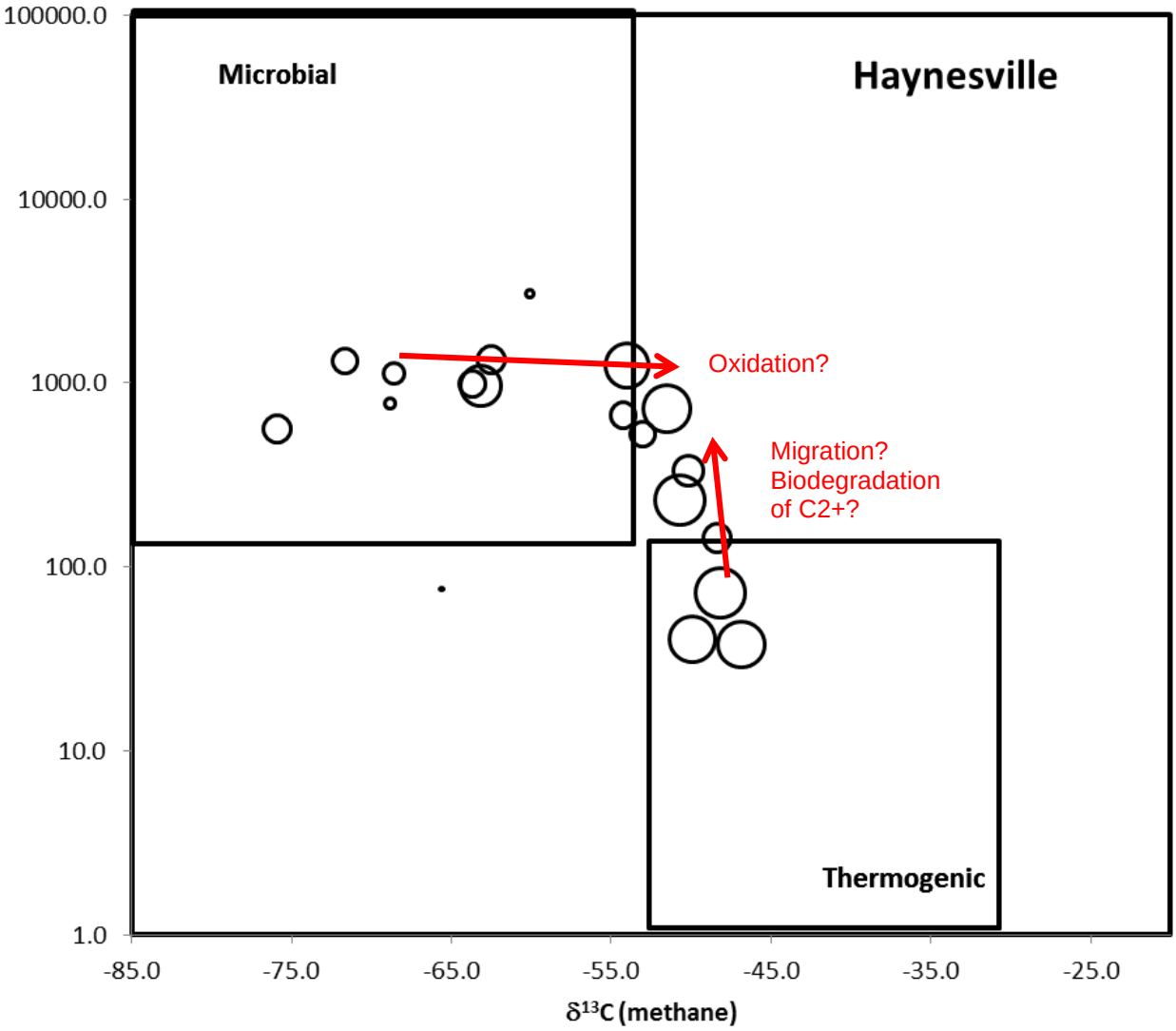

Note: bubble size is related to dissolved methane concentration

Figure 32. Bernard plot of dissolved methane samples (Haynesville)

A Bernard plot (Figure 32) of samples with methane concentration high enough to perform an isotopic analysis shows that the dissolved gas is dry, that some samples are of microbial origin and suggests that the thermogenic gas is being (bio)degraded. The fact that microbial and thermogenic methane samples are spatially associate suggests that oil associated with the gas may be consumed by methanogens to produce microbial methane. Kornacki (2010) emphasized the very dry nature of Haynesville produced gas samples (C1/C2~950-2100), and the relatively heavy C isotopic composition of methane ($\delta^{13}C$ ~ -31.5 to -34.5 ‰). Dryness / wetness needs to be confirmed, Darin and Bowles (2011, their Table 2) mentioned ~1% ethane vs. ~96% methane (volume) and Darling (2015, sl.9) sampled 5 Haynesville producing wells at >1% molar ethane. Warwick et al., 2005 indicated that the CBM gas is very dry with a C1/C2+C3 ratio of 103 with

a methane $\delta^{13}C$ of -55.82‰ and a δD of -194.6‰). Kaiser (1990) shows an abundance of coal beds in the Panola-Shelby cluster area. Our results tend to suggest that the origin of the thermogenic gas is from the Wilcox lignite rather than from the Haynesville shale.

Because they are associated spatially and sampled from the same aquifer, when plotted against depth, high methane samples are constrained to a narrow depth interval of 100+ ft (Figure 33). Plotting methane vs. depth and sulfate concentration does show a conclusive relationship (Figure 34 and Figure 35). Many water samples have low sulfate, some do show some sulfate but all methane-rich samples but one show no sulfate. The most likely origin for the sulfate is the lignite beds (degradation of pyrite, for example) rather than gypsum. All the methane-rich samples are likely subject to sulfate reduction processes. The depth crossplots for Fe are inconclusive as most Fe concentrations are <0.1 mg/L.

On the other hand correlation with Cl is positive (Figure 36 and Figure 37), high-methane water samples also display higher Cl concentrations.

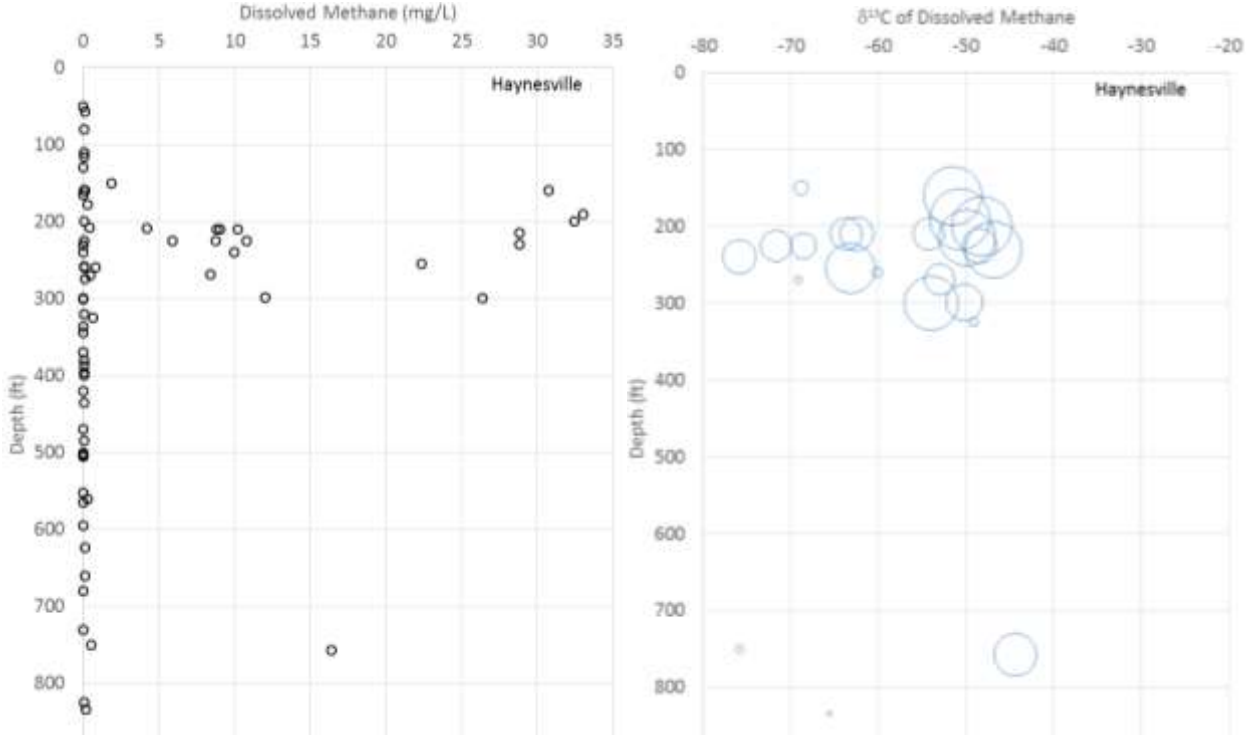

(a) (b)

Note: circle size proportional to methane concentrations; maximum methane concentration is 33 mg/L
(a) 70 dissolved methane water samples including (b) 26 samples with isotope analyses;.

Figure 33. Dissolved methane concentration and its $\delta^{13}C$ as a function of depth (Haynesville)

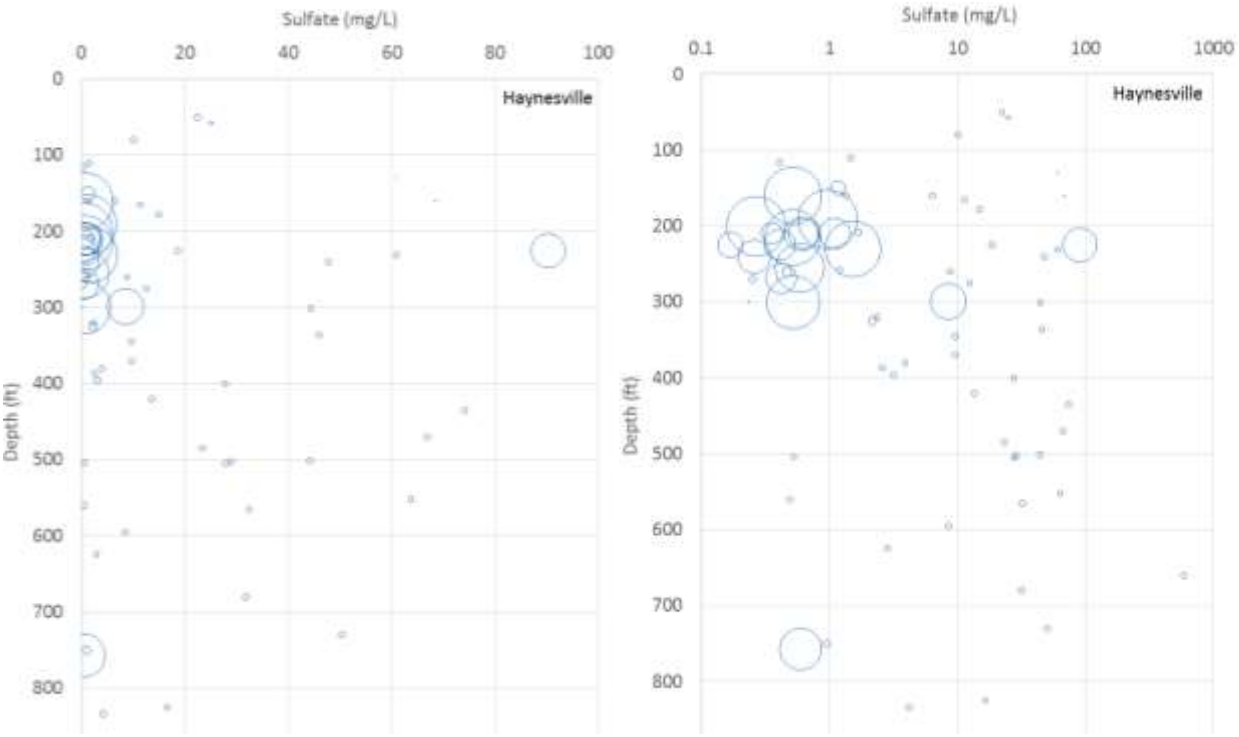

Note: circle size proportional to methane concentrations; all data points with CH_4<0.2 mg/L are plotted as 0.2 mg/L to improve visibility, maximum methane concentration is 33 mg/L; 70 dissolved methane water samples.

Figure 34. Sulfate concentration vs. depth vs. dissolved methane (Haynesville)

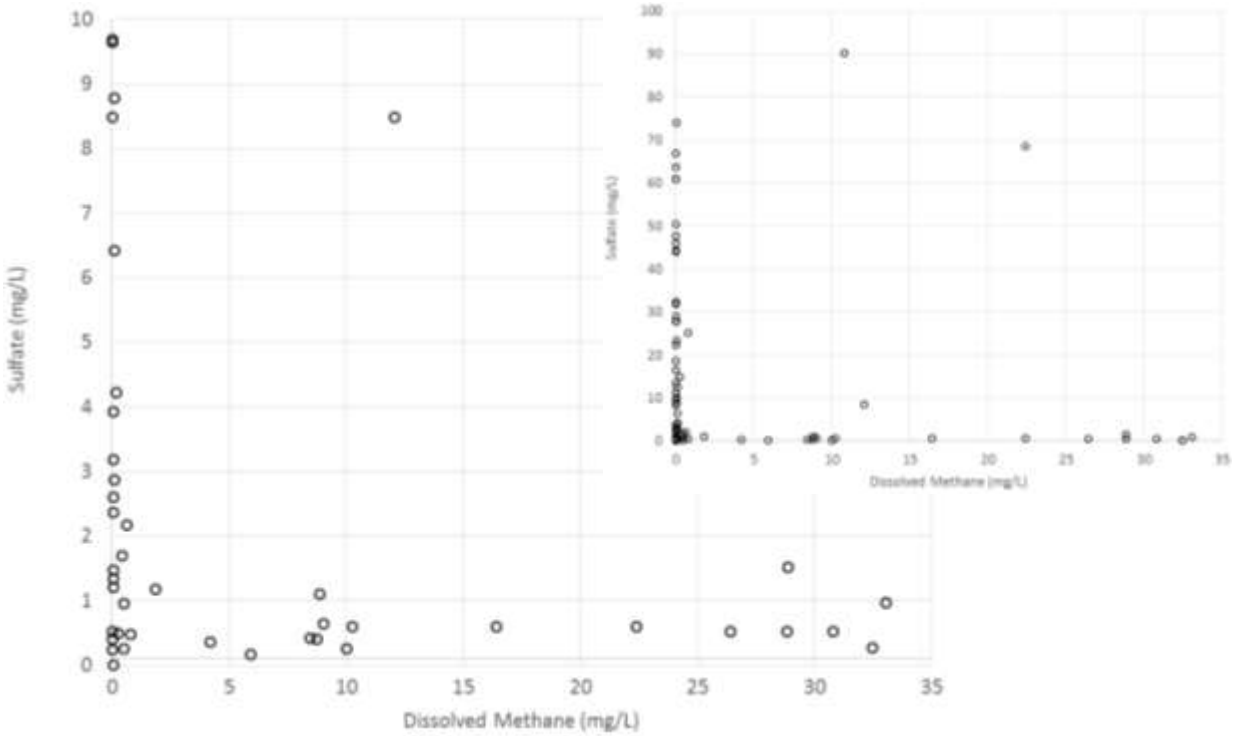

Note: the insert y-axis goes to 100 mg/L

Figure 35. Dissolved methane vs. sulfate concentrations (Haynesville)

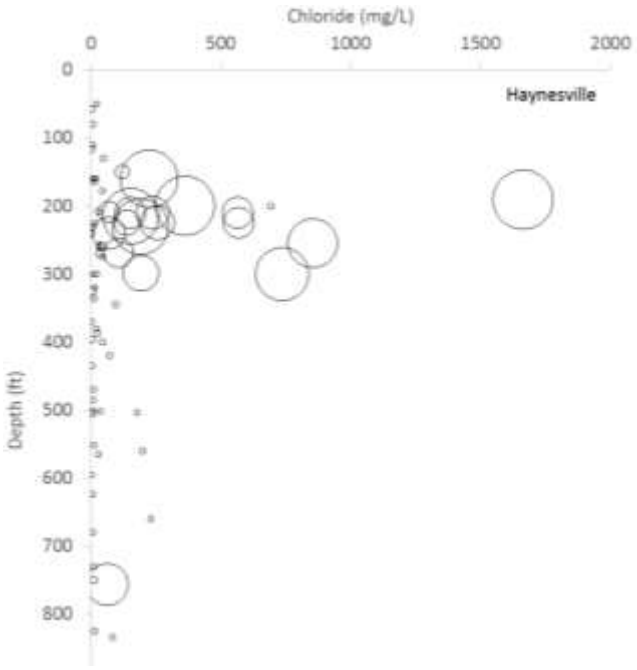

Note: circle size proportional to methane concentrations; all data points with CH_4<0.2 mg/L are plotted as 0.2 mg/L to improve visibility, maximum methane concentration is 33 mg/L
70 dissolved methane water samples.

Figure 36. Chloride concentration vs. depth vs. dissolved methane (Haynesville)

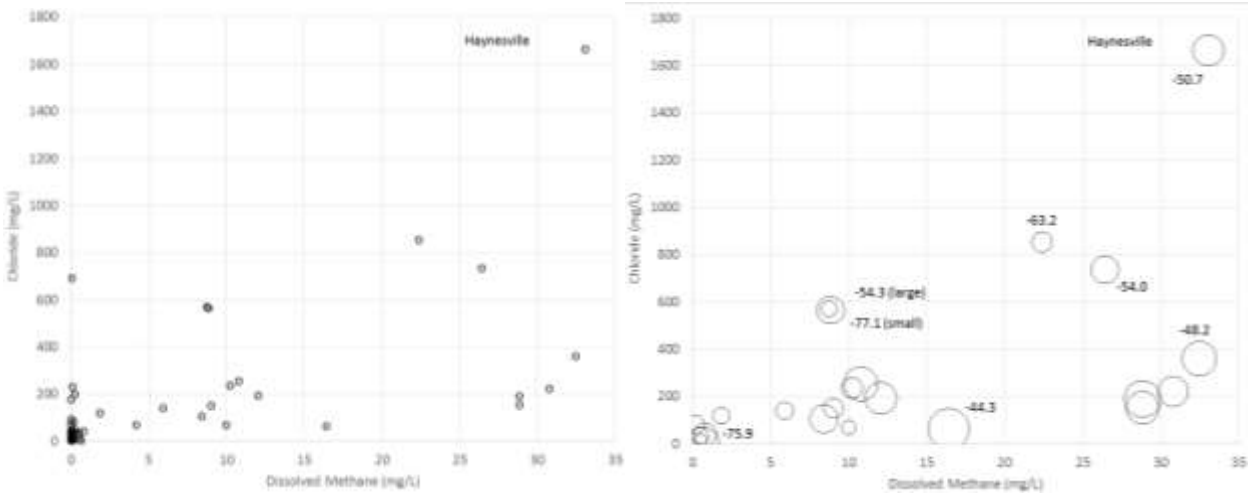

(a) (b)

Note: circle size in (b) proportional to methane $\delta^{13}C$; minimum and maximum values are -75.9 and -44.3

Figure 37. Dissolved methane vs. chloride concentrations (Haynesville)

There is a better correlation between chloride and dissolved methane.

IV-3-2.3 Discussion

The dissolved methane spatial distribution suggests a strong association with the Mount Enterprise Fault system (Figure 38). Plotting of methane concentration vs. distance (Figure 39) confirms quantitatively the association with the highest concentrations closest to the fault zone (distances were calculated as the shortest distance between the sampling point and any of the

individual fault of the system). The samples with the highest thermogenic signal are also the closest to the faults. This fault system has been described in many publications (e.g., Jackson, 1982; Pearson et al., 2012). Dornfeld (2012) and Dornfeld et al. (2012) in a study in Rusk County (just west of Panola County) also suggested that the Mount Enterprise Fault may transmit gas / fluids. The origin of the fault zone is still not well understood but is probably not related to the important salt activity of the East Texas Basin to the west (Jackson, 1982; Dornfeld, 2012) and rather associated with regional basement tectonics related to the Laramide orogeny (Adams, 2009). The fault system has an overall downthrow to the north unlike most fault systems in the Gulf Coast with a downthrow to the Gulf. Other authors have associated the fault system with fluid flow. Reiner and Crocker (1990) described a change in the chemical composition of aquifer water next to the fault in Rusk County. Oliver and Lupton (2013, Fig. 16) also show an increase in TDS in southern Panola County in the vicinity of Gary City (similar to our Figure 37).

Short Conclusion: biogenic methane and methane originating from the Wilcox (not the Haynesville), traveling to aquifers through the Mount Enterprise Faults and being biodegraded.

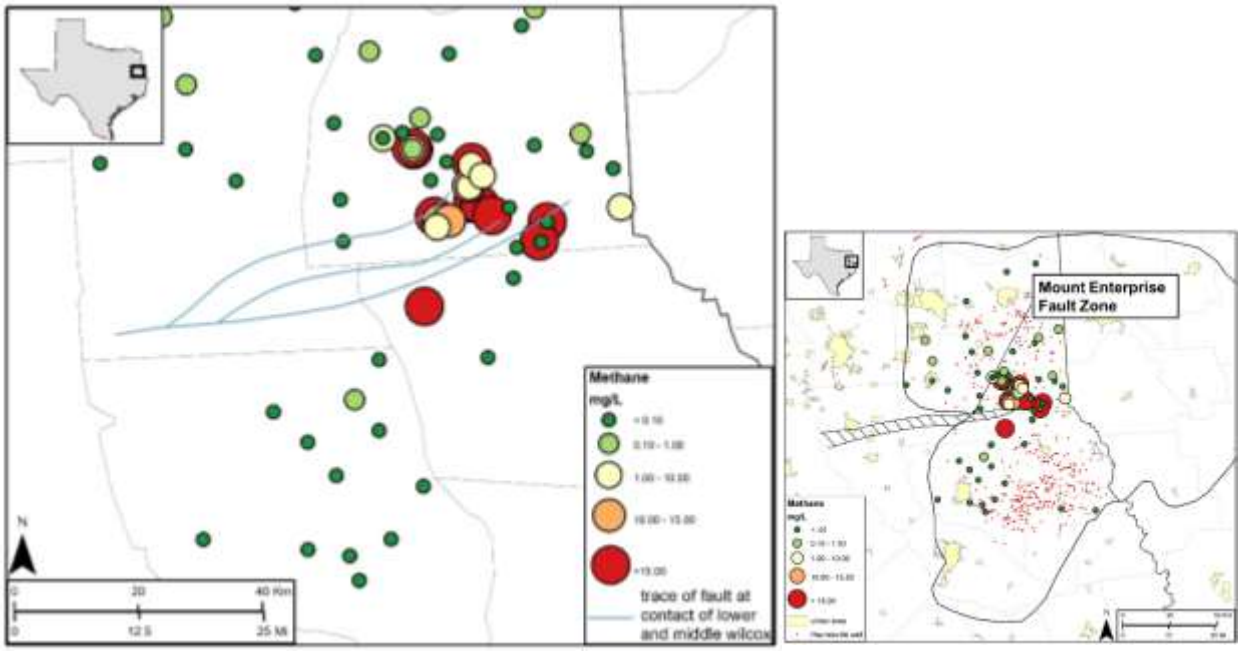

Note: fault trace from Kaiser (1990)

Figure 38. Dissolved methane with a focus on the Panola-Shelby county line (Haynesville)

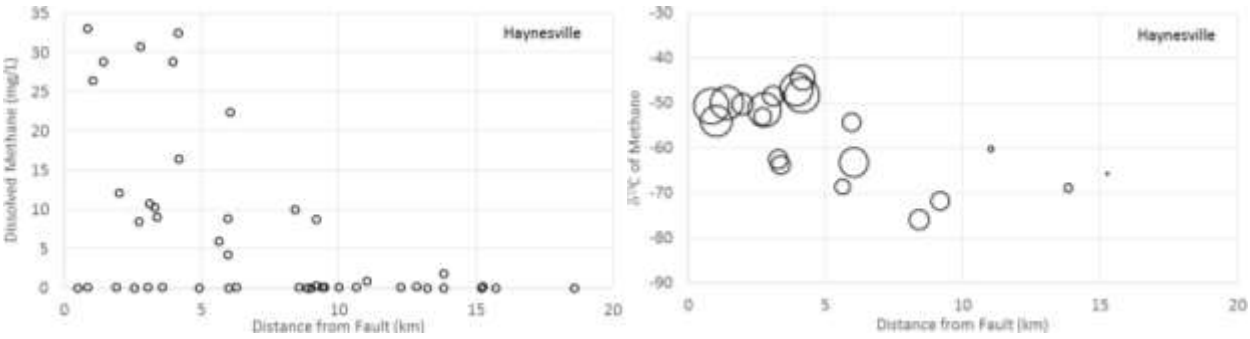

Figure 39. Methane concentration and $\delta^{13}C$ as a function of distance to Mount Enterprise Fault system (Haynesville).

IV-3-3 Eagle Ford Footprint

Eagle Ford activity started in 2008 (Scanlon et al., 2014a,b; Nicot et al., 2013a) and the play is still very active today. Unlike the Haynesville and the Barnett (although the latter contains a condensate section), the Eagle Ford is a gas and oil play which initially produced gas before operators move updip to the oil window to produce oil and condensate. The east and west sections of the Eagle Ford Shale have somewhat different production characteristics (Scanlon et al., 2014). In this study we focused on the eastern section of the Eagle Ford.

IV-3-3.1 Play Characteristics

The Eagle Ford shale is a calcareous mudstone of Cretaceous age present in South Texas. The area geology (Figure 40) consists mostly of Cenozoic age formations with a NE-SW strike and dipping to the Gulf of Mexico with increasing thickness.

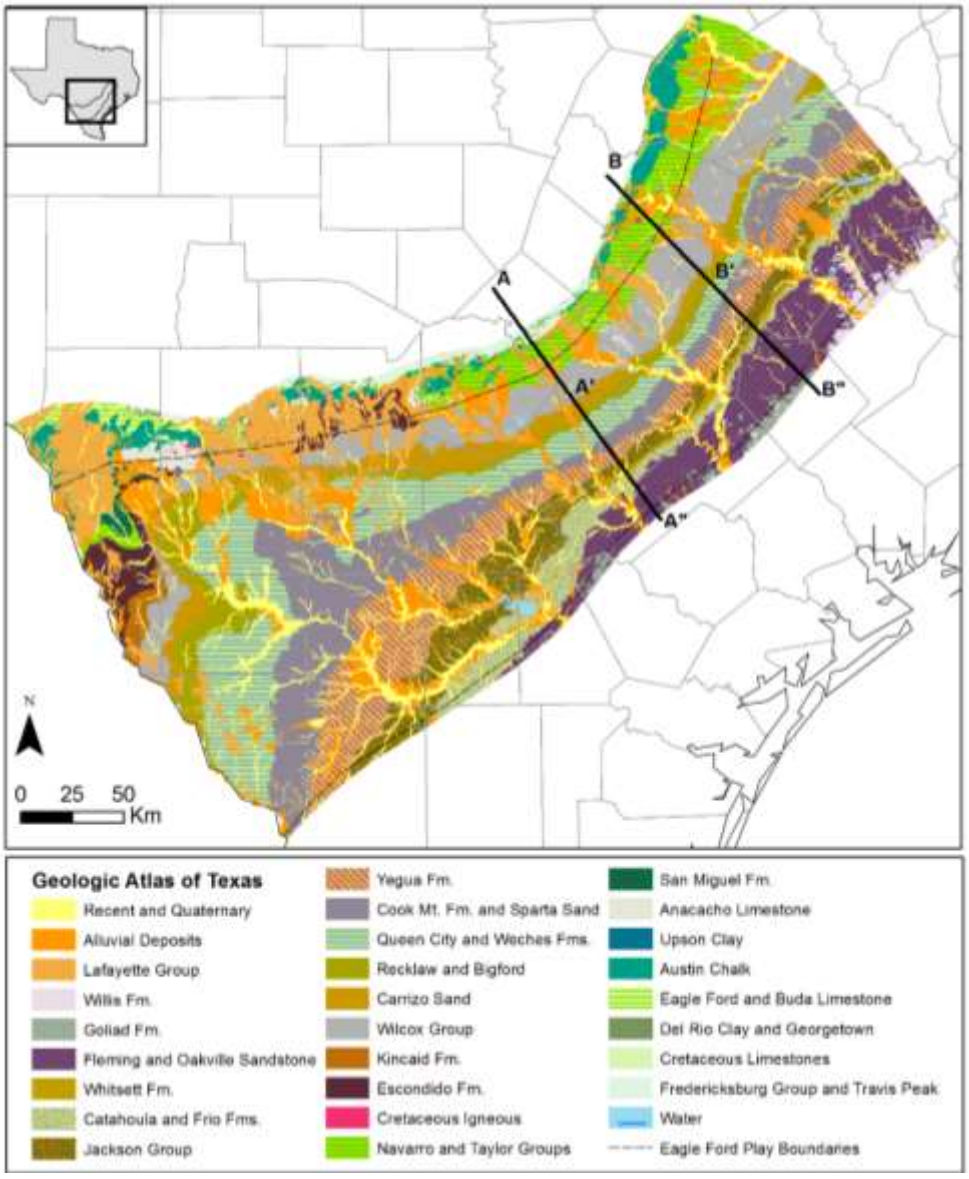

Figure 40. Surficial geology in the Eagle Ford footprint

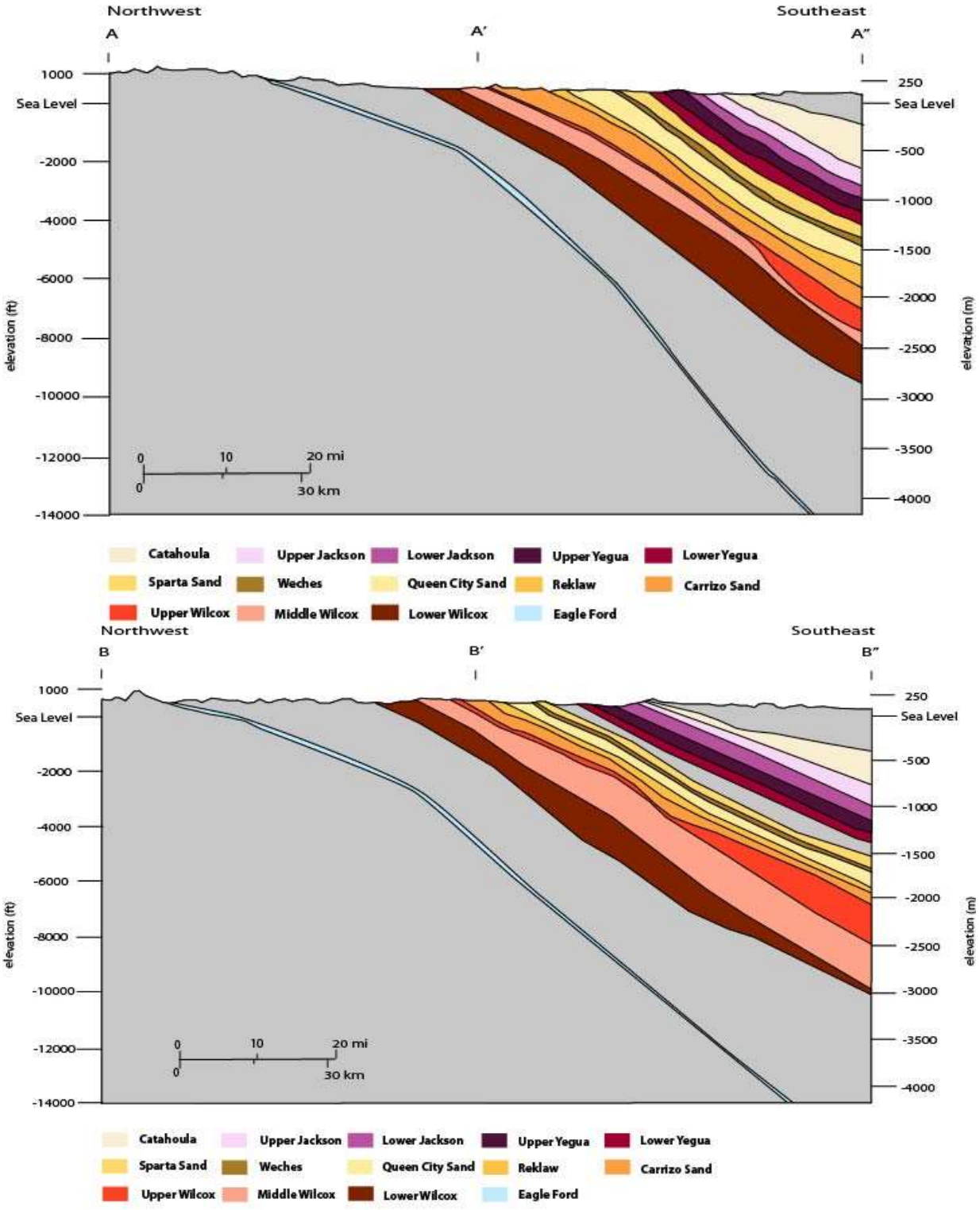

Figure 41. Cross-sections of the Eagle Ford Shale footprint

Shallow subsurface: There are several sandy aquifers separated by shales or clayey layers. They are from the oldest to the youngest: Wilcox, Carrizo, Queen City, Sparta, Yegua, Jackson, and finally Oakville / Jasper, the first aquifer of the Gulf Coast Aquifer System. They are described

in several TWDB reports (Chowdhury et al., 2004; Kelley et al., 2004; Deeds et al., 2010; and references therein).

Presence of Faults: The Gulf Coast basin is impacted by many faults, many listric or growth faults rooted deep in the basin and attenuated within the sediment package with no expression at the surface. The Wilcox fault zone belongs to this group. It was active during Wilcox sedimentation as evidenced by greater sediment thickness on the downthrow side but has been reactivated multiple times.

Natural sources of thermogenic methane: the main source of thermogenic gas is the Eagle ford. There are also younger formations of Eocene age located downdip that could contribute as well as older formations such as the Pearsall Shale (Cretaceous) or the local equivalent to the Haynesville Shale (Jurassic). The Wilcox Fm. also contains abundant lignite resources (Kaiser, 1978; Ayers and Lewis, 1985).

IV-3-3.2 Results

A total of 118 samples were taken in Eagle Ford shale footprint, mostly in its eastern section (Figure 42 and Figure 43). Methane-rich water samples line up along strike along the Wilson-Karnes and Gonzales-Dewitt county lines as most structural features do complicating somewhat the interpretation of the results. In addition, the samples present very little of a thermogenic signature (Figure 44). There is very little C2+ in the sampled gas which is puzzling and not consistent with an origin from the oil and condensate-rich Eagle Ford. Ethane would be impacting the fresh water zones, as it does in the Haynesville with a much drier source. The most likely explanation is that the gas is mostly microbial and evolves to exhibit a thermogenic isotopic signature or originates from the deep lignite beds of the Wilcox. The presence of C2+ alkanes can be explained by this small thermogenic contribution.

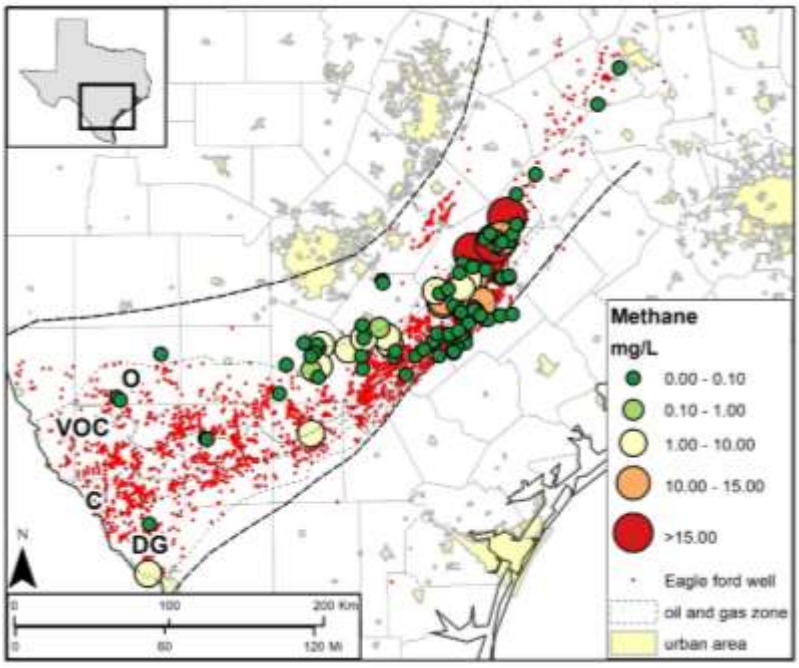

Note: O: oil, VOC: volatile oil, C: condensate, and DG: dry gas zones; source: Scanlon et al., 2014

Figure 42. Spatial distribution of dissolved methane concentration in aquifers (Eagle Ford)

Methane is present at all depths (Figure 45) and becomes slightly lighter at shallower depths (keeping in mind that the amount sampled from depth is only semi-quantitative because of the sampling methodology at ~atmospheric pressure; at these depths saturated methane concentrations are much higher). The relatively consistent isotopic signature suggests communication between the various aquifers or a common carbon source feeding the various aquifers.

As we observed in the Haynesville Shale, high methane concentrations are correlated with lower sulfate (Figure 46a and Figure 47) and higher chloride (Figure 46b and Figure 48) suggesting active sulfate reduction and imprint of brines.

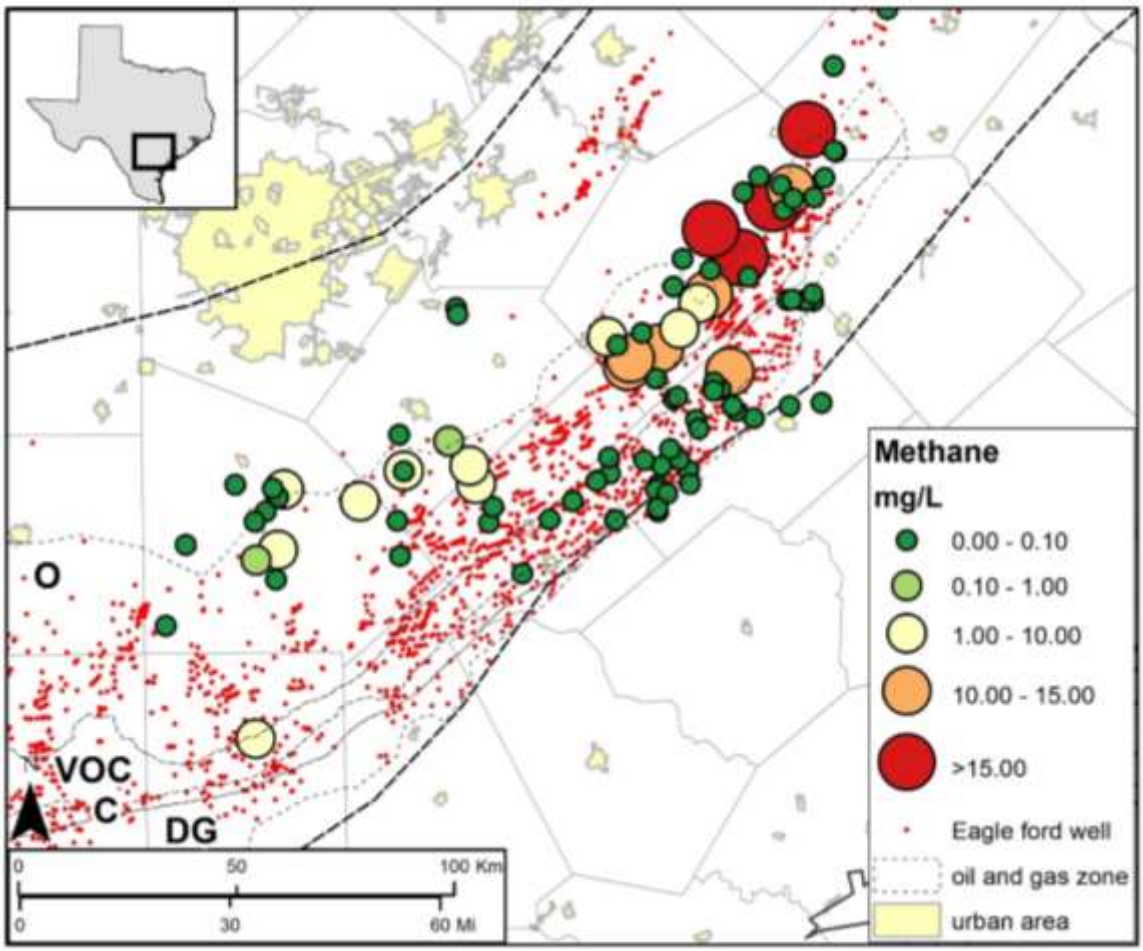

Note: O: oil, VOC: volatile oil, C: condensate, and DG: dry gas zones; source: Scanlon et al., 2014

Figure 43. Spatial distribution of dissolved methane concentration in aquifers (Eagle Ford with a focus on the Eastern section)

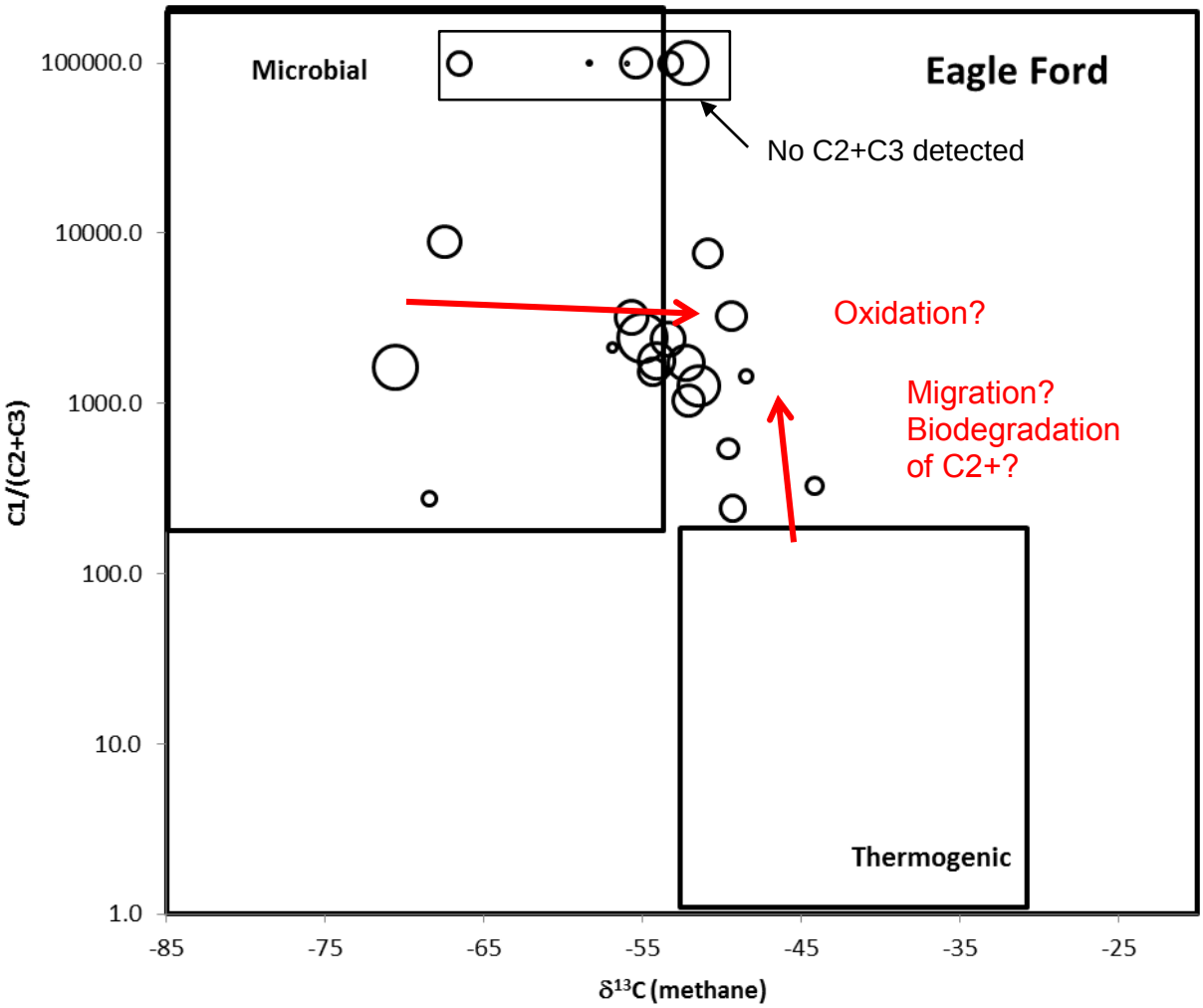

Note: size of the circle correlates to the concentration of dissolved methane

Figure 44. Bernard plot showing methane C isotope vs. ratio of methane, ethane and propane (C1/C2+C3) (Eagle Ford).

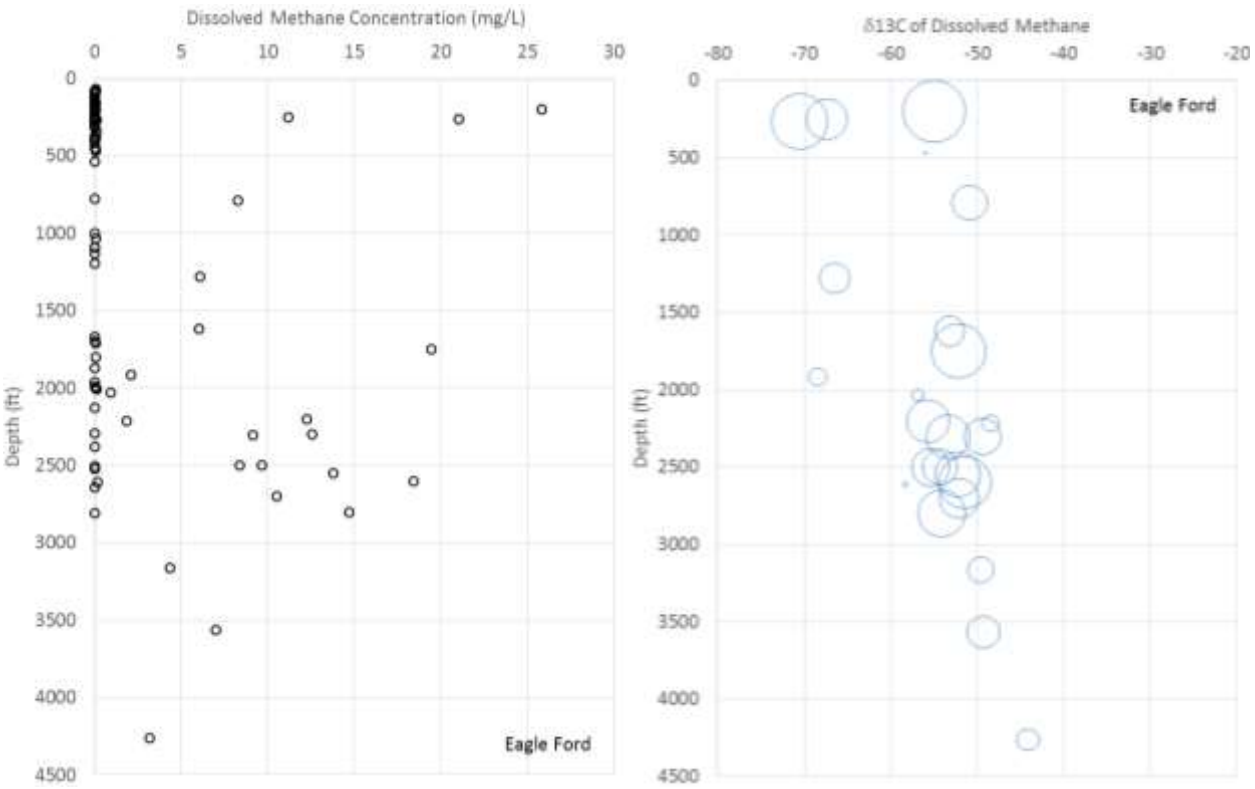

(a) (b)

Note: circle size proportional to methane concentrations; maximum methane concentration is 26 mg/L (EF152), this well is an irrigation well listed with a depth of 200 ft (problematic? It could also corresponds to a contamination case)

(a) 110 dissolved methane water samples including (b) 24 with isotope analyses;.

Figure 45. Dissolved methane concentration and its $\delta^{13}C$ as a function of depth (Eagle Ford)

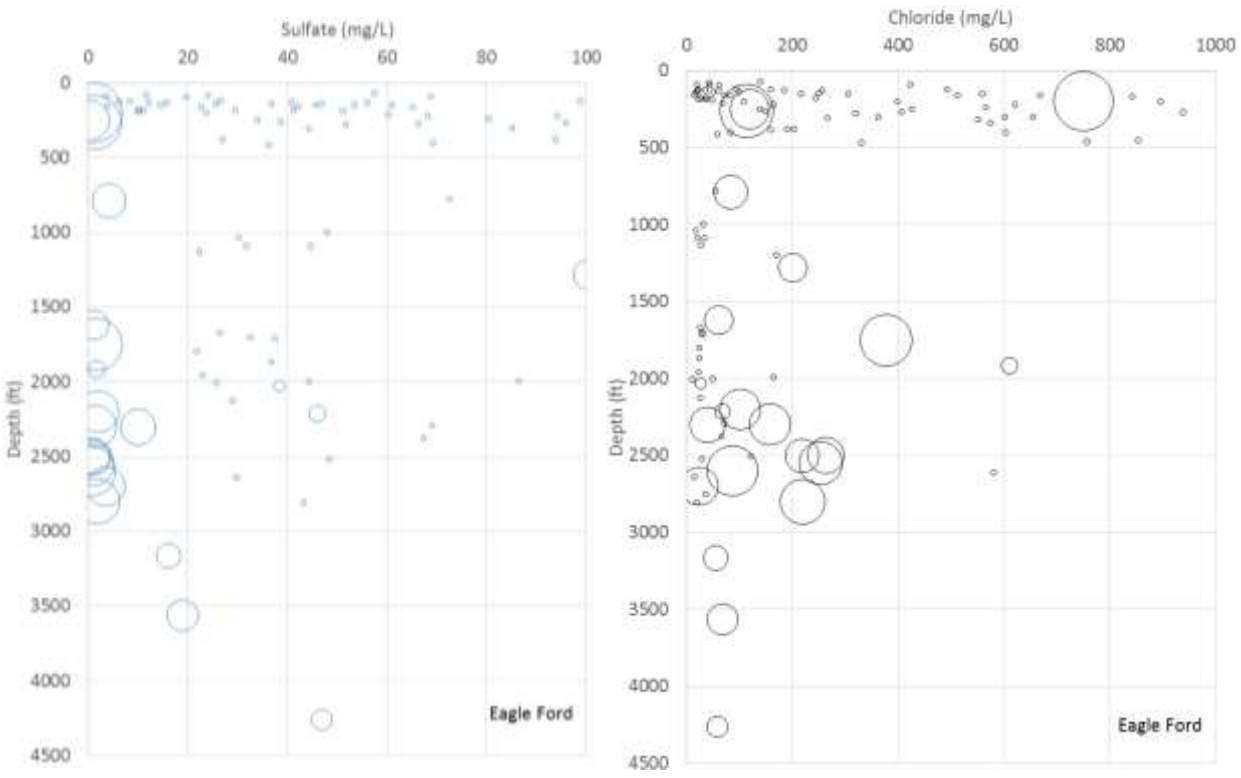

Note: circle size proportional to methane concentrations; all data points with CH_4<0.2 mg/L are plotted as 0.2 mg/L to improve visibility, maximum methane concentration is 26 mg/L
110 dissolved methane water samples.

Figure 46. Sulfate and chloride concentration vs. depth vs. dissolved methane (Eagle Ford)

IV-3-3.1 Discussion

The interesting aspect of the Eagle Ford play results is that no sample shows a clear thermogenic signature, even at depth. Our data points do not cover the play evenly and many are within or close to the gas window. Composition of the Eagle Ford gas was not obtained specifically for this study but it is described in Harrington et al. (2015) from 27 samples taken in the oil window where Frio, Atascosa, McMullen, and Zavala counties meet in the western section of the Eagle Ford. As expected, the gas is wet with a C1/C2+ ratio between 0.3 and 9 and a $\delta^{13}C$ ranging from -48 to -36‰. The current sample distribution suggests that at least two processes could be at play: (1) selective biodegradation of ethane and other C2+ alkanes along with thermogenic methane (lignite), moving the gas composition to the dry end member and to the top of the plot and/or (2) consumption of biogenic methane translating into a heavier $\delta^{13}C$ signature. The presence of biogenic sometimes at great depth is not inconsistent with known behavior of the Wilcox fault zone. Throughout geological times, it has pulsed hydrocarbons coming from various reservoirs at depth that have been recognized at the source of the reducing conditions responsible for the numerous uranium roll-front deposits in the area (south Texas uranium province (Figure 49), see Nicot et al., 2010, and references therein but in particular Galloway, 1982, and Galloway et al., 1982). However, the high-methane band is slightly updip of the Wilcox Fault zone and matches the location of the Karnes Trough, a major structural feature updip of and parallel to the Wilcox Fault zone. The Austin Chalk, an oil reservoir directly overlying the Eagle Ford, is more fractured in the Karnes Trough (Martin et al., 2010) leading to

more oil secondary migration from the Eagle Ford Shale, recognized as the source rock for the chalk. The next structural feature updip of the Wilcox fault zone and Karnes through is the Fashing Karnes trough fault zone which penetrates at least to the top of the Wilcox (Ewing, 20). Although the extent of our dataset is limited, high methane concentrations seem to be updip of and follow the Karnes Trough. Austin Chalk oil resources are the most abundant there (Martin et al., 2011)

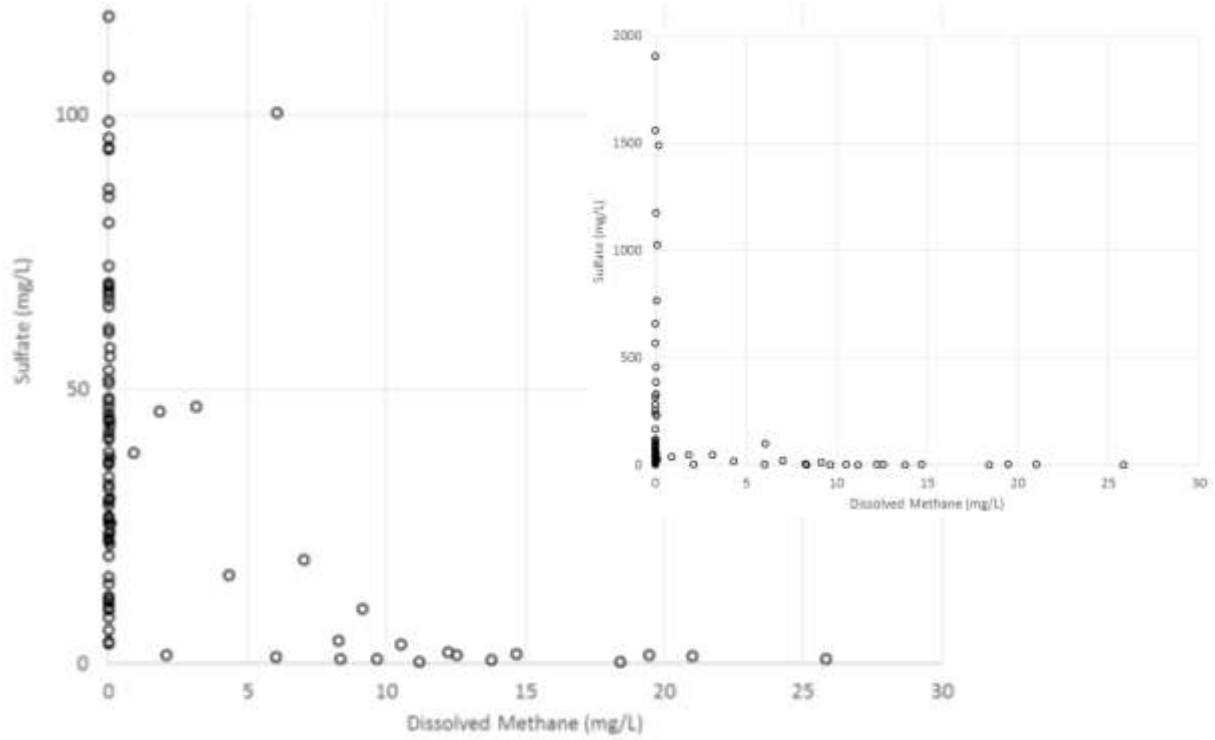

Note: the insert y-axis goes to 2000 mg/L

Figure 47. Dissolved methane vs. sulfate concentrations (Eagle Ford)

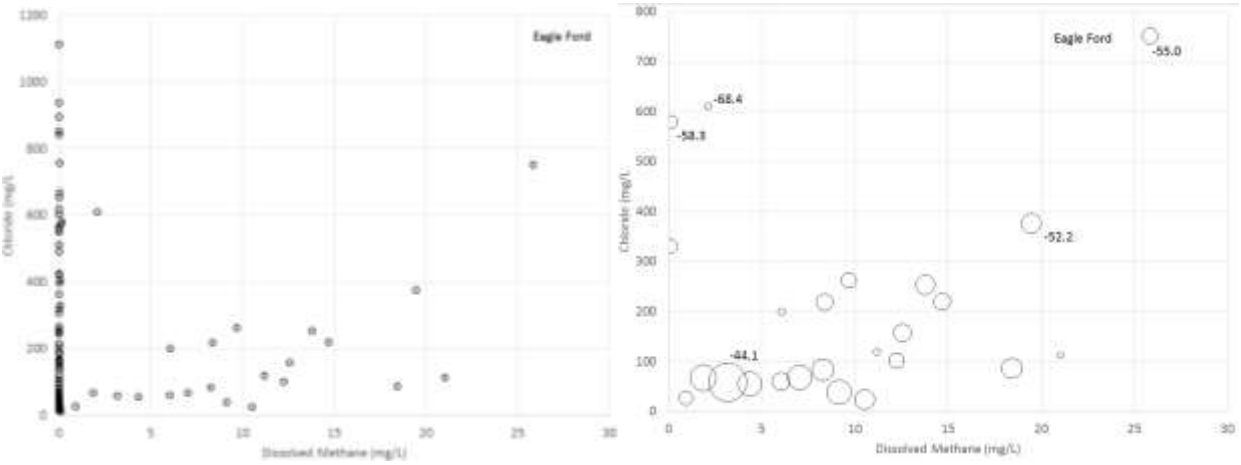

Note: circle size in (b) proportional to methane $\delta^{13}C$; minimum and maximum values are -70.6 and -44.1

Figure 48. Dissolved methane vs. chloride concentrations (Eagle Ford)

Short Conclusion: mostly biogenic methane showing some biodegradation characteristics and possibly originating from the degradation of oil leaking from deeper deposits through vertical features (faults or fractures) combined with some thermogenic methane originating from the lignite beds.

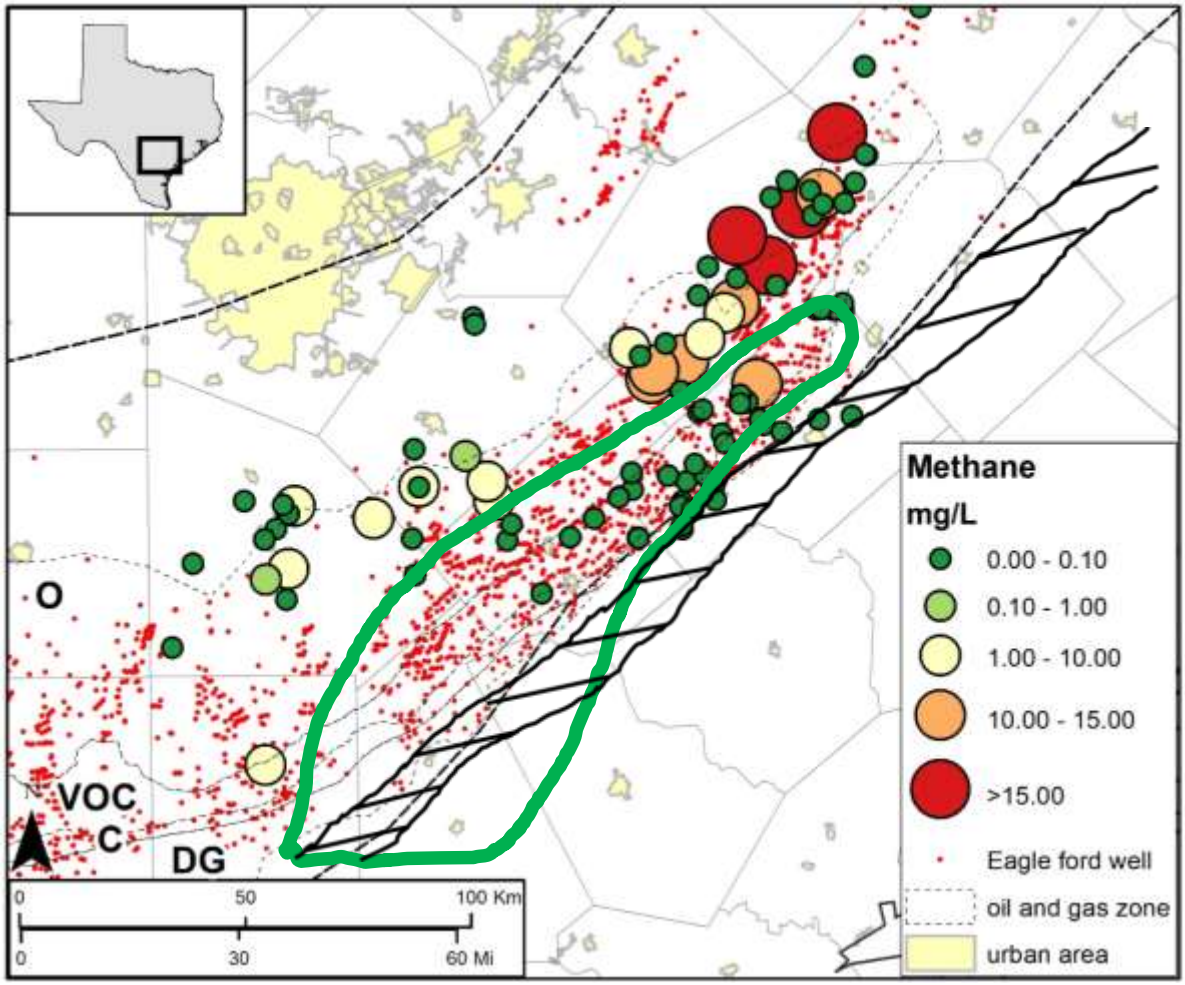

Note: uranium province is highlighted in green whereas the Wilcox fault zone is cross-hatched.

Figure 49. Structural features and Eagle Ford water samples (Eastern section)

IV-3-4 Delaware Basin

See Appendix H: Hydrogeology over Oilfield Operations in Loving County, Texas.

IV-4. Parker County Area

IV-4-1 Historical Background and Previous Studies

Since HF has captured the public interest a few years ago, a few HF-related cases have been highly publicized: Dimock in Susquehanna County, PA, Pavillion in Fremont County, WY (DiGiulio et al., 2011; Wright et al., 2012), and Range Resources in Parker County in TX (Figure 50). The latter has been in the news since Mr. Lipsky and other well owners sued RRC. Expert evaluation and counter-evaluation that followed are a source of information for this study. Drs. Kornacki and McCaffrey, expert geochemists, and Dr. Kreitler, expert hydrogeologist, have presented their findings and position in several presentations, abstracts, and reports (e.g., Kornacki and McCaffrey, 2011; Kreitler, 20102; Kornacki and McCaffrey, 2014; Kreitler, 2014). They assert (1) that the shallow gas is thermogenic; (2) that its N_2 content suggests a Strawn rather than a Barnett origin; and (3) water wells tapping the Trinity Aquifer as opposed to the Strawn show evidence of methane biodegradation. Kornacki and McCaffrey (2014) also commented that biodegradation of dissolved gas is evidenced in some wells by an increase through time of the C1/C2 and C1/C3 ratios (microbes favoring C2+ over methane) as well as an isotopic shift towards heavier methane molecules ($\delta^{13}C$ increases because microbes will process lighter molecules first enriching the dissolved gas in heavier isotopes). They described two along-strike NE-SW trending zones: one including Mr. Lipsky's well, showing little biodegradation, the other zone to the southeast with a significant biodegradation signal (Kornacki and McCaffrey, 2014, p.21) (Figure 50). In addition, they observed changes in composition in some wells through time that they attributed to continued biodegradation or to pulses of "fresh" gas. They explained the zonation by the nature of the underlying Paleozoic rocks. More permeable layers allow pulses to dilute biodegraded gas. Dr. Kreitler also asserted that there is anecdotal evidence that significant water level drop following heavy pumping due to new subdivision development could have depressurized the aquifer and mobilized the methane and other gases. It could have also led to an increase in salinity because of the increasing amount of water being drawn from the saltier Strawn Fm. In this current study we do not try to reproduce their findings but we broaden the spatial scope of the analysis.

RRC (2014) summarizes data collected in the context of the Range Resources lawsuit, first in December 2010 then quarterly (Aug. 2011, May 2012, Aug. 2012, Nov.-Dec. 2012, Feb. 2013). Observed methane concentrations from the Range Resources sampling are in general relatively low. In particular, the sampling after the initial complaint with a maximum value of 2.8 mg/L (Purdue well) is puzzling especially when some wells are described as bubbling. Sampling events by other group (EPA, Duke University, this study) show higher concentrations compatible with historical field observations such as bubbling wells and methane fluxes high enough to keep a flame steady which are more compatible with the general narrative by the Range Resources team. They seem to have used the direct fill method combined with a low-flow sampling. A possible explanation for the relatively low concentrations is some gas loss occurring during sampling as suggested by the higher ethane concentrations relative to methane when compared to the sampling performed during this current study. A correlative conclusion is that there would be

no actual overall increase in dissolved methane concentration through time as asserted in RRC (2014).

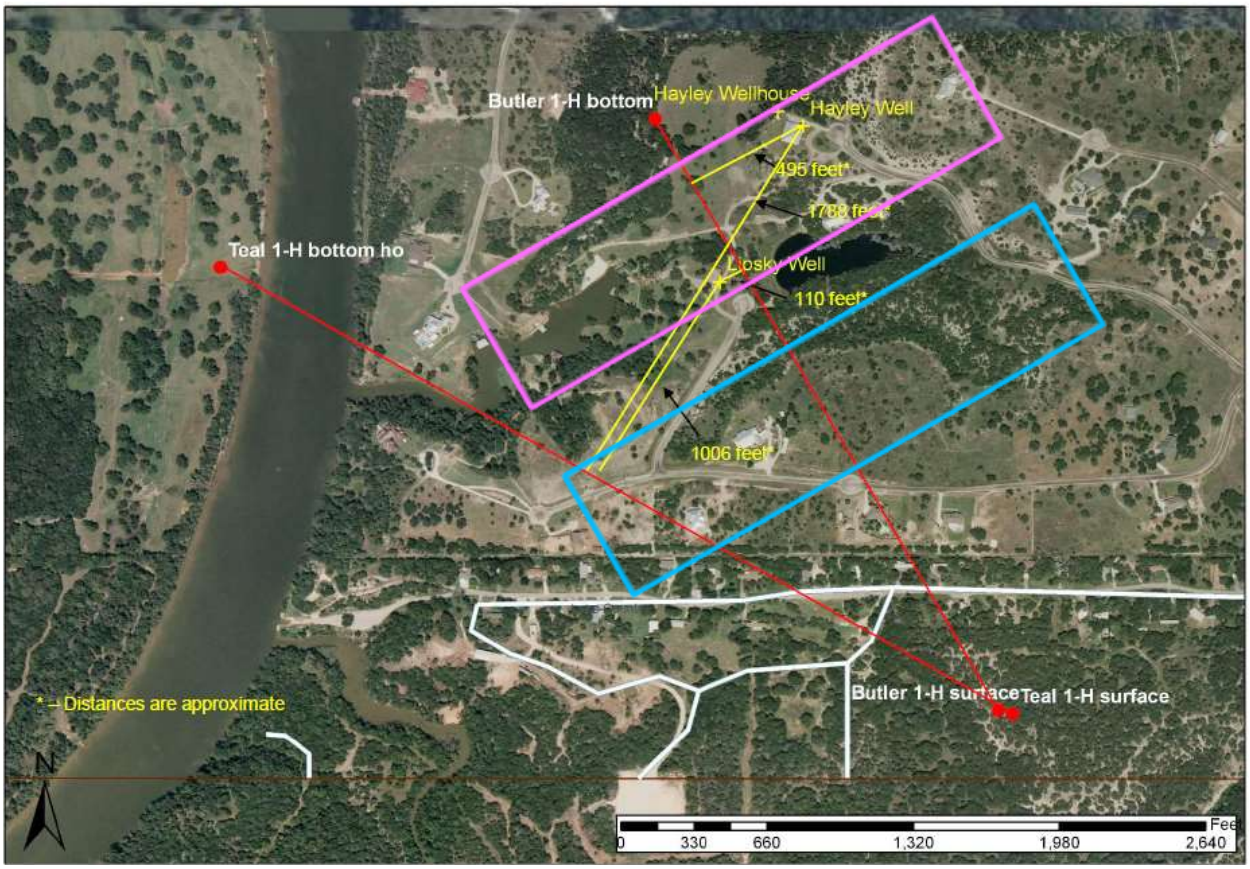

Source: EPA Region 6 file. "Parker County" Range Resources Case: Vol.1 Dec 13, 2010. Map provided by the Range Resources team.
Note: The two contaminated water wells owned by Mr. Lipsky (sampled during this study) are shown. The so-called "Hurst" well now owned by Ms. and Mr. Hayley is also shown (not sampled). This latter well drilled in 2005 is documented as having high dissolved methane concentration at drilling time. The approximate trace of the 2 gas wells (Teal and Butler) is also shown.
Note: also shown are Kornacki and McCaffrey (2014)'s zones with biodegradation (blue) and with little biodegradation (pink).

Figure 50. Location map of the oil and gas and water wells at the center of the Range Resources case

IV-4-2 Area Geography and Geology

In the next subsections, we describe geographic and geologic features of importance to this study.

IV-4-2.1 Cultural Features

Surface contamination from historical oil and gas production or abandoned wells could explain some of the methane. However, the recent EPA report (EPA, 2015a) does not show recent spills in Parker and Hood counties. Pipeline and gathering lines could also be a direct source of thermogenic gas, however none exist in the vicinity of the Parker-Hood cluster (Figure 51).

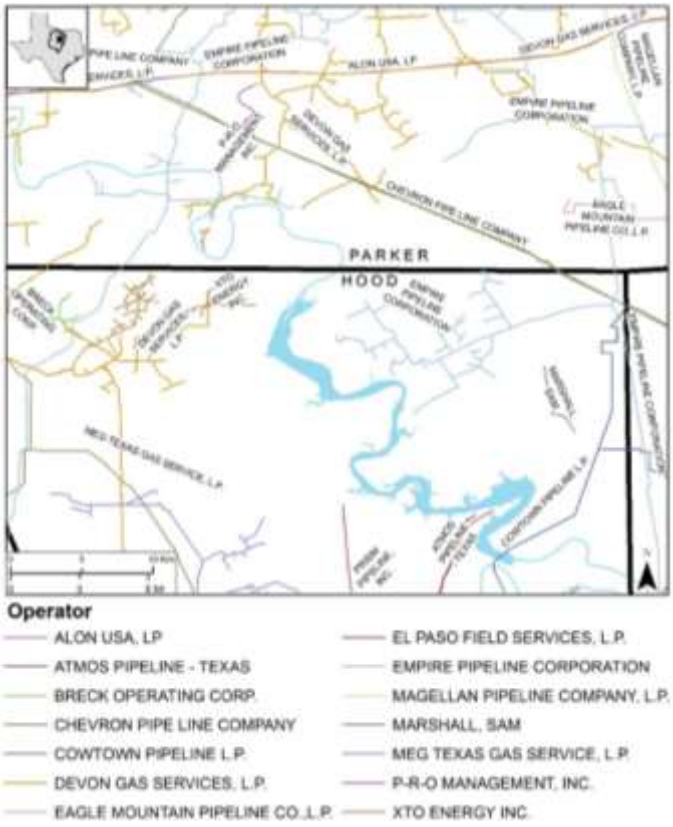

Source: RRC data for purchase: http://www.rrc.state.tx.us/about-us/resource-center/research/data-sets-available-for-purchase/pipeline-data/ (purchased on or before 2013)

Figure 51. Gathering lines in the area of interest.

IV-4-2.2 Surficial Features

Springs: Springs and stream baseflow could be good integrators of average subsurface concentration as any flow lines converge to a single or few locations. Sampling springs is not an uncommon approach and USGS did some experiments and stream measurements that observed the persistence of methane in stream water (Heilweil et al., 2013; Heilweil et al., 2015). The proximity of a gaining and relatively large river (Brazos River) to several high groundwater methane measurements make the Parker County area attractive for such a test, which was discussed but not attempted. Stramel (1951) mentioned the presence of numerous seeps along the Brazos River in Parker County but they have to have mostly disappeared thanks to the historical water level decrease.

Similarly we tentatively looked for springs or seeps along the river as it crosses the high-methane area. There are at least two major bodies of work cataloguing springs in Texas: Brune (2002) and Heitmuller and Reece (2003). The ~35 springs documented in Brune (2002) are mostly small (<0.28cfs in 1980 and did not seem active as seen in recent GoogleEarth images (many could have gone dry after the original settlement of the area in the 19th century). Brune (1975) listed only the "important" springs. Hood and Parker counties each had one but they were described as flooded by Granbury Lake and dry, respectively. The GAM model (Harden et al., 2004) reinforces this point as it did not explicitly include springs but rolled them into the evapotranspiration fluxes.

IV-4-2.3 Geology

The geology of the Parker County area is similar to the rest of the Barnett footprint: a Cretaceous veneer on top of a thick Pennsylvanian sedimentary package that crops out farther to the west. Some of the easternmost outcrops in the region are exposed on the LHS of Figure 52 (Plb, Pkf, Pdb, and Pu, representing the base of the Upper Strawn, i.e., Lazy Bend and other formations). Then starting from the LHS and from the oldest Cretaceous formation in the area: Twin Mountains Fm. (Ktm), Glenrose limestone (Kgr), Paluxy Fm. (Kpa), together forming the Trinity Group partially covered by Quaternary alluvium (Qal) and terrace deposits (Qt), especially in the Brazos River floodplain, and other Quaternary sediments (Qu) and then to the east the base of the Fredericksburg Group (Kgl, Ked, Kdc). Cretaceous layers dip slightly to the east and create small escarpments, bluffs, and mesas. Note that the only aquifer in the area of interest is in the Twin Mountains Fm. (sometimes called Travis Peak Fm.), the Paluxy aquifer is too far to the east and the Glenrose Limestone is an aquitard if part of the vadose zone. Note too that the Twin Mountains aquifer is at least partially confined in the area by the Glenrose and that it can exchange water with the Brazos River (gaining / losing depending on Lake Granbury levels).

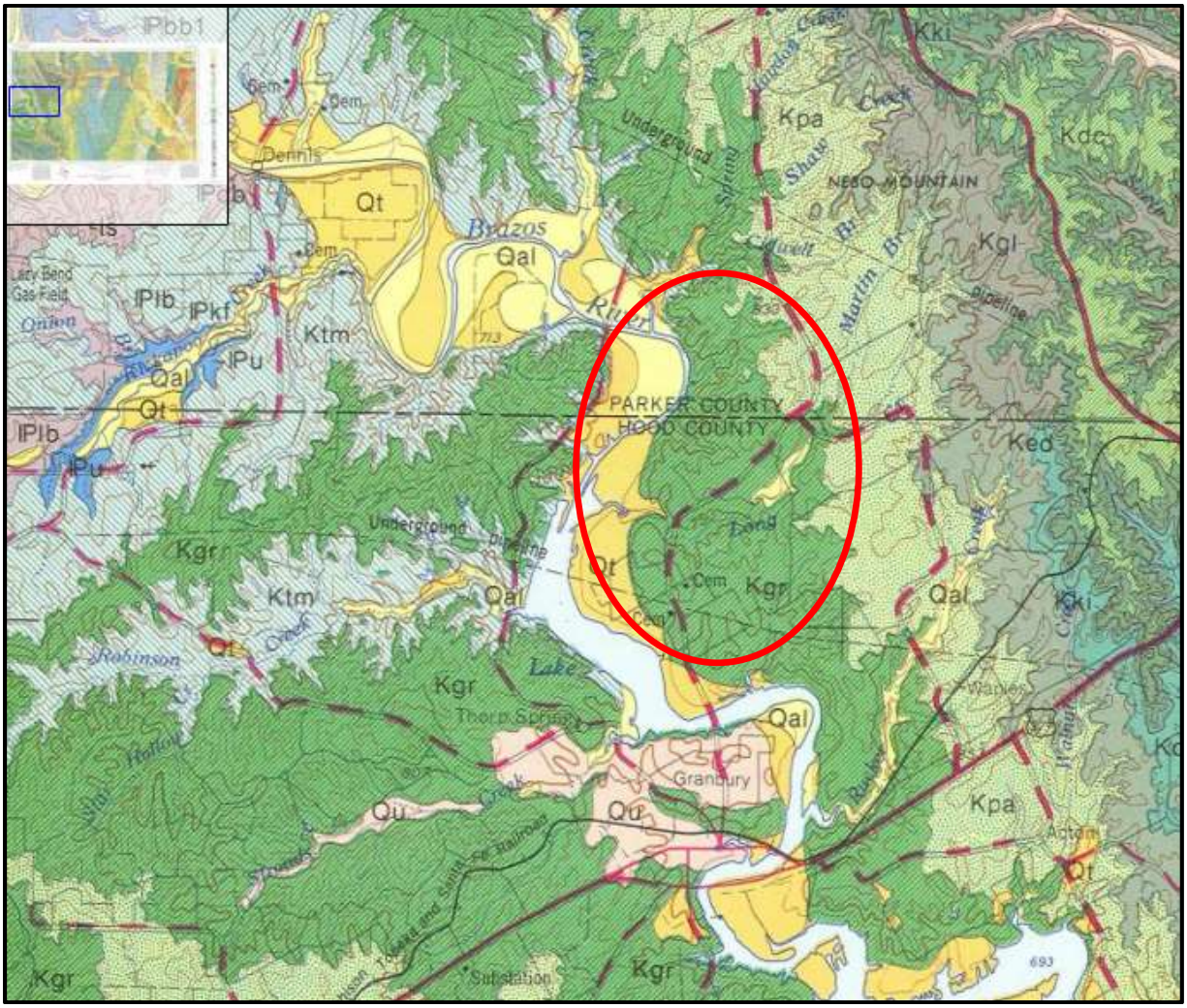

Note: red circle encloses the Parker-Hood cluster. Continuous and dotted red lines represent major roads

Figure 52. Excerpts of Dallas GAT Sheet

By choice, we did not try to reconstruct and better understand the Strawn depositional systems in Parker and Hood counties but, instead, relied on published documents. To our knowledge there is no synthetic study documenting Strawn rocks in Parker and Hood counties. Two large Strawn outcropping areas are known: one along the Brazos River just west of Parker County, mostly Upper Strawn, and another one along the Colorado River, a few counties to the south, mostly Lower Strawn. The Strawn is also known by multiple papers documenting oil and gas fields underneath the Cretaceous unconformity. No doubt that a lot more is known but not in the public domain.

Upper Strawn: In the 1970-80's, Drs. Erxleben and Cleaves studied the paleogeography of the Strawn (oldest), Canyon, and Cisco (youngest) groups where they crop out in the Brazos River Valley, mostly west of the study area , that is, where the Trinity Fm. does not exist. The Pennsylvanian formations trend NNE-SSW to NE-SW at a large scale as indicated by the GAT sheets but the grain of the depositional systems in Parker–Hood counties is mostly EW following the regional topography at the time of deposition (Ouichita Mountains to the east). Erxleben and Cleaves (1985, Fig.5) and Cleaves and Erxleben (1985, Figs.5 and 8) give an overview the paleogeography of the Upper Strawn: elongate fluvio-deltaic centers ("sand") with strandplain-embayment areas in between (mud or "shales"). Cleaves and Erxleben (1985, Fig.13) show 8 separate cycles in Palo Pinto and Wise counties as well as other counties to the west and north deposited during the Upper Strawn. Their work suggests that the neighboring Parker county shows, in the Upper Strawn, similar depositional history with EW to NW-SE trending fluvial channels embedded in a shale matrix.

Lower Strawn: Lower Strawn (Kickapoo Creek Fm.) is not well exposed and outcrops are relatively small. Keyes (1983) and Trice and Grayson (1985) described the Lower Strawn where it crops out in San Saba and Mills Counties. There, they interpreted it to consist mostly of marine deposits (turbidites) that transition to the fluvio-deltaic environments of the Upper Strawn, sediments similar to those observed by Cleaves and Erxleben in the Brazos Valley in Palo Pinto County. The Lower Strawn is fed by deltaic material to east and north ultimately originating from the Ouichita Mountains and thins out quickly to the west Trice and Grayson (1985, p.201). Local studies such as in southeast Parker County show deltaic environments at the top of the Lower Strawn (Ehlmann and Ehlmann, 1985). Shelf carbonates have also been described in the Lower Strawn but further to the West and North in Parker County, not in the vicinity of the Parker-Hood cluster.

Herkommer and Denke (1982) published a map of Strawn formations subcrop in Parker County (Figure 53). From these observations it is logical to infer that the Parker-Hood cluster is included in Upper Lower Strawn Creek Kickapoo Fm. with depositional systems still very shaly but with deltaic or strandplain sand lenses that act as reservoirs. Oil and gas traps may be generated by transitioning to a finer material or by a reduction in permeability of the reservoir sandstone / siltstone.

Coal Seams: Deltaic environments are well-suited to deposition of coal material and several coal seams have been observed and mined in the Upper Strawn. For example, coal beds have been observed in the Lazy Bend Fm. (Upper Strawn). Bituminous coal has been mined in northern Erath and southern Palo Pinto Counties, 20 miles to the west of the Parker-Hood cluster, ("Thurber coal", 12 to 30 inch thick seam) in the Mingus Fm. (Upper Strawn) (Evans, 1974, p.8) deposited in delta-plain deposits (marshes) covered by delta progradation. The Grindstone Creek and Brazos River Fms. also described outcropping coal seams (Evans, 1974, p.8). A possible

extension to the Thurber coal has been recognized in Wise and Jack counties at a depth 1,400 to 1,500 ft below the top of the Strawn (Mapel, 1964, D9). The recognized extent of bituminous coal extends to the north to Palo Pinto, Jack and Wise counties including northwest Parker County but not the Parker-Hood cluster area. Coal has also been encountered in water wells in Parker County (various water driller logs). Coal has also been described in the Atokan below the Strawn (Mapel, 1964, p.D6-D8) mostly in Wise and Denton Counties where the Atoka is several thousand ft thick. When present there, coal seams are more than 4000 ft deep.

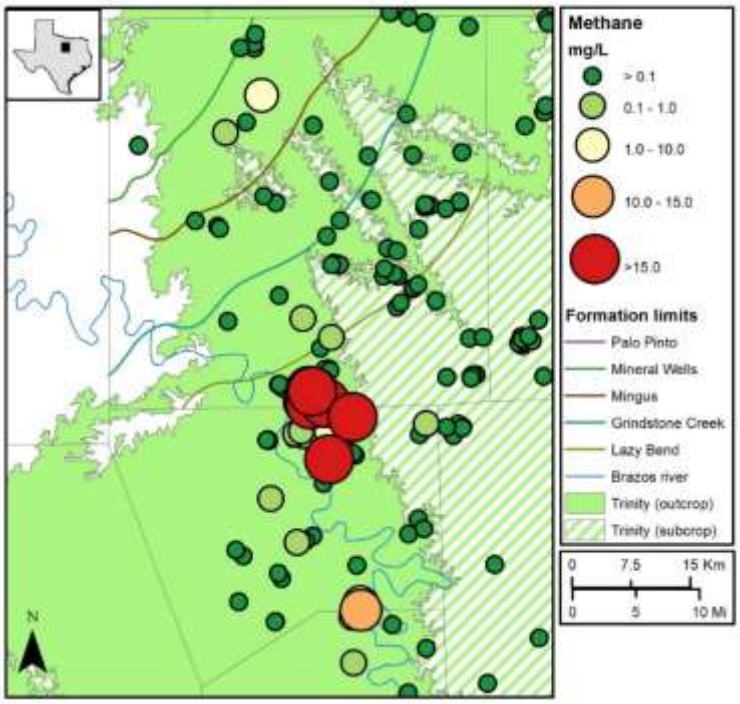

Note: limits shown represent the base of the formation

Figure 53. Strawn subcrop of Parker County with dissolved methane data

Cretaceous: The geology of the Cretaceous has been described in many documents and reports including recently in Intera, 2014 and US EPA. 2015c. In Parker County, the clastic Twin Mountains Fm. directly overlies the Paleozoic formations and is used as a local aquifer. Another aquifer residing in the also clastic Paluxy Fm. overlies the intervening Glenrose limestone considered an aquitard. These three formations form the Trinity Group that holds the Trinity aquifer.

Unconformity: Cretaceous layers dip to the southeast whereas Strawn layers dip to the NW. The unconformity is relatively easy to recognize in well logs and we spent some time trying to determine the formations actually tapped by the water wells. We used oil and gas well logs (black dots on Figure 54) that had used already inspected well logs by a previous project at BEG (Intera, 2014). We added information from the TDLR database, relying of the keyword "red clay" or "red bed" to locate the depth of the unconformity. There is a total of ~1250 TDLR wells out of which ~400 were removed for various reasons. Our initial goal was to determine the topography of the Paleozoic basement on which the base of the Cretaceous was deposited or at least to determine the fluctuations in elevation around the average that may have guided gas migration. The topography at the time of the Cretaceous transgression was likely similar to the

current hilly topography. Unfortunately, the lack of accuracy on the depth to the unconformity in TDLR well logs despite their large numbers preempted such goal.

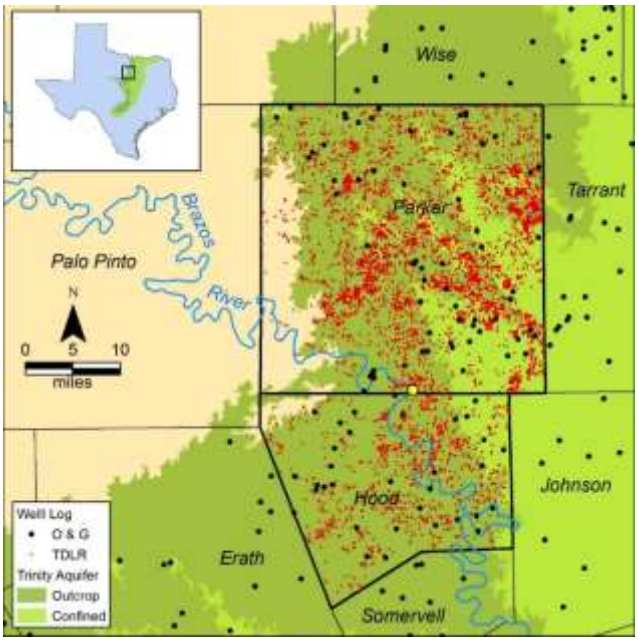

Note: Trinity aquifer outcrop and confined sections showed; TDLT data points represent these wells for which we felt confident that the unconformity was adequately recognized; O&G data points represents those O&G wells for which we were able to accurately defined the unconformity elevation (work by Dr. Scott Hamlin, BEG used in Intera, 2014). The yellow dot illustrates the location of the Silverado area.

Figure 54. Location of wells used to map the Paleozoic-Trinity unconformity

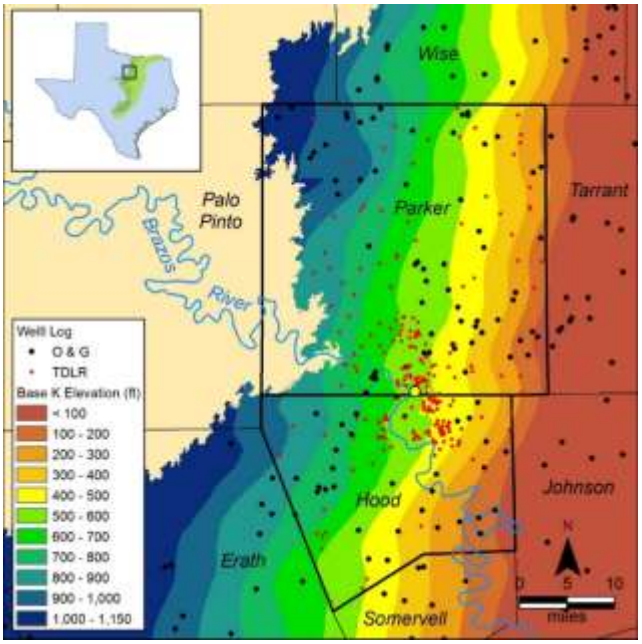

Figure 55. Base of Cretaceous elevation (Parker County area)

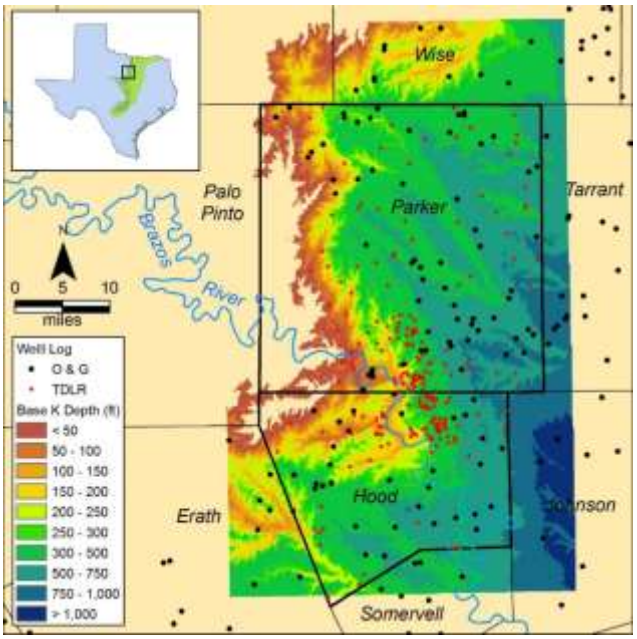

Figure 56. Depth to base of Cretaceous (Parker County area)

Faults: RRC (2014) reported that during the Range Resources investigation it was noted that there is no fault observable in the seismic data provided by Range Resources (data unavailable to us in this study) but several papers have noted the presence of faults impacting at least some of the Paleozoic section. It is not clear if they reach the base of the Cretaceous but the local Geological Atlas of Texas (GAT) map (http://www.twdb.texas.gov/groundwater/aquifer/GAT/ - 1:250,000), west side of Dallas sheet, does not show any fault. Thomas (2003) inferred the presence of two faults in southern Parker County (Figure 57, faults were probably inferred from well log correlation) but west of the area of interest.

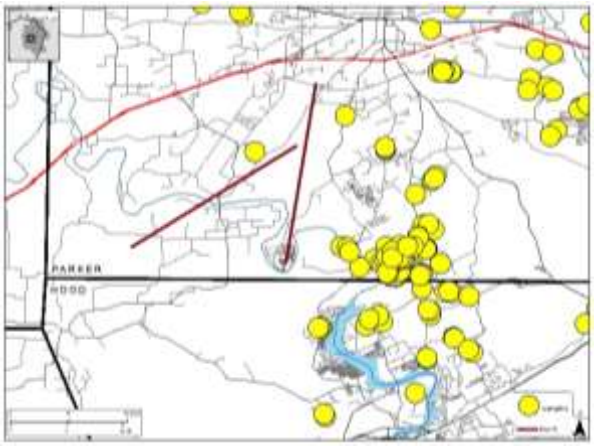

Source: Thomas (2002, Fig.9) – yellow dots represent BEG samples

Figure 57. Example of fault interpretation in southern Parker County

We are able to confirm the existence of the SE-NW trending structural feature by interpreting the geophysical data in the public domain consist of the USGS aeromagnetic and gravity data for Texas (Bankey, 2006). After removing the regional trend (Figure 58a), gravity data reveals a mass deficit trending SW-NE, consistent with the general fault direction as described in Ewing

(1991) where a dropped compartment is also visible on the 1:750,000 tectonic map (faults at top of Ellenburger Fm. shown on map) representing a foundered fault system from the Ouichita orogeny but it is not clear how high they penetrate into the section but its influence does not extend to the Cretaceous.

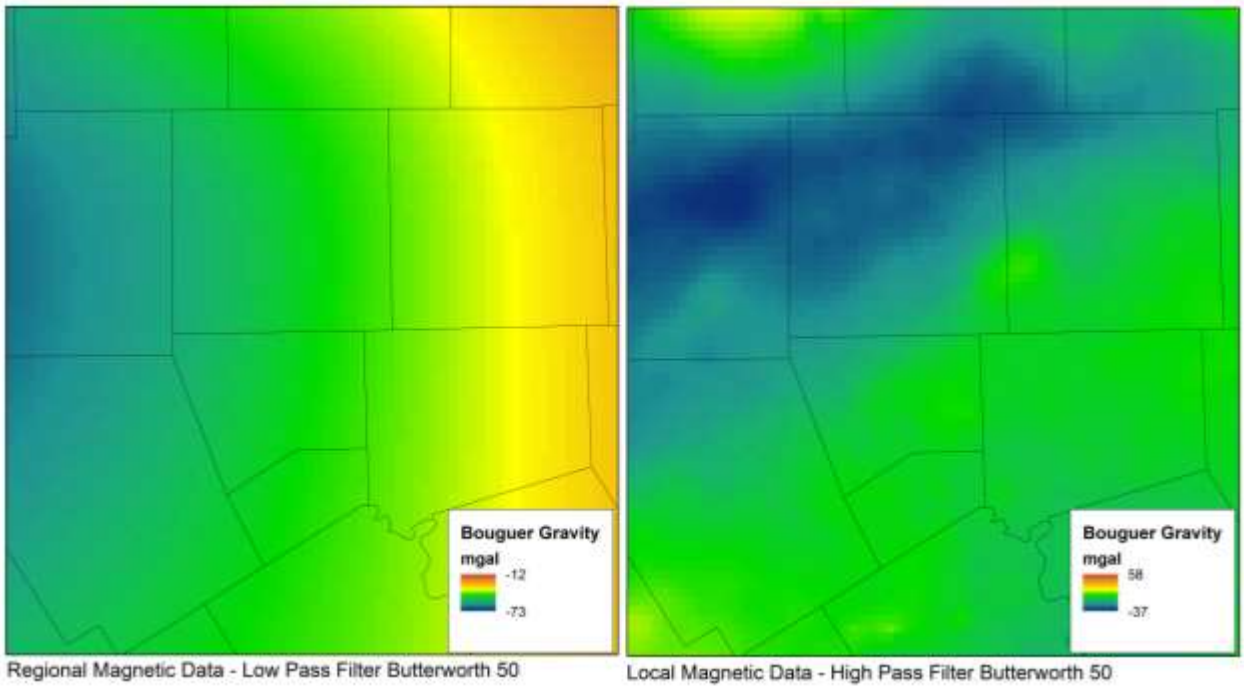

Regional Magnetic Data - Low Pass Filter Butterworth 50

Local Magnetic Data - High Pass Filter Butterworth 50

(a) (b)

Note: A fast Fourier transform was applied to the dataset using Erdas Imagine 2011, which converts the data to an amplitude vs. wavenumber image. A high pass filter was further applied to the dataset. The high pass filter filters for data of a higher frequency. The user specifies the amount of data to be removed by selecting a filtering mask and radius. The Butterworth filtering mask with a radius of 50 was selected for this study.

Figure 58. Local and regional Bouguer gravity maps

IV-4-2.4 Water Wells

We collected information on domestic wells through the TDLR database and assigned their bottom to either the Strawn or the Trinity. Top and bottom of the various layers were obtained from shapes files used to prepare the recent Northern Trinity GAM (Intera, 2014). In addition, we spent a fair amount of time cataloging and collecting information about PWS systems in Hood and Parker counties; the idea being that we would enter the wells when pumps are removed for maintenance. The opportunity never materialized and the closest we came to it was entering two bubbling wells in Hood County (#BS555, sampled for water and gas, and #BS556, sampled only for gas). Wells of the Lake Country Acres PWS, completed to the base of the Trinity (and then for some length into the Strawn), have had a methane problem for many years (i.e., Collier Consulting, 2003). In 2003, a downhole video inspection of 2 of the 4 wells of the well field noted very murky and bubbly water. These two wells also exhibited a faint to strong hydrocarbon smell suggesting that C4+ compounds are present in the wellbore. Our 2014 sampling shows that methane is still produced from these water wells. The Texas Groundwater Protection Committee that summarizes contamination cases every other year for the Texas Legislature has it listed at several occasions as well as another PWS, the Mesa Grande Water

Supply Corporation (WSC), supplying water to a subdivision located on the Brazos just north of the City of Granbury (Hood County). The Mesa Grande well field case is also documented in the RRC files (2004). No methane analysis but propane (110 ppb) and butane (91 ppb) found. On the Hood-Somervell county line on Squaw Creek reservoir, west of the Brazos, another RRC file on potential natural gas contamination with propane at 4.6 ppb (butane not detected).

IV-4-2.5 Oil and Gas Wells and Fields

Herkommer and Denke (1982) provide a list of active oil and gas fields at the time of publication. A check with the IHS database shows that most of the activity had already occurred by the time the paper was published (Figure 59b). Parker and Hood counties produce mostly gas transitioning to mostly oil on the Wise-Parker county line (Figure 59a).

Center Mill well field in Hood County located just south of the county line with Parker County and only 1-2 miles from the Parker-Hood cluster is represented by three vertical wells in the IHS database. Depth to top of Strawn and perforated intervals of wells are 406 ft and 407-414 ft, 418 ft and 418-426 ft, and 362 ft and 358-376 ft. The wells were completed in Feb. 1985 and abandoned in Aug. 1986 after having produced 440, 558, and 600 MCF, respectively (Figure 60). Initial production test yielded 111-152 MCF/day. No oil or water were reported being produced. Note that the field was just below the unconformity and that it was drawn down fairly quickly. There are several shallow wildcat wells in the area very likely looking for similar small accumulations. The abandoned Lake Country Acres water well was reported by Kornacki and McCaffrey (2014, p.8) to flow unchocked at a similar rate at 122 MCF/day when drilled in 2003. As a comparison the Teal and Butler Barnett gas wells in the Parker-Hood cluster yielded 44,194 and 47,712 MCF in their first full month, respectively (their initial production test yielded 2015 and 2390 MCF/day). As a comparison on the other end of the spectrum, we were able to estimate the gas flow rate (that turned out to be mostly methane) from a bubbling water well (drilled in December 2012) when the packer was installed to sample for gas. The estimated rate was 3L/min (in early November 2014) that we measured by timing how long it takes to fill out a sampling gas pouch at atmospheric preesure. A rate of 3L/min corresponds to ~5 MCF/month, equivalent to the flow rate at end of life of the Center Mill Strawn wells, but after almost 2 years of unimpeded production. Some well owners made the comment that keeping these bubbling well wellbores open instead of plugging them help the other water wells in the area as the small natural gas accumulation is blown down. They also noted that a bubbling water well and a water well with no or little methane can be very close (<300 ft) even if drilled at the same depth. A quick calculation shows these small shallow accumulations do not occupy much of a footprint. Assuming that 50% of the gas was recoverable at Center Mill, the original gas in place was 3200 MCF at a depth of 400 ft, that is, a pressure of 170 psi, and a density of 8 kg/m^3, that is, ~10 times more that at standard conditions (online calculator). With a porosity of 30% and an assumed thickness of 5 ft, the footprint of the accumulation would be a square 650 ft across. However, the maximum separation between the wells is 1474 ft, which suggests a more elongated shape compatible with the reservoir type described in Ehlmann and Ehlmann (1985).

At this point, it is not clear if the small reservoirs / accumulations are still charging, that is, small flux of natural gas, either ~constant or by pulses, feeding them.

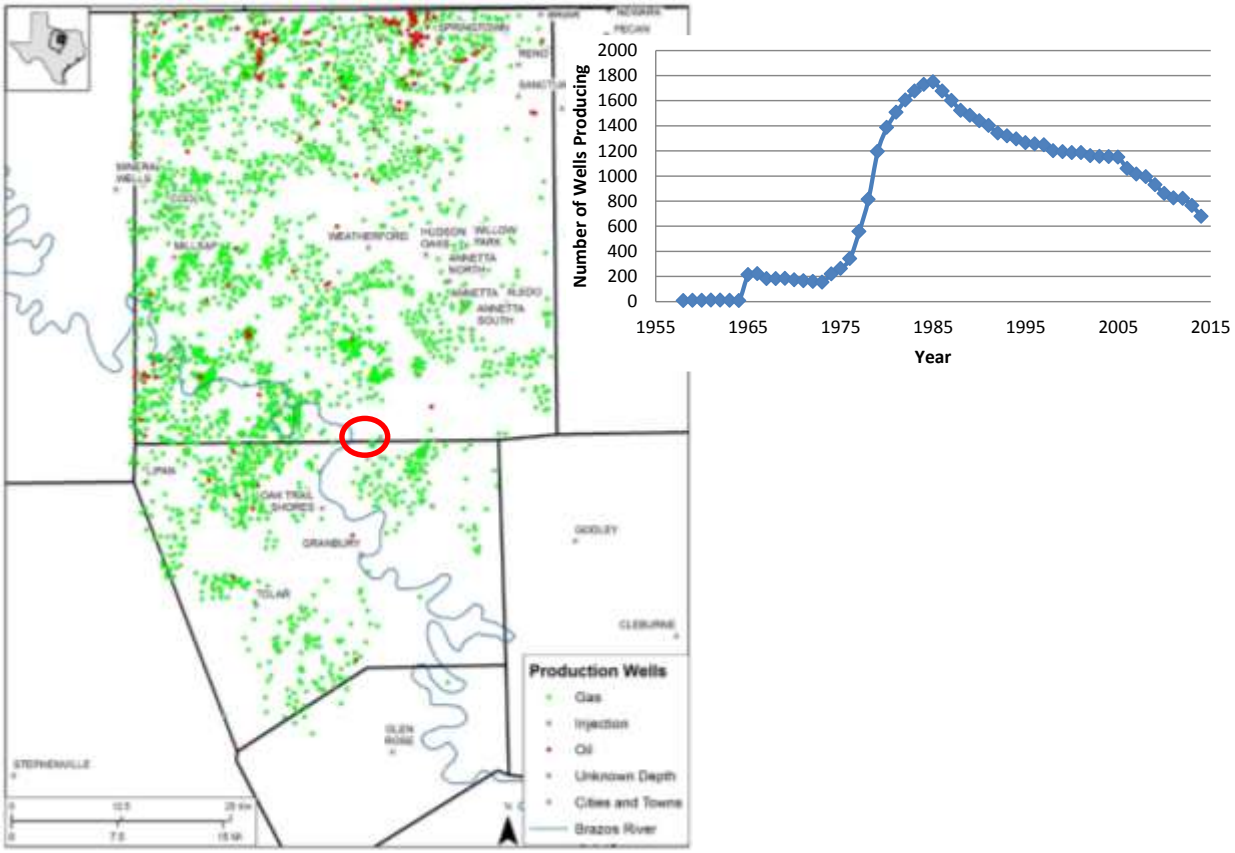

(a) (b)

Note: red circle represents the location of the Parker-Hood cluster; the few green dots contained within the circle represent the Center Mill field

Figure 59. Location (a) and number (b) of non-Barnett wells producing in the Parker, Hood or Somervell counties by year.

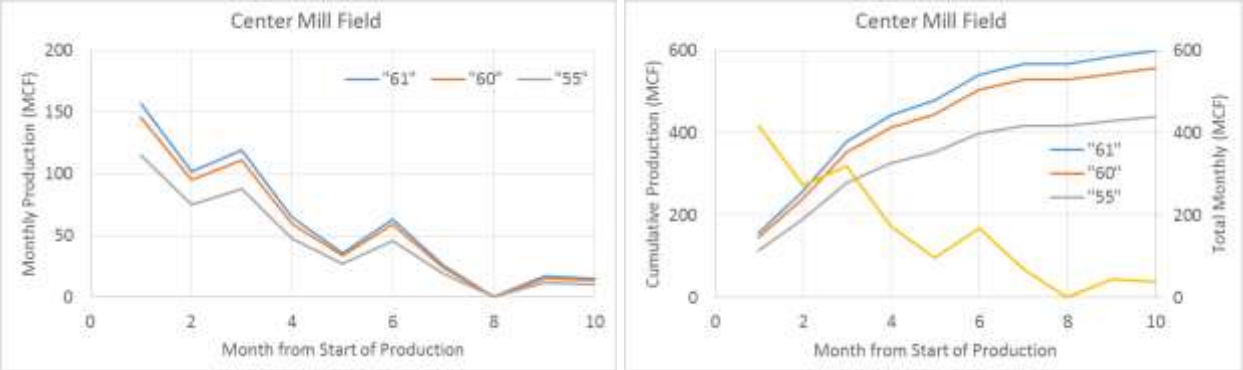

Figure 60. Gas production from Center Mill Field

Other fields in the area generally target deeper formations (Atoka). Another gas field to the ENE in SE Parker County (Aledo SE) is also contained in the Lower Strawn (Ehlmann and Ehlmann, 1985) but at larger depth (1167-2000 ft range for total depth driller) and the reservoir likely presents similarities with that of Center Mill Field and other non-economic accumulations. They described the Aledo (Strawn 1200') gas field as a reservoir contained in E-W trending fluvial

sand channel. Smith (1982) describing the Lipan Gas Field in northwestern Hood County also emphasized the stratigraphic nature of the trap.

The general conclusion of these observations is that there are many small stratigraphic traps in the vicinity of the Parker-Hood county line, some have been commercially tapped and others have been drawn down naturally through open wellbores.

IV-4-3 Other Novel Elements

We were also able to collect data from previous sampling campaigns in the Parker County area to better delineate the area with high methane concentration.

IV-4-3.1 Not a function of distance to wells or topography

In the Marcellus Shale, some authors have postulated that methane concentration is a function of proximity to gas wells (Osborn et al., 2011; Jackson et al., 2013) or of topography (Molofsky et al., 2013). Neither relationship holds in the Barnett. Given the paucity of methane hits in the Barnett it is expected that a region-wide plot of dissolved methane vs. distance to the closest Barnett well will not be very useful (Figure 61). Plots displaying methane vs. distance to Barnett and non-Barnett wells in Parker, Hood, and Somervell counties (Figure 62) show that the highest methane concentration are not necessarily close to gas wells, either Barnett or non-Barnett, and that there is no monotonic increasing function of methane as the sampling point approaches a gas well.

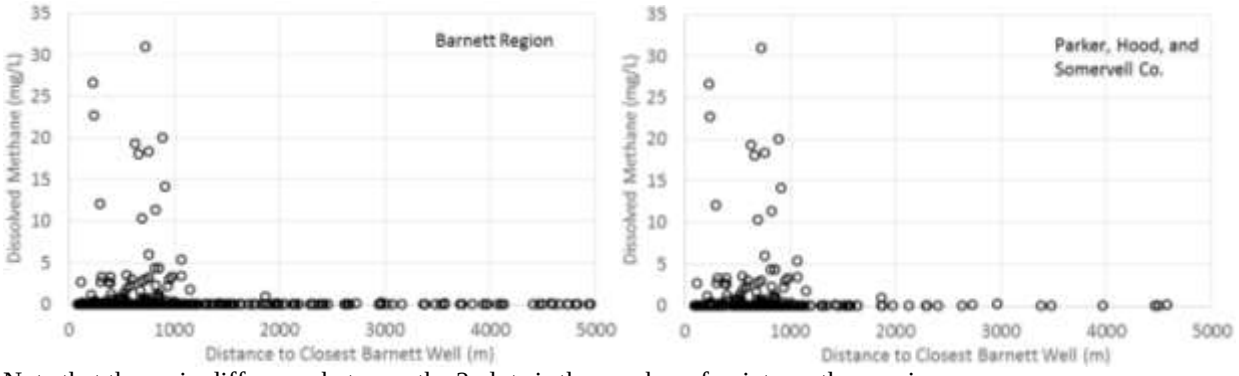

Note that the main difference between the 2 plots is the number of points on the x-axis.

Figure 61. Dissolved methane concentration vs. distance to closest Barnett well

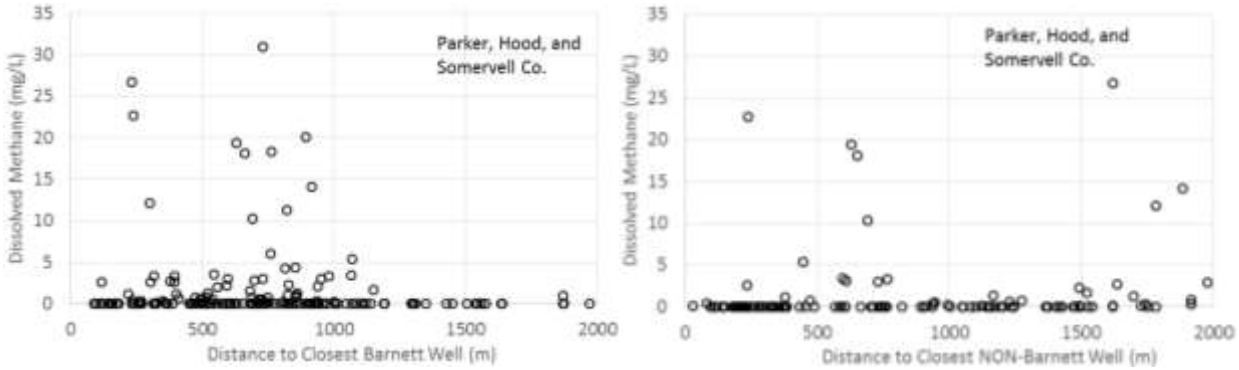

Figure 62. Dissolved methane concentration vs. distance to closest Barnett and NON-Barnett wells

It is also possible to conceive that methane concentration is a function of a more integrated parameter such a spatial well density and lateral density (Figure 63) as the concentration may not be connected by chance to the closest well. However, plots still show no relation with methane concentration (Figure 64) as one would expect methane concentration to increase with well or lateral density. A well-known counterpoint to this observation is that methane has been known to travel far as illustrated by the Hutchinson, KS gas explosion in 2001 (for example, Miyazaki, 2009).

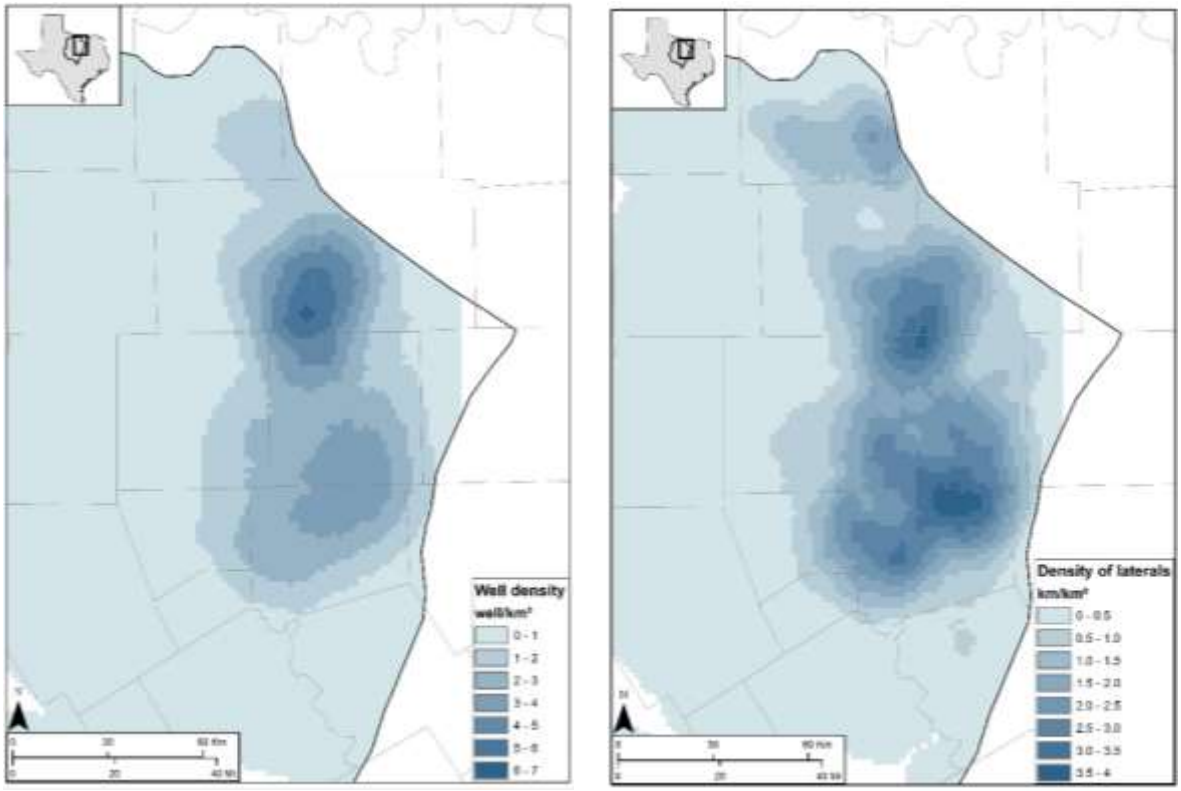

Figure 63. Well and lateral length density (Barnett)

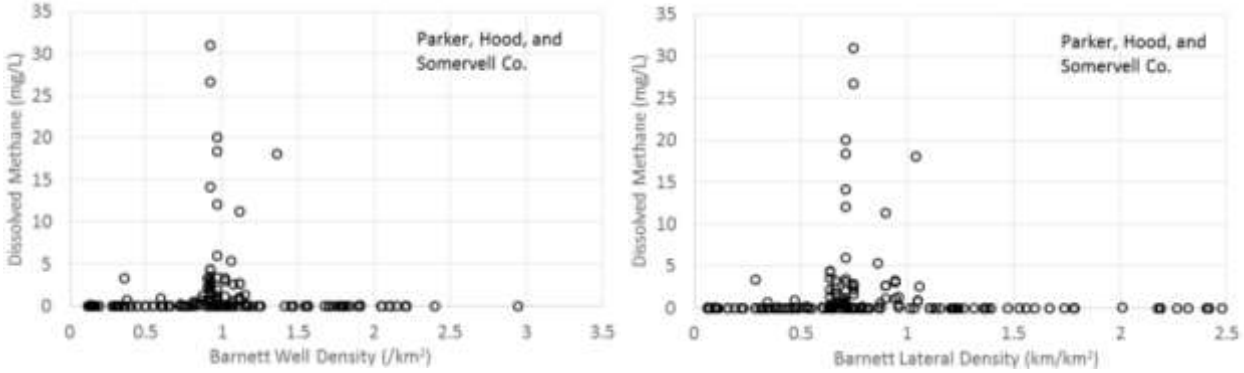

Figure 64. Dissolved methane concentration vs. well and lateral length density (Barnett)

IV-4-3.2 BTEX Analyses

We also analyzed 25 water samples in the Parker-Hood cluster for BTEX (LCRA lab, Austin, TX), all individual BTEX components were non-detect (<2 ug/L). Note that the analyses were

performed a month after sampling, 2 weeks beyond the official holding time but RRC (2014) report similar findings.

IV-4-3.3 Methane

Zooming in on the Parker-Hood cluster (Figure 65) with horizontal well traces shows that methane concentrations do not match high well density.

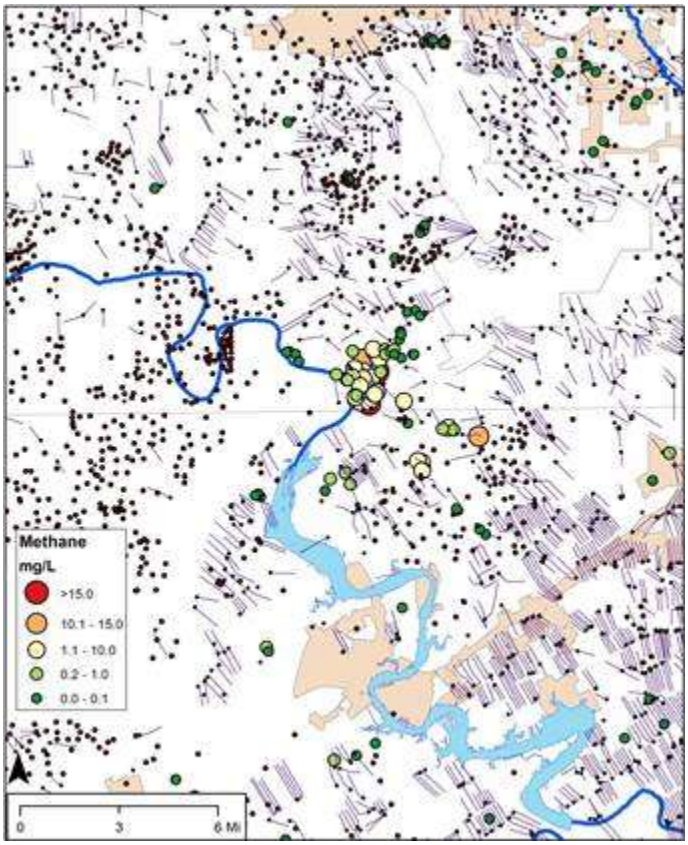

Source: IHS-Enerdeq= well trace and locations; dots= water wells sampled for dissolved methane
Note: simple dots indicate vertical wells; a few horizontal wells with lateral information missing are also included

Figure 65. Oil and gas wells and sampled water well locations

We plotted dissolved methane concentration vs. dissolved elements (major, minor and trace elements). A visual inspection of the plots did not show any obvious trend with which to associate increasing methane concentration (Appendix F: Dissolved methane vs. major, minor, and trace elements concentrations). TDS (small triangles) was also included on the plot y-axis to remove visually the mechanical effect of concentration increase with TDS (Figure 82 to Figure 88). All plots show some higher elemental concentrations at lower methane concentrations related to the slightly brackish nature of some wells. Unlike most, a few elements show an increase in concentration whereas TDS stays constant at higher methane concentrations; they are F and B, to which Al, Zr, and Mo can be added but at lower concentrations. The relative increase in the concentrations of these two elements (F, B) is likely related to the biodegradation of methane and changes in pH conditions as these two elements are not redox-sensitive but exhibit pH-dependent sorption. No detailed explanation of their behavior was attempted for this report. In addition, no rigorous statistical analysis of the data was performed.

We prepared several crossplots with depth, always separating wells completed in the Trinity vs. wells completed in the Strawn as indicated by the interpreted TDLR data. High methane concentrations are mostly found in wells penetrating the Strawn (Figure 66 and Figure 67). The difficulty of acquiring accurate well depth may explain away the presence of a few Trinity wells with high methane but, after specifically checking them, the information about those five Trinity wells seems solid. Nevertheless high methane concentrations are mostly associated with Strawn wells. The methane is mostly of thermogenic origin with a biogenic tail noticeable in the Trinity (Figure 66b). Another trend noticeable especially in the Trinity is that the dissolved methane becomes heavier with decreasing depth, maybe an illustration of the aerobic degradation of methane. Plots contrasting methane concentrations and vertical distance to the unconformity (Figure 67) carry similar information. The unconformity itself and the topography of the surface on which Cretaceous sediments were deposited could also controlled methane distribution in the Trinity aquifer.

There is no obvious evidence of sulfate reduction related to consumption of methane (Figure 68a and Figure 69) as was observed in the Haynesville and Eagle Ford shales, suggesting aerobic degradation. Nor is there strong data demonstrating that higher methane concentrations are associated with high chloride (Figure 68b and Figure 70). Note that chloride can be high because of mixing with deeper Strawn water but also mixing with Brazos River water that tends to be slightly saline because of the presence of salt layers and salt springs upstream. Samples with high dissolved methane concentration tend to have heavier DIC carbon (Figure 71).

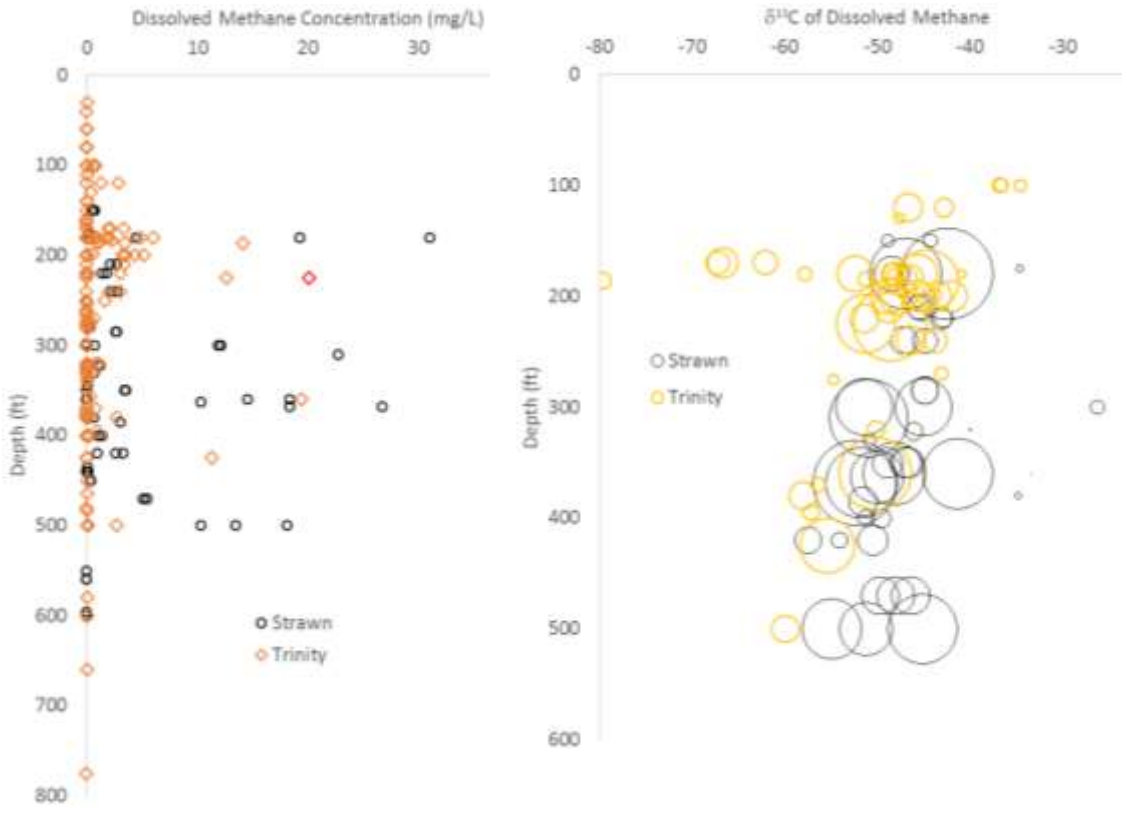

(a) (b)

Note: circle size proportional to methane concentrations
(a) 242 water samples in Parker, Hood, and Somervell counties (that is larger than the P-H cluster); (b) 90 waters in the same counties with isotope analyses.

Figure 66. Dissolved methane concentration and its $\delta^{13}C$ as a function of depth (Barnett)

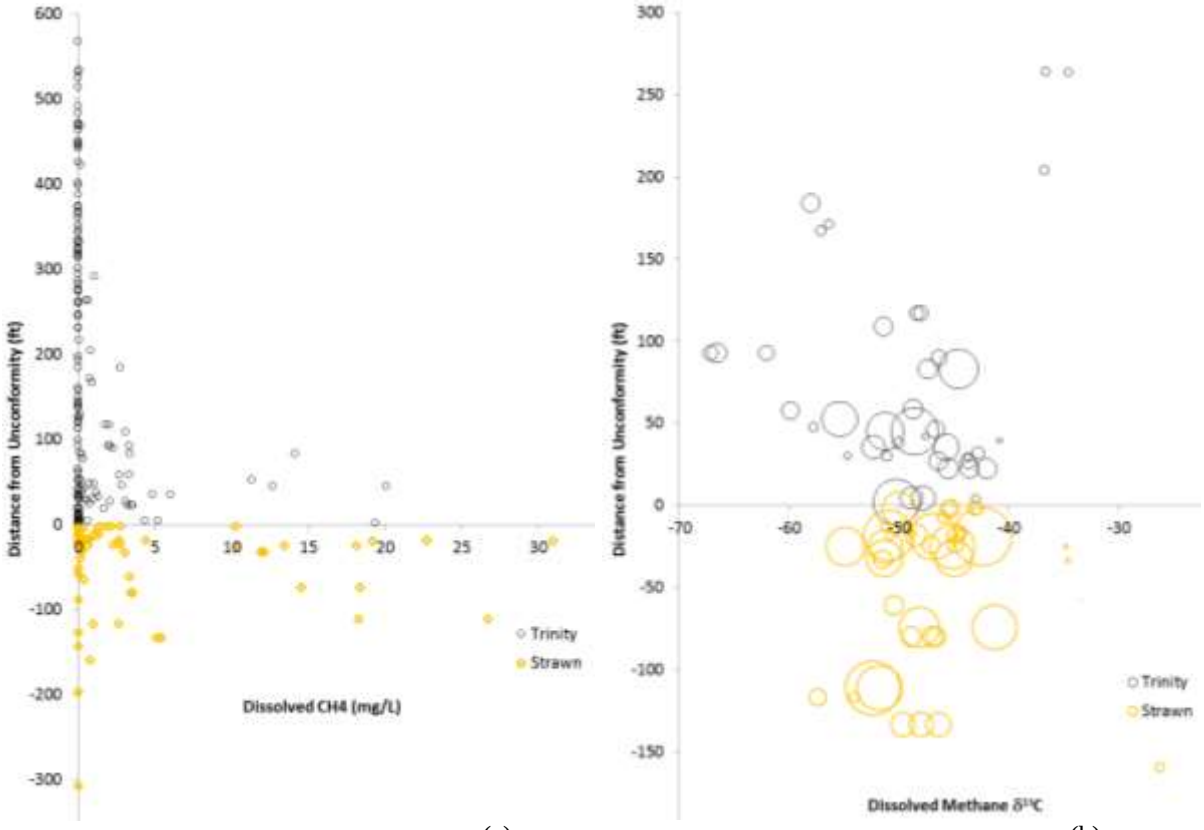

(a) (b)

Note: circle size proportional to methane concentrations
(a) 242 water samples in Parker, Hood, and Somervell counties (that is larger than the P-H cluster); (b) 90 waters in the same counties with isotope analyses.

Figure 67. Dissolved methane concentration and its $\delta^{13}C$ as a function of the vertical distance to the Cretaceous unconformity (Barnett)

The Barnett Bernard plot (Figure 72) unlike that of the Haynesville and Eagle Ford suggests some mixing between thermogenic and microbial gas and relatively little biodegradation. The lower methane concentration in some water samples of the Parker-Hood cluster, the slight shift towards heavier methane (no ethane isotope measurement are available) and their relatively higher C1/C2+C3 ratio argue for limited biodegradation (favoring C2+ alkanes over methane, Kornacki and McCaffrey, 2014).

All the known occurrences of shallow gas occur within the subcrop of the Lower Strawn (Kickaboo Creek Fm.) covered by the Cretaceous layers. The Lower Strawn seems more favorable for trapping hydrocarbons that the Upper Strawn mostly exposed to the West of Parker County. Occurrences include the Center Mill reservoir, the Lake County Acres well field (including a well drilled and abandoned in 2013 because of the high gas flux), the Parker-Hood cluster including 2 wells we did not sample but reported in RRC (2014, p.7), Hurst and Oujesky wells, that flowed natural gas for a period of time, wells BS#555 and BS#556 and another well to the East (confidential), all three wells inoperable because high natural gas flux causes gas lock on the water pumps, Mesa Grande WSC (north of Granbury).

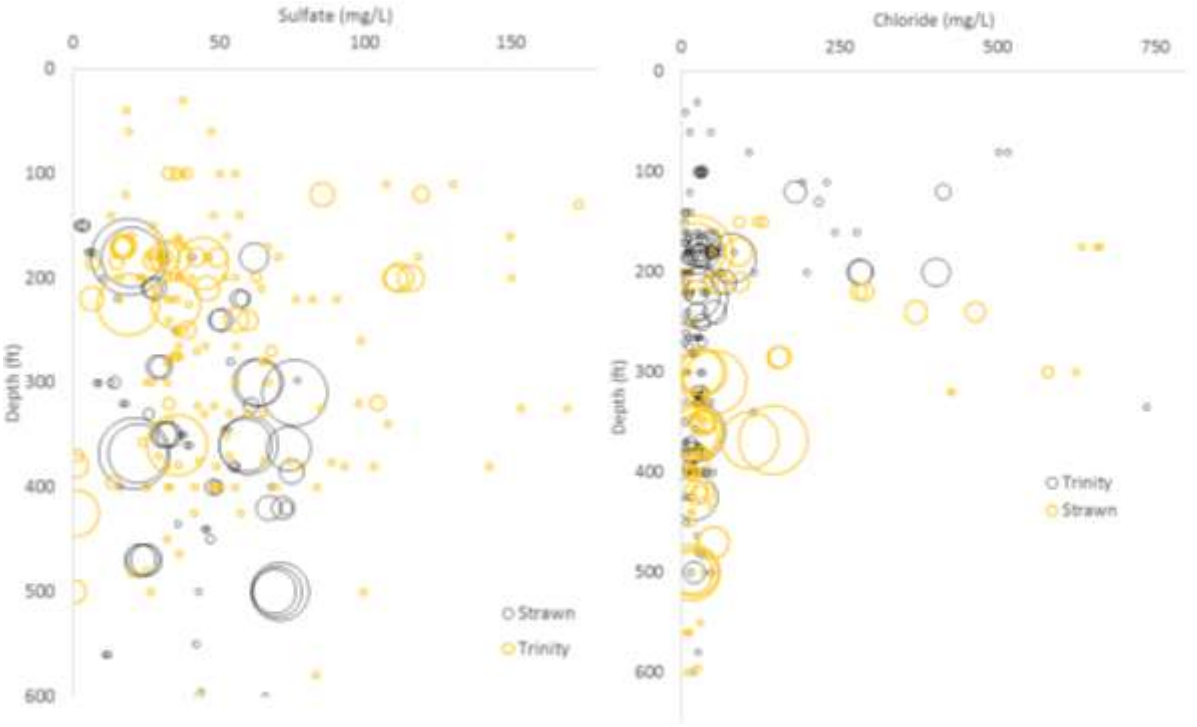

(a) (b)

Note: circle size proportional to methane concentrations; all data points with CH_4<0.2 mg/L are plotted as 0.2 mg/L to improve visibility, maximum methane concentration is
240 water samples in Parker, Hood, and Somervell counties (that is larger than the PH cluster).

Figure 68. Sulfate and chloride concentration vs. depth vs. dissolved methane (Barnett)

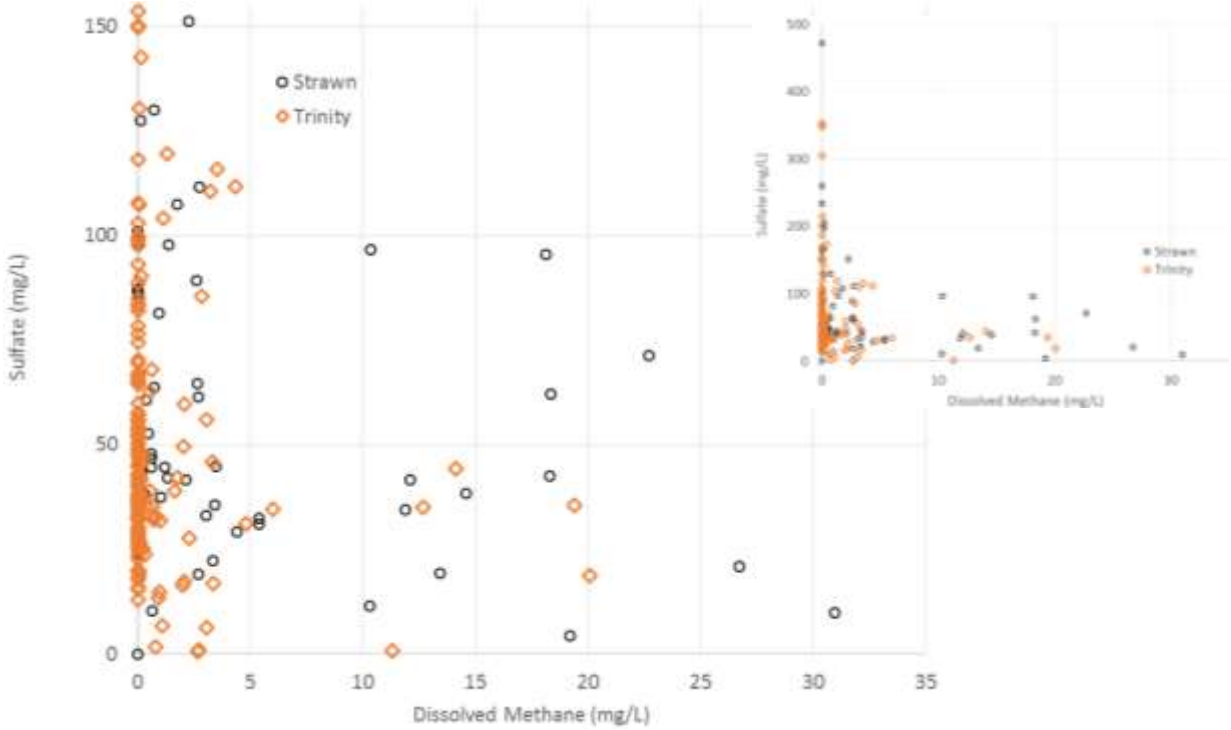

Note: the insert y-axis goes to 500 mg/L

Figure 69. Dissolved methane vs. sulfate concentrations (Barnett)

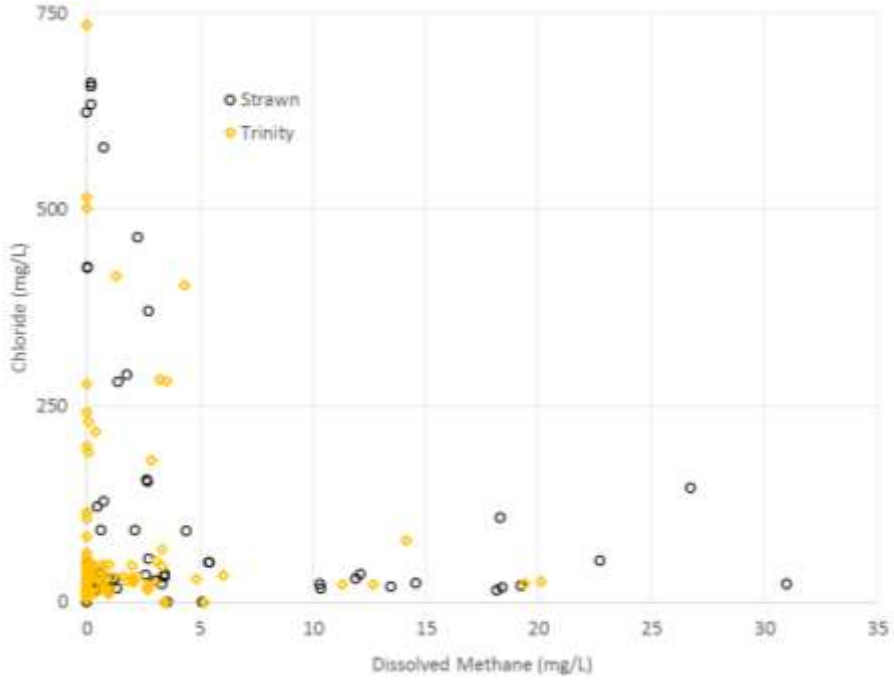

Figure 70. Dissolved methane vs. chloride concentrations (Barnett)

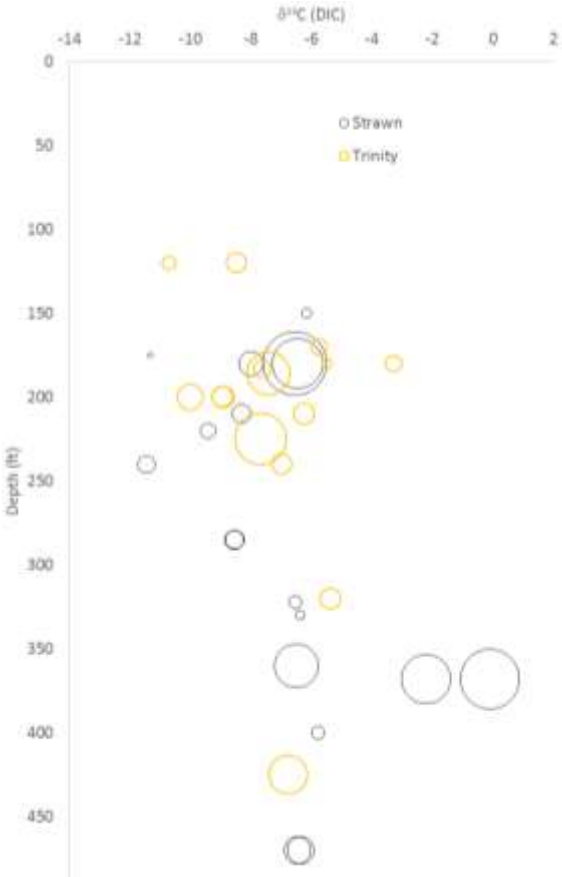

Note: circle size proportional to methane concentrations; 30 water samples from the PH cluster).

Figure 71. $\delta^{13}C$ DIC vs. depth vs. dissolved methane.

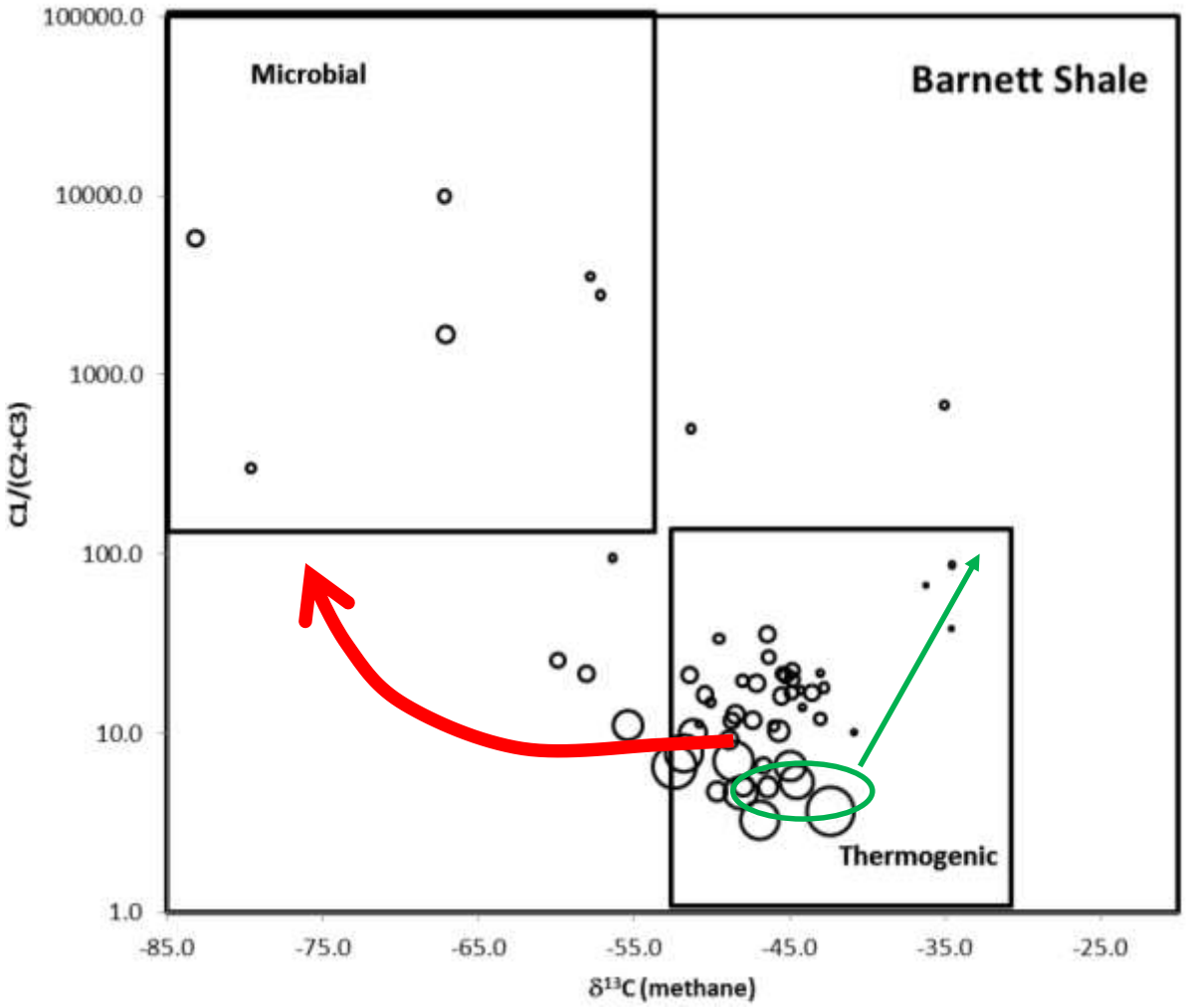

Note: size of the circle correlates to the concentration of dissolved methane; red arrow show the general shape of the mixing lines whereas the green circle demotes location of the Barnett gas on the plot -data from this study and from Zumberge et al. (2012). The green arrow denotes the general direction of the nature of the Barnett gas as the core area is approached (dryer gas and oil cracking resulting in heavier C13 isotopic signature). Strawn gas is slightly dryer than Barnett gas but with similar isotopic composition (this study and Darrah et al., 2014). Some dissolved water samples are wetter than the source possibly because ethane solubility in water is higher than that of methane.

Figure 72. Bernard plot showing methane C isotope vs. ratio of methane, ethane and propane (C1/C2+C3) (Barnett).

IV-4-3.4 Nitrogen

We also measured nitrogen isotopes ($\delta^{15}N$) in 25 well water samples in the Parker-Hood cluster area. In the study area, dissolved nitrogen has two main origins: (1) atmospheric nitrogen dissolved in the recharge water or entrained as tiny air bubbles and (2) deep-sourced nitrogen migrating up with methane and other reservoir gases. The two origins show different isotopic signature, close to 0‰ for atmospheric nitrogen and slightly negative for nitrogen gas in oil and gas reservoirs. In addition, in a multiphase (gas and aqueous phases) multicomponent (water, nitrogen, methane, etc) system, when a gas enters the shallow aquifer system, components present in both phases will partition between them. Dissolved methane that would have a very low concentration from equilibrium with atmosphere will be overwhelmed when a natural gas

stream enters the system. The isotopic signature of the dissolved gas will be that of the natural gas. That is also true of microbial methane that can be overwhelmed by natural gas streams. On the other hand, dissolved nitrogen concentration of atmospheric origin in equilibrium with water can be high compared to the equilibrium concentration due to the much lower nitrogen partial pressure in natural gas (1-5%). It follows that a small amount of natural gas (with a small amount of nitrogen) will imprint its methane isotopic signature to the dissolved methane but not its nitrogen isotopic signature to the dissolved nitrogen. In addition, since the nitrogen partial pressure is low in the gas phase, the dissolved nitrogen of atmospheric origin will tend to exsolve into the gas phase. Figure 73 illustrates these points. It plots the dissolved nitrogen concentration vs. its $\delta^{15}N$. Some samples have excess nitrogen (due to air bubbles) with some methane (small bubbles on the plot) whereas other have been stripped of their nitrogen but still have kept the atmospheric nitrogen signature. It means that there is enough flux (or enough gas relative to the amount of water) to strip some nitrogen from the water but not enough to imprint the natural gas nitrogen signature. For a few water wells with higher fluxes -those we observed in this category clearly show two-phase flow and bubbling methane- dissolved nitrogen shows the isotopic imprint of the natural gas nitrogen. It follows that the samples with atmospheric nitrogen signature and high methane are experiencing fluxes at least one order of magnitude smaller than the BS555 and Lake Country Acres wells. The study did not try to model the processes rigorously but it is a promising avenue to quantify gas migration / leakage when high.

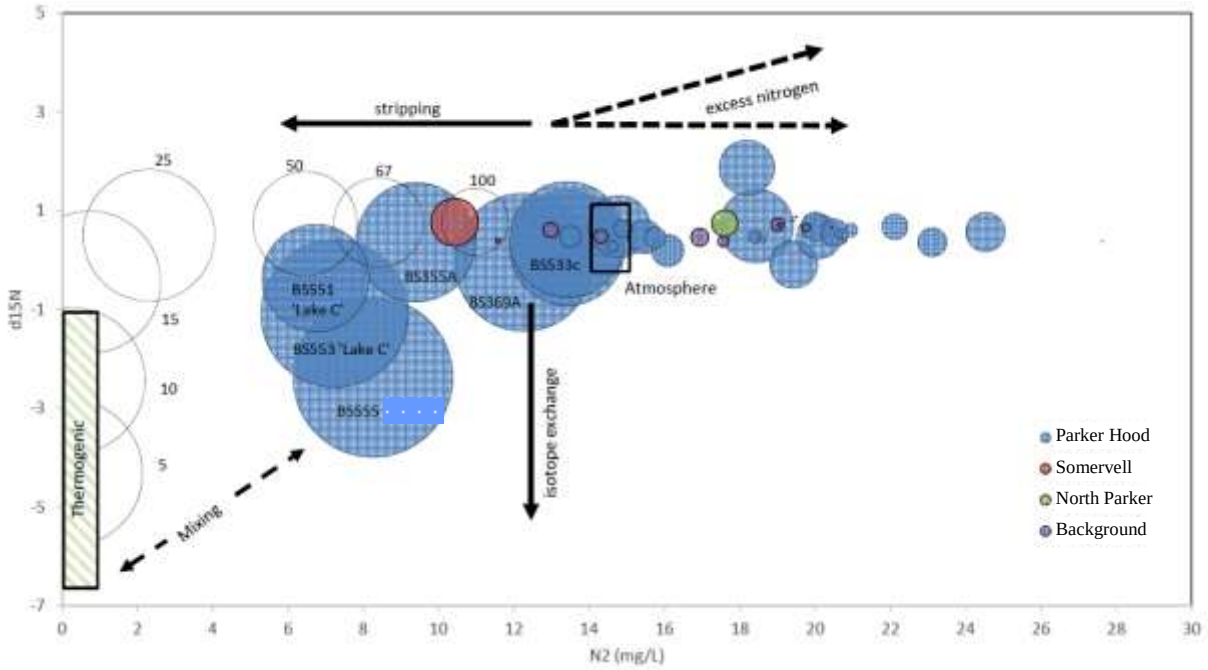

Note: The size of the circle is proportional to the concentration of dissolved methane. Schematics of trends expected for ‘excess’ and ‘stripped’ nitrogen and nitrogen isotope exchange are also illustrated.

Figure 73. Plot showing $\delta^{15}N$ vs. dissolved nitrogen concentration

IV-4-3.5 Noble Gases

See Appendix G: Noble Gases and Stable Isotopes.

IV-4-3.6 Microbial Analysis

Results for the microbial study are not available yet. Table 2 and Figure 74 show nature and location of sampling.

Table 2. Microbial biomass aerobic and anaerobic sampling: well list

Sample ID	Sampling Date	Aer.	Ana.
365	11/7/2014		*
17C	11/7/2014	*	*
367	11/7/2014	*	
357	11/6/2014	*	*
16C	11/6/2014	*	
347	11/6/2014	*	*
355	11/5/2014	*	*
369	11/5/2014	*	*
348	11/5/2014	*	*
211C	11/5/2014	*	*
434	11/5/2014	*	*
207	11/4/2014	*	
447	11/4/2014	*	
351	11/4/2014	*	

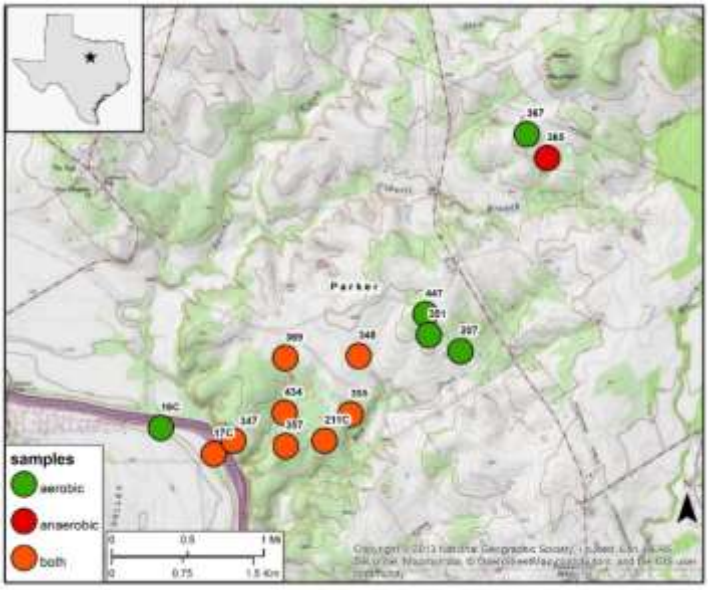

Figure 74. Locations of microbial biomass sampling in water wells

IV-5. Autoclave Experiments

Details on the autoclave and benchtop experiments are given in Appendix J: A Study of Rock-Water Interactions during Hydraulic Fracturing (Barnett Shale). As described earlier, the broad objective of this section of the project is to contribute to the body of knowledge on the geochemical and mineralogical processes operating between hydraulic fracturing (HF) fluids and shales.

IV-5-1 Summary of Methods

The focus was on a well in north Texas in Wise County completed in the Barnett Shale (Blakley lease). The core samples used in the experiments were dominated by quartz, illite, calcite, and chlorite with minor components of plagioclase (albite), K-feldspar, pyrite, kaolinite, ankerite, and dolomite. The relatively reactive mineral phases include calcite (5-10%), albite (~1%), and pyrite (~2%), and to a lesser degree dolomite (0.6%), ankerite (0.6%), and K-feldspar (<1%).

We performed five autoclave experiments on Barnett cores that has been in storage at the BEG repository at ~80°C and 200 bars in which small rock fragments were exposed to various types of artificial HF fluids. The HF fluids used in the experiments range from deionized (DI), to slightly brackish (~2000 mg/L), to brackish (20,000 mg/L) water. We used NaCl salt because brines are typically dominated by Na and Cl complemented by a few runs with $CaCl_2$ or KCl. Similar benchtop experiments (11 total) were also performed at 80°C, atmospheric pressure and under N_2 atmosphere but using ground rock to increase reactivity of the system.

Rock samples were examined before and after reaction using traditional mineralogical techniques (X-ray spectroscopy, SEM) in addition to the more advanced technique of argon milling. The latter enabled us to image in extreme details unreacted and reacted samples and compare the exact same locations before and after reaction. An unreacted and six reacted samples were also sent for mercury intrusion capillary pressure (MICP) tests to provide information about changes in porosity and permeability. Geochemical samples were sent to IC analysis for major ions and to ICP analysis for minor and trace metals. Bicarbonate concentrations were obtained through a carbon analyzer. Approximate pH values were also measured during the experiments. Blanks were performed on an empty autoclave to detect any experimental artefact.

The autoclave experiments consisted in placing 3 or 4 core fragments (~16 g total) into the 250-mL reaction vessel and immersed them in ~160 mL of the synthetic fluid for a period of 3 weeks. Experiments were done under N_2 atmosphere. Aliquots of water were removed periodically from the reaction vessels to form 10 to 15-strong time series over the ~3 weeks of the experiments. Note that the rock-water ratio is smaller (that is, water is more dilute) than during actual HF stimulations. The discrepancy is due to the limited amount of rock available combined with the need to regularly abstract water (3-4 mL) for chemical analysis. Benchtop experiments were performed by exposing ~8g of silt-size ground-up shale rock to 40 mL of the same synthetic fluids.

IV-5-2 Summary of Results

The relatively reactive mineral phases include calcite (5-10%), albite (~1%), and pyrite (~2%), and to a lesser degree dolomite (0.6%), ankerite (0.6%), and K-feldspar (<1%) consistent with descriptions of Milliken et al. (2012). Petrographic observations show that, although no clear

overall major post-reaction changes in mineral composition is revealed by XRD analyses, calcite dissolution was clearly occurring on the reacted samples. The reactions resulted in overall increases in Ca, Sr, and Ba aqueous concentrations. Some feldspar dissolution and limited pyrite dissolution were observed too. More generally, higher ionic strength solutions tended to increase mineral dissolution and reduce mineral precipitation as imposed by thermodynamics. Precipitation reactions are limited with formation of small clay and Fe oxyhydroxide flakes. Organic matter does not seem to be impacted by the rock-water interactions beyond releasing sorbed material. The MICP analyses of the unreacted and reacted samples show a significant increase (at least 50%) in porosity and suggest a two- to three-fold increase in permeability.

Geochemical observations of autoclave runs show that, in general, a few days were needed to reach concentration values often close to final concentrations. The increase for major elements is gradual and concentrations have not fully leveled off at the end of the 3 week-long runs. Benchtop experiments typically display faster release rates. The various experiments at various ionic strengths and ionic compositions show similar behavior of generally increasing concentrations with time for most elements. Notable exceptions are neutral species such as HBO_3 and, to a lesser degree, SiO_2 that both, although increasing with time, show a salting out effect and Fe that likely precipitate/sorb. Given the heterogeneity of the shale rock, experimental results with the same environmental conditions performed on different rock fragments sometimes yielded different but close levels of concentrations and exhibited the same general behavior.

Major elements (Na, Ca, K, Cl, SO_4, HCO_3, Si) display concentrations at the end of the experiments ranging from a few tens of ppm to hundreds of ppm (with a starting point ranging from 0 to sometimes tens of ppm slightly after time zero). A few minor elements (Li, NH_4, Mg, K, F, B, Al, Si, Mn, Fe, Ni, Mo, and Sr) hover around the ppm mark (a fraction of a ppm to a few ppm). The other elements appear only as trace (tens of ppb's: V, P, Cr, Ti, Cu, and Ba; ppb level: Zn, As, Se, Zr, Rb, Cs, Sb, and Tl; and <1 ppb: Ag, Cd, Sn, Pb, Bi, Th, and U) but with explainable behavior for most of them. Minor and trace elements find their source either as impurities in carbonates or as sorbed species, likely mostly on organic matter. Some elements behave in similar fashion as they share similar geochemical properties and originate from the same minerals. For example, Rb and Cs, as well as Tl, follows K; Mg, Sr, Ba, and Mn follow Ca. Some elements are quickly mobilized and then their concentrations drop because of precipitation (Al, Fe, Cr) or sorption (oxyanions such as V, Se, and P). Ionic composition experiments illustrate that the nature of the major cation impacts trace element mobilization. Their concentration is highest in general with Ca but concentrations of some elements are higher with K (NH_4, Rb, Cs, Sb, Tl) or Na (F, V, Cu, Mo, Cd) or indifferent (Ti, Fe, Zn, As, Se).

Overall, from an operational standpoint, experiments demonstrated that HF stimulation leads to an increase in matrix porosity and permeability thanks to geochemical interactions. They also suggested that scaling elements such as Ba and Sr are indeed mobilized The limited number of experiments indicate that these results are preliminary and must be firmed up by (1) repeating the same experiments to eliminate the issue of heterogeneity and build significant statistical results and (2) by devising additional experiments and observations and attending to field produced water sampling.

V. Discussion

In the Results Section we documented that (1) high methane concentrations occur clustered and (2) are likely natural. As mentioned in the introduction, proving a negative in such a complex system is difficult and we cannot exclude that some dissolved methane occurrences could be related to well leakage. However, there is no need to invoke gas leakage to explain field observations. Structural and stratigraphic features explain the presence of thermogenic methane in shallow groundwater in the Haynesville and Barnett shale plays.

It is important to differentiate between the various types of flow that can transport methane: (1) dissolved state in the water and no gas phase, (2) multiphase flow in an independent gas phase as well as dissolved in the water; and (3) bubble flow in which the gas phase occurs in small disconnected bubbles or blobs and does not behave as a coherent phase but rather more as buoyant particles responding to water flow (some methane is also dissolved in the water). Liu et al. (2014) took a look at the time dynamics of phase transfer of methane and CO_2 between gas and aqueous phases. Note that effervescing methane at the surface does not necessarily infer that bubble flow is occurring. Our field observations in the Barnett Shale suggest that there are two types of water wells with methane: (1) wells directly tapping a small non-economic accumulation of the Center Mill type at the top of the Lower Strawn (known examples are the two bubbling wells and the collapsed well, the abandoned PWS Lake County Acres well, and other PWS wells) They are characterized by multiphase flow as seen on the video camera. And (2) wells tapping the Trinity or the Strawn with dissolved methane either at saturation or not at sampling depth (oversaturated at 1 atm). Gas accumulations generate a halo of dissolved methane as seen in produced water and more generally regionally in areas with multiples gas reservoirs (for example, Buckley et al. (1958). The variability in dissolved methane values in the Parker-Hood cluster confirms that natural gas accumulations are small and not large enough to impart high dissolved methane values to the entire aquifer water mass. An issue with well integrity can make a water well behave from a geochemical signal standpoint similarly to a small accumulation drawing down with a nitrogen isotope shift to lighter values. However, observed nitrogen isotopic data suggest this is not the case. Mechanisms other than those related to well integrity have been proposed to explain high methane concentrations: (1) water level drop, (2) (air)drilling (comm. Dan Soeder in GWPC, 2013; Geng et al., 2014).

Water level drop can be characterized by two endmembers: regional drop because of the overall water withdrawal from many wells over many years and local temporary drop because the pump in an individual well has been turned on. Examination of aquifer water levels through time during the past decades in the vicinity of the Parker-Hood cluster and anecdotal historical and current knowledge show that water levels have somewhat fluctuated in the outcrop area of the Trinity aquifers and do not show the massive decline observed in the downdip sections of the aquifer (Kelley et al., 2014, p.4.3-15 and their Table 4.3.8), in particular the large cone of depression centered in Tarrant County. However we know that predevelopment levels from more than a century ago where higher because of the presence of flowing wells (Hill, 1901; Fiedler, 1934; Kelley et al., 2014, Fig. 4.3.23, p.4.7-2) and numerous springs along stream and in river valleys. Flowing wells and springs seemed to be related to relatively short paths along river valleys (Hill 1901, Plate LXVIII). The regrettable habit of not capping flowing wells in the early part of the 20th century led to a general drop in water levels. This likely drop occurred before water level measurements became routine. The more recent water level measurements (Figure 75) suggests that large drawdowns are confined to the pumping well area and does not extend to

the entire aquifer. Such a drop in pressure, both regional historical and local, will nucleate tiny bubbles of exsolving gas when methane becomes oversaturated that would advect with the water towards the low head / pressure area, that is, the well during recovery. The bubbles could collect and coalesce in mini-traps under a small shale or silt stringer. However, the newly created gas pocket will no flow / migrate vertically through the small barriers because of multiphase flow processes (capillary entry pressure). It takes much longer for a gas pocket to shrink than to form it because of the reduced surface area with the flowing groundwater.

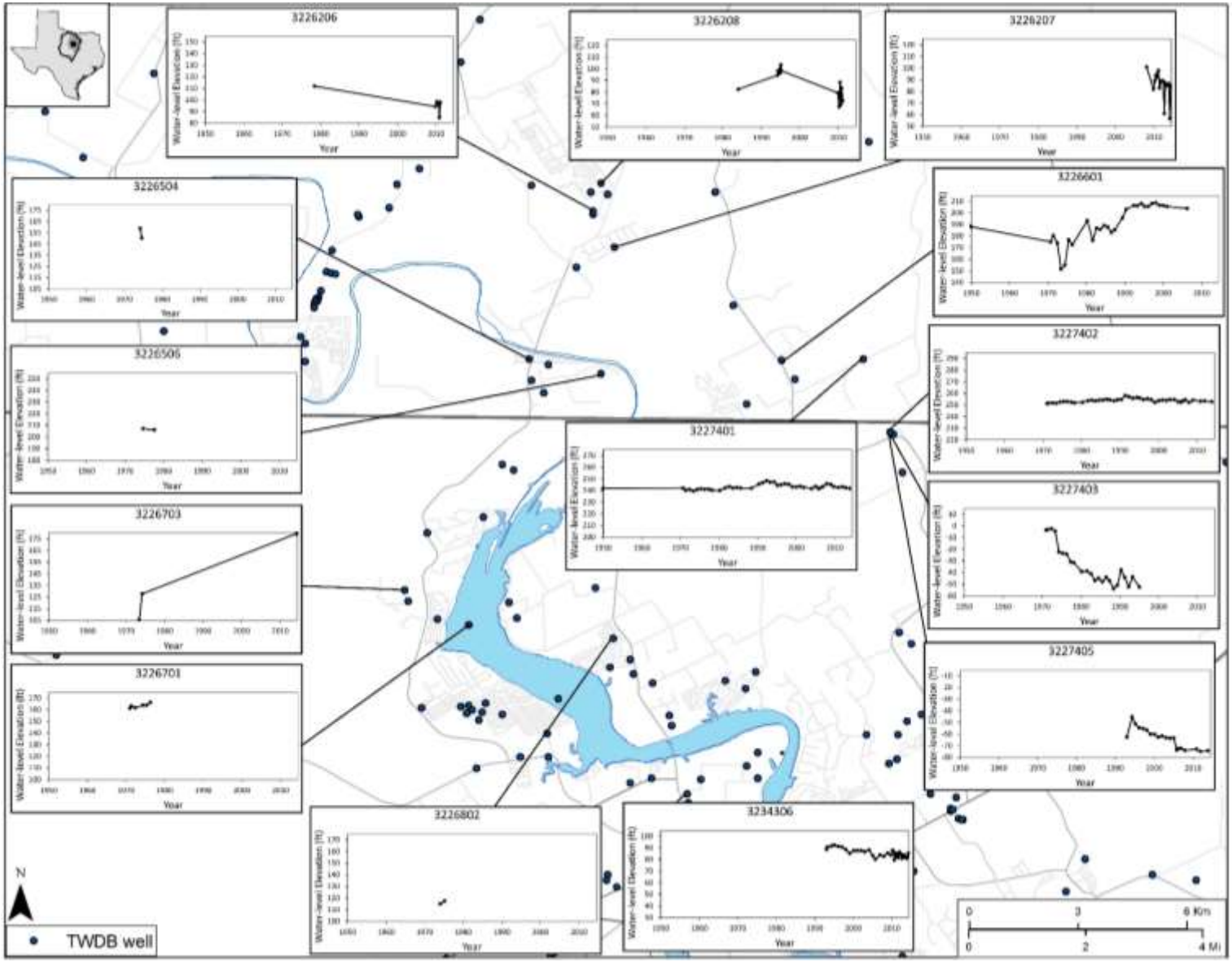

Note: time scale is identical on all plots (1950-2015); all vertical axes span 70ft; vertical axis represents elevation of water level.

Figure 75. Water level measurements through time in the Parker-Hood cluster

VI. Best Management Practices

Best Management Practices (BMP's) should be implemented at several levels: (1) water well construction, (2) oil/gas well construction, and (3) baseline sampling and monitoring

VI-1. Water Wells

Whatever the source of the gas, the most recommended way is to install a venting system to avoid gas accumulation in the well headspace and to locate the well head in a well-ventilated area. This is a standard procedure used by drillers in areas known for stray gas which should be strongly encouraged. Methane forms an explosive mixture between the concentration of 5 and 15% but can be diluted back to flammable levels at concentrations higher than 15%. Two states, Alaska and Pennsylvania, have no standard for water well construction that may exacerbate the problem in the latter state.

VI-2. Oil and Gas Wells

Aquifers are protected by a so-called surface casing when wells targeting deeper formations are drilled through them. A key component of the surface casing is the cement filling the space between the formation and the steel casing. The integrity of the surface casing is not a new topic. The oil and gas industry has been constantly improving well construction. History of oil and gas regulations pertaining to groundwater protection is highlighted in many documents including GWPC (2011) and Nicot (2009). There are many well-documented cases of surface casing failure and the mechanisms are well-known (Dusseault and Jackson, 2014; EPA, 2015b), if not easy to fix. For example, although migration of methane by diffusion or along existing subsurface fractures was possible, the USGS found that manmade conduits accounted for most of the methane found in shallow groundwater in the Animas River Valley of Colorado and New Mexico (Chafin, 1994). The source of methane in the aquifer was attributed to uncemented annuli of gas wells in addition to seepage from deep bedrock water wells (Chafin, 1994). The highest concentration of dissolved methane in groundwater, at 127 mg/L, was found by Harder et al. (1965) in shallow groundwater near active oil and gas fields of southwestern Louisiana. Leaky or defective casing was identified as the source. Faulty casing in the Bammel Gas Field near Houston was found to be responsible for the sudden rise in groundwater elevation, upwards of 20 to 30 feet in some instances, temporarily inducing flowing artesian conditions in several wells in 1943. Water levels rose 4 to 61 feet at distances up to 11.7 miles from one gas well. Shallow water-bearing sands were charged with methane at a depth of about 600 feet, with an estimate of 6 billion gallons of groundwater being displaced due to the gas production well casing failure; the impact on groundwater quality was not reported (Rose and Alexander, 1945).

The flow mechanics of well leakage within the wellbore system are relatively well-known (Hasan and Kabir, 1988; Dusseault and Jackson, 2014). For example, gas accumulates under the surface casing and can move along the casing when the pressure is high enough to overcome the capillary entry pressure of the material / fracture / opening; the current literature suggests that a common mechanism is to have coalesced gas bubbles flow in the wellbore or along string in slugs. This could happen when stray gas is present below the level of the surface casing if the well is not cemented all the way, which is common as most wells are not cemented from wellhead to shoe. The current issue with well leakage seems to be those cases in which the

integrity of the well itself is assured but the connection rock-cement is not sufficient to keep foreign fluids from migrating along the outside of the well system. Such a wellbore will protect the fresh-water aquifers from the fluids circulating within the wellbore as demonstrated by regular pressure tests but will fail to protect them from gas migrating along the failed cement-rock connection as it might have happened in Wise County (see Appendix I: Wise County Litigation) and is suggested to have happened in the Parker-Hood cluster in Darrah et al. (2014).

VI-3. Baseline Sampling and Monitoring

It is important to note that baseline sampling, sometimes called predrill sampling by operators, and monitoring are two different concepts. Baseline sampling is an adhoc approach that uses available wells, often private domestic wells, at non-optimized locations with screen(s) spanning several formations. Baseline sampling achieves the goal of following regulations, gaining a general understanding of the local water quality, and improving relations with residents. It should be done at least before HF stimulation or better before drilling starts. Baseline is also different from background that would represent the pristine environment (that is, without anthropogenic influence that may go back centuries but not necessarily not contaminated as natural contamination is not uncommon). A major drawback of baseline sampling is that it relies mostly on domestic wells whose characteristics and conditions are not well known (unreliable location of screen intervals, intermittent pumping, may not be located in the plume path, that is, downgradient of water flow, downgradient itself may not be well-defined at this location and may be shifting seasonally and according to pumping).

Monitoring on the other hand uses dedicated wells, screened at narrow depth intervals, and located at carefully selected sites. Monitoring wells are typically sampled at regular time intervals for long multiyear periods. They can be broadly divided into two categories: (1) local ("landfill" or "contaminated site" type) to monitor an oil or gas well, a pad or a group of pads and (2) regional to detect distributed contamination. A Canadian expert panel (CCA, 2014, p.162) in its review of impacts of HF also sorted the various types of monitoring into performance, sentry, and receptor monitoring approaches. Receptor monitoring would be approximately equivalent to baseline whereas performance and sentry monitoring would be equivalent to categories (1) and (2) defined above, respectively. Esser et al. (2015, p.63) discussing the CA case proposed the same concepts called area-specific and regional-specific monitoring and went into some details in what they would entail. In any case, it is important to define what the monitoring objectives are: catch offenders, track regional water quality, protect domestic and municipal wells, assess presence of methane or contaminants. Who should do the monitoring?: the operator, the state, the local water agency? Where would the monitoring take place? Within the lease? At the lease boundary?

A staged or tiered approach is also recommended by adding analyses as problems or perceived problems are uncovered. Several states (ODNR, 2012, 2014; WOGCC, 2014; COGCC, 2015), organizations (NGWA, 2012; MSC, 2012; WRF-AWWA, 2015), trade groups (API, 2009), academic or research institutions (Esser et al., 2015) or companies (Chesapeake, McElreath, 2012) have proposed lists of field parameters and chemical elements to analyze. Suggested parameters to measure vary. However, the required/suggested field parameters follow generally accepted sampling practices: Eh, DO, pH, conductivity, temperature, alkalinity to which could be added field turbidity and maybe dissolved H_2S using field probe. These field measurements are to be complemented in the lab by total suspended solids (TSS) and TDS measurements. Also part

of the Tier 1 “general” analysis are the so-called major ions generally analyzed through IC (Na, K, Ca, Mg, Cl, SO_4 to which the anions PO_4 and NO_3 can be added and the minor and trace elements generally analyzed through ICP. These would include elements that could called “regulated” in particular common natural contaminants with a low MCL such as As and Se (10 ppb each) or Cr (100 ppb), or “diagnostic”. As and Se are regulated but they can also be diagnostic. They are released from FeOx coatings when the minerals are dissolved to provide electron acceptors to microbes degrading methane and/or other organics. Diagnostic elements could be natural but they are also frequently associated with oil and gas activities and are compoments of drilling fluids or formation brines (wellbores, equipment, storage pits). Such elements include Br (and I, not typically analyzed), B, Li and Sr, generally indicative of brine / produced water contamination along with higher than expected TDS, Na and Cl; B could also originate from the cross-linkers used in HF gel stimulations. High concentrations of Ca when not expected and certainly of K could also be indicative of the presence of drilling fluids. NO_3 suggests surface or shallow contamination. High pH coud be symptomatic of a cementing issue. High Fe and /or Mn could be symptomatic of active redox reactions maybe degrading organic coumpounds such as light alkanes or associated with oil and gas production (FeOx dissolution). An increase in turbidity may indicate mechanical action from drilling / stimulating, breakthrough of a plume, or a change in chemistry loosening up attached particles.

Other parameters ought to be included in a Tier 1 general analysis are dissolved methane (and light alkanes C2-C5 as appropriate) and BTEX / diesel range organics (DRO) / gasoline range organics (GRO) or TPH or TOC. Benzene is a “regulated’ contaminant (MCL of 5 ppb) that would be indicative of brine or produced water if surface sources (e.g., gasoline) have been ruled out.

Well headspace gas analyses and air methane concentrations next to a water well are important safety measurements but they are qualitative at best in relation with dissolved methane concentrations and should not be relied on for scientific investigations. Some authors have noted a reasonably positive correlation between dissolved and headspace methane concentrations (Mayer et al., 2015).

Tier 2 analysis would kick in if an anomaly is suspected in the Tier 1 results. It would not necessarily require new sampling. For example, if dissolved methane is beyond some threshold, methane C isotopes should be analyzed right away without additional sampling. The technical threshold to routinely access C isotopes of methane is in the 0.1 to 1 mg/L range but this value is likely too conservative for baseline monitoring, a threshold of 1, 2 or even 5 mg/L seems more appropriate. Similarly if the presence of BTEX or of organics is detected, it could be useful to determine the chemical family they belong to (glycols, surfactants, etc.). Ra is of concern only if there is Ba and no sulfate as Ra and Ba share a common chemical behavior.

A Tier 3 analysis will collect information for a scientific evaluation with sampling for C and D isotopes of methane, ethane, and propane, water, Sr and S isotopes, and noble gases.

In Ohio, for conventional oil and gas wells, the regulatory agency, ODNR, recommends analyzing water samples for conductivity, pH, Na, Ca, Fe, Mg, K, Ba, Cl, SO_4, alkalinity, TDS (ODNR, 2012). For Marcellus and Utica unconventional wells, they recommend to add TSS/turbidity, Sr, Mn, Br, BTEX, and CH_4 (ODNR, 2014) for concerned well owners. NGWA and GWPC also suggest the same parameters to which they add As, B, Cr, Se, U as well as DRO, GRO and total petroleum hydrocarbons or oil and grease (“HEM”, N-Hexane Extractable

Material). Chesapeake (McElreath, 2012) has a more complete list of analysis consisting in the same field parameters: pH, conductivity, turbidity to which temperature, DO, Eh, and H_2S are added. They also analyze for the same major and minor elements, Na, Ca, Mg, Ba, Sr, K, Fe, Mn, Cl, Br, SO_4, alkalinity, TDS and TSS but do a longer suite of trace elements: Ag, As, Cd, Cr, Hg, Li, Pb, Se. They also analyze for BTEX and HEM and dissolved C1-C3 and do C isotopic analyses only if CH_4>20mg/L and use the MBAS assay (methylene blue active substance) to detect surfactants. In Colorado, the COGCC (2015) states in its regulation that initial water samples must be analyzed for major anions (Br, Cl, F, SO_4, NO_3 and NO_2, P), major cations (Ca, Fe, Mg, Mn, K, Na), other elements (Ba, B, Se, and Sr), presence of bacteria (iron related, sulfate reducing, slime forming), TPH and BTEX. Field parameters such as pH, specific conductance, TDS, dissolved gases (methane, ethane, propane), alkalinity and observations such as odor, water color, sediment, bubbles, and effervescence have also to be noted. Relative to methane sampling COGCC also indicates that "*If free gas or a dissolved methane concentration greater than 1.0 mg/L is detected in a water sample, gas compositional analysis and stable isotope analysis of the methane (carbon and hydrogen – 12C, 13C, 1H and 2H) shall be performed to determine gas type. The operator shall notify the Director and the owner of the water well immediately if: A. the test results indicated thermogenic or a mixture of thermogenic and biogenic gas; B. the methane concentration increases by more than 5.0 mg/l between sampling periods; or C. the methane concentration is detected at or above 10 mg/l.*" Wyoming (WOGCC, 2014) requires to report BTEX, DRO, GRO, and dissolved gas and isotopic analyses only but requires or suggests (?) analyzing a list of constituents similar to that of Colorado. Esser et al. (2015, their Table 6.2 and p.134ff), in California, presented proposed requirements for baseline sampling. They also proposed monitoring requirements. The recommended approach is tiered with Tier 1 consisting of field parameters (and dissolved H_2S), so-called major anions (Cl, SO_4, NO_3, Br, I, F) and major cations (Na, Ca, K, NH_4), trace elements (e.g., Ba, B, Li, Sr), regulated metals (As, Cu, Cr, Se), radionuclides (Ra, U), BTEX and naphthalene and PAH's, TPH, dissolved light alkanes and their isotopes, isotopes of water, and two unspecified indicators in addition to guar gum components (most HF operations are currently gelled HF stimulations in CA). Unlike other states, CA, through the proposed rules in Esser et al., (2015), targets the additives themselves rather than the proxy chemicals that would accompany them. The Tier 2 analysis would be of compounds actually used in nearby HF stimulations such as various surfactants, alcohols, and biocides (Esser et al., 2015, p.136). .

As we just discussed, several states have regulations or guidelines on how to perform baseline sampling (Table 3) but others such as TX, OK, ND, and LA have no mandatory sampling even if most oil and gas companies do do baseline sampling. The numbers of water wells, the maximum distance from the well to be stimulated, the sampling frequency are very variable. At least one state (PA) puts the burden of proof on the operating company that a water well has not been contaminated by oil and gas operations if water well analyses show contamination although there is no required sampling or required list of constituents. There are still many kinks to solve to improve baseline programs, for example, a concern is seasonal variability and timing relative to the water well use (pumping) (Coleman and McElreath, 2012). The federal government (BLM, 2015, p.228) does not plan to blanket-require baseline sampling. In addition, no state at this point requires monitoring (e.g., Esser et al., 2015, p.52) but several countries have published guidelines suggesting it.

There has been some discussion in the use of introduced tracers to tag individual well or operator (for example, Esser et al., 2015, p.90) as opposed to using natural tracers such as trace element

concentrations, elemental ratios, or isotopes or isotopic ratios. Introduced tracers has been generally accepted as a good research tool but their use run into operational and tracking issues when used on a large scale. More sophisticated but relatively easy to manufacture tracers such as non-biologic DNA strands and nanoparticles have also been suggested. The City of Dallas, TX requires introduced tracers although the drilling activity within the city limits is minor. Minutes from the November 20, 2013 city council reports that "*A (non-radioactive) tagging additive must be added to fracturing fluid that provides a unique identifier for the site*" (City of Dallas, 2013, p.54 and 129). The authors are not aware of any other instance of mandatory tracers.

Table 3. State baseline sampling programs

State	Sampling radius (ft.)	Number of Wells	Timing* (*presumed liability)	Post-Drill Sampling
PA*	2500	All	1 year after*	No
WV*	1000	Owner request	Prior to drilling	TBD
CO	2640	All to 4 max	1 year prior	Yes, 3 (1, 3, 6 years)
OH	1500	All	Prior to drilling	No
ND	2640	All	1 year prior	No
NY	1000	All	Prior to site disturbance	Yes, TBD
CA	1500	All	Prior to drilling	Yes
IL (draft)	1500	All (3 samples)	Prior to drilling	Yes, 3 (6, 18, 30 months)
WY	2640	All to 4 max	Prior to drilling	Yes, 2 (2, 4 years)
MI (draft)	1320	Up to 10	<6 months prior	No
NC (draft)	2640	All	Prior to drilling	Yes

*: the operator is assumed liable if a problem arises unless it can be proven otherwise
Modified from Puls (2014); The following states have no rules, and none appear pending: OK, TX, LA, KS, and AR

Contributions of this work

Overall, the history of the Parker-Hood cluster demonstrates that even with sampling and analyses as suggested in several state rules as described above, the findings for the source of the methane are still being argued. The use of nitrogen isotopes helped constrained the level of exchange between the source of the natural gas and the shallow aquifers, the use of aqueous natural tracers would not have helped because there is no actual change in chemistry with or without methane. The use of a gaseous tracer such as SF6 or PFC's (perfluorocarbons) could have helped establish whether there were more than a hydraulic connection but an actual transport pathway between the shallow sections of the implicated gas wells and the methane-rich water wells. However tracers detectable at minute ppt (part per trillion) concentrations are difficult to work with and it is not clear how the tracer could have been injected in producing wells; it could have been done dissolved in the HF fluids from which it would partition into the gas phase as pressure drops downhole at the onset of flowback.

VI-4. Technology Transfer

BEG has presented partial results of this study at several conferences and workshops. They are listed in Appendix A: Conference Abstracts and Papers.

VII. Conclusions

A total of 784 unique locations and more than 900 water well samples were taken across the state of Texas to test for the presence of dissolved methane. Methane is abundant at low concentrations, likely of microbial origin, and seems to occur in clusters at higher concentrations. It is then mostly of thermogenic origin, that is, it occurs in localized areas where favorable conditions are met. They include a source such as gas reservoirs (Barnett), lignite (Haynesville and Eagle Ford), intense oil degradation (maybe Eagle Ford where the thermogenic origin is less clear) that combined with structural features (unconformity, faults, fractures) can guide the location of the clusters. The same observation is true in the Marcellus Shale footprint where the consensus is also that methane is not sourced from the Marcellus but from higher in the section. Two of the current hypotheses that would explain higher concentration next to gas wells as described in Osborn et al. (2011) and Jackson, Vengosh et al. (2013) within the more general context of topographic influence (Molofsky et al., 2013) are (1) defective casing with methane traveling along the cement-rock contact and (2) mobilization of methane due to the pressure surge during air drilling (comm. Dan Soeder in GWPC, 2013; Geng et al., 2014). Although these two mechanisms do not need to be called upon to explain field observations in Texas, they cannot be ruled out for a specific well unless more detailed study is performed.

Current simple fingerprinting approaches (δD and $\delta^{13}C$ of methane) to link a methane occurrence to a source is not selective enough and is currently done in a holistic fashion that requires the involvement of experts. Adding noble gases and nitrogen isotopes help but there is a need to develop tools that would provide residence time and flux and therefore discriminate between recently introduced material and more long-term processes. For example, nitrogen isotopes show that high methane concentration can be achieved with a low flux and relatively high ^{4}He can suggest a long transit time.

There are several avenues for research to improve our knowledge of the behavior of methane and light alkanes in the subsurface. There is a need to understand the ability of the natural system to process the methane, be it geogenic or anthropogenic contamination. Microorganisms often require an acclimation before being efficient at degrading newly introduced organic molecules. It could be used to differentiate sources of thermogenic methane. Better understand the assimilative capacity of aquifers is also important as it will control the time period in which a slug of natural gas would be degraded / volatilized / dispersed.

VIII. References

Adams, L., 2013, Working with oil and gas in Panola County, presented at 2013 Texas Groundwater, Summit, Texas Alliance of Groundwater Districts (TAGD), last accessed September 3, 2015, https://www.regonline.com/builder/site/tab3.aspx?EventID=1201482.

Adams, R. L., 2009, Basement tectonics and origin of the Sabine Uplift: Gulf Coast Association of Geological Societies Transactions, v. 59, p. 3-19.

Adams, N. and D., Strickland, 1999, Handling a shallow gas blowout in Southeast Texas. World Oil, April 1999. p.137 – 146

Al, T. A., J. Leblanc and S. Phillips, 2013, A Study of Groundwater Quality from Domestic Wells in the Sussex and Elgin Regions, New Brunswick: with Comparison to Deep Formation Water and Gas from the McCully Gas Field, Geological Survey of Canada Open File 7449, 34p.

Almond, S., A. Clancy, R. J. Davies, and F. Worrall, 2014, The flux of radionuclides in flowback fluid from shale gas exploitation, Environ. Sci. Pollut. Res., (21), p.12316–12324. doi:10.1007/s11356-014-3118-y

Alley, B., A. Beebe, J. Rodgers, and J. W. Castle, 2011, Chemical and physical characterization of produced waters from conventional and unconventional fossil fuel resources, Chemosphere, 85(1), p.74-82. doi: 10.1016/j.chemosphere.2011.05.043.

Anaya, R. and Jones, I. C., 2009, Groundwater availability model for the Edwards-Trinity (Plateau) and Pecos Valley aquifers of Texas: Texas Water Development Board Report 373, 103p.

API, 2009, Hydraulic Fracturing Operations—Well Construction and Integrity Guidelines, API Guidance Document HF1, First Edition, October 2009, 24p.

Aravena, R., L.I. Wassenaar, and J.F. Barker, 1995, Distribution and Isotopic Characterization of Methane in a Confined Aquifer in Southern Ontario, Canada. Journal of Hydrology, 173(1-4), p.51-70.

Ayers, W. B., Jr., and Lewis, A. H., 1985, The Wilcox Group and Carrizo Sand (Paleogene) in East-Central Texas: depositional systems and deep-basin lignite: The University of Texas at Austin, Bureau of Economic Geology, 19 p. + 30 pl.

Baker, E.T., 1960, Geology and Groundwater Resources of Grayson County, Texas, Texas Board of Water Engineers Bulletin 6013, 66p., https://www.twdb.texas.gov/publications/reports/bulletins/doc/B6013.pdf.

Baldassare, F. J. and Laughrey, C. D., 1997, Identifying the Sources of Stray Methane by Using Geochemical and Isotopic Fingerprinting, Environmental Geosciences, 4(2), p.85–94.

Baldassare, F. J., M. A. McCaffrey, and J. A. Harper, 2014, A geochemical context for stray gas investigations in the northern Appalachian Basin: Implications of analyses of natural gases from Neogene-through Devonian-age strata, AAPG Bulletin, 98(2), p.341–372.

Bankey, V., 2006, Texas magnetic and gravity maps and data, U.S. Geological Survey Data Series DS-232, http://pubs.usgs.gov/ds/2006/232/

Bené, P. G., Harden, R., Griffin, S. W., and Nicot, J.-P., 2007, Northern Trinity/Woodbine aquifer groundwater availability model: assessment of groundwater use in the northern Trinity aquifer due to urban growth and Barnett Shale development: Texas Water Development Board, TWDB Contract Number 0604830613, 50 p. + apps.

Bernard B.B., Brooks J.M. and Sackett W.M., 1976. Natural gas seepage in the Gulf of Mexico. Earth and Planetary Science Letters, 31(1): 48–54.

Bernard, B.B., Brooks, J.M. and Sackett, W.M. 1977, Light Hydrocarbons in Recent Continental Shelf and Slope Sediments, Journal of Geophysical Research, 83, p.4053-4061.

BGS (British Geological Survey), 2015, National methane baseline survey of UK groundwaters, http://www.bgs.ac.uk/research/groundwater/shaleGas/methaneBaseline/home.html, last accessed September 6, 2015

BLM (Bureau of Land Management), 2015, 43 CFR Part 3160: Oil and Gas; Hydraulic Fracturing on Federal and Indian Lands, http://www.gpo.gov/fdsys/pkg/FR-2015-03-26/pdf/2015-06658.pdf, last accessed October 3, 2015.

Blondes M. S., K. D. Gans, J. J. Thordsen, M. E. Reidy, B. Thomas, M. A. Engle, Y. K. Kharaka, and E. L. Rowan, 2014, U.S. Geological Survey National Produced Waters Geochemical Database v2.1 (provisional), http://energy.usgs.gov/EnvironmentalAspects/EnvironmentalAspectsofEnergyProductionandUse/ProducedWaters.aspx#3822349-data

Brown, L. F., Jr., A. W. Cleaves, II, et al. (1973). Pennsylvanian depositional systems in north-central Texas. Guidebook 14. Prepared for the annual meeting of the Geological Society of America, November, 1973. Austin, Texas, The University of Texas at Austin Bureau of Economic Geology, 122p.

Brune, G., 1975, Major and historical springs of Texas: Texas Water Development Board Report 189, 95 p.

Brune, G., 2002, Springs of Texas: Texas A&M University Press, College Station, TX, Vol.1, 2nd edition, 566p.

Buckley, S. E., Hocott, C. R. and Taggart, Jr M. S., 1958, Distribution of dissolved hydrocarbons in subsurface waters. Habitat of oil: Am. Assoc. Petroleum Geologists, p.850-882.

CAPP (Canadian Association of Petroleum Producers), 1995, Migration of methane into groundwater from leaking production wells near Lloydminster, March 1995, CAPP Pub. #1995-0001, 47p.+Appendices

CAPP (Canadian Association of Petroleum Producers), 1996, Migration of methane into groundwater from leaking production wells near Lloydminster, Report for Phase 2 (1995), March 1996, CAPP Pub. #1996-0003, 75p.+Appendices

Carlson, D. and M. Horn, 2013, Variation of Methane and Ion Concentrations in the Wilcox Aquifer among several Neighborhoods near Bossier City, Louisiana (Abstract), GCAGS and GCSSEPM 63rd Annual Convention, New Orleans, Louisiana, October 6-8, 2013, AAPG Search and Discovery Article #90167.

Carlson, D. and M. Horn, 2014, Methane and VOC concentration within southern Bossier, southern Caddo and northern De Soto Parish (DRAFT), Louisiana Geological Survey Report of Investigation 14-01, 130p.

Carlton, D. P., 1929, West Columbia salt dome and oil field, Brazoria County, Texas, AAPG Bull. 13, 1929, p.451 – 469

Cartwright, M. J., 1987, Continued effects of gas well blowout in Northwestern Harris County, Railroad Commission of Texas, December 22, 1987, 18p.+Figures and Appendices

Council of Canadian Academies (CCA), 2014, Environmental Impacts of Shale Gas Extraction in Canada, The Expert Panel on Harnessing Science and Technology to Understand the Environmental Impacts of Shale Gas Extraction, 262p.

Chacko J. J., G. Maciasz, and B. J. Harder, 1998, Gulf Coast geopressured-geothermal program summary report compilation, report prepared by Louisiana State University submitted to U.S. Department of Energy, 5 volumes.

Chafin, D. T., 1994, Sources and Migration Pathways of Natural Gas in New-Surface Ground Water beneath the Animas River Valley, Colorado and New Mexico. U.S. Geological Survey Water-Resources Investigations Report 94 – 4006. 65 pp.

Cheung, K., P. Klassen, B. Mayer, F. Goodarzi, R. Aravena, 2010, Major ion and isotope geochemistry of fluids and gases from coalbed methane and shallow groundwater wells in Alberta, Canada, Applied Geochemistry, 25, p.1307-1329, doi: 10.1016/j.apgeochem.2010.06.002

Chowdhury, A. H., S. Wade, R. E. Mace, and C. Ridgeway, 2004, Groundwater Availability Model of the Central Gulf Coast Aquifer System: Numerical Simulations through 1999, 108p, https://www.twdb.texas.gov/groundwater/models/gam/glfc_c/glfc_c.asp, last accessed October 4, 2015.

City of Dallas, 2013, November 20, 2013 City Council minutes, last accessed August 19, 2015 http://dallascityhall.com/government/Council%20Meeting%20Documents/2014/FinalBriefing_Combined_11202013.pdf

Cleaves, A. W., II, 1975, Upper Desmoinesian-Lower Missourian depositional systems (Pennsylvanian), north-central Texas. Austin, The University of Texas at Austin, Ph.D. Thesis, 257p.

Cleaves, A. W. and A.W. Erxleben, 1985, Upper Strawn and Canyon cratonic deposition of the Bend Arch, North-Central Texas, Fort Worth Geological Society, Southwest Section, AAPG 1985 Convention, February, 24-26, 1985. Transactions. p.27-46.

CLI (Core Laboratories Inc.), 1972, A survey of the subsurface saline water of Texas: Texas Water Development Board Report 157, 113p.

COGCC (Colorado Oil and Gas Conservation Commission), 2015, Rule 609: Statewide groundwater baseline sampling and monitoring, April 2015, last accessed October 2, 2015, https://cogcc.state.co.us/RR_Docs_new/rules/600Series.pdf

Coleman N. and D. McElreath, 2012, Short-term intra-well variability in methane concentrations from domestic well waters in northeastern Pennsylvania, GWPC Stray Gas Incidence and

Response Forum, July 24-26, 2012, Cleveland, Ohio, last accessed October 2, 2015. http://www.gwpc.org/sites/default/files/event-sessions/Coleman_Nancy.pdf.

Collier Consulting, Inc., 2003, Well videos, cross-section, and recommendations, Lake Country Acres PWS ID # 1110059, Parker and Hood Counties, TX, 10p.

Cozzarelli, I.M., Böhlke, J. K., Masoner, J., Breit, G.N., Lorah, M. M., Tuttle, M.L.W., and Jaeschke, J.B., 2011, Biogeochemical Evolution of a Landfill Leachate Plume, Norman, Oklahoma, Ground Water, 49(5), p.663–687, doi: 10.1111/j.1745-6584.2010.00792.x.

Darin, L. G. and E. B. Bowles, 2011, Shale Gas Measurement and Associated Issues, Pipeline & Gas Journal, July 2011, 238 (7)

Darling, B. K., 2014, Stable isotope forensics as a means of differentiating between thermogenic and biogenic gases in the Wilcox Aquifer, Haynesville Shale trend, Caddo Parish, Louisiana: Gulf Coast Association of Geological Societies Transactions, v. 64, p. 677. Presentation slides at http://www.tapgonline.org/pdf/BruceDarling.pdf.

Darrah, T. H., A. Vengosh, R. B. Jackson, N. R. Warner, and R. J. Poreda, 2014, Noble gases identify the mechanisms of fugitive gas contamination in drinking-water wells overlying the Marcellus and Barnett Shales, PNAS, 111(39), p.14076–14081. doi: 10.1073/pnas.1322107111.

Davis, J. B., and R. M. Squires, 1954, Detection of microbially produced gaseous hydrocarbons other than methane, Science, 119, 381-382,

Deeds, N. E., T. Yan, A. Singh, T. L. Jones, V. A. Kelley, P. R. Knox, S. C. Young, 2010, Groundwater Availability Model for the Yegua-Jackson Aquifer, variously paginated, http://www.twdb.texas.gov/groundwater/models/gam/ygjk/YGJK_Model_Report.pdf

DiGiulio, D. C., Wilkin, R. T., Miller, C. and Oberley, G., 2011, Draft Investigation of Ground Water Contamination near Pavillion, Wyoming., US EPA, 43p. + Appendices, http://www2.epa.gov/sites/production/files/documents/EPA_ReportOnPavillion_Dec-8-2011.pdf. Last accessed October 3, 2015.

Dornfeld, W. A., 2012, Basement control as origins of the Mount Enterprise Fault System (MEFS): A possible degassing mechanism of the Haynesville Shale, Rusk County, Texas, MS Thesis, Stephen F. Austin State University, May 2012, 120p.

Dornfeld, A., Brown, W., and Stafford, K., 2012, Basement control as origins of the Mount Enterprise Fault System (MEFS): A possible degassing mechanism of the Haynesville Shale, Rusk County, Texas (*Abstract*), GSA South-Central Section - 46th Annual Meeting, 8–9 March 2012, Abstracts with Programs, Vol. 44, No. 1, p. 6.

Dusseault M. and R. Jackson, 2014, Seepage pathway assessment for natural gas to shallow groundwater during well stimulation, in production, and after abandonment, Environmental Geosciences, 21(3), p.107–126.

Dutton, A. R., B. Harden, J.-P. Nicot, and D. O'Rourke, 2003, Groundwater Availability Model for the Central Part of the Carrizo-Wilcox aquifer in Texas, 55p. http://www.twdb.texas.gov/groundwater/models/gam/czwx_c/CZWX_C_Full_Report.pdf

Ehlmann, A. J. and R. J. Ehlmann, 1985, The Aledo southeast (1200' Strawn) gas field and associated deeper production, southeast Parker and southwest Tarrant counties, Texas, Southwest Section – AAPG, 1985 Convention, February 24-26. Transactions. P. 100-106.

Eltschlager, K.K., Hawkins, J.W., Ehler, W.C., and Baldassare, F., 2001, Technical measures for the investigation and mitigation of fugitive methane hazards in areas of coal mining: Office of Surface Mining Reclamation and Enforcement, 125 p. last accessed August 30, 2015. http://www.osmre.gov/resources/library/ghm/methane.pdf.

Erxleben, A. W. and A. W. Cleaves, 1985, Strawn-Canyon depositional systems: North-Central Texas, Southwest Section, AAPG. Middle & Upper Pennsylvanian Cratonic Basin Facies Models, North Central Texas. Fieldtrip Guidebook. p.1-12.

Esser, B. K., H. R. Beller, S. A. Carroll, J. A. Cherry, J. Gillespie, R. B. Jackson, P. D. Jordan, V. Madrid, J. P. Morris, B. L. Parker, W. T. Stringfellow, C. Varadharajan, and A. Vengosh , 2015, Recommendations on Model Criteria for Groundwater Sampling, Testing, and Monitoring of Oil and Gas Development in California, Draft Report for Public Release prepared by Lawrence Livermore National Laboratory for California State Water Resources Control Board, LLNL-TR-669645, June 2015, 286p.

Etiope, G., A. Drobniak, and A. Schimmelmann, 2013, Natural seepage of shale gas and the origin of "eternal flames" in the Northern Appalachian Basin, USA, Marine and Petroleum Geology, Marine and Petroleum Geology, 43, p.178–186

Etiope, G.,, 2009, GLOGOS, A New Global Onshore Gas-Oil Seeps Dataset, Search and Discovery Article #70071, last accessed August 19, 2015, http://www.searchanddiscovery.com/documents/2009/090806etiope/

Evans, T. J., 1974, Bituminous coal in Texas: The University of Texas at Austin, Bureau of Economic Geology Handbook 4, 65 p.

Ewing, T. E., 1991, Tectonic Map of Texas (and accompanying text), T. E. Ewing, compiler. Scale 1:750,000. 4 oversized sheets, SM0001. Accompanied by a text booklet, The Tectonic Framework of Texas, 36 p., 1991.

Ewing, J. E., T. L. Jones, T. Yan, A. M. Vreugdenhil, D. G. Fryar, J. F. Pickens, K. Gordon, J. P. Nicot, B. R. Scanlon, J. B. Ashworth, and J. Beach, 2008, Final report groundwater availability model for the Dockum Aquifer: Texas Water Development Board Contracted Report 0604830593, Austin, 510 p.

Ewing, J. E., V. A. Kelley, T. L. Jones, T. Yan, A. Singh, D. W. Powers, R. M. Holt, and J. M. Sharp, 2012, Final groundwater availability model report for the Rustler Aquifer: Texas Water Development Board Contracted Report, Austin, 460 p.

Fiedler, A. G., 1934, Artesian water in Somervell County Texas: U.S. Geological Survey, Water-Supply Paper 660, Washington, D.C., 86p.

Fisher, R. S., 1995, Naturally occurring radioactive materials (NORM) in produced water and scale from Texas oil, gas, and geothermal wells: Geographic, geologic, and geochemical controls, The University of Texas Bureau of Economic Geology Geological Circular #95-3, 43p.

Fisher, R. S., 1998, Geologic and Geochemical Controls on Naturally Occurring Radioactive Materials, Environmental Geosciences, 5(3), p.139–150

Flippin, J., 1982, Stratigraphy, Structure, and Economic Aspects of Paleozoic strata, Erath County, Dallas Geological Society, in Petroleum Geology of the Fort Worth Basin and Bend Arch Area, 2009, p.129-155

Fontenot, B.E., L.R. Hunt, Z.L. Hildenbrand, D.D. Carlton Jr., H. Oka, J.L. Walton, D. Hopkins, A. Osorio, B. Bjorndal, Q.H. Hu, and K.A. Schug. 2013. An evaluation of water quality in private drinking water wells near natural gas extraction sites in the Barnett Shale Formation. Environmental Science & Technology 47, no. 17: 10032–10040.

Galloway, W. E., 1982. Epigenetic zonation and fluid flow history of uranium-bearing fluvial aquifer systems, south Texas uranium province: The University of Texas at Austin, Bureau of Economic Geology Report of Investigations No. 119, 31 p.

Galloway, W. E., C. D. Henry, and G. E. Smith, 1982, Depositional framework, hydrostratigraphy, and uranium mineralization of the Oakville sandstone (Miocene), Texas coastal plain: The University of Texas at Austin, Bureau of Economic Geology Report of Investigations No. 113, 51 p.

Gardner, F. J., 1951, Oil and Gas Field of the Texas Upper Gulf Coast, Five Star Oil Report, Houston, Texas, page 373 of database report provided by the Railroad Commission of Texas, September 20, 2013.

Geng, X., Davatzes, N. C., Soeder, D. J., Torlapati, J., Rodriguez, R. S., and M. C. Boufadel, 2013, Migration of high-pressure air during gas well drilling in the Appalachian Basin, Journal of Environmental Engineering, 46, doi: 10.1061/(ASCE)EE.1943-7870.0000769

George, P. G., R. E. Mace, and R. Petrossian, 2011, Aquifers of Texas, Texas Water Development Board report #380, 172p., last accessed August 22, 2015, http://www.twdb.texas.gov/publications/reports/numbered_reports/doc/R380_AquifersofTexas.pdf

Glass, C. N., 1953, Pierce Junction Field: Harris County, Texas, Houston Geological Society 2007 archived 'Guidebook, Field Trip Routes, Oil Fields, Geology: 1953. p.147 – 150.

Gold, R., 2014, The boom: How fracking ignited the American energy revolution and changed the world, Simon & Schuster, New York, 366p.

Gorody, A. W., 2012. Factors affecting the variability of stray gas concentration and composition in groundwater. Environmental Geosciences, V. 19, no. 1, pp. 17-31.

Gregory, A.R., Dodge, M.M., Posey, J.S., and Morton, R.A., 1980, Volume and accessibility of entrained (solution) methane in deep geopressured reservoirs - tertiary formations of the Texas Gulf Coast. Final report prepared by the Bureau of Economic Geology, The University of Texas at Austin for the U.S. Department of Energy under contract DE-AC08-78ET11397, report #DOE/ET/11397-1, http://www.osti.gov/bridge/product.biblio.jsp?osti_id=5282675

Grossman, E. L., R. W. Hahn, and S. J. Fritz, 1986, Origin of gaseous hydrocarbons in the Sparta aquifer in Brazos and Burleson counties, Texas, Transactions—Gulf Coast Association Of Geological Societies, Vol. XXXVI, p.457-470.

Grossman, E. L., B. K. Coffman, S. J. Fritz, and H. Wada, 1989. Bacterial production of methane and its influence on ground-water chemistry in east-central Texas aquifers. Geology. Vol. 17, pp 495-499.

Grossman, E.L., Zhang, C., Ammerman, J.W., and MacRae, M., 1995, Methane and methanotrophy in Texas aquifers, in Proceedings of the 24th Water for Texas Conference, R. Jensen, ed., Texas Water Resources Institute, College Station, p. 453-456.

Groundwater Protection Council (GWPC), 2013, A White Paper Summarizing the Stray Gas Incidence & Response Forum, July 24-26, 2012, Cleveland, Ohio,48p., last accessed on 8/19/2015, http://www.gwpc.org/sites/default/files/files/stray%20gas%20white%20paper-final(3).pdf

Gutierrez, S. C. and J. C. Bremer. 1990, Occurrence and Distribution of Gaseous Hydrocarbons in the Gulf Coast Aquifer Resulting from a Natural Gas Well Blowout. p.565-575

Gutierrez, S. A. C., 1990, Occurrence and Distribution of Gaseous Hydrocarbons in the Gulf Coast Aquifer Resulting from a Natural Gas Well Blowout, Doctoral dissertation, University of Texas Health Science Center at Houston, School of Public Health, 110p..

GWPC, 2011, State Oil and Gas Agency Groundwater Investigations and Their Role in Advancing Regulatory Reforms: A Two-State Review: Ohio and Texas, last accessed 8/20/2015, Ground Water Protection Council, August 2011, 119p.+Appendices, http://www.gwpc.org/sites/default/files/State%20Oil%20&%20Gas%20Agency%20Groundwater%20Investigations.pdf

Hackley, P. C., Guevara, E. H., Hentz, T. F., and Hook, R. W., 2009, Thermal maturity and organic composition of Pennsylvanian coals and carbonaceous shales, north-central Texas: implications for coalbed gas potential: International Journal of Coal Geology, 77, p.294–309. doi:101016/j.coal.2008.05.006.

Haluszczak, L. O., A. W. Rose, and L. R. Kump. 2013. "Geochemical evaluation of flowback brine from Marcellus gas wells in Pennsylvania, USA." Applied Geochemistry 28:55-61. doi: 10.1016/j.apgeochem.2012.10.002.

Hamlat, M. S., S. Djeffal, and H. Kadi, 2001, Assessment of radiation exposures from naturally occurring radioactive materials in the oil and gas industry, Applied Radiation and Isotopes, 55(1), p.141-146. doi: 10.1016/s0969-8043(01)00042-2.

Hammes, U. and Frébourg, G., 2012, Haynesville and Bossier mudrocks: A facies and sequence stratigraphic investigation, East Texas and Louisiana, USA. Marine and Petroleum Geology, 31(1), 8-26.

Hammes, U., Hamlin, H. S., and Ewing, T. E., 2011, Geologic analysis of the Upper Jurassic Haynesville Shale in east Texas and west Louisiana. AAPG bulletin, 95(10), 1643-1666

Hampton, C., R. B. Coffin, P. S. Rose, T. J. Boyd, and D. Murgulet, 2013, Eagle Ford Shale Play Methane Source and Fate Assessment, American Geophysical Union, Fall Meeting 2013, abstract #H53B-1419.

Harden, R. W. & Associates, 2004, Northern Trinity / Woodbine Aquifer groundwater availability model: Report prepared for the Texas Water Development Board, variously paginated, http://www.twdb.texas.gov/groundwater/models/gam/trnt_n/trnt_n.asp, last accessed September 13, 2015.

Harder, A.H., H.M. Whitman, and S.M. Rogers, 1965, Methane in the Fresh-Water Aquifers of Southwestern Louisiana and Theoretical Explosion Hazards, Department of Conservation Louisiana Geological Survey and Louisiana Department of Public Works, Water Resources Pamphlet, no. 14, 22p.

Harrington, J., C. Whyte, K. Muehlenbachs, and T. Darrah, 2015, Using Noble Gas and Hydrocarbon Gas Geochemistry to Source the Origin of Fluids in the Eagle Ford Shale of Texas, USA, Search and Discovery Article #41710, AAPG Annual Convention & Exhibition, Denver, Colorado, May 31-June 3, 2015, last accessed on November 7, 2015. http://www.searchanddiscovery.com/documents/2015/41710harrington/ndx_harrington.pdf

Harrison, S. S., 1985, Contamination of Aquifers by Overpressuring the Annulus of Oil and Gas Wells. Groundwater. Vol. 23, No. 3. pp. 317-324.

Hasan, A. R. and C. S. Kabir, 1988, A Study of Multiphase Flow Behavior in Vertical Wells, SPE #15138, p.263–272.

Hazen and Sawyer, 2009, Final Impact Assessment Report: Impact assessment of natural gas production in the New-York City water supply watershed, report prepared for the New York City Department of Environmental Protection by Hazen and Sawyer, Environmental Engineers and Scientists, December 2009, last accessed August 19, 2015, http://www.nyc.gov/html/dep/pdf/natural_gas_drilling/12_23_2009_final_assessment_report.pdf

Heilweil, V., M. Bert, J. Stolp, B, A. Kimball, D. D. Susong, T. M. Marston, P. M. Gardner and R. C. Rowland, 2013, A Stream-Based Methane Monitoring Approach for Evaluating Groundwater Impacts Associated with Unconventional Gas Development. Groundwater. Vol. 51, No. 4. pp 511-512.

Heilweil, V. M, P. L. Grieve, S. A. Hynek, S. L. Brantley, D. K. Solomon, and D. W. Risser, 2015, Stream Measurements Locate Thermogenic Methane Fluxes in Groundwater Discharge in an Area of Shale-Gas Development, Environmental Science & Technology, 49 (7), p.4057–4065, doi:10.1021/es503882b

Heisig, P. and Scott, T.-M., 2013, Occurrence of methane in groundwater of south-central New York State, 2012 – systematic evaluation of a glaciated region by hydrogeologic setting, U.S. Geological Survey Sci. Invest. Rep. 2013-5190.

Heitmuller, F. T. and B. D. Reece, 2003, Database of Historically Documented Springs and Spring Flow Measurements in Texas, U.S. Geological Survey Open-File Report 03-315, http://pubs.usgs.gov/of/2003/ofr03-315/

Herkommer, M. A. and G. W. Denke, 1982, Stratigraphy and Hydrocarbons, Parker County, Texas. Dallas Geological Society, Petroleum Geology of the Fort Worth Basin and Bend Arch Area, p. 97 – 127.

Hildenbrand, Z. L., D. D. Carlton, Jr., B. E. Fontenot, J. M. Meik, J. L. Walton, J. T. Taylor, J. B. Thacker, S. Korlie, C. P. Shelor, D. Henderson, A. F. Kadjo, C. E. Roelke, P. F. Hudak, T. Burton, H. S. Rifai, and K. A. Schug, 2015, A Comprehensive Analysis of Groundwater Quality in The Barnett Shale Region, Environ. Sci. Technol., 49 (13), p.8254–8262, DOI:10.1021/acs.est.5b01526.

Hill, R.T., 1901, Geography and geology of the Black and Grand Prairies, Texas with detailed descriptions of the Cretaceous formations and special reference to artesian waters: USGS, 21st Annual Report, Washington, DC, part 7.

Intera, 2014, Updated Groundwater Availability Model of the Northern Trinity and Woodbine Aquifers, contract report prepared for the Texas Water Development Board, variously paginated,

http://www.twdb.texas.gov/groundwater/models/gam/trnt_n/trnt_n.asp, last accessed August 29, 2015

Jackson, M. P. A., 1982, Fault tectonics in the East Texas Basin, University of Texas Bureau of Economic Geology Geologic Circular #82-4, 31p.

Jackson, R.E., A.W. Gorody, B. Mayer, J.W. Roy, M.C. Ryan, and D.R. Van Stempvoort, 2013. Groundwater protection and unconventional gas extraction: The critical need for field-based hydrogeological research. Groundwater, 51(4), p.488–510.

Jackson, R. B., A. Vengosh, T. H. Darrah, N. R. Warner, A. Down, R.t J. Poreda, S. G. Osborn, K. Zhao, and J. D. Karr, 2013, Increased stray gas abundance in a subset of drinking water wells near Marcellus shale gas extraction, Proceedings of the National Academy of Sciences USA, 110(28), p.11250–11255. doi/10.1073/pnas.1221635110

Jackson, R. B., A. Vengosh, J. W. Carey, R. J. Davies, T. H. Darrah, F. O'Sullivan, and G. Petron, 2014, The Environmental Costs and Benefits of Fracking, Annual Review of Environment and Resources, 39, p.7.1–7.36, doi:10.1146/annurev-environ-031113-144051

Jones, V. and R. Drozd, 1983, Predictions of oil or gas potential by near-surface geochemistry, AAPG Bull., 67(6), p.932-952.

Kaiser, W. R., 1978, Depositional system in the Wilcox Group (Eocene) of east-central Texas and the occurrence of lignite, in Kaiser, W. R., ed., Proceedings, 1976 Gulf Coast Lignite Conference: geology, utilization, and environmental aspects: The University of Texas at Austin, Bureau of Economic Geology Report of Investigations No. 90, 276 p.

Kaiser, W.R., 1990, The Wilcox Group (Paleocene-Eocene) in the Sabine Uplift area, Texas: Depositional systems and deep-basin lignite: The University of Texas at Austin, Bureau of Economic Geology Special Publication GF0002, 20p.

Kappel, W.M., and Nystrom, E.A. 2012. Dissolved methane in New York groundwater, 1999—2011: U.S. Geological Survey Open-File Report 2012-1162, 6 p., available online at http://pubs.usgs.gov/of/2012/1162.

Keech, D. K. and M. S. Gaber, 1982, Methane in Water Wells. Water Well Journal, February, 1982. p. 33- 36

Kelley, V. A., N. E Deeds, D. G. Fryar, and J.-P. Nicot, 2004, Groundwater Availability Models for the Queen City and Sparta Aquifers, variously paginated, http://www.twdb.texas.gov/groundwater/models/gam/qcsp/QCSP_Model_Report.pdf,

Kelly, W. R., G. Matisoff, and J. B. Fisher, 1985, The Effects of a Gas Well Blow Out on Groundwater Chemistry. Environ. Geol. Water Sci., 7(4), p.205-213.

Keyes, S., 1983, Sedimentology of the Lower Strawn Formation, Desmoinesean, Central Texas with Particular Emphasis on Reservoir Quality Rock, Abilene Geological Society, Exploration in a Mature Area, p.240-265

Kim, Y., T.T. Tieh, and E.B. Ledger. 1995. "Aquifer Mineralogy and Natural Radionuclides in Groundwater - The Lower Paleozoic of Central Texas." GCAGS Transactions 45:8.

Klass, D.L., 1984, Methane from anaerobic fermentation: Science, 223, p.1021-1028.

Klemt, W. B., R. D. Perkins, and H. J. Alvarez, 1975, Groundwater Resources of Part of Central Texas with Emphasis on the Antlers and Travis Peak Formations, Vol. 1, 22p., http://www.twdb.texas.gov/publications/reports/numbered_reports/doc/R195/R195v1/R195v1_1st_part.pdf

Klusman, R. W., M. E. Leopold, and M. P. LeRoy. 2000. Seasonal variation in methane fluxes from sedimentary basins to the atmosphere: Results from chamber measurements and modeling of transport from deep sources. Journal of Geophysical Research, 105(D20), p.24,661-24,670.

Knowles, R. S., 1978, The Greatest Gamblers, The Epic of American Oil Exploration. Second Edition. University of Oklahoma Press, Norman, OK. 376 p.

Kornacki, A. S., 2010, Composition of Produced Gas and Mud Gas Samples from Greater Sabine Bossier and Haynesville Gas-Shale Reservoirs, Northern Louisiana USA (*Abstract*), AAPG Search and Discover Article #90104, AAPG Annual Convention and Exhibition-11-14 April 2010.

Kornacki, A. S. and McCaffrey, M. A., 2011, Composition, Nature, and Origin of Produced Gas, Well Headspace Gas, and Water Solution Gas Samples; Parker County and Hood County, Texas, last accessed August 20, 2015, http://www.frackinginsider.com/wp-content/uploads/sites/179/2011/01/Range_Expert-Report.pdf

Kornacki, A. S. and McCaffrey, M. A., 2014, Monitoring the Active Migration and Biodegradation of Natural Gas in the Trinity Group Aquifer at the Silverado Development in Southern Parker County, Texas, 2014 AAPG Annual Convention and Exhibition, Houston, Texas, April 6-9, 2014, Search and Discovery Article #80395, last accessed August 20, 2015, http://www.searchanddiscovery.com/pdfz/documents/2014/80395kornacki/ndx_kornacki.pdf.html

Kreitler, C. W., 2012. Lessons Learned from the Barnett Shale Range Resources Litigation. LBG-Guyton Associates presentation to the Texas Association of Professional Geologists (TAPG), Houston, Texas, October 24, 2012, "Truth and Facts on Hydraulic Fracturing and Environmental Implications", PowerPoint, 50p.

Kreitler, C. W., 2014. Lessons Learned from the Barnett Shale Range Resources Litigation. LBG-Guyton Associates presentation to the Texas Association of Professional Geologists (TAPG), Dallas, Texas, November 12, 2014 "Hydraulic Fracturing and Environmental Implications", PowerPoint, 75p.

Kreitler, C. W., J. A. Beach, L. Symank, M. Uliana, R. Bassett, J. E. Ewing, and V. A. Kelley, 2013a, Evaluation of Hydrochemical and Isotopic Data in Groundwater Management Areas 3 and 7, contract report prepared by LBG-Guyton, Austin, Texas for the Texas Water Development Board, May 2013, 265p.+Appendix.

Kreitler, C., R. Bassett, J. Beach, L. Symank, D. O'Rourke, A. Papafotiou, J. Ewing, and V. Kelley, 2013, Evaluation of Hydrochemical and Isotopic Data in Groundwater Management Areas 11,12, and 13, contract report prepared by LBG-Guyton, Austin, Texas for the Texas Water Development Board, July 2013, 454p..

Kresse, T.M., N.R. Warner, P.D. Hays, A. Down, A. Vengosh, and R. Jackson. 2012. Shallow groundwater quality and geochemistry in the Fayetteville shale gas-production area, North-

Central Arkansas, 2011. USGS Scientific Investigations Report 2012-5273, U.S. Geological Survey, 31, Reston, Virginia: USGS.

Laul, J.C., M.R. Smith, and N. Hubbard, 1985, Behavior of Natural Uranium, Thorium and Radium Isotopes in The Wolfcamp Brine Aquifers, Palo Duro Basin, Texas, MRS Proceedings 44 (1984), p.475-482. doi: http://dx.doi.org/10.1557/PROC-44-475.

LeBlanc, R., V. T. Jones, 2004, Assessment of Casing Leaks from Wells in Oil and Gas Fields and Gas Storage Fields to Determine Environmental Hazards in Areas of Urban Development (abstract), AAPG Search and Discovery Article #90026, AAPG Annual Meeting, Dallas, Texas, April 18-21, 2004.

Lee, R.S., D.T. Adamson, M. Vanderford, 2007, Visual Methods for Geochemical Screening of Possible Impacts to Groundwater by Oilfield Brines, 7p., 14th International Petroleum environmental Conference, Houston, TX, November 2007. Last accessed on 06/08/2015 http://ipec.utulsa.edu/Conf2007/Papers/Lee_61.pdf,.

Li, H., and K.H. Carlson, 2014. Distribution and origin of groundwater methane in the Wattenberg oil and gas field of northern Colorado, Environmental Science & Technology 48, no. 3: 1484–1491.

Link, W. K., 1952. Significance of Oil and Gas Seeps in World Oil Exploration in Bulletin of the American Association of Petroleum Geologists. 36(8), p.1505–1540

Liu, Y., Larson, T. E., and Nicot, J.-P., 2014, Theoretical and experimental study of controls on CO_2 dissolution and CH_4 outgassing rates: Energy Procedia, Proceedings of 12th International Conference on Greenhouse Gas Control Technologies GHGT12, October 5-9, 2014, Austin, Texas, v. 63, p. 4773-4781, http://doi.org/10.1016/j.egypro.2014.11.508.

Loucks R. G. and S. C. Ruppel, 2007, Mississippian Barnett Shale: Lithofacies and depositional setting of a deep-water shale-gas succession in the Fort Worth Basin, Texas, AAPG Bull., 91(4), pp.579–601.

Lupton, D. M., T. F. Dale, W. A. Oliver, 2015, Characterization of Wilcox Aquifer Structure, Composition and Hydraulic Properties in Panola County, Texas, contract report by Intera, Austin, Texas prepared for Panola County Groundwater Conservation District, July 2015. 47p. + Appendices, last accessed on September 3, 2015, http://pcgcd.org/wp-content/uploads/2015/09/Intera-Hydro-Study-2015.pdf

Mancini, E. A., P. Li, D. A. Goddard, V. Ramirez, and S. C. Talukdar, 2008, Mesozoic (Upper Jurassic–Lower Cretaceous) deep gas reservoir play, central and eastern Gulf coastal plain, AAPG Bulletin, 92(3), p.283–308

Mapel, W. J., 1967, Bituminous coal resources of Texas: U.S. Geological Survey Bulletin 1242-D, p. Dl–D28.

Martin, R., J. Baihlym, R. Malpani, G. Lindsy, and W. Keith, 2010, Understanding production from Eagle Ford-Austin Chalk System, SPE paper #145117

Mayer, B., P. Humez, M. Nightingale, A. Kingston, J. Ing, and V. Becker, 2015, Isotopic Tools for Groundwater Monitoring to Assess the Potential Environmental Impact of Shale Gas Development, presentation to International Symposium on Isotope Hydrology: Revisiting

Foundations and Exploring Frontiers, 11-15 May, 2015, Vienna, Austria, last accessed September 27, 2015, http://www-naweb.iaea.org/napc/ih/IHS_2015_Symposium.

McElreath, D., 2012, Baseline water quality sampling in shale gas exploration and production areas, presentation by Chesapeake Energy at GWPC Stray Gas Incidence & Response Forum, July 25, 2012, Cleveland, OH, last accessed on 8/19/2015, http://www.gwpc.org/sites/default/files/event-sessions/McElreath_Debby.pdf

McIntosh, J. C., S. E. Grasby, S. M. Hamilton and S. G. Osborn, 2014, Origin, distribution and hydrogeochemical controls on methane occurrences in shallow aquifers, southwestern Ontario, Canada. Applied Geochemistry, 50, p.37-52.

McMahon, P.B., R.R. Caldwell, J.M. Galloway, J.F. Valder, and A.G. Hunt, 2015, Quality and Age of Shallow Groundwater in the Bakken Formation Production Area, Williston Basin, Montana and North Dakota, 53(S1), p. 81–94, April 2015 doi: 10.1111/gwat.12296.

McPhillips, L. E., A. E. Creamer, B. G. Rahm, and M. T. Walter, 2014, Assessing dissolved methane patterns in central New York groundwater, Journal of Hydrology: Regional Studies, 1, p.57–73

Miyazaki, B., 2009, Well integrity: An overlooked source of risk and liability for underground natural gas storage. Lessons learned from incidents in the USA, *in* Evans, D. J. and Chadwick, R. A. (eds) Underground Gas Storage: Worldwide Experiences and Future Development in the UK and Europe. The Geological Society, London, Special Publications, 313, 163–172.

Michaux, Jr. F. W. and E. O. Buck, 1936, Conroe Oil Field, Montgomery County, Texas. Bulletin of the American Association of Petroleum Geologists, 20(6), p.736-773.

Mitchell Energy Corporation v. Bartlett, 1997. Court of Appeals Texas, Fort Worth., No. 2-96-227-CV. http://caselaw.findlaw.com, last accessed 8/4/2014.

Molofsky, L.J., Connor, J.A., Wylie, A.S., Wagner, T. and Farhat, S.K., 2013, Evaluation of Methane Sources in Groundwater in Northeastern Pennsylvania. Groundwater. 51(3): 333–349.

Montgomery, S. L., D. M. Jarvie, K. A. Bowker, and R. M. Pollastro, 2005, Mississippian Barnett Shale, Fort Worth Basin: North central Texas: Gas-shale play with multi-tcf potential, AAPG Bull., 89, p.155–175.

Moritz, A., J.-F. Hélie, D. L. Pinti, M. Larocque, D. Barnetche, S. Retailleau, R. Lefebvre, and Y. Gélinas, 2015, Methane Baseline Concentrations and Sources in Shallow Aquifers from the Shale Gas-Prone Region of the St. Lawrence Lowlands (Quebec, Canada), Environ. Sci. Technol., 49(7), p.4765–4771, DOI: 10.1021/acs.est.5b00443

MSC (Marcellus Shale Coalition), 2012, Recommended Practices: Pre-Drill Water Supply Surveys, MSC RP 2012-3, August 28, 2012, 5p. + Appendix

Murgulet, D., P. S Rose, R. Hay and R. B Coffin, 2015, Shallow Aquifer Methane Gas Source Assessment, AGU Fall meeting, San Francisco, December 18-14, 2015.

Myers, T., 2012. Potential Contaminant Pathways from Hydraulically Fractured Shale to Aquifers. Groundwater. Vol. 50, No. 6, pp 872-882

Nelson, A. W., D. May, A. W. Knight, E. S. Eitrheim, M. Mehrhoff, R. Shannon, R. Litman, and M. K. Schultz, 2014, Matrix Complications in the Determination of Radium Levels in Hydraulic

Fracturing Flowback Water from Marcellus Shale, Environ. Sci. Technol. Lett., 2014, 1 (3), pp 204–208, DOI: 10.1021/ez5000379

NGWA, 2012, Water Wells in Proximity to Natural Gas or Oil Development What You Need to Know, 2p., http://www.ngwa.org/documents/clipcopy/hydraulic_fracturing_info_sheet.pdf, last accessed October 3, 2015

NGWA, 2013, Reduce and Mitigate Problematic Concentrations of Methane in Residential Water Well Systems: NGWA Best Suggested Practice. National Groundwater Association. 11 p. http://www.ngwa.org/Media-Center/press/2013/Pages/2013-11-19-bsp-methane.aspx.

Nicot, J.-P., 2009, A survey of oil and gas wells in the Texas Gulf Coast, USA, and implications for geological sequestration of CO_2: Environmental Geology, v. 57, p. 1625–1638.

Nicot, J.-P., Scanlon, B. R., Yang, C., and Gates, John, 2010, Geological and geographical attributes of the South Texas Uranium Province: The University of Texas at Austin, Bureau of Economic Geology, contract report prepared for the Texas Commission on Environmental Quality, 156 p.

Nicot, J.-P., Hebel, A. K., Ritter, S. M., Walden, S., Baier, R., Galusky, P., Beach, J. A., Kyle, R., Symank, L., and Breton, C., 2011, Current and projected water use in the Texas mining and oil and gas industry: The University of Texas at Austin, Bureau of Economic Geology, Contract Report No. 090480939 prepared for Texas Water Development Board, 357 p.

Nicot, J.-P., Reedy, R. C., Costley, R., and Huang, Y., 2012, Oil & gas water use in Texas: update to the 2011 Mining Water Use Report: The University of Texas at Austin, Bureau of Economic Geology, final report prepared for Texas Oil & Gas Association, 97 p.

Nicot, J.-P., and Scanlon, B. R., 2012, Water use for shale-gas production in Texas, U.S.: Environmental Science and Technology, v. 46, p. 3580–3586.

Nicot, J.-P., Costley, R., and Huang, Y., 2013a, Geographical, geological, and hydrogeological attributes of formations in the footprint of the Eagle Ford Shale: The University of Texas at Austin, Bureau of Economic Geology, contract report prepared for the Houston Advanced Research Center (HARC) Phase III, 200 p.

Nicot, J.-P., Huang, Y., Wolaver, B. D., and Costley, R., 2013b, Flow and salinity patterns in the low-transmissivity upper Paleozoic Aquifers of North-Central Texas, GCAGS Journal, v. 2, p. 53–67.

Nicot, J.-P., B. S. Scanlon, R. C. Reedy, and R. A. Costley, 2014, Source and Fate of Hydraulic Fracturing Water in the Barnett Shale: A Historical Perspective, Environmental Science and Technology, v. 48, p. 2464−2471.

Nicot, J.-P., Mickler, P., Lu, J., and Darvari, R., 2015, A Study of Rock-Water Interactions during Hydraulic Fracturing (Marcellus Shale): Bureau of Economic Geology, The University of Texas at Austin, contract report prepared for Statoil Research and Technology, 194 p.

Nordstrom, P. L., 1987, Ground-water resources of the Antlers and Travis Peak formations in the outcrop area of north-central Texas, 101p., http://www.twdb.texas.gov/publications/reports/numbered_reports/doc/R298/R298_A.pdf,

Nunn, J. A., 2012, Burial and thermal history of the Haynesville Shale: implications for overpressure, gas generation, and natural hydrofracture, GCAGS Journal, 1, p. 81–96.

ODNR, 2008, Report on the Investigation of the Natural Gas Invasion of Aquifers in Bainbridge Township of Geauga County, Ohio, September 1, 2008, Ohio Department of Natural Resources, Division of Mineral Resources Management, 83p.+Appendices, last accessed 8/19/2015, http://oilandgas.ohiodnr.gov/portals/oilgas/pdf/bainbridge/report.pdf

ODNR, 2012, Best management practices for pre-drilling water sampling, September 20, 2012, 8p., Ohio Department of Natural Resources, last accessed 8/19/2015, http://oilandgas.ohiodnr.gov/portals/oilgas/pdf/BMP_PRE_DRILLING_WATER_SAMPLING.pdf

ODNR, 2014, Recommendations for Drinking Water Well Sampling Before Oil and Gas Drilling, January 20, 2014, 4p., Ohio Department of Natural Resources, last accessed 8/19/2015, http://oilandgas.ohiodnr.gov/portals/oilgas/pdf/EPA-fact-sheets/RecommendationsforDrinkingWaterWellSamplingBeforeOilandGasDrilling.pdf

Oliver, W. A. and D. M. Lupton, 2013, Wilcox Structure, Water Levels, and Water Quality in Panola County Groundwater Conservation District, contract report by Intera, Austin, Texas prepared for Panola County Groundwater Conservation District, January 2013. 28p., last accessed on September 3, 2015, http://pcgcd.org/wp-content/uploads/2015/09/Intera-Wilcox-Report-2013.pdf

Osborn, S.G., A. Vengosh, N.R. Warner, and R.B. Jackson, 2011, Methane contamination of drinking water accompanying gas-well drilling and hydraulic fracturing. Proceedings of the National Academy of Sciences USA 108: 8172–8176.

Pearson, O. N., E. L. Rowan, and J. J. Miller, 2012, Modeling the Mesozoic-Cenozoic structural evolution of East Texas, GCAGS Journal, v.1, p.118–130

Pinti, D. L., Y. Gélinas, M. Larocque, D. Barnetche, S. Retailleau, A. Moritz, J.-F. Hélie, and R. Lefebvre, 2013, Concentrations, sources et mécanismes de migration préférentielle des gaz d'origine naturelle (méthane, hélium, radon) dans les eaux souterraines des Basses-Terres du Saint-Laurent, Université du Québec à Montréal, Université Concordia, INRS-ETE, Étude E3-9, FQRNT ISI n° 171083, 94p. [*in French*]

Pollastro, R. M.; Jarvie, D. M.; Hill, R. J.; Adams, C. W., 2007, Geologic framework of the Mississippian Barnett Shale, Barnett-Paleozoic total petroleum system, bend arch-Fort Worth Basin, Texas. AAPG Bull., 91 (4), 405-436.

Puls, R., 2014, State Baseline Water Quality Programs for Oil & Gas Operations, presented at GWPC Annual Forum, Seattle, WA, October 6, 2014, last accessed October 2, 2014, http://www.gwpc.org/sites/default/files/event-sessions/Puls_Bob_Baseline.pdf

Reiner, S. R., and M. C. Crocker, 1990, Some Effects of Groundwater Discharge Through Mount Enterprise Fault Zone on Surface Water Composition in Southern Rusk County, Texas (*Abstract*), AAPG Search and Discovery Article, Annual Convention, San Francisco, California, June 3-6, 1990.

Revesz, K. M., K. J. Breen, A. J. Baldassare, and R. C. Burruss, 2012, Carbon and hydrogen isotopic evidence for the origin of combustible gases in water-supply wells in north-central Pennsylvania, Applied Geochemistry, 27(1), p.360-375. (correction of vol. 25, p.1845–1859, 2010)

Richardson, S., 2014, Evaluating Key Sources of Groundwater Quality Variability in Residential Water Wells for Pre-Drill Sampling, presentation at the NGWA Workshop — Groundwater Quality and Unconventional Gas Development: Is There a Connection?, November 13-14, 2014, Pittsburgh, PA.

Rose, N. A. and Alexander, W. H. Jr., 1945. Relation of phenomenal rise of water levels to a defective gas well, Harris County, Texas: Bulletin of the American Association of Petroleum Geologists, v. 29, p. 253-279.

Rowan, E. L. and T. Kraemer. 2012. Radon-222 Content of natural gas samples from Upper and Middle Devonian sandstone and shale reservoirs in Pennsylvania: Preliminary data. Open-File Report, US Geological Survey. 9 p.

Rowan, E.L., M.A. Engle, C.S. Kirby, and T.F. Kraemer, 2011, Radium Content of Oil- and Gas-Field Produced Waters in the Northern Appalachian Basin (USA): Summary and Discussion of Data, U.S. Geological Survey Scientific Investigations Report 2011–5135, 31p., http://pubs.usgs.gov/sir/2011/5135/.

RRC, 1973, December 13th Letter re: Shallow Gas, Conroe Field Area, Montgomery County, Texas. From Paul Staff, Engineer District 3 to Robert Taylor, District Director. 3 p.

RRC, 1977. Results of Investigation into Gas Contamination of Lower Trinity Aquifer, Springtown Area, Southern Wise County, Texas. Oil and Gas Division, District 9. 44 p.

RRC, 1979. Examiners' Report, Docket No. 9-68, 644 'Commission called Hearing to consider the matter of gas contamination of water sands in southwest Wise County, Texas.' 5 p.

RRC, 1999. Oil and Gas Docket Inquiry, Docket # 09-0218133 / Enforcement. 12/08/1997 to 01/27/1999.

RRC, 2014, Water well complaint investigation report, Silverado on the Brazos neighborhood, Parker County, Texas, May 23, 2014, 19p.

RRC, 2015, Review of analytical data – Murray Complaint (7B-10736) and Singleton Complaint (7B-10612), April 28, 2015, 13p. [Palo Pinto County]

SanFilipo, J. R., C. E. Barker, R. W. Stanton, P. D. Warwick, and L. E. Morris, 2000, A shallow coal-bed methane show in the Gulf Coast of Texas, indication of down-dip commercial potential? (Abstract), 2000 AAPG Annual Convention, New Orleans, Louisiana, AAPG Search and Discovery Article #90914, last accessed August 28, 2015, http://www.searchanddiscovery.com/abstracts/html/2000/annual/abstracts/0593.htm

Saunders, D. F., K. R. Burson, and C. K. Thompson. 1999. Model for hydrocarbon microseepage and related near-surface alterations. AAPG Bull., 83(1), p.170-185.

Scanlon, B. R., Reedy, R. C., and Nicot, J.-P., 2014a, Comparison of water use for hydraulic fracturing for unconventional oil and gas versus conventional oil: Environmental Science & Technology, v. 48, no. 20, p. 12386-12393, http://doi.org/10.1021/es502506v.

Scanlon, B. R., Reedy, R. C., and Nicot, J.-P., 2014b, Will water scarcity in semiarid regions limit hydraulic fracturing of shale plays?: Environmental Research Letters, v. 9, 14 p., http://doi.org/10.1088/1748-9326/9/12/124011.

Siegel, D. I., Azzolina, N.A., Smith, B.J., Perry, A. E., and R.L. Bothun. 2015. Methane Concentrations in Water Wells Unrelated to Proximity to Existing Oil and Gas Wells in Northeastern Pennsylvania. Environmental Science and Technology, 49:4106-4112.

Senior, L.A. 2014. A Reconnaissance Spatial and Temporal Baseline Assessment of Methane and Inorganic Constituents in Groundwater in Bedrock Aquifers, Pike County, Pennsylvania, 2012-2013. USGS, Scientific Investigations Report 2014-5117.

Silva, J. M. et al., 2014, NORM mitigation and clean water recovery from Marcellus produced water, RPSEA Final report project #10122-07, April 2014, 78p. Part I, 52p. Part II

Simoneit, B. R. and B. M. Didyk, 1978, Organic geochemistry of a Chilean paraffin dirt." Chemical Geology, 23(1), p.21-40.

Simoneit, B. R., P. T. Crisp, B. G. Rohrback, and B. M. Didyk, 1980, Chilean Paraffin Dirt – II. Natural gas seepage at an active site and its geochemical consequences. Physics and Chemistry of the Earth, 12, p.171-176.

Sloto, R.A. 2014. Baseline Groundwater Quality from 34 Wells in Wayne County, Pennsylvania, 2011 and 2013. USGS Open-File Report 2014-116.

Small, M.J., Stern, P.C., Bomberg, E., Christopherson, S.M., Goldstein, B.D., Israel, A.L., Jackson, R.B., Krupnick, A., Mauter, M.S., Nash, J., North, D.W., Olmstead, S.M., Prakash, A., Rabe, B., Richardson, N., Tierney, S., Webler, T., Wong-Parodi, G., Zielinska, B., 2014, Risks and Risk Governance in Unconventional Shale Gas Development, Environ. Sci. Technol., 48(15), p. 8289–8297. doi:10.1021/es502111u

Smith, K. G., 1982, Limited Atokan Gas Reservoirs of Hood County, Texas, Dallas Geological Society in Petroleum Geology of the Fort Worth Basin and Bend Arch Area, 1982, p. 231-235

Snavely Jr., E. S, 1989. Radionuclides in Produced Water: A Literature Review, American Petroleum Institute 78p.+Appendices

Stagg, P., 2002, Letter from Exxon Mobil to the RRC, Oct. 25, 2002 RE: intent to sample domestic and public water supply wells and analysis of public wells in 1996 showing presence of benzene, in the Conroe Field, Montgomery County.

Stephenson, M. T., 1992, Components of Produced Water - A Compilation of Industry Studies, Journal of Petroleum Technology, 44(5), p.548-550&602-603.

Stramel, G. J., 1951, Ground-water resources of Parker County, Texas, Texas·Board·of·Water Engineers, Bull. 5103, 55p.

Szabo, Z., Fischer, J. M., and Hancock, T. C., 2012, Principal aquifers can contribute radium to sources of drinking water under certain geochemical conditions: U.S. Geological Survey Fact Sheet 2010–3113, 6 p., available at http://pubs.usgs.gov/fs/2010/3113/.

Taggart, I., 2010, Extraction of dissolved methane in brines by CO_2-injection: Implication for CO2 sequestration. SPE Reservoir Evaluation & Engineering 13 (5), 791-804.

Taylor S.W., Sherwood-Lollar B. et Wassenaar L.I., 2000, Bacteriogenic Ethane in Near-Surface Aquifers: Implications for Leaking Hydrocarbon Well Bores. Environmental Sciences Technology, 34: 4727-4732.

US EPA, 2004, Sample Preparation and Calculations for Dissolved Gas Analysis in Water Samples Using a GC Headspace Equilibration Technique, Standard Operating Procedure RSKSOP-175, Revision No.2, May 2004, 14p., last accessed October 21, 2015,

US EPA, 2012a, The Potential Impacts of Hydraulic Fracturing on Drinking Water Resources: Progress Report, EPA 601/R-12/011, December 2012, 278 pp (http://www2.epa.gov/hfstudy/potential-impacts-hydraulic-fracturing-drinking-water-resources-progress-report-december)

US EPA. 2012b. Quality Assurance Project Plan: Hydraulic Fracturing Retrospective Case Study, Wise, Texas. http://www.epa.gov/hfstudy/barnettqapp.pdf.

US EPA. 2015a. Review of State and Industry Spill Data: Characterization of Hydraulic Fracturing-Related Spills. May 2015, EPA/601/R-14/001. 37p. Last accessed September 10, 2015. http://www2.epa.gov/hfstudy/review-state-and-industry-spill-data-characterization-hydraulic-fracturing-related-spills-1.

US EPA. 2015b. Review of Well Operator Files for Hydraulically Fractured Oil and Gas Production Wells: Well Design and Construction, May 2015, EPA/601/R-14/002. 79p. http://www2.epa.gov/sites/production/files/2015-05/documents/wfr_1_final_5-8-15_508_km_5-13-15_sb.pdf Last accessed September 10, 2015.

US EPA. 2015c. Retrospective Case Study in Wise County, Texas Study of the Potential Impacts of Hydraulic Fracturing on Drinking Water Resources, May 2015, EPA/600/R-14/090, last accessed September 10, 2015, http://www2.epa.gov/hfstudy/retrospective-case-study-wise-county-texas. 171p. + Appendices

Van Stempvoort D., Maathuis H., Jaworski E., Mayer B., and Rich K, 2005, Oxidation of fugitive methane in groundwater linked to bacterial sulfate reduction, Ground Water, 43, p.187–199.

Vengosh, A., Jackson, R.B., Warner, N., Darrah, T.H., Kondash, A., 2014, A Critical Review of the Risks to Water Resources from Unconventional Shale Gas Development and Hydraulic Fracturing in the United States, Environ. Sci. Technol., 48 (15), p.8334–8348, doi:10.1021/es405118y

Warner, N. R., T. M. Kresse, P. D. Hays, A. Down, J. D. Karr, R. B. Jackson, A. Vengosh, 2013, Geochemical and isotopic variations in shallow groundwater in areas of the Fayetteville Shale development, north-central Arkansas, Applied Geochemistry, 35, 207–220

Warner, N. R., C. A. Christie, R. B. Jackson, and A. Vengosh, 2013b, Impacts of Shale Gas Wastewater Disposal on Water Quality in Western Pennsylvania, Environ. Sci. Technol., 47, 11849−11857, dx.doi.org/10.1021/es402165b

Warwick, P.D, Breland, F.C., 2005, Geochemical and Stable Isotope Analysis of the Wilcox Group Coal-Bed Gas and Related Petroleum Systems of Northern Louisiana, U.S.A. (Abstract), 2005 AAPG Annual Convention, Calgary, Alberta, June 16-19, 2005, AAPG Search and Discovery Article #90039.

Warwick, P.D, Breland, F.C., Jr., Ratchford, M.E. and Hackley, P.C., 2004, Coal gas resource potential of Cretaceous and Paleogene coals of the Gulf of Mexico Coastal Plain (including a review of the activity in the Appalachian and Warrior basins), in Warwick, P.D., ed., Selected

presentations on coal-bed gas in the eastern United States, U.S. Geological Survey Open-File Report 2004-1273, 25p.

Warwick, P. D., J. R. SanFilipo, A. W. Karlsen, and C. E. Barker, 2005, Results of coalbed methane drilling in Panola County, Texas, U.S. Geological Survey Open-File Report 2005-1046, 155p.

Warwick, P. D., F. C. Breland Jr., and P. C. Hackley, 2008, Biogenic origin of coalbed gas in the northern Gulf of Mexico Coastal Plain, U.S.A., International Journal of Coal Geology, 76, p.119–137.

Wilson, B., 2012, Geologic and baseline groundwater evidence for naturally occurring, shallowly-sourced, thermogenic gas in northeastern Pennsylvania, AAPG Bull., 98(3), p.373-394

White, J.S. and Mathes, M.V., 2006, Dissolved-gas concentrations in ground water in West Virginia: U.S. Geological Survey Data Series 156, 8 p., available online at http://pubs.water.usgs.gov/ds156/

Whiticar, M.J., 1999. Carbon and hydrogen isotope systematics of bacterial formation and oxidation of methane. Chem. Geol. 161, 291–314.

WRF-AWWA, 2011, Hydraulic Fracturing Issues and Research Needs for the Water Community, Water Research Foundation, 75p., last accessed August 19, 2015, http://www.waterrf.org/PublicReportLibrary/4301.pdf

WRF-AWWA, 2015, Hydraulic Fracturing Workshop Report: Developing Water and Oil & Gas Sector Partnerships, Web Report #4544, report from April 28-29, 2014 workshop, Golden, Colorado, 49p., http://www.waterrf.org/PublicReportLibrary/4544.pdf, last accessed October 3, 2015.

Wright, P. R., McMahon, P. B., Mueller, D. K. and Clark, M. L., 2012) Groundwater-Quality and Quality-Control Data for Two Monitoring Wells near Pavillion, Wyoming, US Geological Survey, April and May 2012: Data Series 718, 23 p. (Revised October 2012), last accessed October 3, 2015, http://pubs.usgs.gov/ds/718/.

WOGCC (Wyoming Oil and Gas Conservation Commission), 2014, Chapter 3. Operational Rules, Drilling Rules Section 46. Groundwater Baseline Sampling, Analysis and Monitoring *and* Appendix K. Sampling and Analysis Procedures for the Wyoming Oil And Gas Conservation Commission Groundwater Baseline Sampling, Analysis, And Monitoring Program, last accessed October 3, 2015, 16p., http://wogcc.state.wy.us/downloads/proposed_rules_2014/K_Sampling_and_Analysis_Procedures_073014.pdf.

Young, S. C., J. Pinkard, R. L. Bassett, and A. H. Chowdhury, 2014, Hydrogeochemical Evaluation of the Texas Gulf Coast Aquifer System and Implications for Developing Groundwater Availability Models, contract report prepared by Intera, Austin, Texas for the Texas Water Development Board, April 2014, variously paginated

Zhang, C., E. L. Grossman, and J. W. Ammerman. 1998. Factors influencing methane distribution in Texas groundwater. Groundwater. Vol. 36, No. 1, pp. 58-66.

Zhang, C., 1994, Microbial geochemistry of groundwater in deep aquifers, central and east-central Texas, Ph.D. dissertation, Texas A&M, 107p.

Zielinski, R. A. and J. K. Otton, 1999, Naturally Occurring Radioactive Materials (NORM) in Produced Water and Oil-Field Equipment—An Issue for the Energy Industry, U.S. Geological Survey Fact Sheet FS–142–99, 4p.

Zumberge, J., K. Ferworn, and S. Brown, 2012, Isotopic reversal ('rollover') in shale gases produced from the Mississippian Barnett and Fayetteville formations, Marine and Petroleum Geology, 31, p.43-52.

IX. Appendix A: Conference Abstracts and Papers

By JPN

Meeting abstracts:

Larson T. et al., Tracing natural gas transport into shallow groundwater using dissolved nitrogen and alkane chemistry in Parker County, Texas: submitted to 2015 American Geophysical Union Fall Meeting, San Francisco, California.

Nicot, J.-P., P. Mickler, T. Larson, R. Darvari, and R. Smyth, Dissolved methane occurrences in aquifers in the footprint of Texas shale plays and their controls: submitted to 2015 American Geophysical Union Fall Meeting, San Francisco, California.

Wen T., M. C. Castro, J.-P. Nicot, C. M. Hall, P. Mickler, and R. Darvari, Identifying the Sources of Methane in Shallow Groundwaters in Parker and Hood Counties, Texas through Noble Gas Signatures: submitted to 2015 American Geophysical Union Fall Meeting, San Francisco, California.

Nicot, J.-P., Mickler, P., Hildenbrand, Z. L., Larson, T., Darvari, R., Uhlman, K., Smyth, R. C., and Scanlon, B. R., 2014, Preliminary results of dissolved methane sampling in the footprint of Texas shale plays (abs.): presented at 2014 Annual Meeting & Exposition, Vancouver, British Columbia, Canada, October 19-22; Geological Society of America Abstracts with Programs, v. 46, no. 6, p. 692.

Nicot, J.-P., Mickler, P., Hildenbrand, Z., Larson, T., Darvari, R., Uhlman, K., Smyth, R. C., and Scanlon, B. R., 2014, Screening for dissolved methane in groundwater across Texas shale plays (abs.): presented at 2014 American Geophysical Union Fall Meeting, San Francisco, California, December 15-19, 2014, no. H23C-0895.

Mickler, P., Lu, Jiemin, and Nicot, J.-P., 2013, Water-shale interactions in bench-top and high pressure/high temperature autoclave experiments: Identifying geochemical reaction controlling flow back water chemistry: presented at 2013 Fall Meeting, AGU, San Francisco, California, 9-13 Dec., no. H53B-1418

Other presentations:

Controls on Methane Occurrences in Aquifers in the Footprint of Texas Shale Plays: presented to American Chemical Society 249th National Meeting & Exposition, presented at Chemistry of Natural Resources, Denver, CO, March 23, 2015 (J.-P. Nicot, invited)

Preliminary results of a dissolved methane sampling campaign in Texas: presented to National Groundwater Association (NGWA) Workshop, presented at Groundwater Quality and Unconventional Gas Development: Is There a Connection?, Pittsburgh, Pennsylvania, November 13-14, 2014. (J.-P. Nicot, invited)

Hot topics in hydraulic fracturing: dissolved methane, NORMs, and seismicity: presented to the Colombian Association of Hydrogeologists, presented at Workshop on aquifers and exploration and production from unconventionals, Bogota, Colombia, August 14-15, 2014. (J.-P. Nicot, invited)

An Overview of Dissolved Methane in Fresh-Water Aquifers in the Footprint of Texas Shale Plays: presented at NGWA Ground Water Summit, San Antonio, Texas, March 17, 2015.

Non peer-reviewed papers:

Liu, Y., Larson, T. E., and Nicot, J.-P., 2014, Theoretical and experimental study of controls on CO_2 dissolution and CH_4 outgassing rates: Energy Procedia, Proceedings of 12th International Conference on Greenhouse Gas Control Technologies GHGT12, October 5-9, 2014, Austin, Texas, v. 63, p. 4773-4781, http://doi.org/10.1016/j.egypro.2014.11.508.

Peer-reviewed manuscripts to be submitted:

Larson, T., J.-P. Nicot, and P. Mickler, Tracing natural gas transport into shallow groundwater using dissolved nitrogen and alkane chemistry in Parker County, Texas [*geared towards the unique information brought out by nitrogen data*]

Mickler, P., J.-P. Nicot, J. Lu, and R. Darvari, Shale-water interactions observed in laboratory experiments: Identifying geochemical controls on flow-back water chemistry in the Haynesville and Barnett shales [*autoclave experiments on Barnett core samples*]

Nicot et al. on Barnett Shale cluster [*detailed work in the Parker County area*]

Nicot et al. on Eagle Ford Shale

Nicot et al. on Haynesville Shale

Nicot et al. on Texas dissolved methane [*overview of dissolved methane in Texas*]

Castro, Wen et al. on Barnett Shale cluster [*detailed interpretation of noble gases in the Parker County area*]

X. Appendix B: RRC Districts - Methane in Well Water

By Kristine Uhlman modified by JPN

The RRC Oil and Gas Division District Offices (Figure 76) were contacted and interviewed (second half of 2013) to obtain data relating to drinking water well complaints and/or anecdotal evidence of methane seepage into water supply aquifers. When a water well complaint would come into the district office, the standard procedure would be to generate a complaint file and/or forward the complaint to the district site remediation field staff for initial assessment. If water sampling was conducted the analysis typically consisted of TPH and could also include BTEX, TDS, MTBE, and Cl. Sampling protocol did not intentionally focus on assuring capture of light volatiles (such as methane gas). At times, complaints address 'gas' in a well did not clarify between free-product floating 'gas' (as in gasoline) or stray gas. Data is typically organized by field/play and county.

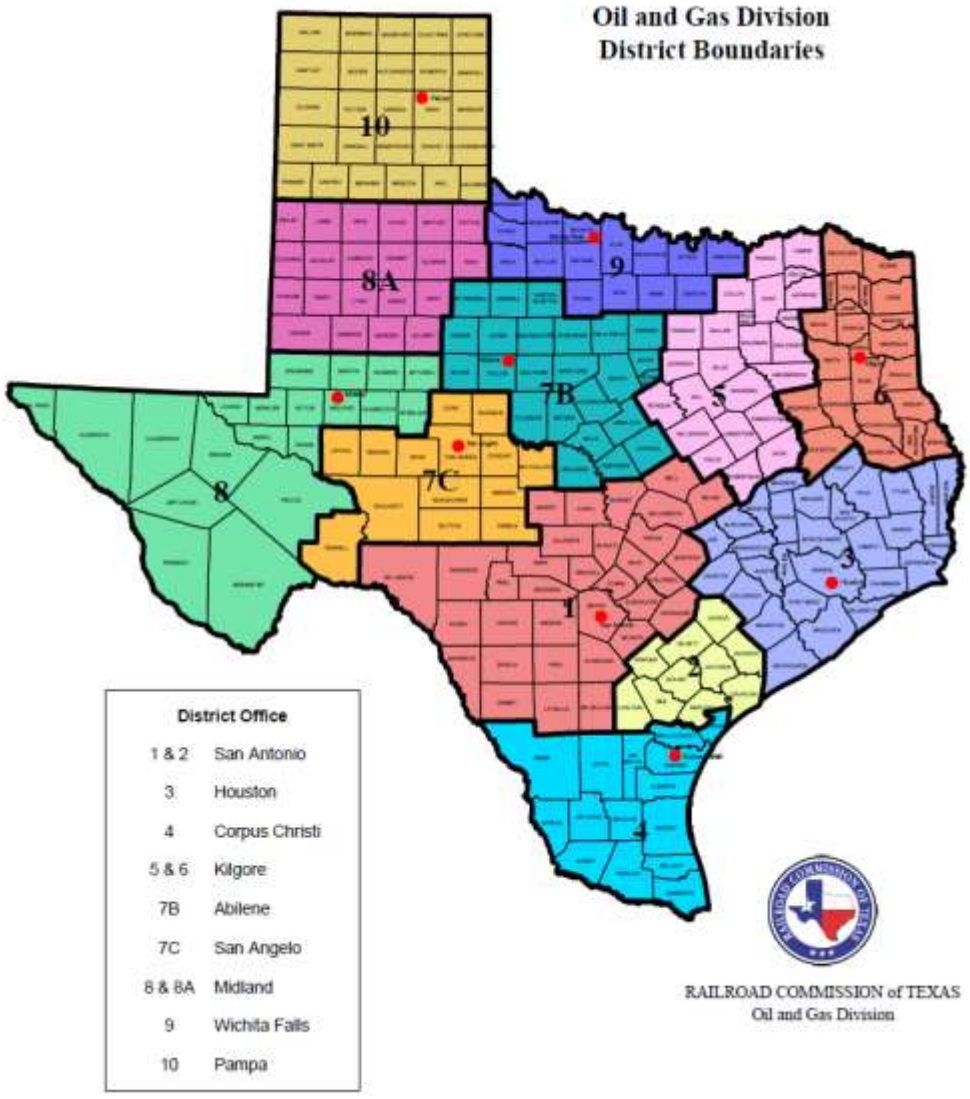

Source: http://www.rrc.state.tx.us/about-us/organization-activities/rrc-locations/counties-by-dist/

Figure 76. RRC regional district boundaries

Well complaint files may – or may not – be forwarded to the Austin Site Remediation Office; some offices reported archiving files in Austin after three years, other offices retained the files in the local office indefinitely. Some water well complaints were the focus of intensive site investigation that could include RRC requests to local producers to remediate a site and/or replace a water well. In general, District Office interviews generated analytical data for those wells with confirmed aquifer impact by petroleum constituents, only a few of which included stray gas. Methane sources were attributed to past producer practices, local 'blow outs', and the presence of subsurface coal-bed methane; none were assumed by the District Offices to be naturally occurring thermogenic methane. ***Isotopic finger-printing of methane has not been a practice of the RRC***. A summary of each District Office interview follows.

District 01 & 02 - San Antonio, covering 43 counties in south-central Texas, including most of the Eagle Ford Shale area: Analytical results for water well complaint locations in seven counties were forwarded for sampling dates in 2012 and 2013. The District office sorted their database of analytical results and forwarded to us those with reports of methane dissolved in water. Methane concentrations were reported in wells located in Caldwell, La Salle, Dimmit, Dewitt, Gonzales, and Victoria Counties, however not all constituents were tested at all wells. The presence of MTBE would suggest well contamination by refined petroleum product for wells reported in Dewitt County. The site in Caldwell County is adjacent to a waste injection well (methane concentrations reported between 3,240 and 8,340 ug/L). It should be noted that the greatest concentration of dissolved methane is from Gonzales County where the well is reported to be an old oil well that has been converted to a water supply well (22,100 ug/L). Of the information provided, the 'Little Ranch' irrigation well in Dimmit County (Carrizo Wilcox Aquifer) is the only report that cites gas leaking from the water well casing annulus (0.50 to 35.4 ug/L). Table 4 provides a summary of well complaint analytical results; full analytical reports and site visit reports are available for most of the listed results. None of the reports included how the complaints were resolved.

District 03 – Houston, covering 28 counties in east Texas along the Gulf: District 03 maintains 30 years of data in their District files. They forwarded to us a summary of 20 cases of water well complaints from 2010- 2012, all but one of which has been closed. All of the complaints were verbally reported to relate to past practices or blow outs, and did not include stray gas, except for the one open case. The open case is in the area of the Danbury Dome field, in Brazoria County, filed under 'Amy Woods' and/or 'Jersey Village' and/or 'Lake Forest Municipal Utility District (MUD)'. The Lake Forest MUD Water Well No. 2, located in Houston, caught fire due to stray gas build-up within the well. We received the January 23, 2013 consultant's report which includes emission test results that indicate ~ 82 to 86 % methane gas (wet), but probable methane source is not identified. Additional analytical reports and site visit reports are available on request.

District 04 – Corpus Christi, covering 14 counties in south Texas, including some of the Eagle Ford Shale area: The site remediation officer verbally reported only one domestic well complaint over the past 7 years; water testing indicated no evidence of petroleum-related contamination (TPH analysis).

District 05 & 06 – Kilgore, covering 46 counties in north east Texas, including the Haynesville Shale (District 6) and eastern section of the Barnett Shale (District 5): It is the district policy to sample and analyze every water well complaint in the region, and there have been over 20 complaints over the past year, however, analysis for TPH found no indication of petroleum-

related contamination. A majority of the complaints were for hydrogen sulfide gas, 'rotten egg smell'.

District 7B – Abilene, covering 24 counties in north central Texas including the southwestern section of the Barnett Shale: The Parker County / Range Resources complaint is included in this district. With every complaint the water well is usually sampled (TPH, BTEX, anions, cations, and salinity) but none of the complaints have included concern for stray gas or methane (until after the Parker County media attention). The District office has over four file drawers of unidentified complaints and no means by which to electronically sort the data.

District 7C – San Angelo, covering 13 counties in west central Texas: The most common water well complaint in this district is salty water, assumed to be the result of past disposal of produced water. Nothing is assumed to be naturally occurring as every complaint resolution has identified a pipeline or tank spill as the cause for TPH in drinking water. Operators are held responsible for clean-up.

District 08 & 8A – Midland, covering 41 counties in west Texas including the Texas section of the Delaware Basin: This district reported that past disposal practices and production spills are the cause of water well complaints. They have found nothing to be naturally occurring due to the number of pipeline breaks and other spills across the District.

District 09 – Wichita Falls, covering 15 counties in north Texas including the northern section of the Barnett Shale: Methane has been flared from domestic and municipal wells, and test results for the 'Brock' domestic well have been provided to us. Interestingly, the analysis reports 'NIL' as the concentration for methane, although propane is present (as well as O_2, N_2 and CO_2). Due to the presence of several coal seams in the region, the District believes the stray gas is due to coal-bed methane.

District 10 – Pampa, covering 26 counties in the panhandle of Texas: A majority of drinking water well complaints in the district are due to hydrogen sulfide gas, and very few complaints have been submitted over the past year. Files archived in the Austin office of the RRC were reviewed and drinking water well contamination was attributed to pipeline leaks. Producers remediated the contamination and replaced domestic wells. The consultant report for the Hinton Well in Gray County includes an analysis of the condensate release from an old booster station, originally reported as 'gas' but actually consisting of LNAPL product floating on the water table.

Barnett Shale:	Districts 5, 7B, and 9
Haynesville Shale:	District 6
Eagle Ford Shale:	Districts 1, 2, and 4
Delaware Basin:	District 8

Table 4. Recent methane contamination complaints in RRC Districts 1 and 2

Complaint Number	INITIAL DATE	Lease	County	Sample Date	Benzene mg/L	Toluene mg/L	Ethylbenzene mg/L	Xylene mg/L	Chloride mg/L	TPH C6-C12 mg/L	TPH >C12-C35 mg/L	Dissolved Methane ug/L	Total Coliform	E. coli	MTBE mg/L	TDS mg/L	pH
3230	10/30/12	H.H. Chapman	Caldwell	11-01-2012	<0.000371	<0.000347	<0.000326	<0.000357	114	<0.539	<1.77	3240	Pos	Neg	NA	NA	NA
				12-11-2012	<0.000310	0.00120	<0.000291	<0.000268	110	<0.539	<1.77	4010	NA	NA	NA	NA	NA
				01-16-2013	<0.000371	<0.000347	<0.000326	<0.000357	111	<0.539	<1.77	8340	NA	NA	NA	NA	NA
				03-07-2013	NA	NA	NA	NA	NA	NA	NA	NA	NA	NA	NA	NA	NA
				07-08-2013	0.0007	<0.000465	<0.000442	<0.000413	115	<0.654	<0.704	4390	NA	NA	NA	NA	NA
3241	2/5/13	Alderman Ranch	La Salle	02-08-2013	<0.000567	<0.000518	<0.000518	<0.000548	191	<0.539	<1.77	NA	NA	NA	NA	1144	7.69
				03-14-2013	NA	NA	NA	NA	183	NA	NA	13.1	Pos	Pos	NA	1102	NA
3248	4/17/13	Little Ranch Well Irrigation	Dimmit	04-18-2013	<0.000567	<0.000518	<0.000518	<0.000548	6160	<0.654	<0.704	35.4	Pos	Neg	NA	NA	NA
				07-10-2013	<0.000387	<0.000465	<0.000442	<0.000413	5780	<0.654	<0.704	5.7	NA	NA	NA	NA	NA
3248	4/17/13	Little Ranch Well Dove	Dimmit	04-18-2013	<0.000567	0.00130	<0.000518	<0.000548	56.0	<0.654	<0.704	2.08	Neg	Neg	NA	NA	NA
				07-10-2013	<0.000387	0.00160	<0.000442	<0.000413	58.5	<0.654	<0.704	2.4	NA	NA	NA	NA	NA
3248	4/17/13	Little Ranch Well House	Dimmit	04-18-2013	<0.000567	0.00110	<0.000518	<0.000548	57.5	<0.654	<0.704	2.05	Neg	Neg	NA	NA	NA
				07-10-2013	<0.000387	0.00330	<0.000442	<0.000413	53.1	<0.654	<0.704	0.50	NA	NA	NA	NA	NA
3255	6/12/13	Franke Water Well	Dewitt	06-17-2013	0.0458	0.130	0.00890	0.203	68.3	<0.654	<0.704	ND	Pos	Neg	0.00350	NA	NA
3255	6/12/13	Becker Water Well	Dewitt	06-17-2013	0.136	0.0449	0.0124	0.171	124	<0.654	<0.704	2.0	Neg	Neg	<0.000549	NA	NA
NA	6/19/13	Harvey WW	Gonzales	06-19-2013	<0.000567	<0.000518	<0.000518	<0.000548	62.6	<0.654	<0.704	1.1	Pos	Neg	NA	NA	NA
3260	7/9/13	Hornstien Water Well Hornstien	Victoria	07-10-2013	0.0899	<0.0232	<0.0221	0.0429	93	<0.654	<0.704	Lab Left Out	Pos	Pos	<0.0251	NA	NA
				08-13-2013	0.0900	0.0117	0.00100	0.0507	109	<0.654	<0.704	317	Pos	Pos	NA	NA	NA
3260	7/9/13	Hornstien Water Well Rig Well	Victoria	08-13-2013	<0.000387	0.000600	<0.000442	0.000500	127	<0.654	<0.704	286	Pos	Pos	NA	NA	NA
3260	7/9/13	Hornstien Water Well Rothen Bach	Victoria	08-13-2013	<0.000387	<0.000465	<0.000442	<0.000413	876	<0.654	<0.704	ND	NA	NA	NA	NA	NA
3262	8/9/13	McKee Water Well Bunkhouse	Gonzales	08-12-2013	<0.000387	<0.000465	<0.000442	<0.000413	161	<0.654	<0.704	5.9	Neg	Neg	NA	NA	NA
3262	8/9/13	McKee Water Well Housewell	Gonzales	08-12-2013	<0.000387	<0.000465	<0.000442	<0.000413	217	<0.654	1.85	2510	Pos	Neg	NA	NA	NA
3262	8/9/13	McKee Water Well Chicken	Gonzales	08-12-2013	<0.000387	<0.000465	<0.000442	<0.000413	185	<0.654	<0.704	22100	Pos	Pos	NA	NA	NA
3262	8/9/13	McKee Water Well Langhoff	Gonzales	08-12-2013	<0.000387	<0.000465	<0.000442	<0.000413	135	<0.654	<0.704	5.4	Neg	Neg	NA	NA	NA

XI. Appendix C: Gas Well Blowouts in Texas

By Sean Porse modified by JPN

XI-1. Introduction and Methodology

Well blowouts can be a potential source for deep subsurface and near-surface contamination in groundwater aquifers. In the United States, state oil and gas agencies are responsible for promulgating rules that prohibit such events from occurring, as well as delineating penalties for violations of these rules. For well blowouts, some state oil and gas regulatory boards keep track of this information to varying degrees available for public analysis. In the case of Texas, the RRC is responsible for regulating oil and gas activities within the state. Current RRC regulations require immediate notification of any fires, leaks, spills, or blowouts (TAC Title 16 Part 1 Chapter 3 Part 3.20). Operators must also submit a report after the incident, including estimated volumes of fluid lost, including hydrocarbons, water, and other fluids. Of particular interest is the incidence of blowouts associated with methane leakage. Since the 1930s, the RRC has tracked the occurrence of blowouts in its respective Districts, including dates, locations, leases, duration, as well as other information reported in incident reports. The standard RRC form to report leaks/well blowouts is the H-8 form.

The goal for this study is to take an initial effort at researching and distinguishing underground blowouts related to natural gas production from existing RRC data found online (http://www.rrc.state.tx.us/data/drilling/blowouts/index.php) and in person at the RRC Offices in Austin, TX (Figure 77). Ideally, this information would include: blowout depth, cause of blowout, duration of blowout, among other pertinent information. However, it is noted where such information is not available.

In order to accomplish this goal, the RRC well blowout records are researched for information regarding the above characteristics and organized into one spreadsheet. In order to distinguish blowouts of interest from others, blowout records noting subsurface depths of blowouts (e.g., 3000 ft. BGS), gas as a component of leaking fluid, as well as types of oil and gas activities such as drilling or pulling out of hole, are separated from the initial list of 1319 blowouts. From there, wells noting gas as a primary fluid indicator, or blowouts occurring in RRC Districts commonly producing natural gas (e.g., District 7B), are further organized. For example, prior to the introduction of CO_2 in Texas as a fluid for enhanced oil recovery purposes in 1972, any records that note gas blowouts are almost certainly methane-related according to RRC staff. Using this final list of methane-related blowouts, a select list of paper records are found for each of the final list blowouts. In particular, this final list focuses on blowouts from RRC Districts 5, 6, 7B, 7C, 8, 8A, 9. Regions 1-4 and 10 are not emphasized due to their geographic location outside the primary areas of interest which includes the Permian Basin, and the Dallas Ft. Worth area. Particular Texas counties of interest are also emphasized, specifically Parker, Loving, and Hood counties. Loving county is located in RRC District 8, while Parker and Hood counties are located in District 7B.

XI-2. Results

Relating specifically to methane derived underground blowouts, a total of 54 records were collected from the RRC database, including 72 pages of paper records obtained from the RRC

paper records from their Austin, TX headquarters. A breakdown by district and depth can be found in Table 5. Those wells included from Districts 3 and 4 were collected from the existing RRC online database; no information was collected via paper records. District 8, a major area of EOR production in the state of Texas, had the largest share of these paper blowouts at 20, along with the largest subsequent amount that occurred due to drilling (16).

Of the 54 wells surveyed for this study, 42 were associated with drilling activities (e.g., air drilling, pulling pipe, logging, perforating). Of these 42 drilling-related gas blowouts, Districts 8 and 7B had the highest share at 16 and 7 respectively. The remaining 13 blowouts occurred during other stages of operation including: completion, workover, production, shut in, and abandoned (Table 6).

Thirty nine blowouts had an estimated depth of origin between 2000 and 7000 feet. Eight of these 54 blowouts were reported to have demonstrated surface leakage nearby (i.e., <0.5 miles) to the injection/production well(s) experiencing the blowout (Table 7). Table 8 notes blowouts associated with cratering, which is the collapse of the immediate ground surrounding a well blowout due to a large influx of fluids, causing a loss of soil and shallow geology structure.

Regarding specific counties, there are no records of blowouts occurring in Hood County in the RRC database. For Loving County, there are fourteen records available for blowouts with associated gas migration. While only one of these fourteen wells had a depth correlation (6100 feet depth), latitude and longitude coordinates were obtained for all entries from the RRC drilling permit database. Parker County had six available well blowout records.

XI-3. Discussion

This study provides a snapshot into the most relevant blowouts researched for the goals of this project: those associated with underground gas blowouts, and is not inclusive of all such occurrences of gas-related blowouts. Such next steps research could follow a similar methodology as outlined in this paper, but would require a significantly more amount of time as well as full access to RRC records. One significant contributor to this time frame is the limitations with RRC's data inquiry procedures. Currently, only RRC staff can copy RRC record files (per official protocol), limiting the efficiency of obtaining a large amount of records. For example, copying 77 pages took roughly 2 weeks to complete under normal scheduling constraints for RRC staff.

Additionally, differentiating underground blowouts from other types of blowouts ended up being a difficult task. In most cases, blowouts were caused not by surface error, but by sudden downhole pressure changes usually during drilling or workovers on a particular well. The most common surface-related blowouts occurred due to human error. For example, "human error" was used to describe incidents such as an energy service truck backing into a well head, improper closing of surface valves, among other errors led to a handful of surface-derived blowouts.

However, there were problems interpreting the available records. Similar to information found on the RRC online database, many paper records lacked quantification for fluid leakage amounts, along with duration of blowouts, despite specific places on standard forms for such information. In speaking with RRC employees in District and HQ offices, some of this information is communicated verbally on site when an inspector arrives during the event. As a consequence, even with follow up reports it may not be necessarily conveyed after the fact.

Overall, next steps could include an expansion of efforts discussed in this summary. Following the procedures outlined above, the only limiting factor is the time required to schedule access to RRC records, and the time it would take to research these records. From the 54 blowouts surveyed for this report, 11 in particular could merit further research consideration (Table 7 and Table 8). These tables outline specific well blowouts that were reported to have multiple surface leakage points away (<0.5 miles) from the immediate well blowout area, as well as those associated with cratering. In both cases, such surface features could equate to contamination and legacy presence of fluids out of the immediate radius of the well blowout. As such, these wells could be good candidates for further study if groundwater sampling campaigns are seeking legacy effects from methane-related blowouts.

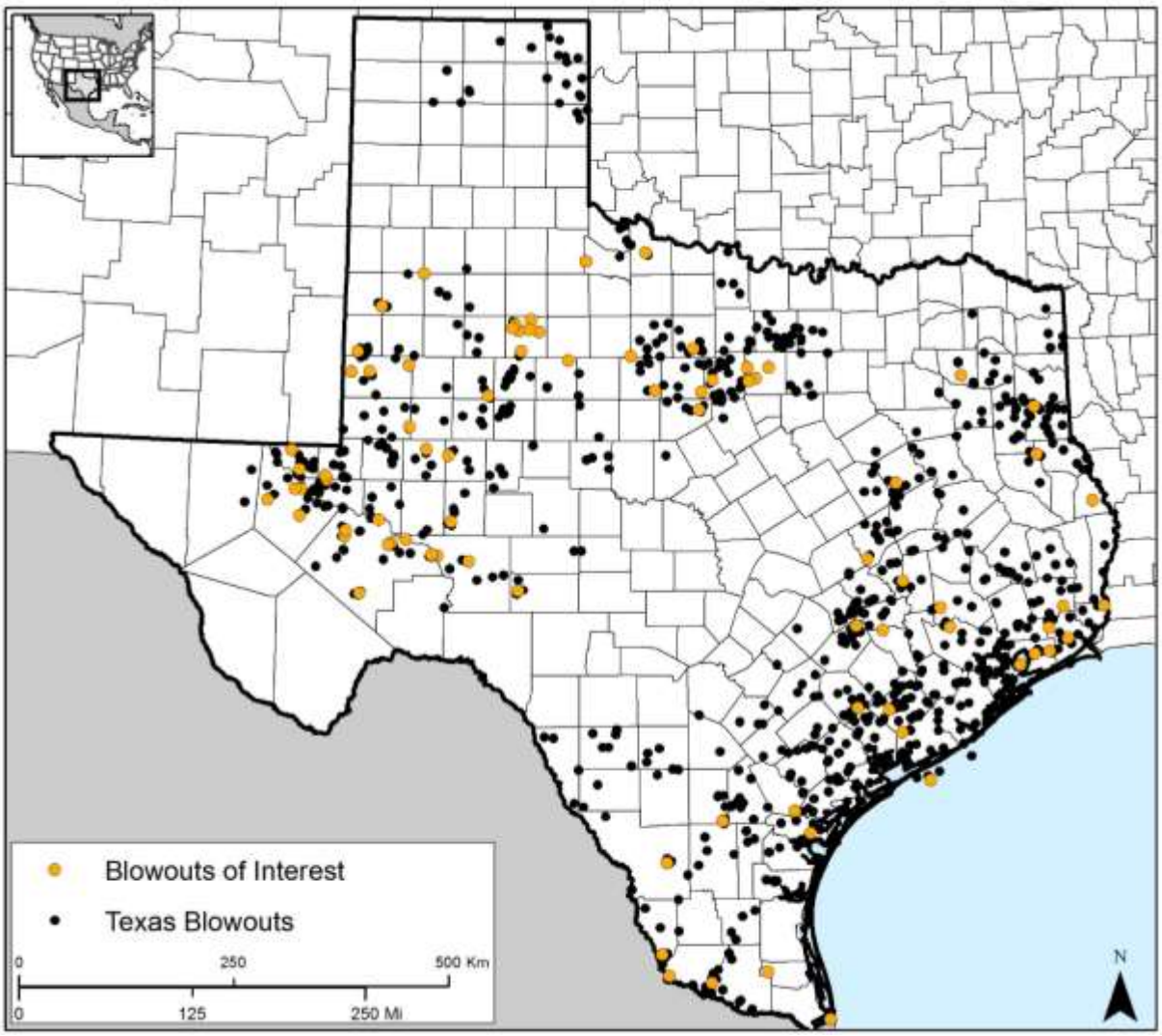

Note: “blowouts of interest” dots represent these subsurface blowouts

Figure 77. RRC-listed blowouts in Texas

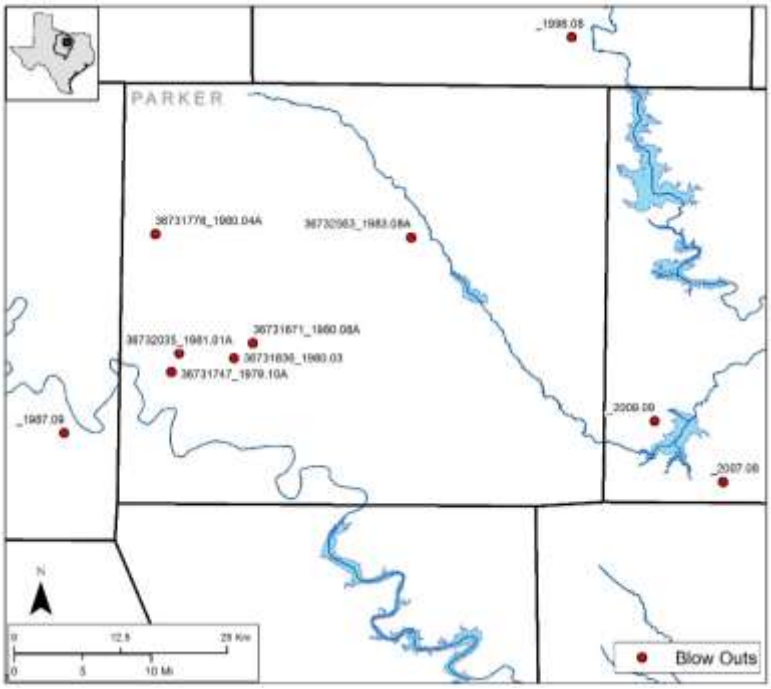

Note: numbering scheme consists of API well number when known (minus the state code) and year and month of the blowout.

Figure 78. Documented blowouts in Parker County

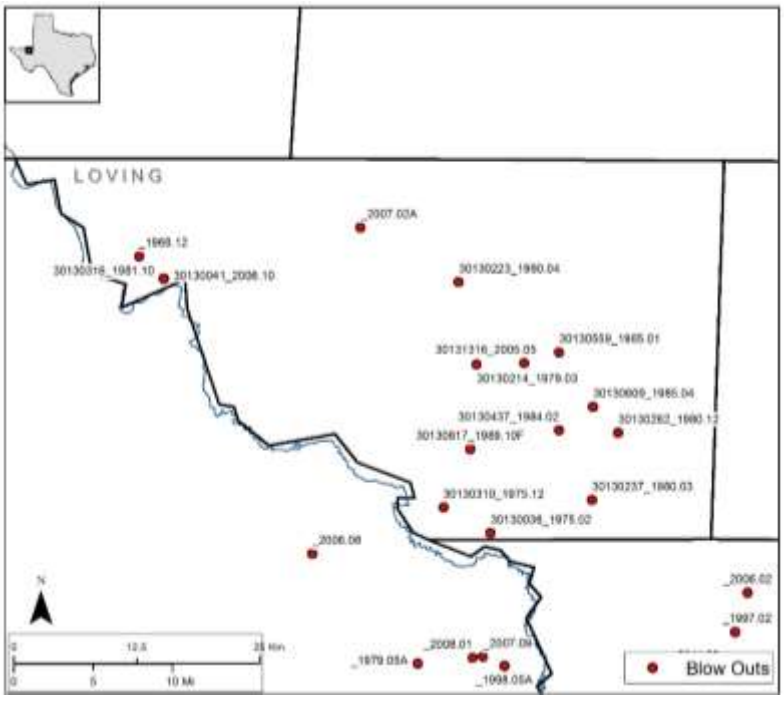

Note: numbering scheme consists of API well number when known (minus the state code) and year and month of the blowout.

Figure 79. Documented blowouts in Loving County

Table 5. Methane-related blowouts by RRC District, depth (ft)

	District 3	District 4	District 5	District 6	District 7B	District 7C	District 8	District 8A	District 9	Total
Total # of Blowouts	344	124	62	118	91	35	182	85	52	1093
Gas-related Blowouts Found at RRC Offices	1	4	4	1	9	5	20	7	3	54
By Depth (ft.)										
0							2	1		3
1000					1	2	4	1		8
2000		1				1	3	1		6
3000				1	1	1	1		2	6
4000					5		4	1	1	11
5000	1	1			2		1	2		7
6000							3			3
7000								1		1
8000		1				1	1			3
9000										0
10000										0
11000							1			1
12000			2							2
13000			1							1
14000										0
15000			1							1
Unknown		1								1

Table 6. Gas-related blowouts sorted by stage of operation and RRC District

	District 3	District 4	District 5	District 6	District 7B	District 7C	District 8	District 8A	District 9	Total
Drilling	1	4	4	1	7	4	16	2	3	42
Completion					1		1			2
Workover					1		2	2		5
Production and Operation								2		2
Shut in						1	1			2
Abandoned								1		1
District Total	1	4	4	1	9	5	20	7	3	54

Table 7. Texas Gas-related blowouts with associated surface leakage features

Dist	Date	Operator	Lease/Facility Name	Lease/ID	Permit #	Well #	Field Name	County	Fire	H2S	Injuries	Deaths	Depth of Blowout (ft)
4	10/31/2000	DOMINION EXPL. & PROD., INC.	Kenaf Industries Unit		496647	1	Wildcat	Willacy	N	N	0	0	2300
4	5/16/2001	COASTAL OIL & GAS CORP.	Samano		508219	21		Starr	N	N	0	0	5423
5	1/17/2000	ANADARKO PETROLEUM CORP.	Stephens A-1				Dew	Freestone					13289
7B	12/14/2005	Telesis Operating Co., Inc	Ritchie-37-		610032	2		Palo Pinto	Y		1	0	3700
7C	6/1/1989	MARATHON OIL COMPANY	University	00228		125	Big Lake	Reagan	N	Y	0	0	2875
8	1/20/2011	Endeavor Energy Resources L.P.	Lewellen		708322	2	Brasher (Atoka)	Midland	N	N	0	0	2319
8A	8/18/1997	MOBIL PRODUCING TX & NM INC	Mallet Unit	18149		199	Slaughter	Hockley	N	Y	0	0	5000
9	7/29/1990	R. M. HILL	Choate "A"	27781	375659	1	Minta	Young	N	N	0	0	3080

Table 8. Texas gas-related blowouts with associated cratering

Dist	Date	Operator	Lease/Facility Name	Lease/ID	Permit #	Well #	Field Name	County	Fire	H2S	Injuries	Deaths	Depth of Blowout (ft)
7B	12/14/2005	Telesis Operating Co., Inc	Ritchie-37-		610032	2		Palo Pinto	Y		1	0	3700
8	5/25/1979	TEXACO, INCORPORATED	Cornell Knight	45043		1	Greasewood (Siluro-Dev.)	Reeves	N	Y	0	0	11392
5	9/19/1990	SAMEDAN OIL CORP.	Winfree	117405		2	Teague (Cotton Valley)	Freestone	N	N	0	0	12450

XII. Appendix D: Water Type Analysis

by Roxana Darvari modified by JPN

In this appendix, we compare major ion chemistry of samples taken during this study to historical samples taken by TWDB (oldest sample in the database taken in 1919). If multiple samples are available from the same well, we used the most recent. We used the same counties in which BEG samples are present and we tracked the samples per aquifer. The samples are distributed throughout the year but mostly between the months of September and November. The TWDB groundwater database is available at: http://www.twdb.texas.gov/groundwater/data/gwdbrpt.asp (last accessed on 04/30/2015).

Overall the description that follows shows that BEG sampling is representative of and consistent with the larger TWDB database in the aquifers of interest. Box plots are provided for all TWDB and BEG total dissolved solids (TDS). The box plots summarize the distribution of formation water TDS for each formation. Some plots have insufficient data to construct proper box plots and they are included only for completeness. Generally the BEG and TWDB plots are similar. But there are some differences in which are listed below (using t-test in "SigmaPlot"). "AquaChem" was chosen to manage the water quality data and analyze the geochemistry of each formation.

XII-1. Barnett Shale

More than 2624 wells were sampled from 1919 to 2014 by TWDB in the Barnett footprint and a total of 5591 water samples were collected from these wells but this report only considers the most recent sample from each well. 302 wells have incomplete analyses or are not charge-balanced so they are not considered in this study. Total number of TWDB wells considered in this study is 2322. BEG sampled from 556 water wells in the Barnett footprint.

Comparing TDS distribution in different formations:

The following plots (units are mg/L) display results for the 3 aquifers in the Barnett Shale footprint: (1) Paleozoic group; (2) Trinity aquifer system composed of several aquifers (most of the BEG data belong to this group); and (3) Woodbine aquifer.

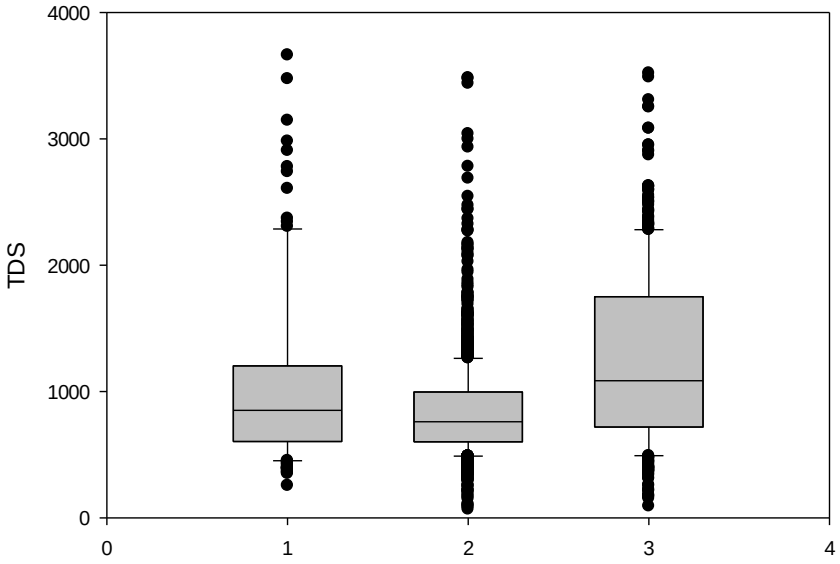

[TDS; TWDB data]

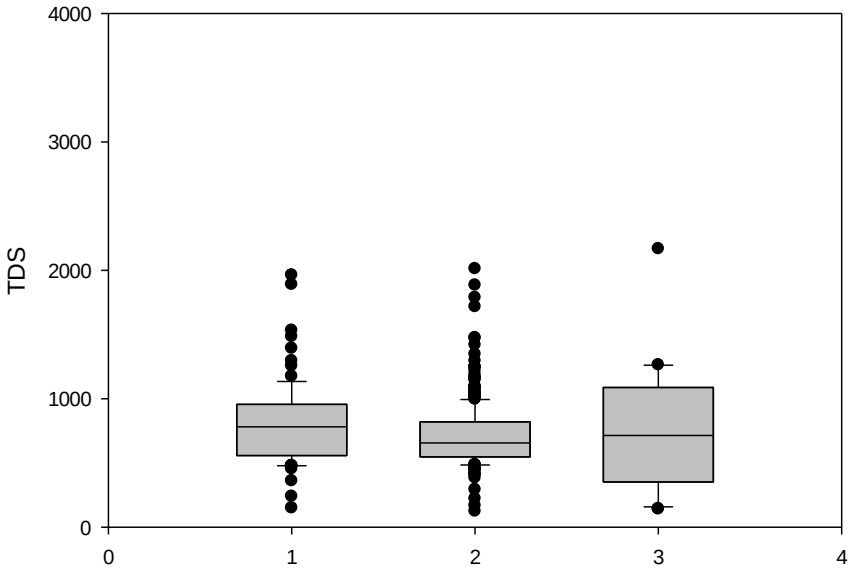

[TDS; BEG data]

Paleozoic: BEG and TWDB boxes overlap but not both medians. The sample mean of TWDB data exceeds the sample mean of BEG by an amount of 371 mg/L, which is greater than would be expected by chance. It is likely that overall TWDB samples have greater TDS than BEG samples. By using t test statistics to determine the two tailed p-value of 0.008 (which is less than 0.05), it fails the hypothesis that the BEG population mean is equal to the TWDB population mean. It indicates that it is likely that there is a relationship between TWDB and BEG results.

Trinity: There is a statistically significant difference between TWDB and BEG dataset, with two tailed P-value of 0.000127. So it fails the hypothesis that the BEG population mean is equal to the TWDB population mean.

Woodbine: The difference in the mean values of the two groups is greater than would be expected by chance; t test result with two tailed P-value of 0.003 indicates that there is a statistically significant difference between BEG and TWDB sample results.
The 3 t-tests failed but they passed the Mann-Whitney test, similar test for non-normally distributed data.

Group Name	Number of samples	Mean	Std Dev	SEM*
Paleozoic				
TWDB	140	1169.70	1252.73	105.875
BEG	85	798.42	314.41	34.103
Trinity				
TWDB	1667	874.17	834.76	20.445
BEG	351	709.43	238.89	12.751
Woodbine				
TWDB	514	1285.49	827.89	36.552
BEG	23	762.09	480.89	100.272

***:** SEM = standard error of the mean

Water Type Comparison:

Paleozoic*:* The plots below show that the water type of groundwater drawn from TWDB wells was Na-HCO_3, which is consistent with BEG dataset with Na-HCO_3 as the most dominant water type in the groundwater. [number of samples on the y-axis and water type on the x-axis]

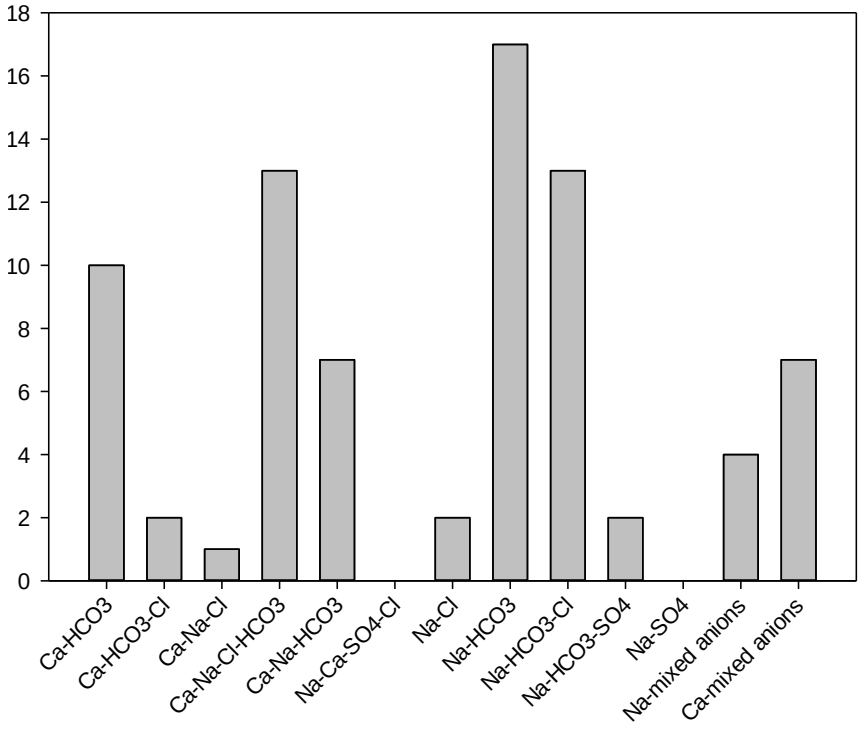

[Paleozoic; TWDB data]

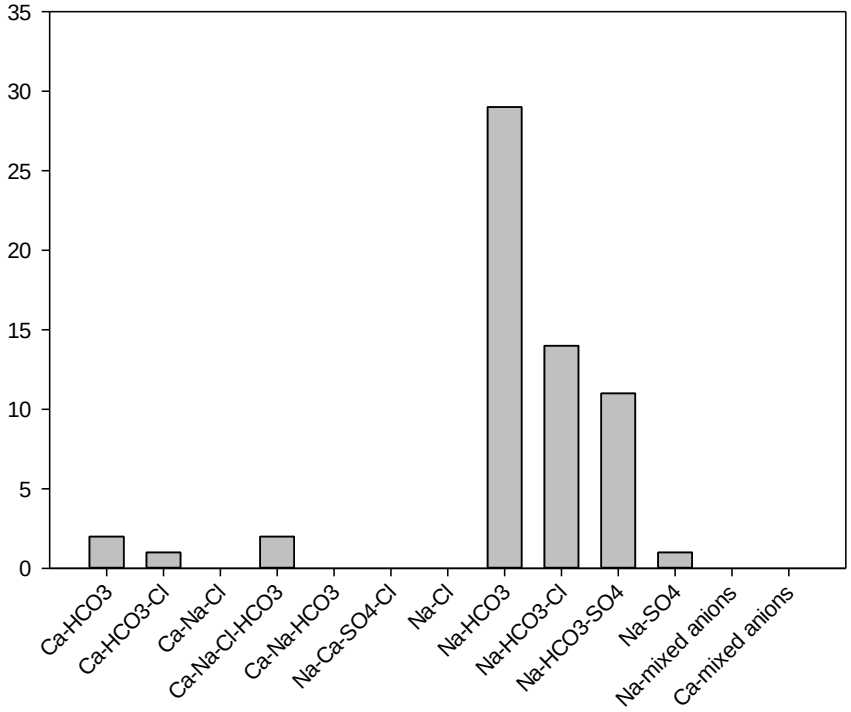

[Paleozoic; BEG data]

Trinity: As shown in the following plots, the dominant water types in the wells sampled by TWDB is Na-HCO_3 which seem to be consistent with the BEG results. This is also consistent with information from the literature. The water type in Twin Mountain as part of the Trinity group formation is Ca-HCO_3 (Beynon 1991). Water type from Antlers-Travis Peak outcrop is generally Na-HCO_3 type (Nordstrom, 1987). Baker (1960) stated that "the Trinity group generally yields soft water that is high in Na-HCO_3 content". [number of samples on the y-axis and water type on the x-axis]

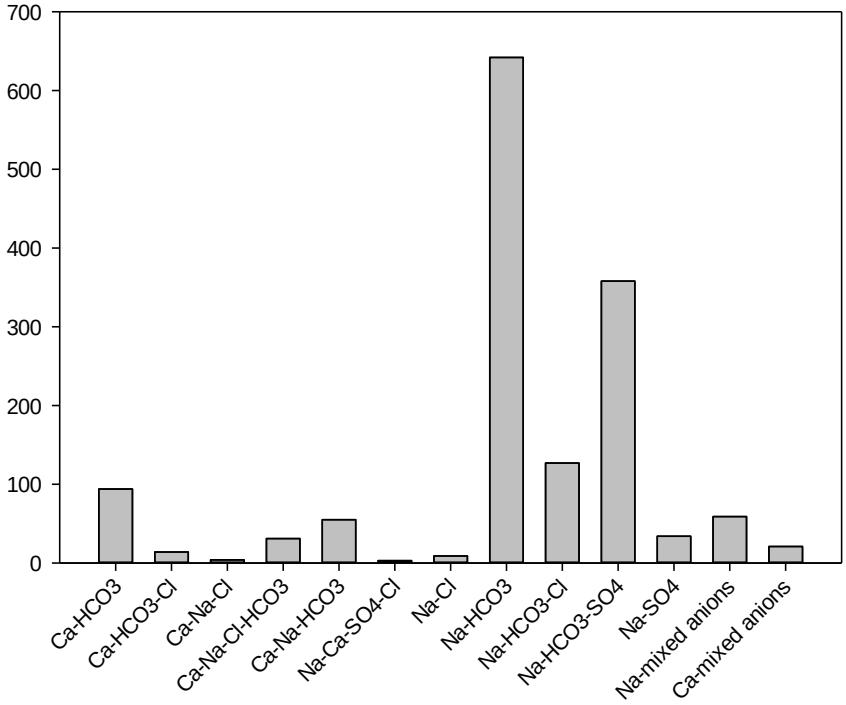

[Trinity; TWDB data]

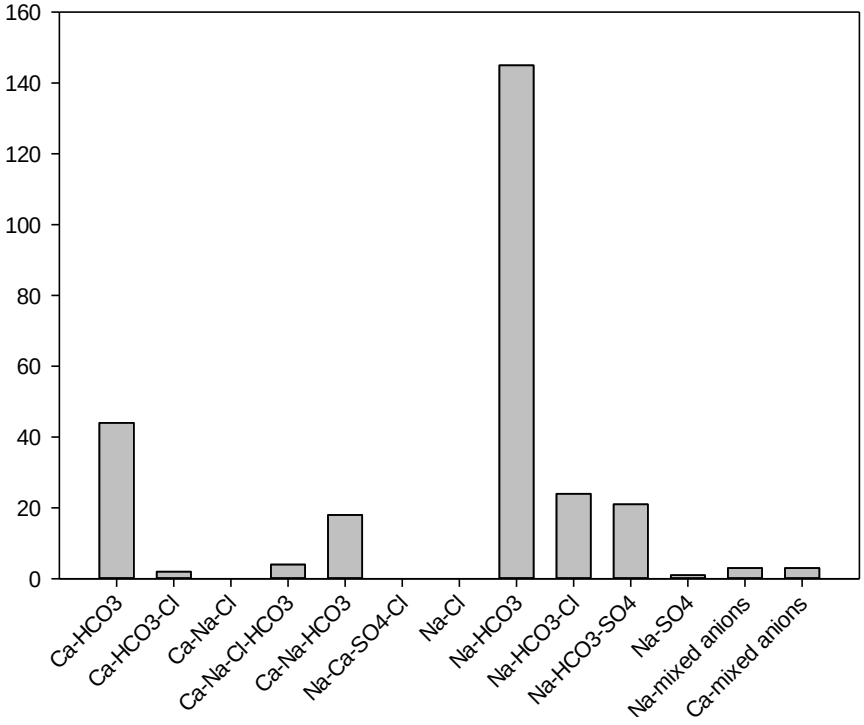

[Trinity; BEG data]

Woodbine: Both TWDB and BEG results show that Na-HCO_3 and Na-HCO_3-SO_4 are the most dominant water type composition. According to Klemt et al. (1975) "the water in the Woodbine is usually a soft, sodium bicarbonate type of fair quality, except in the immediate outcrop area where it is a hard, calcium bicarbonate type of good quality". [number of samples on the y-axis and water type on the x-axis]

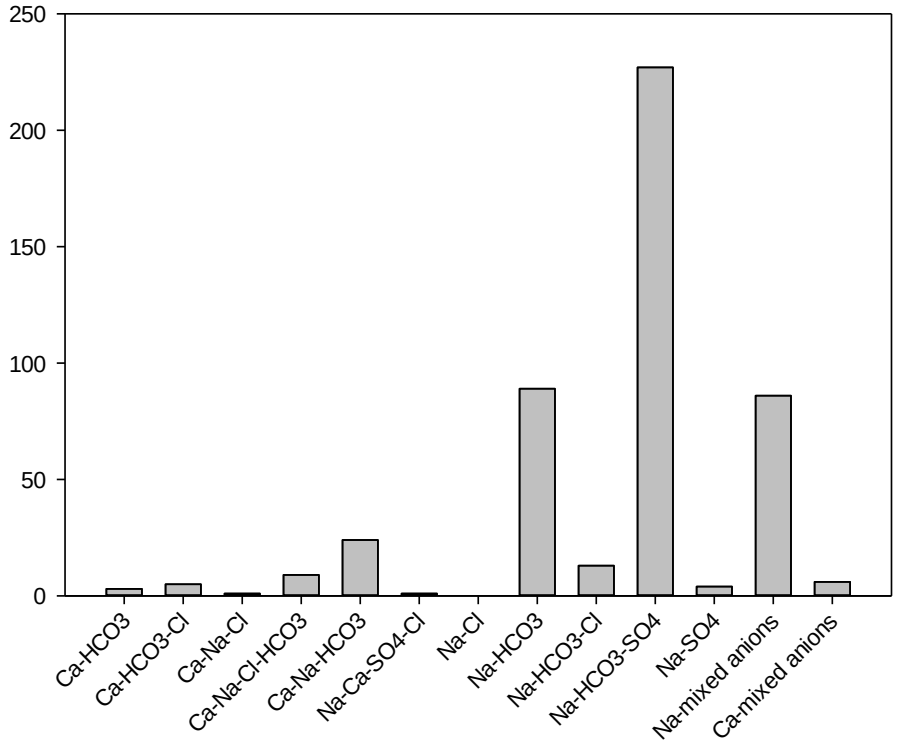

[Woodbine; TWDB data]

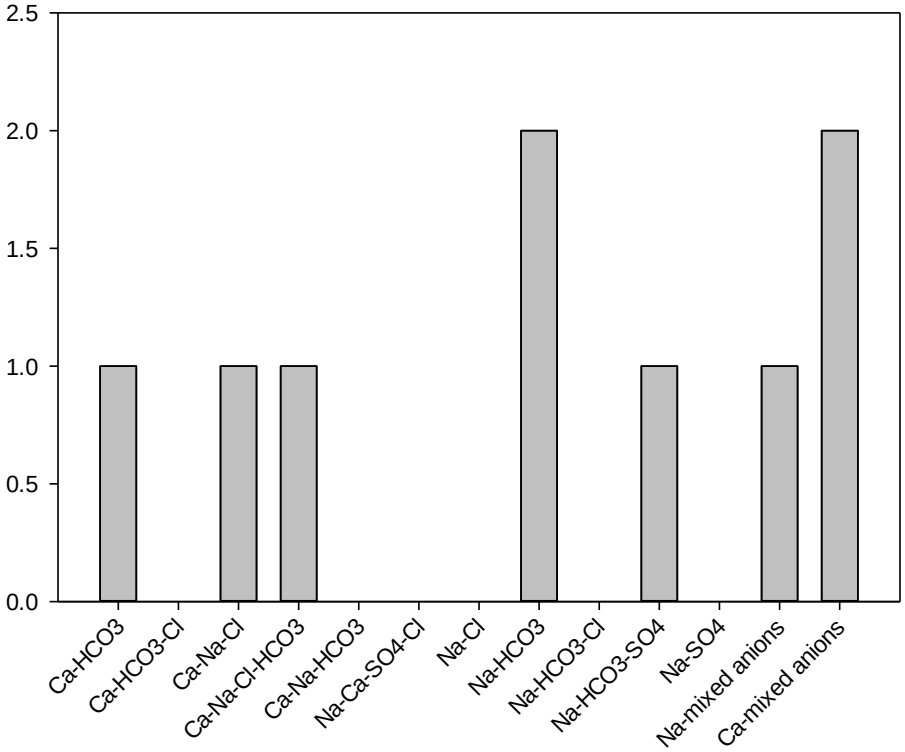

[Woodbine; BEG data]

XII-2. Haynesville Shale

More than 990 wells were sampled from 1934 to 2014 by TWDB in the Haynesville Shale footprint. A total of 2257 water samples were collected from these wells but this report only considers the most recent sample from each well. 196 wells with incomplete analyses or with no charge-balanced removed from the wells list. BEG study sampled 70 water wells in Haynesville footprint.

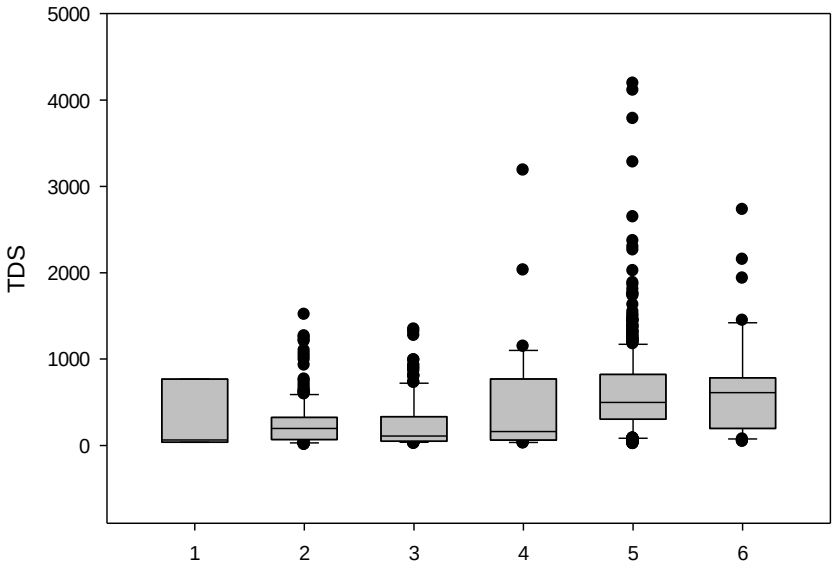

Formations (1=Alluvium-Quatenary with 3data points , 2=Carrizo with 217 data points, 3=Queen City-Sparta with 147 data points,4=Reclaw with 36 data points, 5= Wilcox with 542 data points, 6=Yegua-Jackson with 44 data points)

[TDS; TWDB data]

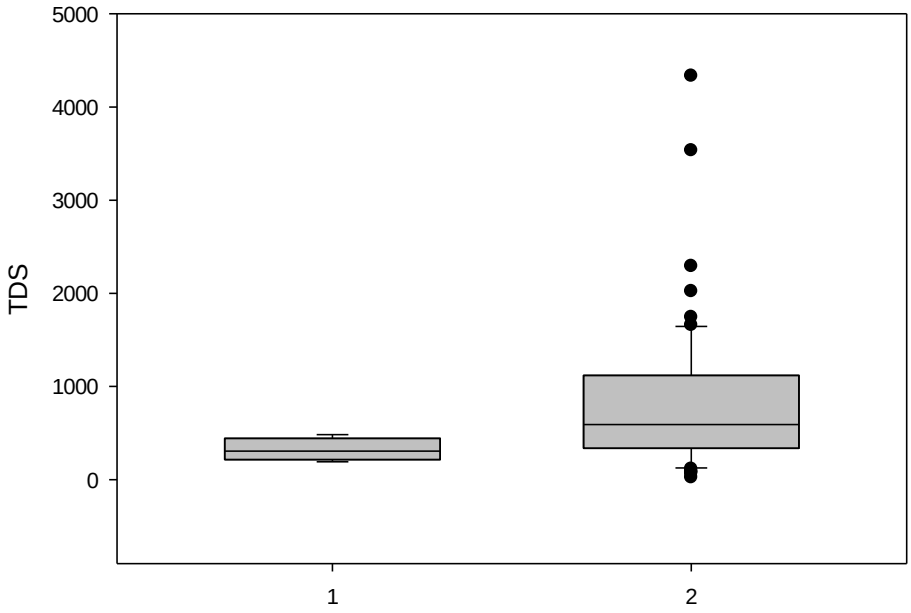

Formations (1=Carizzo with 4data points , 2=Wicox with 66 data points)

[TDS; BEG data]

Comparing TDS distribution in different formations:

The following plots (units are mg/L) display results for the 2 aquifers sampled in the Haynesville Shale footprint: (1) Wilcox aquifer; (2) Carrizo aquifer. Other aquifers exist in the footprint but there were not sampled during this study.

Wilcox: t test result with P-value of 0.051 shows that there is not a statistically significant difference between BEG and TWDB data.

Carrizo: There is not a statistically significant difference between the TWDB and BEG groups. As a result of t test with P-value of 0.656. The difference in the mean values of TWDB and BEG is not great enough to reject the possibility that the difference is due to random sampling variability.

Group Name	Number of samples	Mean	Std Dev	SEM*
Wilcox				
TWDB	529	605.340	510.526	22.197
BEG	66	810.751	757.644	93.260
Carrizo				
TWDB	205	261.551	268.531	18.755
BEG	4	321.655	121.054	60.527

***:** SEM = standard error of the mean

Water Type Comparison:

Wilcox: As shown in the following plots, the dominant water type of the samples taken from wells in Wilcox, both by BEG and TWDB, are Na-HCO3 and Na-HCO3-Cl type composition. . [number of samples on the y-axis and water type on the x-axis]

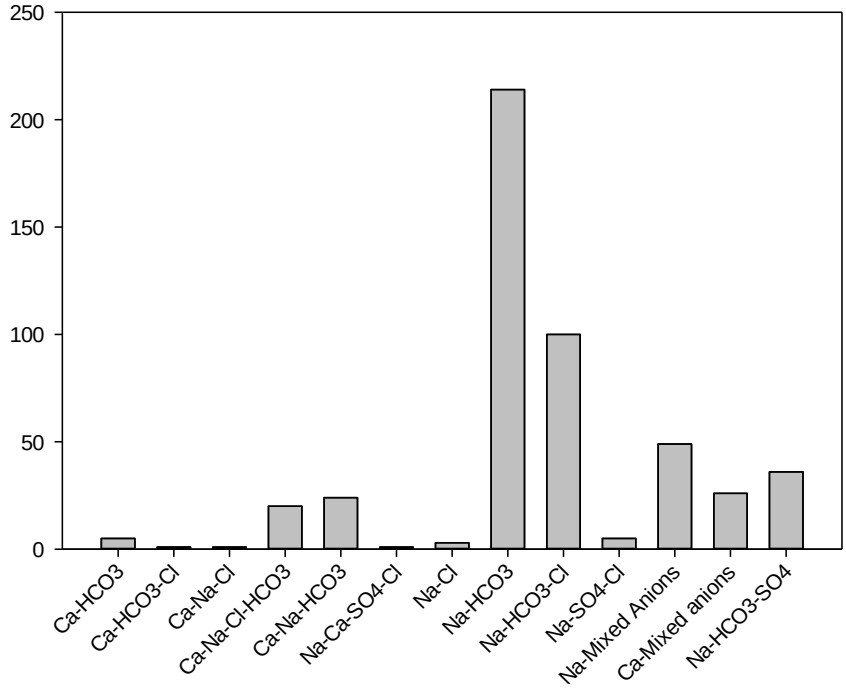

[Wilcox; TWDB data]

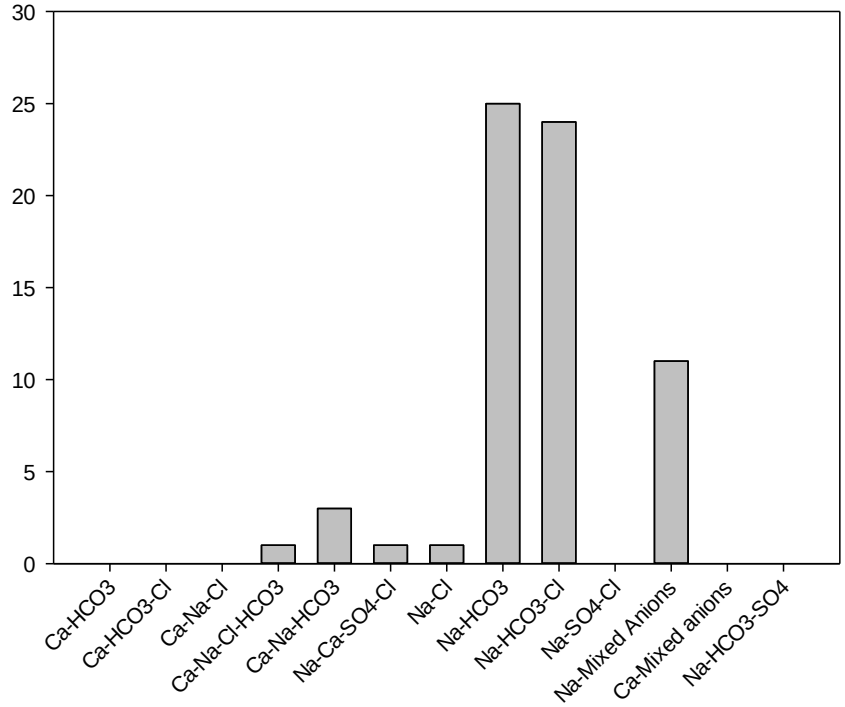

[Wilcox; BEG data]

Carrizo: the plots below, as results of both TWDB and BEG, show that water type in Carrizo is more Na-HCO_3 and Na-HCO_3-SO_4 type composition. [number of samples on the y-axis and water type on the x-axis]

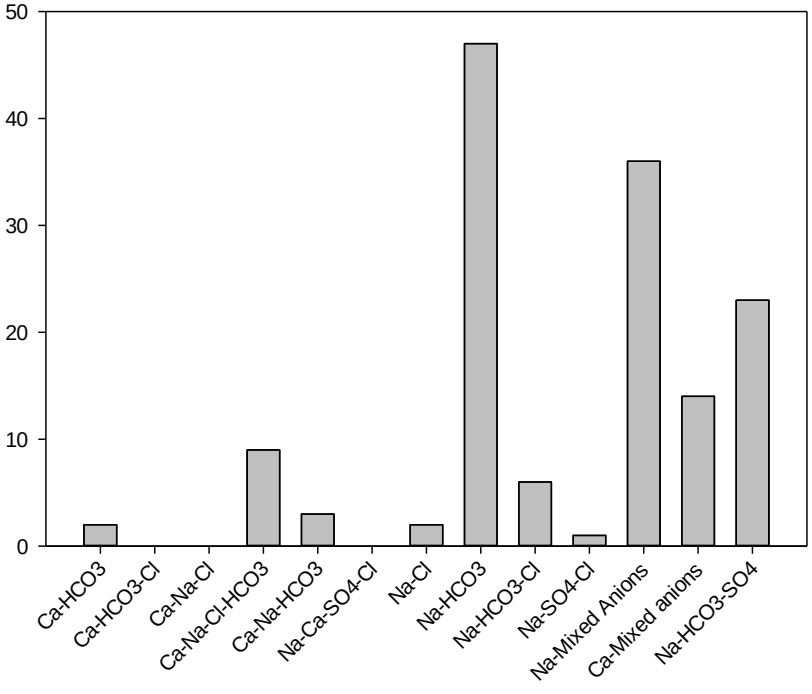

[Carrizo; TWDB data]

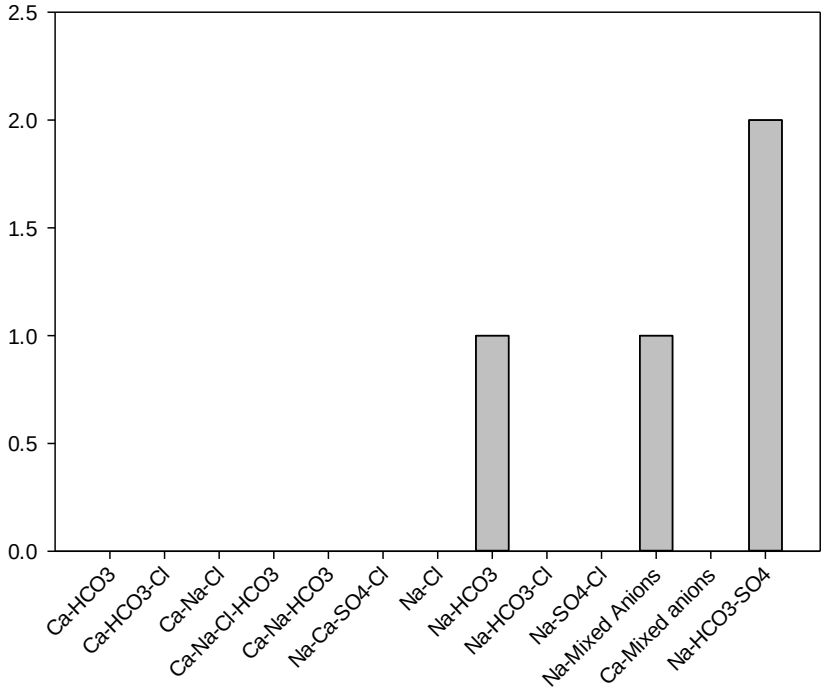

[Carrizo; BEG data]

Kreitler et al. (2013b) state that the water type at shallower depths is Ca-mixed anions and changes to Na-HCO3 with increasing depth. Since most of the wells sampled by BEG in the Carrizo-Wilcox are deeper than 500 ft., so the Na-HCO3 type composition is expected to be the dominant water type.

XII-3. Eagle Ford Shale

More than 2903 wells were sampled from 1919 to 2014 by TWDB in the Eagle Ford Shale footprint. A total of 6233 water samples were collected from these wells but this report only considers the most recent sample from each well. Some wells have incomplete analyses or are not charge-balanced so they are not considered in this study (number of removed data points in each formation: Catahoula: 70, Carrizo- Wilcox: 63, Queen City-Sparta: 67, Reklaw: 2, Yegua Jackson: 72). BEG sampled 110 water wells in the Eagle Ford footprint.

The following plots (units are mg/L) display results for the 4 aquifer systems in the Eagle Ford Shale footprint BEG sampled: (1) Catahoula; (2) Carrizo-Wilcox; (3) Queen City-Sparta; and (4) Yegua-Jackson aquifers.

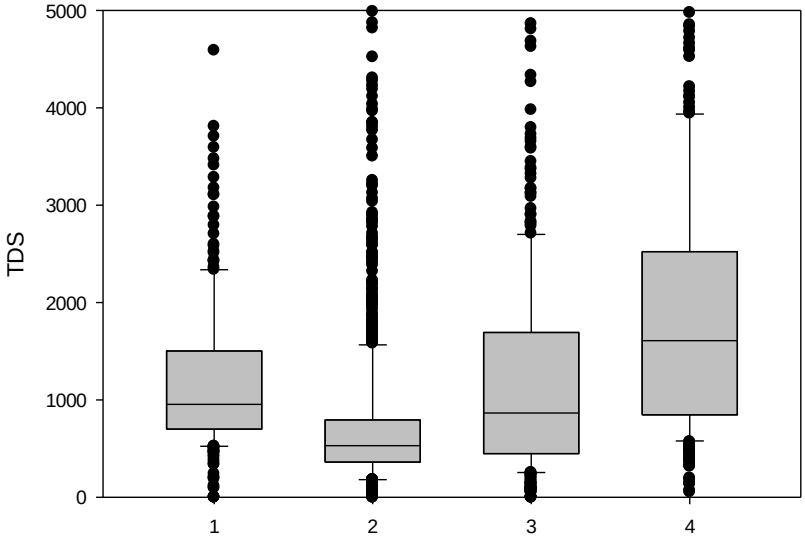

Formations (1=Catahoula with 288 data points, 2=Carrizo-Wilcox with 1079 data points, 3= Queen City- Sparta with 468 data points,4=Yegua-Jackson with 313 data points) [TDS, TWDB data]

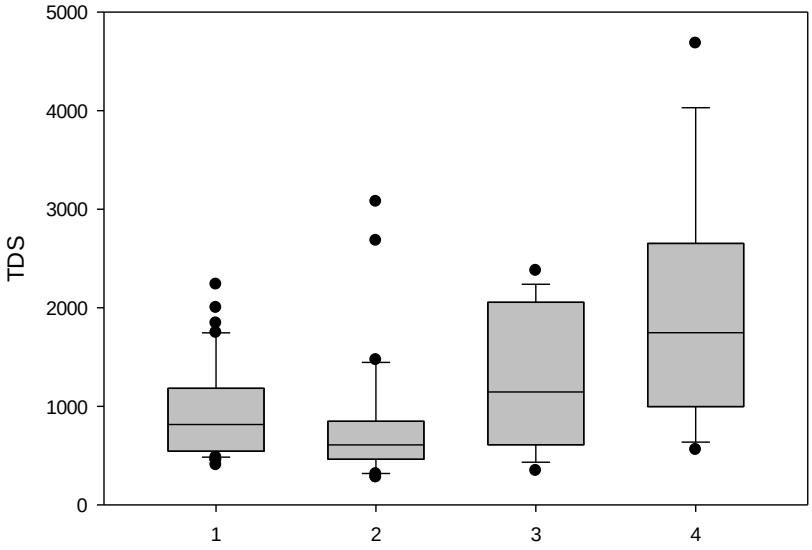

Formations (1=Catahoula with 48 data points , 2=Carrizo-Wilcox with 30 data points, 3=Queen City-Sparta with 16 data points , 4=Yegua-Jackson with 16 data points) [TDS; BEG data]

Comparing TDS distribution in different formations:

Generally the BEG and TWDB plots are the same. But there are some particular differences in different formations which are listed below:

***Catahoula*:** boxes overlap but not both medians. The sample mean of TWDB data exceeds the sample mean of BEG by an amount of 307 mg/L. It is likely that overall TWDB samples have greater TDS than BEG samples. By using t-test statistics to determine the two tailed p-value of 0.0276 (which is less than 0.05), it indicates that it is likely that there is a relationship between TWDB and BEG results.

***Carrizo-Wilcox**:* boxes overlap with both medians. No difference can be claimed. Also t-test with the two tailed p-value of 0.946 suggests that there is not a statistically significant difference between BEG and TWDB data.

***Queen City-Sparta*:** boxes overlap but not both medians. The difference in the median values between the two groups is not large enough to exclude the possibility that the difference is due to random sampling variability. The TWDB average is 64 mg/L larger than the BEG average. Performing the t test (p-value of 0.862) rejects the possibility that there is a statistically difference between two groups.

Yegua-Jackson: boxes overlap with both medians. And we cannot tell if there is a difference. t test (p-value of 0.971) also confirms that no difference can be claimed.

Group Name	Number of samples	Mean	Std Dev	SEM*
Catahoula				
TWDB	288	1228.61	943.74	55.61
BEG	48	921.08	458.55	66.19
Carrizo-Wilcox				
TWDB	1079	793.42	1019.06	31.02
BEG	30	780.69	633.67	115.69
Queen City-Sparta				
TWDB	468	1323.66	1425.68	65.90
BEG	16	1259.59	704.36	176.09
Yegua-Jackson				
TWDB	313	1991.12	1830.91	103.49
BEG	16	2007.71	1176.17	294.04

***:** SEM = standard error of the mean

Water Type Comparison

Catahoula: The plots below show that the water type of groundwater drawn from TWDB wells is Na-Cl-HCO_3, which is consistent with BEG dataset with Na-Ca-Cl-HCO_3 as the most dominant ions in the groundwater. According to Lee et al. (2007), the water chemistry of wells from Catahoula is characterized by high dissolved solids content and Na-Cl is the most dominant water type composition. [number of samples on the y-axis and water type on the x-axis]

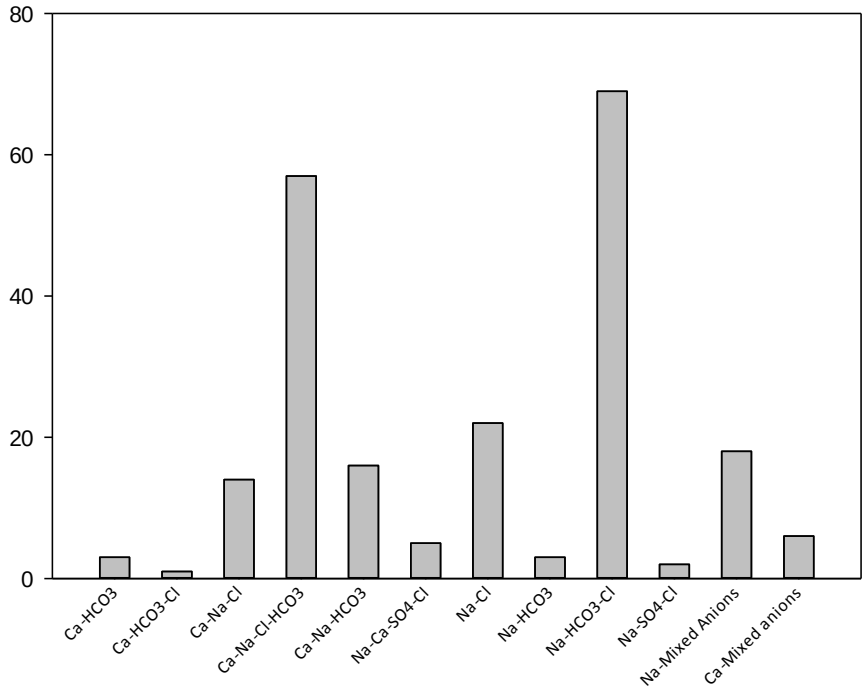

[Catahoula; TWDB data]

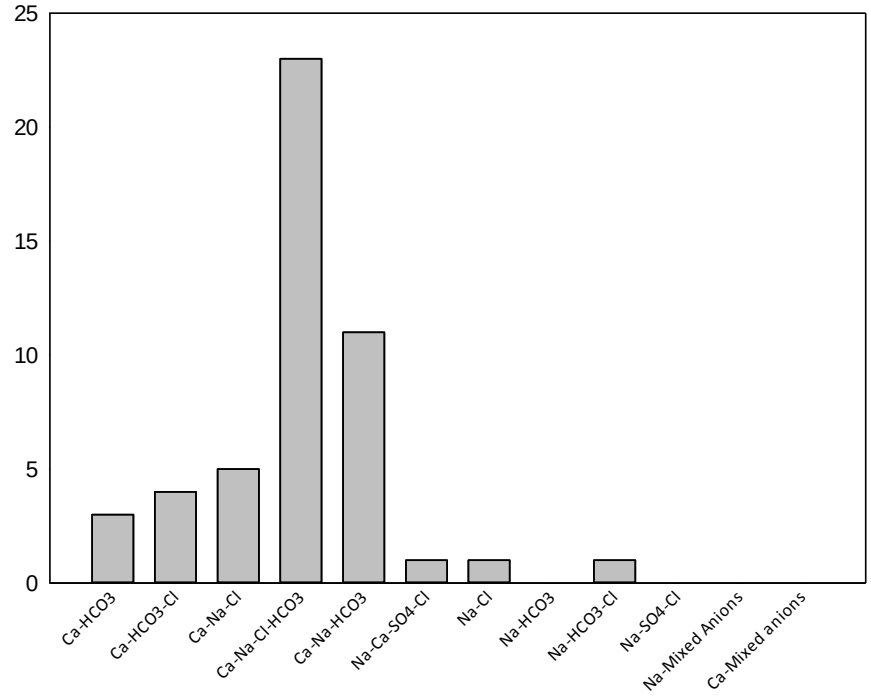

[Catahoula; BEG data]

Carrizo-Wilcox: the dominant water type in the wells sampled by TWDB is Ca-Na-HCO_3-Cl consistent with the BEG results. The CZWX GAM report also confirms the findings. It indicates that as groundwater moves farther downdip the water type tend toward the Na-HCO_3 type (Dutton et al., 2003). Kreitler et al. (2013b) shows that the water type at shallower depths (<500 ft.) is Ca-mixed anions tending to Na-HCO_3 with increasing depth (>2000 ft.). The well depths BEG sampled in Carrizo-Wilcox ranges from 1000 ft to 4000 ft, so the NaHCO3 type composition is expected. [number of samples on the y-axis and water type on the x-axis]

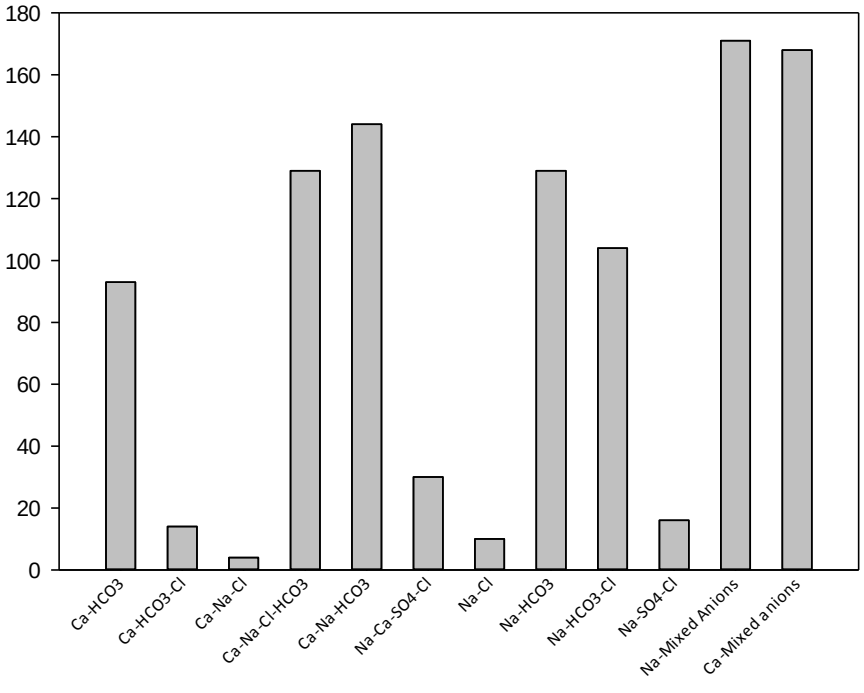

[CZWX; TWDB data]

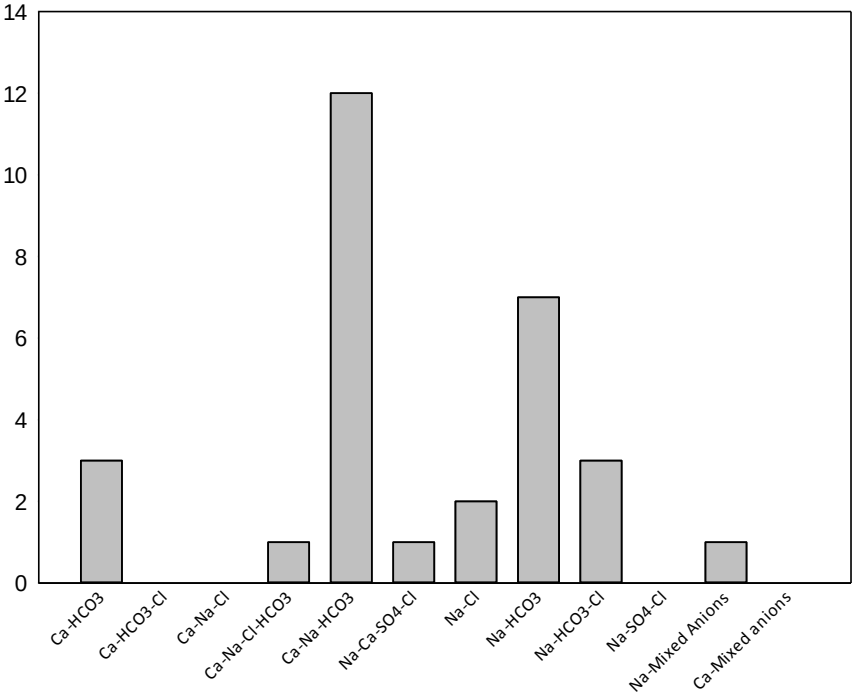

[CZWX; BEG data]

Queen City-Sparta: the Na-HCO_3-Cl type is dominant in the BEG samples consistent with TWDB water types. QCSP GAM model describes Ca-HCO_3, Na-HCO_3, or Na-mixed anion are the most dominant water types in QCSP aquifer with "the single most prevalent type in either aquifer is the Na-HCO3 type" (Kelley et al., 2004). Kreitler et al. (2013b) also confirms that the water chemistry in QCSP changes from mixed cations (Ca-Mg-Na) and mixed anions (Cl-HCO_3-SO_4) in shallow depths to Na-HCO_3 type at depth (>500ft.). Since almost all of the BEG samples range in depth from 700 ft to 2500 ft, Na and HCO3 are expected to be the dominant ions. [number of samples on the y-axis and water type on the x-axis]

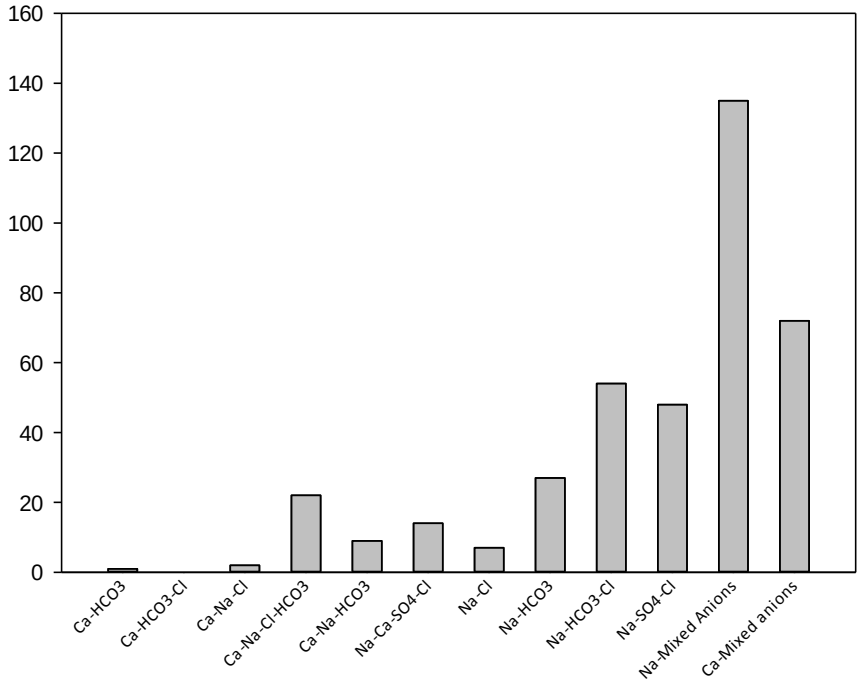

[QCSP; TWDB data]

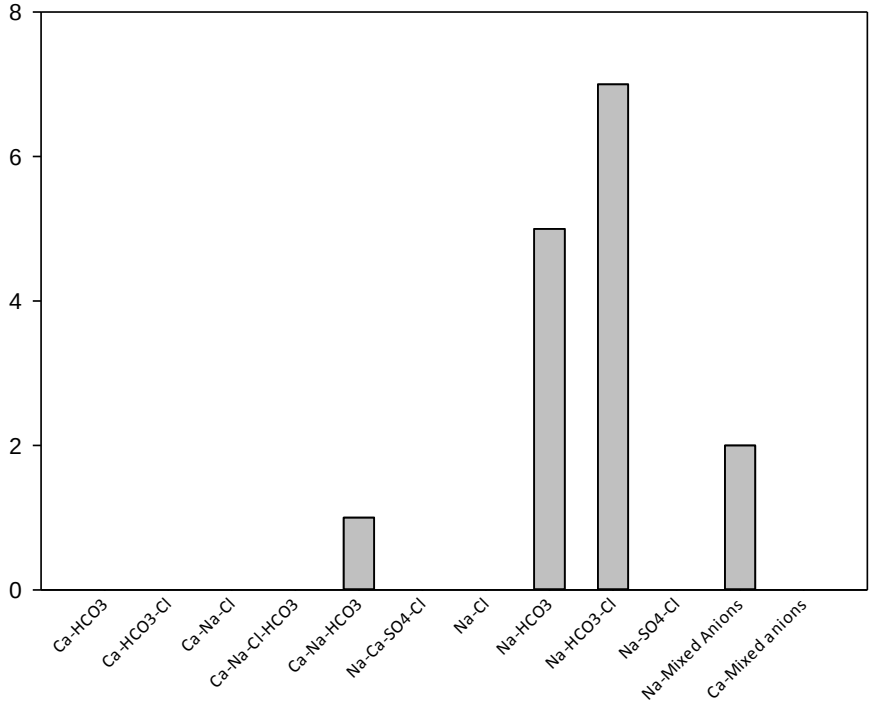

[QCSP; BEG data]

Yegua-Jackson: both TWDB and BEG results show that the most dominant ions are Na-Ca-SO_4-Cl which is confirmed by Kreitler et al. (2013b) and Deeds et al. (2010), indicating that Na-mixed anions (Cl-SO_4-HCO_3) water type is the dominant. [number of samples on the y-axis and water type on the x-axis]

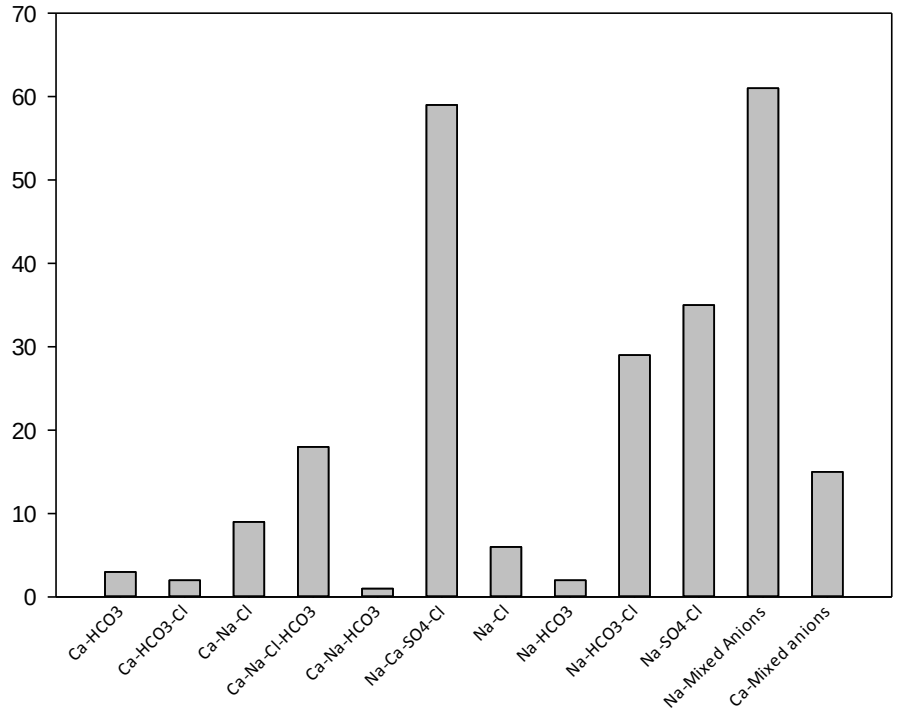

[YGJK; TWDB data]

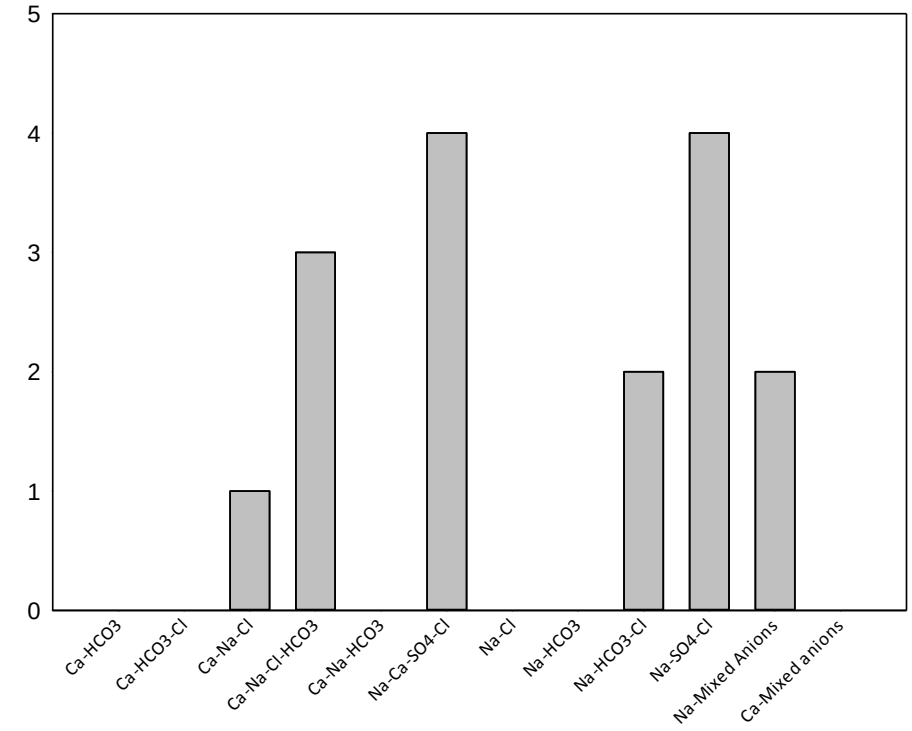

[YGJK; BEG data]

References:

Baker, E.T., 1960, Geology and Groundwater Resources of Grayson County, Texas, Texas Board of Water Engineers Bulletin 6013, 66p., https://www.twdb.texas.gov/publications/reports/bulletins/doc/B6013.pdf.

Deeds, N. E., T. Yan, A. Singh, T. L. Jones, V. A. Kelley, P. R. Knox, S. C. Young, Groundwater Availability Model for the Yegua-Jackson Aquifer, variously paginated, http://www.twdb.texas.gov/groundwater/models/gam/ygjk/YGJK_Model_Report.pdf

Dutton, A. R., B. Harden, J.-P. Nicot, and D. O'Rourke, 2003, Groundwater Availability Model for the Central Part of the Carrizo-Wilcox aquifer in Texas, 55p.. http://www.twdb.texas.gov/groundwater/models/gam/czwx_c/CZWX_C_Full_Report.pdf

Kelley, V. A., N. E Deeds, D. G. Fryar, and J.-P. Nicot, 2004, Groundwater Availability Models for the Queen City and Sparta Aquifers, variously paginated, http://www.twdb.texas.gov/groundwater/models/gam/qcsp/QCSP_Model_Report.pdf,

Klemt, W. B., R. D. Perkins, and H. J. Alvarez, 1975, Groundwater Resources of Part of Central Texas with Emphasis on the Antlers and Travis Peak Formations, Vol. 1, 22p., http://www.twdb.texas.gov/publications/reports/numbered_reports/doc/R195/R195v1/R195v1_1st_part.pdf

Kreitler, C., R. Bassett, J. Beach, L. Symank, D. O'Rourke, A. Papafotiou, J. Ewing, and V. Kelley, 2013b, Evaluation of Hydrochemical and Isotopic Data in Groundwater Management Areas 11,12, and 13, contract report prepared by LBG-Guyton, Austin, Texas for the Texas Water Development Board, July 2013, 454p..

Lee, R.S., D.T. Adamson, M. Vanderford, 2007, Visual Methods for Geochemical Screening of Possible Impacts to Groundwater by Oilfield Brines, 7p., 14th International Petroleum environmental Conference, Houston, TX, November 2007. Last accessed on 06/08/2015 http://ipec.utulsa.edu/Conf2007/Papers/Lee_61.pdf,.

Nordstrom, P. L., 1987, Ground-water resources of the Antlers and Travis Peak formations in the outcrop area of north-central Texas, 101p., http://www.twdb.texas.gov/publications/reports/numbered_reports/doc/R298/R298_A.pdf,

[also listed in the Reference section of the main text]

XIII. Appendix E: BEG-Isotech Methane and Isotope Comparison

by Roxana Darvari modified by JPN

In the context of a QA analysis some duplicates were sent to Isotech Labs, Champaign, Illinois (http://www.isotechlabs.com/). Dissolved methane measurements from IsoFlask samples sent to Isotech Labs are systematically higher than samples analyzed at BEG and taken following the BEG procedure but both are consistent with each other (Figure 80). It is unclear whether one lab underestimates concentrations whereas the other lab overestimates them and what the impact of the sampling method is on the final results. One can be certain though that measured low concentrations are low and that measured high concentrations are high. All bubbling and fizzy wells have "high" methane values. We also compared isotopic results of standards (Figure 81a) and selected samples high in methane (Figure 81b) to Isotech results from the same dissolved methane analysis samples. Results from both labs differ by a few $\delta^{13}C$ units at most.

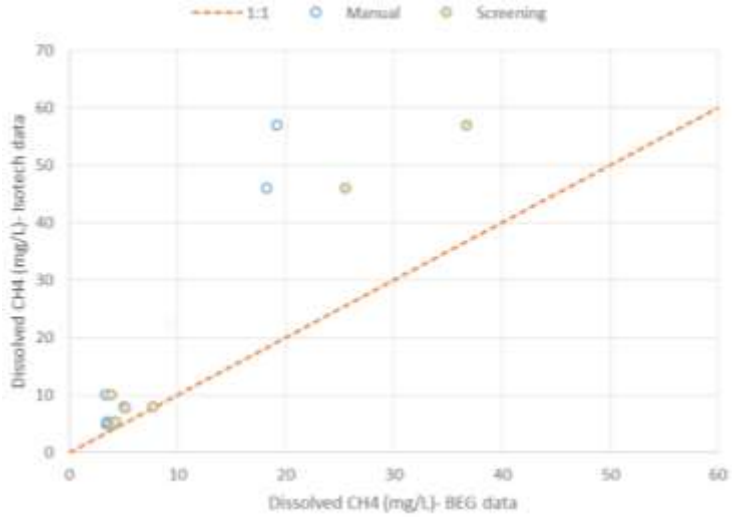

Figure 80. Comparison Isotech-BEG sampling and dissolved gas analysis

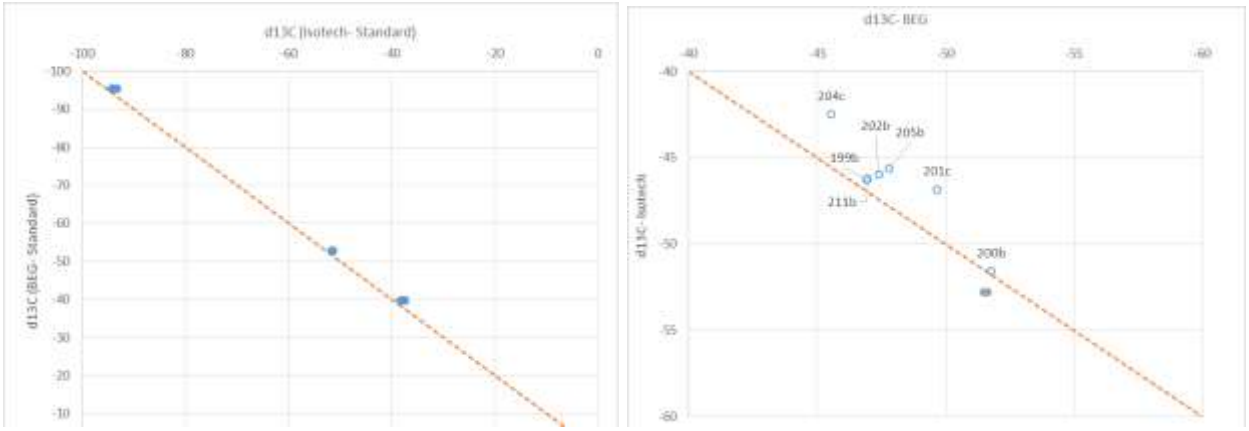

Figure 81. Comparison Isotech-BEG isotope analysis with standards (a) and collected samples (b).

XIV. Appendix F: Dissolved methane vs. major, minor, and trace elements concentrations

by Roxana Darvari modified by JPN

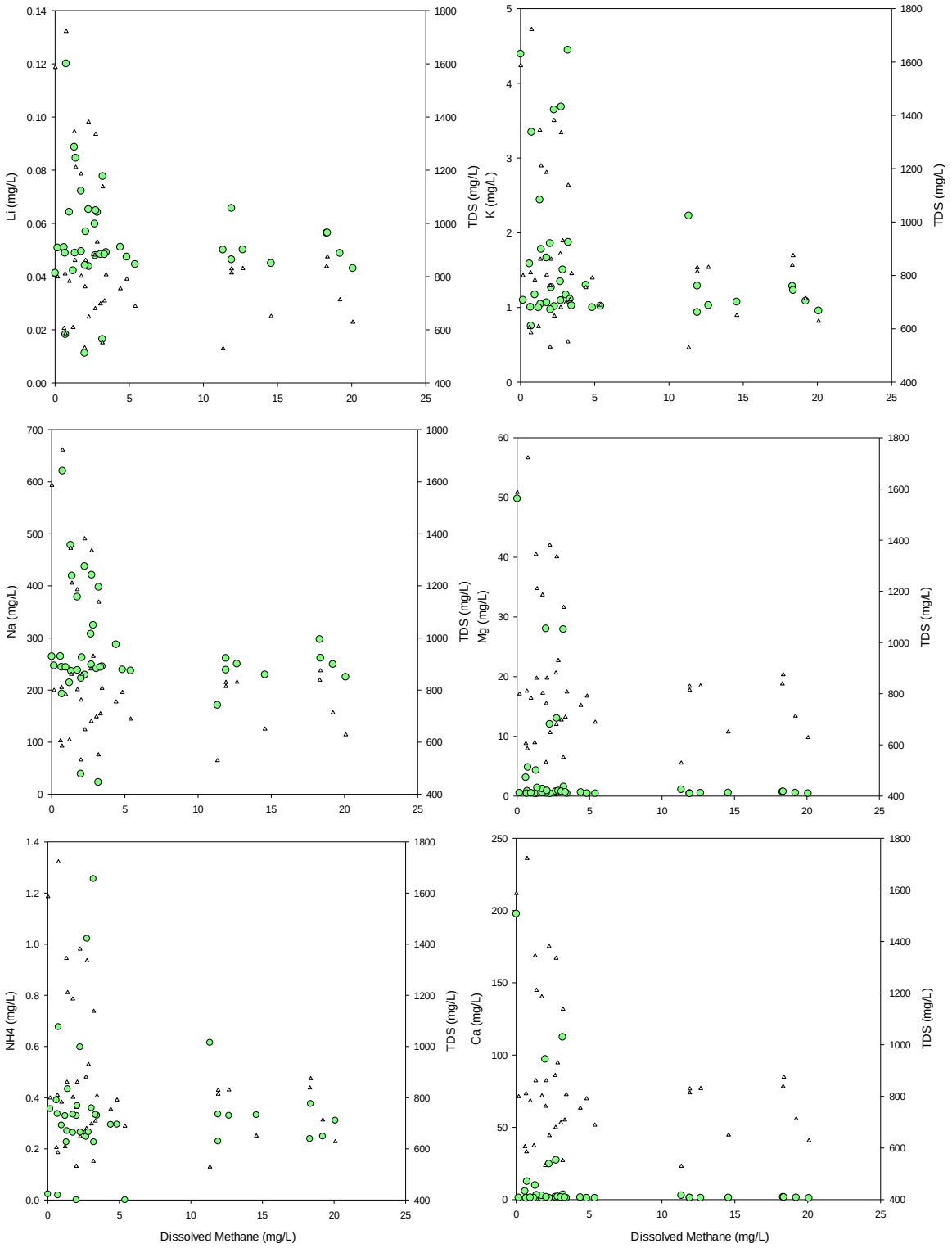

Figure 82. Diss. methane vs. major and trace elements concentrations: Li, K, Na, Mg, NH_4, Ca.

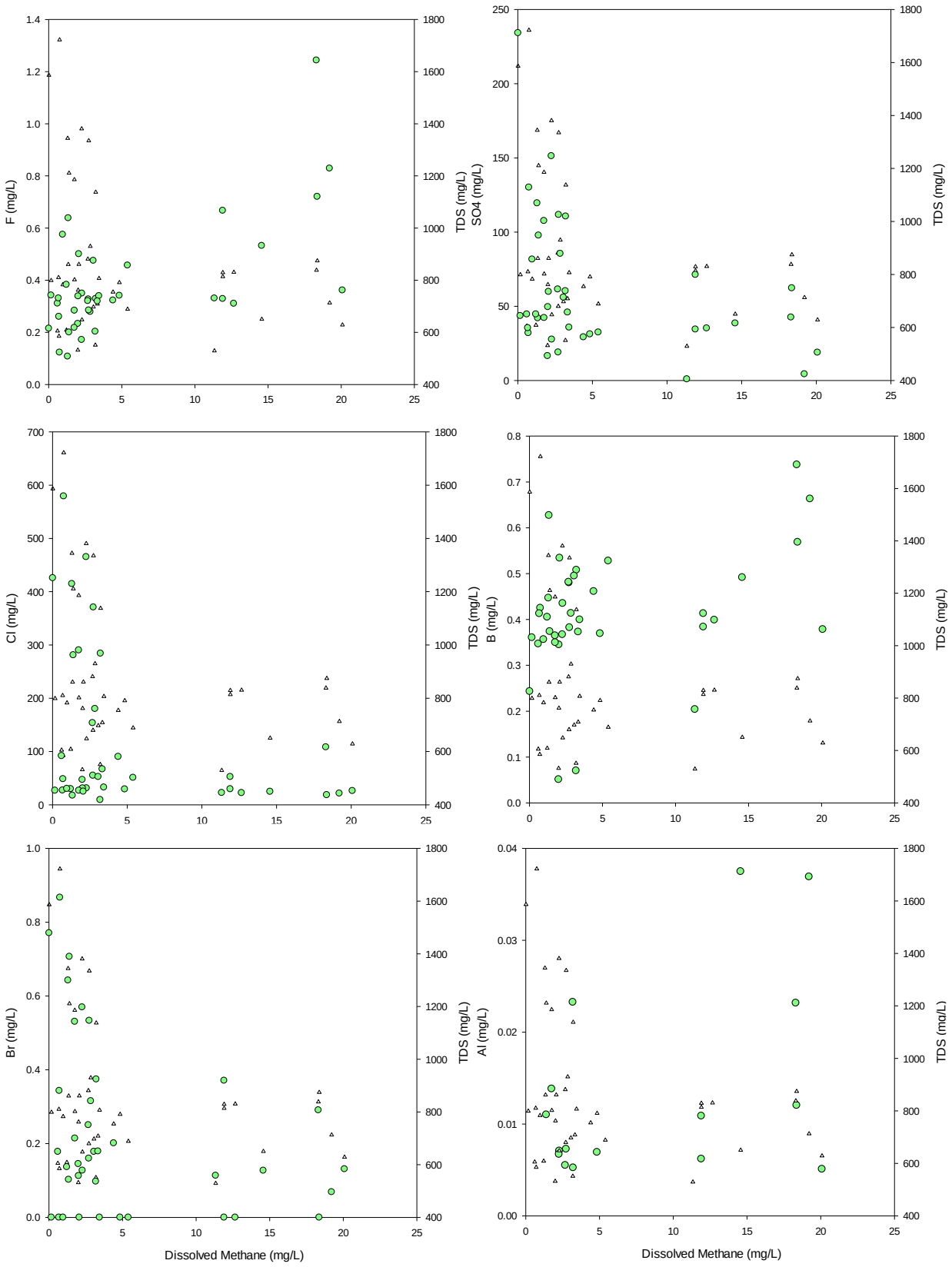

Figure 83. Diss. methane vs. major and trace elements concentrations: F, SO_4, Cl, B, Br, Al.

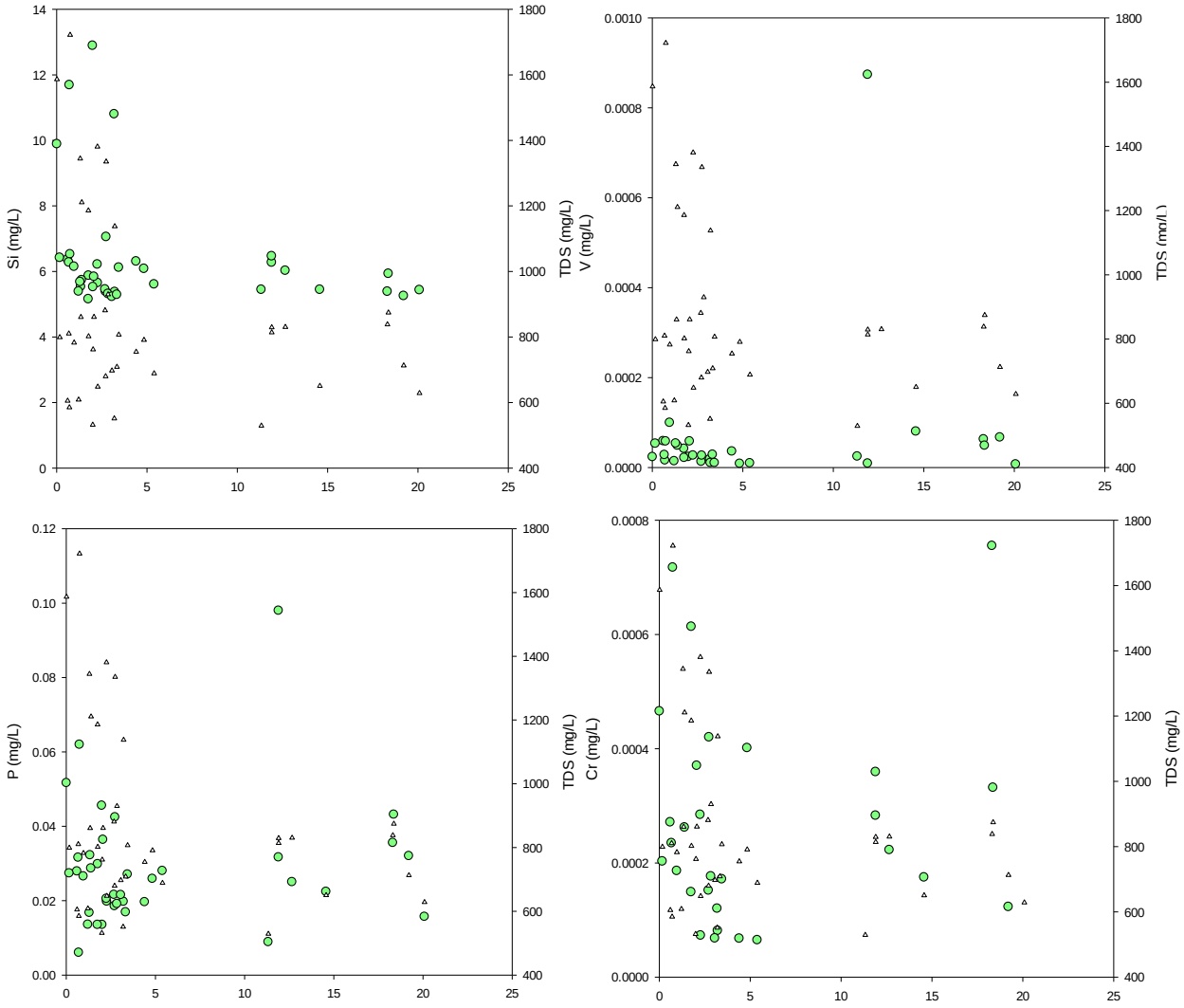
Si (mg/L)
TDS (mg/L)
V (mg/L)
P (mg/L)
TDS (mg/L)
Cr (mg/L)
TDS (mg/L)

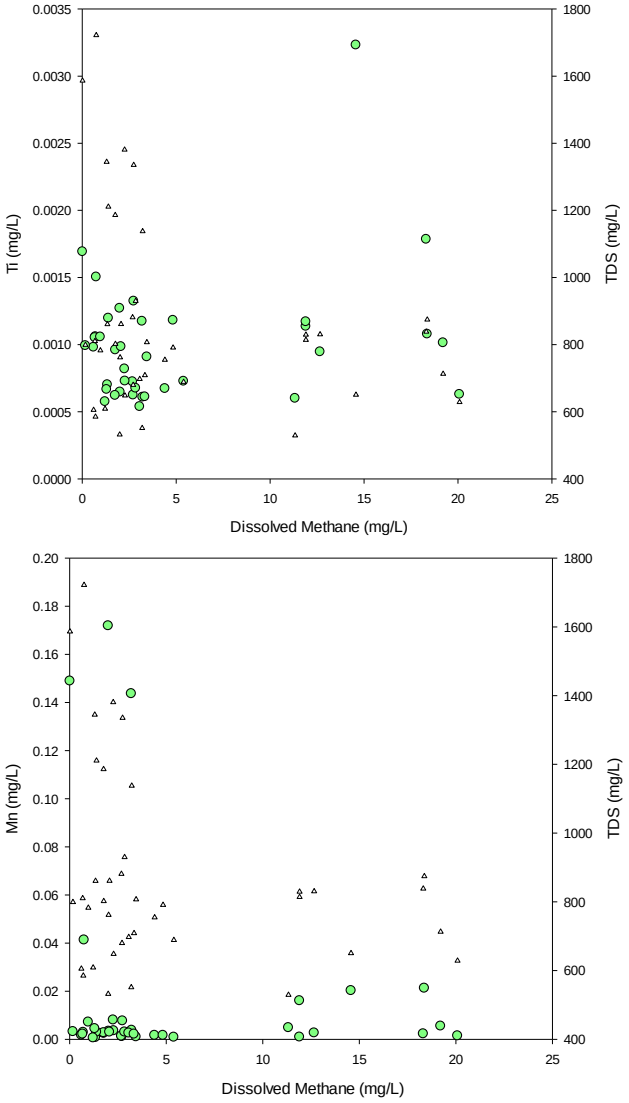

Figure 84. Diss. methane vs. major and trace elements concentrations: Si, V, P, Cr, Ti, Mn.

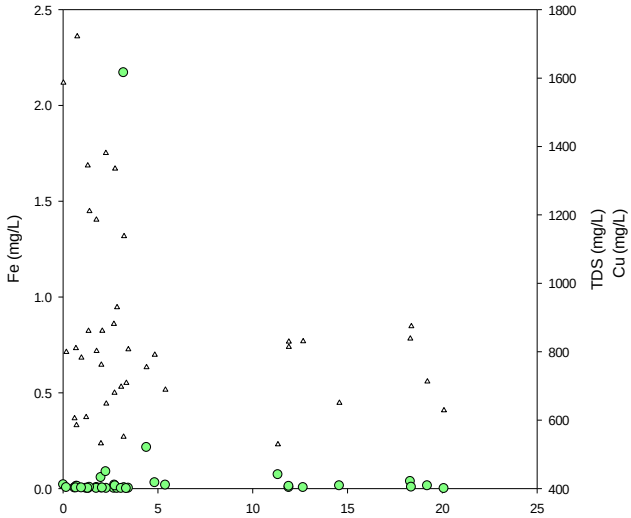
Fe (mg/L)
TDS (mg/L)
2.5
2.0
1.5
1.0
0.5
0.0
1800
1600
1400
1200
1000
800
600
400
0
5
10
15
20
25

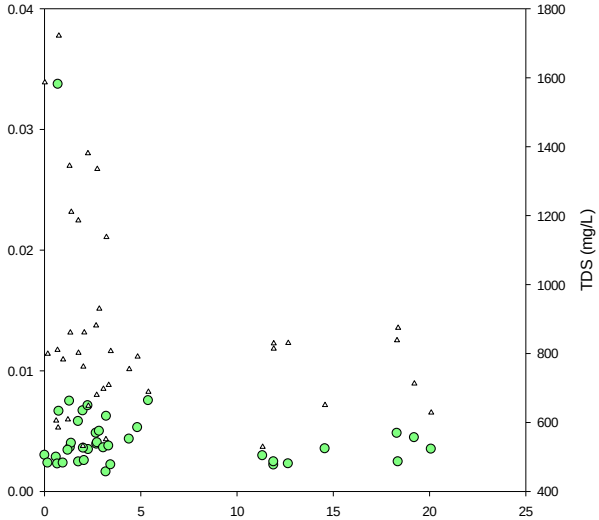
Cu (mg/L)
TDS (mg/L)
0.04
0.03
0.02
0.01
0.00
1800
1600
1400
1200
1000
800
600
400
0
5
10
15
20
25

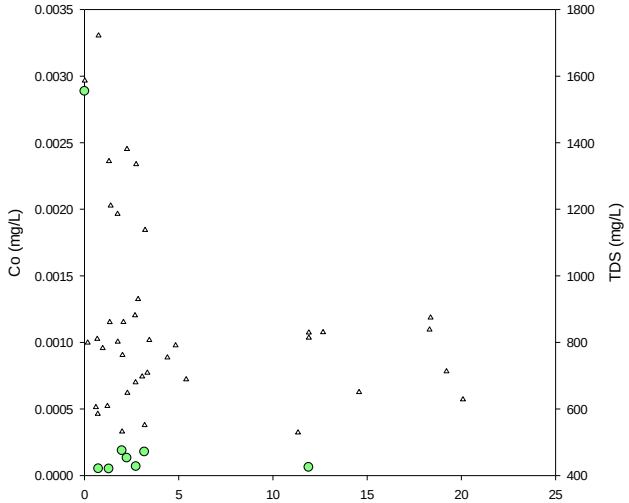
Co (mg/L)
TDS (mg/L)
0.0035
0.0030
0.0025
0.0020
0.0015
0.0010
0.0005
0.0000
1800
1600
1400
1200
1000
800
600
400
0
5
10
15
20
25

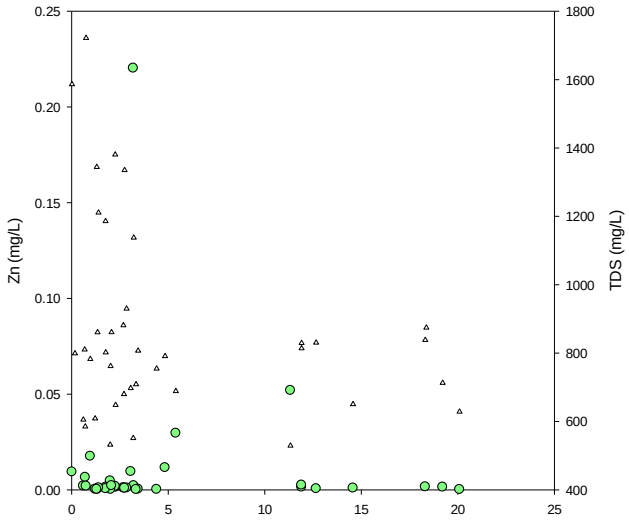
Zn (mg/L)
TDS (mg/L)
0.25
0.20
0.15
0.10
0.05
0.00
1800
1600
1400
1200
1000
800
600
400
0
5
10
15
20
25

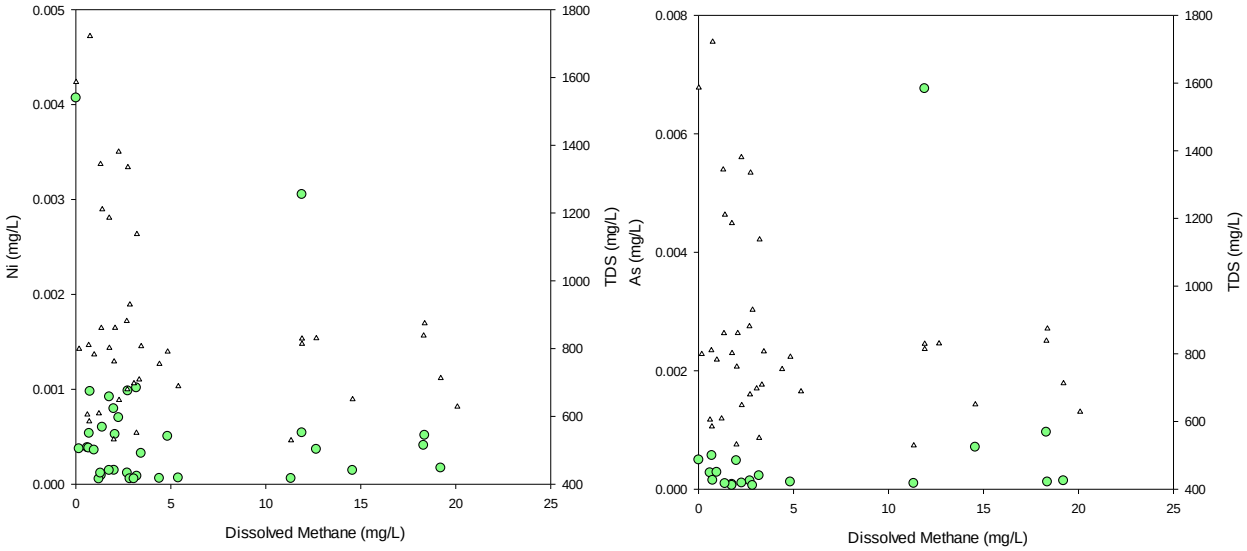

Figure 85. Diss. methane vs. major and trace elements concentrations: Fe, Cu, Co, Zn, Ni, As.

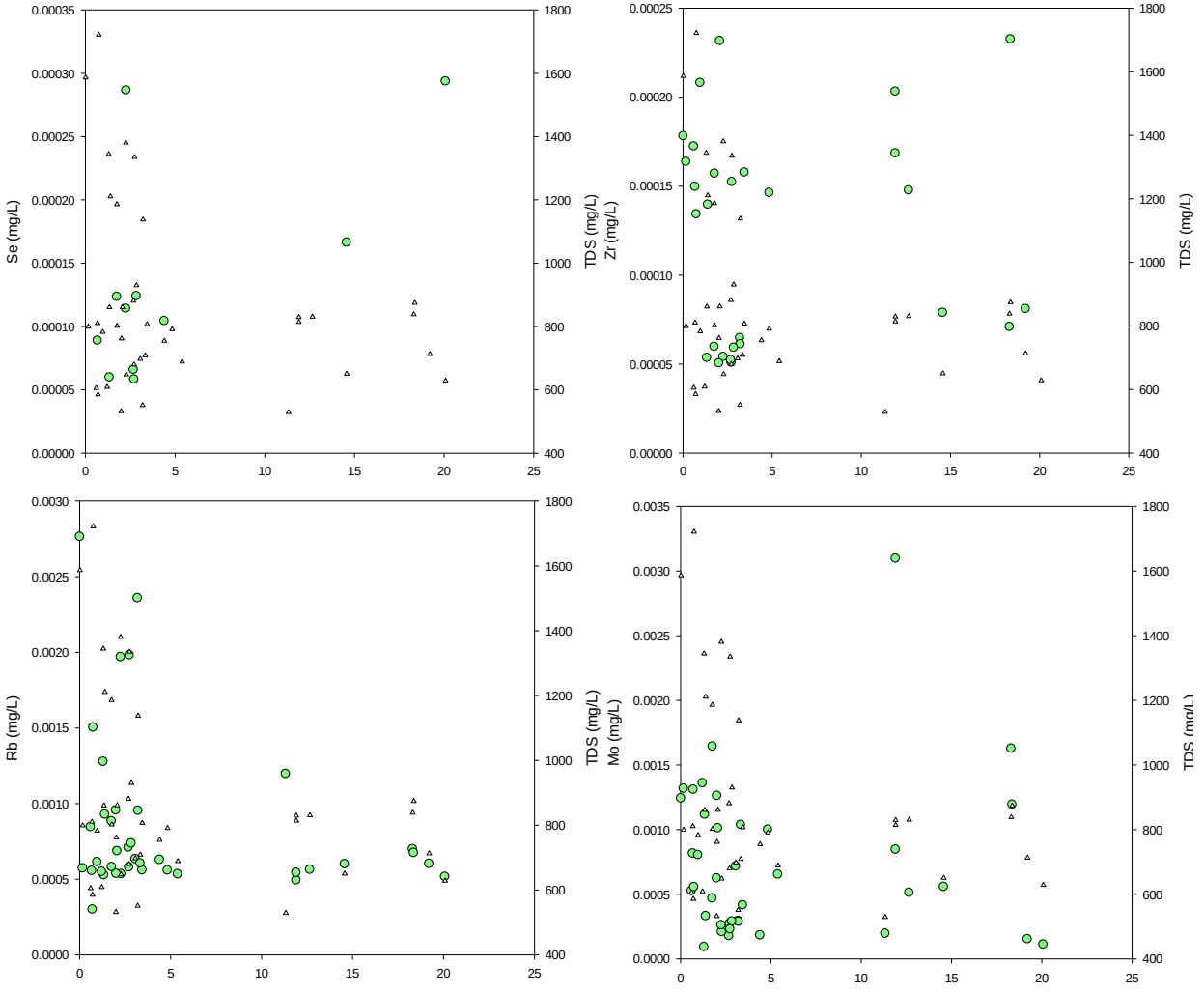

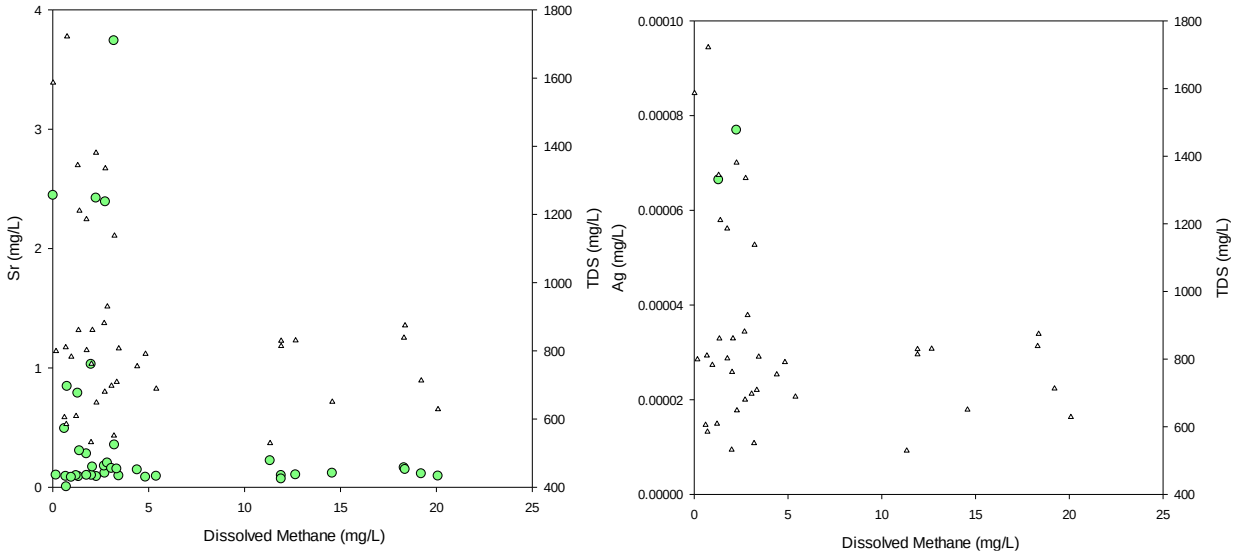

Figure 86. Diss. methane vs. major and trace elements concentrations: Se, Zr, Rb, Mo, Sr, Ag.

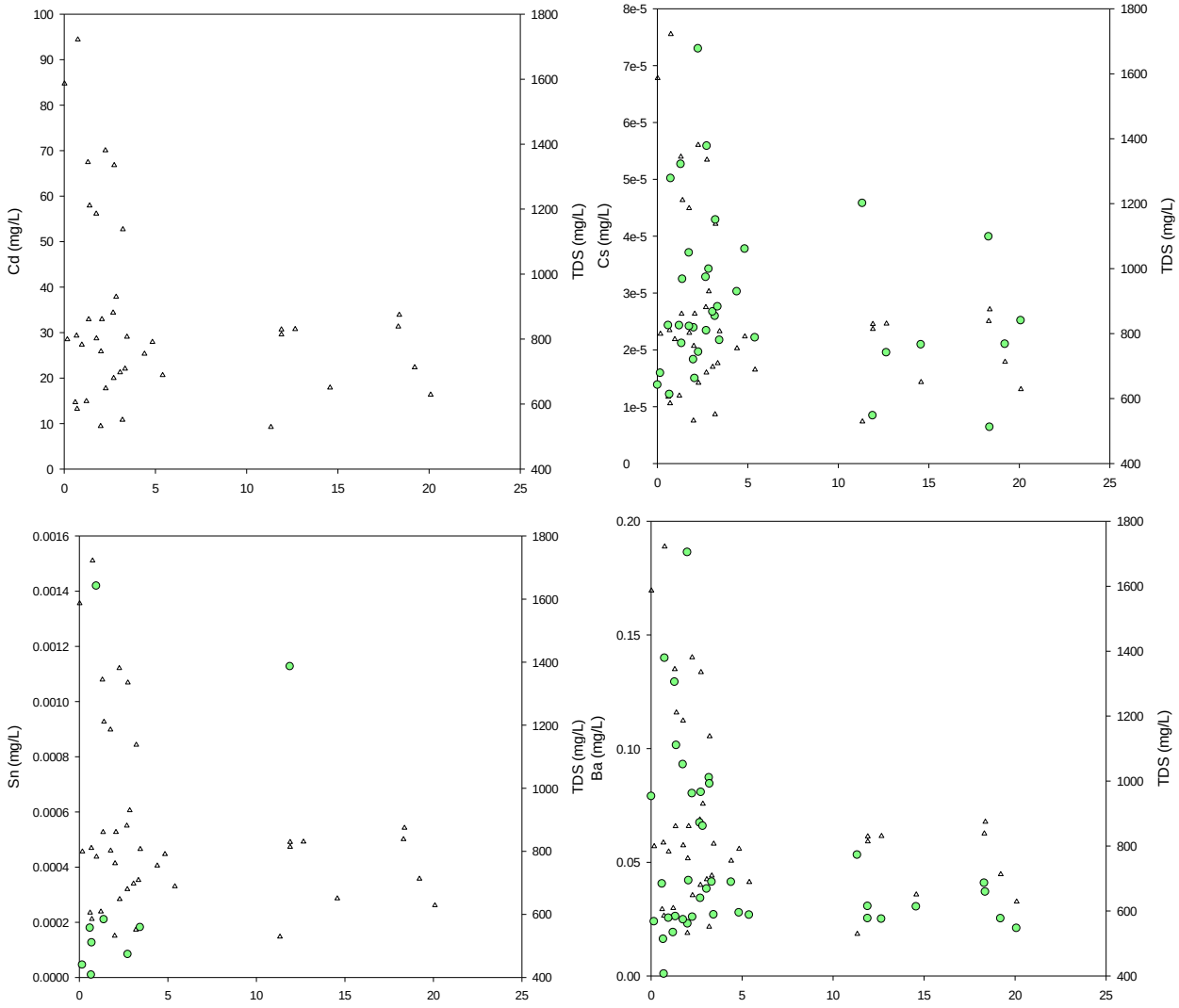

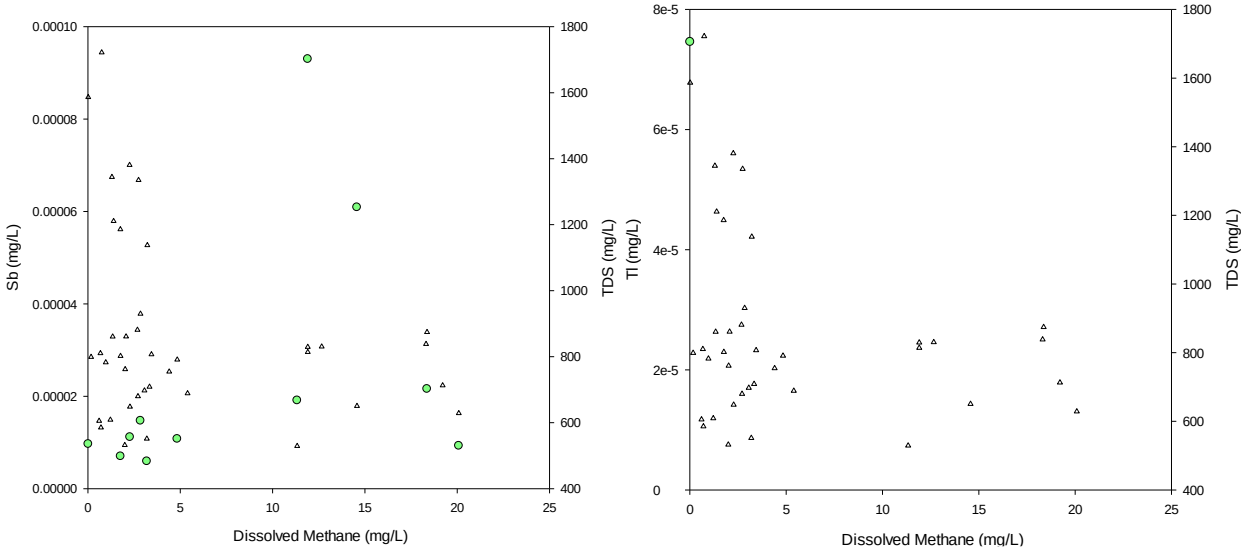

Figure 87. Diss. methane vs. major and trace elements concentrations: Cd, Cs, Sn, Ba, Sb, Tl.

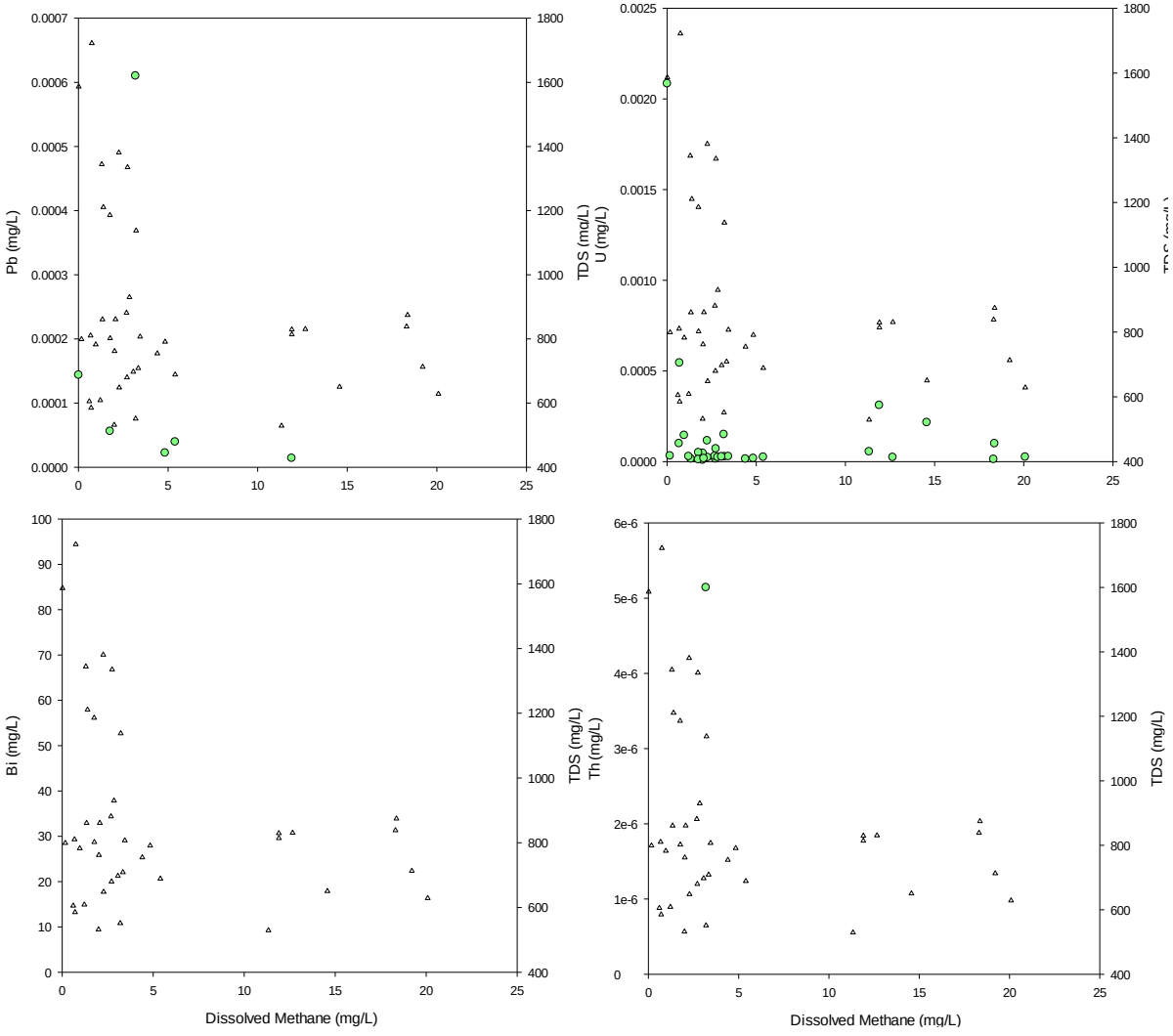

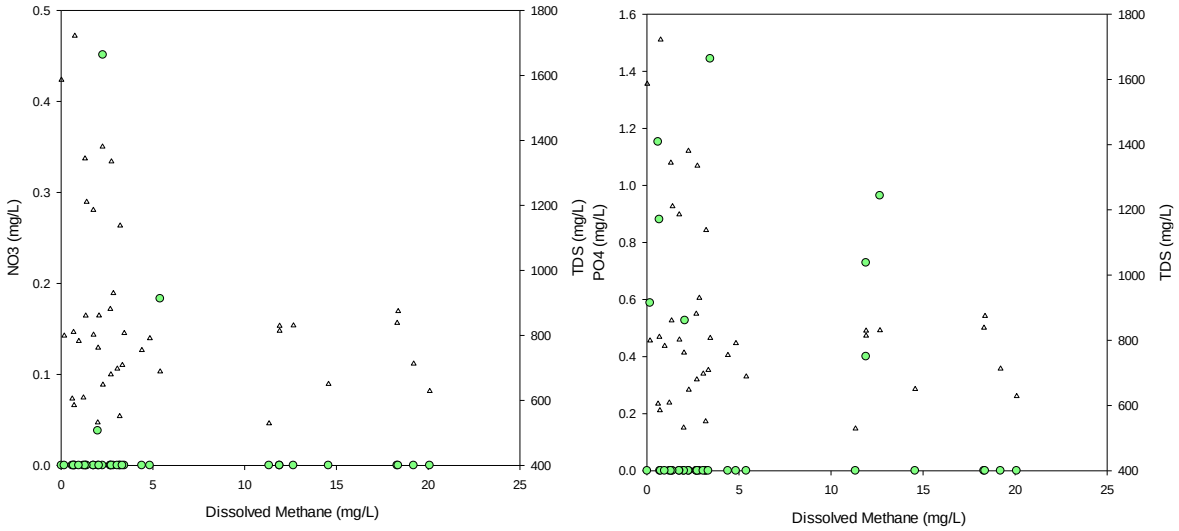

Figure 88. Diss. methane vs. major and trace elements concentrations: Pb, U, Bi, Th, NO_3.

XV. Appendix G: Noble Gases and Stable Isotopes

By M. Clara Castro, Tao Wen and Chris M. Hall, UMI

XV-1. Introduction

Stable noble gases (Helium – He, Neon – Ne, Argon – Ar, Krypton – Kr, Xenon - Xe) are chemically inert and are thus transported without being affected by chemical reactions or microbial activity (Ballentine, 1991; Hilton and Porcelli, 2003a; Ozima and Podosek, 2002). Moreover, noble gases in subsurface fluids (*e.g.*, freshwater, natural gas) are derived from the atmosphere, crust and mantle, all of which show distinct isotopic and elemental signatures (Castro, 2004; Hilton and Porcelli, 2003b; Ozima and Podosek, 2002; Pinti et al., 2012; Porcelli et al., 2002; Saar et al., 2005). Thus, noble gases are ideal natural tracers to study the origin and evolution of crustal fluids in sedimentary basins (Castro et al., 1998a; 1998b; 2009; Hilton and Porcelli, 2003b; Kulongoski et al., 2005; Ma et al., 2009a; 2005; Oxburgh et al., 1986; Pinti and Marty, 1995; Warrier et al., 2013). In most subsurface fluids of sedimentary systems, noble gases are dominated either by an atmospheric origin (Air Saturated Water or ASW), containing Ne, Ar, Kr and Xe in solubility equilibrium with the atmosphere or by crustal components (*e.g.*, ^{4}He*, ^{21}Ne*, ^{40}Ar*, ^{136}Xe* resulting from radioactive decay of U/Th and ^{40}K - Crustal He, Ne, Ar, Kr, and Xe are indicated with the a "*" notation, e.g., crustal ^{4}He is ^{4}He*) (Ozima and Podosek, 2002). Mantle contributions are generally minor but not negligible (Castro et al., 2009; Ma et al., 2005; 2009b; Pinti and Marty, 2000; Wen et al., 2015).

Components of different origin, i.e., atmosphere, crust or mantle, present specific characteristics, which allow identification of their sources and sinks (Castro, 2004; Hilton and Porcelli, 2003b; Saar et al., 2005; Stute et al., 1992). Concentrations of He isotopes (^{3}He, ^{4}He) in groundwater frequently exceed those expected for water in solubility equilibrium with the atmosphere (air-saturated water: ASW). These excess He can result from different sources: 1) an excess air component resulting from dissolution of small air bubbles caused by fluctuations of the groundwater table (Heaton and Vogel, 1981); 2) the β-decay of natural background and bomb tritium (tritiogenic ^{3}He); 3) the ^{6}Li(n, α)^{3}H (^{3}He) reaction (Morrison and Pine, 1955) (i.e., nucleogenic ^{3}He); 4) the α-decay of the natural U and Th decay series elements (i.e., radiogenic ^{4}He), and; 5) mantle contributions to both ^{3}He and ^{4}He (e.g., Castro et al. 2009). Excess He (He_{exc}) is calculated by removing the ASW (He_{eq}) and excess air (He_{ea}) components (Kipfer et al., 2002) from total measured He concentrations (He_{meas}) in groundwater samples (Castro et al., 2000; Stute et al., 1992). He_{eq} and He_{ea} are estimated following Ballentine and Hall (1999) based on measured Ne, Ar, Kr and Xe concentrations. A detailed analysis of both the helium concentrations and the ^{3}He/^{4}He (R) ratios measured in groundwater allows the separation of the different components (Castro, 2004; Stute et al., 1992; Wen et al., 2015).

XV-2. Sampling Techniques and Experimental Methods

Water samples were collected in copper tubes (i.e., standard refrigeration grade 3/8" Cu tubing) from 35 groundwater wells in the study area after temperature, pH, and electrical conductivity reached equilibrium. While the water flushed through the system for approximately 10 min, the absence of gas bubbles that could potentially indicate gas fractionation in the samples was checked through a transparent plastic tube mounted at the end of the Cu tube. The Cu tubes were

then sealed by steel pinch-off clamps (Weiss, 1968). Specific requirements for well sampling were followed. We ensured that sampled groundwater wells were (1) drilled to shallow groundwater aquifers and (2) did not contain any type of filtration device. Homeowners were contacted ahead of time and asked to purge the wells. The entire well volume was purged of its standing water to remove any pockets of air that may have accumulated through time and to obtain water samples that are representative of groundwater. Natural gas samples were also collected in copper tubes at the wellhead of 9 production wells, one from the Strawn Group and all other from the Barnett Shale. Atmospheric contamination during sampling was minimized by allowing the gas to flush through the system for approximately 5 min.

The complete measurement procedure for both water and gas samples carried out in the Noble Gas Laboratory at the University of Michigan comprises estimation of He, Ne, Ar, Kr, and Xe concentrations for groundwater and volume fractions for gas samples in addition to their respective isotopic ratios. Standard errors for concentrations and volume fractions are 1.5, 1.3, 1.3, 1.5 and 2.2%, respectively. Analysis procedures are described below.

Water and gas samples in Cu tubes were attached to a vacuum extraction and purification system. The copper tube is connected to a vacuum system at a pressure of ~2×10^{-5} Torr. Once this pressure is achieved and the system isolated from its turbo-molecular vacuum pump, the lower clamp is opened to release the water/natural gas into a low He diffusion glass flask. Specifically, for water samples we have to extract the dissolved gases from water in two stages: the first uses water vapor as a carrier gas to transport all dissolved gases through a tubing constriction into a liquid N_2 cold trap; the second stage uses water vapor from warming the small quantity of water in the cold trap to transport the dissolved gases into a section of the system with a 3 Å molecular sieve. This part of the system is dried by the water adsorption properties of the molecular sieve and most active gas components are removed by inletting samples to the first getter with Ti sponge at 600°C for ~60 minutes. For natural gas samples, extraction of the dissolved gases is not necessary and thus natural gases can be inlet into the molecular sieve and the first getter for the removal of water and active gases. Gases from the water/natural gas sample are subsequently admitted into a cleanup section of the line equipped with the second getter pump to remove the remaining active gases.

Noble gases are then quantitatively extracted and sequentially allowed to enter the Thermo Scientific® Helix SFT (for He and Ne isotopes) and ARGUS VI (for Ar, Kr and Xe isotopes) mass spectrometers using a computer-controlled cryo-separator. Ar, Kr and Xe are pumped into the high temperature (high-T) chamber of the cryo-separator at a temperature of 104K while He and Ne are pumped into the low temperature (low-T) chamber of cryo-separator at a temperature of ~10 K. The cryo-temperature is subsequently increased sequentially to release He, Ne, Ar, Kr, and Xe, at temperatures of 49 K, 84 K, 210 K, 245K, and 290 K, respectively. Specifically, at the He release temperature, He is introduced into the SFT mass spectrometer and the signal intensity of ^{4}He is determined for the He concentration estimate. This estimate is then used by the automated system to optimize the amount of He that should be introduced for measurement of the ^{3}He/^{4}He ratio.

Complete measurement procedures involve estimating the concentration of each noble gas component, as well measuring the isotopic ratios for He, Ne, Ar, Kr, and Xe. First, a portion of a known volume of air is introduced into the molecular sieve section of the extraction system, and all noble gases are measured in turn with the Helix SFT and ARGUS VI mass spectrometers. This calibrates the mass spectrometer signal size for each noble gas. Subsequent to the air

calibration run, the same measurement procedure is performed on a portion of the unknown sample. All noble gas isotopes are measured using a Faraday detector, except for ^{3}He which is measured using an electron multiplier in ion counting mode.

Water samples were also collected from each of the 35 sampling wells for measurement of δD and $\delta^{18}O$ in the Stable Isotope Laboratory at the University of Michigan following procedures as described below.

For analysis of δD, 1 ml of water per sample or standard is injected into a chromium reactor maintained at 800C via A CTC Analytics PAL autosampler. Samples are allowed to react for two minutes and then equilibrated in the dual inlet for one minute. Samples are run at 8 volts against a reference gas of known composition in a Thermo Finnigan H-Device coupled to the dual inlet of a gas source Thermo Finnigan Delta V Plus mass spectrometer. Samples are run in triplicate to account for memory effects, and are bracketed with suites of standards (VSMOW/VSLAP or USGS 45/46/47, and in-house standards) throughout the run. Samples are normalized relative to the VSMOW/VSLAP scale and expressed relative to VSMOW. Accuracy and precision is better than +/-1 per mil on replicate analyses, and analytical error on standards over time is better than +/-1.3 per mil.

For analysis of $\delta^{18}O$, 0.5 ml of water per sample or standard is injected into a pre-evacuated Labco exetainer and loaded into the Finnigan Gas Bench II sample tray. A CTC Analytics PAL Autosampler flushes the samples with a 0.3% CO_2 in Helium mixture for 8 minutes each, and samples are allowed to equilibrate for two days at 30 °C. Samples are then flushed with pure (UHP grade) helium for 8 minutes. The sample gas is carried via helium flow and cleaned of water via the Gas Bench water traps, and fed through a GC column maintained at 70 °C. The CO_2 is then admitted through a capillary to the inlet of the mass spectrometer where multiple sample peaks are measured against the CO_2 reference gas peaks in a Thermo Finnigan Delta V Plus mass spectrometer. Data are normalized and reported relative to the VSMOW/VSLAP scale, and accuracy and precision are ±0.1‰.

XV-3. Overall Results

Thirty five groundwater samples, two gas samples from groundwater wells and nine shale gas samples, eight from the Barnett Shale Fm. and one from the Strawn Fm. were analyzed for noble gas concentrations and isotopic ratios (He, Ne, Ar, Kr and Xe), Stable isotopes (δD and $\delta^{18}O$) were also analyzed for the thirty five groundwater wells.

XV-3-1 Groundwater Samples

XV-3-1.1 Noble Gas Isotopic Ratios

Overall groundwater samples can be divided into two groups based on their sampling locations: 1) "south cluster" – located close to the boundary of Parker and Hood counties (Parker-Hood cluster); and 2) "north cluster" – located in the northern portion of Parker county (North Parker cluster).

$^{3}He/^{4}He$ (R) ratios in groundwater samples vary from 0.030 ± 0.001 times the atmospheric ratio Ra to 0.882 ± 0.007. Because the atmospheric He contribution is significant in these shallow waters, measured R/Ra ratios represent a mixture of atmospheric, crustal and mantle He components. Typical crustal R/Ra production values are low (0.01 – 0.05; Oxburgh et al., 1986)

due to the dominant ^{4}He production from U and Th decay. Mantle R/Ra ratios are far higher due to the presence of primordial ^{3}He in the mantle, with R/Ra values of ~8 in Mid Ocean Ridges Basalts (MORB) and ~50 in Ocean Island Basalts (OIB) (Graham, 2002; Starkey et al., 2009). Measured R/Ra ratios in our groundwater samples are greater than typical crustal values, and point to the presence of an atmospheric component and, to a lesser extent, of a mantle He component. Since these groundwater samples with high R/Ra values are at shallow depths and have relatively low ^{4}He concentrations close to those of ASW (altitude of 250 m and a temperature of 17.5 °C), atmospheric derived He is the component contributing the most to these higher R/Ra values for some of our samples. Using a mantle R/Ra value of 8 and a crustal production value of 0.05, a He component separation analysis (Castro, 2004; Stute et al., 1992) shows that crustal ^{4}He contributions in these samples vary between 0% and 99.8% of total measured ^{4}He, with a mantle ^{4}He contribution of up to ~2%. No obvious correlation between R/Ra and depth is observed. Simultaneous analysis of R/Ra and methane concentrations in the groundwater samples shows a strong negative correlation. The relationship between He signatures and methane concentrations are discussed further below.

Measured $^{20}Ne/^{22}Ne$ ratios are very close ($\pm 1\sigma$) to the atmospheric value (9.8) for most samples and thus, the presence of mantle Ne in these samples is not suggested. $^{21}Ne/^{22}Ne$ ratios range from 0.0290 ± 0.0002 to 0.030 ± 0.0001 reflecting the addition of minor but non-negligible crustally produced ^{21}Ne through the nuclear reactions $^{18}O(a, n)^{21}Ne$ and $^{24}Mg(n, a)^{21}Ne$ (Wetherill, 1954). Simultaneous analysis of both $^{20}Ne/^{22}Ne$ and $^{21}Ne/^{22}Ne$ ratios allows for the separation of the atmospheric, crustal, and mantle Ne components as the three sources all have distinct end-member values. Analysis of Ne isotopic ratios in these groundwaters indicates an atmospheric ^{21}Ne contribution varying from 97.8% to 100% of total measured ^{21}Ne and a crustal ^{21}Ne contribution varying between 0% and 2.2%. No clear correlation between $^{21}Ne/^{22}Ne$ ratios with depth is observed.

$^{40}Ar/^{36}Ar$ ratios of some groundwater samples are above the atmospheric value of 295.5, reflecting the addition of crustally produced, radiogenic ^{40}Ar. These vary between 294.6 ± 0.1 and 309.7 ± 0.5. However, no obvious correlation is observed between $^{40}Ar/^{36}Ar$ and depth. Similar to ^{4}He, excesses of ^{40}Ar are commonly observed in old crustal fluids due to natural decay of ^{40}K in rock formations (Ballentine et al., 1994; 1991). Unfortunately, the exact crustal and mantle contributions of ^{40}Ar cannot be effectively separated due to current uncertainties of both $^{40}Ar/^{36}Ar$ and $^{38}Ar/^{36}Ar$ end-member values. However, the contribution of crustally produced ^{40}Ar can be estimated by assuming that ^{36}Ar in the groundwater comes mainly from the atmosphere with the atmospheric $^{40}Ar/^{36}Ar$ ratio being 295.5. The contribution of atmospheric derived ^{40}Ar varies from 95.2% to 100%, with crustally produced ^{40}Ar varying between 0% and 4.8%. Similar to ^{4}He, $^{40}Ar/^{36}Ar$ ratios correlate well with methane concentrations (Figure 89) and may indicate the same external noble gas source for both radiogenic ^{4}He and ^{40}Ar.

Kr isotopic ratios (e.g., $^{86}Kr/^{84}Kr$) are all indistinguishable from the atmospheric values. Kr will thus not be the object of further discussion in the present document.

$^{136}Xe/^{130}Xe$ groundwater ratios show values above the atmospheric ratio (2.176), up to 2.206 ± 0.004, and point to the presence of excess ^{136}Xe. Similar to R/Ra, $^{136}Xe/^{130}Xe$ ratios display no correlation with depth. These elevated Xe isotopic ratios suggest the presence of crustal and/or mantle Xe components in these groundwaters in addition to the atmospheric component. Similar to $^{40}Ar/^{36}Ar$, the highest $^{136}Xe/^{130}Xe$ ratios are found at an intermediate depth of ~107 m among all these groundwater samples.

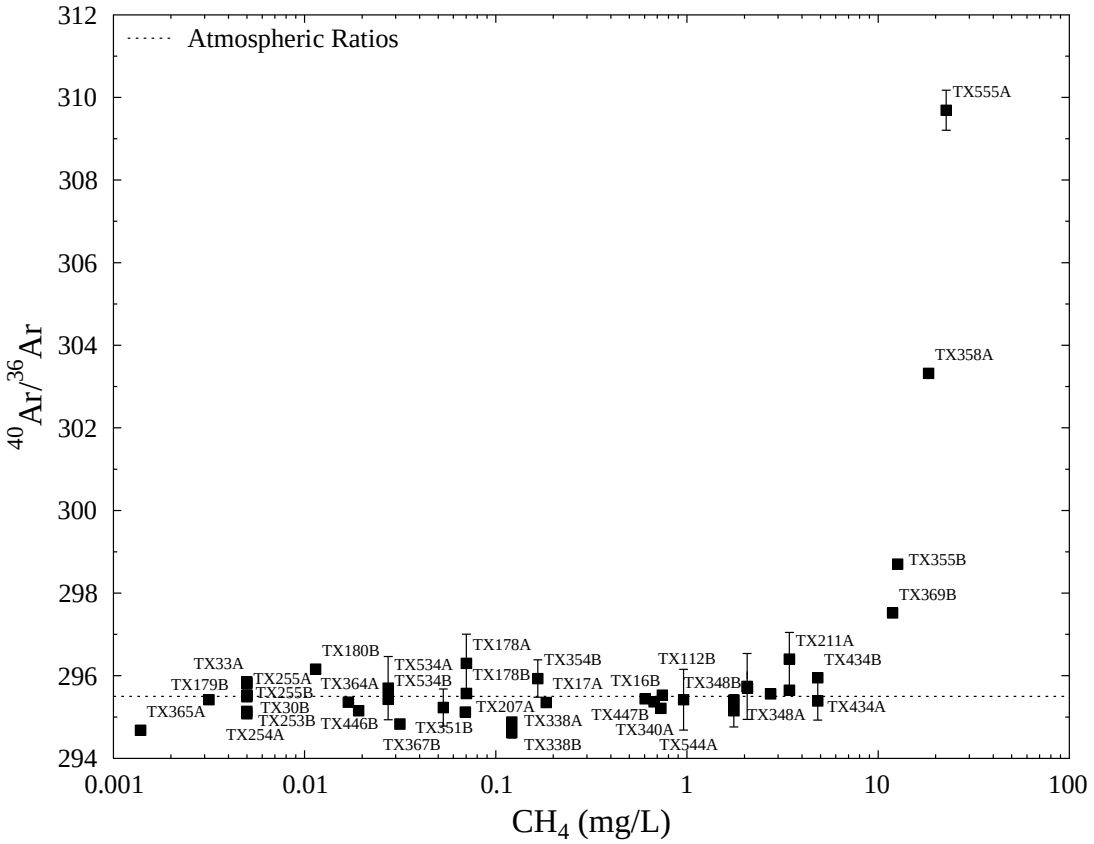

Note: Dashed line represents the corresponding atmospheric $^{40}Ar/^{36}Ar$ value

Figure 89. $^{40}Ar/^{36}Ar$ ratios versus methane concentrations for all groundwater samples.

XV-3-1.2 Separation of Crustal Noble Gas Components

Most groundwater samples in this study display ^{4}He concentrations in excess of ASW values. These He excesses reach values of over three orders of magnitude above that of ASW for ^{4}He, and are particularly high for samples TX544, 358, 555, 369 and 355, located at the proximity of Parker and Hood counties' boundary. Obvious correlations are observed for most samples between He signatures (total He concentrations, excess He - He_{exc}, R/Ra and R_{exc}/Ra) and methane concentrations in groundwater, strongly suggesting that fugitive methane and helium in these groundwaters have a common source (Figure 90). Thus, helium signatures can be used as a tool to fingerprint the source and migration of fugitive methane in groundwater.

R_{exc}/Ra values vary from 0.028 to 0.203 for these groundwater samples (Figure 91), and are far greater for samples from the 'north cluster' as compared to samples from the "south cluster".

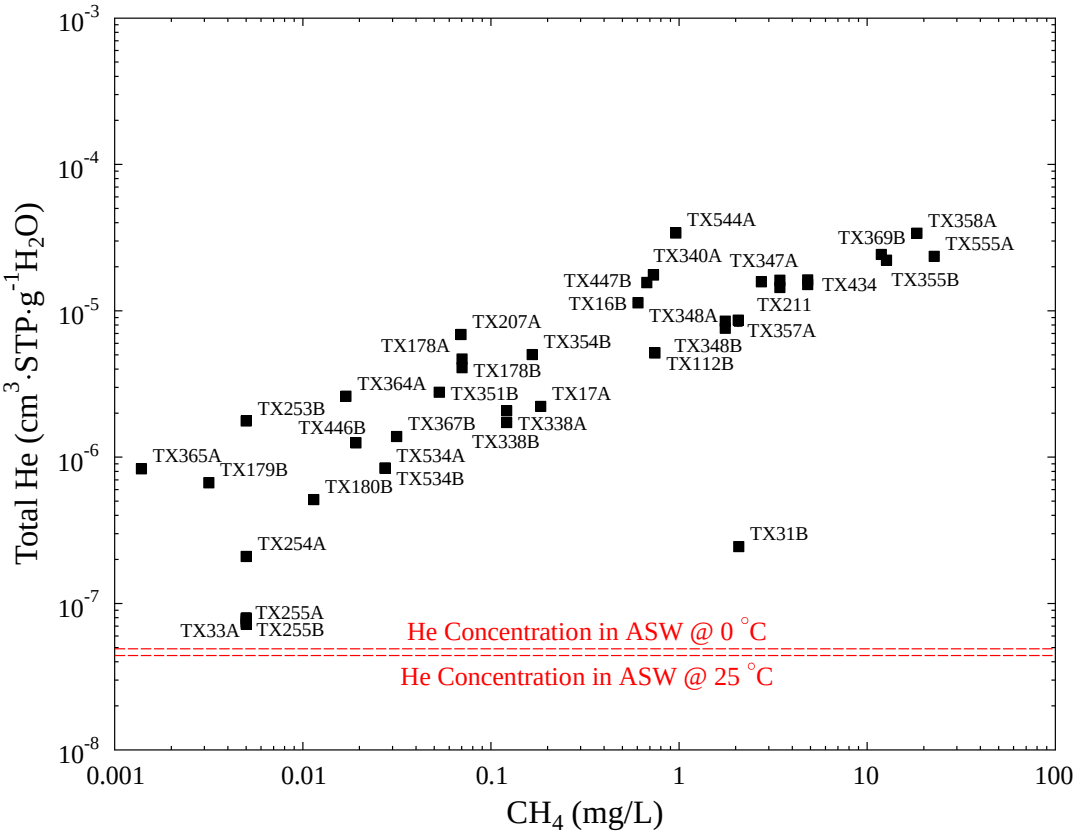

Note: Red dashed lines represent corresponding ASW values at temperatures of 0°C and 25°C, respectively

Figure 90. Total He versus methane concentrations for all groundwater samples.

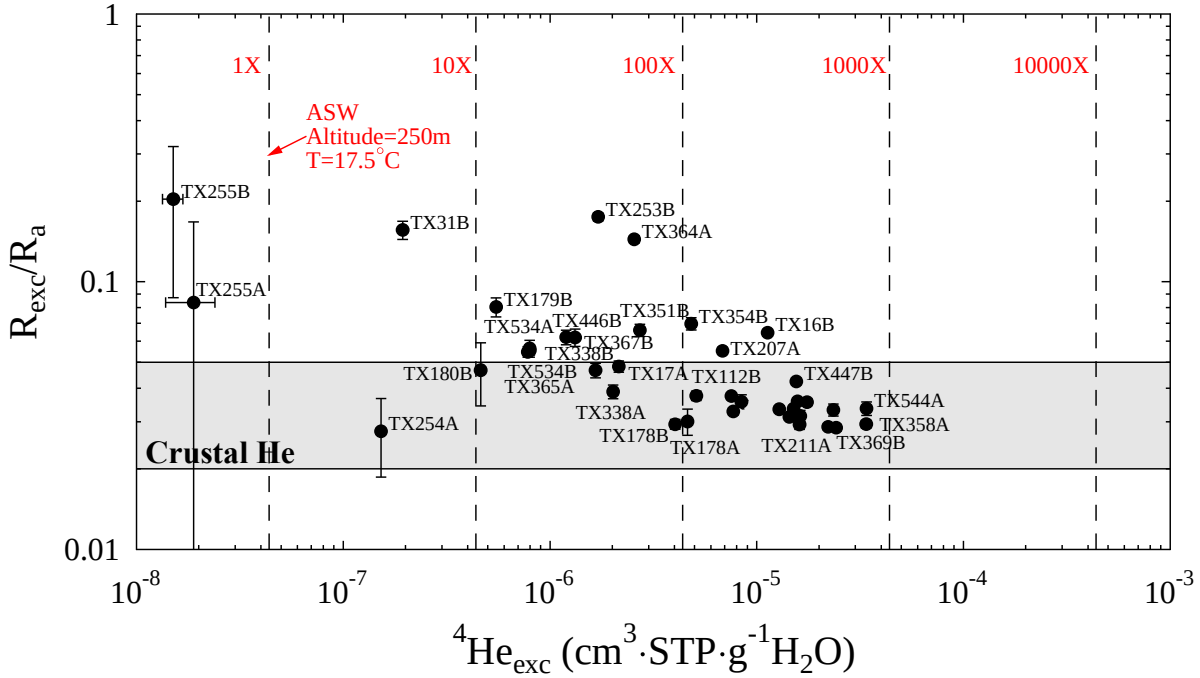

Note: Shaded areas indicate typical crustal R/Ra values

Figure 91. R_{exc}/Ra values versus $^4He_{exc}$ concentrations for all groundwater samples.

Noble gas isotopic concentrations (^{4}He, ^{21}Ne and ^{40}Ar) and their crustally produced components in the groundwater samples are discussed. Crustal He volume fractions ($^{4}He^{*}$) in these groundwaters are estimated by using the He isotopic ratios as discussed above. He is found to be essentially of crustal origin, while Ne and Ar are treated as a two-component mixture, with an atmospheric and a crustal end-member. Crustal ^{21}Ne and ^{40}Ar contributions ($^{21}Ne^{*}$, $^{40}Ar^{*}$) are estimated as follows (Ballentine, 1991):

$$^{21}Ne^{*} = {}^{21}Ne_{measured} \times \left(1 - \left(\frac{^{21}Ne}{^{22}Ne}\right)_{air} \Big/ \left(\frac{^{21}Ne}{^{22}Ne}\right)_{measured}\right) \quad (1)$$

$$^{40}Ar^{*} = {}^{40}Ar_{measured} \times \left(1 - \left(\frac{^{40}Ar}{^{36}Ar}\right)_{air} \Big/ \left(\frac{^{40}Ar}{^{36}Ar}\right)_{measured}\right) \quad (2)$$

where $(^{21}Ne/^{22}Ne)_{air} = 0.029$ and $(^{40}Ar/^{36}Ar)_{air} = 295.5$ (Ozima and Podosek, 2002). Neglecting the presence of a potentially minor mantle Ne and Ar contributions would not affect the discussion and conclusions that follow.

$^{4}He^{*}$ volume fractions vary over three orders of magnitude, from 1.47×10^{-8} to 3.39×10^{-5} cc STP/g_{H2O}. A plot of $^{4}He^{*}$ and depth points to a lack of correlation between crustally produced ^{4}He and depth. Concentrations of both total ^{4}He and $^{4}He^{*}$ are identical with an overall increase from "north cluster" samples towards "south cluster" samples. These identical distribution patterns and volume fractions suggest that crustally produced ^{4}He dominates almost entirely over any other component. Unlike He signatures, atmospheric ^{21}Ne and ^{40}Ar component dominate total ^{21}Ne and ^{40}Ar concentrations.

XV-3-1.3 δD and $\delta^{18}O$ in Groundwater Samples

δD values of all groundwater samples vary from -32.15‰ to -10.39‰, with an average of -26.68‰. $\delta^{18}O$ values correlate well with δD values, varying from -8.60‰ to -1.78‰. δD and $\delta^{18}O$ values are further discussed below.

XV-3-2 Gas Samples from Groundwater Wells, Barnett and Strawn Formations

Natural gas samples were collected from 2 groundwater wells (TX555 and 556) and 9 currently active production wells. These 9 production wells are highly variable with respect to depths, ranging from 544 m to 2929 m, with one production well belonging to the Strawn Group (TXBG3) and eight to the Barnett Shale (TXBG1, 2, 4, 5, 6, 7, 8 and 9)

R/Ra ratios in gas samples vary from 0.021 ± 0.001 to 0.143 ± 0.001. Measured R/Ra ratios represent a mixture of crustal and mantle He components for most gas samples. Highest R/Ra ratios are found in samples TX556GA2 and TX556GA3 with R/Ra values of 0.143 and 0.133, respectively. Excluding these two samples, R/Ra ratios range from 0.021 to 0.042, for all other gas samples including TX556GA1 and TX556GB2, which overlap the typical crustal R/Ra production values are 0.01 – 0.05 (Oxburgh et al., 1986). Highest R/Ra ratios in two TX556 replicates may indicate air contamination while R/Ra ratios (0.021 to 0.042) of all other samples suggest dominant crustally produced He in these gases. The average R/Ra values for the Barnett Shale is 0.032 which is not significantly distinct from the only measured sample value of 0.022 in the Strawn Fm. No obvious correlation is observed between R/Ra and depth for these produced gas samples. Although a detailed He separation component analysis is not applicable to

natural gas samples due to the difficulty in comparing water and gas samples with respect to noble gas volume fractions, crustal He can be estimated if total He in the gas samples is treated as a two-gas component, in this specific case, a mantle and crustal components. Using a mantle R/Ra value of 8 and a crustal production value of 0.02 (Ballentine et al., 1991), crustal ^{4}He contributions in these samples vary between 98.5% and 100% of the total measured ^{4}He, strongly suggesting the dominance of crustally produced He in all natural gas samples.

Measured ^{20}Ne/^{22}Ne ratios for most gas samples are greater than the air value of 9.8, strongly suggesting the presence of mantle Ne. ^{21}Ne/^{22}Ne ratios range from 0.0295 ± 0.0001 to 0.0582 ± 0.0020 reflecting the addition of crustally produced ^{21}Ne through the nuclear reactions of ^{18}O(a, n)^{21}Ne and ^{24}Mg(n, a)^{21}Ne (Wetherill, 1954). Comparing gas samples from the Barnett and Strawn formations, we find that average ^{20}Ne/^{22}Ne and ^{21}Ne/^{22}Ne ratios are 10.18 and 0.0315 for the Barnett Shale, both of which are significantly different from the Strawn Group with 9.59 and 0.0542, respectively. Following equation (1), crustally produced ^{21}Ne is calculated, indicating an atmospheric ^{21}Ne contribution varying from 49.8% to 98.3% of the total measured ^{21}Ne and a crustal ^{21}Ne contribution varying between 1.7% and 50.2%.

^{40}Ar/^{36}Ar ratios of most gas samples are above the atmospheric value of 295.5), reflecting the addition of radiogenic ^{40}Ar, with values between 325.1 ± 0.1 and 803.7 ± 11, the highest value being found in the shallower Strawn Group. ^{40}Ar/^{36}Ar ratios of Barnett Shale gases vary from 287.5 to 695.1, and are significantly lower than that of our Strawn Group sample. Similar to ^{4}He, excesses of ^{40}Ar are commonly observed in old crustal fluids due to natural decay of ^{40}K in the rock formation (Ballentine et al., 1994; 1991). The contribution of crustally produced ^{40}Ar is estimated by assuming that ^{36}Ar in the gas samples derives mainly from the atmosphere and the ^{40}Ar/^{36}Ar ratio in the atmospheric component is 295.5. The contribution of atmospheric derived ^{40}Ar varies between 36.7% and 90.7%, with the crustally produced ^{40}Ar contribution varying from 9.3% to 63.3%.

Kr isotopic ratios (e.g., ^{86}Kr/^{84}Kr) are all indistinguishable from the atmospheric values.

^{136}Xe/^{130}Xe ratios of Texas gas samples show values above the atmospheric ratio (2.176), up to 2.210 ± 0.044, clearly showing the presence of excess ^{136}Xe. Similar with R/Ra, ^{136}Xe/^{130}Xe ratios do not correlate with the depth. ^{136}Xe/^{130}Xe ratios of natural gas samples from the Barnett and Strawn formations are indistinguishable. These elevated Xe isotopic ratios suggest the presence of crustal and/or mantle Xe components in these gas samples, in addition to the atmospheric component.

XV-4. References (NOT in main reference list)

Ballentine, C.J., 1991. He, Ne, and Ar Isotopes as Tracers in Crustal Fluids. Cambridge University Press.

Ballentine, C.J., Hall, C.M., 1999. Determining paleotemperature and other variables by using an error-weighted, nonlinear inversion of noble gas concentrations in water. Geochimica et Cosmochimica Acta 63, 2315–2336. doi:10.1016/S0016-7037(99)00131-3

Ballentine, C.J., Mazurek, M., Gautschi, A., 1994. Thermal constraints on crustal rare gas release and migration: Evidence from Alpine fluid inclusions. Geochimica et Cosmochimica Acta 58, 4333–4348.

Ballentine, C.J., O'nions, R.K., Oxburgh, E.R., Horvath, F., Deak, J., 1991. Rare gas constraints on hydrocarbon accumulation, crustal degassing and groundwater flow in the Pannonian Basin. Earth and Planetary Science Letters 105, 229–246. doi:10.1016/0012-821X(91)90133-3

Castro, M.C., 2004. Helium sources in passive margin aquifers—new evidence for a significant mantle 3 He source in aquifers with unexpectedly low in situ 3 He/ 4 He production. Earth and Planetary Science Letters 222, 897–913.

Castro, M.C., Goblet, P., Ledoux, E., Violette, S., de Marsily, G., 1998a. Noble gases as natural tracers of water circulation in the Paris Basin: 2. Calibration of a groundwater flow model using noble gas isotope data. Water Resources Research 34, 2467–2483.

Castro, M.C., Jambon, A., de Marsily, G., Schlosser, P., 1998b. Noble gases as natural tracers of water circulation in the Paris Basin: 1. Measurements and discussion of their origin and mechanisms of vertical transport in the basin. Water Resources Research 34, 2443–2466.

Castro, M.C., Ma, L., Hall, C.M., 2009. A primordial, solar He–Ne signature in crustal fluids of a stable continental region. Earth and Planetary Science Letters 279, 174–184.

Castro, M.C., Stute, M., Schlosser, P., 2000. Comparison of 4He ages and 14C ages in simple aquifer systems: implications for groundwater flow and chronologies. Applied Geochemistry 15, 1137–1167.

Graham, D.W., 2002. Noble Gas Isotope Geochemistry of Mid-Ocean Ridge and Ocean Island Basalts: Characterization of Mantle Source Reservoirs. Reviews in Mineralogy and Geochemistry 47, 247–317. doi:10.2138/rmg.2002.47.8

Heaton, T.H.E., Vogel, J.C., 1981. "Excess air" in groundwater. Journal of Hydrology 50, 201–216. doi:10.1016/0022-1694(81)90070-6

Hilton, D.R., Porcelli, D., 2003a. 2.06 - Noble Gases as Mantle Tracers, in: Turekian, H.D.H.K. (Ed.), Treatise on Geochemistry, Treatise on Geochemistry. Pergamon, Oxford, pp. 277–318. doi:10.1016/B0-08-043751-6/02007-7

Hilton, D.R., Porcelli, D., 2003b. Noble gases as mantle tracers, in the Mantle and Core, in: Holland, H.D., Turekian, K.K. (Eds.), *Treatise on Geochemistry*. Elsevier, New York.

Kipfer, R., Aeschbach-Hertig, W., Peeters, F., Stute, M., 2002. Noble Gases in Lakes and Ground Waters. Reviews in Mineralogy and Geochemistry 47, 615–700.

Kulongoski, J.T., Hilton, D.R., Izbicki, J.A., 2005. Source and movement of helium in the eastern Morongo groundwater Basin: The influence of regional tectonics on crustal and mantle helium fluxes. Geochimica et Cosmochimica Acta 69, 3857–3872. doi:10.1016/j.gca.2005.03.001

Ma, L., Castro, M.C., Hall, C.M., 2009a. Atmospheric noble gas signatures in deep Michigan Basin brines as indicators of a past thermal event. Earth and Planetary Science Letters 277, 137–147.

Ma, L., Castro, M.C., Hall, C.M., 2009b. Crustal noble gases in deep brines as natural tracers of vertical transport processes in the Michigan Basin. Geochemistry Geophysics Geosystems 10, Q06001.

Ma, L., Castro, M.C., Hall, C.M., Walter, L.M., 2005. Cross-formational flow and salinity sources inferred from a combined study of helium concentrations, isotopic ratios, and major elements in the Marshall aquifer, southern Michigan. Geochemistry Geophysics Geosystems 6, Q10004.

Morrison, P., Pine, J., 1955. Radiogenic origin of the helium isotopes in rock. Ann NY Acad Sci 62, 71–92. doi:10.1111/j.1749-6632.1955.tb35366.x

Oxburgh, E.R., O'nions, R.K., Hill, R.I., 1986. Helium isotopes in sedimentary basins. Nature 324, 632–635. doi:10.1038/324632a0

Ozima, M., Podosek, F.A., 2002. Noble Gas Geochemistry. Cambridge University Press, New York.

Pinti, D.L., Castro, M.C., Shouakar-Stash, O., Tremblay, A., Garduño, V.H., Hall, C.M., Hélie, J.F., Ghaleb, B., 2012. Evolution of the geothermal fluids at Los Azufres, Mexico, as traced by noble gas isotopes, δ18O, δD, δ13C and 87Sr/86Sr. Journal of Volcanology and Geothermal Research 249, 1–11.

Pinti, D.L., Marty, B., 2000. Chapter 7. Noble gases in oil and gas fields: origins and processes, in: Fluids and Basin Evolution. Mineral Soc Can Short Course, pp. 160–196.

Pinti, D.L., Marty, B., 1995. Noble gases in crude oils from the Paris Basin, France: Implications for the origin of fluids and constraints on oil-water-gas interactions. Geochimica et Cosmochimica Acta 59, 3389–3404. doi:10.1016/0016-7037(95)00213-J

Porcelli, D., Ballentine, C.J., Wieler, R., 2002. An Overview of Noble Gas Geochemistry and Cosmochemistry. Reviews in Mineralogy and Geochemistry 47, 1–19. doi:10.2138/rmg.2002.47.1

Saar, M.O., Castro, M.C., Hall, C.M., Manga, M., Rose, T.P., 2005. Quantifying magmatic, crustal, and atmospheric helium contributions to volcanic aquifers using all stable noble gases: Implications for magmatism and groundwater flow. Geochemistry Geophysics Geosystems 6, Q03008. doi:10.1029/2004GC000828

Starkey, N.A., Stuart, F.M., Ellam, R.M., Fitton, J.G., Basu, S., Larsen, L.M., 2009. Helium isotopes in early Iceland plume picrites: Constraints on the composition of high 3He/4He mantle. Earth and Planetary Science Letters 277, 91–100.

Stute, M., Sonntag, C., Deak, J., Schlosser, P., 1992. Helium in deep circulating groundwater in the Great Hungarian Plain: Flow dynamics and crustal and mantle helium fluxes. Geochimica et Cosmochimica Acta 56, 2051–2067. doi:10.1016/0016-7037(92)90329-H

Warrier, R.B., Castro, M.C., Hall, C.M., Lohmann, K.C., 2013. Large atmospheric noble gas excesses in a shallow aquifer in the Michigan Basin as indicators of a past mantle thermal event. Earth and Planetary Science Letters 375, 372–382. doi:10.1016/j.epsl.2013.06.001

Weiss, R.F., 1968. Piggyback sampler for dissolved gas studies on sealed water samples. Deep Sea Research and Oceanographic Abstracts 15, 695–699.

Wen, T., Castro, M.C., Hall, C.M., Pinti, D.L., Lohmann, K.C., 2015. Constraining groundwater flow in the glacial drift and saginaw aquifers in the Michigan Basin through helium concentrations and isotopic ratios. Geofluids n/a–n/a. doi:10.1111/gfl.12133

Wetherill, G., 1954. Variations in the Isotopic Abundances of Neon and Argon Extracted from Radioactive Minerals. Physical Review 96, 679–683. doi:10.1103/PhysRev.96.679

XVI. Appendix H: Hydrogeology over Oilfield Operations in Loving County, Texas

By Rebecca Smyth

XVI-1. Introduction

There is controversy over whether fracking to produce oil and gas impacts overlying groundwater resources. The study area for the Permian Basin portion of the RPSEA Stray Gas study, Loving County (Co.), lies within the central Delaware basin of southeastern New Mexico and far west Texas. Here BEG researchers had the opportunity to sample groundwater from wells being used to support oilfield operations, plus limited domestic and public water supply wells. In Figure 92, Loving Co. is located near the center of the Bone Spring play within the Delaware Basin just below the Texas-New Mexico border.

Below we briefly present the history of oil and gas activity in the study area followed by discussion of regional geologic setting and analytical results of BEG groundwater sampling from March 2014 through January 2015. BEG-sampled water wells are completed in multiple shallow (< 1,000 ft depth) aquifers that overlie historical oilfields (Delaware play) and areas currently under development for oil shale fracking (Bone Spring and Wolfcamp plays). It is fortuitous that the timing of our groundwater sampling nearly corresponded with the beginning of fracking activity, providing what may be considered "background" water quality data for the region.

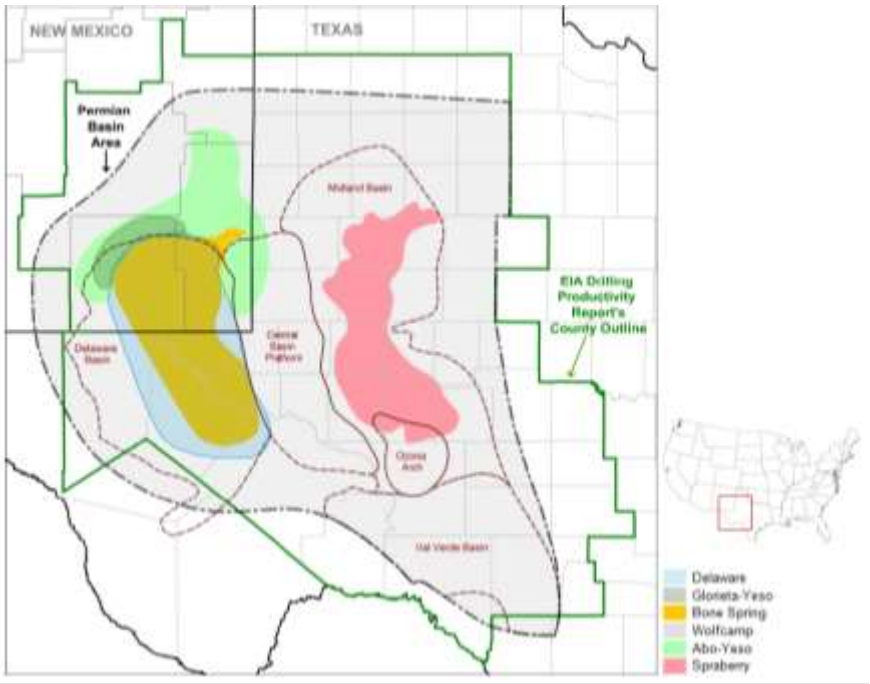

Note: Locations of Permian Basin and subsidiary structural components, selected oil-producing formations, and boundary of EIA information included in next section. Source: http://www.eia.gov/todayinenergy/detail.cfm?id=17031.

Figure 92. Map of Elements of Permian Basin

XVI-1-1 Oil and Gas Activity in Loving County, Texas

Conventional oil production (i.e., primary recovery, secondary water flooding, and tertiary carbon dioxide enhanced oil recovery) from the Delaware sandstone has been ongoing in Loving County, Texas since the mid-1920s (e.g., Reiter, 1952; Galloway et al. 1983). However unconventional recovery of oil from Bone Spring and Wolfcamp shale plays[1] only became active in this area between 2011 and 2013. Figure 93 and Figure 94 show locations of recently spudded wells near Mentone, Texas, which is the county seat of Loving County (and only town in the county), and a plot of oil production in barrels per year (bbl/yr) for the same areas between 1994 and 2015.

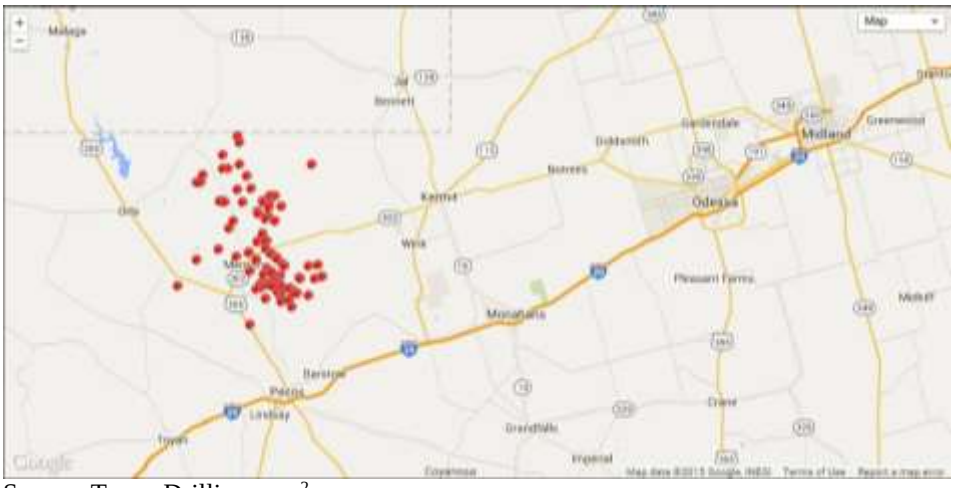

Source: Texas-Drilling.com[2]

Figure 93. Most recently spudded wells near Mentone, Texas

Oil production in the Permian Basin of Texas and New Mexico increased by 60% from 2007 through 2014 from production in six low-permeability geologic formations, three of which: Wolfcamp, Bone Spring, and Delaware, underlie our Delaware Basin study area (EIA, 2014). The production methodology is hydraulic fracturing via horizontal wells. In March 2013 the volume of oil produced from the Permian Basin exceeded that from federal offshore Gulf of Mexico (EIA, 2014).

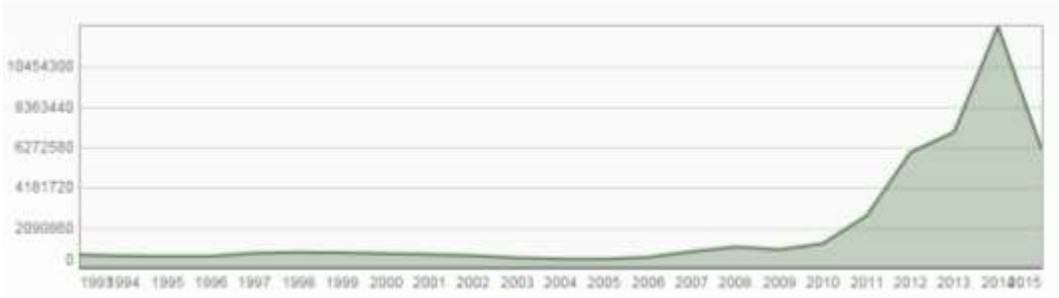

Source: Texas-Drilling.com[3]

Figure 94. Oil production in bbl/yr near Mentone, Texas from 1993 to 2015.

[1]Map showing extent of Avalon-Bone Spring and Wolfcamp plays in TX-NM http://www.ogfj.com/content/dam/ogfj/shale-maps/2014-shale-maps/OGJPermianBasinMap201410-20-14.pdf

[2]Mentone area maps and production plot: http://www.texas-drilling.com/loving-county/mentone

[3]Ibid.

XVI-1-2 Blowouts

The Railroad Commission of Texas maintains a database of blowouts and well control issues by year[4]. Figure 95 shows locations of blowouts that have occurred in the region through 2015. The database contains incidents for Loving County through 2007. Through personal communication with Judge Jones of Loving County (February 2014) we know there was a blowout on the Wheat Ranch ~1 mi south of Mentone on August 11, 2008. This incident caused the casing to part at a depth of ~700 ft. Hydrocarbon gas migrated to a water well just east of the Loving County courthouse, and caused an ~100 ft high gas-charged geyser, which ignited from static electricity. Water quality studies were undertaken and the well was subsequently capped. BEG sampling of other nearby water wells, results of which are presented below, show persistence of hydrocarbon gas-charged groundwater in the vicinity of the courthouse. Some other local blowouts have been documented in the news[5]

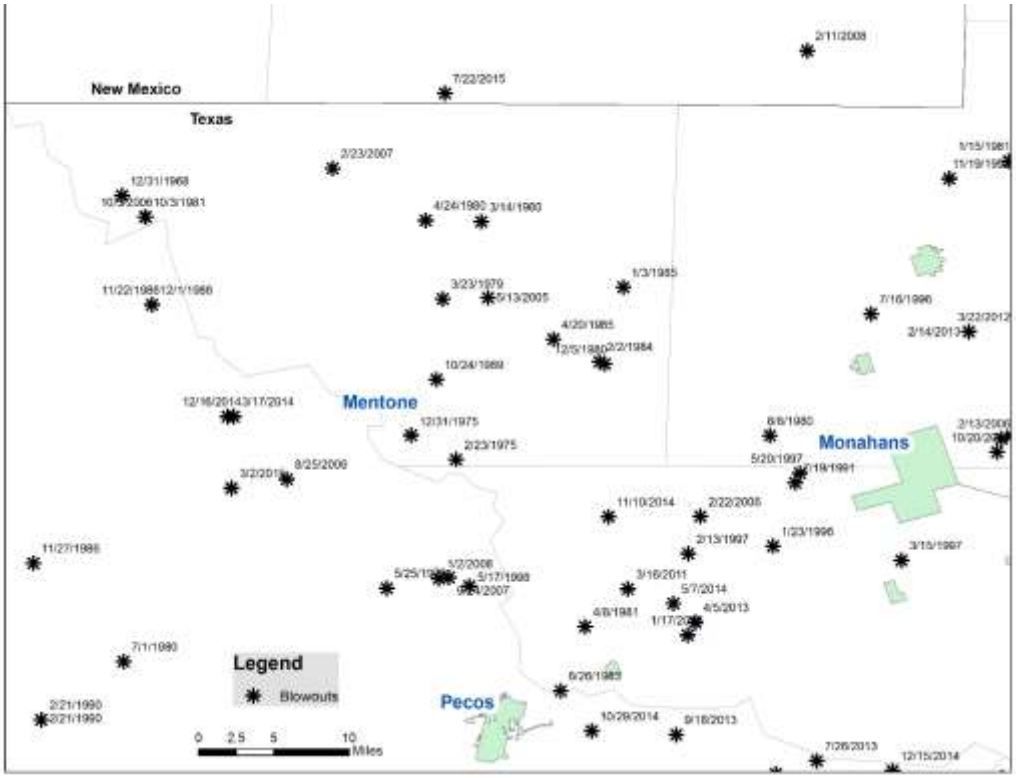

Source: RRC database

Figure 95. Regional oil and gas wells with blowouts or other well-control issues.

XVI-1-3 Frack water supply

Slightly to moderately saline water (i.e., 1,000 to 3,000 mg/L total dissolved solids [TDS] and (3,000 to 10,000 mg/L TDS, respectively[6]) is pumped from ~500-800 ft deep industrial water

[4] http://www.rrc.state.tx.us/oil-gas/compliance-enforcement/blowouts-and-well-control-problems/

[5] News articles on blowouts near Mentone: http://www.latimes.com/nation/nationnow/la-na-nn-oil-well-explosion-texas-20140430-story.html; http://www.oaoa.com/news/business/article_993139be-aee5-11e3-b1b7-0017a43b2370.html

[6] http://water.usgs.gov/edu/saline.html

supply wells for oilfield fracking operations in Loving County, TX. The wells are completed in at least three laterally discontinuous water-bearing zones within up to five geologic rock units. Hydrogeology of the area is discussed further below.

Loving County lies within an arid region where only 12-inces per year of precipitation was measured between 1961 and 1990 (Anaya and Jones, 2009). Despite average annual evaporation of 80 to 82-inches, which was documented for lakes in the region between 1950 and 1979 (Anaya and Jones, 2009), frack supply water is stored in above ground, plastic-lined impoundments, which are locally referred to as frack tanks. Figure 96 shows a typical Loving County oilfield operations area with a frack tank in the left foreground. Figure 106 is a close up photo of a frack tank in north western Loving County showing steel water distribution lines with oilfield operations in the distance.

XVI-2. Geologic Setting

XVI-2-1 Basin History

The Delaware Basin is a long-lived structural basin that originated in the Proterozoic (i.e. Precambrian time) when this region was on the southwestern edge of the North American continent (Muehlberger, 1980; Hills, 1984). With the exception of late Paleozoic deformation along older Precambrian faults, this basin has been tectonically stable throughout its ~1 billion year history (e.g., Hills, 1970, 1984; Keller et al., 1980) The Paleozoic deformation resulted in (1) uplift of the Central Basin Platform, (2) associated division of the Permian Basin into multiple sub-basins, of which the Delaware Basin is one (Figure 92), and (3) slight eastward tilting Delaware Basin strata.

The Delaware basin contains up to 24,000 ft of sediments deposited during the Phanerozoic (i.e., Paleozoic, Mesozoic, and Cenozoic time) (Hentz et al., 1989). During earlier stages of Delaware Basin history it was rimmed by broad limestone shelves (e.g., Hentz et al., 1989). In places the carbonate platforms developed into significant reefs; for example, formations in the Guadalupe Mountains ~50 mi west of the Loving-Reeves county border. Intermittent influx of terrigenous sediment into the basin resulted in thick sequences of interlayered sand and shale with occasional carbonate gravity flow deposits in deeper parts of the basin while reefs were building along the margins (Playton and Kerans, 2002; Playton, 2008; Stolz, 2014). During later stages of basin history sea level apparently dropped and several thousand feet of evaporite minerals (i.e., halite and anhydrite that later converted to gypsum) were deposited. (Galloway et al., 1983). Variations in thickness and continuity of intra-basin sedimentary units resulted from (1) thinning of layers being deposited along the basin margins, (2) faulting associated with late Paleozoic tectonism (e.g., Hills, 1984), and (3) post-depositional dissolution of evaporite layers causing collapse of overlying strata (Bachman, 1984; Hentz et al., 1989).

Note: Looking NE from mile marker 15 on County Road 300, north of Mentone, Texas in February 2014. Frack tank with plastic-lined berms is on left. Pump jack is ~10 ft tall; flare is ~25 ft tall; drilling rig ~100 ft tall.

Figure 96. Illustrative photo of oil activity in Loving County (1/2)

Note. Frack tank on left with distribution/feeder lines, and oilfield activity in background; taken near intersection of CR 300 and State Hwy 652 in Loving Co., February, 2014.

Figure 97. Illustrative photo of oil activity in Loving County (2/2)

The entire Permian Basin, including the Delaware Basin hosts abundant hydrocarbon-bearing intervals. Hills (1984) surmised that ocean circulation must have been fairly restricted throughout Paleozoic time as evidenced by the thick accumulations of organic-rich shales. Hills (1984) further states that there were four periods of hydrocarbon generation in the Delaware Basin. Hydrocarbons generated during early to middle Paleozoic were structurally trapped as gas accumulations. The latest Permian age period of hydrocarbon generation resulted in stratigraphically trapped "light sweet oils"; most of which probably migrated to the carbonate shelves around the perimeter of the Delaware Basin (Hills, 1984).

In Late Permian to Early Triassic time, deposition in the Delaware Basin transitioned from marine tidal flat or hypersaline arid environments to more humid fluvial, deltaic, and lacustrine environments (McGowan et al., 1979; Schiel, 1994). There is disagreement over whether deposition was continuous across this transition from Permian to Triassic time. Regardless, thick accumulations of red beds overlie late Permian evaporite deposits throughout the Permian Basin of Texas and New Mexico. There is no record of Jurassic deposition in the Delaware Basin, and only thin layers of Cretaceous marine carbonates are preserved. This is a result of extensive erosion during the Laramide Orogeny near the end of Mesozoic time.

XVI-2-2 Oil-bearing horizons

Local stratigraphy is described in Figure 98 and the oil-bearing horizons from the deepest to shallowest are:

Wolfcamp –conventional and recent fracking

Bone Spring – conventional and recent fracking

Delaware Mountain group – older conventional hydrocarbon recovery

Wolfcamp

Lower Permian-age Wolfcamp deposits in the Delaware Basin consist of organic rich shale and interbedded carbonate detritus. The shales serve as both hydrocarbon seals and source rock; trapping is stratigraphic (Dutton et al., 2004). Deeper completions of horizontal wells for fracking operations in Loving County are tapping Wolfcamp strata.

Bone Spring

Hydrocarbons in the Leonardian age (Lower Permian) Bone Spring Fm. of the Delaware Basin have been produced from multiple sand and carbonate units (Figure 98) using conventional recovery methods (Dutton et al., 2004). More recently the Avalon Shale interval within the first carbonate unit of the Bone Spring has yielded oil using unconventional recovery methods (Loving County land owner, 2014 personal communication). Stolz (2014) notes that some operators call Avalon Shale the Leonard Shale, and that the names refer to different sub-horizons within the Bone Spring Fm. depending on location within the Delaware Basin. The highest potential for unconventional oil recovery is in the mudstone versus carbonate intervals (Stolz, 2014).

Delaware Mountain Group

Significant amounts of oil have been produced by conventional methods from at least 78 sandstone reservoirs of the Upper Permian age Delaware Mountain Group (DMG) in northern

and eastern portions of the Delaware Basin. All three formations within the DMG have been productive, but the highest yield has been from the uppermost Bell Canyon Fm. (Figure 98) (Dutton et al., 2004). Good description of Delaware Sandstone and distribution and geological setting of oilfields in Loving County is available in Galloway et al. (1983, p.131).

XVI-2-3 Miscellaneous oilfield information

The following information is from an example location in northwestern Loving county of a well being drilled for oil-shale fracking during a BEG sampling reconnaissance visit:

- Hit pressurized water at ~150-200 ft; had to mud up to continue drilling
- Surface casing - ~800 ft depth
- Shallow gas shows at multiple depths – industry mud log shows minor hydrocarbon gas at 440 and 800 ft depths, then significant gas at ~4,400 ft near base of salt
- Vertical drill - down to ~8,000 ft then curved to target horizontal completion at ~9,000 ft in Leonardian-age strata.

The BEG maintains a database of geophysical logs from oil and gas wells drilled in the state of Texas. Many of the older logs cover the shallow subsurface interval and provide information valuable to hydrogeological studies such as this. Table 9 contains a summary of log header information from four wells completed in the El Mar field in north central Loving County. Completion depths are between 4,500 and 4,700 ft below surface, which roughly corresponds to the Bell Canyon Fm. (Figure 98). Note that depths of surface casing installed to protect groundwater resources range between ~550 and 820 ft, which means they extend down into Dewey Lake or Rustler Fms.

Table 9. Summary of header information on selected oil and gas well geophysical logs in Loving County

API #	Date drilled	TD (ft bKB)	Surf Csg base (ft bKB)	Logged interval (ft bKB)	Sands on gamma log (ft bKB)	BH temp (^{o}F)	Surf elev (ft)	KB (ft agl)
42-301-30849	8/23/1989	4,540	549	40 - 4537	40 - 70, 390 - 650	101	3,052	?
42-301-31073	6/4/1997	4,706	778	100 - 4701	500 - 750	111	3,049	14.5
42-301-31074	6/21/1997	4,710	775	100 - 4701	430 - 690	113	3,052	15
42-301-31075	6/12/1997	4,710	822	90 - 4701	90 - 100, 510 - 770	113	3,050	14.5

Era	System	Series	Group	Stratigraphic Unit	Lithology	Approximate Base (ft bgl)
Cenzoic	Quaternary			Pecos Alluvium	Unconsolidated to partially consolidated sand, silt, gravel, clay, and caliche	100 - 400
	Tertiary					
Mesozoic	Cretaceous	Gulf		Undifferentiated	Limestone interbedded with shale	not present in Loving Co.
		Comanche		Undifferentiated	Limestone with interbedded marl, shale, and sandstone	
			Fredericksburg	Undifferentiated		
			Trinity	Undifferentiated		
	Triassic		Dockum	Undifferentiated	Reddish-brown and gray sandstone & cong. w/intbed red and green shale and siltstone; calcite and silica cement	500 (eastern side of county only)
Paleozoic	Permian	Ochoan		Dewey Lake	Red siltstone and shale with gypsum and calcite cement	500
				Rustler Formation	Dolomite, anhydrite, sandstone, conglomerate, and shale w/ halite and ls.	800 - 1,000 (central and western side of county only)
				Salado Formation	Mostly halite, with anhydrite and some dolomite	
				Castile Formation	Mostly calcareous anhydrite, with halite and associated salts and some limestone.	~4,400
		Guadalupian	Delaware Mtn	Bell Canyon	Porous limestone and dolomite, bedded limestone, and reef talus.	~7,500
				Cherry Canyon		
				Brushy Canyon		
		Leonardian		Bone Spring Formation	1st Carbonate/Avalon Shale	~9,500
					1st Sandstone	
					2nd Carbonate	
					2nd Sandstone	
					3rd Carbonate	
					3rd Sandstone	
					Lower Carbonate	
		Wolfcampian		Wolfcamp		~12,000?

Note: the table shows geologic units from which oil and gas (Permian-age Wolfcamp, Bone Spring and Bell Canyon Fms.) and frack supply water (Permian-age Rustler and Dewey Lake Fms.; Triassic-age Dockum Group; and Quaternary-age Pecos Valley Alluvium) are produced. The approximate depths of units defined in the far right column are based on BEG interpretation of multiple sources of information in the vicinity of the study area.

Figure 98. Stratigraphy in Delaware Basin

XVI-2-4 Evaporite and frack water supply horizons

Geologic units of interest in this study that overlie the oil-producing zones are from oldest to youngest the (1) Late Permian-age Castile, Salado and Rustler Fms., (2) Late Permian to early Triassic Dewey Lake Redbeds, (3) Triassic-age Dockum Group, and (4) Quaternary Pecos Alluvium.

Castile and Salado formations

Because of the similarity of these two halite-, anhydrite-, and gypsum-bearing evaporite rock units, they are commonly not distinguished in subsurface mapping using geophysical logs. In outcrop and cores, the underlying Castile Fm. (Figure 98) is distinguished by fine laminated interbeds of anhydrite/gypsum, halite, and limestone (Hentz et al., 1989). According to Armstrong and McMillan (1961), the Salado Fm. contains more halite than anhydrite, especially in more northern regions of the Delaware Basin. Together these two units comprise thousands of feet of low-permeability strata from ~1,000 to 4,000 ft depth, below frack water supply and above oil-bearing zones in Loving County. In the Rustler Springs area of Culberson and Reeves counties, just west of Loving County, significant but discontinuous biogenic sulfur deposits occur within these evaporite formations, and to a lesser degree, the underlying Rustler Fm.

Rustler Formation

The late Permian aged Rustler Fm. unconformably overlies the Salado Fm. (Figure 98). It is primarily composed of dolomite and anhydrite with minor amounts of salt and limestone, and conglomerate, sand, and shale near the base (Armstrong and McMillan, 1961). The Rustler is the youngest unit with bedded evaporites in the Delaware Basin (Hentz et al., 1989). It is the oldest and most prolific geologic unit from which water for fracking operations is obtained in Loving County. The Rustler Fm. occurs throughout the Delaware Basin and crops out within 10 to 25 miles west of Loving County in an area called the Rustler Hills. Here Hentz et al. (1989) subdivided the Rustler into multiple distinct units as part of their characterization of the origin of sulfur mineralization.

Dewey Lake Redbeds

Schiel (1994) describes the age, depositional environment, and paleogeographic history of the Dewey Lake Fm. (also called Dewey Lake Redbeds) completed earlier during her thesis research. The rocks are mostly reddish brown, finely laminated siltstone to silty claystone with some unfossiliferous, medium to fine-grained sandstone. Gray reduction spots on Dewey Lake rocks are thought to result from contact with hydrogen sulfide gas (Hentz et al., 1989). Lateral thickness variations indicate that the Delaware Basin was still subsiding during Dewey Lake deposition. The thickness of this unit may reach up to 100 ft, but it is difficult to distinguish from the overlying Dockum Group rocks (Armstrong and McMillan, 1961; Schiel, 1994).

Dockum Group

Dockum Group rocks vary in lithology, but are all terrigineous clastics deposited in fluvial-deltaic or lacustrine environments across west Texas, eastern New Mexico, and southeastern Colorado during Triassic time (McGowan et al., 1979). Dockum Group rocks are most commonly red in color, but occasional bluish colored shales indicating deposition under reducing conditions in deep lacustrine settings (Armstrong and McMillan, 1961). Deposition of Dockum Group rocks was restricted to the eastern half of Loving County where the environment is

thought to have yielded more coarsely grained channel fill sediments than are found in deeper portions of the "Dockum Basin" (McGowan et al., 1979). Dockum Group rocks are present at the surface in eastern Loving County as indicated by reddish coloring of soils.

Pecos Alluvium

Deposition of the Pecos River alluvium occurred during Quaternary time in topographic troughs that are thought to have resulted from dissolution of evaporite layers (Castile and Salado Fms.) and subsequent collapse of overlying Triassic, Cretaceous, and Tertiary age rocks (Malley and Huffington, 1953; Armstrong and McMillan, 1961). The Pecos alluvium is the youngest water-bearing unit utilized for frack water supply in Loving County; it is only present on the western side of the county coincident with the westernmost trough. The character of the sediment is very fine-grained, gypsum-rich windblown sand, which locals refer to as "sugar sand". The Pecos alluvium extends to depths of 100 to 400 ft below our study area in Loving County (Figure 98).

XVI-3. Regional hydrogeology

The Texas Water Development Board (TWDB) is a state agency responsible for management of groundwater resources. In fulfilling these responsibilities, the TWDB defines major and minor aquifers of the State[7], conducts sampling and maintains an online database of water levels and water quality in statewide wells[8], and conducts or supports groundwater availability modeling[9]. Below we discuss the two minor and one major aquifers that occur within our Delaware Basin study area, useful information from the TWDB online database, and BEG groundwater sampling activity.

XVI-3-1 Properties of aquifers in Loving County

Boundaries of aquifers usually do not coincide with the full extent of the geologic units for which they are named. This is because by definition the term aquifer usually implies minimum water quality conditions. For example, even though the Rustler Fm. exists below all of Loving Co., the down dip edge of the aquifer, which is defined by the 5,000 mg/L TDS contour (Boghici and Van Broekhoven, 2001), nearly bisects the county a northwest-southeast oriented curve. The Dockum aquifer only underlies the eastern half of Loving Co (Figure 99).

Rustler aquifer

The Rustler aquifer is one of the six TWDB minor aquifers in far west Texas (Figure 99). It is recharged by infiltration of precipitation on the outcrop to the west in Culberson Co., infiltration of irrigation water, primarily in Pecos Co, and cross-formational flow from deeper aquifers. There is no primary flow direction because of diverse recharge, and compartmentalization from faulting and cavernous porosity of the dolomite, anhydrite/gypsum, and vuggy limestone aquifer matrix (Armstrong and McMillan, 1961; Boghici and Van Broekhoven, 2001; Ewing et al., 2012).

Yield of wells completed in the Rustler varies greatly due to the type of porosity; however, acidizing has been used since the mid-1950s to enhance groundwater recovery. TDS of Rustler groundwater is generally around 3, 000 mg/L, so it is often mixed with lower TDS water from

[7] http://www.twdb.texas.gov/groundwater/aquifer/
[8] Add groundwater data page
[9] http://www.twdb.texas.gov/groundwater/models/gam/

the overlying Pecos alluvial aquifer before being used for irrigation (Armstrong and McMillan, 1961; Boghici and Van Broekhoven, 2001). More detailed information on the Rustler aquifer can be found in the TWDB GAM (Ewing et al., 2012).

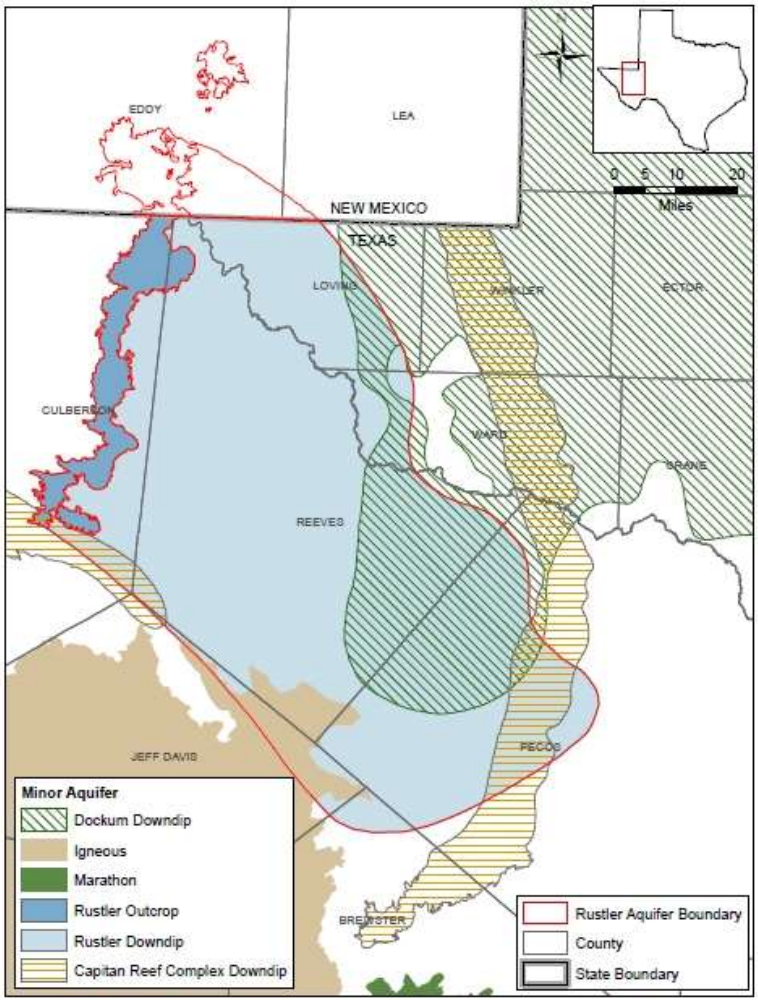

Source: Ewing et al., 2012, fig.2.0.6.
Note: the Rustler aquifer underlies western two thirds and Dockum aquifer underlies eastern portions of Loving County. These aquifers both underlie the Pecos Valley aquifer shown in Figure 100.

Figure 99. TWDB-defined minor aquifers in general region of BEG study area

Dockum aquifer

The Dockum is another one of the TWDB minor aquifers of west Texas, but it is more widespread than the Rustler, extending northward through the Texas panhandle up into New Mexico and southeastern Colorado. This aquifer overlies the Rustler, but is only present in the eastern part of Loving Co. Of the multiple formations within the Dockum Group rocks, the Santa Rosa is the most prolific water-bearing unit (Ashworth, 1990). However, the heterogeneous distribution of fine and coarse-grained sediments make it difficult to correlate Santa Rosa zones between distant localities. Thick accumulations of mudstone in middle and upper parts of the Dockum result in confined groundwater conditions (McGowan et al., 1979). There are no outcrops of Dockum rocks in the vicinity of Loving Co. Recharge from precipitation is thought

to have been disrupted by incision of the Pecos and Canadian rivers during Pleistocene time (Dutton and Simpkins, 1986).

Dockum groundwater is primarily of poor quality because of high TDS; however, it is used for water supply in Pecos, TX in Reeves Co., just south of Loving Co. (Ashworth, 1990; Bradley and Kalaswad, 2001). More detailed information on the Dockum aquifer can be found in the TWDB GAM (Ewing et al., 2008).

Pecos Valley aquifer

The Pecos Valley is considered a major TWDB aquifer even though it is of limited aerial coverage (Figure 100). According to Anaya and Jones (2009), the base of the Pecos Valley alluvial aquifer in Loving County is between 2, 500 to 3,000 ft elevation. Hence this unit is present from surface to a depth of ~400 ft in our study area (Figure 98 and Figure 100) and overlies the Dockum and Rustler aquifers (Figure 99). Note that the aquifer is not present in central Loving Co. between the two sections of the aquifer, which were defined by Ashworth (1990) as the Pecos Trough on the west and the Monument Draw Trough on the east (Figure 100). Groundwater quality is generally higher in the Monument Draw Trough of the Pecos Valley aquifer.

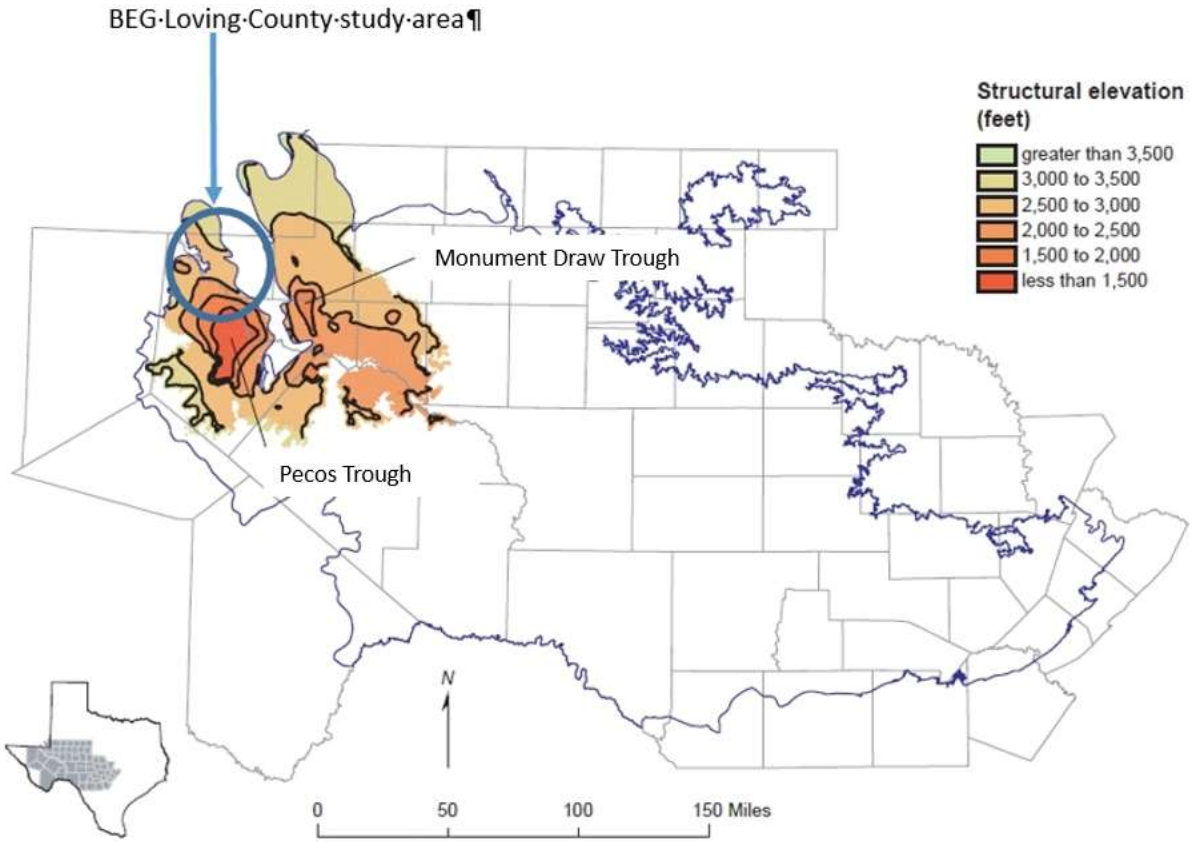

Note: the map shows BEG study area in blue oval. Figure modified from: Anaya and Jones (2009, fig 5-11

Figure 100. Elevation of base of TWDB-defined Pecos Valley aquifer

Prior to widespread irrigation in the late 1950s around Pecos, TX, the Pecos Valley aquifer fed numerous freshwater springs. Farther north the aquifer water contained higher TDS concentrations Quality and availability of the groundwater is in part influenced by presence of

caliche and other types of cementation of the alluvial deposits (Armstrong and McMillan, 1961). Most of the groundwater in the Pecos Trough of the Pecos Valley aquifer exceeds the drinking water standard of 500 mg/L TDS (). In Loving Co, TDS concentrations in the Pecos Valley aquifer are elevated as a result of contamination from oilfield brine (Ashworth, 1990). More detailed information on the Pecos Valley aquifer can be found in the TWDB GAM (Anaya and Jones, 2009).

XVI-3-2 TWDB data

Two forms of Texas Water Development Board (TWDB) data contributed to our early understanding of groundwater conditions in the Loving County study area (1) drillers logs from wells recently installed for rig supply water and (2) wells that are monitored for water levels and water quality. Table 10 summarizes driller's logs for wells drilled in Loving Co. in 2011 through 2013.

Table 10. Summary of Loving County recent drillers logs found in TWDB online database.

TWDB Tracking No.	Date drilled	Total depth (ft bgl)	Cement intervals (ft bgl)	Yield (gpm)	Static WL (ft bgl)	First water depth (ft bgl)	Annular completion	Screened Interval (ft bgl)	Use	Lat.	Long.	Drilling method
276724	11/19/2011	500	0 - 125	100	na	330	open	400 - 500	Rig supply	31° 59' 55"	103° 38' 52"	air rotary
276733	12/12/2011	475	0 - 65	na	na	325	open	375 - 475	Rig supply	31° 59' 56"	103° 38' 51"	air rotary
276738	1/7/2012	500	0 - 85	30	na	325	open	400 - 500	Rig supply	31° 59' 13"	103° 38' 14"	air rotary
276738	1/11/2012	500	0 - 75	80	na	275	open	400 - 500	Rig supply	31° 59' 10"	103° 38' 00"	air rotary
277672	1/5/2012	900	0 - 75	50	400	na	na	625 - 725	Rig supply	31° 59' 10"	103° 38' 43"	air rotary
313512	2/3/2013	653	0 - 10	15	300	550	open	510 -650	Rig supply	31° 59' 03"	103° 39' 12"	air rotary
313516	2/1/2013	715	0 - 10	15	300	650	open	590 - 700	Rig supply	31° 59' 03"	103° 39' 12"	air rotary
313518	2/5/2013	653	0 - 10	15	300	630	open	510 - 640	Rig supply	31° 59' 06"	103° 39' 21"	air rotary
331388	7/11/2012	430	0 - 10	na	155	na	open	260 - 430	Industrial	31° 58' 17"	103° 40' 06"	mud rotary

na = information not available

Most, if not all, new wells in Loving County are being installed for industrial water supply. The population is very small (2013 Census: 82 people[10], making this the least populated county in the U.S.) and there is much ongoing oil and gas activity (Figure 101). Most of the wells are open-hole completions with annular cement only occupying the upper most 10 ft (Table 10). In some cases water well drillers install surface casing down through the base of the unconsolidated Pecos alluvium sediments to keep the borehole open during installation of well casing (Loving Co. landowner personal communication, 2013).

XVI-3-3 BEG groundwater sampling

BEG collected groundwater samples from 36 water wells in Loving and Reeves counties in March and April 2014, plus an additional 5 wells in January 2015. In January 2015, we also resampled two of the wells that were found or suspected to contain methane (CH_4) during 2014 sampling. The methodology used was the same as that described for BEG groundwater sampling in other parts of this RPSEA study. All except two of the wells sampled in the Delaware Basin are located in Loving Co; two are located in Reeves Co., near Pecos, TX.

[10] http://www.census.gov/popest/about/terms.html

Figure 101. Traffic jam in downtown Mentone, TX.

Many of the sampled wells have been installed since 2012 when fracking operations in the Bone Spring oil shale play. The reason for drilling and completing the new wells was to supply water for drilling and fracking operations. In addition to sampling the industrial supply wells, BEG also sampled some older domestic and public water supply wells. The hydrogeologic setting of the Loving Co. wells is the northern flank of the Pecos Trough of the Pecos Valley alluvial aquifer where is only several hundred feet thick (Figure 100, Figure 102). Note that the north-south oriented, A-A' cross section (Figure 102) passes through eastern side of Loving Co. east of the westward pinch out of the Dockum Fm.

XVI-4. Results

Since most, if not all, of the water wells in our study area are completed with open annuli, they are potentially sourced from multiple water-bearing zones: Rustler, Dewey Lake, Dockum, and Pecos alluvium (Figure 102). Locations of the 40 wells sampled by BEG in 2014 and 2015 are shown in Figure 103. The points are color-coded by deepest geologic formation to which total depth (TD) of wells extend. The process used to match TD with subsurface horizon was to (1) obtain surface elevation of each well location using the USGS National Elevation Dataset (NED)[11]. (2) convert well TD to elevation below land surface, (3) compare well TD elevations to grids of top and bottom of aquifers used in the various TWDB GAM models, and (4) double-check lateral extent of TWDB aquifers against unit assignment using model grids of unit structure contours. Note that the two wells near Pecos, TX TD in the Pecos Valley aquifer not

[11] http://nationalmap.gov/elevation.html

Edwards-Trinity as might be indicated by Figure 102. This is because the town of Pecos lies west of the Edwards-Trinity aquifer, extents of which are shown in Figure 99.

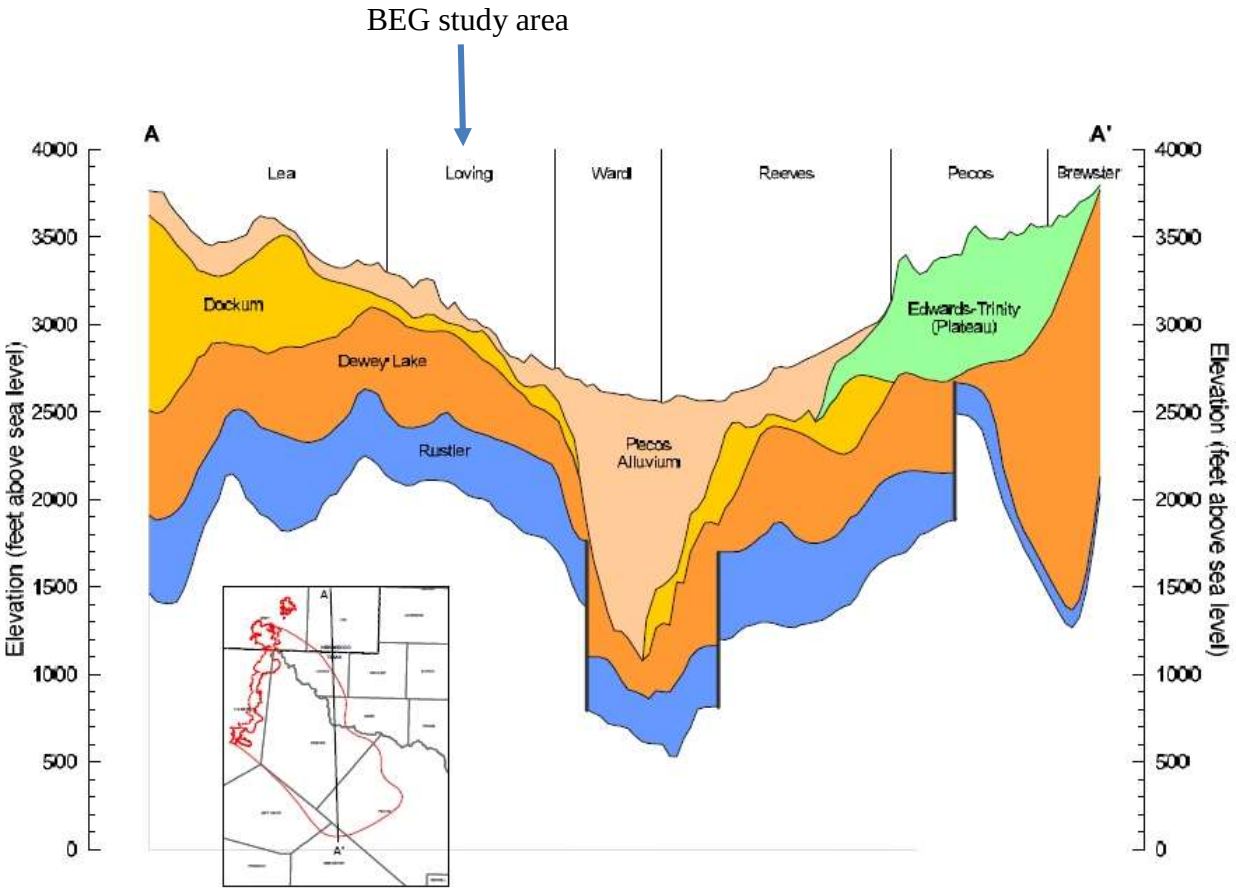

Note: Cross section A-A' from Ewing et al. (2012, fig.2.2.4). BEG groundwater sampling area is on northern flank of the Pecos Trough.

Figure 102. NS cross-section through Loving County

A summary of (1) geologic unit of well TDs, (2) groundwater chemistry results from samples collected by BEG and representative values from Loving Co., and (3) general chemistry of oilfield brines from the Delaware Mountain Group is presented in Table 11. The point of looking at shallow oilfield (Figure 98) brine chemistry is to see if impacts to overlying aquifers might be indicated from brine concentrations, primarily TDS, sulfate (SO_4^{2-}) or chloride (Cl^-). Results using this simple method of inspection are inconclusive, and further analysis is needed.

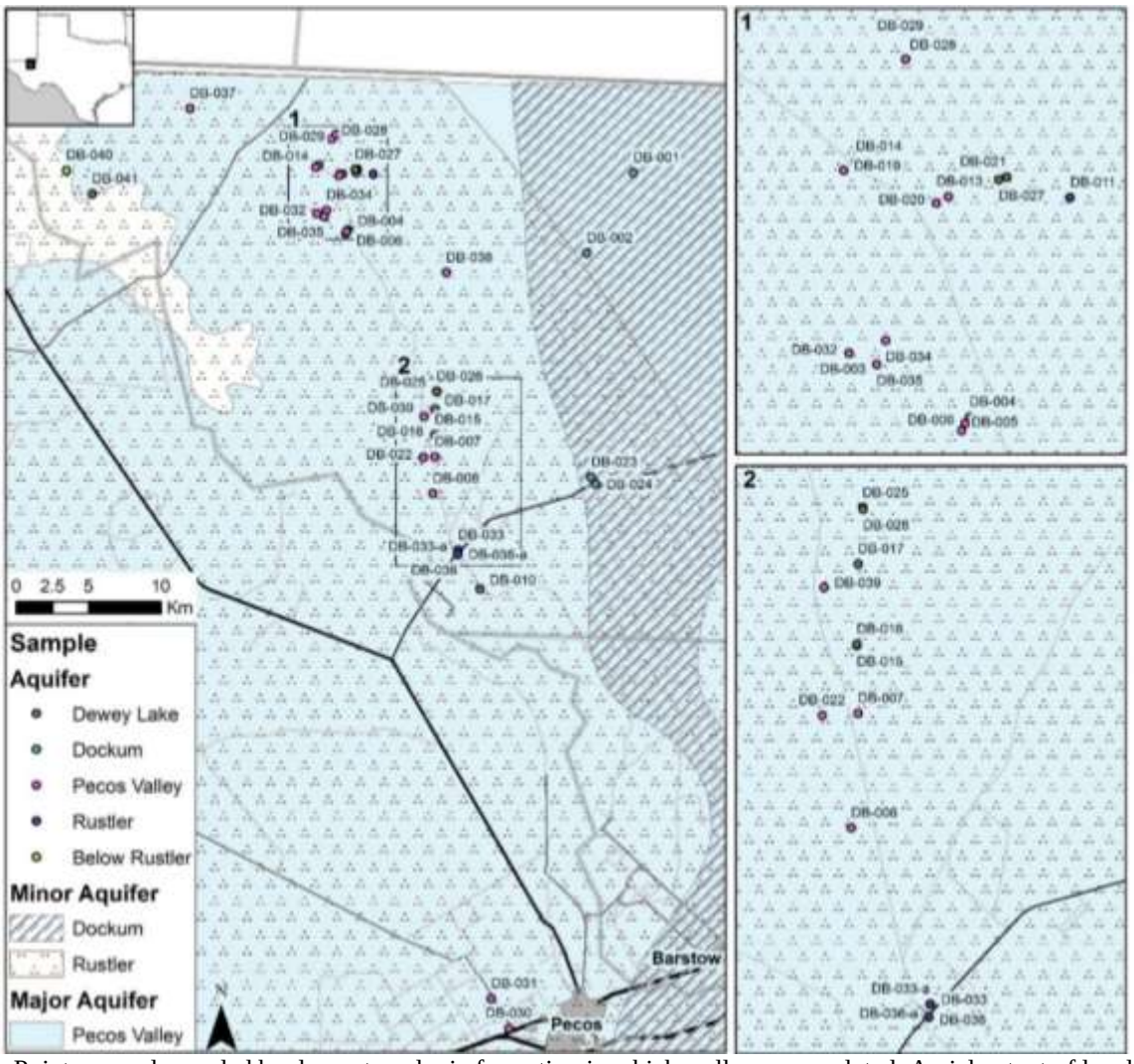

Note: Points are color-coded by deepest geologic formation in which wells are completed. Aerial extent of local TWDB major and minor aquifers are also shown.

Figure 103. Locations of 40 water wells sampled by BEG in Loving and Reeves counties

Table 11. Summary of BEG groundwater sampling results from Loving and Reeves counties

	Number of samples	Well depth (ft bgl)	TDS (mg/L)	pH	Dominant cation	Dominant anion	Median SO_4^{2-}	Median Cl^-
Pecos	21	90 - 400	1,009 - 4,381	6.4 - 7.5	Ca^{2+}, Na^+	SO_4^{2-}, Cl^-	1,018	429
Dockum	4	250 - 400	602 - 2,216	6.9 - 7.7	Ca^{2+}	SO_4^{2-}	612	55
Dewey Lake	10	125 - 500	1,034 - 4,980	6.2 - 7.5	Ca^{2+}	SO_4^{2-}	1,241	134
Rustler	5	250 - 560	3,381 - 5,390	7.1 - 7.7	Ca^{2+}, Na^+	SO_4^{2-}, Cl^-	2,018	763
Below Rustler (DB-040)	1	800	6,348	7.1	Na^+	Cl^-	1,868	1,644
High TDS frack water (DB-018)	1	200	17,781	6.5	Na^+	SO_4^{2-}	8,819 single value	3,351 single value
USGS Delaware Mtn. Fm. Brine (Loving County median values)	25	4,590	232,280	6.3	Na^+	Cl^-	140,964	555

In Figure 104, we show a Piper plot of groundwater chemistry from BEG groundwater samples symbolized by TD of geologic unit. This is a way of evaluating chemical trends of groundwater from different sources. Given the potential for mixing of groundwater in Loving Co. wells, it is not surprising that there are no clear groupings of samples with TDs in the same units. However, there is an indication of cation exchange in samples from the Pecos Valley aquifer (cation triangle on left side of Piper plot, Figure 104). This could be indicative of mixing between oil field brine and Pecos Valley aquifer water.

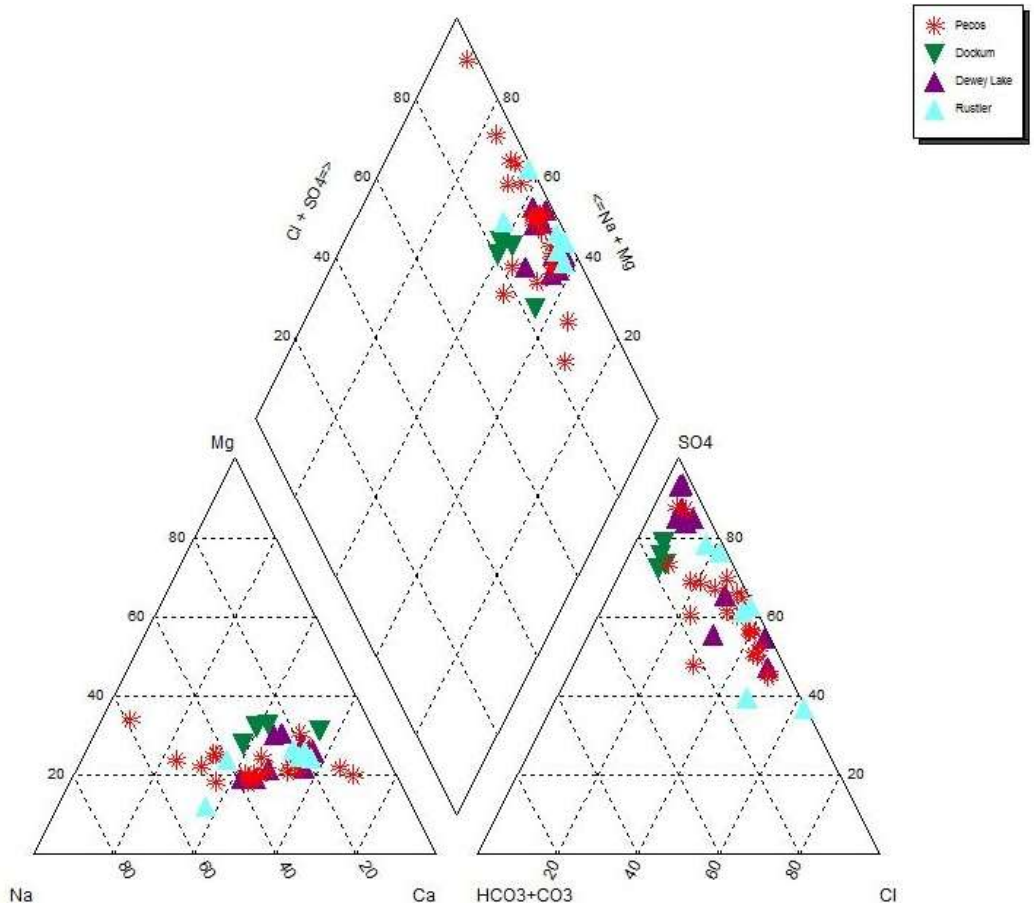

Figure 104. Piper plot of BEG groundwater samples from Loving Co.

Another parameter besides pH that is measured in the field after groundwater parameters have stabilized, immediately prior to sampling, is total alkalinity. Total alkalinity, or acid-neutralizing capacity, of groundwater is commonly used to estimate concentration of carbonate species, which is usually bicarbonate (HCO_3^-) for water near neutral pH. In this study we also measured concentration of HCO_3^- in the laboratory. Total alkalinities calculated from field parameters are consistently higher than the laboratory HCO_3^- values. This indicates the possibility of other processes contributing to total alkalinity of Loving Co. groundwater such as sulfate reduction or addition of organic acids.

Analysis of methane in groundwater samples from Loving Co. shows detection of a significant concentration (~9 mg/L) in only one well near the Loving County courthouse in Mentone, TX. This well is in close proximity to the water well that was impacted by the blowout at the Wheat

Ranch in August 2008. Three other wells (noted by blue circles in Figure 105) have screening values of methane between ~0.1 and 0.3 mg/L.

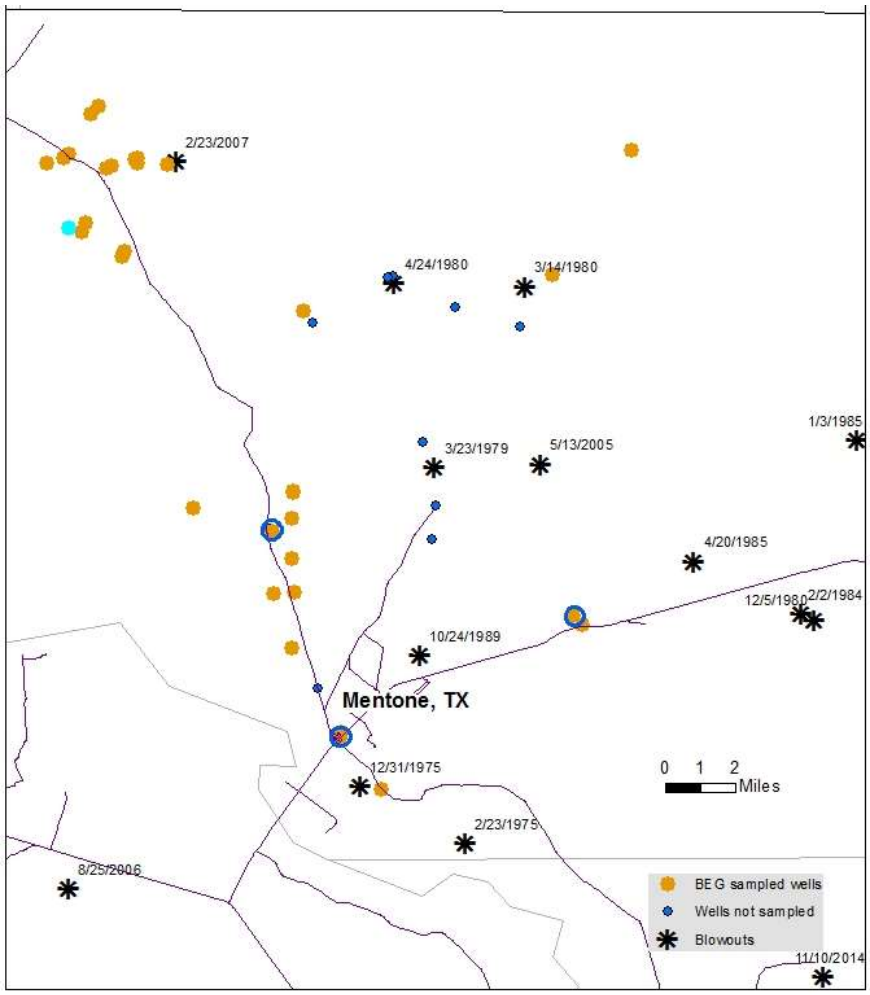

Note: Blue rings around BEG sampled locations indicates wells with methane concentrations over 0.1 mg/L.

Figure 105. Location of blowouts and water wells (both sampled and not sampled) near Mentone, TX

XVI-5. Discussion

Results presented here allow us to provide a preliminary evaluation of groundwater conditions near the beginning of regional hydraulic fracturing for hydrocarbon recovery in the northern Delaware Basin of far West Texas. BEG sampling of a subset of accessible water wells in Loving and Reeves counties shows that water used by oilfield operators for oil shale fracking comes from multiple subsurface water-bearing intervals. Data indicate the possibility of impacts to groundwater from mixing with oilfield brine; however, geochemical modeling, and sampling of additional parameters may be needed to prove this hypothesis. Of the 40 water wells sampled by BEG, a significant concentration of hydrocarbon gas was detected in only one well. This well is located in an area known to have been impacted by a blowout in August 2008. Otherwise, there is no indication of impacts to groundwater from ongoing fracking activities.

References (NOT in main reference list)

Anaya, R. and Jones, I. C., 2009, Groundwater availability model for the Edwards-Trinity (Plateau) and Pecos Valley aquifers of Texas: Texas Water Development Board Report 373, 103p.

Ashworth, J.B., Evaluation of Groundwater Resources in Parts of Loving, Pecos, Reeves, Ward, and Winkler Counties, Texas. 1990, Texas Water Development Board. p. 13-14, 30.

Bachman, G.O., 1984, Regional geology of Ochoan evaporates, northern part of Delaware Basin: New Mexico Bureau of Mines and Mineral Resources Circular 184, 24p.

Boghici, R., and Van Broekhoven, N.G., 2001, Hydrogeology of the Rustler Aquifer, Trans-Pecos, Texas, in Mace, R.E., Mullican, III, W.F., and Angle, E.S., eds, Aquifers of west Texas: TWDB, Report 356, p. 207-225.

EIA, 2014, Today in Energy, Six formations are responsible for surge in Permian Basin crude production: U.S. Energy Information Agency, http://www.eia.gov/todayinenergy/detail.cfm?id=17031

Ewing, J. E., T. L. Jones, T. Yan, A. M. Vreugdenhil, D. G. Fryar, J. F. Pickens, K. Gordon, J. P. Nicot, B. R. Scanlon, J. B. Ashworth, and J. Beach, 2008, Final report groundwater availability model for the Dockum Aquifer: Texas Water Development Board Contracted Report 0604830593, Austin, 510 p.

Ewing, J. E., V. A. Kelley, T. L. Jones, T. Yan, A. Singh, D. W. Powers, R. M. Holt, and J. M. Sharp, 2012, Final groundwater availability model report for the Rustler Aquifer: Texas Water Development Board Contracted Report, Austin, 460 p.

Galloway, W.E., Ewing, T.E., Garrett, C.M., Tyler, N. and Bebout, D.G., 1983, Atlas of Major Texas Oil Reservoirs: The University of Texas at Austin, Bureau of Economic Geology, 139p.

Hills, J.M., 1970, Late Paleozoic structural directions in southern Permian Basin, West Texas and southeastern New Mexico: AAPG Bulletin, v. 54, p.1809-1827.

Hills, J.S., 1984, Sedimentation, tectonism, and hydrocarbon generation in Delaware Basin, West Texas and southern New Mexico: AAPG Bulletin, p. 250-267.

Jones. I.C., 2001, Cenozoic Pecos Alluvium aquifer, Chapter 9 in Mace, R.E., Mullican, III, W.F., and Angle, E.S., eds, Aquifers of west Texas: TWDB, Report 356, p 120-134.

Keller, G.R., Hills, J.M and Djeddi, R., 1980, A regional geologic and geophysical study of the Delaware Basin, New Mexico and West Texas, in Dickerson, P.W. and Hoffer, J.M., eds., Trans-Pecos region, southwestern New Mexico and West Texas: New Mexico Geological Society Guidebook, 31st Field Conference, p. 105-111.

Maley, V.C., and Huffington, RM., 1953, Cenozoic fill and evaporite solution in the Delaware Basin, Texas and New Mexico: Geol Soc. Amer. Bull. v. 64, no. 5, pp. 539-546.

Meyer, J.E., Wise, M.R., and Kalaswad, S., 2011, Pecos Valley aquifer, west Texas: Structure and brackish groundwater; contract report for TWDB, 85 p.

Muelhberger, W.R., 1980, Texas lineament revisited in Dickerson, P.W. and Hoffer, J.M., eds., Trans-Pecos region, southwestern New Mexico and West Texas: New Mexico Geological Society Guidebook, 31st Field Conference, p. 113-121.

Playton, T. E., 2008, Characterization, variations, and controls of reef-rimmed carbonate foreslopes, unpub. PhD dissertation: University of Texas, Austin, 302 p.

Playton, T. E., and C. Kerans, 2002, Slope and toe-of-slope deposits shed from a late Wolfcampian tectonically active carbonate ramp margin, in Dutton, S. P., S. C. Ruppel, and T. F. Hentz, eds., Gulf Coast Association of Geological Societies Transactions, v. 52, p. 811– 820.

Schiel, Kathryn, A., 1994, A new look at the age, depositional environment, and paleogeographic setting of the Dewey Lake Formation (Late Permian?): West Texas Geological Society Bulletin, v. 33, no. 9, p. 5-13.

Stoltz, D.J., 2014, Reservoir character of the Avalon Shale (Bone Spring Formation) of the Delaware Basin, west Texas and SE New Mexico: Effect of carbonate-rich sediment gravity flows: unpublished thesis, The University of Kansas, 155 p.

Trentham, R. Melzer, L. S., and Vance, D., 2012, Commercial exploitation and the origin of residual oil zones: Developing a case history in the Permian Basin of New Mexico and west Texas, Final contract report for RPSEA 81.089 08123-19-RPSEA,

XVII. Appendix I: Wise County Litigation

By Kristine Uhlman modified by JPN

The Trinity and overlaying Paluxy formations are the source of groundwater for domestic and agricultural wells in the south-central portion of Wise County. Well depths to approximately 130 ft for the Paluxy and 370 ft for the Trinity are common, with mineralized water quality averaging 1,000 ppm TDS (calculated from recent sampling). Mitchell Energy had initiated exploration and conventional gas production in the region by 1953 in the Boonsville (Bend Conglomerate), at an average depth of 6,000 ft below land surface (bls) and from the Cal-Tex (Cado Field) at approximately 3,850 ft bls (RRC, 1977). Unconventional, horizontal production from the Barnett Shale at depths from 9,000 to 12,000 feet bls is relatively recent.

RRC District 9 initiated an investigation following the report of a well house fire of the Darwin White domestic water well in early 1977. During their investigation another local well owner, Jack Jackson, complained about what appeared to be bubbling gas from his well. Both the White and Jackson water wells were 300 ft deep into the Lower Trinity Sand. Although the odor of H_2S was reported at the Jackson well, and the odor of hexane (an odorless gas) was reported at the White well, only methane was found in both samples (the report does not identify if the methane was dissolved in water or contained within the headspace of the sample collection bottle). The RRC immediately initiated an investigation on September 12, 1977 and inspected all active oil and gas wells within a one mile radius of the complaints, and surveyed all fresh water wells owners within the study area, reporting the results of their investigation by December of 1977 (RRC, 1977).

Sixty-eight (68) water wells were investigated and two other occurrences of gas were discovered. A well owned by Dr. T. C. Mayo was verbally reported to exhibit combustible gas after a nearby gas well was squeezed to repair a casing leak at 1,560 feet bls in April of 1976. A second well owned by Lee Gibson had been abandoned and replaced ‘some time ago’ after he had discovered gas. Other than the mention in the 1977 RRC report, no other documents for these two wells are available (RRC, 1977).

Of the 68 water wells investigated, only nineteen (19) wells were completed in the Lower Trinity Sand, the other wells were producing water from the Paluxy. None of the Paluxy well sites had complaints of gas, suggesting the vertical confinement of gas within the Lower Trinity Sands below the Glen Rose limestone. The report concluded that the gas contamination was confined solely to the lower Trinity Fm. and was isolated to southern Wise County (RRC, 1977).

Although in compliance with RRC regulations in force at the time, the RRC report identified the likely source of stray gas as the insufficient casing depth of 325 feet reported for the Mitchell Energy Corporation’s D. A. Pearson No. 1 (I.D. No. 32554) well, allowing basal Trinity sands to be exposed to the well bore. An apparent casing leak occurred between March of 1975 when the well was shut in and the RRC bradenhead survey in 1977. Over the period of investigation, pressures between 20 to 30 psi were repeatedly measured by RRC staff between the surface pipe and production casing of the Pearson No. 1 well (Figure 106). Numerous gas wells owned and operated by Mitchell Energy, as well as other producers in the area, were found by the RRC to be equipped with insufficient surface casing to protect the Trinity aquifer. The recommendation of

the Commission report was to consider requiring operators in the Boonsville Bend Conglomerate field to initiate surface casing repairs.

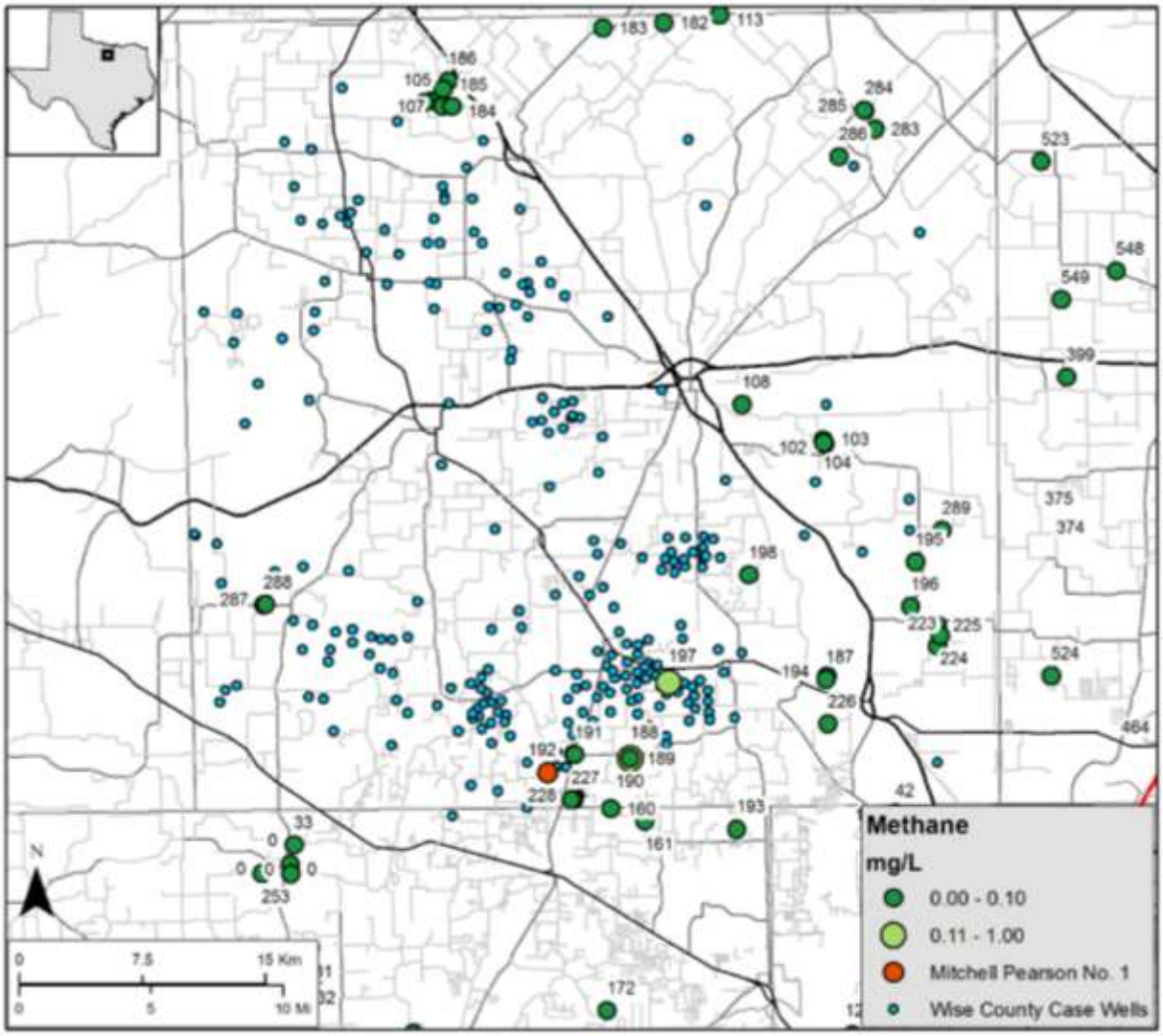

Note: concentration of dissolved methane in water well samples collected in December 2013 through March 2014 also displayed on the map

Figure 106. Gas production wells and water wells in Wise County,

During a May 12th, 1978 hearing at the RRC (Docket No. 9-68, 644) RRC District 9 office recommended that operators be required to permanently isolate the fresh water aquifer by casing to 450 feet bls (RRC, 1979). Mitchell Energy had a total of 90 wells in the area, 68 of which were drilled prior to 1966 and in compliance with the 300 foot surface casing rule in effect at the time. Mitchell also testified that 17 of their wells had experienced casing leaks, and eleven of those leaks had been isolated by setting packer. The Commission ruling from this hearing was that surface casing pressure on all wells be monitored and reported and that if pressure were found the producer must initiate repair. In addition, all future gas wells drilled in the Boonsville field must have sufficient cement to isolate all productive zones in the well bore. The Commission approved the new rule by hearing on June 4, 1979.

In April of 1987, a Wise County land owner sued Mitchell Energy Corporation. By January 1995 eight other family land owners joined and the cases consolidated under Bartlett v. Mitchell Energy Corporation. The complaint alleged that domestic well water had been polluted by twelve of Mitchell's gas wells, citing the RRC investigation and testimony of experts. The record showed that Mitchell was one of 22 operators with gas wells in the area, and it operated less than half the wells. The focus of the case was that H_2S gas had migrated from Mitchell gas wells into the water wells, causing a 'rotten egg' odor and general pollution. Other possible causes of H_2S were not ruled out by the expert testimony. It should be noted that the RRC had sampled one of the complainant's water wells and reported in 1993 that there was "no evidence" of oil-field contamination. The RRC also reported that it suspected that the rotten egg odor was caused by natural sources (Mitchell Energy Corporation v. Bartlett, 1997).

The jury found that Mitchell's conduct constituted gross negligence and was committed with malice, and awarded $204 million. Mitchell appealed, contending that under the discovery rule, the test is not discovery of the cause of the injury; rather, the test is the discovery of the injury itself. Mitchell, in its appeal, noted that the appellees knew of their injuries between three to sixteen years prior to filing, and that the statute of limitations expired two years preceding the date the lawsuit was filed. The Fort Worth Court of Appeals of Texas agreed with Mitchell and reversed the lower court, judging that the appellees recover nothing from Mitchell on November 13, 1997 (Mitchell Energy Corporation v. Bartlett, 1997).

The lawsuit triggered another investigation by the RRC in June of 1996, and by March of 1998 a Commission staff attorney stated that Mitchell Energy "deliberately misreported" the actual depth of protective casing for all but two of the 112 Mitchell Energy wells in Wise and three other nearby counties (Gold, 2014). The December 1998 Compromise Settlement Agreement and Final Order following the RRC investigation (Docket # 09-0218133) noted the cost to Mitchell for repair work had been approximately $2.8 million to date (RRC, 1999). The Commission ordered Mitchell to pay into the Oil Field Cleanup Fund the sum of $100,000.- and assessed an administration penalty of $100,000.- The final order concluded that there had been no admission of violation and no finding of violation in the docket and stipulated the Order not become a part of Mitchell's compliance history.

Accessible water wells near the Mitchell Pearson No. 1 (I.D. No. 32554) well location (Figure 106) were sampled between December 2013 and March of 2014, and analyzed for dissolved methane. Dissolved methane can be from many sources, including deep geologic sources from which natural gas is extracted, coal beds, and biological activity that breaks down organic material. Wells with methane concentrations below 10 mg/L are generally considered safe for use. All of the results of testing in south-central Wise County showed concentrations less than 1.0 mg/L in the well water [However, a witness testified that he saw a water well set on fire in the 1920's because of gas in the aquifer (Gold, 2013, p.110)]

References:

Gold, Russell, 2014. The Boom: How Fracking Ignited the American Energy Revolution and Changed the World, Simon and Schuster, New York.

Mitchell Energy Corporation v. Bartlett, 1997. Court of Appeals Texas, Fort Worth., No. 2-96-227-CV. http://caselaw.findlaw.com. Accessed 8/4/2014.

Texas Railroad Commission (RRC), 1999. Oil and Gas Docket Inquiry, Docket # 09-0218133 / Enforcement. 12/08/1997 to 01/27/1999.

Texas Railroad Commission (RRC), 1979. Examiners' Report, Docket No. 9-68, 644 'Commission called Hearing to consider the matter of gas contamination of water sands in southwest Wise County, Texas.' 5 pages.

Texas Railroad Commission (RRC), 1977. Results of Investigation into Gas Contamination of Lower Trinity Aquifer, Springtown Area, Southern Wise County, Texas. Oil and Gas Division, District 9. 44 p.

XVIII. Appendix J: A Study of Rock-Water Interactions during Hydraulic Fracturing (Barnett Shale)

By J.-P. Nicot, P. Mickler, J. Lu, and R. Darvari

XVIII-1. Approach, Background and Methodology

XVIII-1-1 Plays and Sample Sources

The focus of this research was on a cored well targeting the so-called core area of the *Barnett shale* and located in Wise County, Texas (Figure 107), API# 42-497-33041 Blakley #1 cored and completed in 1985 as a vertical well to the Ellenburger Fm. (top and bottom of Barnett interval cores at 7104 and 7224 ft, respectively), targeted the Viola Limestone, and produced ~140,000 MCF to year 2000. The core is 114 feet long, containing the lower section of the upper Barnett shale, the Forestburg limestone, and the upper part of the lower Barnett shale. Cores from the well have been thoroughly studied by BEG researchers (Loucks and Ruppel, 2007; Loucks et al., 2009; Zhang et al., 2014). The well, by then a Mitchell Energy well, was subsequently stimulated through HF in December 2000 (IHS and FracFocus data), still as a vertical well in a heydays of vertical HF in the Barnett (see Nicot et al., 2014) with 120,000 gal of water and 114,500 lbs of sand. It has produced ~760,000 MCF from 2000 to 2014 (Figure 108). The amount of water produced back after HF (flowback + produced water) amounts to ~80% of the amount injected, making the well fairly typical of Barnett wells (Figure 109).

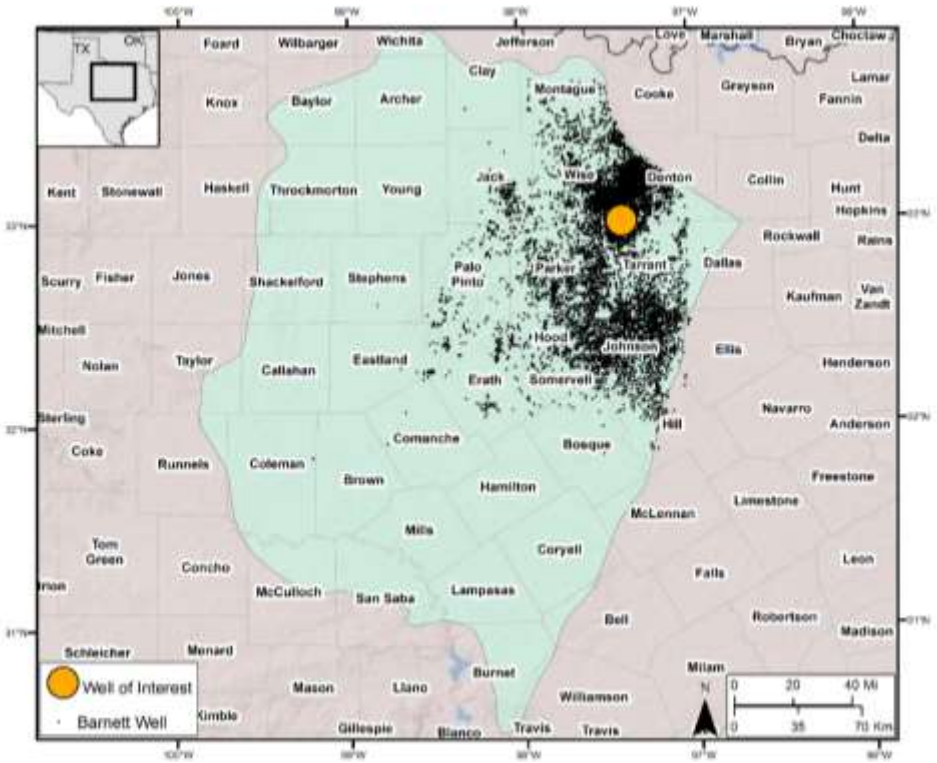

Note: Barnett well locations from IHS (data download on 7/13/2015); Barnett footprint from EIA shape file (http://www.eia.gov/pub/oil_gas/natural_gas/analysis_publications/maps/maps.htm, accessed on 7/13/2015).

Figure 107. Location map of Blakley #1 well

The well (now operating by Devon Energy) was refrac'ed in February 2015 (1,408,480 gal according to FracFocus, possibly off by one order of magnitude; no data yet in IHS) . See Attachment A for FracFocus details about some of the 2015 HF stimulation parameters.

IHS reported a pressure of 3747 psi (258 bar) at a depth of ~7450 ft and a temperature gradient of 1.69, that is, a temperature of 1.69°F / 100 ft × 7200 ft / 100 ft + average temperature in Decatur of 62°F (http://www.usclimatedata.com/climate/decatur/texas/united-states/ustx1873) = 184°F (84°C).

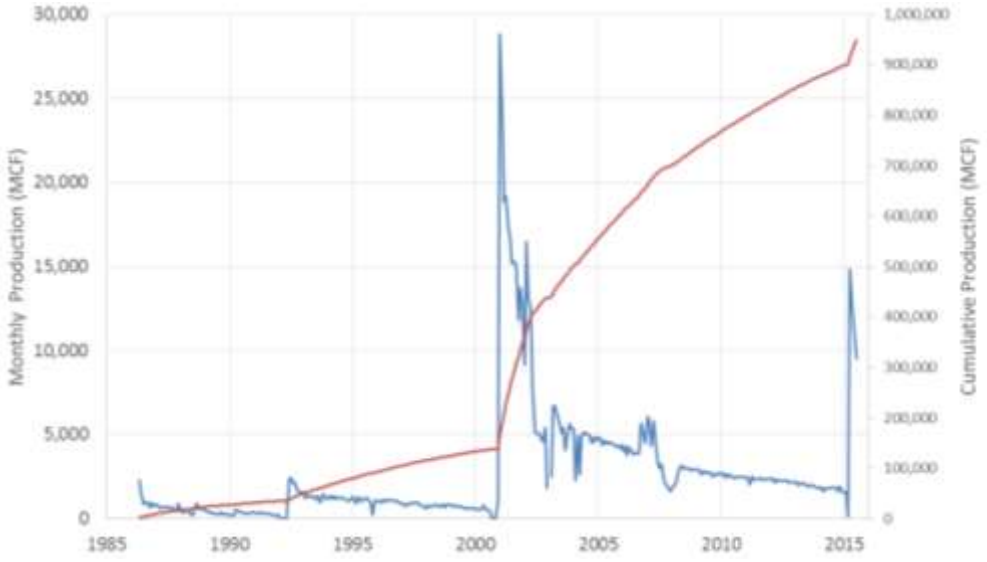

Figure 108. Monthly and cumulative gas production of Blakley #1 well

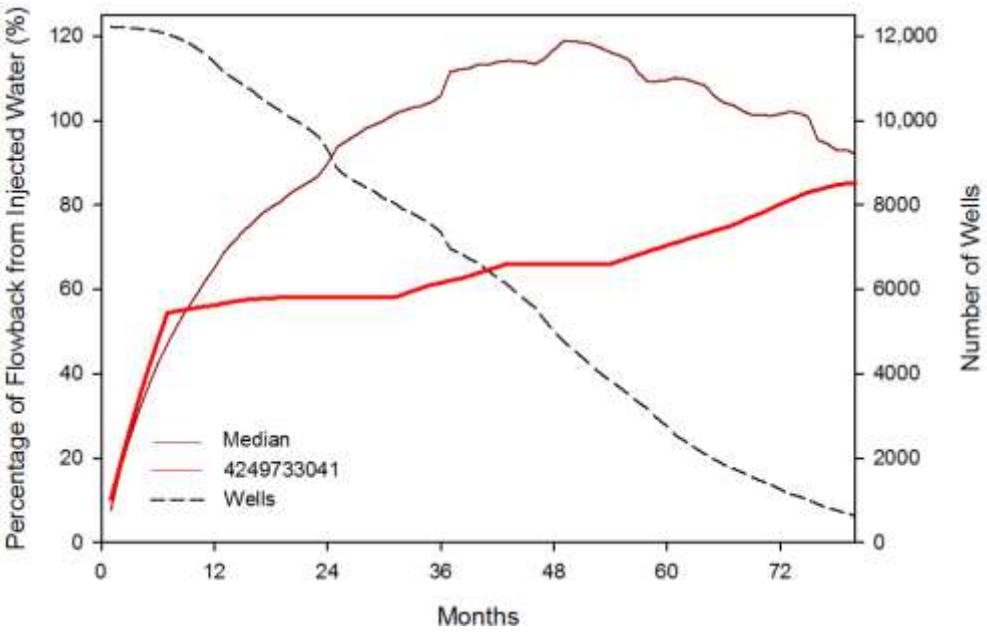

Note: RHS y-axis corresponds to number of wells available to calculate the median percentage of all wells some number of months after HF.

Figure 109. Cumulative flowback volume as a function of HF volume (Blakley #1)

The core used for the experiments was taken from the lower Barnett section at a depth of 7197 ft. Location within the entire Barnett section is shown in Figure 110.

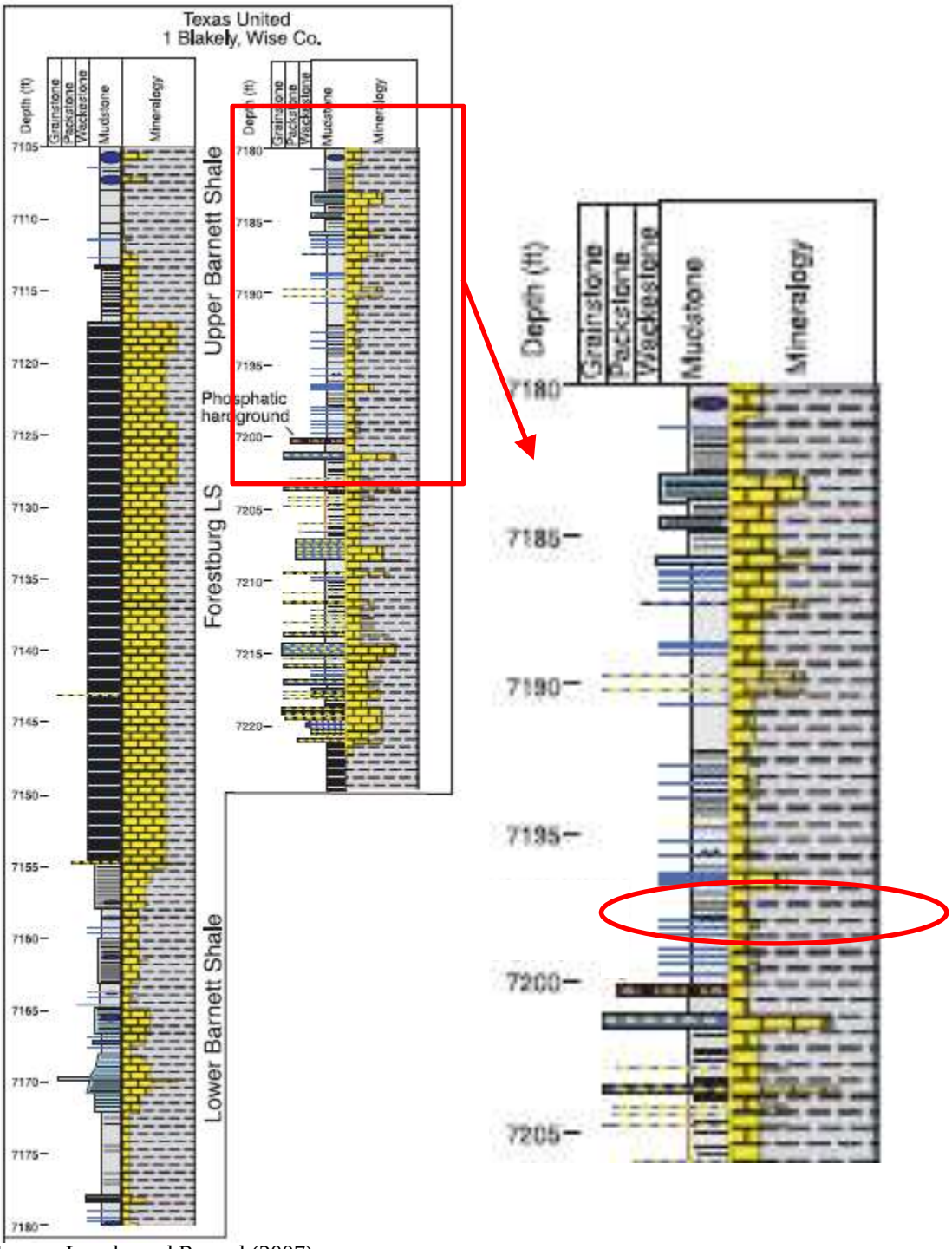

Source: Loucks and Ruppel (2007)

Figure 110. Stratigraphic location of experimental core.

XVIII-1-2 Sample Characterization Methods

The samples were analyzed using a variety of tools, first on a fresh sample, then on reacted samples: X-ray diffraction (XRD), scanning electron microscope (SEM) coupled with energy dispersive X-ray spectroscopy (EDS) analyses complemented by argon-ion milling for sample preparation and MICP analyses. Quantitative X-Ray Diffraction (XRD) analysis of spray dried random powders provides good estimates of the amount of the most abundant minerals (for example, quartz, feldspars, carbonates, clays) but not necessarily of minerals in minute amount (less than ~1-2%) such as pyrite or maybe anhydrite. SEM on ion-milled samples produces sharp images showing the topography of a microscopic surface allowing the visual determination of mineralogy and texture. EDS gives the elemental composition of the surface of a sample and allows to create maps of the element of interest, for example, Fe or Ca distribution. No particular precaution was taken when handling the cores and rock fragments. Sample-preparation methods and analytical parameters can be found in Lu et al. (2011), Lu et al. (2012), and Lu et al. (2014).

XVIII-1-2.1 X-Ray Diffraction Mineralogy

Samples for XRD analyses were prepared the following way. Bulk powders of the original and reacted rock samples were prepared by means of wet grinding and spray drying. The samples were first disintegrated using a TEMA ball mill before further grinding in a McCrone Micronizing Mill. The samples were ground for 16 minutes in 0.5% (wt./vol) aqueous solution of polyvinyl alcohol to reduce particle size sufficiently to less than 10 μm. The resulted slurry samples were sprayed from the top of a spray drier and the dry and randomly oriented powders were collected at the bottom. X-ray diffraction analysis was conducted on a Bruker AXS D8 diffractometer at the University of Texas at Austin. The powder samples were scanned from 4° to 70° 2θ, at a scan rate of 1.5 s per 0.015° step with Cu Kα radiation. Bruker's Eva software was used to identify mineral phases. Quantitative analysis was conducted using Topas 3, a personal computer software based on the Rietveld method (Bish, 1994). Quantitative phase analysis results from this method are accurate to within 2% absolute error (Hillier, 1999).

XVIII-1-2.2 Scanning Electron Microscopy, Energy Dispersive X-ray Spectroscopy, and Argon Ion Milling

Both unreacted and reacted core chips with rough surface of approximately 8 mm in size were examined by SEM. The samples were air-dried and a conductive coating of iridium was sprayed onto sample surface to limit charging during FE-SEM imaging. The samples were examined under secondary electron (SE) mode for topography using a field-emission SEM, an FEI Nova™ NanoSEM 430. Typically, accelerating voltage of 15 kV and working distance of ~9 mm were used. Backscattered electron (BSE) and energy dispersive spectroscopy (EDS) point analyses were conducted for mineralogy. EDS element distribution maps were also acquired using two EDS detectors. The EDS maps are rendered as false color images overlying SEM images to show mineralogical variation in the examined area.

In addition, for some autoclave experiments, a piece of unreacted shale was shaped into a cuboid of approximately 10×8×5 mm in size. The unreacted samples were first polished by a Triple Ion Beam Miller (Leica EM TIC020) using an accelerating voltage of 8 kV, a current of 2.8 mA, and a milling time of 10 hr. The polished surfaces were perpendicular to the beddings and showed as shallow triangles of ~5 mm long and ~1 wide. Iridium was sputtered on the ion-milled surfaces to create a conductive coating to limit charging during SEM imaging. The unreacted samples

were examined by SEM with the aid of an X-ray energy dispersive spectroscopy (EDS) system. Secondary electron (SE) images, backscattered electron (BSE) images, and EDS elemental maps were obtained with location reference. Then, the coated surfaces were re-milled using a broad-ion-beam miller (Leica EM TIC 3X) to remove the iridium coating. The re-milled surfaces were examined using a low-vacuum SEM detector in a water-vapor environment. After two rounds of SEM imaging, the polished, uncoated shale cuboids were placed in the reaction vessel with other core fragments (16 g in total) to react with the brine for over 3 weeks.

After the reacted sample was retrieved from the reactor, the ion-milled surface was examined using the low-vacuum SEM detector without a conductive coating. SEM images were taken at the exact same areas of the pre-reaction images. By directly comparing the topography of the same areas of unreacted and reacted rock samples without a veil of coating material, we were able to identify mineral dissolution and precipitation that occurred during the reaction experiments.

The samples with iridium coating were examined on an FEI NovaNano SEM 430 using SE and BSE modes at an accelerating voltage of 10–15 kV and a working distance of 7–9.5 mm. X-ray EDS mapping was conducted using dual Bruker 30-mm^2 detectors. Mineral composition was documented by BSE and EDS images in the pre-reaction samples. The uncoated samples were examined under low-vacuum conditions (chamber pressure = 0.35 Torr) with water vapor as conductive media. Low accelerating voltage (4 kV) of the electron source beam was used. Working distance was set at 3.2 mm. Mineralogical identification is greatly hindered in this mode because low accelerating voltage leads to a weak BSE signal and incomplete EDS spectra. However, without a layer of coating material overlying the polished surface, the low-vacuum detector (LVD) images reveal more topographic and textural details, and the boundaries of fine grains and contacts between different components are more readily observed. A different charging effect helps identify calcite, which usually shows a bright charging effect in larger grains; smaller calcite grains do not glow as much, and lower water-vapor pressure is required for the charge effect to show up.

For quantitative measurement of mineral dissolution, geometry of the newly formed pores in the reacted samples was traced manually using a digital drawing pen on a touch screen (Wacom Cintiq 22” HD), a method similar to Milliken et al. (2013) and Lu et al. (2015). Five LVD–SEM images were traced and analyzed for the reacted sample. The LVD images were taken at an instrument magnification of 6,000×, covering an area of 49.74×42.90 μm. The single image area is 2133.83 μm^2, and the total measured area for each sample is 10669.13 μm^2. Each image contains 1024×883 pixels excluding the information bar, and the image resolution is 49 nm/pixel. Edges of the secondary pores were marked out manually. Tracing and analyses of the pore geometry were carried out using NIS-Elements by Nikon Instruments Inc., microscope image software that calculates object size and shape parameters of the marked secondary pores (e.g., area, length, width, equivalent circular diameter). Porosity generated during the experiments was calculated as the total area of the secondary pores divided by image area.

XVIII-1-2.3 MICP Analyses

MICP analyses were conducted by an outside vendor (PoroTechnology). Pore systems and capillary properties of the reacted samples were characterized using high-pressure MICP measurements at PoroTechnology using techniques similar to Shafer and Neasham (2000). MICP permeability was calculated using the Modified Purcell method (Comisky et al., 2007). MICP

data were acquired by injecting mercury into cleaned and dried rock samples. All samples were dried at ~100°C prior to MICP tests. MICP was increased in a stepwise manner, and the percentage of rock volume saturated by mercury at each step was recorded, after sufficient time for equilibrium to be established was allowed.

XVIII-1-3 Rock-Water Interaction Experiments

In this section we described the material and apparatus used in the experiments as well as the various types of measurements performed in the course of the study.

XVIII-1-3.1 Experiments

Two sets of experiments were conducted; bench top experiments and high temperature/high pressure experiments. Samples slated for experiments were extracted from core samples and chosen in such a way that interactions with and contamination by drilling muds were limited. The shale samples from cores were reacted with several aqueous solutions chosen both for their scientific interest and for mimicking actual HF fluids: (1) de-ionized (DI) water that was produced from a nanopure water purification system; (2) ~2,000 ppm NaCl, KCl, and $CaCl_2$ solutions that were produced by mixing the appropriate salt with DI water; and (3) an approximately 20,000 ppm NaCl solution that was produced by mixing NaCl salt with DI water and 20,000 KCl and CaCl2 solutions (benchtop only). It is recognized that an acid slug is often injected before initializing HF proper, we assume the acid is consumed and neutralized and that pH is back to pre-injection level (for example, Morsy et al., 2013). NaCl was used because Na brines are very common and even dominant in the subsurface and blending with flowback / produced water would pull the HF fluid towards a Na composition. $CaCl_2$ was used because Ca water are frequent in the shallow subsurface and often used as base fluid for HF (however, operators tend to remove Ca from blended water because of the detrimental effect of divalent ions on generic friction reducers). KCl was used because of its common use in the industry.

Both the benchtop and autoclave experiments are designed to be free of O_2 and are done under a N_2 headspace. However, despite the precautions taken, in instances in which we see pyrite oxidation, it is likely that some minor O_2 may be left in the experimental water and rock from air trapped in the pores during storage; especially for the benchtop experiments where the purge cannot be as thorough. Other possible explanations for pyrite oxidation are presented later in this report.

XVIII1.3.1.1 Benchtop Experiments

In benchtop experiments 8 grams of freshly ground/pulverized shale samples were placed in a 60 ml serum vial filled with 40 mL of the aqueous solution. Material used for the experiments was prepared in a single batch. Pulverization to silt size particles was done with a tungsten carbine ball mill. A variable amount of pre-heated water with distinct chemistry was added to the serum vial and a septum cap was sealed onto the vial. A hypodermic needle attached to a N_2 tank was inserted through the septum and into the head space of the serum vial. A second needle was inserted to allow the head space gas to exit the bottle. A strong flow of N_2 gas from a compressed N_2 tank was allowed to flow through the headspace such that the total volume of gas used was many times the volume of the initial headspace suggesting all the original gas was replaced by N_2 and no O_2 was left. The vial was then placed in an oven at 80°C (on ice for the temperature experiments) and the aqueous solution was incrementally sampled during the course of the

experiment by removing approximately 3 ml of fluid from the vial using a syringe and hypodermic needle (no atmosphere was introduced to the vial during sampling). The fluid was filtered through a 0.45 µm syringe filter. Aliquots were then taken for dissolved inorganic carbon (DIC) measurements or alkalinity titrations (performed at BEG), pH analysis, IC analysis (major cations and anions; performed at BEG) and acidification for ICP-MS analysis (trace metals; performed at the UT Department of Geological Sciences). After sampling the serum vials were re-pressurized using compressed N_2 gas and returned to the oven, vials were out of the oven approximately 15 minutes. Typically several vials were prepared for each experiment with powder from the same batch and the same fluid. Only a few samples were taken from each vial to limit the slight decrease in fluid volume due to sampling.

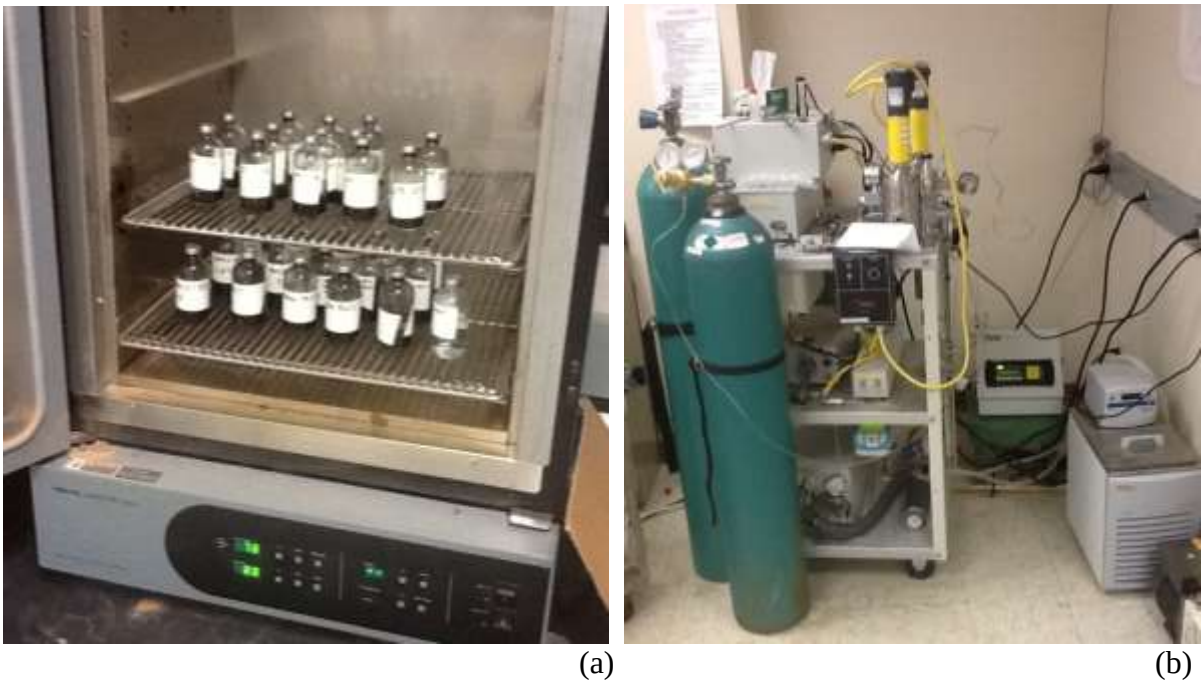

(a) (b)

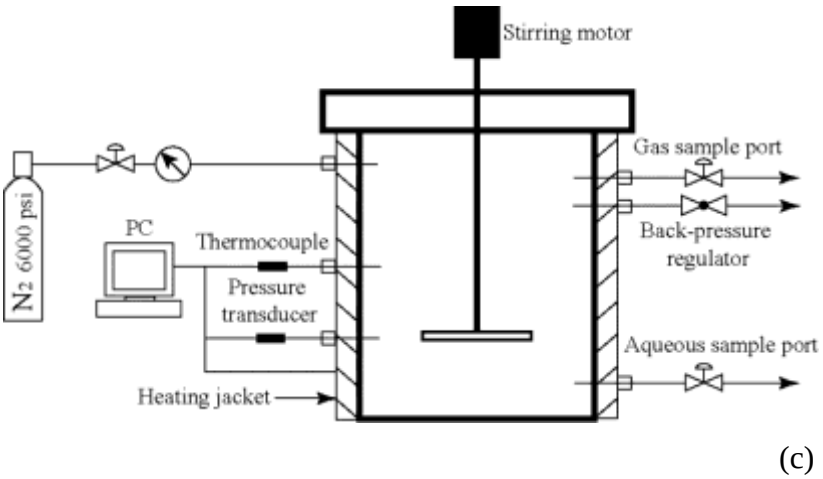

(c)

Figure 111. View of (a) oven for benchtop experiments showing racks with vials; (b) of autoclaves and related equipment; reactors are underneath the yellow-jacketed stirring mechanisms. (c) is a schematic diagram of the autoclave system.

XVIII1.3.1.2 Benchtop Temperature Experiments

In order to assess the impact of temperature, particularly at early times, and with the goal of slowing down geochemical interactions, we performed a few benchtop experiments on ice at 0°C with DI water for a maximum of 5 days.

XVIII1.3.1.3 Autoclave Procedure

The autoclave reactor and related equipment represent a state-of-the-art apparatus that was recently installed and tested at the BEG (in 2013). The stainless-steel reactor cell volume is approximately 250 ml and we performed batch, not column experiments. Experiments were conducted at 80°C and 200 bar with synthetic solution of various salinities.

In the autoclave experiments approximately 16 grams of shale fragments, usually consisting of two to four pieces, were loaded into the reaction vessel with water of distinct chemistry. The rock pieces were not disintegrated in order to keep mineral surface area relatively unchanged and to minimize the risk of plugging the lines of the sampling system. The synthetic solution (~160 mL) is then added. A fluid volume of 160 mL and ~16g rock chips in the reactor initially gives a bulk brine/rock ratio in volume about 30 times higher than in a typical HF operation (see further discussion in Attachment C). Nitrogen (N_2) was flushed through the reaction vessel for 5-10 minutes to remove residual atmospheric gasses such as O_2. The vessel was then sealed and pressurized using a high pressure N_2 tank and the temperature was increased. The aqueous solution was sampled through a capillary tube without changing the experimental conditions. The collected aqueous solution was then sampled for pH, DIC, IC and ICP-MS analyses. The fluid was filtered through a 0.45 μm syringe filter. Aliquots were then taken for dissolved inorganic carbon (DIC) measurements or alkalinity titrations (performed at BEG), pH analysis, IC analysis (major cations and anions; performed at BEG) and acidification for ICP-MS analysis (trace metals; performed at the UT Department of Geological Sciences).

Temperature and pressure are automatically controlled by regulators. The reaction temperature was maintained by a computer controlled heater with a thermocouple positioned in the reaction chamber. The magnetic stirrer homogenizes the system and speeds reactions by removing slow diffusion-based controls; this is an apparatus which is not commonly implemented in autoclave reactors. It gives us confidence that the solution is well-mixed and that aqueous samples are representative of the rock-water interactions. Once the temperature is reached, a liquid sample (~2 mL) is taken through a dip tube in the reactor. For each sample, approximately 1.5-2 mL of water was purged through the sampling port to remove the old fluid that was isolated in the sampling tubing (that is, a total of 3.5-4 mL). The purged fluid was set aside and used for pH measurement. A sample is then taken every 2 hours for the first 6-8 hours, then once daily, then every few days for a total of approximately 3 weeks. No additional fluid is added during the experiment. As little water as possible (<4 mL per sample for alkalinity measurement, chemical analyses, and purging the lines) is taken from the solution. It follows that the solution volume cannot be assumed constant. However, no correction for evaporation was needed. In earlier experiments not related to this project, we used Br as a tracer to assess evaporation and other leaks that turned out to be very limited. We also used blanks as control. A potential problem that was not resolved in the course of this research is the possibility that some precipitation occurs because of relatively rapid decompression and temperature decrease and that some of the minerals observed at the surface of the reacted samples are actually artefacts. Remaining fluids at the end of experiments were filtered (0.45 μm) and sent for NORM analyses.

A concern during the experiments was avoiding corrosion of the reactor, especially when O_2 is introduced through inadequate purging of the air, as it could bias trace element concentrations. The vessel body is made of 17-4PH stainless steel whereas the vessel cap is made of Nitronic 60 (literature from the vendor "Thar"). In addition to iron, the stainless steel reactor components are composed of Cr and Ni to which Mn, Mo, and Cu can be added (Table 12).

Table 12. Typical composition of autoclave vessel components

17-4PH Stainless Steel (main vessel body)		**Nitronic 60 Stainless Steel (vessel cap)**	
Element	**Composition (weight %)**	**Element**	**Composition (%)**
Iron	>75	Iron	~60
Chromium	15.5	Chromium	16-17
Nickel	4.5	Nickel	8-8.5
Manganese	0.40	Manganese	7.5-8.5
Silicon	0.50	Silicon	3.7-4.2
		Molybdenum	0.75
Copper	3.50	Copper	0.75
		Vanadium	0.20
		Tungsten	0.15
		Nitrogen	0.1-0.18
Columbium + Tantalum	0.30	Columbium	0.10
	0.04	Carbon	0.06-0.08
		Titanium	0.050
		Tin	0.050
Phosphorus	0.020	Phosphorus	0.040
Sulfur	0.005	Sulfur	0.030
		Aluminum	0.020
		Boron	0.0015

Source: vendor information

The amount of core available limited the number of experiments that could be performed (Table 14).

Table 13. Summary of benchtop runs.

Experiment	Rock (g)	Brine (mL)	Brine composition	Press. (bar)	Temp. (°C)	Run start and end dates and comments
A	7.99	40	DI water	1	80	06/11 to 06/24/2013 (14 days)
B	7.99	40	2000 ppm NaCl (0.5044 g NaCl in 250 ml)	1	80	06/11 to 06/24/2013 (14 days)
C	7.99	40	2000 ppm KCl (0.6366 g KCl in 250 ml)	1	80	06/11 to 06/24/2013 (14 days)
D	8.00	40	2000 ppm CaCl2 (0477 g $CaCl_2$ in 250 ml)	1	80	06/11 to 06/24/2013 (14 days)
E	8.00	40	20,000 ppm NaCl (5.0086 g NaCl in 250 ml)	1	80	06/12 to 06/24/2013 (13 days)
F	7.99	40	20,000 ppm KCl (6.3770 g KCl in 250 ml)	1	80	06/13 to 06/24/2013 (12 days)
G	8.01	40	20,000 ppm $CaCl_2$ (4.7472 g $CaCl_2$ in 250 ml)	1	80	06/13 to 06/24/2013 (12 days)
H	8.015	40	DI water	1	0	08/09/2013 at 1:32 pm to 3:15 pm (1h 43 min)
I	8.01	40	DI water	1	80	08/09/2013 at 1:32 pm to 3:15 pm (1h 43 min)
J	8.06	40	DI water	1	0	08/19 to 08/23/2013 (5 days)
K	8.01	40	DI water	1	80	08/19 to 08/23/2013 (5 days)

Table 14. Summary of autoclave runs.

Experiment	Rock (g)	Brine (mL)	Brine composition	Press. (bar)	Temp. (°C)	Run start and end dates and comments
Blak-A	16.27	160	DI water	200	80	06/13 to 07/01/2013 (19 days)
Blak-B	16.04	160	2000 ppm NaCl (2.0082 g NaCl/L)	200	80	08/08 to 08/26/2013 (19 days)
Blak-C	16.06	160	2000 ppm $CaCl_2$ (1.8915 g $CaCl_2$/L)	200	80	08/27 to 09/03/2013 (8 days) Stopped prematurely because of a leak
Blak-D	16.09	160	2000 ppm $CaCl_2$ (1.8915 g $CaCl_2$/L)	200	80	09/23 to 09/23/2013 (20 days) Repeat of Black-C
Blak-E	16.04	160	2000 ppm KCl (2.5519 g KCl/L)	200	80	09/24to 10/13/2013 (20 days)
Blak-F	16.04	160	20,000 ppm NaCl (20.0002 g NaCl/L)	200	80	10/14 to 11/04/2013 (22 days)

Another major concern was the purity of the salts used during the experiments (NaCl and $CaCl_2$). They could contain traces of other ions such as K, Mg, Ca, Na etc that would bias the experimental results. We analyzed 2 samples of the NaCl and $CaCl_2$ solution (~100 ppm each) (Table 15).

Table 15. Typical composition of the synthetic salt solutions used (salt baseline)

	Li	Na	NH_4	K	Mg	Ca	F	Cl	Br	NO_3	PO_4	SO_4
NaCl												
run 1	0.0012	**95.1**	0	0.032	0	0.0093	0	140.4	0	0	0	0
run 2	0	**95.4**	0	0.017	0	0	0	140.9	0	0	0	0
Ave.	**0.0006**	**95.2**	0	**0.025**	0	**0.0047**	0	140.7	0	0	0	0
DL	**0.0077**	**0.0207**	**0.0013**	**0.0348**	**0.0003**	**0.6723**	**0.0752**	**0.0136**	**0.489**	**0.5259**	**0.0976**	**0.065**
$CaCl_2$												
run 1	0.0646	1.8181	0	3.51	0	**85.7**	0	149.6	2.06	0	0	0
run 2	0.0638	1.7949	0	3.50	0	**85.9**	0	150.2	2.10	0	0	0
Ave.	0.0642	1.8065	0	3.51	0	**85.8**	0	149.9	2.08	0	0	0
DL	**0.0077**	**0.0207**	**0.0013**	**0.0348**	**0.0003**	**0.6723**	**0.0752**	**0.0136**	**0.489**	**0.5259**	**0.0976**	**0.065**

NaCl solution:

Each 1 ppm of Na in brings 0.00026 ppm of K, 0.000049 ppm of Ca, and 0.0000063 ppm Li but no Mg, phosphate or sulfate

$CaCl_2$ solution:

Each 1 ppm of Ca in brings 0.0408 ppm of K, 0.021 ppm of Na, and 0.00075 ppm Li but no Mg, phosphate or sulfate

Table 16. Significant levels of K, Ca, Na, and Li in the experiments (ppm)

	ppm Na/Ca	K	Ca	Na	Li
Na 2k	786 Na	0.2	0.04	n/a	0.005
Na 20k	7863 Na	2.1	0.38	n/a	0.05
Na 50k	19,658 Na	5.1	9.60	n/a	1.24
Ca 2k	721 Ca	29.4	n/a	15.2	0.54
Ca 20k	7207 Ca	294.4	n/a	151.7	5.4

XVIII-1-3.2 Produced Water Sampling

In order to somewhat calibrate the experimental results, we sampled the flowback of another well tapping the Barnett Shale. A total of four produced water and one fresh water samples were taken. A field blank was taken as well.

XVIII-1-3.3 Chemical Analyses

Major and other cations (Li, Na, NH_4, K, Mg, Ca) and anions (F, Cl, Br, NO_3, PO_4, SO_4) of water samples were analyzed on two Dionex ICS-1100 Ion Chromatography systems equipped with an AS-AP auto sampler at the BEG. Na and Cl concentrations were largely outside analytical calibration, and brine samples were diluted after collection by a factor of up to 100 using de-ionized water for ion chromatography (IC) such that Ca and SO_4 concentrations did not exceed 500 ppm. Trace and other elements (B, Mg, Al, Si, P, K, Ca, Ti, V, Cr, Mn, Fe, Co, Ni, Cu, Zn, As, Se, Rb, Sr, Zr, Mo, Ag, Cd, Sn, Sb, Cs, Ba, Tl, Pb, Bi, Th, U) were analyzed on an Agilent 7500ce quadrupole inductively coupled plasma-mass-spectrometer (ICP-MS) at the UT Department of Geological sciences http://www.geo.utexas.edu/isochem/default.htm). Samples for trace metals were acidified with 2% HNO_3 immediately after collection and diluted so that the total dissolved solid content was close to 500 mg/L.

Due to the small amount of solution used in these experiments pH and alkalinity were not determined for every sample. The pH was always measured around 7 or slightly higher so not all samples were analyzed for pH. The pH was determined using an Orion 3-star pH meter and gel-filled pH/ATC Triode by transferring ~1 mL of sampled reaction fluid into a 15-mL centrifuge tube. The centrifuge tube allowed the smallest possible volume of water to cover the pH electrode allowing the pH determination. Dissolved inorganic carbon (DIC) was analyzed in a carbon analyzer.

XVIII-1-3.4 Isotopic Analyses

The water isotopic analyses were performed by Dr. Toti Larson at the UT Department of Geological Sciences. Filtered and unacidified water samples were analyzed for $\delta^{18}O$ and δD values. $\delta^{18}O$ values were measured using CO_2 equilibration with a ThermoScientific Gas Bench II coupled to a ThermoScientific MAT253 isotope ratio mass spectrometer (IRMS). 1-ml samples were equilibrated with 3000 ppm CO_2 at 40°C for 12 hours. Measured $\delta^{18}O$ values of CO_2 gas from IAEA-SMOW, IAEA-GISP and internally calibrated standards were used to generate a $\delta^{18}O$ calibration curve. All analyses are reported in standard 'permille' notation with respect to $\delta^{18}O_{VSMOW}$=0‰. δD values were measured using ThermoScientific temperature conversion elemental analyzer (TCEA). 1 microliter aliquots of water were injected into a heated septum injection port and reduced to hydrogen gas at 1440°C in the presence of glassy carbon. Measured δD values of H_2 gas from IAEA-SMOW, IAEA-GISP and internally calibrated standards were used to generate a δD calibration curve. All analyses are reported in standard 'permille' notation with respect to δD_{VSMOW}=0‰.

It should be noted that the method for $\delta^{18}O$ is straightforward and rarely effected by contaminants but that the method for δD is easily effected by organics, so the water needs to be pure; hence larger error bars on δD.

XVIII-2. Results

In this section we describe unreacted samples (Figure 112) and samples reacted with waters of various salinities. Then follows a description of aqueous composition results of the autoclave experiments (Section XVIII-2-2). We then examine other relevant analyses (Cl/Br ratios) and porosity / permeability measurements).

Source: BEG_Blak Sh MICP_PR131122-008.xls

Figure 112. Photographs of unreacted core segments.

XVIII-2-1 Description of Unreacted and Reacted Samples

A core sample of Barnett shale was selected at depth of 7197ft from the Blakley #1 well. The shale can be described as a dark grey siliceous mudstone. In total, six reaction experiments were started and five of them went to completion. One of them failed because of leakage. For the DI (Blak-A) and 20k NaCl (Blak-F) autoclave experiments, an argon ion-milled shale block was used and examined using SEM before and after the reaction experiment. The flat surface of the ion-milled area allowed us to locate and examine the same area imaged before the experiment. SEM on ion-milled samples provides the clearer evidence of mineral dissolution and precipitation by detailed comparison of the same mineral grains before and after reaction.

The Barnett Shale samples are relatively consistent in mineral compositions between the samples suggesting small mineralogical heterogeneity (Table 17). The Barnett shale sample chosen for the experiment is dominated by quartz, illite, calcite, and chlorite with minor components of plagioclase (albite), K-feldspar, pyrite, kaolinite, ankerite, and dolomite (Table 17). The relatively reactive mineral phases include calcite (5-10%), albite (~1%), and pyrite (~2%), and to a lesser degree dolomite (0.6%), ankerite (0.6%), and K-feldspar (<1%) consistent with descriptions of Milliken et al. (2012).

Mineral compositions of the reacted samples are similar to the unreacted for most mineral phases (within 3% analytical error 3% of the XRD method). However, the reacted samples from Exp. C and F show >3% of calcite increase and illite decrease compared to the unreacted sample. Calcite was dissolved during the experiment based on the results from aqueous chemistry and SEM examination, which would lead to lower calcite abundance in the reacted sample. The addition of

calcite to the reacted samples can only be attributed to sample heterogeneity which is still significant even on centimeter scale. Because the destructive nature of the XRD method, different rock chips from the same sample block were used for each analysis. Mineralogy variations across shale laminations and beds are notable and can lead to different XRD results.

Table 17. XRD Mineral Composition of Unreacted and Reacted Shale Samples

Sample	Quartz	Illite	Chlorite	Kaolinite	Calcite	Dolomite	Ankerite	Albite	K-feldspar	Pyrite
Unreacted	43.99	36.56	6.20	0.88	6.27	0.61	0.6	1.1	1.32	2.47
Blak-A	43.66	37.82	6.14	1.86	5.00	0.61	0.58	1.29	0.25	2.79
Blak-C	43.47	32.27	7.02	1.32	11.14	0.65	0.86	0.79	0.34	2.14
Blak-F	41.55	34.19	6.54	1.65	10.77	0.81	0.77	1.28		2.44

XVIII-2-1.1 Unreacted Barnett Shale Sample

The unreacted sample is abundant in clay minerals. SEM images of rough sample surface show dominant fibrous clays and clay-sized quartz with occasional silt-sized mineral grains (Figure 113A). Silt-sized mineral grains are usually surrounded and isolated by clay matrix (Figure 113B-D). Clayey matrix and elongated mineral grains align along the bedding (Figure 113A, B, D). Most calcite occurs as isolated grains (Figure 113B, C, E). Calcite grains sometimes show smooth surface. Rare calcite cements were observed (Figure 113F). Except quartz and calcite, other mineral grains, such as albite, K-feldspar, and pyrite, often occur as euhedral or sub-euhedral crystals (Figure 113B-F). K-feldspar and plagioclase (mostly albite) generally appear as sub-euhedral tabular crystals with relatively smooth surfaces (Figure 113B, D, F). Pyrite usually occurs as framboids (Figure 113E, F), however, large pyrite crystals of several micrometer in size also exist (Figure 113B).

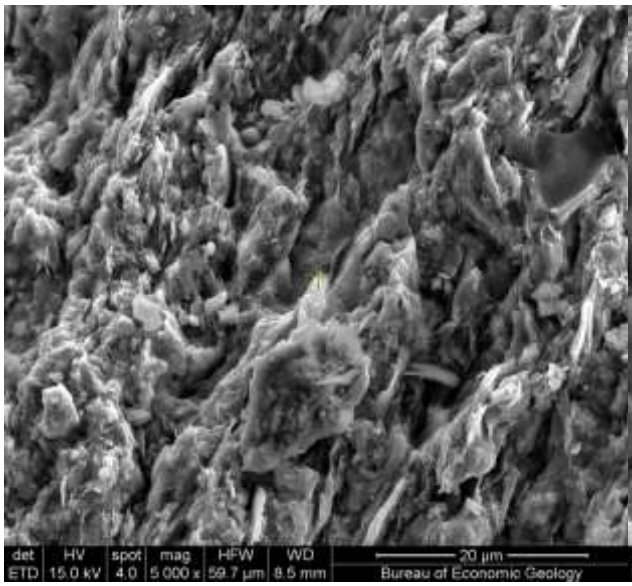

A) Typical view of rough surface with fibrous clay covering and surrounding other mineral grains. SE image.

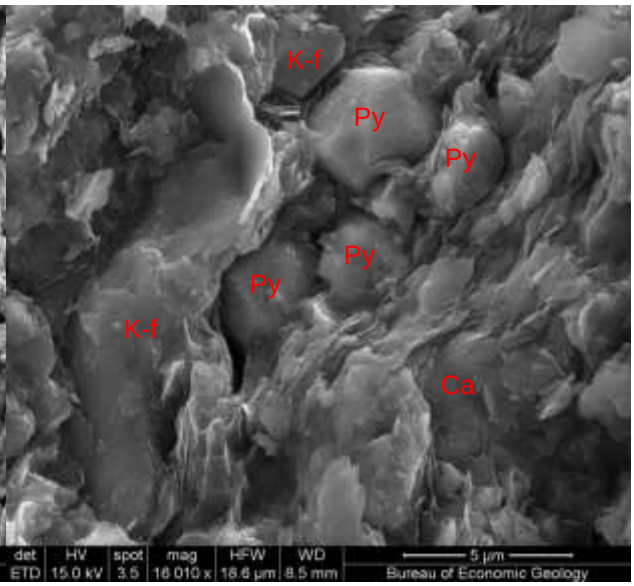

B) pyrite crystals (Py), K-feldspar (K-f) and calcite grains (Ca) are surrounded by clay minerals. SE image.

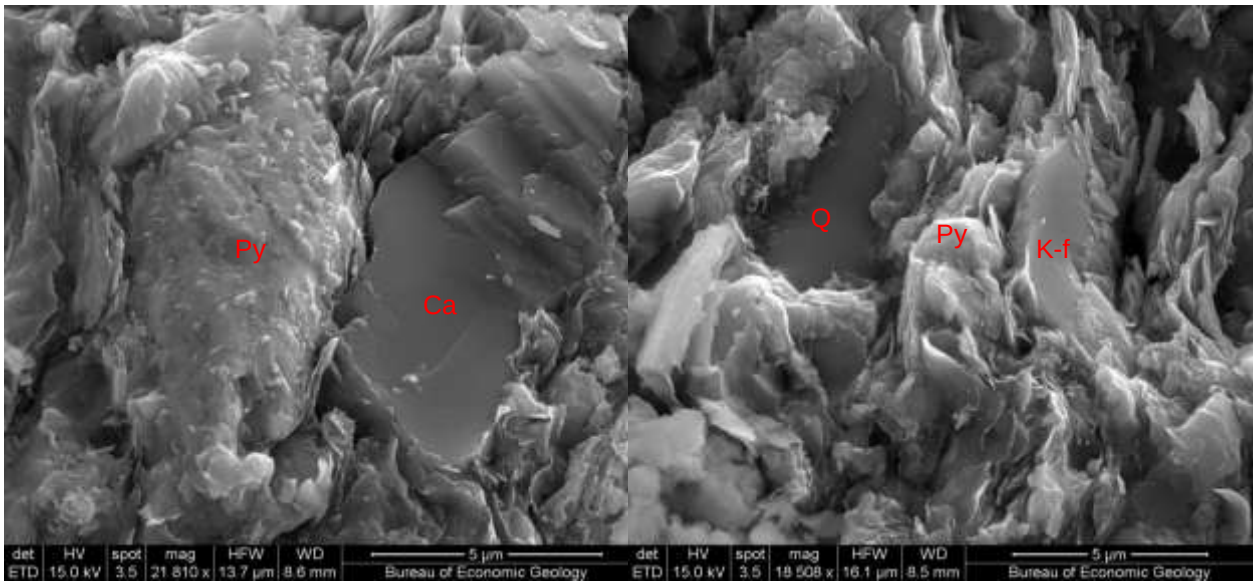

C) A calcite grain with a fresh-looking surface next to a pyrite grain. SE image.

D) K-feldspar grain with a fresh smooth surface. SE image.

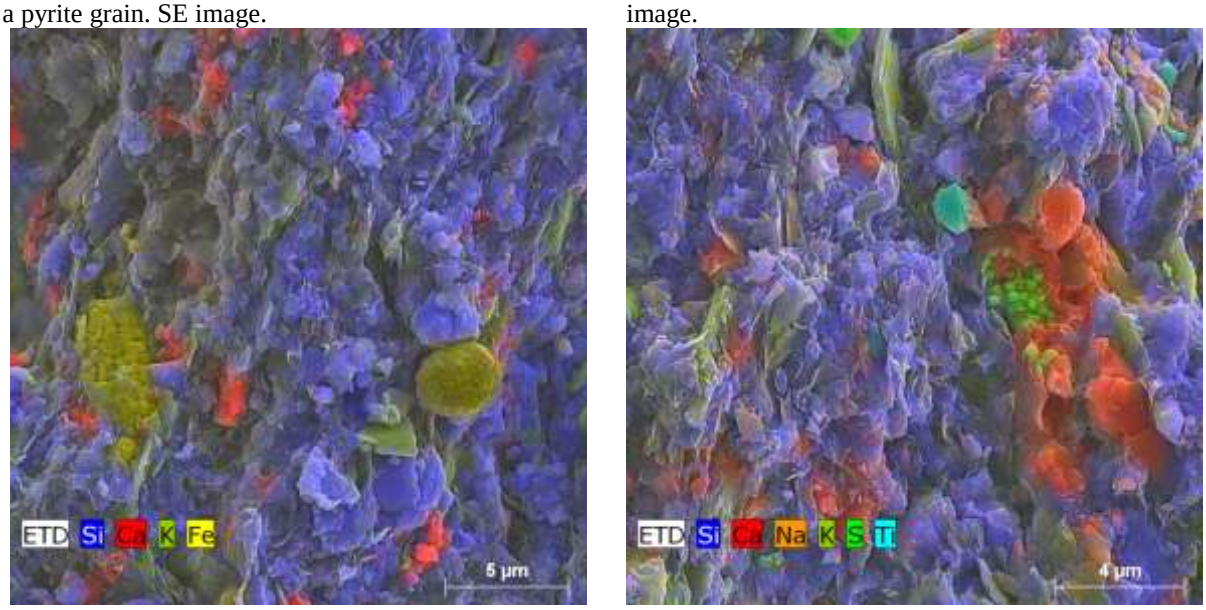

E) The view area dominated by quartz and clays (blue) and dotted with calcite (red), K-feldspar (light green) , pyrite (yellow). EDS map overlying SE image.

F) Calcite grains and cements (red) surrounding pyrite framboid (green) in a silicate dominated rock. EDS map overlying SE image.

Figure 113. SEM and EDS images of the unreacted rough sample Barnett sample

SEM of ion milled surface is a better approach to show intergranular texture and porosity. With the aid of ESD mapping, spatial distribution of minerals is also easier to study. The ion-milled area is shallow cone shape about 5 mm wide and 1 mm high. Considering the small grain size of the Barnett sample (<20 µm), such an area may stride across several laminations, therefore, offer a good representation of the heterogeneity of the bulk rock. Figure 114A shows a polished area adjacent to the ion-milling scarp. The polished surface contains sufficient diversity of minerals and the observation on this area offers a good proxy to the rock-water reactions of the bulk rock.

The ion-milled unreacted sample was studied with and without iridium coating. With the coating, higher magnification and EDS analysis can be used. However, without the conductive coating

concealing some of the fine details of the rock texture, the SE-SEM images reveal considerably more details of the matrix. One of the drawbacks of using non-coated sample is that resolution suffers and the images become too noisy at magnification higher than ×20,000. However, such magnification is sufficient for observation of grain dissolution.

Figure 114B-F reveals more clearly the texture of the silt grain and matrix. Silt-sized grains are commonly floating in clay-sized particles which mainly consist of quartz and clay minerals (Figure 114B-D, F-H). Organic matter appears as dark-gray to black particles and can be easily differentiated from pores (Figure 114B, E). Clay plates and fibers are better revealed on ion-milled surface. Large clusters of clay with significant volume of pore spaces between the clay platelets were also observed (Figure 114C, D). These relatively large pores are significant host sites of the formation water which will be release to the flow back water after hydraulic fracturing. Organic matters (OM) in the Barnett shale often contain nanometer-sized pores (Figure 114E).

EDS maps overlying SE images display mineral composition and distribution within the view area. The maps aids greatly in characterizing the distribution of the reactive mineral phases, such as calcite, pyrite, albite, and K-feldspar by signing the bright artificial colors to the elements of Ca, Fe, Na and K. Consequently, these minerals stand out against a blue background of the silicate matrix when Si is tagged as blue. Calcite occurs as grains of >10 μm in size (Figure 114F, G) as well as aggregates of grains <1 μm (Figure 114H). Pyrite framboids and single crystals are sparsely distributed, but it is ubiquitously present in the sample. Dolomite mostly exists as rhombic grains which commonly contains Fe as EDS analysis shows. Trace amount of titanium oxide were also observed in EDS maps (Figure 114G).

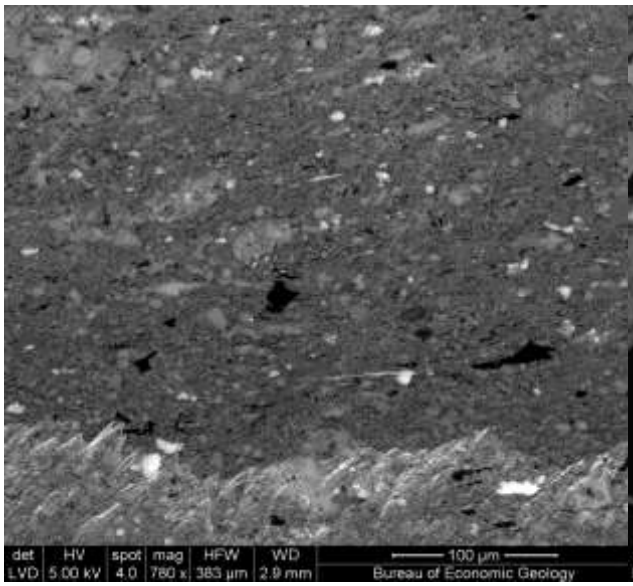

A) Typical ion-milled surface with edge of the milled area visible at the bottom. Milled surface perpendicular to bedding. No coating applied.

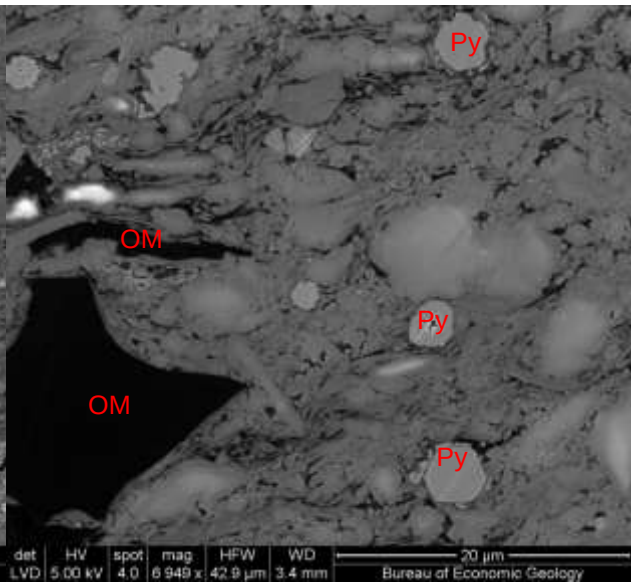

B) Organic matter (OM) shows up as dark areas on milled surface. More texture details of intergranular areas can be seen on uncoated surface. No coating applied.

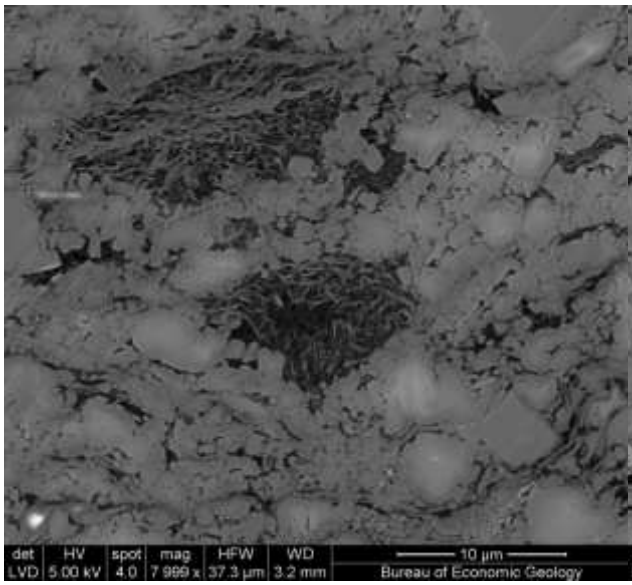

C) Large intergranular spaces filled with fibrous clays. No coating applied.

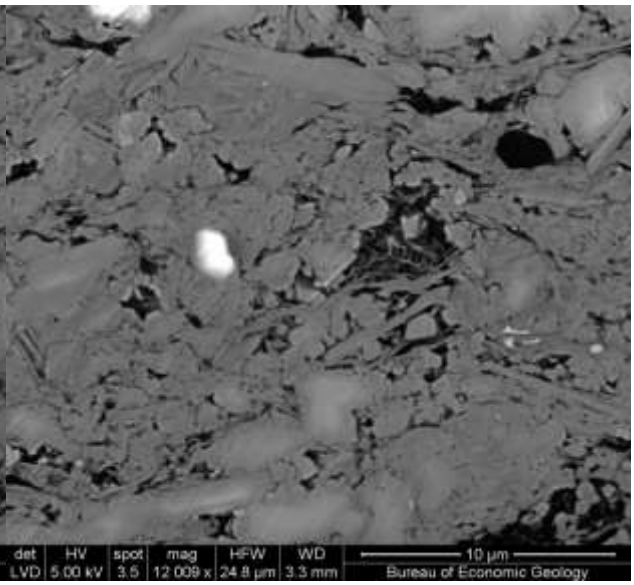

D) Large intergranular spaces filled with fibrous clays. No coating applied.

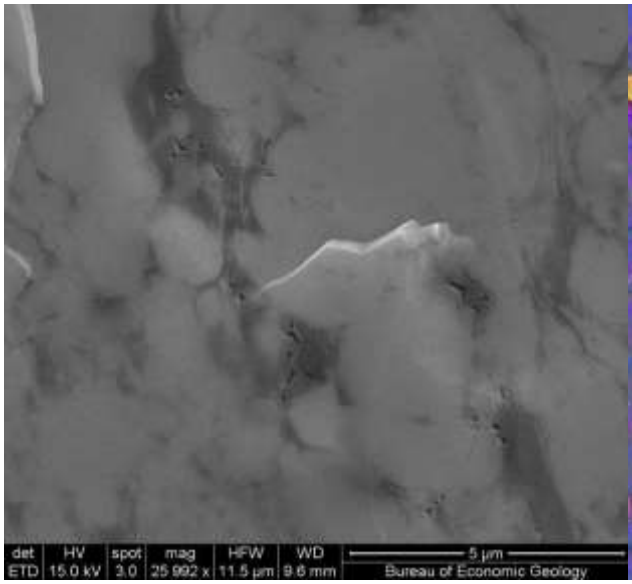

E) High magnification SEM image of coated sample showing nanometer-sized pores developed in organic matter (dark gray). With iridium coating.

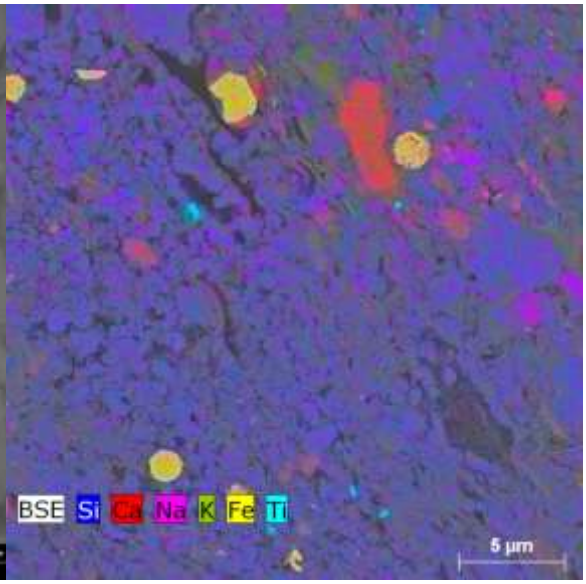

F) EDS map showing a typical silicate mineral (blue)-dominated view area with occasional calcite (red) and pyrite (yellow). Organic matters show as dark area. With iridium coating.

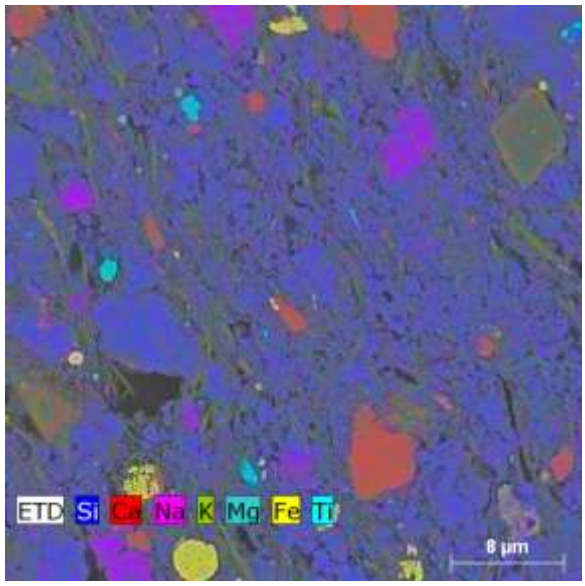

G) EDS map showing several calcite (red), dolomite (olive green), pyrite (yellow), and albite (purple) grains among quartz and clay materials (blue). With iridium coating.

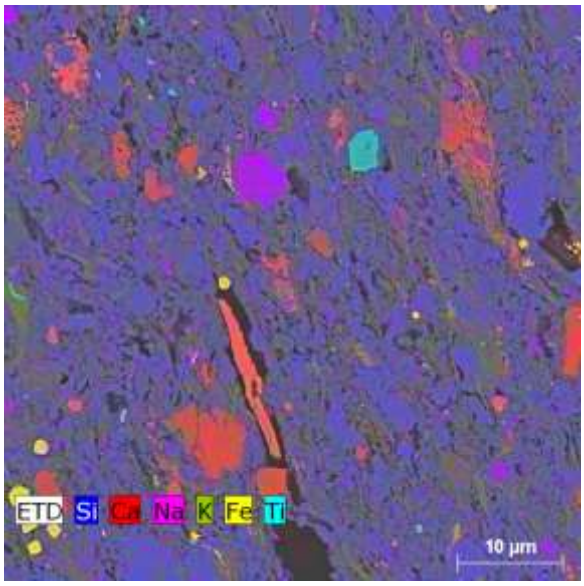

H) EDS map showing prominent beddings. Calcite (red), albite (purple) and quartz (blue) several calcite (red) are the major silt sized grains. A titanium oxide crystal shows up as cyan. With iridium coating.

Figure 114. SEM and EDS images of the unreacted ion-milled Barnett sample

XVIII-2-1.2 Reacted Samples

SEM examination of rough surface is able to show 3D views of individual mineral grains and better characterize topography of the grain surfaces. By characterizing and comparing surface topography of minerals before and after the reaction, one can deduce potential dissolution and precipitation of mineral phases occurred during the experiments. SEM images of reacted rough samples are shown in Figure 115.

One ion-milled core block was reacted with 20g/L NaCl solution at 80^0C and 200 bar in experiment Blak-F. At the end of the experiment, the polished sample block was carefully retrieved and rinsed with DI water. Then it was dried in oven at 70^0C overnight. The sample was examined using a low vacuum detector without conductive coating applied on its surface. The SEM images in Figure 116 were taken from the untreated reaction surface. Because a layer of deposits formed during the experiment and covered the previously ion-milled surface, the sample was subjected to ion-milling again to remove the layer of precipitates so that the underlying minerals are exposed for comparison with those in the unreacted sample. The re-milled surface was examined without iridium coating and then, with a coating applied (Figure 117).

On rough rock surfaces, it is difficult to identify dissolution-derived intergranular pores; therefore it is difficult to determine mineral dissolution when the whole grains are removed. This is the case for carbonate minerals whose remaining was rarely found on the reaction surface. Most calcite grains have been completely dissolved leaving no traces behind.

Only evidence of mineral dissolution in the reacted rough samples exists at the sites of dissolution relics. Figure 115A shows that a partially dissolved K-feldspar grain with distinct dissolution steps and kinks. Dissolution of pyrite may have occurred too as some pyrite framboids show crystal pits suggesting partial dissolution (Figure 115B, C). However, pyrite in

the reacted ion-milled sample does not show evidence of dissolution as most pyrite framboids remain physically intact.

Reacted surfaces are often littered newly formed clay flakes and iron oxide droplets and disks (Figure 115D-F). New precipitates tend to form clusters or chains on rough surface (Figure 115D-F), while they cover the polished sample surface ubiquitously (Figure 116).

The reacted samples from different experiments do not show notable differences. Evidence for geochemical reaction was found in the fresh dissolution features associated with the reactive minerals. Qualitative observations suggest that the samples reacted in DI water show relatively more distinct dissolution features than those reacted in brines. Water chemistry results are more diagnostic to quantify dissolution.

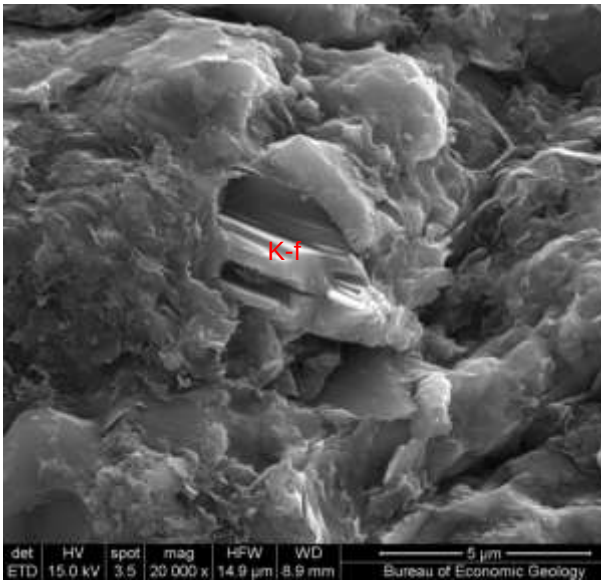

A) A K-feldspar grains showing corrosion features. Exp. A (DI water, 80 ^{0}C, 200 bar).

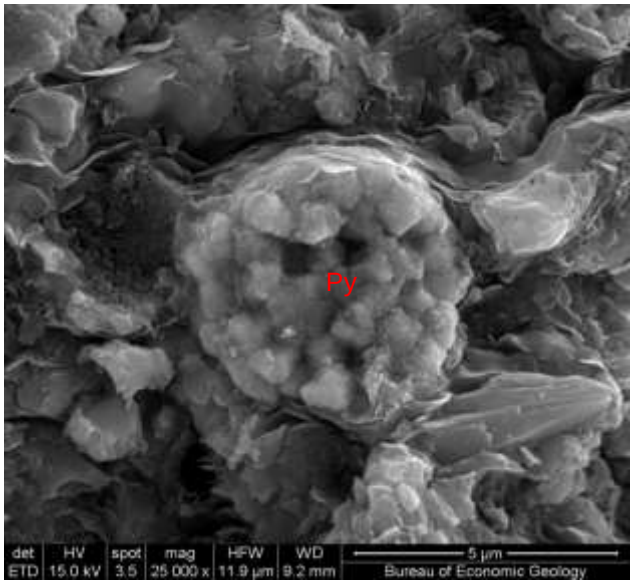

B) A pyrite framboid (Py) may have been partially dissolved. Pyrite crystals no longer showing smooth dotted with new precipitates, most likely iron oxides. Exp. A (DI water, 80 ^{0}C, 200 bar).

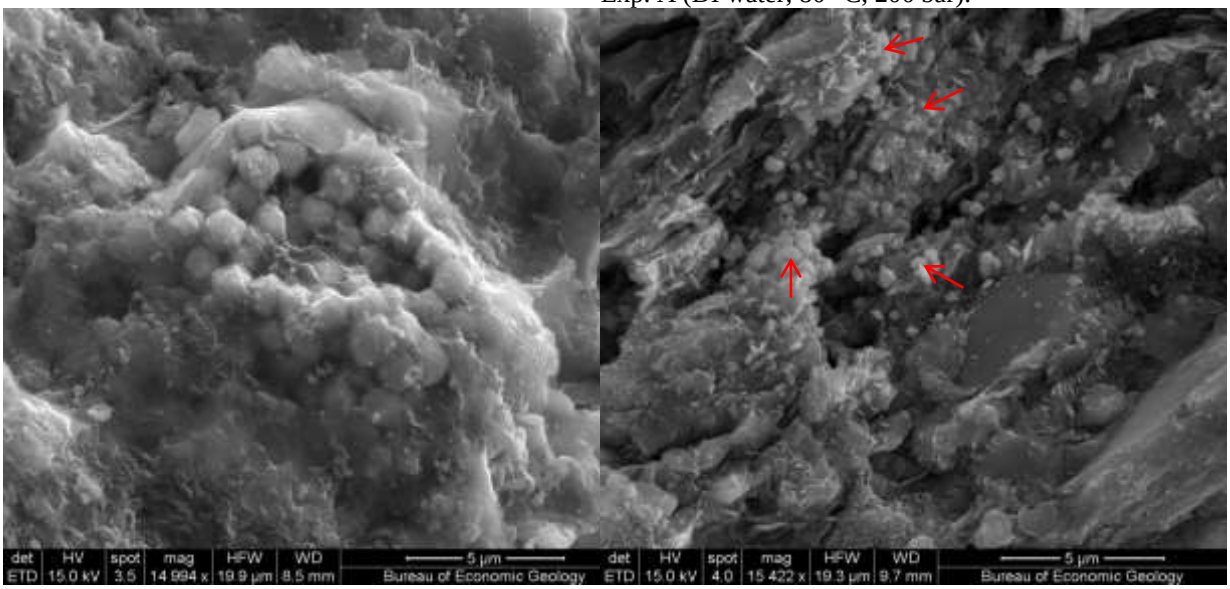

C) Pyrite framboid with missing crystals, littered with new precipitates. Exp. E (2k KCl, 80 ^{0}C, 200 bar).

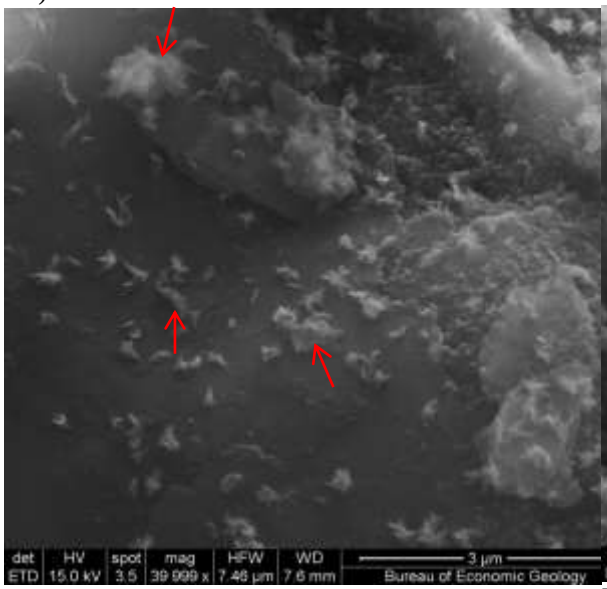

E) Flaky clay minerals precipitated on mineral surfaces. Exp. E (2k KCl, 80 ^{0}C, 200 bar).

D) Reacted mineral surfaces littered with disks of iron oxides (arrows) and clay flakes. Exp. A (DI water, 80 ^{0}C, 200 bar).

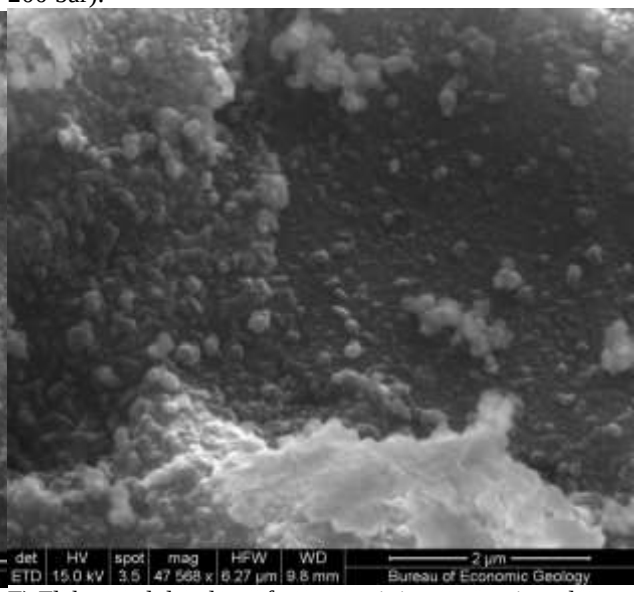

F) Flakes and droplets of new precipitates on mineral surface. Exp. D (2k $CaCl_2$, 80 ^{0}C, 200 bar).

Figure 115. SE-SEM image of reacted rough surfaces (Blak-A, -D, -E)

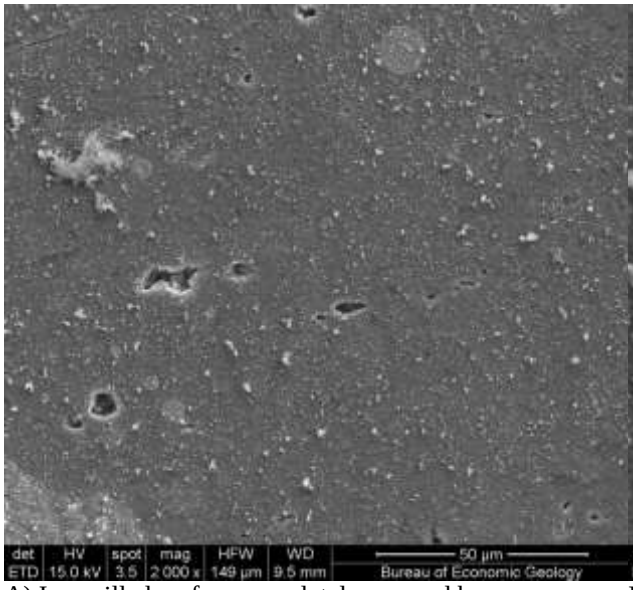

A) Ion-milled surface completely covered by new precipitates and dotted with dissolution pits. Original petrographic texture is no longer seen. Reacted with 20g/L NaCl solution at 80°C and 200 bar (Blak-F).

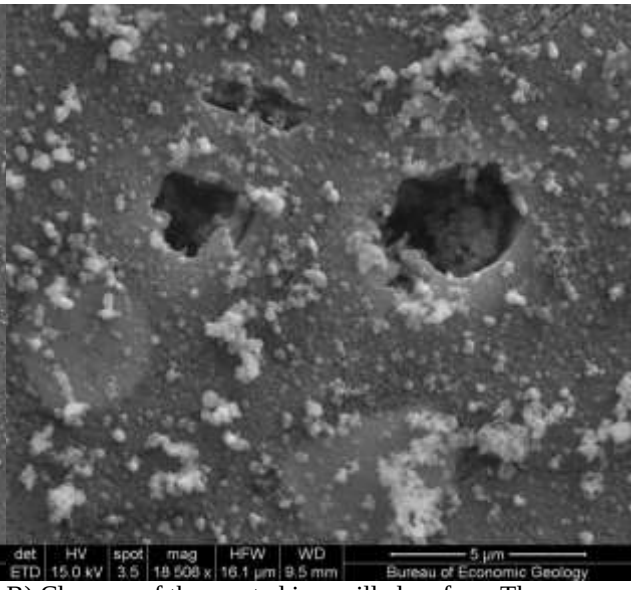

B) Close up of the reacted ion-milled surface. Three micrometer-sized holes indicate dissolution of mineral grains. The whole area is covered by spherical and fibrous precipitates of nanometer size. Original minerals under the layer of the new precipitates is vaguely visible.

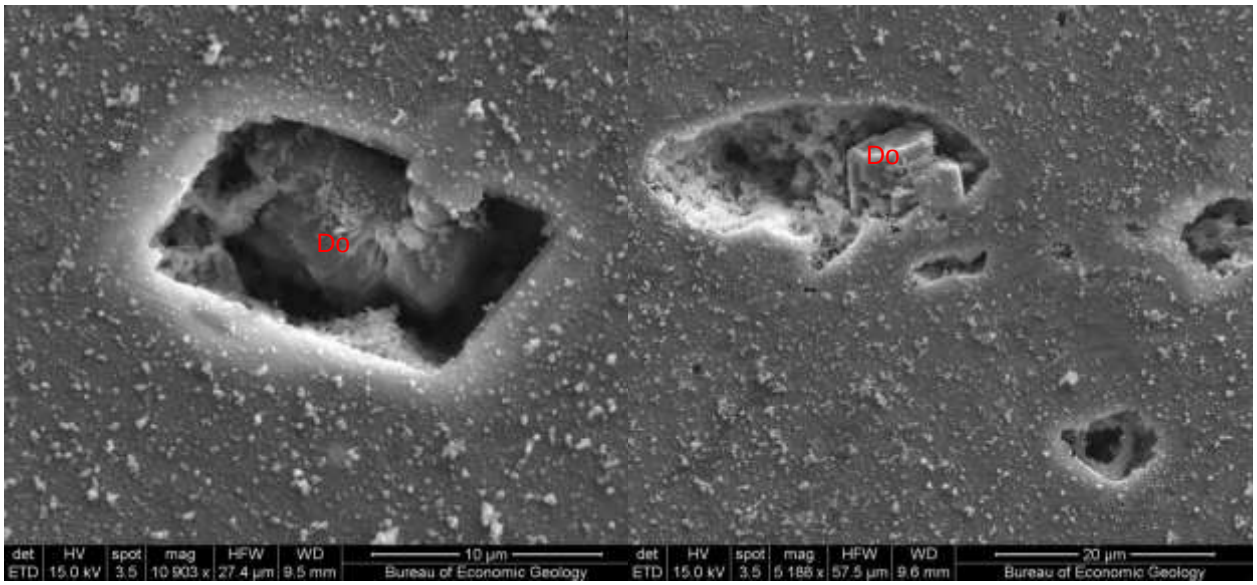

C) A rhombic hole with remaining dolomite (Do) at the bottom, indicating it was formed from dolomite dissolution.

D) Dolomite (Do) relic in a dissolution pit.

Figure 116. SEM images of reacted ion-milled surface after Exp. Blak-F (20k NaCl, 80 ^{0}C and 200 bar). No coating applied.

By far, the ion-milled sample provides the clearer evidence of mineral dissolution and precipitation during the experiment. After the experiment, the polished surface was completely covered by a layer of nanometer-sized precipitates and dotted with holes up to tens of micrometer (Figure 116A). The original surface underneath the layer of newly-formed clays, iron oxides and possibly other minerals is no longer visible. The outlines of mineral grains and mineral contacts are vaguely discernible at places. The precipitates appear as spheres, disks, and flakes of 10s to 100s nanometer in size (Figure 116B).

The dissolution holes and pits tend to inherit the outlines of the dissolved minerals (Figure 116B-D). The most distinctive ones are those formed from dolomite dissolution which produced diamond shaped holes (Figure 116C). Dolomite relics were detected by EDS scan at the bottom of some dissolution sites, suggesting origin of the dissolution pits (Figure 116C, D). Calcite dissolution was more complete and little calcite was left in the dissolution holes. Calcite grains usually has anhedral to subhedral outlines, therefore the shape of the dissolution holes is less diagnostic for determined their origin.

To remove the layer of new precipitate and reveal the original polished surface, the reacted sample was subjected to a short period of ion-milling for 2 h. The layer of new precipitates was largely milled away while some part of the surface is still covered by a much thinned layer (Figure 117A-C). The remilled surface show better views of the dissolution features. It also shows that dissolution did not occur to mostly of mineral phases, rather it focused on certain mineral grains. Individual dissolution pits ranging from < 1µm to 10s µm in size are all bounded by the extent of the precursor mineral grains which are carbonates in most cases (Figure 117A-C, G). Other mineral phases and organic matters do not show evidence of alteration (Figure 117H).

The new precipitates in the dissolution pits were protected from the remilling. EDS scans show that these materials contains strong signal of iron and weak signals of Al, K and Na (Figure 117C, F), suggesting iron oxides are the major components with smaller amounts of clays.

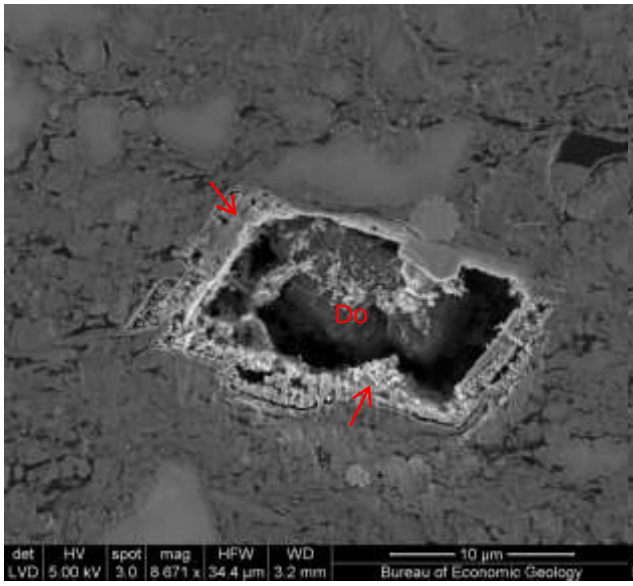

A) New precipitates partially removed from the surface by secondary ion-milling. Dolomite remaining was detected at the bottom of the diamond shaped dissolution pit whose edge is lined with newly precipitated iron oxides and clays (arrows). The surrounding area shows no signs of dissolution. Same view area as Figure 116C. No coating applied.

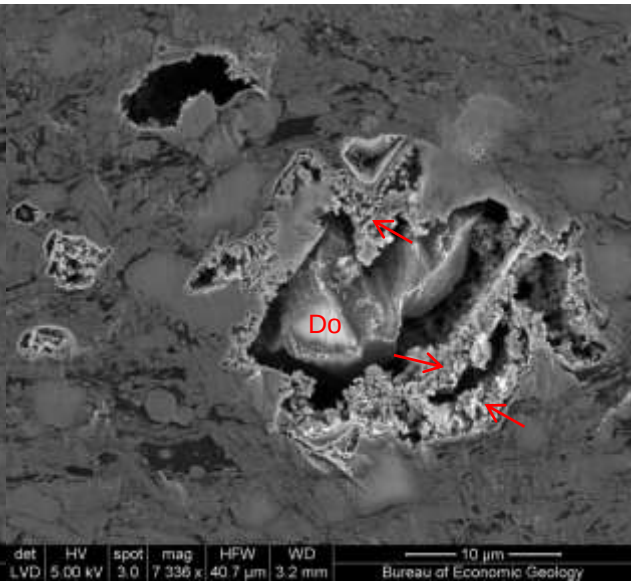

B) A newly formed dissolution pit partially filled with iron oxides and clays (arrows). Dolomite at the center of the pit indicates that the pit was derived from dolomite dissolution. No coating applied.

C) EDS map showing FeOx precipitates partially filling a rhombic pore derived from dolomite dissolution. With iridium coating.

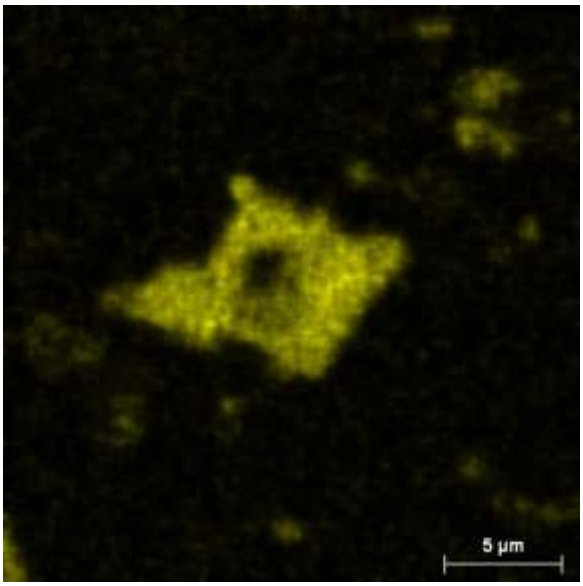

D) EDS map showing distribution of Fe in the same view area of C).

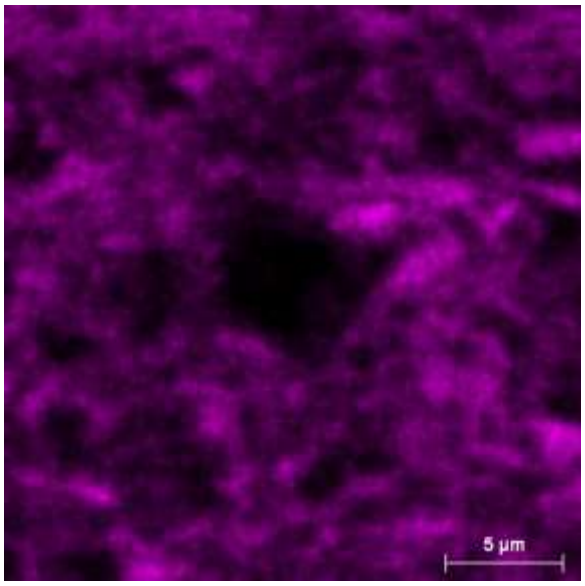

E) EDS map showing distribution of Al in the same view area of C).

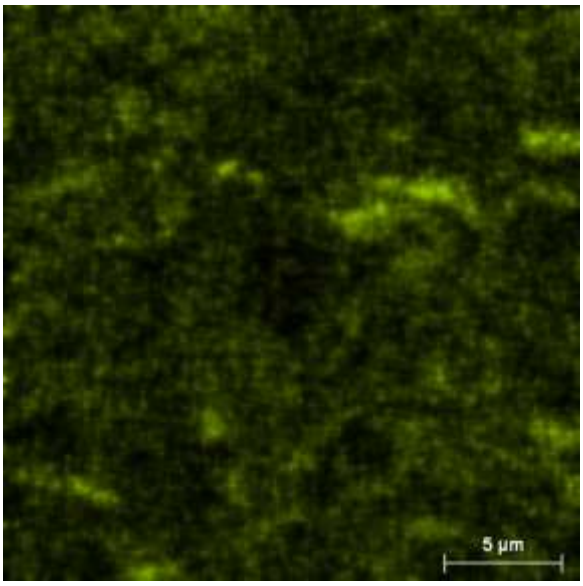

F) EDS map showing distribution of K in the same view area of C).

Figure 117. SEM images of re-milled reacted sample after Exp. F (with 20g/L NaCl solution, at 80 ^{0}C and 200 bar)

Efforts were made to relocate the examined areas before and after the reaction experiment sample and compare the surface topography. It was made possible by the short period of remilling which revealed the original surface. By locating the characteristic mineral grains and organic matters, SEM image were taken at the exact view areas that were previously imaged before the reaction experiment. The comparison can be made between the two sets of images (Figure 118). The major alteration on the reacted surface is the formation of the dissolution pits. Judging from their location and shape, it can be determined that most dissolution occurred on calcite and dolomite grains. Carbonate grains appear to be bright and glowing in the LVD-SEM images (Figure 118A, C, E) and those white grains all disappeared and replaced by holes on the reacted surface. Almost all calcite grains were completely consumed in the experiment, while some dolomite grains partially survived because dolomite dissolution rate is two orders of magnitude slower than calcite.

Figure 118 shows that dissolution is limited to carbonate minerals. Pyrite framboids were mainly kept intact, as well as other mineral phases. No alteration of organic matter was detected, no additional pores were created in the large OM grains, suggesting they are solids.

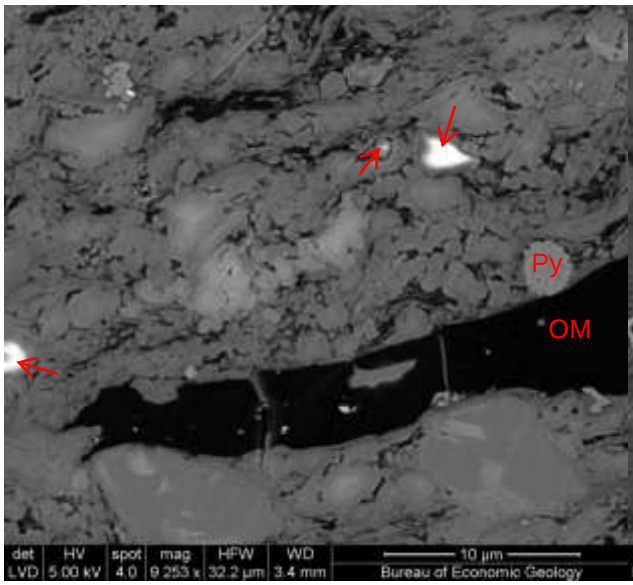

A) Unreacted ion-milled surface. Calcite grains are easily identified as they show up as the brightest grains (arrows). No coating.

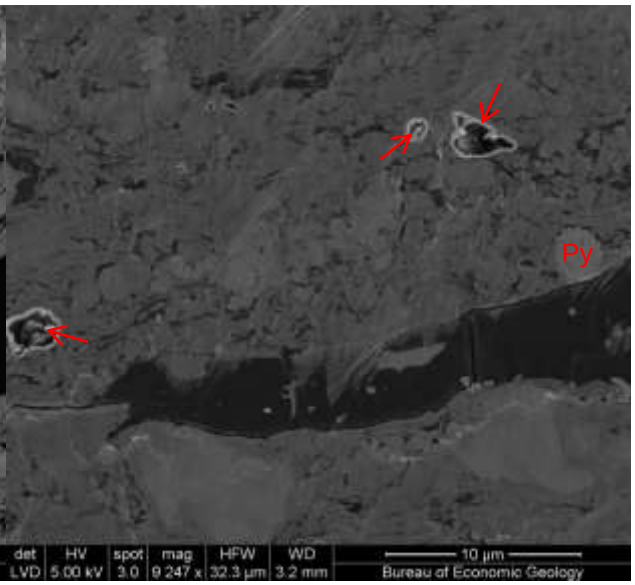

B) Reacted remilled, still partially covered by new precipitates. Some dissolution pits are visible compared to the unreacted surface. The large dissolution holes (arrows) were formed from carbonate minerals. No coating applied.

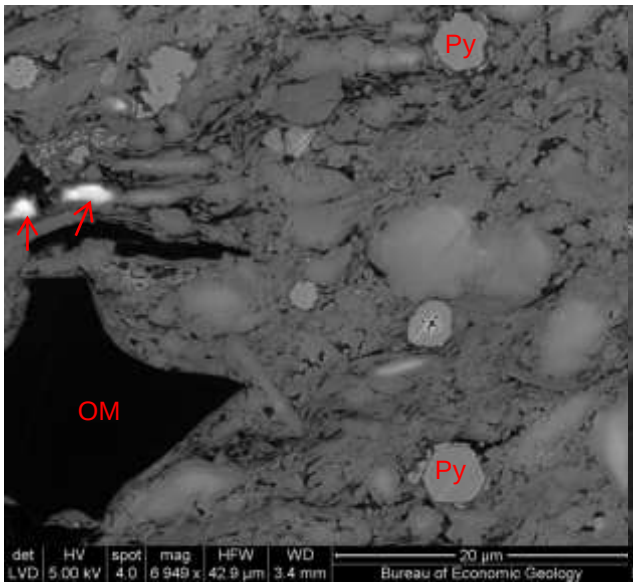

C) Unreacted ion-milled surface. No coating.

D) Remilled reacted surface, still partially covered by new precipitates. Some dissolution pits formed from the previous sites of calcite. Pyrite framboids do not show signs of alteration. No coating applied.

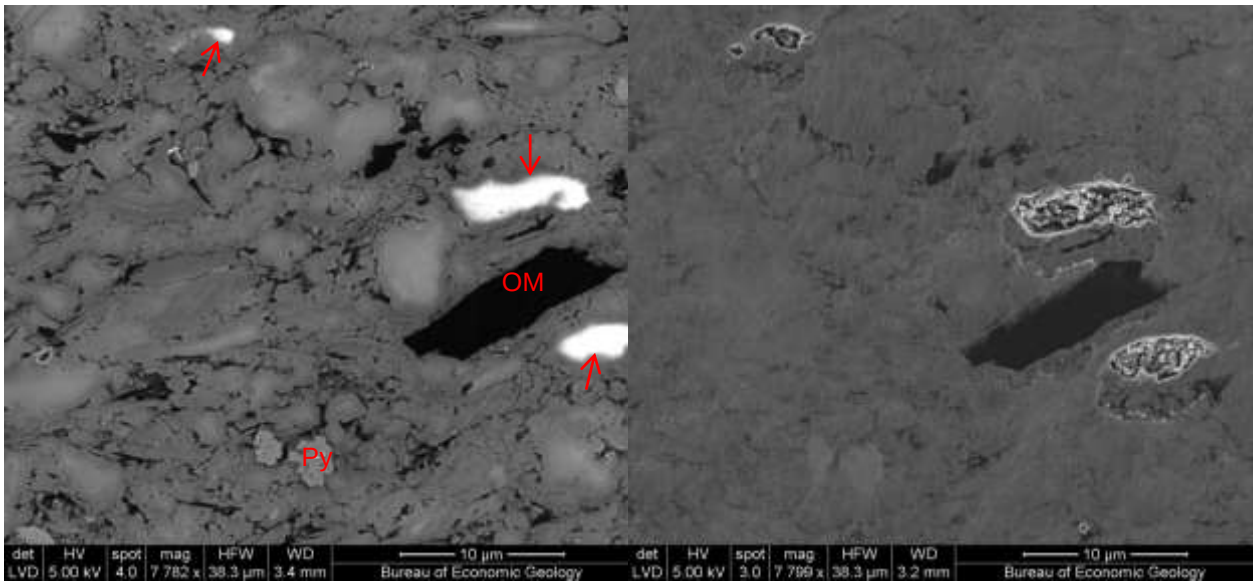

E) Unreacted ion-milled surface. Calcite grains show up as the brightest grains. No coating applied.

F) Remilled reacted sample surface, partially covered by new precipitates. Dissolution pits are derived from carbonate dissolution. No coating applied.

Figure 118. SEM images obtained from the same view areas of the unreacted and the reacted remilled surface after Exp. F.

XVIII-2-2 Experimental Results of Aqueous Chemistry

We performed a total of five complete autoclave experiments (+ 1 failed run). Time-evolution plots of individual element concentrations are displayed in Attachment B. In these experiments the ionic strength of the reaction solution were changed to explore the effects of these changes on the elemental release rates. The ionic strengths of the solutions were changed from DI water, to ~2,000 ppm solution, to 20,000 ppm NaCl. Some experiments also tested the impact of the ionic makeup using NaCl, $CaCl_2$, and KCl. Autoclave experiments use ~16 g of rock and ~160 ml at 80°C and 200 bar, conditions close to bottom hole conditions.

XVIII-2-2.1 General observations:

Major elements (Na, Ca, K, Cl, SO_4, HCO_3) display concentrations at the end of the experiments ranging from a few tens of ppm to hundreds of ppm (Figure 119). Concentrations of the first sampling point slightly after time zero range from 0 to sometimes tens of ppm for Na and Cl as can be observed in DI experiments (Figure 121). Mg and K are the only "major" element with low ppm-level concentrations in these experiments. A few minor elements hover around the ppm mark (a fraction of a ppm to a few ppm): Li, NH_4, Mg, K, F, B, Al, Si, Mn, Fe, Ni, Mo, and Sr. Concentration values for the following trace elements range in the tens of ppb: V, P, Cr, Ti, Cu, and Ba whereas Zn, As, Se, Zr, Rb, Cs, Sb, and Tl are generally present at the ppb level and Ag, Cd, Sn, Pb, Bi, Th, and U at the <1ppb level. Concentrations of some trace elements are low because either they are not present in the system or they sorb strongly to the rock substrate. Some elements could have been leached from the autoclave reactor walls (Table 12) mostly Fe, Cr, and Ni. Other results in the autoclave A experiments show also high values suggested contamination. B, Al, Si, V, Mn, Fe, Cu, and Ni are much higher than in the benchtop temperature experiments (the only benchtop experiments with ICP trace metal analyses).

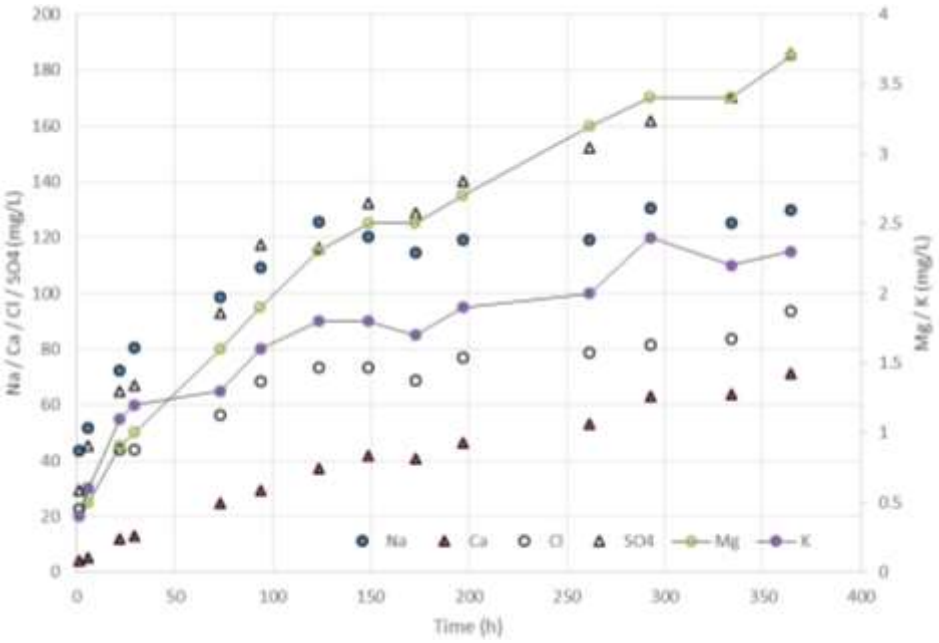

Note: Na, Ca, Cl, and SO_4 concentrations are on the primary y-axis (LHS) where K and Mg which much lower concentrations are on the secondary y-axis (RHS).

Figure 119. Major ion concentration (DI autoclave run – A)

Overall, the time trends of the major cations and anions are similar among all the experiments. Release of K, Ca, Sr, SO_4, Cl and Si are the dominant changes with time (Attachment B). The release rates of these ions (steep slope) were the highest during the first day of reaction and later gradually declined, but concentrations were still increasing at the end of the experiments. The release rate is also faster in the benchtop experiments (higher surface area with ground rock). The alkali metals (Group I of the periodic table) such as K, Rb and Cs (Figure 130b, Figure 134c, and Figure 135b) often exhibits similar behavior as do the alkali-earth elements (Group II) such as Ca, Mg, Sr and Ba (Figure 130f, Figure 130d, Figure 134e, and Figure 135d).

Higher salinity is associated with higher mineral dissolution as demonstrated by the increase in concentrations of major cations at the end of the experiments by a factor of 2 to 3 or higher compared to the DI experiments. Note that Na and Cl (and associated Br) cannot be accurately evaluated because they are the main components of the added salinity in the experiments.

Pyrite oxidation is driving some of the experimental observations such as the increase in SO_4 (Figure 131) and maybe some carbonate dissolution as calcite buffers the pH. It may or may not happen in the field depending on the presence and amount of deliberate (thiosulfates, sulfites) or incidental (gel stabilizers such as amine alcohols) oxygen scavengers.

Approximate pH values (Figure 120) stay relatively stable during most of the experiments. The experiments exhibit pH values ranging approximately from 7 to 8 with a slight downward trend towards neutral pH but still slightly alkaline. Recall that the neutral pH of water goes down with increasing temperature (~6 at 100°C and 7.5 at 0°C). pH was measured only at the beginning and end of the experiment in the DI run A.

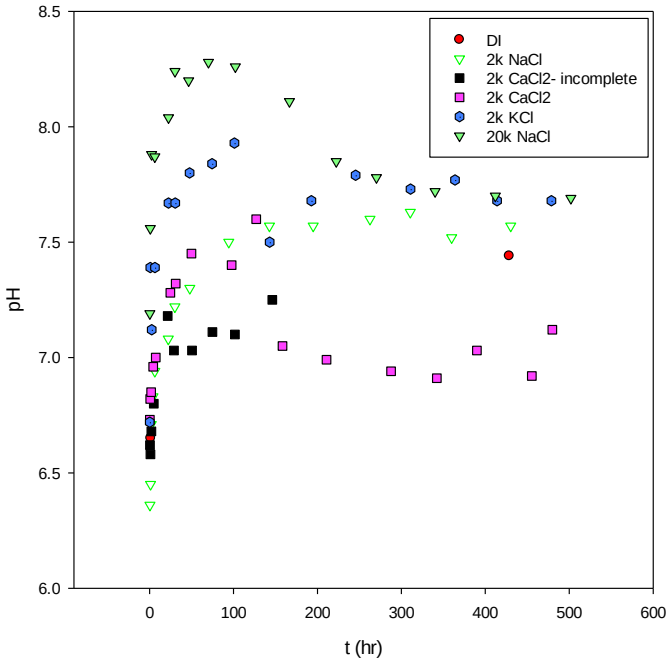

Note: See Methods section for details on how pH was measured; data on Table 18

Figure 120. Approximate pH values during autoclave experiments

Table 18. Approximate pH values during autoclave experiments

DI		2k NaCl		2k $CaCl_2$		2k $CaCl_2$		2k KCl		20k NaCl	
Blak-A		Blak- B		Blak-C		Blak-D		Blak-E		Blak-F	
t (h)	pH	t (h)	pH	t (h)	pH	t (h)	pH	t (h)	pH	t (h)	pH
1.3	6.65	0.5	6.36	0.5	6.62	0.3	6.73	0.23	6.72	0.3	7.19
5.7		1.1	6.45	1.0	6.58	0.8	6.82	0.90	7.39	0.9	7.56
21.8		2.0	6.71	2.2	6.68	1.8	6.85	2.57	7.12	2.4	7.88
29.4		4.1	6.83	5.0	6.80	4.3	6.96	6.35	7.39	6.2	7.87
73.3		6.3	6.94	21.5	7.18	7.3	7.00	22.48	7.67	22.5	8.04
93.6		22.3	7.08	29.1	7.03	24.7	7.28	30.60	7.67	30.3	8.24
123.4		30.1	7.22	50.5	7.03	31.0	7.32	47.62	7.80	46.6	8.20
148.9		48.0	7.30	74.8	7.11	49.8	7.45	74.42	7.84	70.1	8.28
172.6		94.3	7.50	101.6	7.10	97.8	7.40	101.07	7.93	102.2	8.26
196.9		142.7	7.57	146.2	7.25	127.0	7.60	142.98	7.50	166.7	8.11
261.7		194.9	7.57			158.3	7.05	192.75	7.68	222.3	7.85
292.6		262.7	7.60			210.7	6.99	245.40	7.79	270.3	7.78
333.9		310.6	7.63			287.8	6.94	310.95	7.73	340.1	7.72
364.4		360.0	7.52			342.3	6.91	363.93	7.77	412.0	7.70
428.5	7.44	430.3	7.57			390.1	7.03	414.08	7.68	502.0	7.69
						455.4	6.92	478.73	7.68		
						479.8	7.12				

Note: See Methods section for details on how pH was measured
Data plotted on Figure 120

Table 19. Charge-balance-estimated bicarbonate concentrations

t (h)	Time (hr)	HCO_3 (ppm) (calculated)	HCO_3 (ppm) (measured)
A-1	1.3	54.3	
A-2	5.7	47.5	
A-3	21.8	76.3	
A-4	29.4	99.2	
A-5	73.3	131.4	13.9
A-6	93.6	124.9	
A-7	123.4	186.2	19.2
A-8	148.9	167.3	18.4
A-9	172.6	161.5	21.9
A-10	196.9	163.9	23.3
A-11	261.7	167.4	22.6
A-12	292.6	213.3	26
A-13	333.9	186.9	29.4
A-14	364.4	186.3	

Data plotted on Figure 122. The DIC analyzer operates close to its detection limit and values cannot be trusted

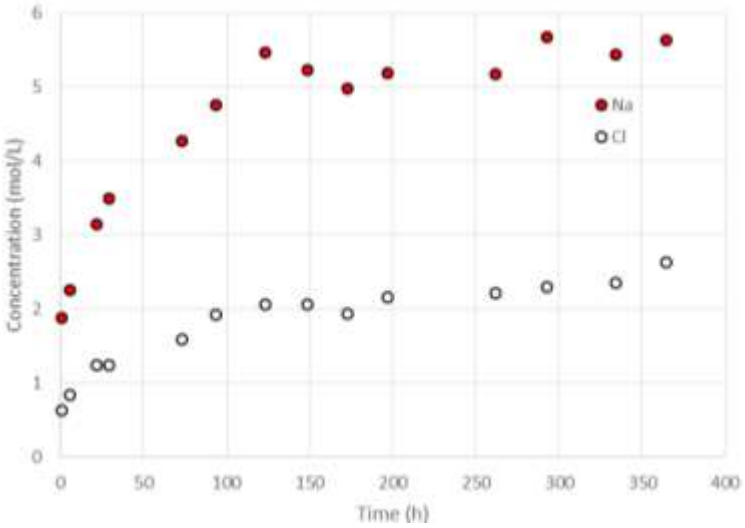

Figure 121. Na and Cl concentrations in NaCl-free experiments (DI).

XVIII-2-2.2 A Note on Heterogeneity

Because of the time-consuming nature of the autoclave experiments, we did not systematically run duplicate or triplicate experiments. Experiments on samples from other shale plays show that consistency between experiments is good. Note that benchtop run cannot be used to test heterogeneity because the ground rock is well mixed and the same batch is used in all benchtop runs. A comparison can be made in this Barnett study between run C that was interrupted because of a leak and run D. Both runs were with 2k $CaCl_2$. A few elements show different concentrations but same trend. They are Co, Cr, Fe, Ni, and Ba. All are related to the presence of O_2 and oxidation of pyrite. The amounts of O_2 impacts oxidation of the metals and indirectly Ba sulfate precipitation.

XVIII-2-2.3 Impact of salinity / Ionic strength

Concentrations of elements increase as the ionic strength increases including for major elements (Figure 130 to Figure 136). Na and Cl cannot be tested because they are added to the solution. Similarly, bicarbonate concentrations (Figure 122) have been estimated through charge balance calculations, which do not work well with added salt because the uncertainties on Na and Cl are larger than the absolute value for bicarbonate. Elemental concentration increasing with salinity is consistent with accepted rock-water interaction geochemical models [note: contamination by reactor material in DI run (A) does not conform to this]. Activity of charged solutes decreases with increasing ionic strength (~salinity), translating into higher concentrations as the solubility product of the dissolved mineral stay constant. SO_4 is not much impacted by salinity (Figure 131b) as it would have if it resulted, for example, from anhydrite dissolution but rather it is likely caused by the oxidation of pyrite controlled by the amount of O_2 in the system. Fe (Figure 133a) follows a similar trend. Other elements whose concentration go down with increasing ionic strength are typically associated with Fe: Cr (Figure 132d), Mn (Figure 132f), Co (Figure 133c), Ni (Figure 133e), and Mo (Figure 134d) although the relationship is not simple in the details. Concentrations of neutral species such as Si (H_2SiO_4 or $SiO_2.2H_2O$) and B (H_3BO_3) show an inverse relationship with salinity as expected (salting out) (Figure 131d and Figure 132a) although the Si curves are not as well expressed as in some other shale play experiments.

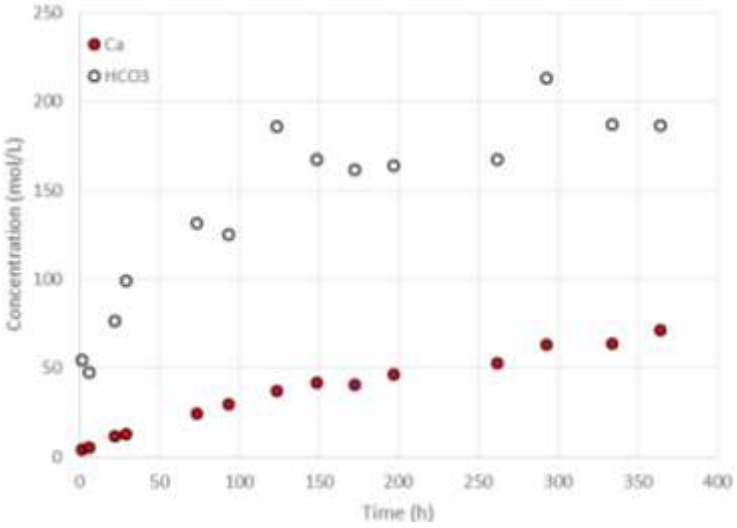

Note: bicarbonate data on Table 19; the 2 high HCO3 values slightly out of trend correspond to the same Na points on Figure 121

Figure 122. Ca and Charge-balance-estimated bicarbonate concentrations (DI experiment A).

Most element concentrations increase through time regardless of salinity (that is, even if increasing salinity brings down overall concentrations, they are still increasing for a given salinity) [with the contamination caveats for DI run A]: Li, K, Na, Mg, NH_4, Ca, F, SO_4, B, Si, Mn, Co, Zr, Ni, Rb, Mo, Sr, Ag, Cd, Cs, Sb, and Ba. Exceptions are Al, V, P, Cr, Ti, Fe, Cu, and Se, that show an initial peak then downward concentrations. Some elements shows the same general trend but with a fatter peak (As) or slow decrease after the peak (Tl). Some elements show non-monotonic behavior for a single salinity: Mn in the DI experiment and Cd in the 50k experiment. A decrease in concentration for Fe can be attributed to precipitation of FeOx minerals that will then accept sorption from V and As, oxyanions negatively charged at the

slightly alkaline pH's of the experiments. Al goes into building new clay minerals and Tl, which belongs to the same group as B and Al but behaves similarly to K, goes with it. However, P and particularly Mo do not conform to the oxyanion explanation as it keeps increasing to multi-ppm values (Figure 134d). P increase may be related to phosphorite layers in the shale and Mo is likely sorbed to organic matter, that is, easily mobilized. Note that other oxyanions have concentrations in the tens of ppb level: As = ~5 ppb (Figure 133f), Se = ~20ppb (Figure 134a), V = ~2 ppb (Figure 132b), 2 or 3 orders of magnitude less than Mo, for which the sorption sites may be saturated.

SEM and related observations infer that Ca and Mg (Figure 130d, f) come from the dissolution of calcite and possibly dolomite. Group II elements generally associated with carbonates (Sr, Ba) show a behavior similar to Ca (Figure 134e, Figure 135d). NH_4 (Figure 130e) is very sensitive to the salinity of the solution and is mobilized by DI but drops to lower concentrations as solution salinity increases. Although contamination by NH_4 from drilling fluids is a possibility, it is unlikely as other associated contaminants such as K and Ba do not show undue concentrations. In addition, it has been described that NH_4-rich clays are not uncommon in source rocks (e.g., Drits et al., 2002; Nieto, 2002; Holloway and Dahlgren, 2002).

XVIII-2-2.4 Impact of Ionic Composition

The impact of salinity on element mobilization and mineral dissolution and precipitation was performed on NaCl solutions. In this section, we analyze the impact of the ionic makeup using ~2000 ppm of NaCl, KCl, and $CaCl_2$ of approximate similar ionic strength. Most elements (Li, Mg, B, Mn, Co, Ni, Sr, Ag, Ba) reach higher concentrations when $CaCl_2$ is used, a few reach their maximum with KCl (NH_4, Al, Si, Rb, Cs, Sb, Tl) or NaCl (F, V, Cu, Mo, Cd) and a few are indifferent to the composition of the solution (SO_4, P, Ti, Fe, Zn, As, Se). Some show opposite behaviors such as Cr that displays high earlier concentrations with $CaCl_2$ that drop below that of NaCl and KCl whereas these start low and increase to higher values than that of CaCl2 (especially KCl) (Figure 139d). Sb also shows a complex behavior.

In general, concentrations increase with time for most elements. Plateau is reached fairly quickly (1day) for, for example, Li, P, Co, Zn, As, Rb, Sr, Ag, Cs, Sn, Pb, and U, or still growing after 3 weeks for Mg, F, SO_4, B, Mn, Mo, Cd, and Sb. Other elements are about to plateau after 3 weeks (NH_4, Si, Ti). Some elements show a consistent peak for the 3 curves either early and sharp (for example, Cr,) or broader (Ni, Se, Ba, Tl). Other element concentration go consistently downward (Al). Some concentrations decrease then up and down again (V, Cu, Fe) suggesting complex interactions.

XVIII-2-2.5 Impact of Temperature

We initially designed the temperature experiments to test the practicality of performing experiments at slower kinetics to better access residual fluids or their associated salts (possibly precipitated while the core was in storage). Using DI water (that typically generates less mobilization of major elements), the experimental run at 80°C consistently showed only slightly higher elemental release rates than the experimental run at 0°C (Figure 123 and Attachment B). Note that the experiments were benchtop experiments, that is, the same thoroughly mixed and finely ground powder is used. Although outside of natural reservoir conditions, the 0°C experiments suggests that temperature does not significantly affect elemental release rates.

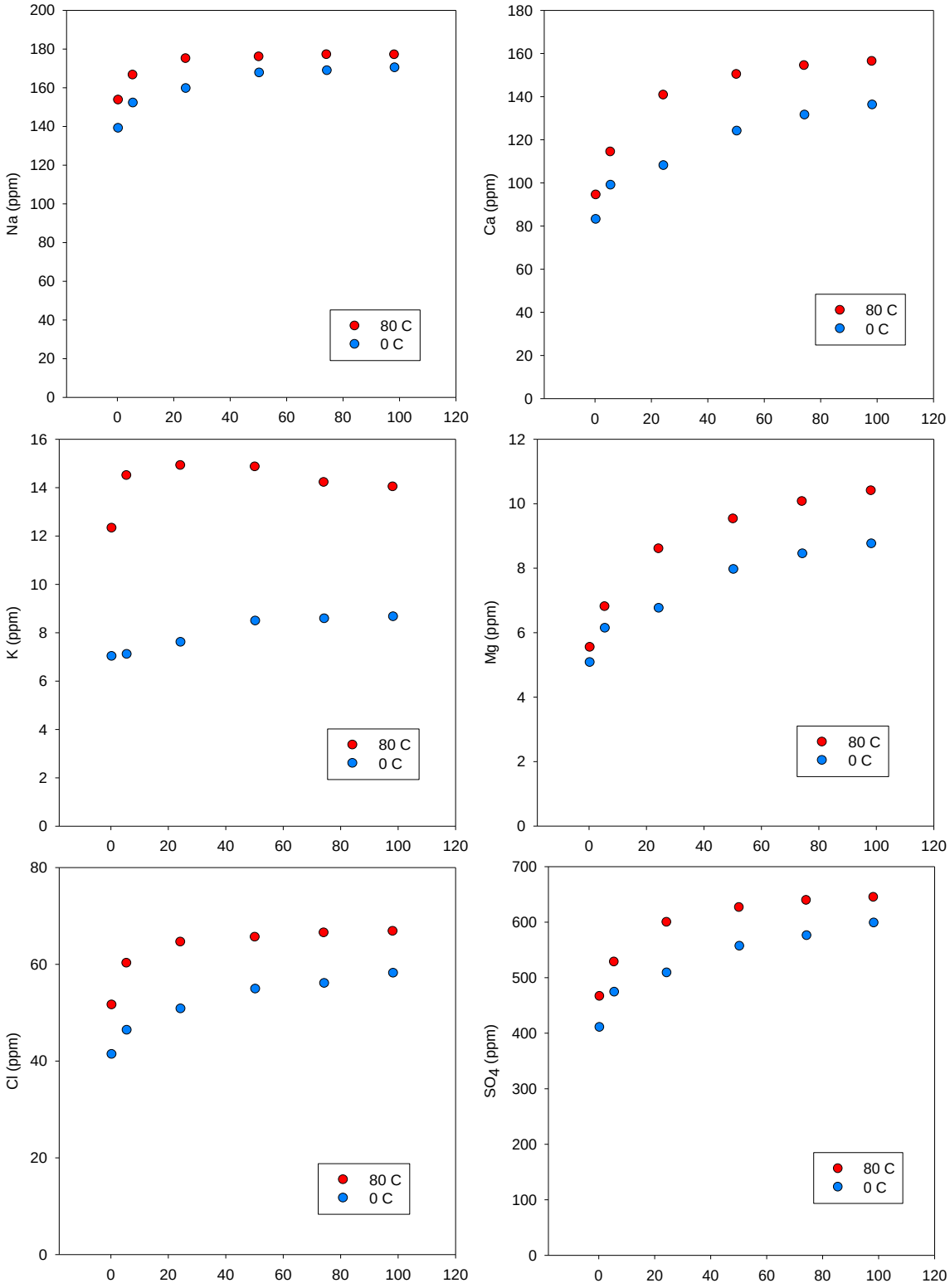

Figure 123. Barnett Shale benchtop experiments with DI at 0°C and 80°C for major species (Na, Ca, K, Mg, Cl, and sulfate)

XVIII-2-3 Other Results

XVIII-2-3.1 Cl/Br Ratios

Cl/Br ratios are useful to determine the source of the chloride. A ratio close to 300 or lower suggests that the origin of Cl is a brine whereas a high ratio close to 1000 suggest that the source of Cl is halite because the NaCl mineral (halite) does not easily incorporate Br in its crystal lattice and the brine becomes enriched in Br. Samples with Cl/Br ratios in the intermediate range suggest a mixture of both. In modern seawater the Cl/Br weight ratio is 293. The Cl/Br ratios of the solution produced in the shale water reactions studies could be determined only for the experiment run with DI water (Blak-A). Because Cl salts were used to prepare the higher ionic strength solutions, Cl/Br ratios were not useful in determining ratios of Cl and Br released from the shale. However, Br concentrations are very close to detection limits such that an accurate concentration could not be easily determined. For several samples, Br fell below the detection limit of the IC's, and this for typical Cl values suggesting a halite origin (that has not been observed), an interpretation opposite to what would be expected. The halite is unlikely to be natural though and would results from contamination. Results of the Cl/Br ratios are outlined in Table 20.

Table 20. Cl/Br weight ratios in DI experiments (Blak-A)

Sample	Cl (mg/L)	Br (mg/L)	Cl/Br w. ratio
Blak-A-1	22.7	BDL	
Blak-A-2	30.0	BDL	
Blak-A-3	44.1	BDL	
Blak-A-4	44.1	BDL	
Blak-A-5	56.5	BDL	
Blak-A-6	68.3	BDL	
Blak-A-7	73.5	BDL	
Blak-A-8	73.5	BDL	
Blak-A-9	68.7	BDL	
Blak-A-10	76.8	BDL	
Blak-A-11	78.8	BDL	
Blak-A-12	81.4	BDL	
Blak-A-13	83.6	BDL	
Blak-A-14	93.5	BDL	
Blak-A-15	22.7	BDL	

XVIII-2-3.2 Porosity / Permeability (MICP results)

MICP porosity and calculated permeability results are listed in Table 21. Porosity of the unreacted sample is 2.28% and permeability is 1.34×10^{-5} mD. Measured porosity of the reacted samples is higher (by >50%) than that of the unreacted samples (Figure 124). Permeability is also higher in the reacted samples than the unreacted (two- to three-fold increase). The cross-plot of MICP porosity and permeability shows consistently higher porosity and permeability of the reacted samples compared to the unreacted. The average porosity of the reacted samples is 3.99% and average permeability is 3.61×10^{-5} mD, over 2 times higher than the unreacted sample. The reacted samples from the different experiments are plotted close to each other in Figure 124, suggesting the reaction conditions and brine chemistry did not cause significant variations in mineral reactions. It should be noted that during MICP data processing, the dissolution pits and holes formed at the sample surface are excluded as surface roughness. MICP tests probe the pore

systems beneath the reaction surface. Therefore, porosity measured by MICP is much lower than that observed porosity at the reacted surface by SEM.

Pore size distribution of the samples is shown in Figure 125. The pores < 3.6 nm are not access by mercury intrusion due to limited intrusion pressure (60,000 psi). These smaller pores apparently constitute of a significant portion of total pore in the shale because the pore size distribution trends indict higher percentile of the pores smaller than the detection limit (Figure 125). Most of sample trends show mode pore size of 5-6 nm.

The unreacted sample clearly shows smaller pore size with the mode pore size of 4.5 nm and higher abundance of pores < 4.5 nm in size. The reacted samples show similar pore size distribution with slightly higher abundances of pore > 4.5 nm. Again, note that during data processing, those large dissolution pores of micrometer in size formed at reacted surfaces are excluded from results as surface roughness. The increase of matrix porosity and permeability may be significant for enhancing gas/oil flow through the matrix to hydraulic fractures.

Table 21. Results of MICP porosity and permeability tests for unreacted and reacted samples

Sample	Experiment	Porosity (%)	Permeability (md)	Density (g/cc)
Unreacted		2.28	1.34E-05	2.379
Blak-A	DI	4.00	3.67E-05	2.369
Blak-B	2k NaCl	3.80	3.42E-05	2.404
Blak-C	2k $CaCl_2$ stopped	3.69	3.20E-05	2.399
Blak-D	2k $CaCl_2$	3.99	3.44E-05	2.416
Blak-E	2k KCl	4.14	3.89E-05	2.378
Blak-F	20k NaCl	4.31	4.02E-05	2.393

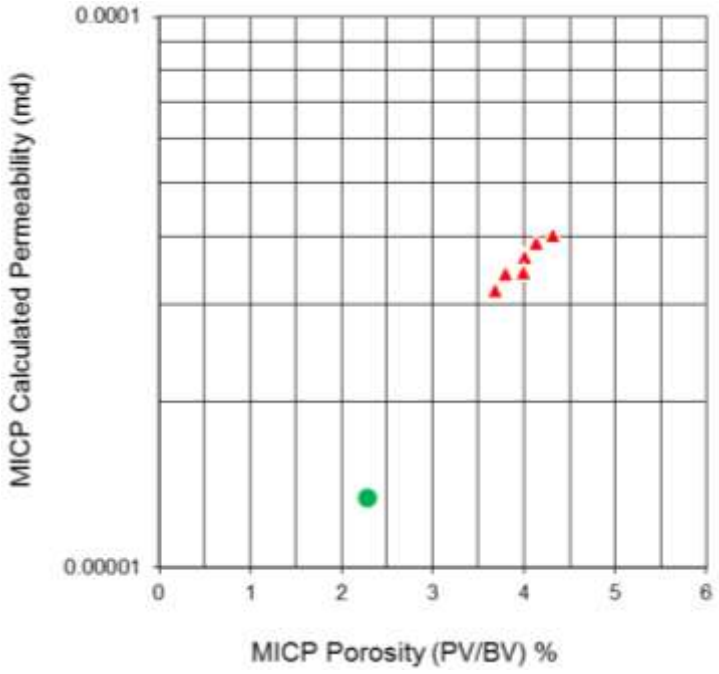

Figure 124. Porosity and permeability of unreacted and reacted shale samples measured in mercury intrusion capillary pressure tests.

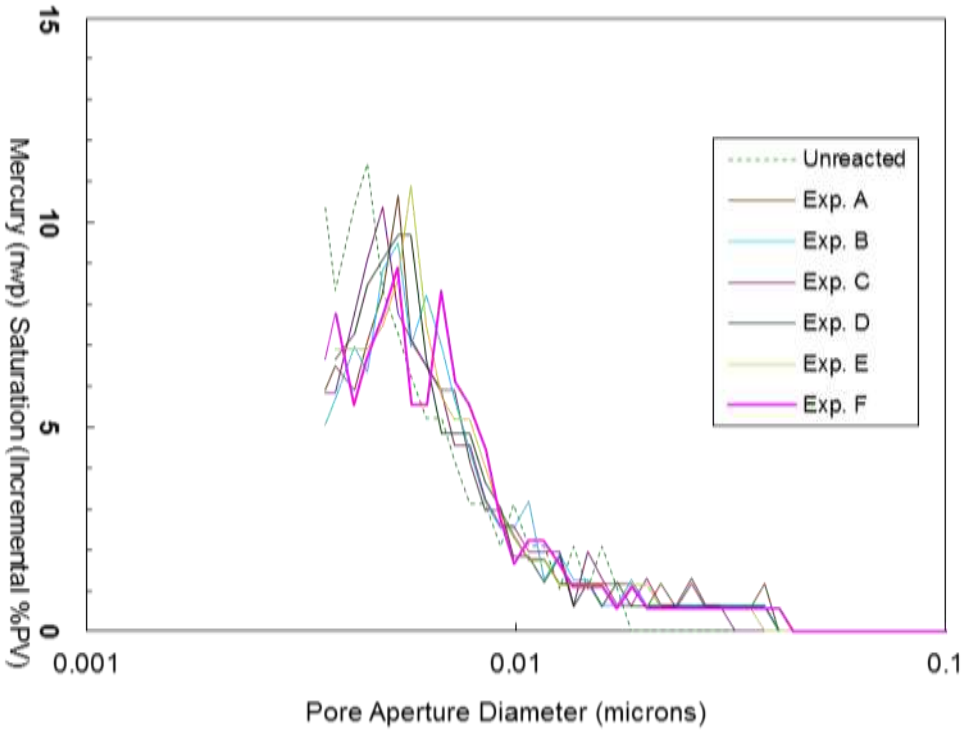

Figure 125. Pore-throat-size distribution of unreacted and reacted shale samples from mercury intrusion capillary pressure tests.

XVIII-2-4 Produced Water Sampling

XVIII-2-4.1 Major Element Analysis and Cl/Br Ratio

Produced water from a Wise County gas well was sampled after being re-HF'ed. The HF water came from a nearby pond (likely surface water) with a Ca-Na bicarbonate composition and a low TDS of ~250 ppm. The four produced water samples were taken at short intervals and they share the same chemical composition of Na-Cl waters with a relatively low TDS of 15,000-18,000 ppm. The Cl/Br ratio is indicative of brine mixing and not halite dissolution (Table 23).

Table 22. Flowback major element composition

Sample ID	Date and time	pH	T(°C)	TDS	Li	Na	NH_4	K	Mg	Ca	F	Cl	Br	NO3	PO4	SO4	HCO3 (Est.)
BW-S	4/21/15 11:00 AM	7.65	17.7	243	0.00	14.9	0.15	7.86	7.8	36.3	0.36	17.3	0.10	0.71	0.00	49.5	108.0
BW-1	4/21/15 11:45 AM	7.35	28.7	16,761	2.48	5387	27.8	51.2	84.0	788	2.35	9768	81.1		0.00	568.7	
BW-2	4/21/15 12:45 PM	7.15	30.0	14,974	2.41	4945	26.4	42.4	71.3	633	1.87	8618	66.3		0.00	566.7	
BW-3	4/21/15 1:55 PM	7.28	30.2	16,899	2.57	5519	28.7	44.4	82.9	735	1.76	9831	76.1		0.00	578.1	
BW-4	4/21/15 2:25 PM	7.46	30.6	17,921	2.69	5728	29.7	54.5	98.9	875	1.84	10,439	90.4		0.00	600.7	
Detection Limits																	
BW-S					0.00	0.01	0.00	0.00	0.02	0.05	0.10	0.07	0.04	0.50	0.84	0.05	
BW-1					0.32	1.45	0.20	0.46	1.94	4.78	10.50	7.48	4.62	51.77	86.93	4.90	
BW-2					0.32	1.47	0.20	0.47	1.96	4.83	10.62	7.57	4.68	52.38	87.95	4.96	
BW-3					0.31	1.42	0.19	0.45	1.89	4.67	10.26	7.31	4.52	50.59	84.94	4.79	
BW-4					0.32	1.47	0.20	0.47	1.96	4.83	10.61	7.56	10.25	4.67	52.33	87.88	

Note: BW-S = pond water sample used as HF water

No ICP (/metals / trace elements) analyses were performed on these water samples

Table 23. Flowback Cl/Br ratio

Sample ID	Cl	Br	Cl/Br
BW-S	17.3	0.10	168
BW-1	9768	81.1	120
BW-2	8618	66.3	130
BW-3	9831	76.1	129
BW-4	10,439	90.4	115

XVIII-2-4.2 Isotopic Analyses

Water isotopes can help in determining the source of the water in the flowback / produced water. The HF water, if not blending with flowback / PW water, will fall on the global / local meteoric water line (LMWL) whereas water isotopes from resident brine, especially $\delta^{18}O$, will fall away from the line. The flowback water isotopes may then reside somewhere on the mixing line between these two members. The LMWL is well-known as many samples have been taken by many different entities in the past decade. Our fresh water sample (Table 24) fall close to the GMWL.

The ponded HF water has a $\delta^{18}O$ and δD value (-3.6‰ and -18.3‰) distinct from the flowback water (-1.95‰ to -2.17‰ and -11.49‰ to -12.25‰). Isotopic composition of the produced water can be used as a tracer to because of the distinct signatures of the surface water used for HF on the one hand and of the original formation water on the other hand. Recently US EPA also sampled surface water and produced water in the Barnett Shale play (EPA, 2015).

Table 24. Produced water isotopic composition

	$\delta^{18}O$	$\delta^{18}O$ error	δD	δD error	Comments
BW-1	-2.17	0.2	-12.25	0.06	
BW-2	-2.12	0.2	-11.76	0.08	
BW-3	-1.95	0.2	-11.94	0.18	
BW-4	-2.12	0.2	-11.49	0.65	
BW-Surface	-3.64	0.2	-18.3	0.33	From nearby pond

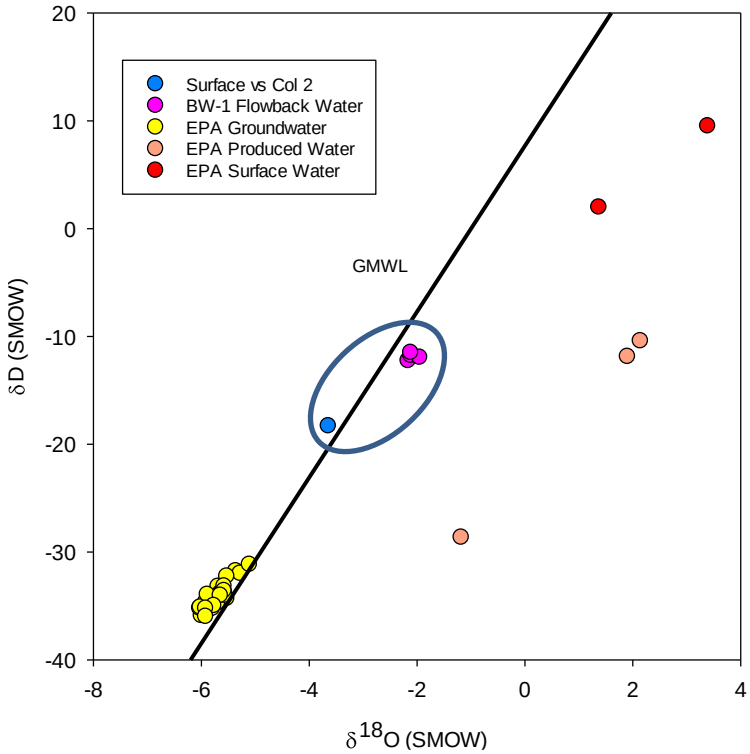

Note: blue circle contains samples taken during this study; other groundwater, surface water, and produced water samples are extracted from EPA (2015, Table B7) and include multiple sampling vents at the same locations.

Figure 126. Water isotope plot

XVIII-3. Discussion

The origin of the overall TDS increase through time of flowback / produced water has generated many discussions. Some researchers insist that the increasing TDS results from progressive mixing with resident brine (Laughland et al., 2014; Blauch et al., 2009) whereas others maintain that the flowback retain the injected water imprint. The details of the flow processes (capillary drive, osmosis, diffusion, pressure) cannot be discussed here. For example, the brine would have to flow towards the fracture, in the direction of which it would be impeded by the ingress of HF water.

In any case, several researchers have suggested that the chemical composition of flowback / produced water is due to more than mixing with residual water in the shales or mixing with formation waters of more permeable intervals that have been inadvertently or willingly stimulated. For example, Blauch et al. (2009) attributed the high salinity of the Marcellus flowback / produced water to halite dissolution (bromide data are not provided in their paper) or a breach of surrounding aquifers during the HF process. Others have suggested that, in the Marcellus Fm. brines are the source of the high salinity of the flowback. It has become clear that there is no universal answer. For example, a tight formation such as those in the Permian basin can contains substantial amount of brine. On the other hand, a gas shale holds little water. A mass balance for the Barnett shale with a porosity of 3% and a saturation of 25% translate into <1% only of its volume as brine.

Work similar to the one presented here has also been performed at DOE NETL (Wall et al., 2013) and at other academic institutions (Balashov et al. 2015; Herz-Thyhsen and Kaszuba, 2013; Bank and Staub, 2013). Wall et al. (2013) used crushed Marcellus cores under high pressure (27.5 MPa) at high temperature (130°C) exposing them to brine and HF fluids. Bank and Staub (2013) also used Marcellus samples but exposed them at standard pressure and temperature conditions for six months. They observed that pH stayed neutral to slightly alkaline and that cation exchange played a role in the composition of the leached fluids. Herz-Thyhsen and Kaszuba (2013) tested the Niobrara and another formation at 115°C and 350 bars pressure for at least 28 days. Balashov et al. (2015) did some benchtop experiments on Marcellus samples.

Several non-mutually exclusive processes can explain the observed changes in composition of the solution in contact with the shale and the origin of the solutes. These include: (1) mixing of added water with formation brines; (2) dissolution of major mineral phases present in the shale; (3) pyrite oxidation buffered by carbonate dissolution; and (4) cation exchange and sorption/desorption from newly hydrated clay minerals.

XVIII-3-1 Geochemical Processes

XVIII-3-1.1 Dissolution and Precipitation of Minerals

The main reactive minerals contained in the Barnett cores are calcite and pyrite, to which can be added plagioclase and K-feldspars and dolomite and ankerite. Soluble minerals such as halite and anhydrite do not seem to be present naturally. Initial XRD analysis (Table 17) and other observations did not find evidence of any. Formation water contains mostly Na and Cl and we added NaCl in most experiments, it follows that only the DI autoclave experiment can be used to evaluate the presence of halite (Figure 127a). Na vs. Cl crossplot (Figure 127a) does not show

the 1:1 ratio characteristic of halite dissolution but displays a considerable excess Na with a molar ratio / slope between 1:3 and 1:2 even at early time. On the other hand the Ca vs. HCO_3 crossplot (Figure 127b) shows a deficit of Ca. Ca and HCO_3 result from the dissolution of calcite. The conventional explanation to a Ca deficit and an excess Na is cation exchange. Crossplots Ca vs. SO_4 (Figure 127c) does not show evidence of anhydrite dissolution; the early time slope is not 1:1. The figure also shows considerable deficit of Ca even if SO_4 concentrations are mostly related to pyrite oxidation. Equations (1) and (2) of the next section in addition to $CaCO_3 + H^+ = Ca^{2+} + HCO_3^-$ illustrate that calcite dissolution combined with pyrite oxidation yields 2 moles of Ca for each mole of SO_4. Such a slope is indeed approximately observed for the autoclave experiments even if at early time the processes are more complex (Figure 128).

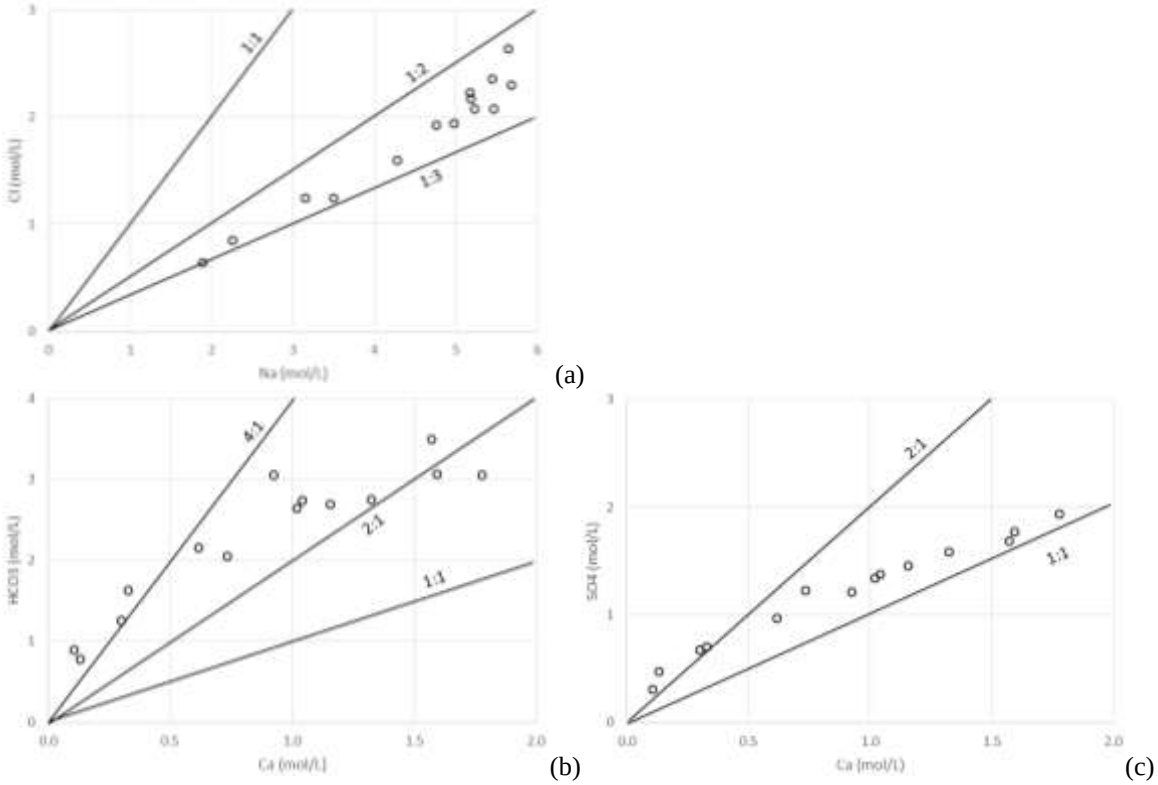

Figure 127. Na vs. Cl and HCO_3 and SO_4 vs. Ca molar crossplots (DI experiment)

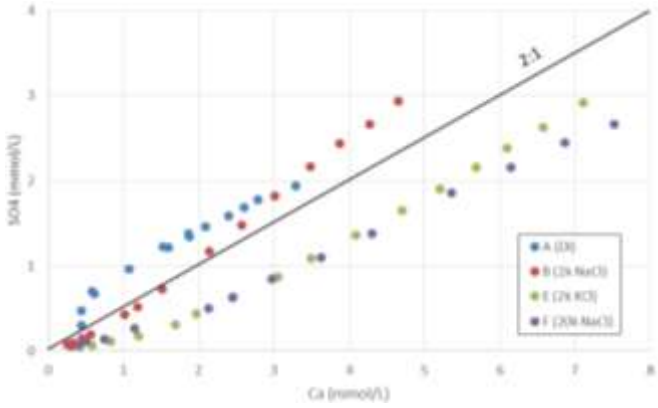

Note: $CaCl_2$ experiments not included

Figure 128. Ca vs. SO_4 crossplot for autoclave experiments

XVIII-3-1.2 Cation Exchange

There are several elements indicating ion exchange: (1) the presence of abundant illite (~35%, Table 17) that is typically accompanied by some mixed-layer clays; (2) excess Na and Ca deficit although ion exchange is masked by additional processes as the classic ion exchange plot (Na-Cl vs. Ca-SO_4 or Ca-HCO_3) does not show a typical relationship (Figure 129); and (3) Another good indication ion exchange occurs is evidenced by the increase in Mg in the 2k $CaCl_2$ experiment (Figure 137) and increase in NH_4+, Tl, Rb, Cs when exposed to the 2k KCl solution (Figure 137, Figure 141, and Figure 142)

Ion exchange explanation is valid only if the exchange is approximately 2 moles of Na for 1 mole of Ca, which is not exactly the case here (Figure 129) although the trend is in the right direction.

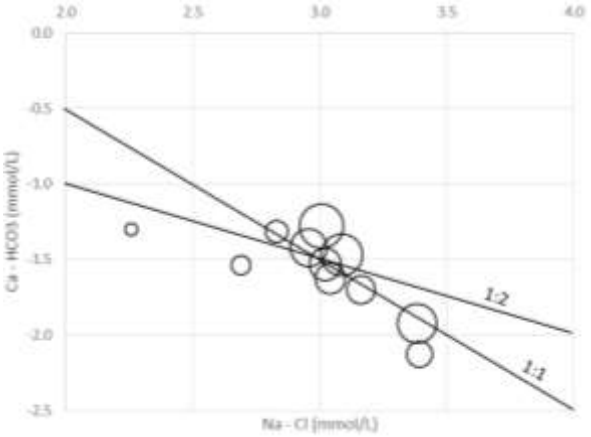

Note: dot size represents increasing experimental time

Figure 129. Na-Ca ion exchange crossplot

XVIII-3-1.3 Pyrite Oxidation Buffered by Carbonate Dissolution

Though most of the precipitated materials were unidentified because of their small sizes, the larger clusters of spherical materials were identified as Fe oxyhydroxide by X-ray EDS. Fe is derived from pyrite oxidation (Equations 1 and 2).

$$2FeS_2 + 7O_2 + 2H_2O \rightarrow 2Fe^{2+} + 4SO_4^{2-} + 4H^+ \quad (1)$$

$$2Fe^{2+} + 1/2O_2 + 5H_2O \rightarrow 2Fe(OH)_3 + 4H^+ \quad (2)$$

Sulfate concentrations at the end of the experiments are within a range of 180 to 280 ppm. Assuming all aqueous sulfate in solution is produced from pyrite oxidation, dissolution of 18–28 mg of pyrite is required [180-280 ppm is 1.87-2.92 mmol/L of sulfate, that is, 18-28 mg of dissolved pyrite into 160 mL]. Sixteen grams of Barnett shale contains an average of 400 mg pyrite (~2.5%, Table 17). Therefore, the amount of pyrite dissolved during the experiments is ~5 to 7% of the available pyrite. Approximately 17-28 mg of O_2 is needed by pyrite oxidation. The amount of O_2 exceeds O_2 solubility in water at atmospheric pressure and room temperature (~8 mg/L in 160 mL). In addition, we flushed the reactor using ultrapurity N_2 gas to remove O_2 in the headspace and water before the reactor was sealed. In a perfectly flushed system, O_2 in the reactor should be completely removed. We could also hypothesize that the ultrapure N_2 gas contains some impurities. It is nominally 99.999% pure, that is, 165 mL of headspace would

contain 165 times 1×10^{-5} = 0.0017 mL at 200 bars and 85°C. Applying ideal gas law, the resulting maximum amount of O_2 (assuming no other impurities and neglecting non-ideal behavior) is 0.011 mmol or 0.36 mg, much less than the required amount. Another possibility is that a small amount of O_2 may remain in the rock chips. The maximum amount of trapped air in a 16 g-rock sample with a porosity of 3% is 0.26 mg, again much less than the required amount. Other mechanisms or sources of oxidation agents must be considered. It is possible that pyrite oxidation occurred right after the core was retrieved from subsurface and that reaction products were stored in shale matrix and pores before the experiments. The cores were stored for years before the experiments were conducted and had been exposed to O_2 during that time period. A certain amount of acid may have already been generated by pyrite oxidation (e.g. Pye and Miller, 1990). Pyrite oxidation and calcite dissolution could have occurred at the interfacial contact of minerals and the remaining pore water. Reaction products such as H^+ and SO_4 were stored in the pore water, which was subsequently released into the reaction fluid during the experiments. Before the experiments, pyrite in the shale samples appeared to be fresh looking and no calcite corrosion and gypsum was observed at the ion milled surface. It follows that some of the observed chemical changes in the experiments could be partially accounted for by mixing the preexisting reaction products with the reaction solutions.

Ca released during the experiments was clearly sourced from calcite dissolution observed by SEM. Therefore, pyrite oxidation may have occurred during core storage, but the acid products largely remained in the pore water and had not been in contact with carbonate minerals. Only when the pore water mixed with the reaction solutions, the acids started reacting with the carbonate and feldspar minerals.

XVIII-3-2 Water Behavior

Simple mixing of added water with formation brines can explained some but not all of the observed geochemical trends. A simple way to assess mixing would be to examine the behavior of Cl, a conservative ion. We can perform a mass balance calculation on the DI experiment Cl concentrations (run A). A total of 16g of core with a density of 2.4 translates into a rock volume of 6.67 mL that is exposed to 160 mL of DI water. The resulting solution has an approximate concentration slightly less than 100 mg/l (Figure 121 and Figure 123). Assuming a porosity of 3% and a water saturation of 25% yields a water volume of 0.05 mL. If all the Cl came from the brine, Cl would have a concentration of 100×160/0.050 = 320,000 mg/l, an impossibly high Cl concentration. Since Cl is a conservative ion that does not sorb or enter into silicate mineral structure, it follows that the only origin in addition to the residual brine is halite or some other soluble salts. The source of the halite is likely contamination because it has not been described as a constitutive mineral of the Barnett Shale. Unfortunately this also means that there is no easy way to quantify mixing with residual water.

The relatively low concentrations observed in the experiments compared to typical flowback / produced water is largely due to the low rock-water ratio. In the field, concentrations of major ions in produced water are much higher. However, mixing cannot fully explained the high concentrations. Other mechanisms such as diffusion (Balashov et al., 2015) and osmosis (Engelder et al., 2014) must be invoked. Those same mechanisms must be at play in the autoclave experiments. The previous description of the experiments does not preclude that the solutes reached the dilute solution through diffusion / osmosis rather than through true physical mixing.

XVIII-4. Conclusions

We performed autoclave experiments exposing Barnett rock fragments to simple synthetic fluids of various ionic strengths. Mineral composition of the Barnett shale consists mostly of quartz and illite with minor amounts of more reactive minerals such as carbonates (calcite, dolomite, ankerite), feldspar (K-feldspar and plagioclase), and pyrite. The reacting fluids consisted of DI water and of 2k NaCl, $CaCl_2$, KCl, and 20k ppm NaCl solutions. Because of experimental constraints, it was not possible to reproduce the approximate field rock-water ratio. However, the main geochemical reaction has been validated: dissolution of calcite and ion exchange. In addition, pyrite oxidation seems to occur possibly when O_2 is introduced into the system or before the experiments, in storage. There is also minor precipitation of likely clays and Fe oxyhydroxides and little ion exchange. MICP analyses show that dissolution / precipitation reactions on balance increase the shale porosity and permeability.

Overall most elements displays an increase in concentration through time. The increase grows larger with increasing fluid salinity. Reactions are relatively quick with concentrations >80% of their asymptotic final concentrations after a few days. Some reactive elements (Al) show a concentration decrease after the initial peak. The origin of the flowback salinity could be explained by mixing with residual brine and possibly halite contamination but the water composition is altered by the carbonate dissolution and pyrite oxidation, and, to a lesser degree, ion exchange reactions.

This research represents one of the first attempts to understand which parameters and processes impact the chemical composition of the flowback water with an ultimate goal of limiting surface treatment and preventing scaling. It will also eventually help explaining the fate of the water during hydraulic fracturing. However, there is still a considerable amount of work to be accomplished to fully understand the results of these experiments, in particular the lack of field data limits the interpretation of the results. In addition, several system components of importance have not been tested yet. Currently the limited number of experiments and of samples used is not enough to lift ambiguity in terms of the results. Systematic duplicate and triplicate experiments are needed in order to develop results more convincing from a statistical standpoint because of the known extreme heterogeneity of shales. Additional experiments are also needed to understand the impact of actual HF fluids. Results presented in this study concern only fresh and brackish water. More reactive additives (gel breakers) could translate into more geochemically active systems and must be tested individually then together. In addition, the action mechanisms of the various additives need to be researched and understood. In this research, pH has been slightly alkaline to neutral but experiments do not control pH and let it drift. Deviations from this range toward higher or lower pH values could translate in a different evolution of the system. Another set of experiments should be done at controlled (alkaline) pH. Addition of O_2 scavengers would also help in determining the timing of pyrite oxidation. The experimental set-up can also be made more realistic by doing something akin to core flooding instead of the batch experiments presented in the report.

From a field standpoint, results from flowback / produced water sampling are needed, in particular, from wells that underwent their first HF stimulation with little shut-in time. Ultimately, experiments are only a help to understand the field data and collecting field data has to be a major component of any thorough study. An ideal test to prove or disprove some of the arguments presented in this report would be to drill and core a horizontal well close to and

parallel to the lateral of a producing well intersecting fractures and matrix that can then examined as well as their contained fluids.

Geochemical reactions are only one aspect of the downhole processes, other such as fluid flow, diffusion, and osmosis are also important. Progress in the understanding of the other processes is needed to better grasp rock-water interactions. Thorough isotopic work (water isotopes, Sr) can help in elucidating these processes. Some of the progress can be accomplished by modeling various aspects of the system. In particular, a thorough geochemical modeling exercise is needed to put together microscopic observations combined with water chemical analyses.

XVIII-5. References (NOT in main reference list)

Balashov, V. N., T. Engelder, X. Gu, M. S. Fantle, and S. L. Brantley, 2015, A model describing flowback after Marcellus Shale hydraulic fracturing, AAPG Bulletin, 99(1), p143–154.

Bank, T., Giese, R., and Staub, P. L., 2013, The evolution of salinity in fluid rock reactions with the Marcellus Shale, Geological Society of America Abstracts with Programs. Vol. 45, No. 7, p.76.

Bish, D.L., 1994. Quantitative x-ray diffraction analysis of soil, in: Amonette, J.E., Zelazny, L.W. (Eds.), Quantitative Methods in Soil Mineralogy. Soil Science Society of America, Wisconsin, pp. 267-295.

Blauch, M.E., R.R. Myers, T. R. Moore; B.A. Lipinski, and N.A. Houston, 2009, Marcellus Shale Post-Frac Flowback Waters - Where is All the Salt Coming From and What are the Implications? Society of Petroleum Engineers #125740, 20p.

Comisky, J. T., K. Newsham, J. A. Rushing, and T. A. Blasingame, 2007, A comparative study of capillary-pressure-based empirical models for estimating absolute permeability in tight gas sands: Society of Petroleum Engineers Annual Technical Conference and Exhibition, Anaheim, California, November 11–14, SPE Paper 110050-MS, 18 p., doi: 10.2118/110050-MS.

Drits, V. A., H. Lindgreen, B. A. Sakharov, H. J. Jakobsen, A. L. Salyn and L. G. Dainyak, 2002, Tobelitization of smectite during oil generation in oil-source shales; application to North Sea illite-tobelite-smectite-vermiculite, Clays and Clay Minerals, 50(1), p.82-98

Engelder T., L. M. Cathles, L. T. Bryndzia, 2014, The fate of residual treatment water in gas shale, Journal of Unconventional Oil and Gas Resources (7), p.33–48

U.S. EPA. 2015. Retrospective Case Study in Wise County, Texas Study of the Potential Impacts of Hydraulic Fracturing on Drinking Water Resources, May 2015, EPA/600/R-14/090, last accessed September 10, 2015, http://www2.epa.gov/hfstudy/retrospective-case-study-wise-county-texas. 171p. + Appendices

Herz-Thyhsen, R. J. and Kaszuba, J., 2013, Evaluation of fluid-rock interaction between hydraulic fracturing fluids and unconventional reservoirs of the Powder River Basin, Wyoming, Geological Society of America Abstracts with Programs. Vol. 45, No. 7, p.758

Hillier, S., 1999. Use of an air brush to spray dry samples for X-ray powder diffraction, Clay Minerals, 34, p.127-135

Holloway, J. M. and R. A. Dahlgren, 2002, Nitrogen in rock: Occurrences and biogeochemical implications, Global Biogeochemical Cycles, 16(4), 1118, doi:10.1029/2002GB001862.

Laughland, M. M., D. E. Nelson, P. Wilson, E. Eastridge, 2014, Uncharted Waters: What Can We Learn From Waters Produced From Horizontal Wells in the Permian Basin?: presented at URTeC conference, Denver, CO, August 25-27, 2014, #1926712, 9p.

Loucks R. G. and S. C. Ruppel, 2007, Mississippian Barnett Shale: Lithofacies and depositional setting of a deep-water shale-gas succession in the Fort Worth Basin, Texas, AAPG Bull., 91(4), pp.579–601.

Loucks,R. G., R. M. Reed, S. C. Ruppel, and D. M. Jarvie, 2009, Morphology, genesis, and distribution of nanometer-scale pores in siliceous mudstones of the Mississippian Barnett Shale, Journal of Sedimentary Research, 79, p.848–861

Lu, J., Milliken, K., Reed, M.R., Hovorka, S., 2011. Diagenesis and sealing capacity of the middle Tuscaloosa mudstone at the Cranfield carbon dioxide injection site, Mississippi. Environ. Geosci. 18, 1-19.

Lu, J., Kharaka, Y. K., Thordsen, J. J., Horita, J., et al., 2012, CO_2-rock-brine interactions in Lower Tuscaloosa Formation at Cranfield CO2 sequestration site, Mississippi, U.S.A., Chemical Geology, v. 291, p. 269-277.DOI: 10.1016/j.chemgeo.2011.10.020.

Lu, J., P. J. Mickler, J.-P. Nicot, C. Yang, K.D. Romanak, 2014, Geochemical impact of oxygen on siliciclastic carbon storage reservoirs: International Journal of Greenhouse Gas Control, v. 21, p. 214-231.

Lu, J., S. C. Ruppel, and H. D. Rowe, 2015, Organic matter pores and oil generation in the Tuscaloosa Marine Shale: AAPG Bulletin, v. 99, p. 333–357, doi: 10.1306/08201414055.

Mickler, P., J.-P. Nicot, J. Lu, and R. Darvari, Shale-water interactions observed in laboratory experiments: Identifying geochemical controls on flow-back water chemistry in the Haynesville and Barnett shales, to be submitted

Milliken, K. L., M. Rudnicki, D. N. Awwiller, and T. Zhang, 2013, Organic matter-hosted pore system, Marcellus Formation (Devonian), Pennsylvania: AAPG Bulletin, v. 97, p. 177–200, doi: 10.1306/07231212048.

Milliken, K. L., Esch, W. L., Reed, R. M., and Zhang, T., 2012, Grain assemblages and strong diagenetic overprinting in siliceous mudrocks, Barnett Shale (Mississippian), Fort Worth Basin, Texas, AAPG Bull., 96(8), p.1553-1578.

Morsy, S., C. J. Hetherington, and J. J. Sheng, 2013, Effect of low-concentration HCl on the mineralogical, mechanical, and physical properties of shale rocks, SPE paper # 165689, 12p.

Nicot, J.-P., B. S. Scanlon, R. C. Reedy, and R. A. Costley, 2014, Source and Fate of Hydraulic Fracturing Water in the Barnett Shale: A Historical Perspective, Environmental Science and Technology, v. 48, p. 2464−2471.

Nicot, J.-P., P. Mickler, J. Lu, and R. Darvari, 2015 A Study of Rock-Water Interactions during Hydraulic Fracturing (Eagle Ford), Bureau of Economic Geology, The University of Texas at Austin, contract report prepared for ExxonMobil Exploration Company, 100 p.

Palmer, I. D., Moschovidis, Z. A., and Schaefer, A., 2013, Characterizing stimulation domains for improved well completion in shale gas, RPSEA final report 09122-02, 160p., http://www.rpsea.org/projects/09122-02/

Palmer, I. D., Moschovidis, Z. A., Schaefer, A., and Mcketta, S., Southwestern Energy, 2014, Case Histories From Fayetteville Shale: SRV Sizes, Fracture Networks, Spacing, Aperture Widths, and Implications for Proppant, SPE# 169015

Pye, K., and J. A. Miller, 1990, Chemical and biochemical weathering of pyritic mudrocks in a shale embankment: Quarterly Journal of Engineering Geology & Hydrogeology, v. 23, p. 365–381.

Shafer, J., and J. Neasham, 2000, Mercury porosimetry protocol for rapid determination of petrophysical and reservoir quality properties: Proceedings of the International Symposium of Society of Core Analysts Paper SCA2000-21, 12 p., http://www.ux.uis.no/~s-skj/ipt/Proceedings/SCA.1987-2004/1-SCA2000-21.pdf. Last accessed on May 29, 2014.

Wall, A. J., Hakala, J. A., Marcon, V., and Joseph, C., 2013, Using Sr isotopes to track the dissolution of Marcellus Shale by hydraulic fracturing fluids, Geological Society of America Abstracts with Programs. Vol. 45, No. 7, p.

Warner, N. R., C. A. Christie, R. B. Jackson, and A. Vengosh, 2013, Impacts of Shale Gas Wastewater Disposal on Water Quality in Western Pennsylvania, Environ. Sci. Technol., 47, 11849−11857, dx.doi.org/10.1021/es402165b

Zhang, T., Yang, R., Milliken, K., Ruppel, S. C., Pottorf, R. J., and Sun, X., 2014, Chemical and isotopic composition of gases released by crush methods from organic rich mudrocks: Organic Geochemistry, 73, p.16-28, http://doi.org/http://dx.doi.org/10.1016/j.orggeochem.2014.05.003.

XVIII-6. Attachment A: FracFocus data on wells of interest

This attachment displays FracFocus data on well Blakley #1 (refrac)

Job Start Date:	2/16/2015
Job End Date:	2/16/2015
State:	Texas
County:	Wise
API Number:	42-497-33041-00-00
Operator Name:	Devon Energy Production Company L.P.
Well Name and Number:	Blakley 1
Longitude:	-97.39942900
Latitude:	33.00561900
Datum:	NAD27
Federal/Tribal Well:	NO
True Vertical Depth:	7,370
Total Base Water Volume (gal):	1,408,480
Total Base Non Water Volume:	0

Hydraulic Fracturing Fluid Composition:

Trade Name	Supplier	Purpose	Ingredients	Chemical Abstract Service Number (CAS #)	Maximum Ingredient Concentration in Additive (% by mass)**	Maximum Ingredient Concentration in HF Fluid (% by mass)**	Comments
Fresh Water	Operator	Base Fluid					
			Fresh Water	7732-18-5	100.00000	95.48674	Density = 8.330
Common White - 100 Mesh	Halliburton	Proppant					
			Crystalline silica, quartz	14808-60-7	100.00000	2.20067	
Premium White - 40/70	Halliburton	Proppant					
			Crystalline silica, quartz	14808-60-7	100.00000	2.19742	
FE ACID - >10% HCL	Halliburton	Solvent					
			Hydrochloric acid	7647-01-0	30.00000	0.01324	
Baktron K139	Champion	Biocide					
			Quaternary Ammonium Compounds, Benzyl-C12-16-Alkyldimethyl, Chlorides	68424-85-1	10.00000	0.00383	
			Ethanol	64-17-5	5.00000	0.00191	
			Glutaraldehyde	111-30-8	5.00000	0.00191	Density = 8.37
FR-76	Halliburton	Friction Reducer					
			Hydrotreated light petroleum distillate	64742-47-8	30.00000	0.00705	
FE-1A ACIDIZING COMPOSITION	Halliburton	Additive					
			Acetic anhydride	108-24-7	100.00000	0.00182	
			Fatty acids, tall oil	Confidential		0.00009	
		Other Ingredient(s)					
			Reaction product of acetophenone, formaldehyde, thiourea and oleic acid in dimethyl formamide	68527-49-1		0.00009	
		Other Ingredient(s)					
			Alcohols, C14-C15, ethoxylated	68951-67-7		0.00009	
		Other Ingredient(s)					
			Oxyalkylated phenolic resin	Confidential		0.00005	
		Other Ingredient(s)					
			Oxyalkylated phenolic resin	Confidential		0.00002	
		Other Ingredient(s)					
			Olefins	Confidential		0.00002	
		Other Ingredient(s)					
			Olefins	Confidential		0.00002	
		Other Ingredient(s)					
			Olefins	Confidential		0.00000	
		Other Ingredient(s)					
			Olefins	Confidential		0.00000	

* Total Water Volume sources may include fresh water, produced water, and/or recycled water

** Information is based on the maximum potential for concentration and thus the total may be over 100%

XVIII-7. Attachment B: Result Plots of Autoclave Experiments

This attachment contains plots of chemical analyses. The plots are presented 6 a page with elements in no particular order with IC results followed by ICP results:

Li, K, Na, Mg, NH_4, Ca

F, SO_4, Cl, B, Br, Al

Si, V, P, Cr, Ti, Mn

Fe, Cu, Co, Zn, Ni, As

Se, Zr, Rb, Mo, Sr, Ag

Cd, Cs, Sn, Ba, Sb, Tl

Pb, U, Bi, Th

All plots are showed for each experiment even if they are empty for consistency of format.

XVIII-7-1 Autoclave Experiments – NaCl (0, 2k, 20k) Series

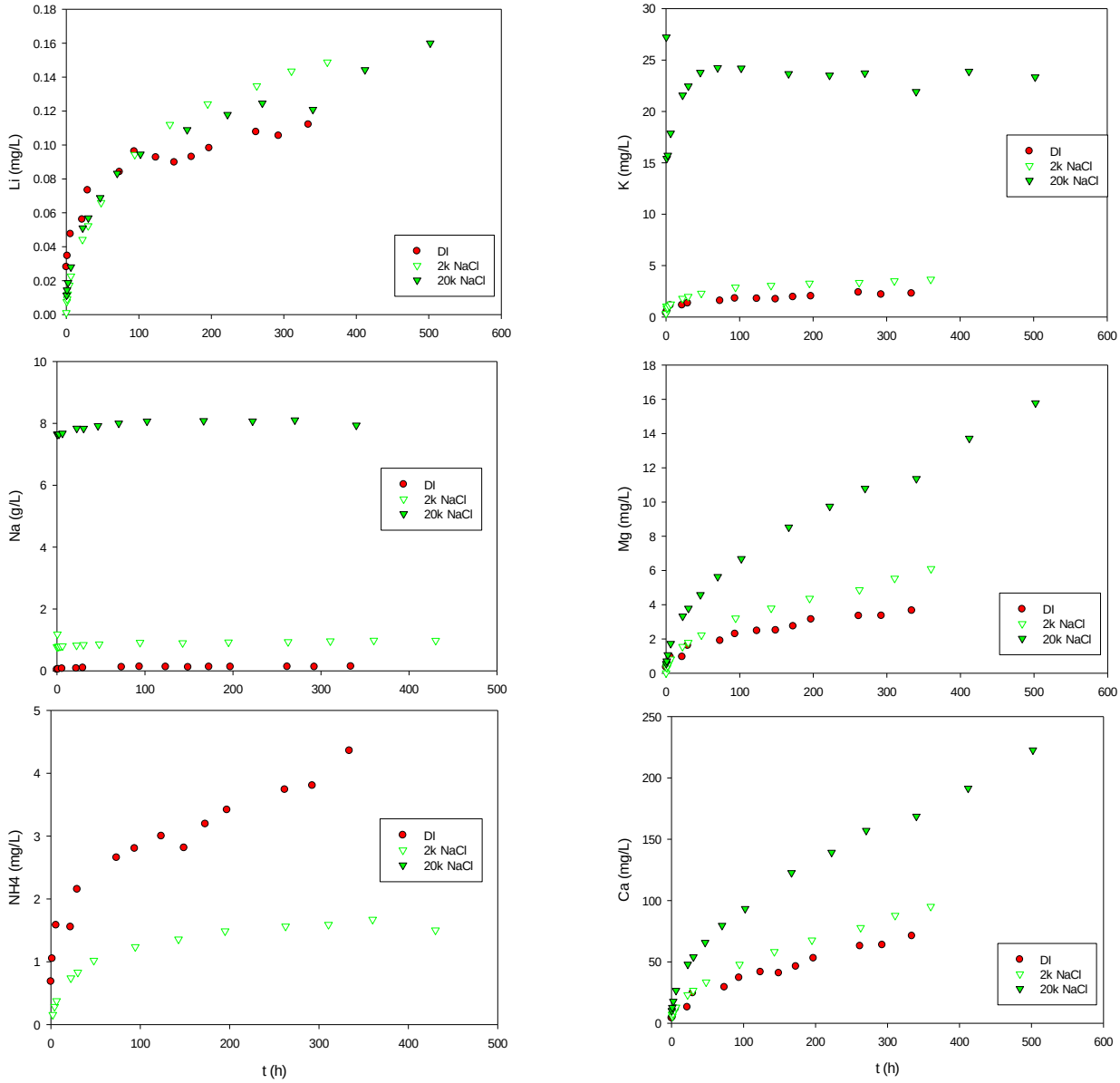

Figure 130. Barnett, NaCl series. Li, K, Na, Mg, NH_4, Ca

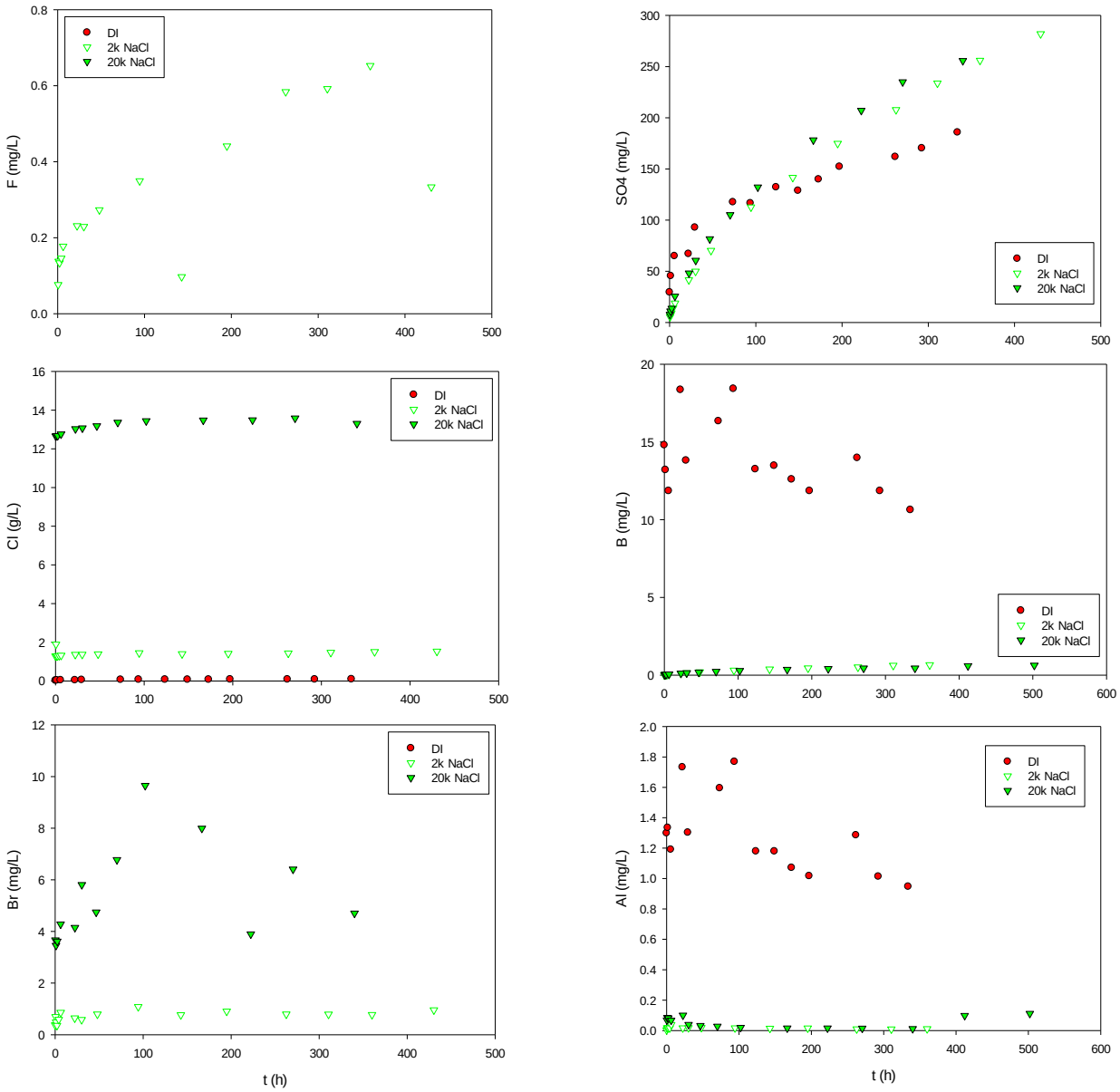

Figure 131. Barnett, NaCl series. F, SO_4, Cl, B, Br, Al

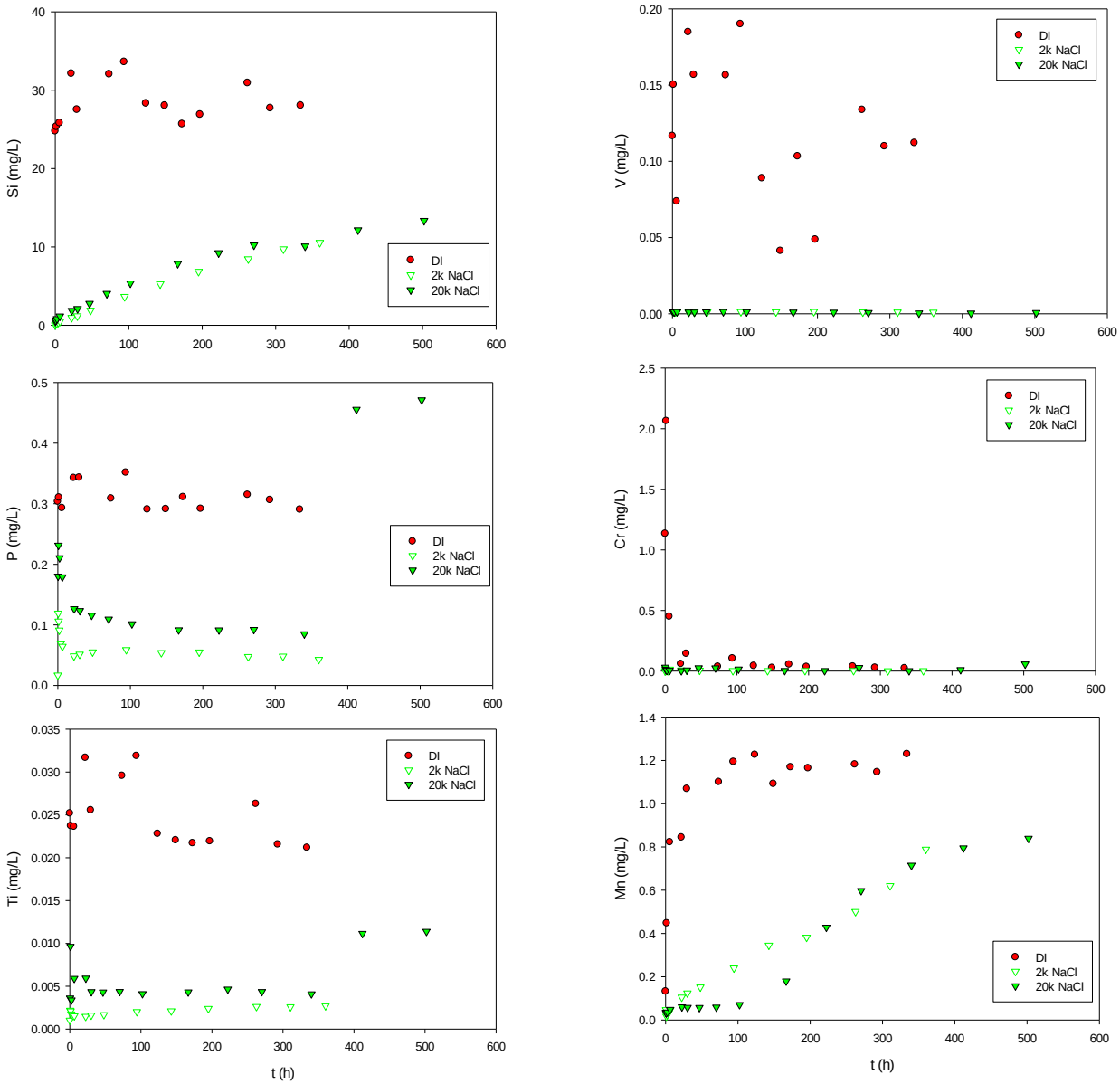

Figure 132. Barnett, NaCl series. Si, V, P, Cr, Ti, Mn

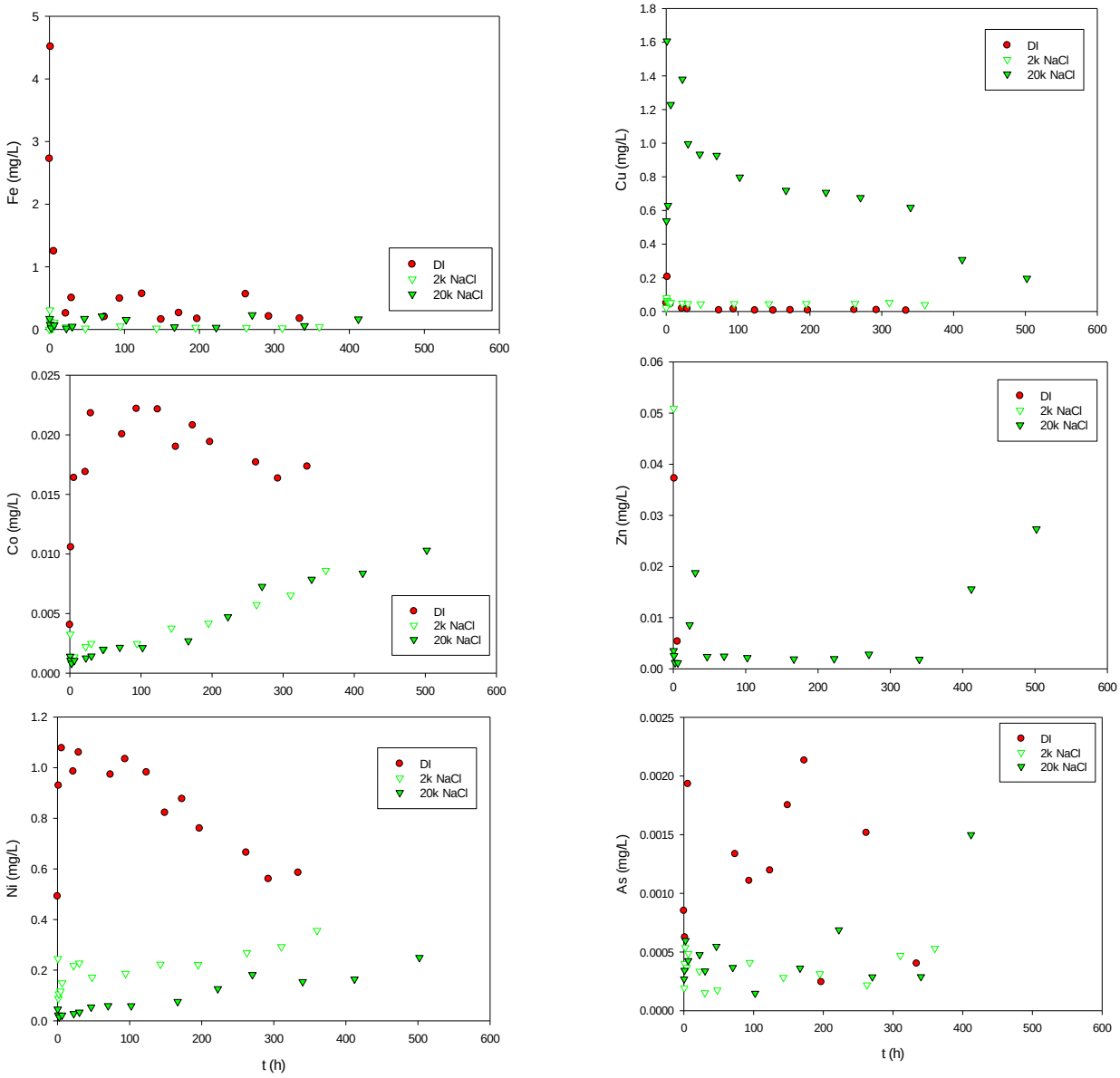

Figure 133. Barnett, NaCl series. Fe, Cu, Co, Zn, Ni, As

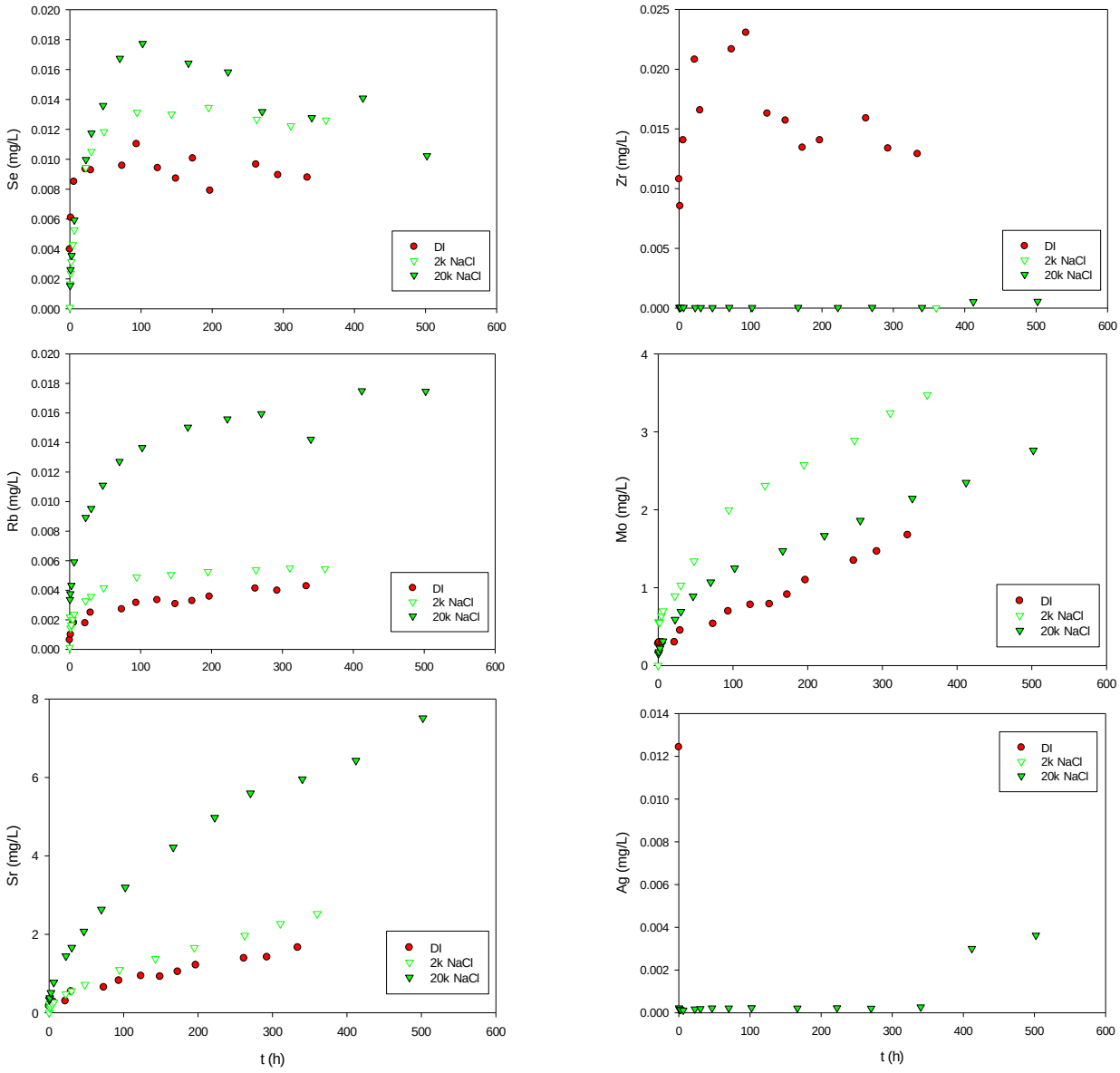

Figure 134. Barnett, NaCl series. Se, Zr, Rb, Mo, Sr, Ag

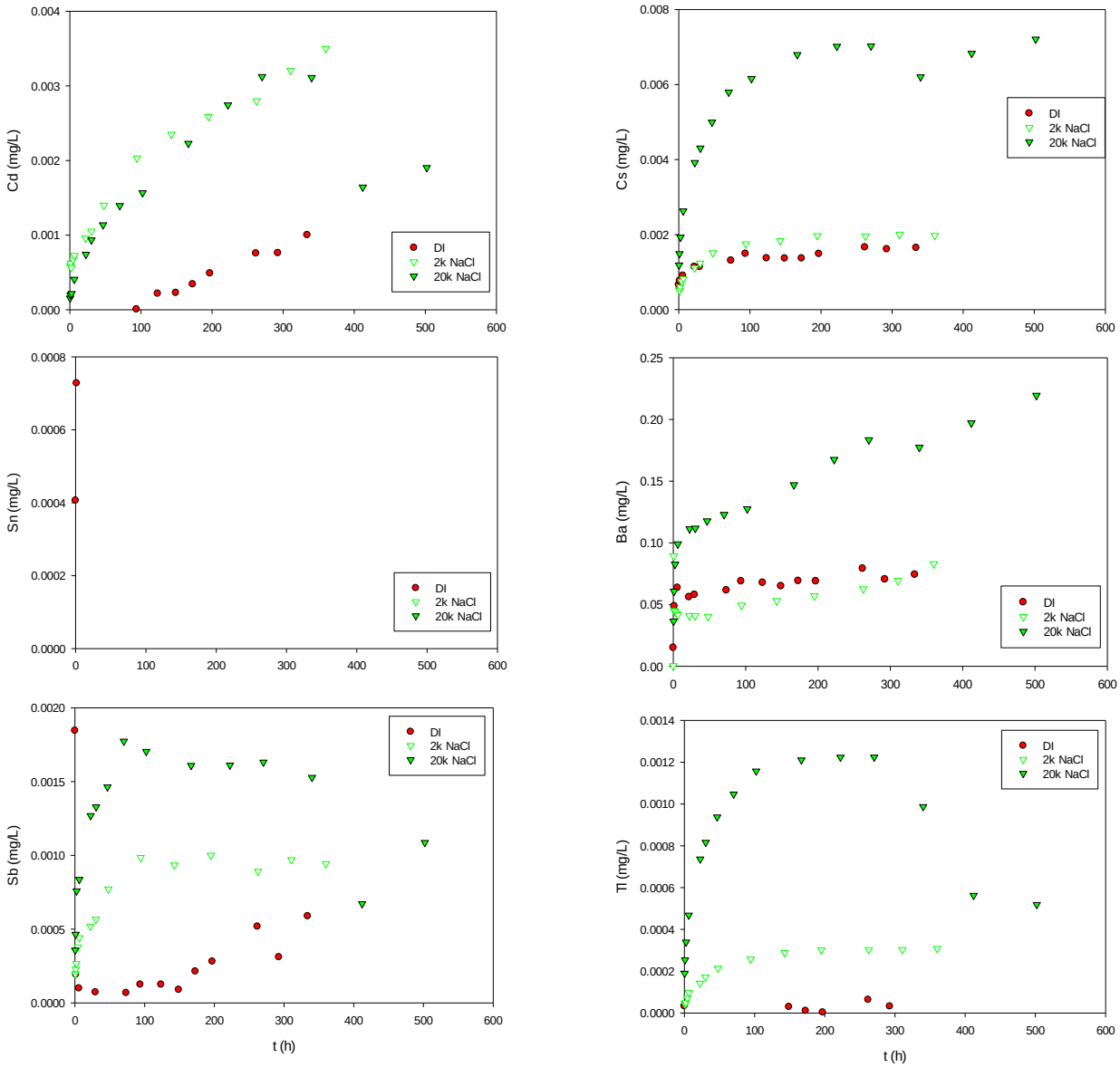

Figure 135. Barnett, NaCl series. Cd, Cs, Sn, Ba, Sb, Tl

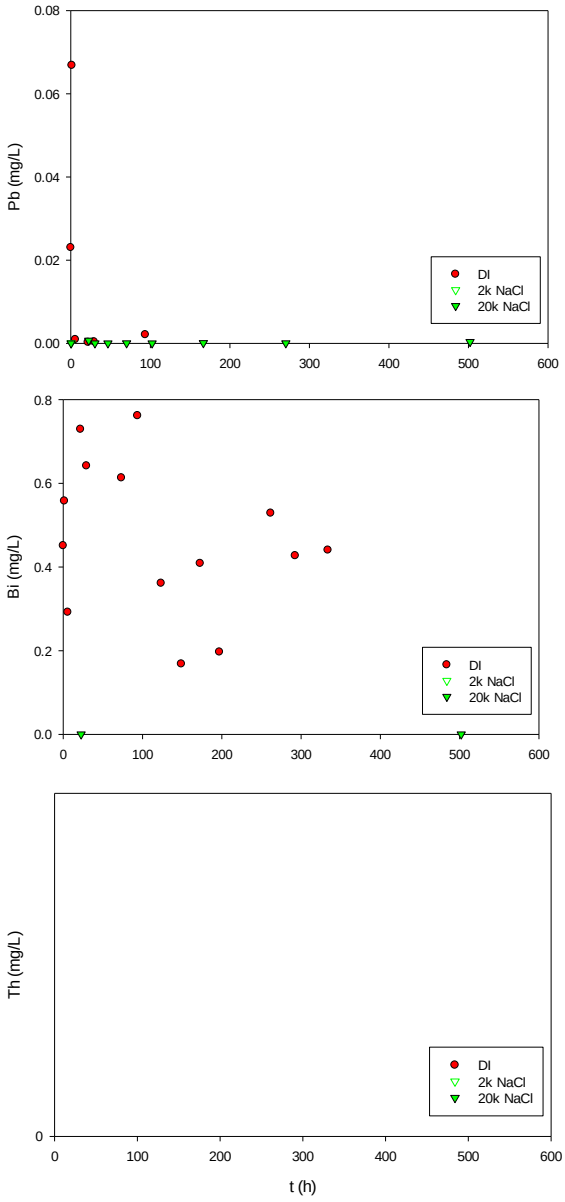

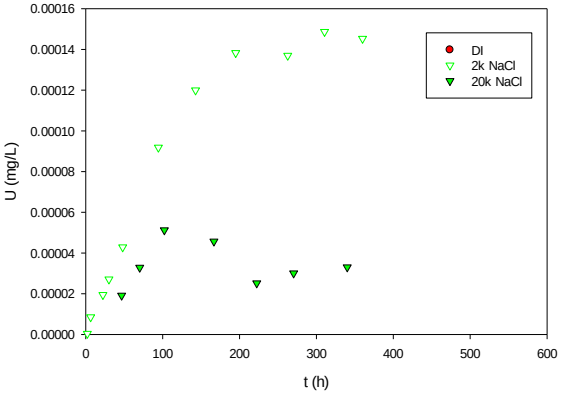

Figure 136. Barnett, NaCl series. Pb, U, Bi, Th

XVIII-7-2 Autoclave Experiments – 2k (Na, Ca, K)Cl Series

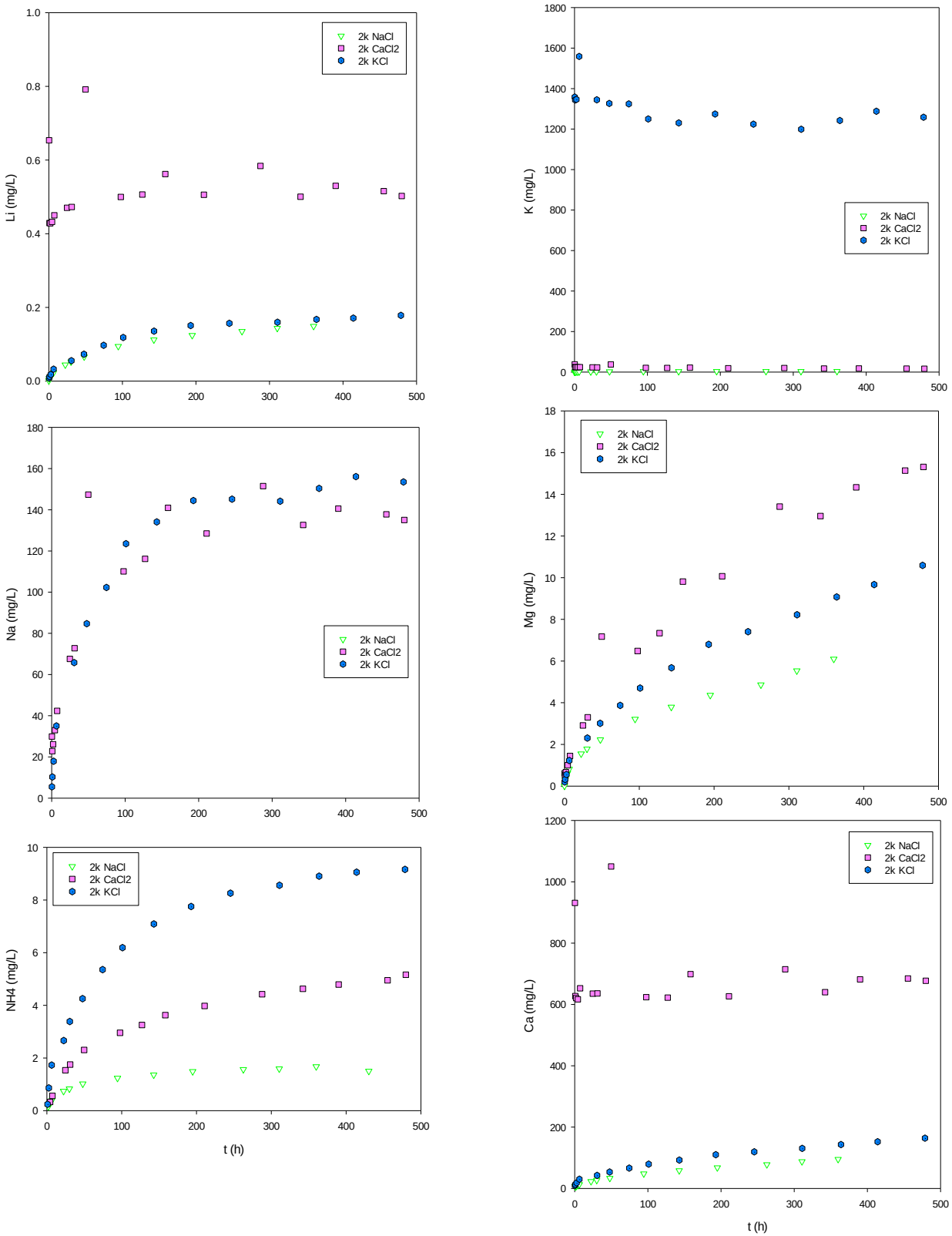

Figure 137. Barnett, 2k series. Li, K, Na, Mg, NH_4, Ca

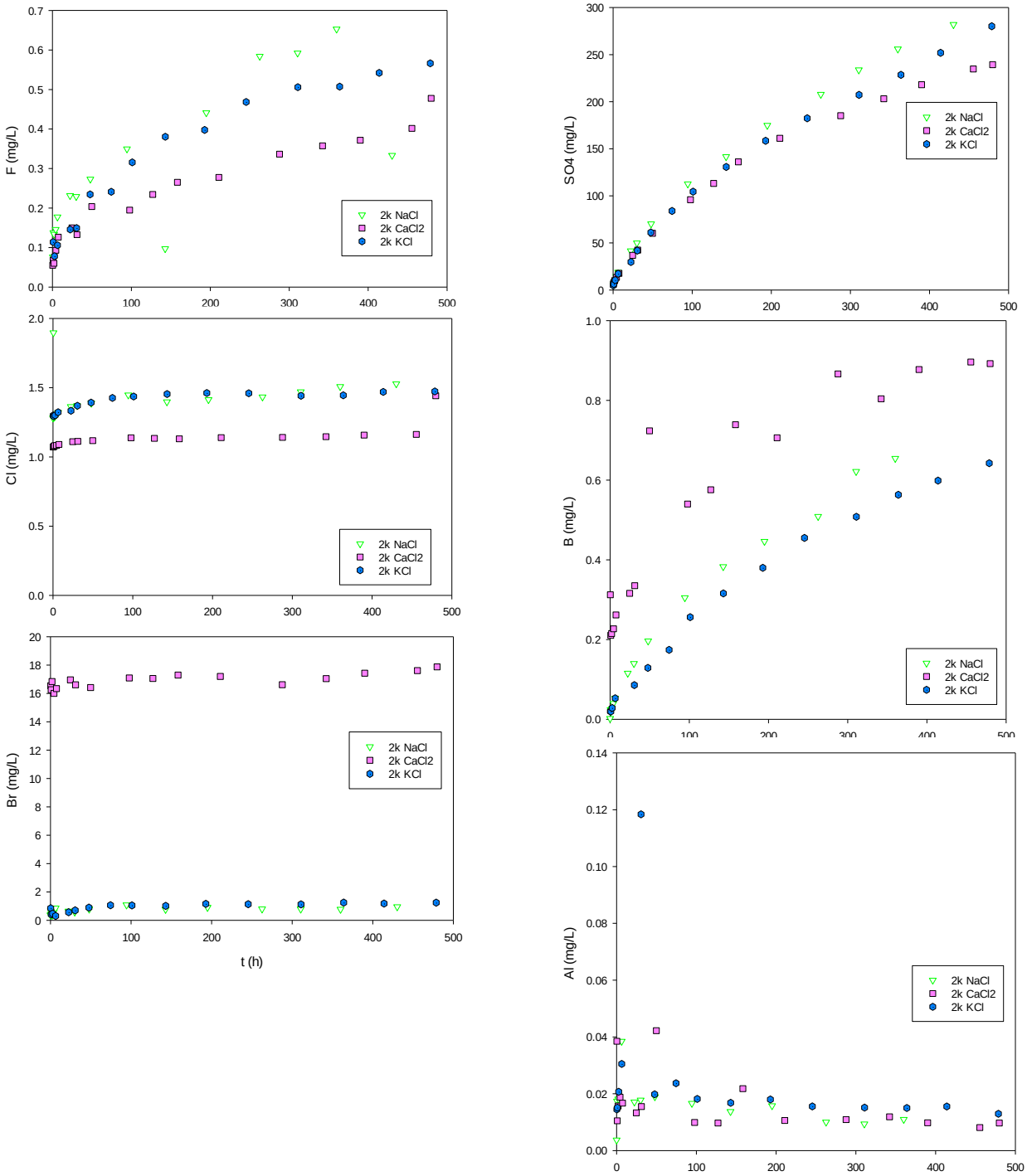

Figure 138. Barnett, 2k series. F, SO_4, Cl, B, Br, Al

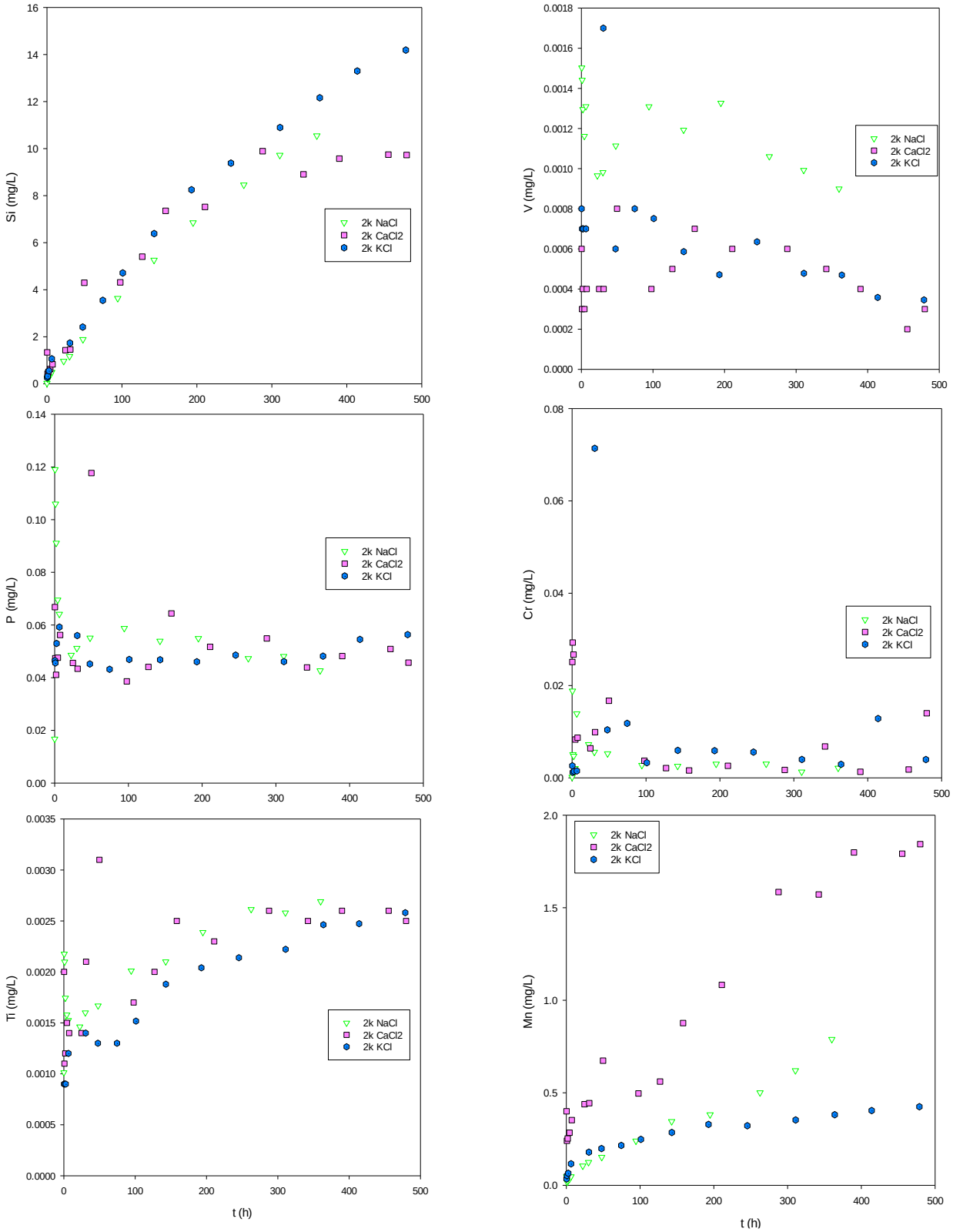

Figure 139. Barnett, 2k series. Si, V, P, Cr, Ti, Mn

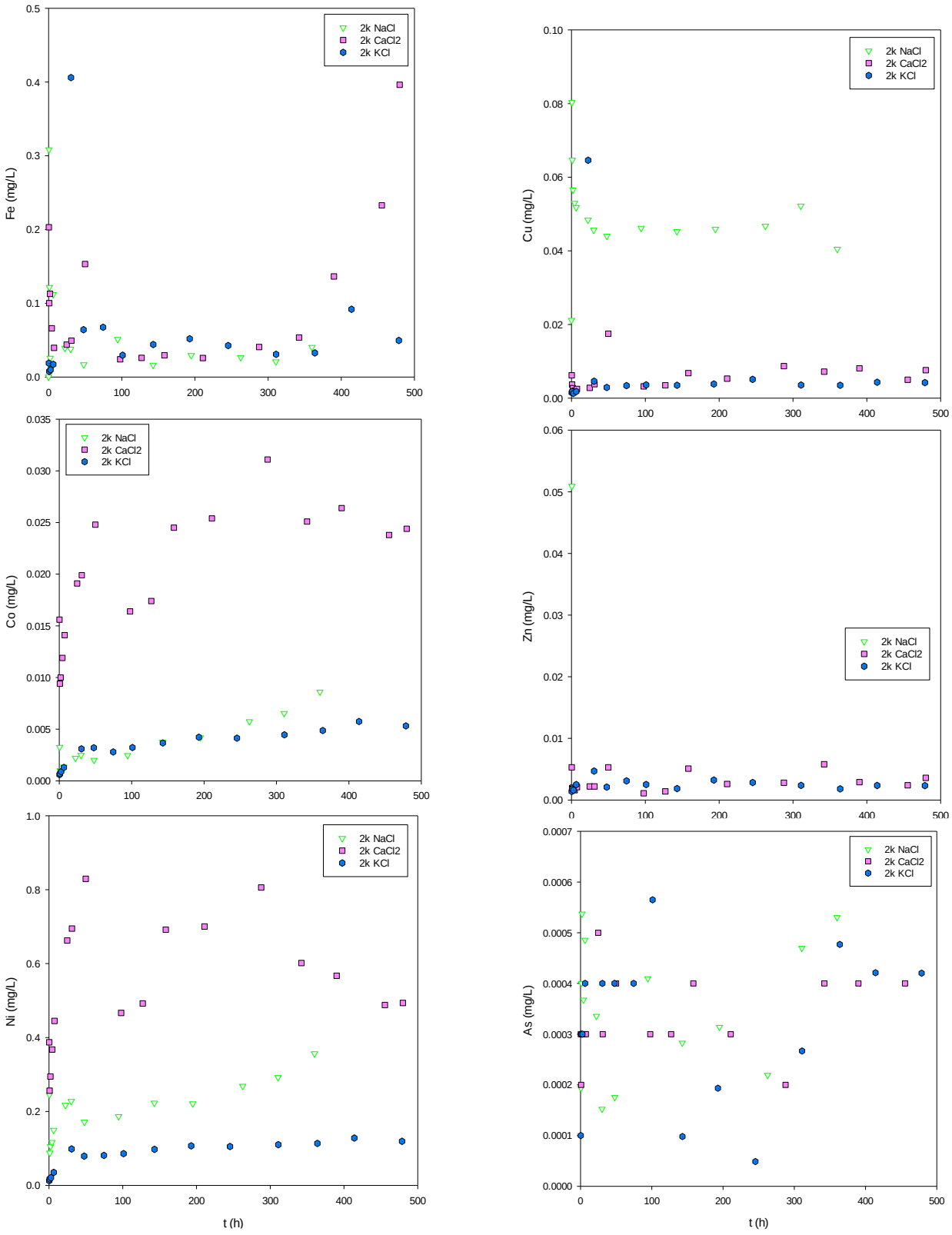

Figure 140. Barnett, 2k series. Fe, Cu, Co, Zn, Ni, As

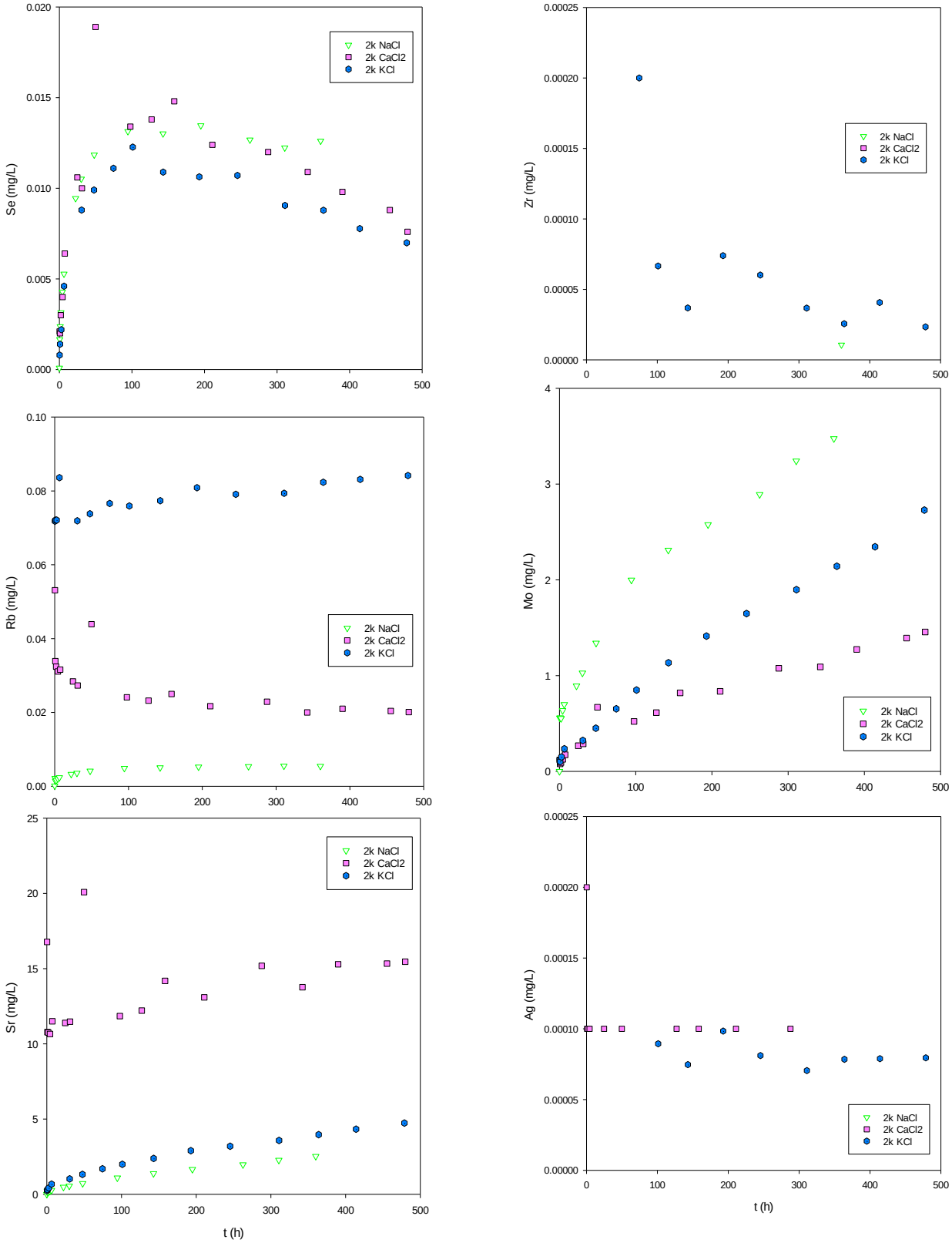

Figure 141. Barnett, 2k series. Se, Zr, Rb, Mo, Sr, Ag

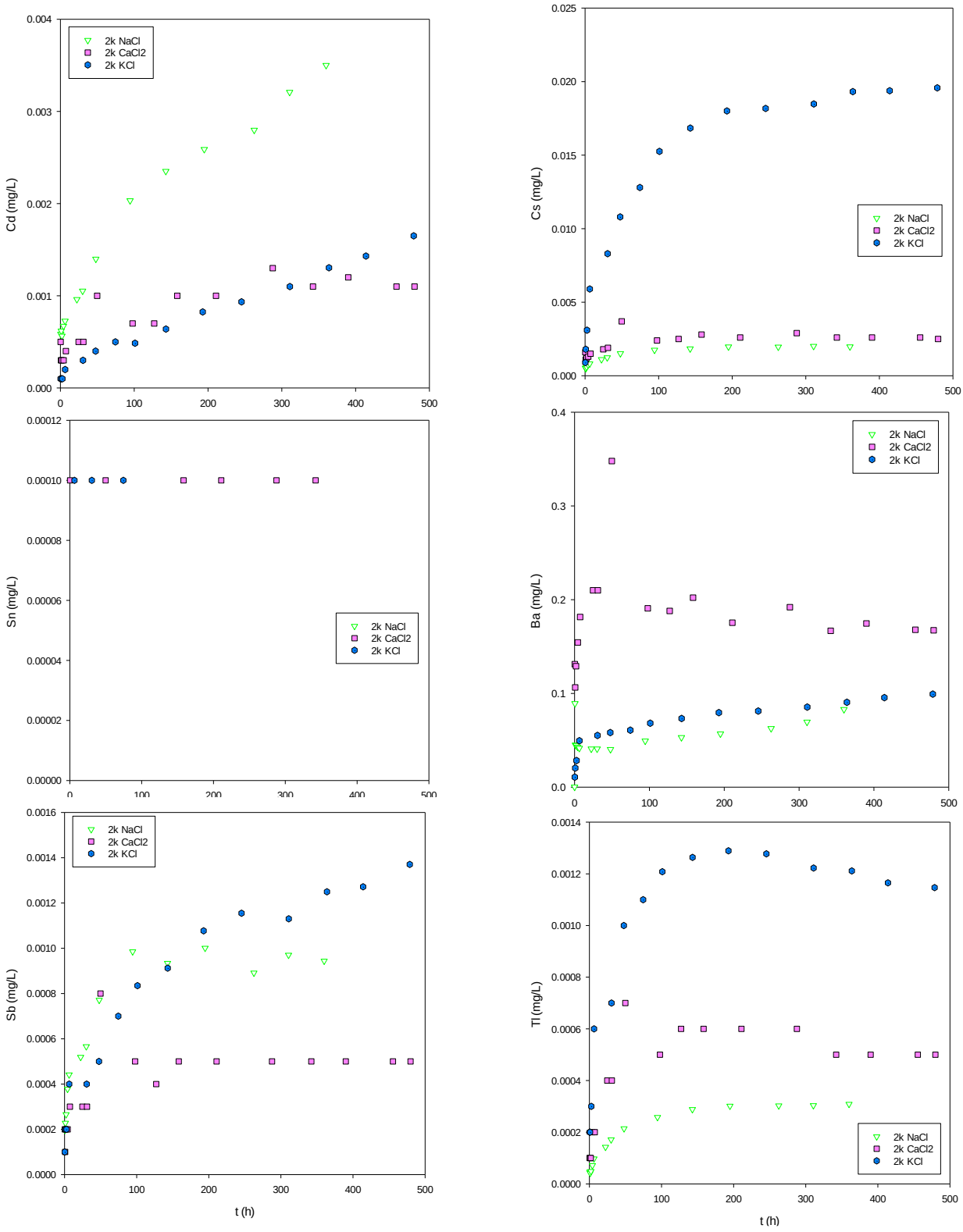

Figure 142. Barnett, 2k series. Cd, Cs, Sn, Ba, Sb, Tl

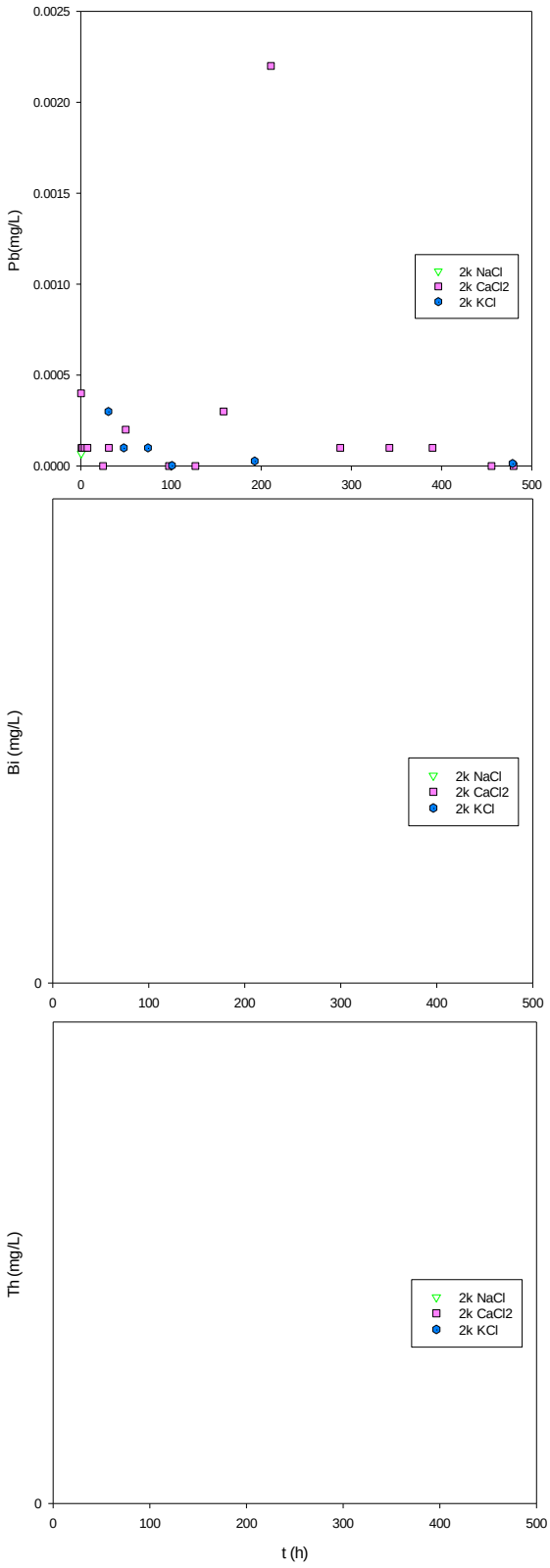

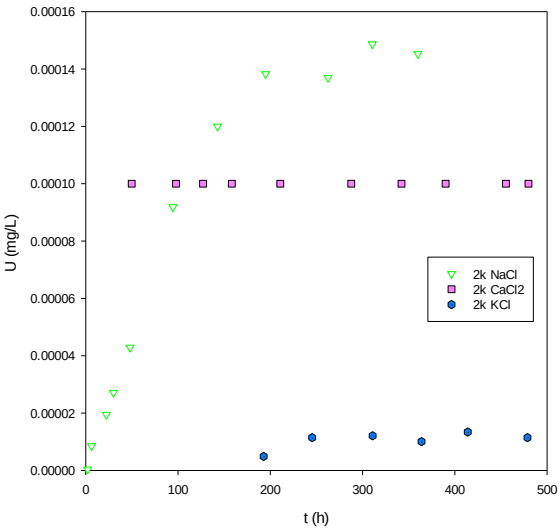

Figure 143. Barnett, 2k series. Pb, U, Bi, Th

XVIII-7-3 Benchtop Experiments Series (IC only)

XVIII-7-3.1 NaCl (0, 2k, 20k) Series

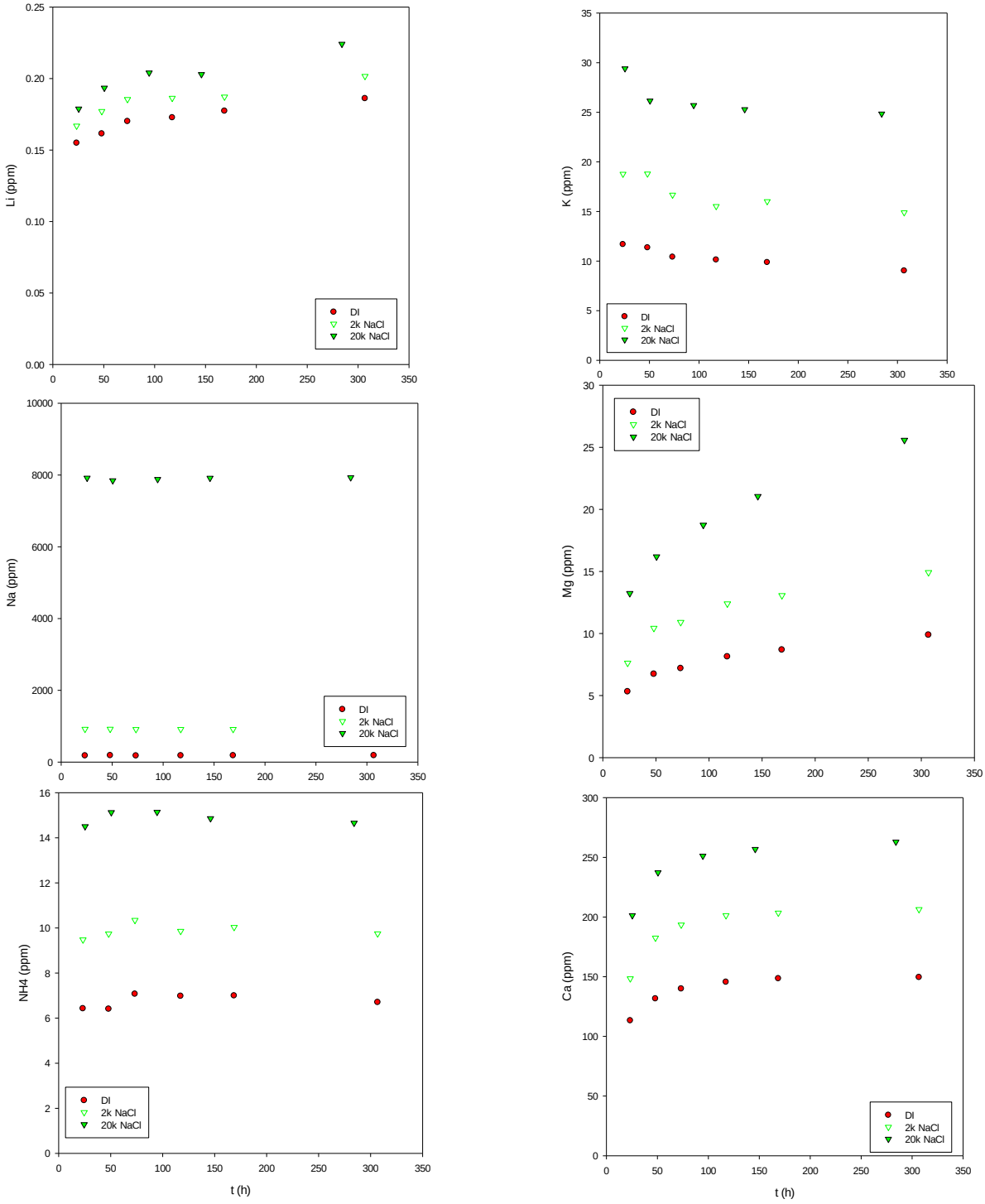

Figure 144. Barnett benchtop Na series (Li, K, Na, Mg, NH_4, Ca)

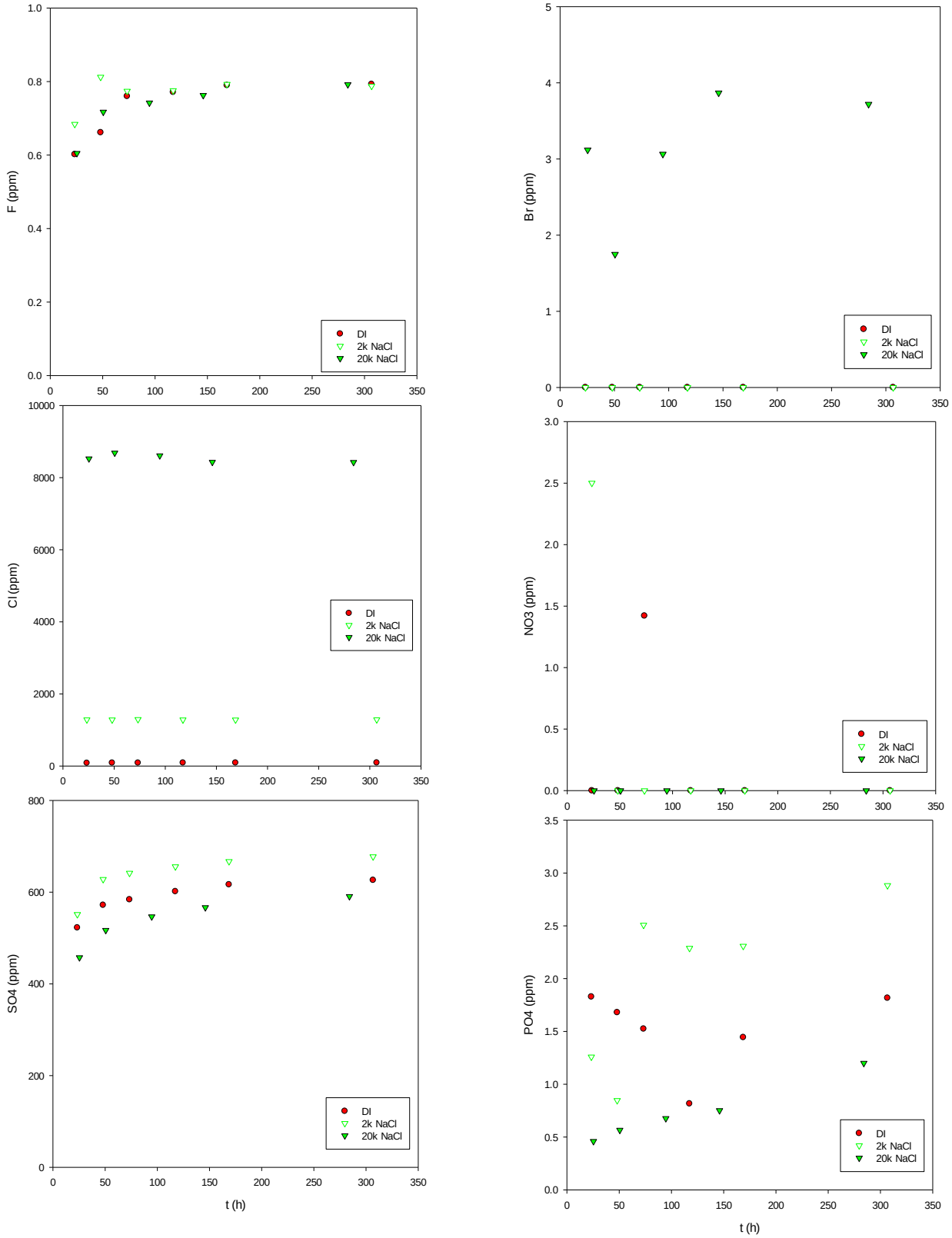

Figure 145. Barnett benchtop Na series (F, Br, Cl, NO_3, SO_4, PO_4)

XVIII-7-3.2 2k (Na, Ca, K)Cl Series

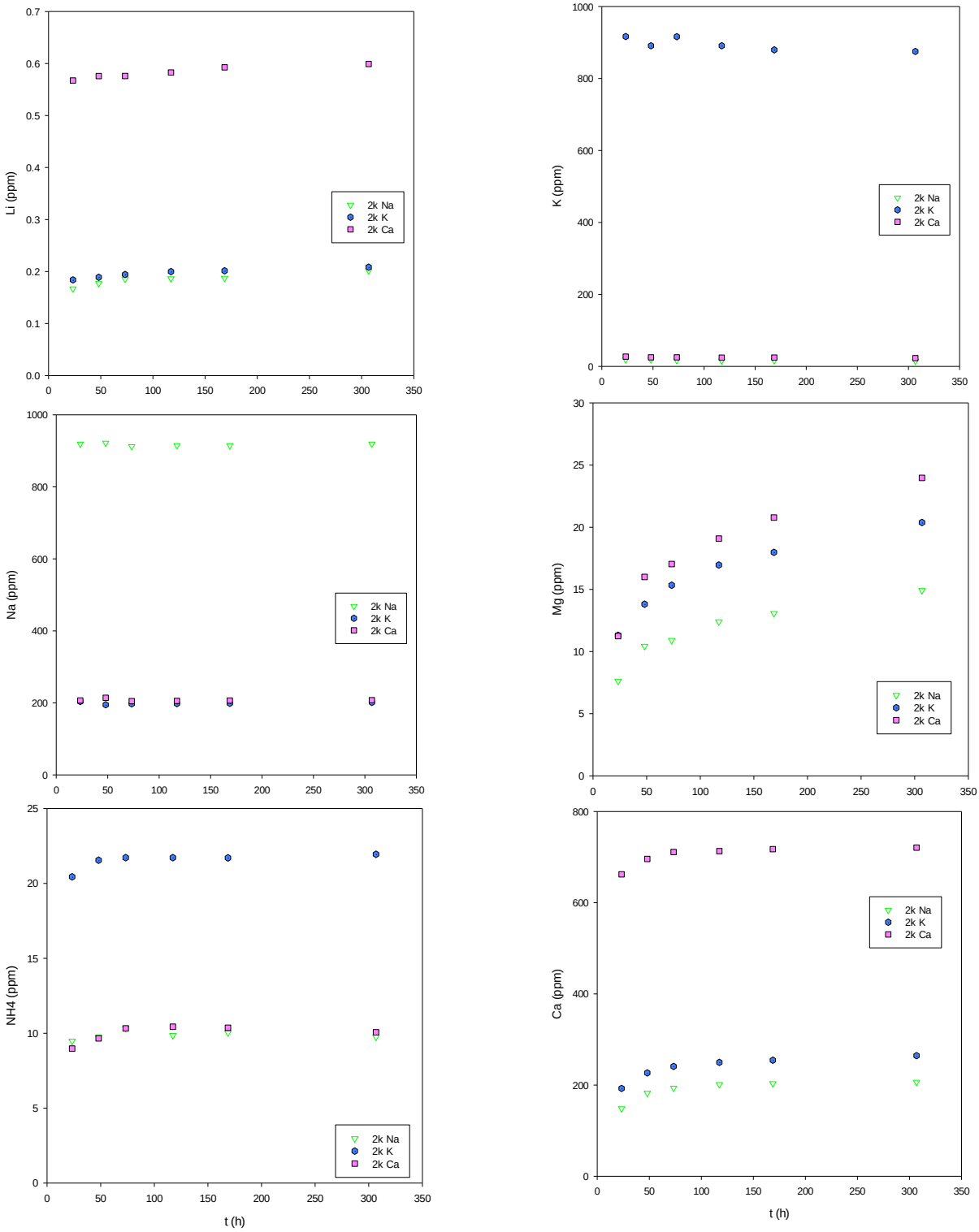

Figure 146. Barnett benchtop 2k series (Li, K, Na, Mg, NH_4, Ca)

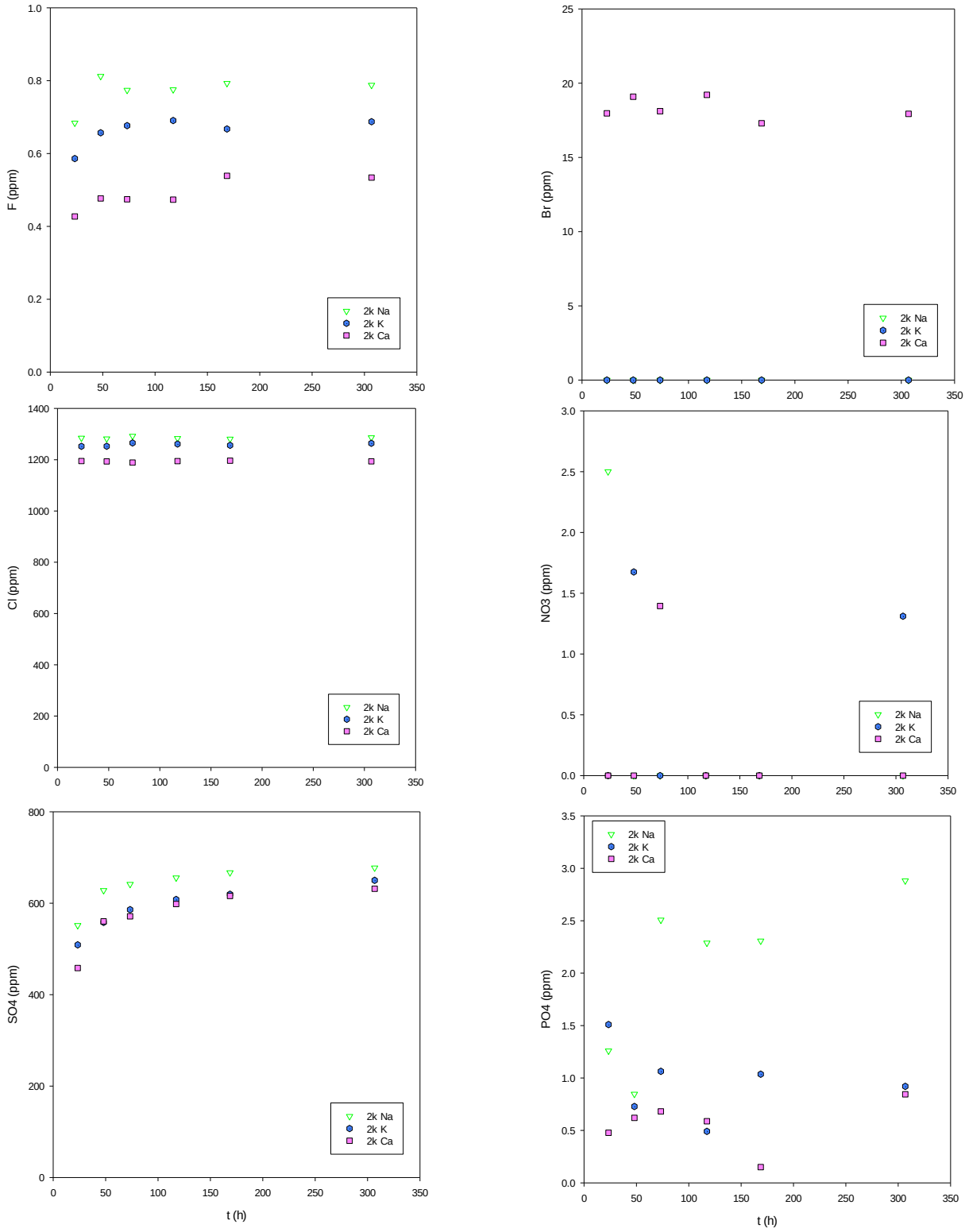

Figure 147. Barnett benchtop 2k series (F, Br, Cl, NO_3, SO_4, PO_4)

XVIII-7-4 Benchtop Experiments – Temperature Series

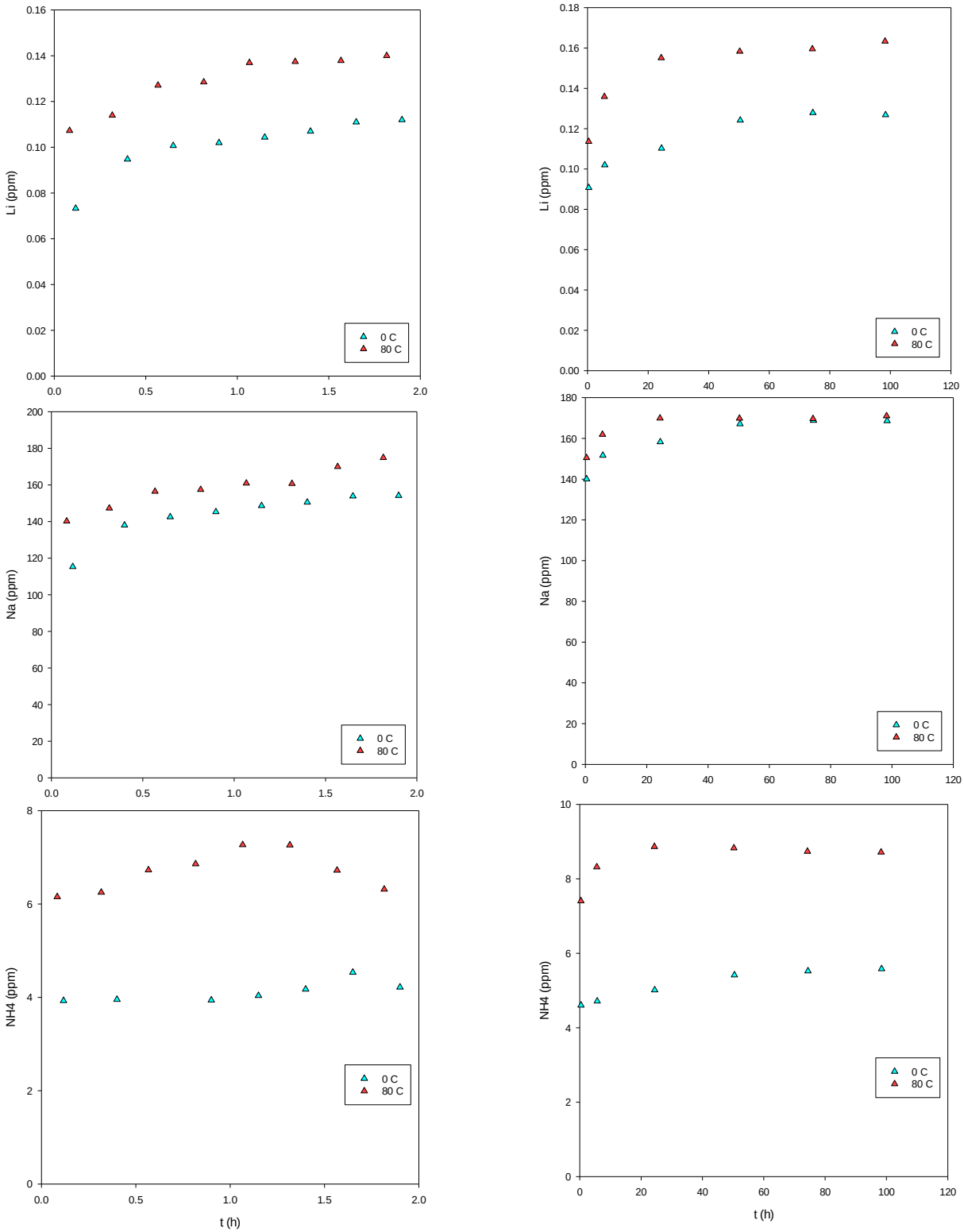

Figure 148. Barnett benchtop temperature series (Li, Na, NH_4)

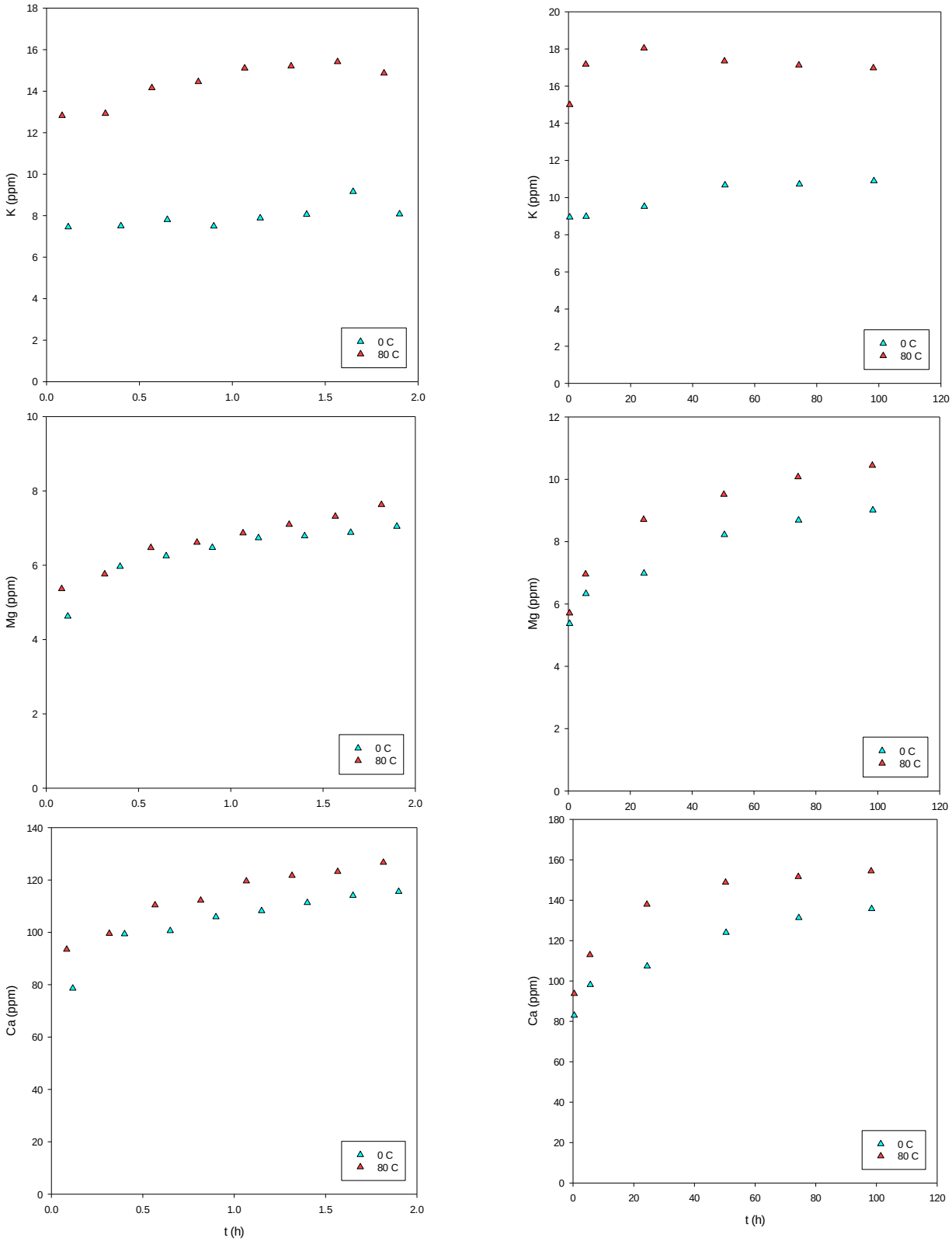

Figure 149. Barnett benchtop temperature series (K, Mg, Ca)

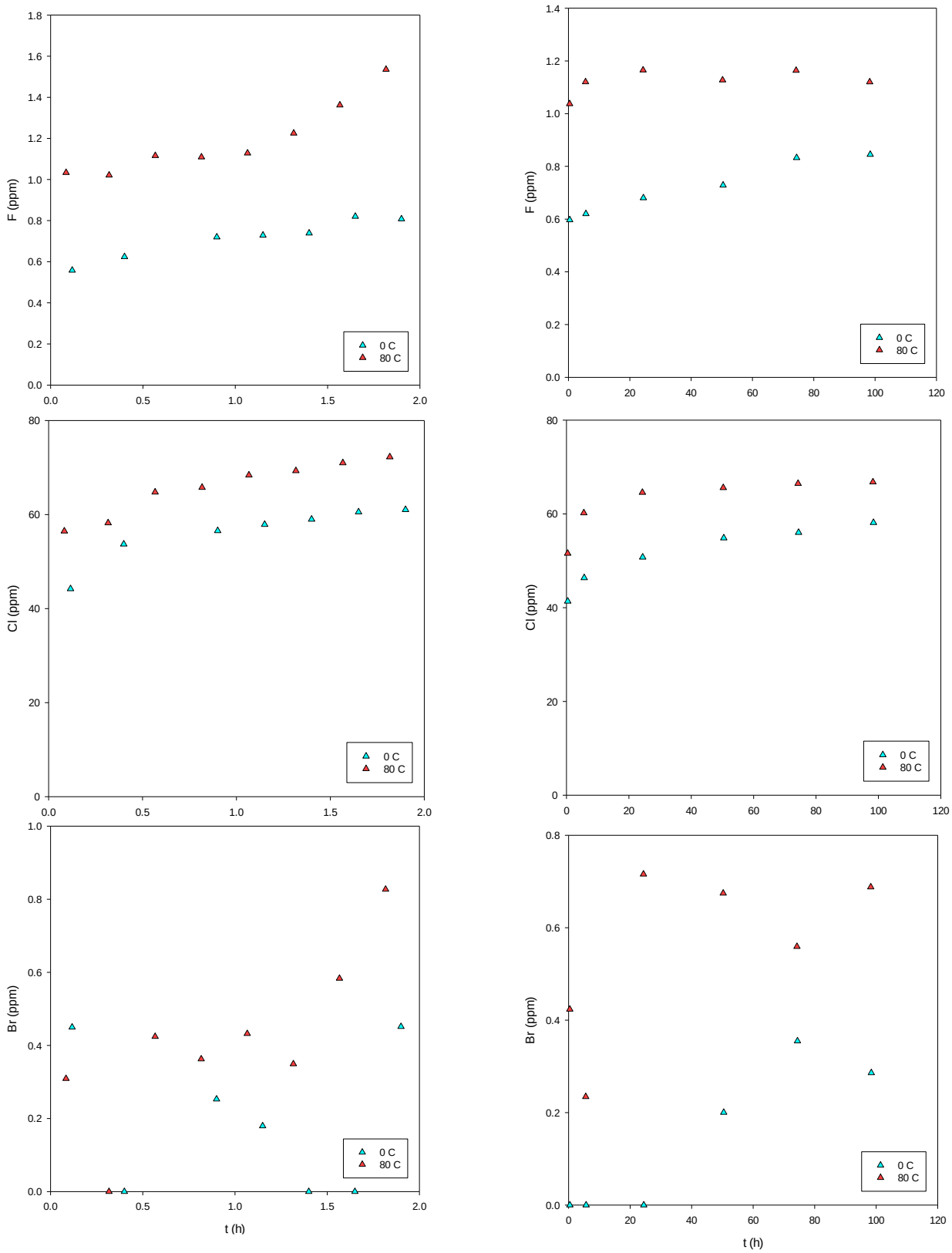

Figure 150. Barnett benchtop temperature series (F, Cl, Br)

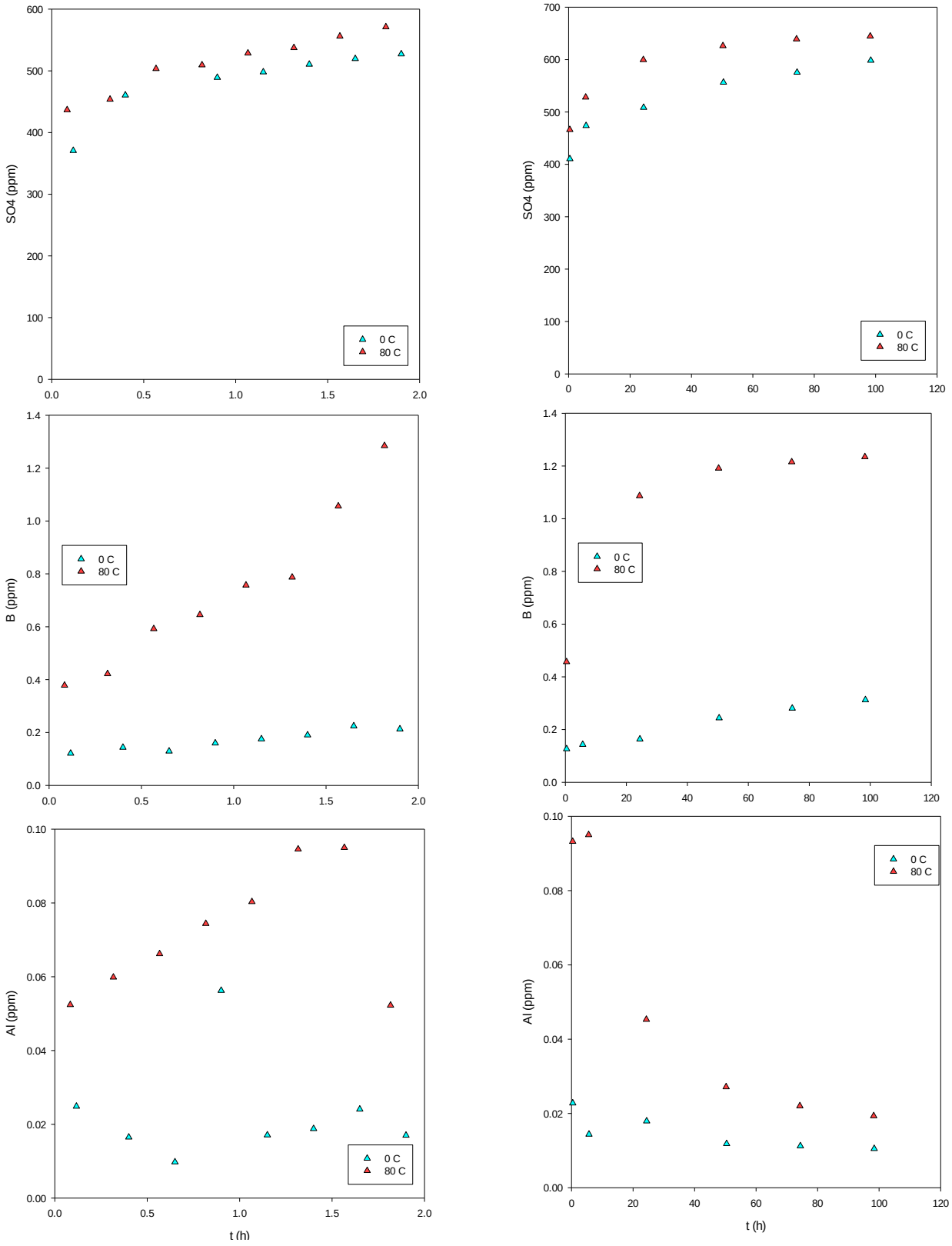

Figure 151. Barnett benchtop temperature series (SO_4, B, Al)

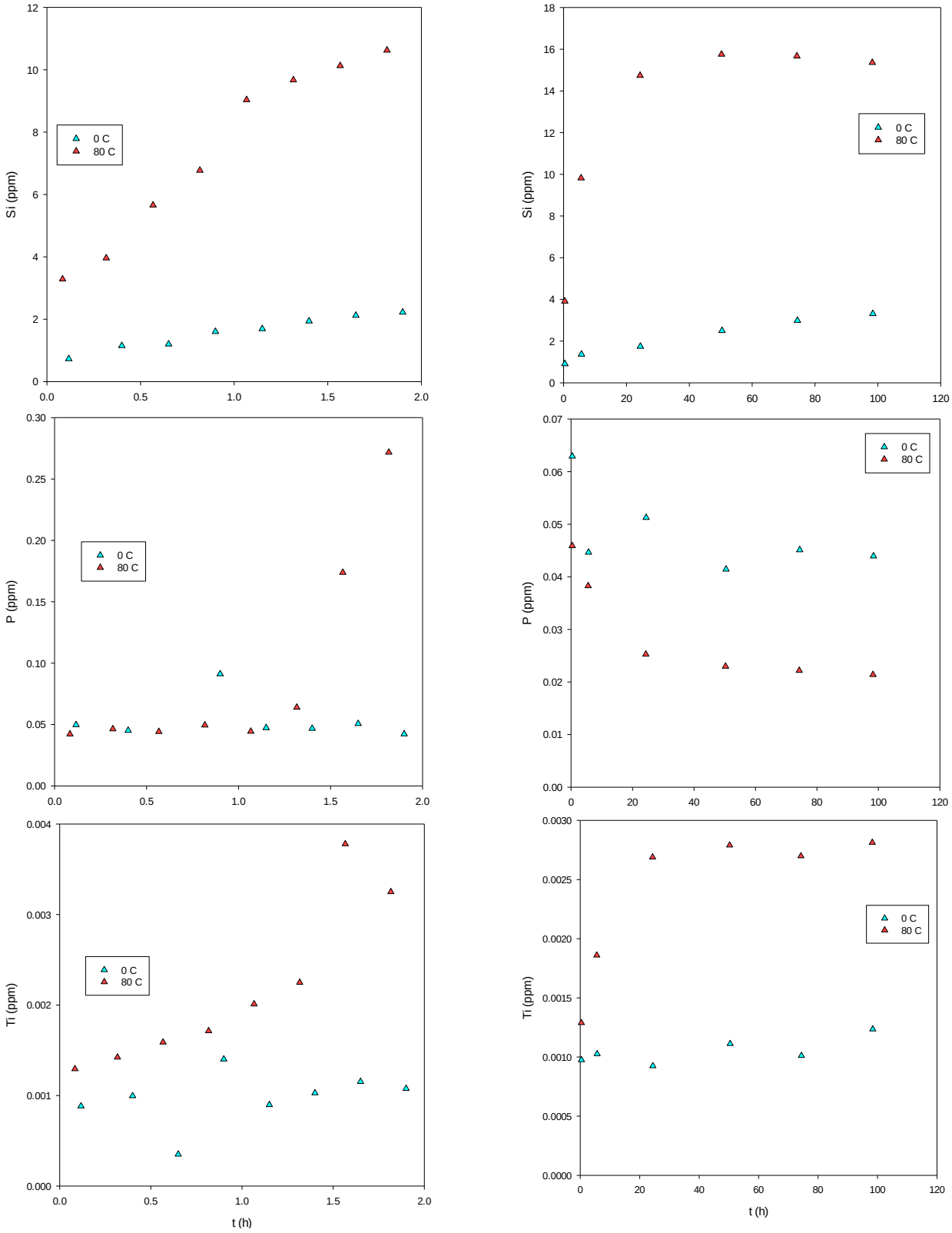

Figure 152. Barnett benchtop temperature series (Si, P, Ti)

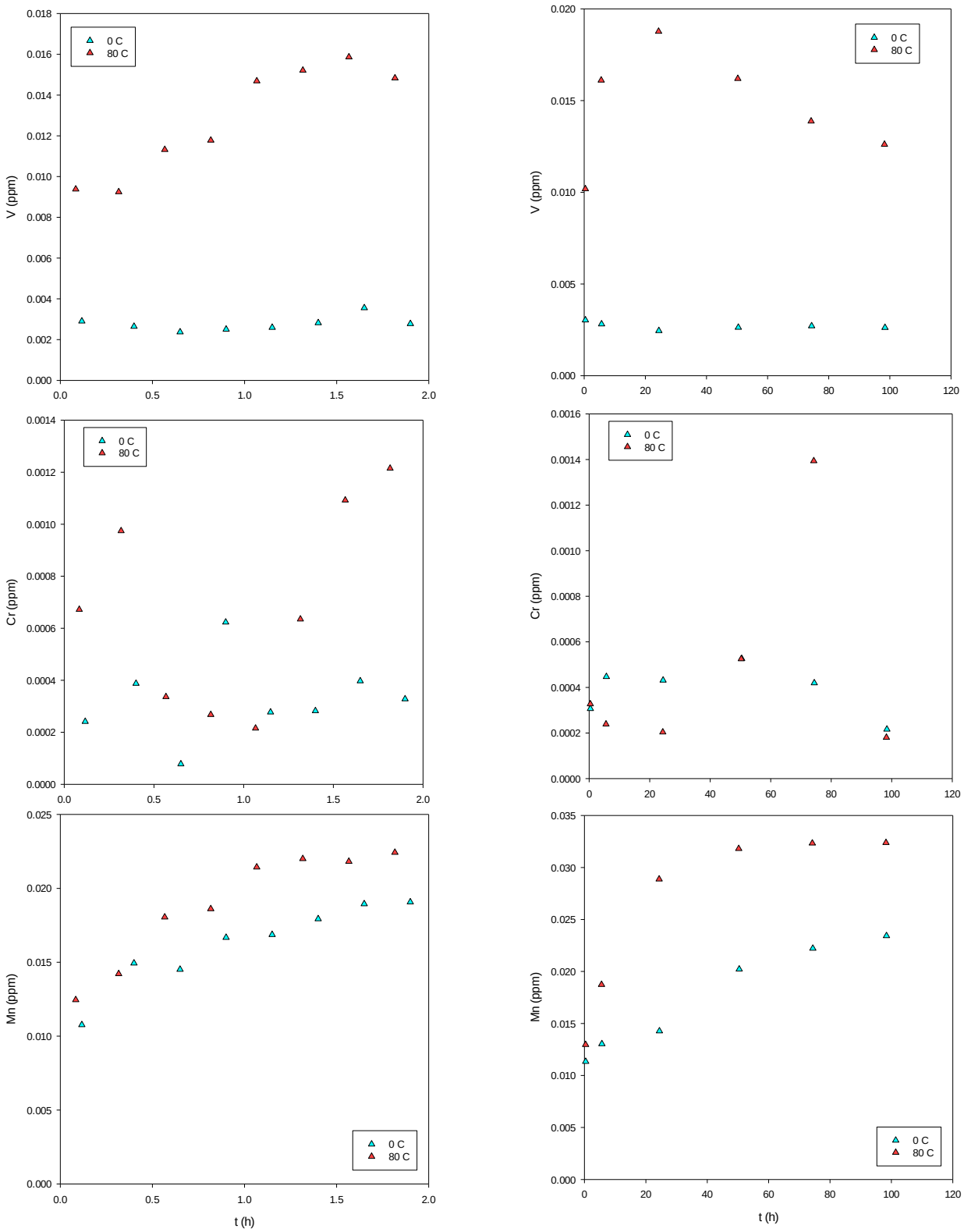

Figure 153. Barnett benchtop temperature series (V, Cr, Mn)

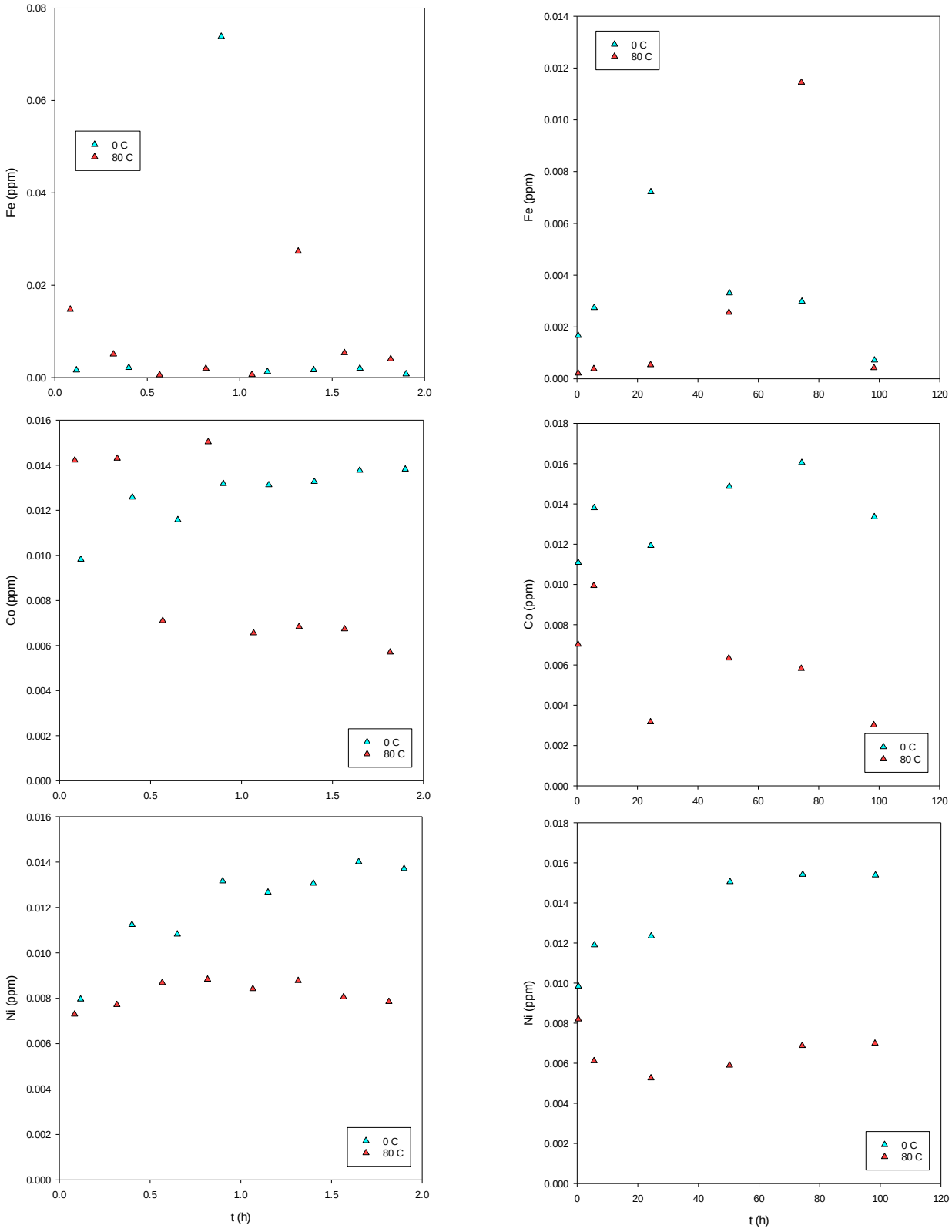

Figure 154. Barnett benchtop temperature series (Fe, Co, Ni)

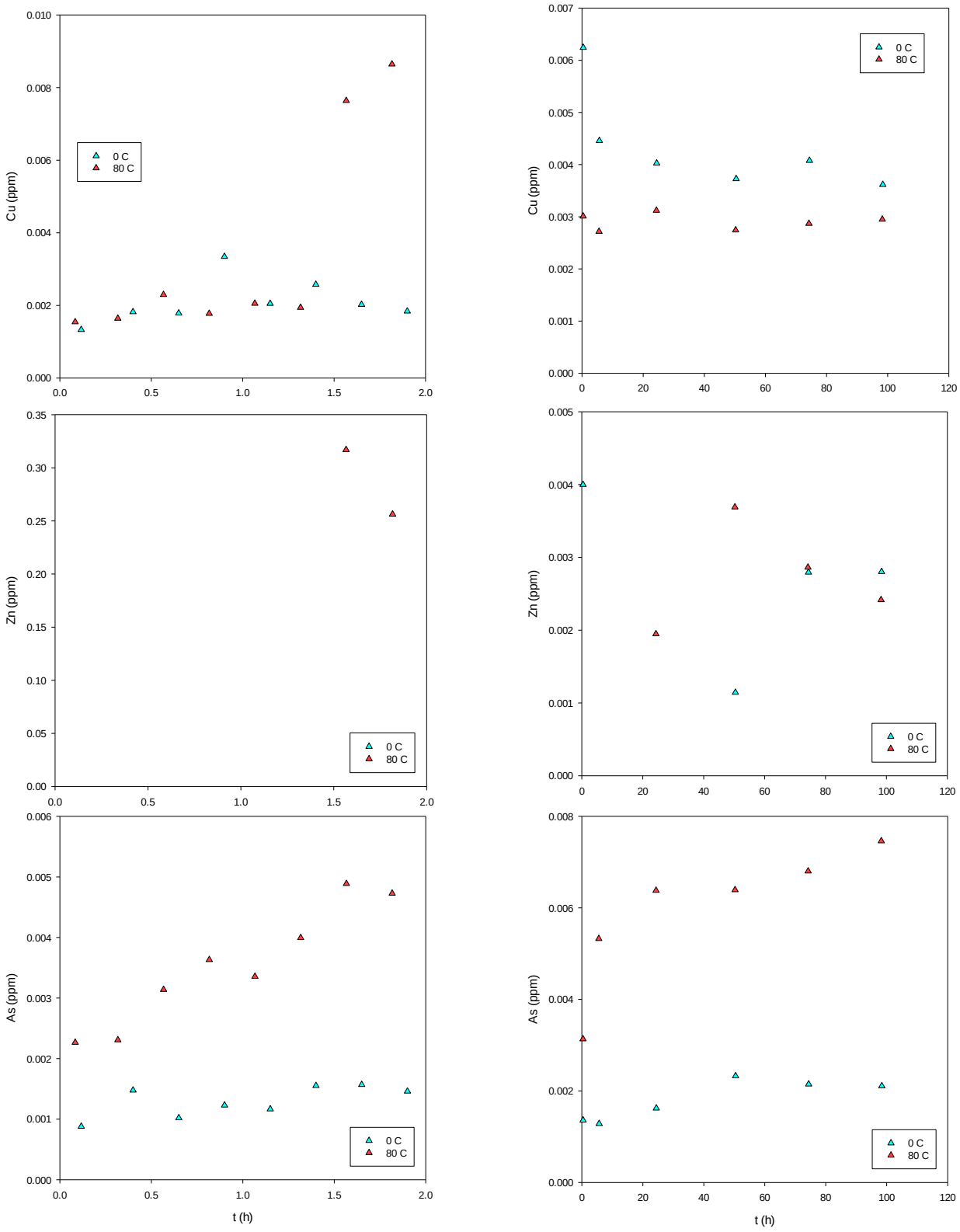

Figure 155. Barnett benchtop temperature series (Cu, Zn, As)

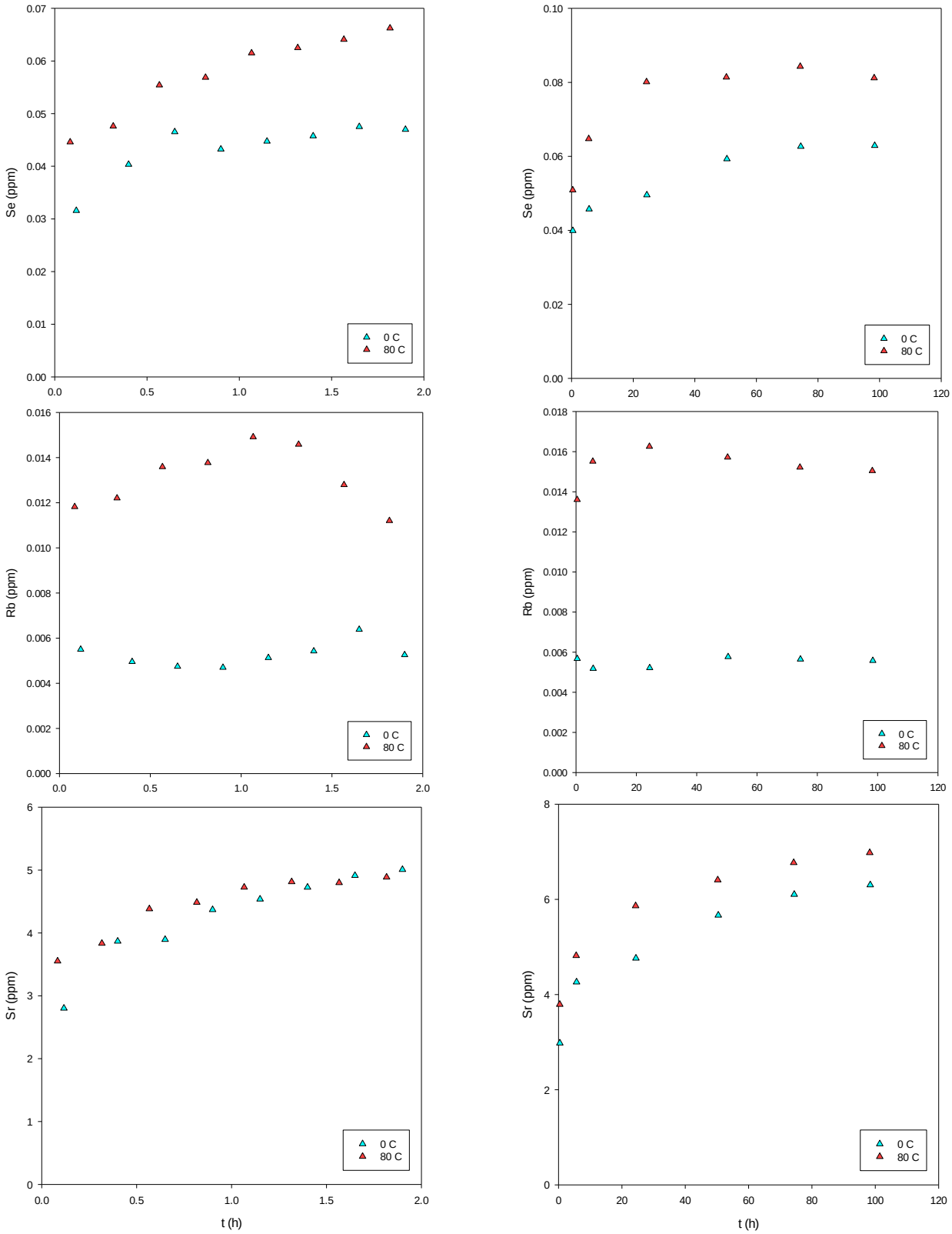

Figure 156. Barnett benchtop temperature series (Se, Rb, Sr)

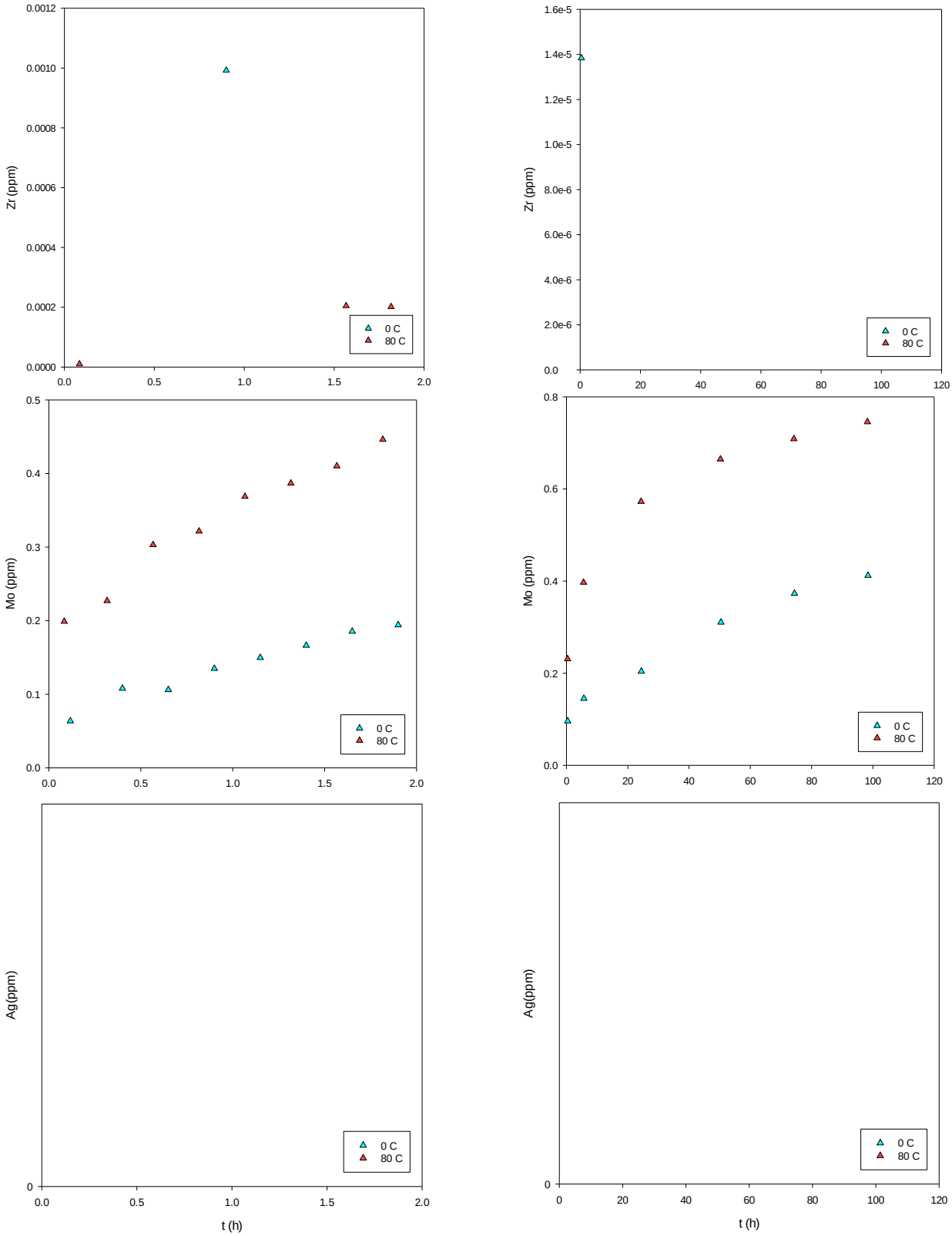

Figure 157. Barnett benchtop temperature series (Zr, Mo, Ag)

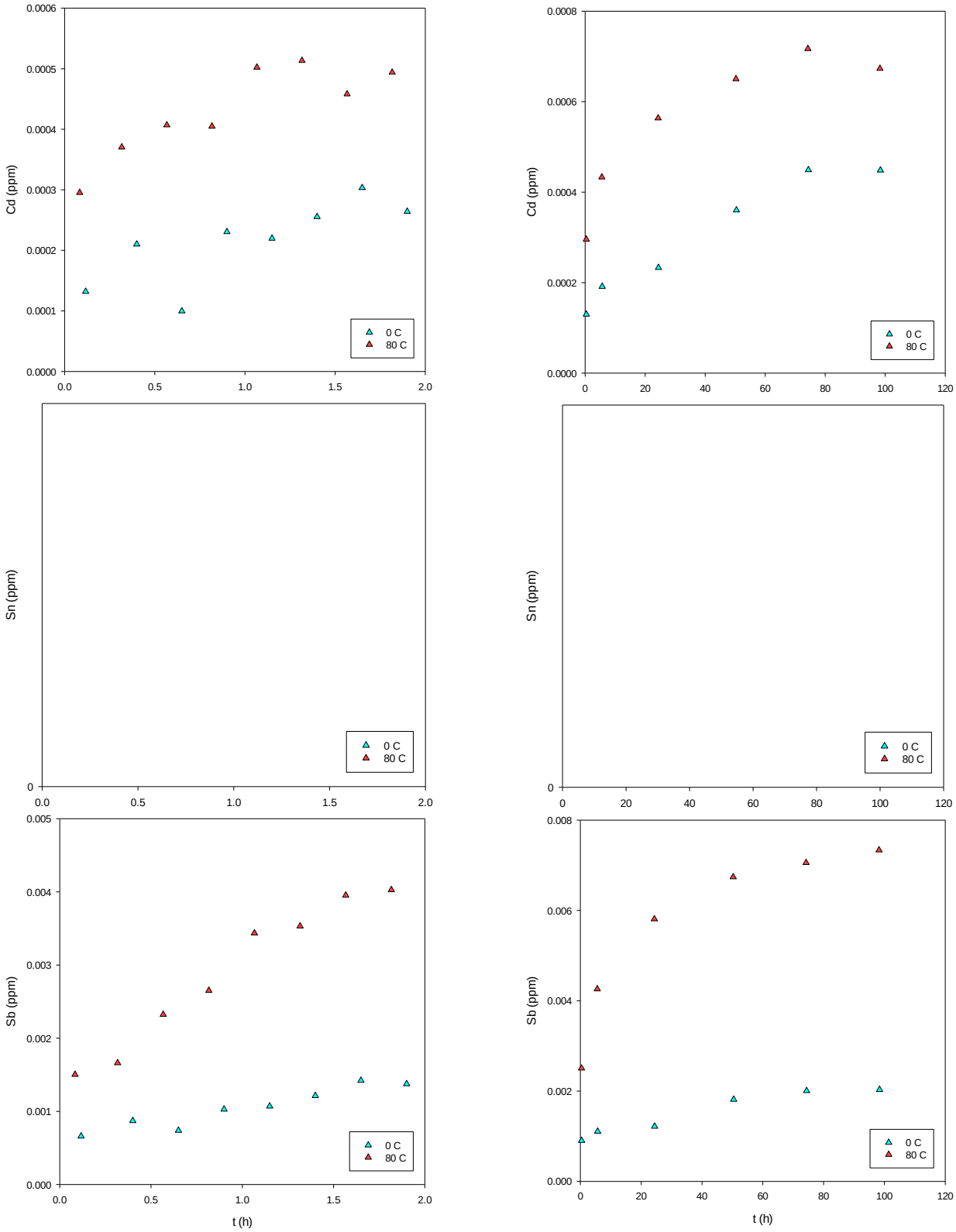

Figure 158. Barnett benchtop temperature series (Cd, Sn, Sb)

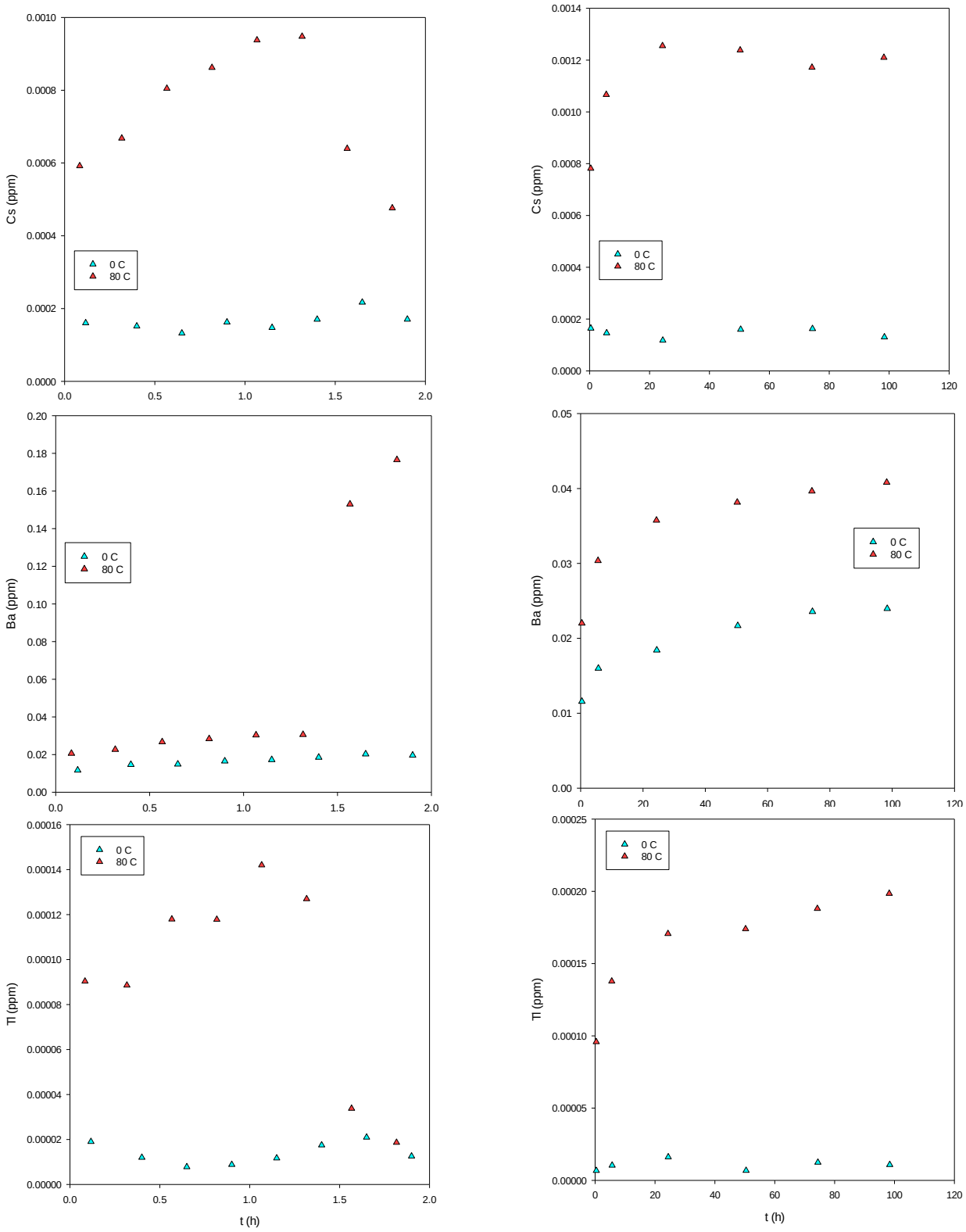

Figure 159. Barnett benchtop temperature series (Cs, Ba, Tl)

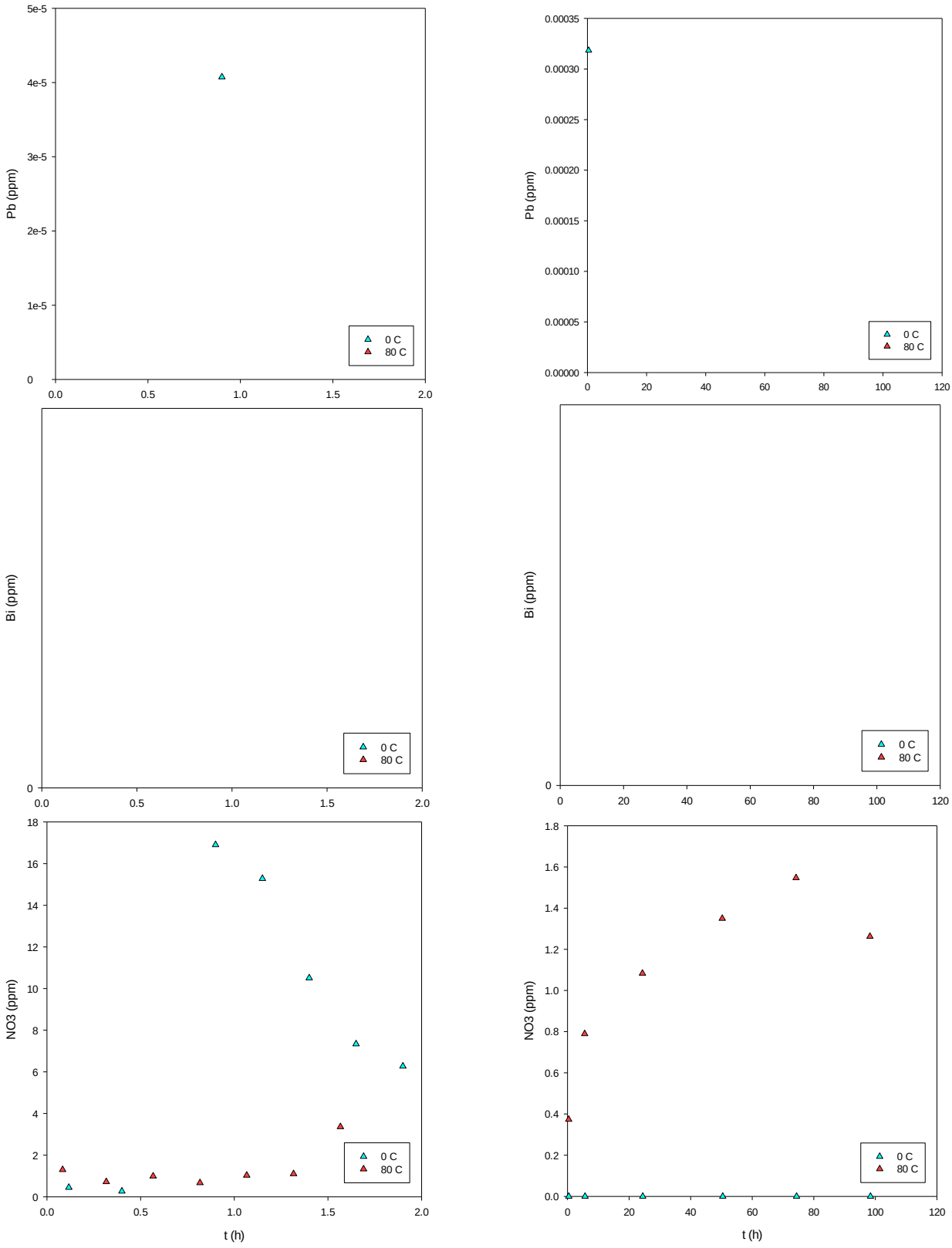

Figure 160. Barnett benchtop temperature series (Pb, Bi, NO_3)

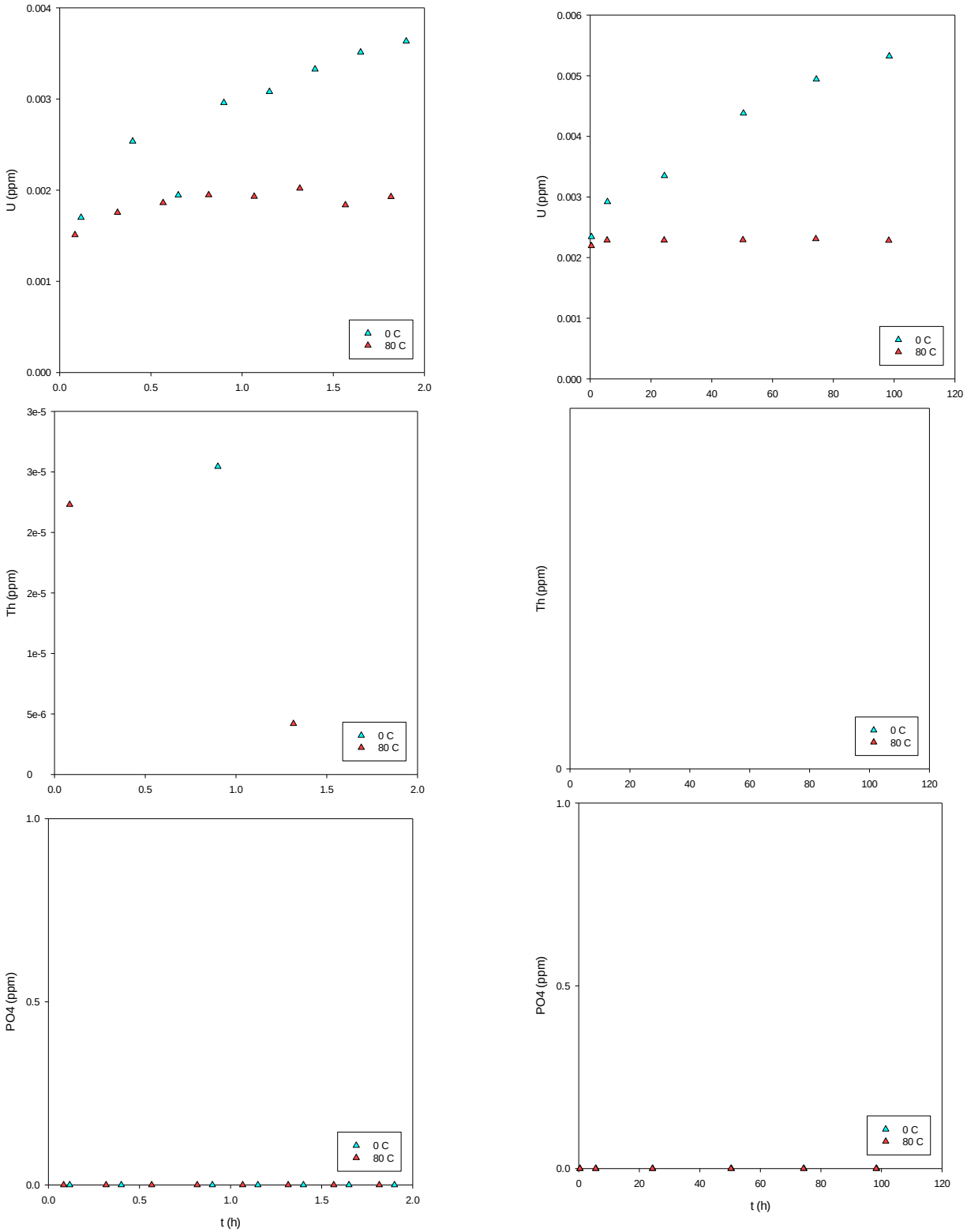

Figure 161. Barnett benchtop temperature series (U, Th, PO_4)

XVIII-8. Attachment C: Discussion on Rock-Water Ratio

Table 13Table 14